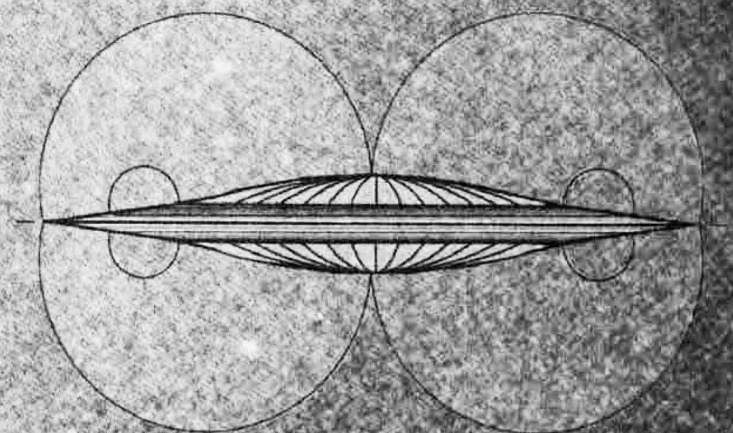




StarDrive Engineering

by Mark R. Tomion



StarDrive Engineering

by Mark R. Tomion



StarDrive Engineering



All rights reserved.
Copyright © 2001 by Mark R. Tomion
This book may not be reproduced in whole or in part,
by photocopy or any other means,
without the express written permission
of the publisher.

This *First Edition* manuscript independently published
by

 **Archer Enterprises**
2938 Ferguson Crs. Rd.
Geneva, NY 14456
Custom Engineering Design

and printed in the United States of America
by

Cayuga Press of Ithaca, Inc.
1650 Hanshaw Rd.
Ithaca, NY 14850

Chapter 8 and the Appendices of this text were originally
copyrighted by the author in unpublished form ©1999, as
Basic Specifications for the Electrodynamic Field Generator.

Library of Congress Cataloging-in-Publication data

Tomion, Mark R.
StarDrive Engineering.

Summary: describes development of, and specifications for, a
novel electrodynamic field generator and starship.
Includes special glossary.

1. electrical engineering 2. aerospace propulsion

I. Title.

Library of Congress Control Number (LCCN): 2001118702 [nonfiction]

ISBN 0-9713727-0-5 paperback

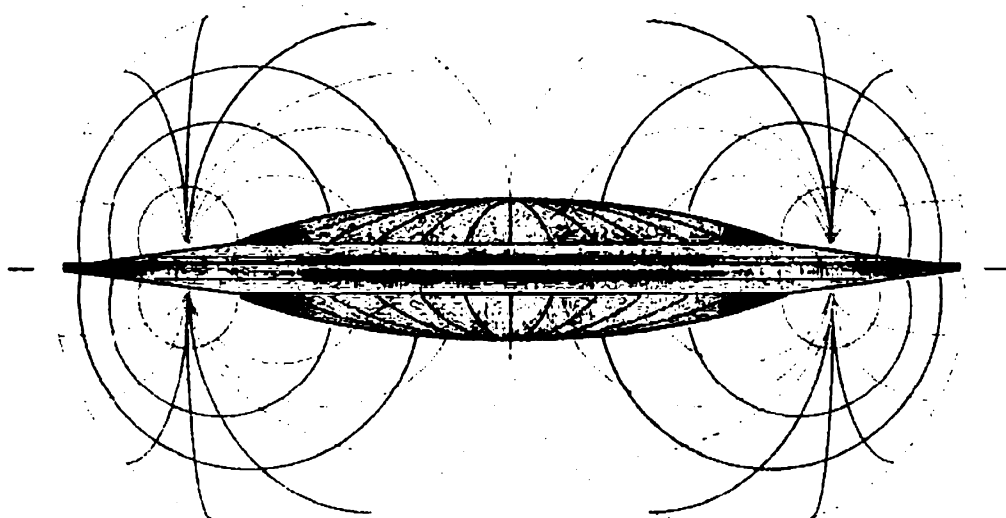
Acknowledgements

I would like to extend special thanks to Mr. Richard Neufang, who taught me that advanced algebra is the absolute standard against which all other forms of mathematics are measured, and that achieving intellectual excellence in one's chosen field can be the superlative experience in life.

Also, I am very grateful for permission to use the material listed below (in text order).

- Pgs. 2-3: (quote) pgs. 13-14, Ether Technology by 'Rho Sigma', ©1977; 1st edition published by the author.
- 2nd edition published in 1996 by Adventures Unlimited Press. Kempton, IL 60946
- Pgs. 5-6: (quote) excpt. pgs. 37-39, How to Build a Flying Saucer by T.B. Pawlicki, ©1981.
- published by Prentice Hall, Inc., Upper Saddle River, NJ 07458; *usage pending inquiry*.
- Pg. 8: (lyrics) "Time", The Turn of a Friendly Card by Alan Parsons & Eric Woolfson (Arista); copyright ©1980.
- all rights o/b/o Woolfsongs, Ltd.; admin. by Careers-BMG Music Publishing (BMI). Used by permission.
- Pg. 20: (Fig. 3) pg. 103, Electricity Made Simple by Henry Jacobowitz, B.A. (from the *Made Simple Books* series)
- published by Doubleday & Co., Inc., ©1959; a div. of Random House, Inc. New York, NY 10036
- Pg. 22: (Fig. 4) pg. 7, Receiving Tube Manual by RCA Corp., ©1971. All rights reserved.
- published by RCA Corporation, Electronic Components Div., Harrison, NJ 07029
- Pg. 23: (quote) pg. 89, Vol. 8, *The Book of Popular Science* by the Grolier Society, ©1958.
- published by The Grolier Society, Inc.; a div. of Grolier Publishing, Danbury, CT 06816
- Pg. 29: (libretto) "Music is the Best", Joe's Garage: Acts I, II & III by Frank Zappa (Rykodisc). Published by Munchkin Music, copyright ©1979 The Zappa Family Trust. All rights reserved. Used by permission.
- Pg. 34: (Fig. 6) pg. 74, Ether Technology by 'Rho Sigma', ©1977 (as above).
- Pg. 41: (quote) pg. 41, Permanent Magnet Design & Application Handbook by Lester R. Moskowitz.
- published by Cahners Books Int'l., Inc., ©1976; a div. of Cahners Business Info., New York, NY 10014
- Pg. 74: (quote) excpt. pgs. 144-145, The Complete Venus Equilateral by George O. Smith, ©1976.
- published by Ballantine Books; a div. of Random House, Inc., New York, NY 10036
- Pg. 98: (lyrics) "Rocket Man", Honky Château; words and music by Elton John & Bernie Taupin (MCA Records).
- copyright ©1972 Universal/Dick James Music Ltd.; administered by Universal-Songs of Polygram International, Inc. (BMI) International copyright secured. All rights reserved. Used by permission.
- Pg. 174: (photo) Nikola Tesla; used by permission, courtesy of Culver Pictures, New York, NY 10011
- Pg. 234: (lyrics) "Space Oddity", Space Oddity; words and music by David Bowie (Virgin Records).
- copyright ©1969 (renewed) Onward Music Ltd., London, England. Used by permission.
- Pg. 248: (Fig. 58) pg. 76, How to Build a Flying Saucer by T.B. Pawlicki, ©1981 (as above).
- Pg. 265: (Fig. 60) pg. 60, April '93 issue *Discover* magazine, ©1993 The Walt Disney Company.
- Discover Publications, Inc., New York, NY 10011; courtesy of Josef Astor, New York, NY.
- Pg. 270: (lyrics) "If", by David Gates (Manna, on Elektra); copyright ©1971 Sony/ATV Tunes LLC. All rights admin. by Sony/ATV Music Publishing, Nashville, TN (ASCAP). All rights reserved. Used by permission.
- Pg. 289: (Fig. 65) pg. 56, April '86 issue *Radio Electronics* magazine, ©1986 Gernsback Publications, Inc.
- Gernsback Publications, Inc., Farmingdale, NY, 11735; courtesy of Gregory Hodowanec, Newark, NJ.
- Pg. 290: (lyrics) "I'm Your Captain", Closer to Home by Grand Funk Railroad (Capitol Records).
- copyright ©1970 Storybook Music, Yuma, AZ (BMI). Used by permission.
- Pg. 321: (quote) pg. 81, reprinted with the permission of Scribner, a division of Simon & Schuster, Inc., from The Lathe of Heaven by Ursula K. LeGuin. Copyright ©1972 by Ursula K. LeGuin.
- Pg. 333: (graph) The Cosmological Constant by Sean M. Carroll, William H. Press, & Edwin L. Turner.
- published in Annual Review of Astronomy and Astrophysics, pg. 506 (Fig. 1), Vol. 30, 1992 and used by permission; ©1992 Annual Reviews, Palo Alto, CA 94300
- Pg. 348: (graphs & drws.) pgs. 47-48, Permanent Magnet Design & Application Handbook
by Lester R. Moskowitz; ©1976 (as above).
- Pg. 349: (graph) pg. 42, Permanent Magnet Design & Application Handbook
by Lester R. Moskowitz; ©1976 (as above).
- Pg. 351: (graph) pg. 79, Permanent Magnet Design & Application Handbook
by Lester R. Moskowitz; ©1976 (as above).

Pg. 355: (Fig. 30) pg. 31, Receiving Tube Manual by RCA Corp., ©1971 (as above).
 Pg. 357: (Fig. 31) pg. 29, Receiving Tube Manual by RCA Corp., ©1971 (as above).
 Pg. 358: (Fig. 32) pg. 32, Receiving Tube Manual by RCA Corp., ©1971 (as above).
 Pg. 359: (Fig. 33) pg. 27, Receiving Tube Manual by RCA Corp., ©1971 (as above).
 Pg. 361: (Fig. 34) pg. 26, Receiving Tube Manual by RCA Corp., ©1971 (as above).
 Pg. 379: (Fig. 36) pg. 203, Vol. 8, Encyclopædia Britannica, 14th Edition.
 - ©1968 by Encyclopædia Britannica, Inc., Chicago, IL 60604; reprinted with permission.
 Pg. 381: (Fig. 38) pg. 176, Receiving Tube Manual by RCA Corp., ©1971 (as above).
 Pg. 412: (Fig. 51) courtesy of Dr. Thomas R. Shrout, Penn State University, Materials Research Laboratory.
 Pg. 413: (Fig. 52) courtesy of Dr. Thomas R. Shrout, Penn State University, Materials Research Laboratory.
 Pg. 417: (Fig. 54) pg. 282, Permanent Magnet Design & Application Handbook
 by Lester R. Moskowitz; ©1976 (as above).



Materials Source References

Metals: ***Allegheny Ludlum Corp.***
 Pittsburgh, PA 15200 {stainless steel hull sectors}
Mi-Tech Metals Inc.
 Indianapolis, IN 46218 {field emitters} *many thanks to Jeff Keeler
MWS Wire Industries
 Westlake Village, CA 91362 {rotor segments, field coils}
Westinghouse Electric Corp.
 Metals Division; Blairsville, PA 15717 {magnetic rings}

Ceramics: ***CeramTech, NA***
 Laurens, SC 29360 {power resistors, segment separators} *special thanks to Jon Scott
Keramos Inc.
 Indianapolis, IN 46268 {dielectric & space charge buffers}
NTK Technical Ceramics
 Arlington Heights, IL 60004 {ballrace components} *many thanks to Joe Tajima
Radio Materials Corp.
 Attica, IN 47918 {ballast capacitors} *many thanks to Dale Klausen

NM Composites: ***Advanced Composite Products & Technology, Inc.***
 Huntington Beach, CA 92649 {superstructure} *special thanks to Lee Truong

Table of Contents

* Preface	xi
** Forward	xii
*** Introduction	xv

Book I: A Dream

[1] Perspective and Purpose	1
[2] Tales of Starships	9
[3] Historical Background	18
[4] Design Parameters	30
[5] Magnetics: Rings & Coils	42
[6] Hull Configuration	58

Book II: The Way

[7] Electrostatics: Rings & Grids	75
[8] Basic Specifications	91
[9] Field Electrodynamics	215

Book III: The Stars

[10] Exceeding the Limits	235
[11] The Quest for Quantum Gravity	254
[12] Field Resonance & Communications	271
[13] Navigation & Sensor Capability	291
[14] Dual Continuum Cosmology	322
- Appendix A (Technical DataSheets)	345
- Appendix B (Material SpecSheets)	387
- Bibliography	421
- Special Glossary	423
- Table of Illustrations	440

Bold Text Cues

In order to give you all a synoptic overview of the course of discussion taken in **StarDrive Engineering**, the following listing of bold-faced **text cues** is provided, and these should hopefully also assist each reader to navigate their own course therein.

Book I: A Dream

<i>Preface:</i>	- a Dream	<i>xi</i>
	- the Way	<i>xi</i>
	- the Stars	<i>xi</i>
<i>Forward:</i>	- "the key to the universe"	<i>xii</i>
	- mysterious point of light	<i>xiii</i>
<i>Intro.:</i>	- StarDrive	<i>xiv</i>
<i>Chapter 1:</i>	- electric field theory	4
	- powered electrostatic induction	5
	- the most spectacular artificial lightning storm ever	5
	- to artificially transcend the speed of light	6
	- the Universe's actual upper speed limit is c^2	7
	- reactionless electric drive	7
	- the dc disk dynamo	7
	- the Gateway to the Stars	7
<i>Chapter 2:</i>	- a glowing field of force	10
	- a "semi-polarized capacitive arc-discharge envelope"	16
	- a great, charged, flywheel	16
<i>Chapter 3:</i>	- utilizing vacuum tube techniques	24
	- to boost Primary Power System voltage	25
	- Searl and his levity disc	26
	- the Apocrypha	26
<i>Chapter 4:</i>	- operative characteristics which have been rejected	30
	- valid design elements of a workable StarDrive system	33
	- rotor segments	33
	- electrode rings	33
	- field emitters	35
	- field coils	38
	- magnetic rings	38
<i>Chapter 5:</i>	- Variable Inductor Arrays	46
	- secondary rotor magnetic field	48
	- flux initiator coils	50
	- annular power field	51
	- transflection coils	52
	- flux reductor	52
<i>Chapter 6:</i>	- the Field Hub	59
	- Central Chamber	60
	- the Drive Ring	61
	- radial Drive Field	64
	- Field envelope configuration	64
	- hull static capacitance	66
	- uniform Field intensity	68
	- Field specific impulse	71

Book II: The Way

Chapter 7:	- induction electrode arrays	75
	- transfer triode arrays	75
	- stage voltage balance	78
	- <i>primary voltage expansion ratio</i>	81
	- field ballast capacitors	83
	- electric Primary Arrays	84
	- Field current bias	87
	- field power resistors	88
Chapter 8:	- design hull configuration	93
	- Field and rotor voltages	99
	- advanced rotor design	125
	- magnetic ring arrays	131
	- field coil design	138
	- electrode array voltages	151
	- Field Voltage Control System	182
	- dielectric buffers	200
	- thermal conduits	200
	- Structural Intercooler System	200
	- closing hardware considerations	214
Chapter 9:	- displacement current	216
	- field dynamic capacitance	216
	- selector plane	218
	- the StarDrive integral Field	220
	- the electrophysics of lightning	226
	- Field ignition	228

Book III: The Stars

Chapter 10:	- power and over-unity	239
	- on the right track	245
	- pushing the envelope	249
	- an unlikely hero	250
	- the time-light barrier	251
Chapter 11:	- quantum potential loop-space	257
	- quantum vacuum fluctuations	261
	- negative quantum time-space	264
	- trans-light mechanics	266
Chapter 12:	- oscillatory apparent mass effect	271
	- linear oscillating amplifier	281
	- tuned gravity wave cavity detector	288
Chapter 13:	- warp jump turnaround sequence	300
	- galactic coordinates	306
	- hull precessional torque	314
	- induced X-ray emissions detection	317
Chapter 14:	- universal architecture	338
	- the no-boundary universe	340
	- Eternity	342

Book I: *A Dream*

Preface

Children really are amazing, aren't they? In particular, their incredible innate potential makes it virtually impossible to predict what special interests and abilities each one might manifest later on in life.

An almost universal tendency among the young in my time, though, much like the very common fascination with 'dinosaurs!' at an early age, was to experience a phase of fascination with 'flying saucers!' and other "outer space stuff".

Almost all of us, it seems, grew out of this at some point as the seeming impossibilities of traveling between the stars were impressed upon increasingly *adult* minds. A rare few, however, are even at this time leading lives spent dedicated to the pursuit of the actual knowledge which might yield *a viable means of star travel*, dominated by a **Dream** that such means must exist. Perhaps only the child in us is capable of sustaining the sure and certain faith that **the Way** can be found.

I would like to believe that my work will become a valued legacy to the Children of Man, who for uncounted centuries have gazed at the heavens in wonder and who may indeed inherit **the Stars** one day if they want to or need to badly enough.

When I was a young boy, growing up in the central Finger Lakes region of New York State, my father had a little shop out behind our house where he fixed electric motors nights and weekends. This was, and remains, a fairly rare trade and it requires more than a little aptitude for physics. I would sit for hours on a tall stool near his workbench, watch my father work on various electro-mechanical marvels, and no doubt drive him to distraction with endless questions of “how?” and “why?”.

My dad is a Korean War veteran and at that time in my life, the early 1960's, he didn't much care to talk about it. At times, however, he would elaborate on certain remarks he had occasionally made: that sometimes at night (after heavy ground fighting) he and his compadres would see strange “points of light” in the sky. These remote yet brightly glowing objects moved at incredible speeds and executed maneuvers which would be impossible under ordinary aerodynamic and inertial conditions. Among themselves, they came to the consensus that they were observing, and perhaps being observed by, alien aerospace craft which technologically were orders of magnitude beyond the early jet fighters of that period.

He went on to say that in his belief these craft were all-electrically powered, and hence their brightness and speed were more readily understandable. He also thought that they no doubt incorporated some very sophisticated magnetic engineering because a proper understanding of applied magnetics was very probably **“the key to the universe”**. In his opinion, the greatest human intellectual achievement of all would be to discover the principles which would allow Man to cross the gulf between the stars in just such craft.

Well, this indeed seemed to me, even at that time, an irresistibly lofty and noble challenge and it remains one which has profoundly influenced my life more than I could possibly have imagined then. I began to keep a voluminous scrapbook of UFO and ‘saucer’ stories gleaned from newspapers and tabloids throughout the ‘60's. This was, of course, not too difficult as the world was then-currently enjoying a great wave of UFO-mania. I delved passionately into astronomy and soon knew all the major constellations and many of their

important stars and celestial distances. My parents fostered this interest by getting me a rather fine amateur telescope, which I used for hours with rapt attention.

One particularly clear winter night I just happened to be observing the planet Mars, which had appreciable 'disk' within the 'scope's field, when I saw my own **mysterious point of light**. It emerged, to my astonishment, from behind the Martian silhouette and sling-shotted around the planet at a celestially incredible speed! It left my field in a mere few seconds, quickly leaving Mars and both its moons far behind (on a visibly hyperbolic trajectory), and ufology had another confirmed believer/advocate.

In the years that followed, I became a voracious reader of great science fiction stories and was, of course, a devoted "Trekkie". My days were filled with college, work, family, and friends, like other young people my age in the pleasant 1970's. But as the '80's unfolded, I realized that my increasingly rarified life lacked something somehow undefined. And so, after many years of unfulfilled Wandering in the adult world, the Man returned to the skilled trade of his father and to the inescapable Quest for the Way. This work is thus dedicated to my dad, Wesley: it is to him I owe my life and my Dream.

Introduction

I must hope at this point that the sincere reader begins to feel the spirit of intellectual wonder and total commitment that underlies this textual offering, despite the obviously controversial nature of the subject matter. Properly introducing a work of this type may well represent some of the most difficult and important non-technical writing I could ever do. It is my intent, however, that this book be made accessible to all of the good people whose world view allows them to appreciate the pursuit of this life's dream of mine: the design and eventual construction of an electromagnetic machine with the real capacity to travel among the stars.

Every effort has been made herein to create a basic and logical framework of scientific conceptual reasoning which is sufficient to guide any serious reader to a clear understanding of what is proposed, regardless of their having an advanced educational background. The following material is therefore written and presented on a variety of levels so that it may appeal to the broadest possible audience. No attempt will be made, though, to defend this project against the broad negativism it may engender in those persons who are either incapable of understanding the truly imminent need for a working 'star drive' system or unable to believe that one is possible - today!

I don't think that such a dream arises solely of its own accord or suddenly becomes the focus of a lifetime. Without digressing unduly into philosophy, I feel it's safe to say that forces beyond our full understanding shape and guide the destiny of true pioneers in any frontier of the human experience. One day, someone *must* develop, build, and test the world's first **StarDrive**, based on the application of a *unified quantum field theory*, or mankind will be unable to achieve its own greater Destiny and may perhaps be unable even to survive.

I have never been an especially religious man, but perhaps even our own Creator awaits us, out there, at the ends of the Universe and the limits of our comprehension. You see, I refuse to believe that a loving God would create us, with such open-ended evolutionary potential, in a Cosmos with physical laws which doom us to be trapped here forever . . . It would require hundreds of years of objective time to reach the nearest star other than our own, even with the greatest conventional sublight space technology possible, and return. Who would ever volunteer for such a trip?

I have also come to believe of late that the enormous social and political problems our race has always suffered will not be conquered until all our peoples live in the light of a common knowledge - that there are innumerable green worlds, out among the stars, for us to explore with a faster-than-light space drive. Until then, the Earth will be for Mankind like a high-tech prison from which we have no hope of parole.

Chapter 1

Perspective and Purpose

During the early and intermediate stages of my search for a provable trans-light technology, I was driven by the powerfully uplifting conviction that the successful completion of my work – and its subsequent unveiling to the world – would be entirely for the common good and benefit of all humanity. I was at that point (of course) still unsure about a great many details, but I abided faithfully the “hardships of the ways of knowledge” – certain that I could find the Truth and that it should set us free to roam the heavens forever *in starships*.

Much later, as I could see my sacred scientific destination on the horizon and realized I was also arriving at a more *mature* understanding of my own work, a strange and melancholy apprehension almost made my final decision to publish a difficult one. I didn't fear rejection slips, as I'd already endured and survived every type of negative response to my ideas possible (from gentle chiding to outright ridicule). I realized what scared me was that my life's work might be used for purposes quite removed from what I intended: Einstein and the famous letter to F.D.R. came to mind at a certain point.

What really confused me for a time is how a race so technologically advanced can still display such emotional and moral retardedness. Sometimes I'd swear that our society is actually evolving backwards in matters of real 'civilization'. I have come to understand, however, that my principal responsibility is just to reveal something marvelous that I have been allowed to see, which is unequivocally intended for “the good of the many”, and not how that knowledge *might* subsequently be misapplied by a few.

Therefore, let us pray that we may all journey together safely, facing a new and awesome level of responsibility, into and beyond the 21st century and the Unknown. It's time mankind grew up, anyway: an infinity awaits and beckons us, commanding that we choose our own common destiny in how we utilize the new StarDrive technology I'm about to reveal. I'll just have to have faith that we choose well; like the aliens in Whitley Streiber's best-selling book Communion? When he was asked what they actually do with StarDrive, with all of time and space to wander around in, he replied, “work for God”.

Many of the great theoretical physicists of our time (including Einstein) felt that the closer we approach a truly comprehensive understanding of the Universe's innermost secrets, the more we must be prepared to address certain philosophical and even religious concepts. This theme will reappear at times within the pages that follow, and it is in keeping with the mood of this premise that I offer the following material. It's an address which was written for and presented to a scientific convention in Amsterdam in 1972 by former Apollo 14 astronaut Capt. Edgar D. Mitchell, Ph.D., quoted in its entirety:

"The view from space which I was priveleged to have of our planet is an event which has profoundly affected my life. The pictures you have seen in books, magazines, and on television help give some sense of that awesome but magnificent sight. But photography has its limits and a photograph cannot tell you of the way my philosophy and my commitment to philosophy have been changing since that voyage to the moon.

"To see a small, majestic planet Earth floating in a black sky in its blue and white splendor is something you cannot forget. It stays with you profoundly, long after the splashdown, the hero's welcome, and the parades have been forgotten. Because the view from space has shown me – as no other event in my life has – how limited a view man has of his own life and that of the planet.

"Man fancies himself the highest development in nature – the ruler and most intelligent of creatures on Earth. About that notion, I have strong reservations. If animals could communicate with us, and some experiments going on now indicate they might someday, I will suggest that the first thing they would say is: how glad they are not to be human. Because no other animal commits the atrocities and stupidities that men do. In our surfeit of knowledge but paucity of wisdom, we've come near the brink of global destruction. The possibility of nuclear Armageddon is very real. The possibility of our extinction due to environmental pollution is just as real and only a little bit slower than using fission or fusion. Certainly these man-made threats to life on Earth cast some doubt on the supremacy of human intelligence.

"So the situation is desperate, and I became truly aware of that as I gazed at Earth from a quarter of a million miles away. It put a new perspective on things far beyond just the visual dimension. I could see the potential of the planet, if it were to function in accordance with the natural design of the Universe. I could see what the Earth can be if Man could choose to make it so. Yet I knew back on Earth people were fighting, stealing, raping, deceiving – totally unaware of their individual part [in], or responsibility for, the possible future of the planet – just living unconsciously or distrustfully or greedily or callously or apathetically. And at the same time other people were living in poverty, ill-health, near-slavery, starvation, fear, and misery from prejudice and outright persecution, because as individuals and as a planet we have not had the will to change these conditions.

"As I said, those thoughts and perceptions stayed with me and worked on my mind. I could see the problem; but even more importantly, I began to see a solution. It's the only possible solution but it will be enormously difficult to achieve. The solution is: a global change of consciousness. Man must rise from his present ego-centered consciousness to sense his intimate participation in the planet's functioning, and beyond that, in the functioning of the Universe. Otherwise, we're doomed. It's as simple as that. It is not for the Universe to bow itself to man. It is for man, who inhabits an insignificant little planet, to find within himself, individually and collectively, ways to bring his consciousness into attunement with the Universe."⁽¹⁾

* * *

I believe that Capt. Mitchell's 'view' of our Earth carries with it a very specific and ominous corollary: perhaps the spaceship captain's telling implication is that, 'at the rate we're going', it's more than likely we will not have a viable *starship* program before we foolishly use up our world and then ourselves. We certainly face a great number of critical transitionary processes and challenges as a global society, at the advent of this new and uncertain millenium, and sheer overpopulation is almost undoubtedly the worst and most obvious.

Most of us would agree, I think, that of any of the crises now facing our planet, what we are to do when the world's petroleum reserves are gone is also one of the most imminent and potentially volatile. I myself believe that the development of a new (electric) power production technology, which eliminated the need for any dependence on fossil fuel combustion or atomic fission, would be a veritable god-send at this point in history. Cheap, clean, and abundant electric power could at least enable us to remake and maintain our world, and it might just help us survive long enough as a race to achieve that viable starship program before it's too late. As C. West Churchman (a former NASA research consultant) points out in The Systems Approach, if we put off logically assessing a problem for too long, it may not be possible to adequately address that problem at all.

The life work and philosophy of no one great physicist of our time perhaps better counterpoints the message inherent in Capt. Mitchell's address, especially in light of the inevitable depletion of the world's oil, than that of Nikola Tesla. In his mind's eye, he saw a quite different aspect of the view Mitchell saw from space. Tesla, a poor Russian who emigrated to the United States in 1884, was a brilliant physicist and electrical engineer. During his lifetime, he was awarded 111 patents, and is generally credited with being the father of radio broadcasting, AC power production and transmission, and the AC induction motor. It is he who designed the country's first working large-scale hydroelectric plant at Niagra Falls, and thus he was also one of the pre-eminent magnetic engineers of his day. The standard unit of magnetic flux density (Wb/m²) has been named the *tesla* in his honor.

(1) QUOTE: pgs. 13-14, Ether-Technology by 'Rho Sigma', © 1977.

As AC power distribution subsequently won general acceptance in the early 20th century, Tesla was bothered by what he saw as the unsightly proliferation of transmission towers, poles, and lines. In a bold effort to eliminate the need for a physical power distribution grid, he worked at breakthrough ideas in **electric field theory**, derived from his pioneering achievements in radio, which would allow the safe broadcast (wireless) transmission of electrical energy itself!

Tesla was a great visionary who believed that certain electrical principles he had discovered could also be utilized, by the 21st century, to solve the world's energy problems and *to make all forms of warfare obsolete*. He firmly believed in the indomitable creative spirit of Man and that we would overcome the present-day derangement of our civilization once we became adjusted to being masters of "the machine age". He felt the arcane principles of environmentally-safe power production and distribution he was working to engineer would, when coupled with the broad-based development and use of industrial robotics in the 21st century, enable us to free ourselves to pursue higher aspirations and inaugurate an "electric millenium".

Tesla was an eccentric loner, and unfortunately a poor businessman, who did little to profit from his inventions. His genius was perhaps too far ahead of his time and undoubtedly created animosities among his peers which often impeded the achievement of his ideas. Securing financing or investment capital for some of his later work many times proved to be difficult if not impossible. The Tesla Tower, an uncompleted large-scale project on Long Island, was to have publicly demonstrated the radial long-distance transmission of *household electric power* in a manner analogous to the broadcasting of a mere radio signal as information. What an incredible accomplishment this might have been . . .

Tesla's belief that his work could also make warfare obsolete apparently stems from some knowledge he must have had that he could also cause the direct *linear* transmission of electrical energy, with extreme destructive potential, at short range. His Long Island broadcast power designs are based on ultra-high electron charge as the operative element, and a *phase-polarized arc discharge* of quasi-lightning proportions is truly a sobering concept.

Above and beyond the visionary yet ironically naive views Tesla held, a careful analysis of his later work reveals that he believed (and I think could demonstrate) that a veritable "sea of energy" permeates all of existence which can be tapped for nearly illimitable electric power. Please note that what Tesla had in mind was the first electrical device in human history whose total output would be very much greater than its *apparent* input by absorbing ambient electric charge and even radiant electromagnetic energy itself!

This type of device has in recent years earned the appellation "over-unity", meaning that it operates with an apparent total efficiency over a classically-calculated 100% (and thus would seem to violate the Conservation of Energy Principle as it is presently understood) although "perpetual motion" and/or "free energy" are specifically *not* claimed.

What he proposed (in its preferred embodiment for operation in air) was a machine which could generate more total electrical energy than it consumed through the proper usage of a self-sustaining capacitive electric field discharge.

To this end, he erected a steel pole with a large pointed copper ball at the top and a partially-buried steel chain link fence encircling it at a given fixed distance. According to accounts, when the fence was properly energized (by impressing a small AC signal on a huge dc voltage) incandescent ball lightnings would stream down, from the sky to the copper ball, at regular intervals. Rather like the mad scientist's stereotypical "Jacob's ladder" (in one of those old-movies), only in *reverse* . . .*

The following account of one of Tesla's experiments in this type of over-unity 'inverse' broadcast power technology, **powered electrostatic induction**, is one of the best I've ever discovered; and it captures one of those beautiful moments in science that you'd give anything to have seen. This charming biographical vignette also has a certain dark wit and an all-too-plausible ending, though:

"Tesla knew there is a powerful [dc] voltage between the Earth and the upper atmosphere; this is what causes lightning to discharge . . . [we'll talk about lightning and its electrophysics later]. When an antenna is raised, this voltage climbs it, in a gradient to be concentrated at its tip. Any *fluctuation* in the natural voltage between Earth and sky generates a flow of [AC] voltage in the antenna. This is how a radio receiver works.

"In radio's early days, the current generated in the receiving antenna was fed into a resonating circuit that would filter out the wavelength of the broadcasting station to which it was tuned [the carrier wave] and amplify the signal until it had enough energy to actuate headphones.

"Tesla figured that the Earth would filter out its resonant frequency, amplify the current by its resonance, and function as a capacitor in a circuit as big as the entire planet. He pumped an electric current into the Earth, and tuned to a precise harmonic length of the Earth's resonant frequency [thought to be 7.5 Hz]. As he expected, the electric wave travelled to the antipodes and bounced back in time to coincide with its own following wave, doubling its amplitude. After repeated amplification in this manner, the electric energy burst from the top of Tesla's pyramidal tower to illuminate the entire countryside with **the most spectacular artificial lightning storm ever** seen. The surge melted the wiring in . . . power generators serving the whole county. No one would supply Tesla with electricity after that . . .

"Undaunted by superabundant success, Tesla continued his experiments to prove that when his antenna was pumping electric waves into the Earth, a standing wave

* Note: As will be explained further, the StarDrive device is fundamentally a dc (not AC) technology but utilizes this same Tesla technique - impressing a small AC signal on a huge dc voltage - to achieve extraordinary results.

pattern was generated in the planet's geo-electromagnetic structure. At precise intervals, or harmonic fractions thereof, all Tesla had to do was drive a metal rod into the ground and plug in the electric frying pan, hair dryer, or washing machine . . .

"It was Nikola Tesla who electrified the world with alternating current. To the end of his life, Tesla dreamed of recycling all those unsightly high-voltage electric power transmission towers and replacing them with broadcast power generated and received from the Earth. But if power could be tapped from the Earth, how would Consolidated Edison - General Electric - Standard Oil bill you for it . . .

"When he died in New York City on a winter night in 1943, Tesla was alone in a hotel room, possessing little more than when he had arrived as an immigrant with four cents in his pocket. The Secret Service immediately sealed his room, and whatever papers he had were transferred to government vaults where they remain to this day." (2) [excerpted pgs. 37-39, How to Build a Flying Saucer by T.B. Pawlicki, © 1981.]

I have a good friend and former research compadre from Long Island, named Joe Suda, whose childhood home happens to be quite near the place where Tesla's broadcast power station was to have been built. It is Joe who reinterested me in the life and work of this amazing inventive genius. Joe has a wonderful preoccupation with theoretical over-unity devices and, before the twin spectres of free energy and perpetual motion invoke themselves, I must say that he and I have seen published evidence that New Age over-unity electric motor-generators have already been successfully and independently demonstrated (by a Japanese researcher and a University of Maryland physics professor) in the late 1980's. Both designs, although somewhat different in conception, incorporate high-powered rare-earth magnets to produce both electric power and torque!

Joe also introduced me to the work of two little-known engineers (one electrical, the other magnetic) whose insights are utterly essential to the foundation of this book: this will be explored later on in depth. At this point, however, we must move directly to a fundamental clarification of the over-all premise of **StarDrive Engineering** and its relationship to over-unity technology.

It is therefore the premise of this text to show conclusively that:

[1] a new non-nuclear method of producing cheap, clean, and abundant electric power as well as a directly-related *all-electric aerospace vessel design* are now achievable, using a number of commonplace 20th century technologies *best exemplified by the magneto, the vacuum tube, and the cyclotron*;

[2] such a power-plant/vessel combines Tesla-type electrical engineering and New Age magnetic theories so that *a set of specifications* is developed for an exotic high-voltage dc over-unity motor-generator incorporating permanent magnets, powered electrostatic induction capability, and a densely-charged hull; and

[3] such a machine could readily achieve near-light speed and indeed perhaps be made to **artificially transcend the speed of light**.

In the pages to come, we will therefore also investigate certain mathematical and cosmological principles which suggest that, given just the right hardware, **the Universe's actual upper speed limit is c^2** – the speed of light squared – and not c as Einstein believed. Some rules are, after all, just meant to be broken.

* * *

Before a comprehensive examination of this formidable theoretical premise may be undertaken, it will be necessary to briefly review (in Chapter 3) the work of Michael Faraday – the greatest electrical researcher of the 19th century. Even the most brilliant theories are of questionable value without the *hardware* to practicably test, prove, and apply them. Faraday not only developed much of our understanding of the laws of electromagnetism, but also designed and built most of the experimental electrical apparatus of his time.

The author is greatly indebted to a number of other great scientists whose individual work contributed integral parts to the theories and design concepts set forth in this book: New Age magnetic engineer and inventor John Ecklin, and Lee deForest, electrostatics expert and inventor of the triode vacuum tube (both Americans); the mysterious Englishman John R.R. Searl, who is thought to have developed the bulk of the fundamental principles of **reactionless electric drive**; and, of course, Nikola Tesla.

My deepest appreciation, however, goes to M. Faraday. Without his intuitive genius for electrical hardware, and his invention of **the dc disk dynamo**, my StarDrive system would be without its formative mechanical design basis.

May I therefore now present ***StarDrive Engineering*** to you all, in honor of: the spirit and ideals of Nikola Tesla, who so sadly was unable to leave the world an even more magnificent legacy; my old friend Joe Suda, without whose initial guidance and encouragement this book would not exist; and Michael Faraday: I pray that I live to see if he has helped me open **the Gateway to the Stars**.

Prelude

Goodbye, my friends,
maybe for forever:
goodbye, my friends -
the Stars wait for me.

Who knows when
we shall meet again - if ever -
but Time keeps flowing,
like a river, on and on,
to the sea . . .

Alan Parsons Project
The Turn of a Friendly Card

Chapter 2

Tales of Starships

Many years ago, when I started making a really thorough study of the vast body of UFO lore this world has produced, it became apparent that most of the intelligent speculation concerning these presumably extraterrestrial craft revolved around two essential issues: the shape of the hull and the nature of the “field” surrounding it.

The bulk of reported sightings which have a believable ring to them attribute the ‘classical’ flying saucer or domed disk shape (of course) to these devices, which almost *all* true enthusiasts agree do not make use of the rocket principle our own space scientists appear hopelessly hung-up on. The only other hull configurations reported with any significant regularity are the cigar shape, often associated with very large craft, and a triangular wedge design sometimes observed.

At one time some researchers thought that starships having the sleek saucer shape, shown in Fig. 1 below, originate in the Epsilon Eridani star system about 11 light-years away. It has never to date been established, however, whether this or any other extra-terrestrial star system actually has a “Class M” planet (to use StarTrek™ terminology for a green world such as our own). Nevertheless, researchers using the Arecibo radio telescope obtained the first purportedly irrefutable evidence of a planet outside our own star system in 1994: a pulsar star 1,500 light-years distant appears to have at least three planets!

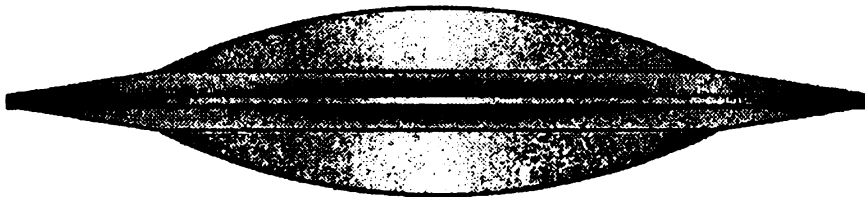


Fig. 1: side view of ‘Eridani’ hull design.

On a related note, scientists using images from the repaired Hubble space telescope at about this same time developed the world’s first conclusive proof of the existence of a rotating black hole, in the constellation Virgo. We’ll get back to the very relevant significance of rotating black holes later . . .

Another interesting hull design which shows up occasionally (see Fig. 2) is a truncated conical variant of the saucer which a once-prominent UFO group claimed in the ‘70’s came from the Pleiades, a constellation some 430 light-years distant. However, astrophysicists now know that the 400 to 500 suns which comprise this dense star cluster are far too “young” to have *any* planets which support life, let alone an advanced civilization.



Fig. 2: side view of 'Pleiades' hull design.

Regardless of which of these special hull shapes is sighted, eye-witness accounts invariably describe a **glowing field of force** which envelops the vessel. Although these accounts contain many common points-of-observation regarding the effects attributed to this field, there is (to my knowledge) virtually no written speculation in existence which succeeds in explaining scientifically what this drive field is or how it is produced – until now.

I'm afraid people have, in general, been content to assume that the StarDrive field comprises something totally unknown and perhaps beyond the reach of mere human understanding. In much the same way, scientists have failed (as far as we know) to develop *cogent* faster-than-light drive theory simply because Einstein said it can't be done.

What can be found in quantity, though, is a great deal of off-the-wall conjecture about "anti-gravity". This is indeed convenient, as it helps to keep that flying saucer mystique alive. However, humans as yet don't even know what gravity really is, and some of the speculation regarding supposed anti-gravity propulsion is nothing short of ludicrous. Besides, anti-gravity does little to explain the weird electromagnetic effects generally associated with the drive field or the withering crystallization of soil and vegetation at purported saucer landing sites. Or all those cows (in the '60's) going belly-up in the pasture . . .

Interlude: Weight

When I was a young man, I had a small off-road motorcycle which I rode with reckless abandon in the farm fields and lanes near my parents' rural home. One night in late summer I was out riding and stopped on a hilltop, quite a distance from any roads or houses, to smoke a cigarette and enjoy the evening sky.

As I sat facing east, I saw a light moving over the horizon and thought it was an airplane. As it got nearer, over a period of some minutes, I realized that it had no flashing running lights and that I could not hear any typical engine noise. Still not thinking that much was all *that* out of the ordinary, I put my helmet back on and started the bike.

When I looked up again, I could see that what I'd been watching was definitely *not* a plane, for it had no wings. It glowed a dark blood red and I began to hear a sound so deep that the fillings in my teeth ached, and the soles of my feet tingled uncomfortably. Whatever this thing was, it was cigar-shaped and immense. I could

tell it was very high up, but it had to be easily as large (and heavy) as an aircraft carrier. To see something *That Big* gliding lazily across the sky was just uniquely unnerving; and no, it was *not* a zeppelin!

A strange feeling of dread and panic overcame me and when I tried to exercise a sincere desire to flee, I realized the bike had quit. I kicked and kicked, but my ever-reliable motor just wouldn't start. By now, this other-worldly monstrosity was passing almost directly overhead and the oddest thing about the whole experience struck me: that great and terrible fusilage was oriented at a 45° angle with respect to its flight path!!

I was completely mesmerized, and couldn't help but stare open-mouthed as the ship gained speed and disappeared over the western horizon in just about 15 seconds. Beside myself with excitement, I tried my motor again (which started on the first kick) and raced home to tell my parents what had happened. When I had finished my heartfelt narrative, my usually-supportive folks poo-poo'd the tale of the starship and wryly accused me of having watched too much StarTrek™...

One of the broadest logical assumptions regarding the nature of interstellar travel harkens back to the aforementioned discovery of 'nearby' alien planets: the average distance to the next-closest habitable world from any given planet which *is* in fact inhabited must everywhere be such that a trans-light ship, under a constant and reasonable apparent acceleration, could still traverse that distance in an acceptable amount of *objective* time. Even with the enormous subjective relativistic time dilation which would be involved (as we'll see), due to the unfathomable immensity of the cosmos an alien ship would otherwise almost never appear in *anyone's* skies...

The late Dr. Carl Sagan, of Cornell University, is justly accredited as one of the first eminent astrophysicists to attempt any accurate probabilistic calculations regarding the odds that such a starship might so-appear. Even with the most discriminatory variables imaginable, his careful conclusions imply that such an appearance must be possible. It is generally accepted that the Universe comprises roughly 100 billion galaxies each of which contains about 100 billion stars, on the average. Thus, with potentially 10^{22} stellar systems or more *Out There*, it is virtually inconceivable that star-faring races do not exist.

Many years ago, my father expressed the opinion that ancient Earth peoples, the Egyptians in particular, may actually have had some contact with extra-terrestrials. This is, of course, not a unique theory by any means. In support of this contention, however, he cited as just one example the incredible precision with which these 'primitive' humans erected intricate and enormous pyramids for an ultimate purpose which *must* transcend serving merely as royal tombs. As he liked to point out, they would have been the only artificial structures visible from space at that time. Strangely enough, the Pyramids at Giza also happen to lie at the exact center of a Mercatur projection of the Earth's entire land mass, and are aligned to the true north pole.

Many books have obviously been written exploring this and other similar ideas which may admittedly be somewhat far-fetched, and it is not within our purview to discuss or debate these conjectures here. However, it is interesting to

note that an American research scientist who claims to have been attached for a time to the Air Force's top-secret Galileo Project*, at Nellis Air Range in central Nevada, came forward a few years ago publicly stating that in 1988 he was given Q-level security clearance to begin evaluating a captured saucer propulsion system. He says that in one government briefing document he read, the craft involved was alleged to have originated in the Zeta Reticuli star system (37 light-years distant) and the race that built it had supposedly been coming here for 10,000 years to externally correct and accelerate Man's evolution . . .**

In any event, two fundamental precepts of starship design just happen to be related to the type of engineering evidenced by the Pyramids: (1) such feats are not accomplished without extraordinary mathematical savoir-faire; and (2) the specific shape chosen is a pure-math expression of its *loftiest true purpose*. In the case of the Giza Pyramids, we will probably never know the full story of what such a higher purpose might have been. As regards starships, however, we must logically assume that the exact shape of the vessel hull is inextricably linked to the nature and purpose of the drive field upon it.

I have always been, as I'm sure *some* of you readers are, a person fascinated with the subtle interplay of patterns of numbers. I also happen to be one of those rare birds who actually enjoy (and are very good at) the devilish art of fractions. I have elected therefore (as we'll see) to define the large majority of my StarDrive specifications in terms of fractional mathematics, and the ratio $1/5$ is of particular significance. I'm not sure I myself could fully explain why. Anyway, the masterful Egyptian builders of antiquity used a fractional math system and I believe that this is perhaps the best way to give StarDrive students a clear 'feel' for the relative proportions of *major systems components*, as well as to achieve an optimum in design precision. The latter consideration is surely necessary in something as powerful and unbelievably dangerous as a starship in operation.

StarDrive technology, and the resultant ability to warp the fabric of space-time, indeed represents a form of near-absolute Power; and because of this I unfortunately feel that present-day humankind may not really yet be ready for its possession. There is a certain amount of historical evidence to support legends that Atlantians of old possessed electric airships, called Voilixi, and that they destroyed themselves with this and other advanced technologies through apathy, vice, and moral indifference. I guess we'll have to see if we have risen above historical repetitions of this nature, for the StarDrive device has the very real capability of being used as an instrument of Armageddon.

* * *

I'm not exactly sure when I became totally convinced that an actual faster-than-light drive simply begs our discovery. My preoccupied obsession with theoretical UFO propulsion systems eventually just included that logical presumption. Down through the years, I have been greatly influenced in this respect by

* Project Galileo was (is?) purportedly devoted to the study of nine disk-shaped alien space vessels which were somehow acquired by the US government.

** See OMNI Magazine, April 1994 issue.

masterful works of science fiction which fortuitously found their way into my library: Cities in Flight by James Blish is an excellent example.

Very probably, however, this concept took hold in me during the run of the original StarTrek™ series: I hardly ever missed a show. Gene Roddenberry, the extraordinarily far-sighted and gifted creator of the series, had a great concern for scientific realism within the context of what was (for him) a labor of love. He also had many expert technical advisors working on the show, and I guess I figured if he accepted the possibility of trans-light velocity as a matter of course, then that was good enough for me. At least it helped propel me onto a course of conceptual and mathematical investigation not often pursued.

The fundamental obstacle to attaining (let alone breaching) light speed is, of course, Einstein's Special Theory of Relativity. It has been irrefutably established via high-energy particle physics experiments that c is in fact the upper velocity limit for a positive-mass object when accelerated by an *outside force* which: [1] arises from a relatively stationary reference frame (e.g. synchrotron or cyclotron accelerator fields); and [2] rises *linearly* against asymptotically increasing objective (relativistic) mass. The same type of restriction inevitably applies as well to an object which is inherently self-accelerating by means of any rocket-principle *reactionary force* that must also rise linearly to a fixed finite maximum value!

My own thought experiments eventually led me to consider the following: what if an object is self-accelerated by an inherent non-reactionary force wherein the near-light velocity component of the *subjective* thrust must remain constant even while such a mass body's *objective* momentum rises toward infinity?! Such object should "bypass" the exact value of $v = c$ at some point due to sufficiently large Heisenberg uncertainty *as to its relative position*, based on two postulates: that *space itself is quantized* and *time may exhibit dual relativistic dilation!!*

This will bear explaining; but such an object could conceivably cause itself to 'disappear' intact into a local spatio-temporal warp of its own generation, rather similar to what happens to a black hole, by presenting the normal 'fabric' of the Universe's structure with an impossibly untenable set of physical conditions.

It was Roddenberry's StarTrek™ which first made "space warp", a strange infolding of the fabric of our space-time continuum, a household phrase. The space warp is caused by a super-intense gravitational field, or gravity "well", which has the theoretical capacity to draw two distant points (departure point and destination, for instance) relatively closer together. It has been pretty much verified scientifically by the work of bona fide physicists like Prof. John A. Wheeler, who coined the term "wormhole" for this effect, and constitutes in general terms any form of *Einstein-Rosen bridge*.

While traversing a space warp, at $v > c$, our starship (let's say the Enterprise) *must* technically be outside our dimensional continuum: but if this is indeed the case, where *are* we? Prior to Wheeler's work with super-gravity and wormholes, the late Dr. Isaac Asimov had formulated the concept of "hyperspace": an alternate quantum energy continuum mistakenly thought of by many as a 'parallel universe'. Here, objects may only move *faster* than light, relative to *our* space-time.

A very useful analogy I've found to envision this concept is that of a surfer "shooting the tube". The normal space-time continuum is the sea, upon the surface boundary of which our Enterprise and crew (board and surfer) are riding a tubular wave. This wave moves toward the shore – the time-light barrier – at speeds always less than that of light. However, the surfer who is temporarily suspended in an adjacent rarer medium (the air) may *fall* down the infolding side of the wavefront at a transverse velocity much greater than that of the forward-moving wave itself.

I'm virtually certain that Mr. Roddenberry had access to some very sophisticated and then-recent research related to trans-light velocity while developing StarTrek™. For instance, physicist Olexa-Myron Bilaniuk and associates were able to show in 1962 that mass objects which might travel faster than light do *not* violate Einstein's Special Theory of Relativity as do objects at $v = c$. In this theoretical condition, the object merely has imaginary mass (representing the square root of a negative number) and negative kinetic energy. The Lorentz transformation which governs the object's relativistic momentum and position will still yield meaningful results above light speed!

In an article published in 1969, Dr. Asimov further suggests an important concept which is necessary to reconcile faster-than-light theory with accepted particle physics. Using physicist Gerald Feinberg's term "tachyonic" to describe an object with hyper-light velocity relative to our continuum, he proposed that such objects still travel at $v < c$ with respect to the foreshortened distance (between departure point and destination) which exists in hyperspace, or what I prefer to term *the time-energy continuum*. In this dual-continuum model, objects in both the space-time continuum and the time-energy continuum would each appear to have tachyonic velocities with respect to the other. In 1971, Bilaniuk published an article called Space-Time wherein this two-fold relationship is indeed mathematically corroborated.

As regards my conviction that the true upper speed limit for a tachyonic mass object (relative to a given point in the space-time continuum) is actually c^2 , I must confess that once again I have looked toward the intersecting of science fiction and science fact to attempt the derivation of missing components of the Truth. Here, I have none other than Arthur C. Clarke to thank for reminding me that everything in the Universe is indeed comprised of waves, and that in classical wave mechanics (without relativity) there is no upper speed limit on transmitted wave motion.

During WWII, Mr. Clarke was instrumental in the top-secret development of radar for the British Royal Corps of Engineers. A remarkable effect his team observed within the rectangular copper wave guides used as radar antennae was that each sub-light radar signal was accompanied by an electromagnetic wave pattern which always moved *faster* than light (at what is called phase velocity), such that the product of the two speeds always equalled c^2 ! If we take this real observed relation as being indicative somehow of the constraints imposed on wave motion by relativity, it cannot be arbitrary or accidental that the product of the velocity of a signal waveform and that of its traveling wave counterpart happens to equal this particular number!

Another British scientist and sci-fi author who was a wartime colleague of Clarke's, George O. Smith, also implied (as long ago as 1944, believe it or not) that an unidentified principle which causes gravity might *itself* propagate at c^2 . This view is of course at odds with the graviton theory, which proposes that gravity is somehow effected by the exchange of virtual particles called gravitons (which no one to date has ever detected) and thus its speed of propagation is limited by relativity to that of light. However, a very interesting thing happens when we combine the concept that *gravity is induced at c^2* with Clarke's group-and-phase-velocity c^2 product and a Bilaniuk tachyonic mass object.

In the rather elegant scenario contemplated, a mass object moving at relativistic velocity is thought of as *a deBroglie elliptical* wave quantum energy pattern* (*having a longitudinal pulse signal component). Associated with this signal waveform will be a supra-light 'carrier wave' moving at phase velocity, a sort of quantum energy mirror image if you will. Should such an object actually cross the *time-light barrier*, these two complement waveforms would merely switch 'places' (or continuums), with gravity's causal agent propagating at c^2 to ensure that all local *quantum wave mechanics* on both "sides" conform to the proper physical laws. Inertial mass would be an inductive property still limited to $v < c$.

Finally, it is interesting to note that in an early 'technical manual' published for fans of the original StarTrek™ series, the Enterprise's top (and not quite attainable) design speed was, of course, Warp Factor 10. In terms of this early velocity scale, c^2 was equivalent to an impossible Warp Factor 54.7 (according to my friend Joe's calculations). It was gratifying to see that a more recent StarTrek™ technical manual, arising of the "Next Generation" series, indeed ascribes a re-scaled Warp Factor 10 to the new (and not quite attainable) maximum speed of c^2 .

Perhaps the good people at Paramount really are helping move us a little closer to a world where starships are much more than just a good story! In any event, the warpage of space-time which is responsible for a starship's relative trans-light velocity can only be produced by the glowing field of force . . .

* * *

For two thousand years, the only viable aerospace propulsion systems developed by Man have all utilized the rocket principle, representing Newton's law of equal and opposite action and reaction, in one form or another. Unfortunately, there are two completely insurmountable problems in trying to apply this linear propulsion method to interstellar space travel: (1) the tremendous bulkiness and weight of the types of fuel ordinarily used, in the huge amounts that would be required; and (2) the fact that the vehicle's top speed is limited to the velocity of an exhaust stream composed of relatively heavy particles, which require vast amounts of energy to accelerate even to any appreciable sub-light velocity.

To develop a true 'reactionless' space drive, which has never been practicably (or publicly) demonstrated to date on this world, we therefore need to use a fuel or energy source of ultimate compactness and absolutely minimal weight which can be made to produce a net longitudinal thrust *without producing an oppositely-vectored exhaust stream*.

No known 'substance' in the universe is more compact, lightweight, and abundant than the electron, and realizing that this elementary particle can be made to serve as a tappable energy source in and of itself is fundamental to an understanding of what the StarDrive field really is. This is the single most important axiom of both advanced magnetic engineering and StarDrive technology. In addition, no other mass object known can be more readily accelerated to ultra-high relativistic velocities or more precisely controlled in doing so.

Therefore, we will make the not-unrealistic deductive assumption that the field of force surrounding "real" UFOs is actually composed of electricity itself: fantastic numbers of orderly-moving electrons which are harnessed and directed in such a manner that they yield an asymptotically rising level of thrust with no significant 'backward' exhaust. As we'll see, this is accomplished in large part by means of a specially-shaped charged hull and magnetic fields, and the StarDrive *electrodynamic field* is perhaps best described as a "**semi-polarized capacitive arc-discharge envelope**". And, as Poul Anderson suggests in his essay Our Many Roads to the Stars⁽³⁾, an ultra-dense toroidal field of electrons spinning at extreme relativistic speed in the manner of a smoke ring should theoretically be able to produce a *Kerr metric space warp*.

Once we realize that the field envelope about a starship hull is not some mysterious anti-gravity or quasi-nuclear machination, the aforementioned drive field effects become much easier to understand as a logical consequence of two things which are surely more familiar to us: a *rotational dc electric field encompassing a stationary magnetic field*. Thus, the StarDrive hull and field combination to a certain extent mimics in macrocosm the electron itself! With this in mind (and after a great deal of deliberation), the 'official' name which I selected during the Patent application process for my StarDrive system as a whole is **Electrodynamic Field Generator**. And I think that sums it up nicely.

Assuming that we can develop the necessary hardware inside a starship to produce and control our external electromagnetic drive field, we then need only select a proper hull shape. Because of its pure symmetry and beauty, I have confined my design analysis to the 'Eridani' configuration. I'm afraid that I am just not ready for anything cigar-shaped, thank you.

I think many serious flying saucer buffs have long suspected that something solid in there must be rotating. Before we get into hardware in depth, suffice it to say that this is indeed the case. It may sound a bit simplistic, and is, but inside that thin saucer wing is a **great, charged, flywheel** . . .

(3) FOOTNOTE: published in Faster Than Light , ACE Books, © 1976 by J. Dann & G. Zebrowski.

Prelude

And I looked, and behold,
a whirlwind came out of the north,
and a fire infolding itself, and
a brightness was about it, and out of
the midst thereof as the colour of amber,
out of the midst of the fire.

Ezekiel 1:4

Chapter 3

Historical Background

In the early 19th century, when electricity was still a little-understood laboratory curiosity, there occurred a concentrated burst of scientific insight and creativity rarely seen in human history. The men responsible for giving the world the bulk of our proven electromagnetic theories, which still govern our production and use of energy, are familiar to us yet today having bestowed their names to many of the important units and laws of electromagnetism. And, justly enough, a brief review of their work will serve to illuminate certain 'simple' terms and concepts which will still be important in *StarDrive Engineering*.

The Danish physicist Hans Oersted was the first person to study the relationship between electricity and magnetism, starting in 1807, and in 1821 he published a paper defining basic rules concerning their interaction. His name is given to the standard cgs unit of *magnetic field intensity* (and, the demagnetizing force experienced by a magnet under load).

Based on Oersted's work, Frenchman D. Francois Arago built the world's first electromagnet in 1820 and noted that the magnetism thus imparted to the iron or steel core (or armature) was many times greater than that produced by the coil wound upon it acting alone. This is due to the fact that ferromagnetic materials have a far higher *permeability* or "ease" of magnetization than air or vacuum. He also observed that the magnetic field produced by the armature was temporary in soft iron and permanent in hard steel alloys.

Another French physicist, André Ampère, also studied the magnetic effects of electric current at about this same time and formulated the *inverse-square magnetic force relationship* known as Ampère's Law. The unit of electric current flow still in use today is the amp, of course, in his honor.

Similarly, in 1827 the German physicist Georg Ohm formulated and published Ohm's Law of electrical resistance, governing the relationships between voltage, current, and resistance in an electrical circuit. And, in 1834, Russian scientist Emil Lenz postulated Lenz's Law, concerning the nature of the *magnetic losses* within an electric motor or generator.

By far the greatest name in the early history of electrical research is, however, that of Michael Faraday. The son of a poor rural English blacksmith, who never went beyond elementary school, Faraday was nevertheless possessed of the boundless curiosity that is the hallmark of a true scientist. When his family moved from Surrey to London, he apprenticed at a book binding shop where he voraciously read every scientific treatise he could find. He was especially fascinated with the few articles available on electricity.

Faraday began taking a course in "natural philosophy", as the study of science was still called in that day, and attended lectures given by the then-famous scientist Sir Humphry Davy. Davy was the Director of the Royal Institution and he impressed Faraday so much that the young genius applied for a job as his lab assistant. Years later, when asked to name his greatest scientific discovery, Davy would wryly reply, "Michael Faraday".

Although Oersted and Ampère worked out the basic relationships between magnetism and electricity, it was Faraday who built the world's first crude (dc) electric motor in 1821. He also formulated the fundamental interrelationships between these forces and motion: the *law of three mutual perpendiculars*, or Faraday's Law of Induction. This essential electromagnetic principle governing the generation of electrical power and his practical demonstration of Ampère's Law relating current and electric motor torque subsequently made possible the development of all modern electric generator and motor technology, changing our world forever.

He also expanded on the work of Arago by winding two separate coils on an iron ring and energizing one with a battery while the other was connected to a galvanometer (an early ammeter). He found that whenever he connected or disconnected the battery, a brief current would flow in the secondary coil, and that the polarity of the battery connection determined the polarity of the secondary current. Thus, Faraday had discovered *magnetic induction without relative motion*, using the world's first primitive transformer!

Faraday developed the concept of "lines of force" to represent a magnetic field and conducted the first systematic experimentation into the magnetic properties of various types of substances. He was the first to call such substances as bismuth and glass, which exhibit a force in a magnetic field which tends to align the material perpendicular to the lines of force, "diamagnetic"; and substances like iron or steel (which tend to align parallel to the field) "ferromagnetic".

He also developed many of the known laws of electrolysis and terms thereof: "electrode", "anode" (+), "cathode" (-), "electrolyte", and "ion". Furthermore, (and rather amazingly) his experiments with the magnetization of a beam of light led him to postulate, for the first time ever, *the electromagnetic theory of radiant energy*. [Scottish scientist James Clerk Maxwell is credited with developing modern EM wave theory.]

Of particular importance to the application contemplated here is Faraday's discovery of the basic principles of *electrostatic* induction in 1838. His 'charged ice-pail experiment' is perhaps his most famous and demonstrates the principle of *Faraday shielding*: any net electric charge on a hollow conductor must reside on its outer surface. This is why people in a car struck by lightning are relatively safe, as are the people onboard a starship with a densely-charge hull! It is also relevant to our purposes to note that the standard unit of capacitance, or ability to store electrical charge, is the farad.

Etude

Faraday's most important experiment, in relation to StarDrive technology, took place in late 1831 and is based on one form of his Law of Induction: a voltage is induced in any conductor which is moving perpendicular to (or "cutting") magnetic lines of force (or "flux"), and the magnitude of this voltage is proportional to the rate at which these lines of force are being cut. Therefore, the induced voltage is proportional to the speed of relative motion, the total strength of the magnet(s) used, and the number of conductors or turns of wire involved. This relation yields the simple formula: $V = N\Delta\phi/\Delta t$, where $\Delta\phi$ is the change of flux per unit time (Δt) times the number (N) of turns or conductors.

In a manner analogous to the early ignition magneto, we will use this formula later on to design a primary generating circuit capable of delivering a very high dc voltage for the purpose of developing a sustained electric arc field.

The device Faraday built to demonstrate this principle has come to be known as 'Faraday's disk dynamo' (see Fig. 3): he rotated a 1-ft. copper disk on a re-fitted hand-cranked ax grinding mechanism and held a horseshoe magnet over the edge so that the poles were on opposite sides of the disk. A voltmeter was connected via brushes to the edge of the disk and to the axle, but the dc voltage thus created upon rotation was very small for three reasons: [1] in essence, only the "leakage" flux between the horseshoe legs was being utilized, not the directed primary field normal to the pole faces; [2] he could only crank so fast by hand!; and [3] electricity generated in this fashion within a massive solid conductor tends to dissipate its energy in small circular pathways known today as "eddy" currents.

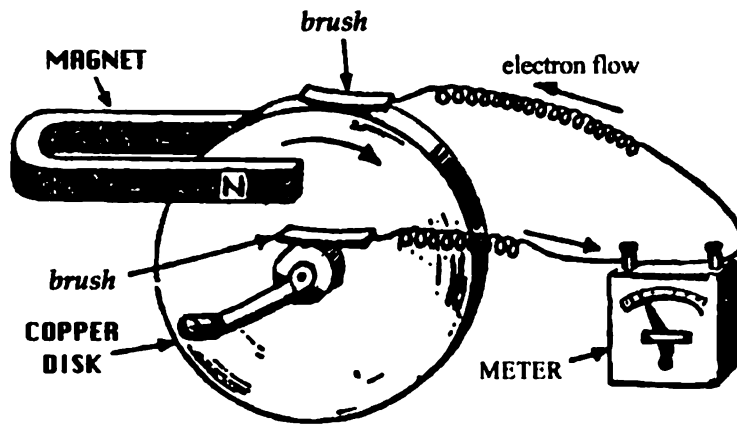


Fig. 3: *Faraday's disk dynamo* - for producing continuous (pure) dc voltage. This was the world's first electrical generator.

The refinements to Faraday's disk dynamo which are necessary to adapt it for use as the basis of a working StarDrive system (or commercial power plant) will be discussed later on in detail. That neither he nor any other scientist (with the possible exception of John Searl) ever did discover these design changes is fairly understandable although unfortunate. The far-ranging nature of Faraday's interests, the complexity of the necessary modifications, and the fact that certain key materials, theories, and industrial techniques would not exist until years later readily account for his simple "new electrical machine" not being developed further by Faraday himself.

The fact that others since his day have not done so can also easily be explained by a simple and sad sociological fact: our race has always been quick to ignore

that which is not conducive to making the most money in the fastest and easiest way. When Edison soon discovered that direct current was not suitable for even local power distribution (due to heavy line losses), and Tesla later proved that alternating current was, the research and development of sophisticated dc power systems virtually ceased.

Since Faraday's time, it has become increasingly difficult for inventors and pure scientists like him to acquire R&D funds, both from the private sector and the government, for anything that can't be readily understood and quickly turned to profit or military use. Today, the very word *dynamo* is virtually obsolete and the following anecdote, showing an uncharacteristically cynical side of Faraday's nature, perhaps best sums up this brief review concerning the disk dynamo and our current lack of a StarDrive system based thereon: When Faraday had himself risen to the Directorship of the Royal Institution, Chancellor William Gladstone could not comprehend the functioning of one of his experimental devices and asked, "But what good is it?". "Why, sir," Faraday replied, "presently you will be able to tax it."

* * *

Although Michael Faraday was the first to demonstrate the mechanical generation of electrical current, scientists of his day did not yet understand the actual nature of current as the motion of electrons within a conductor. It wasn't until 1897 that the English physicist Sir J. J. Thomson announced to the world that he had discovered the elemental unit of negative charge, the electron, and subsequently it became known that electrons are the constituent components of electrical current.

Prior to this knowledge, in 1883, Thomas Edison constructed an experimental light bulb with a small metal plate sealed inside near the hot negative filament. When this plate was grounded, a faint *blue glow* was observed in the region between the filament and the plate. Edison couldn't explain this phenomenon, later termed the "Edison effect", and didn't pursue the matter further as he was (of course) extremely busy with his many other projects.

Twenty years later, in 1903, the English electrical engineer John Fleming built a modified version of Edison's two-element bulb and applied a positive voltage to the plate. After numerous experiments, he came to understand that the Edison effect was caused by electrons emanating into space from the hot filament and traveling to this plate. He found that the device was not only a good rectifier of electricity – allowing current to flow in only one direction – but also a good detector for the wireless telegraph signals being investigated at that time. This two-element bulb was the world's first "electron tube": the diode. The term "electronic" was soon applied to devices like the diode which control the motion of electrons outside of a conductor – in vacuum. Such devices are therefore also called *vacuum tubes*.

The dawn of the Electronic Age actually occurred in 1907 with the invention of the three-element electron tube by Iowa-born Lee deForest. A Yale graduate with a Ph.D. earned in the study of electromagnetic radiation, deForest recognized at

the turn of the 20th century that the newborn field of wireless telegraphy was essentially wide-open. At that time, the major problem confronting pioneers in the art (like Marconi) was that signal strength diminished with the square of the distance and the effective range of transmission was therefore quite limited.

DeForest decided to concentrate his efforts on the career opportunity afforded to one who could overcome this transmission range problem. After a great number of experiments, he added a fine wire mesh electrode element, or grid, to one of Fleming's diodes midway between the filament (or cathode) and the plate. When a small negative voltage was applied to this *control grid*, it greatly diminished the number of electrons reaching the plate (and therefore plate current) by repelling them back to the cathode (see Fig. 4). Thus, small changes in the negative grid voltage could control relatively large changes in plate current (a kind of electric leverage) and the three-element vacuum tube, or **triode**, could not only detect radio waves or AC signal voltages but also *amplify* them as well!

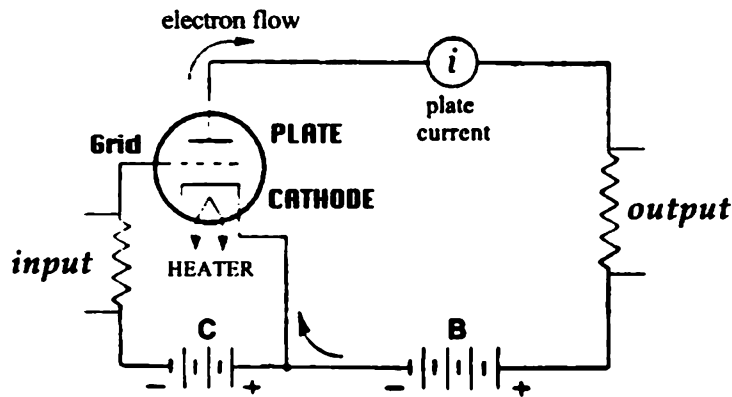


Fig. 4: *triode vacuum tube* and basic circuit diagram.

A small negative voltage applied to the grid can control a comparatively large plate current.

DeForest was eventually responsible for over three hundred inventions in the field of electronics. He made significant contributions to the development of radio, building high-powered stations for the U.S. Navy, and sent the world's first news broadcast in 1916. His triode tube also made transcontinental telephone communications possible. Triodes soon found their way into millions of domestic radio receivers and television sets all over the world, and were of course incorporated into hundreds of military and civilian radar installations.

By 1950, the vacuum tube industry had grown to employ over a million people in production, distribution, and sales worldwide and had a major positive impact on the economies of many countries, especially the United States. Lee deForest's triode vacuum tube revolutionized civilization in the first half of the 20th century and a Nobel Prize winner in physics once called it "so outstanding in its consequences that it almost ranks with the greatest inventions of all time".

Improvements were made in the triode over the years which greatly increased the ratio of the change in plate current to the change in control grid voltage, this ratio being the *amplification factor*. By placing the grid much closer to the cathode than the plate, for instance, significant improvements in amplification can be achieved. It was also discovered that if an alkaline rare-earth oxide coating was applied to the cathode, the number of electrons emitted (and hence *power output*) could be increased enormously even at lower cathode operating temperatures. [Note: A comprehensive discussion of this important breakthrough's vital relevance to the Electrodynamic Field Generator is provided in DataSheet #13 {Instantaneous Charge Differential}.] DeForest's original triodes could manage amplification factors of about 10. With modifications such as those described above, factors as high as 100 or more were made possible.

Many electrostatic engineering principles (representing proven vacuum tube theory) which are employed in electron tubes having 3 or even more electrodes will be incorporated into the StarDrive system. For example, when plate current was to be maximized, it was found that a properly placed control grid which was positively charged (an accelerator grid) would greatly enhance cathode emission. Conversely, when plate current was to be minimized, the standard negative dc control grid voltage could be increased to a value called "*cutoff*" bias where virtually no primary dc plate current could flow.

Also, it was observed that clouds of electrons were knocked from the plate surface by incoming cathode-emitted electrons, and rebounded into the space near it. This effect is called "secondary emission" and creates a negative *space charge* between grid and plate which acts to inhibit plate current. To further promote plate current and tube efficiency, a negative "suppressor grid" could be placed near the plate which would drive these rebounded electrons back to it.

Toward the end of his career, deForest realized that vacuum tubes would soon be replaced, except for very specialized tasks, by another new and revolutionary device: the transistor. In his own words: "Of recent years the transistor, invented and perfected in the Bell Telephone Laboratories, has begun to take over many of the duties of the electron tube. It offers many advantages: it is small; its weight is negligible; it requires only the B-battery [one][power] source; its power requirement is modest indeed. The transistor – a three-electrode device wholly electronic in nature – is obviously an offspring, and a most ingenious one, of my grid electron tube".⁽⁴⁾

For purposes of StarDrive development, the transistor unfortunately had the same effect on the evolution of vacuum tube technology as Tesla's work had on the evolution of Faraday's disk dynamo: a device which might have yielded many further valuable returns was allowed to wander into a cul-de-sac. However, *unlike* the disk dynamo, the triode and other multi-electrode vacuum tubes were indeed developed to a high degree of sophistication.

Our aim at this point is then to raise the disk dynamo to a comparable level of refinement and combine it with the vacuum tube's specialized capabilities, as a device which is also fundamentally dc in nature, to create the Electrodynamic

(4) QUOTE: The Book of Popular Science, Vol. 8, pg.89, Grolier Society © 1958. [LCCC #58-5005]

Field (EDF) Generator's Primary Power System. This power system's hardware is therefore comprised of a highly-modified Faraday disk dynamo that is made brushless with pairs of plane-parallel electrode arrays **utilizing vacuum tube techniques**, and will be used to charge negative and positive exterior sections of an evacuated hull to an extremely high potential difference.

To wit, please observe carefully the following side cross-sectional diagram (Fig.5). It shows a flat conductive rotor across which a very high dc voltage is impressed using brushless pairs of *electrode rings*, and the two inner ring pairs have triodic control grids (g) as shown. The positive inner edge of this rotor is coupled by electrostatic induction to two central positive hull sections, via two 5-element (pentode) *primary induction ring arrays*, whereas its negative outer edge is allowed to 'short' to the single peripheral negative hull section across an empty vacuum chamber. Once this negative hull section in turn shorts to the two positive sections, by ionizing corona discharge, the field envelope circuit is completed and the machine is entirely enclosed in a powerful arc field. [The field envelope configuration is shown in SpecSheet I of Chapter 8.]

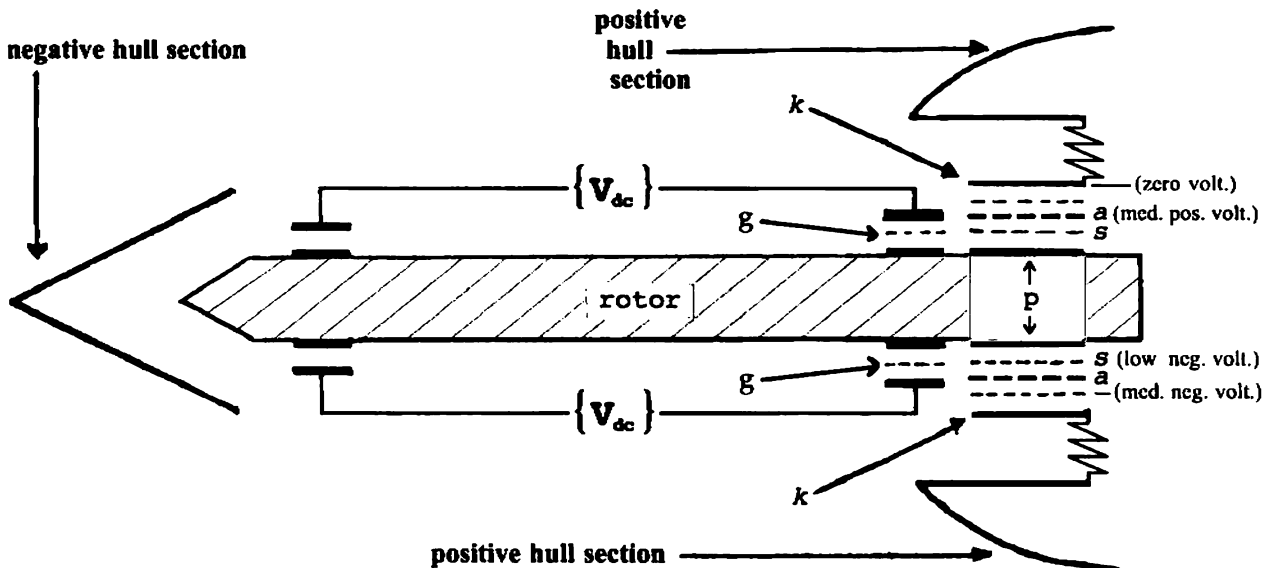


Fig. 5: primary & rotating electrode arrays

It can clearly be seen here that the Generator's rotor assembly directly combines essential aspects of both the disk dynamo and the triode tube (as shown in the preceding two Figures).

Note: grids shown between (a) and (k) are *control grids*, as in (g), but are stationary.

Specialized vacuum tube design features we'll employ in the EDF Generator's combined Primary Power System and field envelope circuits parallel those previously discussed, and are as follows:

- the field envelope circuit's two (2) major rings of *cathode elements* (k) will be made of thorium-adsorbed tungsten to maximize electron emission.* {next page}
- two (2) *positive grid element rings* (a) in the field envelope circuit may be used to maximize major rotor plate element (anode) current, and thus function as *accelerator grids* with respect to adjacent field cathode emission.

- two (2) negative *suppressor grid* element rings (s) will be used to minimize secondary emission from the surfaces of the two (2) major anode rings (p).**
- rotating *control grid* element rings (g) will be operated at a sufficient negative voltage (or bias) to effectively block almost all Primary Power System dc current between minor cathode rings and their adjacent rotor anode rings.

In the present day, the type of creative electrostatic engineering represented by vacuum tubes *may* soon be a lost art, should TV picture tubes go obsolete (!). Many readers will be largely unfamiliar with some of the tube-related terms and concepts introduced above, but these will be expanded upon as we go.

Before we move on to the next (and most intriguing) portion of our background on design development, I would like to return briefly to the term 'capacitance': the ability of a device to store electrical charge. Such a device is of course called a *capacitor*, and is electrostatic in nature like a vacuum tube. When vacuum tubes were used to amplify a signal, the capacitances which were found to exist between the tube's electrodes were design-engineered to be minimized because they could cause undesirable radio frequency effects.

One of the effects a vacuum tube can exhibit is that the actual voltage present across its terminals can be elevated (by control grid biasing) to a value which is *higher* than the voltage of the main dc power source applied between cathode and plate! This effect is due to the electrostatic force exerted by capacitively-stored space charge itself, in this case located between grid and cathode, and is very like a "voltage dam" which causes the grid and cathode dc voltages to behave as if they were variably coupled in series and not in parallel. The ancillary purpose of the two rotating triode arrays shown in Fig. 5 is then *not only to amplify any AC signal voltage present*, but to interact with the rotor in such a way as **to boost Primary Power System voltage** and therefore outer hull potential difference!!

* **Note:** An alkaline rare-earth oxide coating cannot be used due to the high current density.

** **Note:** Above 10^3 volts, secondary emission is effectively quenched, so the suppressor grids' primary function above very low rotor speeds will be to regulate the distribution of stored negative charge to the rotor as part of a Field Voltage Control System (see SpecSheet IX of Chap. 8).

Interlude: Levity

In late 1971, when I was a high school freshman, I remember reading an article in The Star about a British gentleman named John R.R. Searl. The Star, by way of reference, is a supermarket tabloid of somewhat dubious veracity having articles which sensationalize such improbable subject matter as 'the boy with the dog face' and UFO abduction stories.

The article I saw described Mr. Searl's work with what he called a "levity disc": an electric device which looked like a flying saucer and which could purportedly defy gravity by exhibiting 'levity' or lift. Apparently, Searl had put together a Consortium, or investor group, to promote the commercial development of his invention as a transportation system.

Given the source, I paid little attention to this admittedly interesting information. At that time I was quite involved in pursuing musical studies in the hope of one day

becoming a concert pianist. My fundamental obsession with flying saucers had not entirely abated, however, as I continued my casual yet persistent research on the subject (in my spare time) throughout high school and then college.

After leaving Ithaca School of Music in 1980, having discovered that music was perhaps not my truest calling, I had a difficult time finding and holding down a job that suited my off-beat nature. I drifted from one short-term employment situation to another for a few years, not knowing quite where my life was headed.

Then, in August of 1984, a friend I had met in college came to visit me at my parents' home. We talked for a time, sipping iced tea under a shade tree, before the conversation came around to a shared interest we had discussed on numerous occasions while at Ithaca: theoretical UFO propulsion systems.

My friend, Joe Suda, wanted to know if I had ever heard of John Searl. I told him, "yes", I had read an article about him years before but that it contained no hint of how his device worked. Joe, as it turned out, had gotten a job with an aerospace firm, and in his spare time had accumulated quite a dossier of information about Searl and his levity disc.

He said that when he got home, he would send me copies of everything he'd collected about Mr. Searl and suggested that perhaps I could find some renewed sense of meaning and purpose in life if I studied his files and endeavored to derive a scientifically sound all-electric propulsion system from them.

This event rekindled my passion to fully understand something I believed few people, if any, really knew very much about. My life since that day assumed a new and unique direction and the work contained herein is the legacy of the real avocation I presently enjoy.

* * *

In the years which have elapsed since I rediscovered the work of John Searl, I've learned that so much has been written about him (and so much blatant misinformation disseminated regarding his work) that an entire separate book would be necessary to adequately analyze and collate all of the various data and conjecture involved! **The Apocrypha** surrounding Searl is amazing, and vast. A great number of alleged scientists and acknowledged writers have contributed to the virtual legends concerning Searl and the levity disc. For instance, "fluid dynamicist" Jan Roos and W. P. Donovan (a fringe-area science analyst) have some very interesting but largely speculative hypotheses to offer regarding this whole strange affair; their views, however, seem to have little firm basis in demonstrable physics.

American inventor and science editor D. A. Kelley and alternative energy researcher Ron E. Hall have cited Searl's work and presented some relevant insights thereunto yet little in the way of feasible hardware proposals, let alone any good specifications. As a matter of fact, I contacted Mr. Hall by phone at his Hall Research offices in Arizona in the spring of '94, and tried to establish a working correspondence with him about the levity disc. Oddly enough, he seemed nervous and extremely hesitant to do any such thing, and all attempts at such communications were basically unsuccessful.

Even a former NASA scientist writing under the pseudonym 'Rho Sigma', the late Dr. Rolf Schaffranke, has contributed to the huge body of information arising from the career of John Searl: a family man whose main credentials seem to be having been a municipal electrical engineer and gifted experimenter.

If not for a little personal substantiation, I would have discounted much of what I've learned of Searl's scientific efforts as being largely mythical. However, I have a copy of a signed letter from Joe's files (from a William T. Sherwood of Rochester, NY), dated July 6, 1983, stating that the correspondent had indeed "worked with Searl on a volunteer basis from 1970 to 1976, editing and distributing his [Consortium] Newsletters". He went on to say that since that time, he had been virtually out of touch with Searl and revealed that the progress of his work during the time of their association was "very slow".

By all accounts, John Roy Robert Searl was born May 2, 1932 in Wantage, Berkshire, England. It is believed that his father was stationed in India then as a sergeant in the British Army. Apparently he was a fragile child, and lived for a time in a home for the elderly and infirm under a doctor's care. For reasons uncertain, he was later placed in a foster family in Suffolk with whom he lived until the end of WWII. Throughout the war period, Searl was plagued by strange recurring dreams of an unusual glowing machine with the capacity to hurtle straight up off the ground into space. He was also troubled by severe headaches.

After the war, his first job (at age 14) was with an electric motor shop in London where it is presumed he learned the basic principles of electromagnetic engineering. During his spare time he supposedly began a series of experiments with early versions of the levity disc. In 1950, Searl was conscripted into the British military; but by 1952, he had been released from duty (once again amid circumstances unclear). He then went to work for the Midland Electricity Board, a municipal power authority, as a meter reader and electrical fitter.

At this time, it is believed by some that he began work on a modified Faraday generator which was designed to capitalize upon an obscure phenomenon known as the "Hooper effect". A professor at Berkeley University, one Dr. W. J. Hooper, had discovered that a thin rapidly-rotating disk of conductive material would polarize electrically, building a negative charge at its outer rim and a positive charge at its center. This effect grows in proportion to increases in rotational speed and temperature but otherwise immediately reaches equilibrium. I have applied the term "inertiomotive force" to this mechanical centrifuging of electrons and the term "electrocentripetal force" to the resultant internal electric field which causes equilibrium; and we will return to *this* topic later on.

In any event, the first real levity disc was completed in '52. This permanent magnet field-generator was about a meter in diameter and was slip-shaft-coupled to a gas engine. Searl and a minister friend decided to test it in an open field, presumably just in case it actually worked *too well*, and not long after starting the motor they noticed the smell of ozone. Wisely, they backed away from the device as it continued to speed up on its own. It soon broke loose from the motor, by this time being enveloped in a noticeable pinkish corona, and began to hover. It slowly rose to a height of about 50 feet, where the corona suddenly turned blue, and the disc shot straight up into the sky and disappeared forever!

During the next twenty years, Searl and his associates supposedly built over 30 experimental discs of various sizes; most of these devices were also lost, but eventually a satisfactory form of remote control was developed. In 1970, the "Searl National Space Research Consortium" was founded and shares were sold to investors, purportedly raising millions of pounds. Research and development continued more intensively than ever until 1978, when Searl dropped out of sight for four years.

From 1978 to 1982, there were no more articles, seminars, interviews, or Newsletters, nor information of any kind either from or about Mr. Searl. Then in May of 1982, British authorities raided his home in Mortimer, Berkshire and confiscated everything even remotely related to his work. He was arrested for allegedly utilizing electricity not purchased from the municipal grid. [Note: In England, it can be a criminal offense to generate and use one's own unauthorized electric power.] In what could only be a suspicious travesty of justice, he was detained for almost a year; and during this time an arsonist burned his home, destroying nearly all of his remaining notes and equipment.

By one account I've read, John R. R. Searl next surfaces in September of 1983 under the pseudonym of "Dr. Bill Bates" in Smethwick, West Midlands, when he forms a new company: the "International Institute of Advanced Technology". Interestingly enough, I recently discovered an Internet website devoted to the "Searl International Space Research Consortium". This site reveals that Searl's technology is actually based on *an anomalous magnetic effect*, and subsequent investigations suggest that Searl himself has had trouble achieving satisfactory performance of his devices *since 1983* because no one has been able to adequately reproduce the original magnetic alloy and specialized magnetization process he had used prior to the destruction of his lab!

The only further information I'm going to offer at this time regarding Searl came in the form of a rather disturbing letter, dated March 1, 1991, from a European gentleman named Anders Heerfordt. Apparently, he had attended a lecture given by Searl in Denmark in early December 1990, regarding Searl's claims about the levity disc. The skeptical yet enthusiastic Heerfordt spent no little time and expense investigating these claims and, indeed, the whole Searl legend. He *states* that he could find no one who had witnessed any actual levity demonstration, or in fact anyone who could substantiate *any* of Searl's claims . . .

Prelude

**"Information is not Knowledge.
Knowledge is not Wisdom.
Wisdom is not Truth.
Truth is not Beauty.
Beauty is not Love.
Love is not Music.
Music is *the Best*."**

Frank Zappa

Joe's Garage: Acts I, II & III

Chapter 4

Design Parameters

Many researchers would be put off, and no doubt have been, by the singularly peculiar aspects of the Searl story as related thus far. The full nature of the mystery surrounding this man will probably never be unravelled. After years of painstakingly reviewing and analyzing all available accounts of his work itself, though, I found many fascinating common threads emerged – which jointly convinced me that this strange saga is much more than just an elaborate hoax.

Before we move on to a discussion of StarDrive design elements which were selected from levity disc research as being valid, including the only published *second-hand* instructions in Searl's own words I believe to be true, I'd like to begin with a brief accounting of design components and **operative characteristics which have been rejected** as constituting either unscientific speculation or deliberate misinformation. They represent points-in-common between most of the inferior related Searl writings, and are rebutted one at a time.

Excessive Operating Voltage: As the StarDrive device is being powered-up, an ultra-high static potential difference is created across the outer hull. When this potential difference reaches the insulation breakdown value of air (or vacuum, approximately) at 3 million volts per meter of effective (arc trajectory) separation, the negative hull section flashes over or "shorts" to the two positive sections.

The goal is to then maintain this corona discharge, or field envelope current flow, such that the machine is continuously enclosed in an impenetrable bubble of electric arc. At first the field envelope is a pale violet in color as its current is passed through air. In Electrodynamic Field Generators intended for use as *Thermal Power Units* (involved in the commercial production of electricity), the above-stated voltage gradient is sufficient as a base design value. Were such a machine operated in vacuum, without impeding kinetic collision with the atmosphere, field current at this point is already being accelerated to about 99% of the speed of light (and is at the 'knee' of its asymptotic momentum curve).

In EDF Generators designed for use as *Impulse Drive Units*, the StarDrive system voltage gradient must be many times higher to achieve significant thrust. Because the energy density of a Drive Unit field envelope is sufficient to ionize and expel almost all of the air within it, a virtual vacuum quickly develops (under the theory of *kinetic occlusion*), and the field turns a deeper whitish-blue. It requires, by ordinary standards, an enormous voltage for this to occur. As can be seen in Chapter 8, a 4ft. diameter prototype Drive Unit would have a specification field potential difference of about 35.1 million volts.

Many writers have expressed the view that the potential difference on the hull of Searl's levity discs was on the order of 10^{10} (10 billion) to 10^{14} (100 trillion) volts. This is flatly impossible. Anyone who has studied cyclotrons and other types of atom smashers knows that the structural integrity of most ordinary substances begins to break down at the molecular level under electron bombard-

ment at voltages around 10^9 . At voltages of over 10^9 , the electron energies involved are sufficient to disrupt the atomic nuclei themselves. I have calculated (according to the formulas given in WorkSheet I(a) in Chapter 8) that the required field voltage of a starship 100ft. in diameter is approximately 4.4×10^9 , and we can see therefore that this is about the upper limit on the size of any StarDrive system which can be built using this technology.

What I believe these Searl writers are referring to with numbers on the order of those stated above is in fact what I call the *peak inherent field power*, or the gross electrical product of Drive Unit field voltage and current in watts. In the 4ft. prototype Drive Unit, this field power is 1.474 terawatts (1.474×10^{12}) – a truly astonishing figure {see WorkSheet II(c)}. In the 100ft. Drive Unit, the figure is 20.7×10^{15} watts or over 20 thousand *terawatts*; and this is beyond what we could conceive of as even a planetary level of power by present standards.

Freedom from Inertia: One of the effects attributed to the levity disc, and usually to flying saucers in general, is freedom from the operation of Newton's law of inertia. Although the notion of shielding a starship from the full effects of inertia ("inertial damping") will be briefly referred to in a later Chapter, no known means of obviating the law of inertia has ever been found.

Perhaps one reason an inordinately high hull voltage has repeatedly been postulated in the Searl Apocrypha is that it provides a handy 'deus ex machina' to explain this implausible concept. Besides, it sure sounds impressive.

It should be noted that the incredible acceleration exhibited by *smaller* UFOs in countless sightings, which no large physical organism onboard could withstand, can more readily be accepted if such craft are in fact unmanned probes. The asymptotic reactionless drive contemplated and disclosed in *this book* can be shown capable of achieving multi-*g* acceleration if necessary.

Slotted Iron Rotor: Some writers have implied that the levity disc incorporated a rotor which was a slotted solid piece of iron. It is now known that a *stator* of similar structure is actually used, and that Searl's basic *generator* variant has no rotor per se! Nevertheless, in any feasible *Faraday-type* StarDrive device, such a choice of rotor material would have to be rejected for the following reasons:

- the *electrical resistivity* of iron is high enough that, after careful mathematical analysis, the rotor would not be able to carry a requisite level of current without unacceptable weight and heating;
- iron's valence electrons, which are responsible for all current conduction, are too tightly bound to take full advantage of the Hooper effect; and
- the use of iron in the rotor would cause undesirable *magnetic coupling* with other necessary components of the Primary Power System.

Rotor Rim Electromagnets: The supposed placing of wound C-shaped iron motor cores about the outer rim of a rotor element is the most common and misleading false design parameter found in levity disc writings. These "motor coils" were surely conceived to explain its self-operation without stored onboard power, but they really represent only a diversionary parody of the disk dynamo.

In reality, the levity disc's *generator* coils are similarly positioned around the

periphery of its *stator*, and in fact it utilizes dynamic permanent magnet rollers but no electric motor coils. An important reason exists why motor coils could not be positioned about the rotor's periphery in any feasible Faraday-type StarDrive device, and this should be self-evident: they'd be hard-pressed to survive such direct immersion in the raw arc-flame emanating off the rotor's edge!

The EDF Generator does indeed use wound iron armatures to produce torque on the rotor, but these armatures are located quite a bit further inboard in two circular arrays (one above and one below the vessel's radial centerline). They are moreover axial in shape, and only one (opposite) pole set of each array is used to provide the uniform field required for torque production. These armatures, or *variable inductors*, are intended as a secondary source of rotational torque used to alter the local angular acceleration of the rotor (for lateral maneuvering) in Drive Units, or as a means of basic torque-assist in ground-based Thermal Units.

The other pole of each armature is used to semi-polarize the field envelope itself, primarily to *promote a uniform distribution of the field current's energy* which aids in rendering the envelope quasi-coherent. This very important usage of electromagnetic fields is mentioned nowhere in *any* of the Searl Apocrypha.

Lack of Hull Anti-Rotation Provisions: Finally, it was found that not one rotor-based levity disc design analysis addressed the problem of hull rotation due to rotor bearing friction. Such a device would have had *excellent gyroscopic stability* (due to the rotor's geometry) provided that its hull and superstructure could be maintained in a non-rotational aspect. Without an adequate means of assuring this relationship, bearing drag would impart a small but constant rotational force to the superstructure until rotor and housing tended to rotate as one.

In a StarDrive device, there are two sources of hull counterrotational torque: the rotor drive motors themselves (low-voltage dc units similar to those in large electric trains), and the inductor arrays described above. To the extent that counterrotational force may actually exceed 'forward' rotational bearing drag, a small portion of the rotor's angular momentum may be tapped using reserve AC generators to apply added forward load: a *dynamic braking* technique which imparts a controllable amount of torque balance upon the hull. Such generators could then be used to power the onboard cryogenic and heat transfer systems.

* * *

Other speculative, erroneous, or obviously-omitted design parameters are evident in the Searl Apocrypha but those discussed above are the most noteworthy. These will hopefully serve to adequately debunk the levity disc myth in the form that has been so widely promulgated. Therefore, we'll move on to much more exciting revelations of greater value to the serious StarDrive student.

Uncovering the many nuggets of real engineering worth in the legacy of John Searl's career has been like sifting through tons of sediment. Although one might think from the preceding material that little of true importance could underlie such a bewildering tale, this is definitely not the case. After a great deal of careful scientific and mathematical detective work, I have found so many details of undeniable significance that I'm almost inclined to believe an insidious effort has been made to confuse and conceal the truth.

The most logical theory to explain the unusual and unfortunate circumstances surrounding Mr. Searl is that the intense nature of his vision became an overwhelming force which caused him to 'put the cart before the horse', and he endeavored to actively promote his invention before he could provide suitable proof of its viability. I feel his work really is far ahead of its time and that the only thing he was actually guilty of was unwisely pressing a sensitive issue in such a publicly visible way that it 'rocked the boat' a little too much to suit the British government! I have also failed to find any Searl levity disc Patent, by the way.

A working StarDrive device can readily be built today with existing materials, technology, and computers, although an enormous prototype development budget would be required which might well be beyond the reach of all but the wealthiest non-governmental individuals or group. At that time, however, certain of these crucial late 20th century resources were simply not yet available, and Searl most likely found that as soon as he had raised enough money to overcome one critical design or construction problem, another seemingly insurmountable obstacle presented itself.

For example, certain *specialized ceramic compounds* are essential to meet the unique engineering requirements inherent in the EDF Generator's unusual construction. Silicon Nitride (Si_3N_4), Zirconia (ZrO_2), and especially Sodium Bismuth Titanate ($\text{Na}_{0.5}\text{Bi}_{4.5}\text{Ti}_4\text{O}_{15}$) are commercially available today, but in the late '60's or early '70's similarly-exotic materials Searl may have needed might have been either incredibly expensive or not obtainable at all. Also, without the aid of sophisticated engineering computer programs, designing individual parts and components to the precise tolerances the disc's design requires would be a very difficult and time-consuming process. Quite likely, all of the above considerations jointly explain Mr. Sherwood's revelation regarding Searl's slow progress.

Anyway, the balance of this Chapter will be devoted to an examination of the design characteristics associated with Searl's levity disc which are related to his *alleged* adoption of a Faraday-type rotor as the central component. Like the parameters discussed in the next Chapter, this material has been selected as representing **valid design elements of a workable StarDrive system** and is constituted of points-in-common between virtually all of the superior Searl articles and various associated writings from my friend Joe's files.

Segmented Disk with Rotating Rings: *If* Searl truly did adapt the Faraday dynamo for incorporation into his levity disc, he would first have addressed the issue of eddy currents. Thus, instead of using a solid rotor, he would have divided the rotor into a *uniform radial assembly* comprising a large number of individual conductive "segments". It is known that the reduction in an armature's eddy current losses, and its subsequent increase in electron conduction efficiency, is proportional to the increase in number and decrease in thickness of its individual layers or laminations: or, in my case, **rotor segments** made of copper.

A photograph I studied of a *purported* levity disc rotor reveals what seems to be a total of 64 identical segments, which were all connected in parallel by means of attached **electrode rings** near the inner and outer circumferences. Since only a few readers may already be familiar with the shape of a "Searl" rotor as opposed

to that of an original Faraday disk, please realize that such a segmented rotor would've had a hollow center, like the turntable of a carousel, and two separate axles which were electrically insulated from the inner edge of the rotor (unlike the photograph of Fig. 6 below appears to suggest). This allows for a small "open" non-evacuated *central chamber* to accomodate instrumentation and payload.

In the EDF Generator, I have elected to eliminate the use of the somewhat impractical axles, and instead use a split-frame centrifuge-style *carrier assembly* whose two halves are welded directly to two large ring gears. These ring gears may in turn be supported by pillow block and pinion gear bearing assemblies affixed to the superstructure. This results in a much stronger and more compact over-all rotor mounting arrangement, and actually allows the use of *direct gearmotor drive and rotor support* (as is probably optimal in this application).

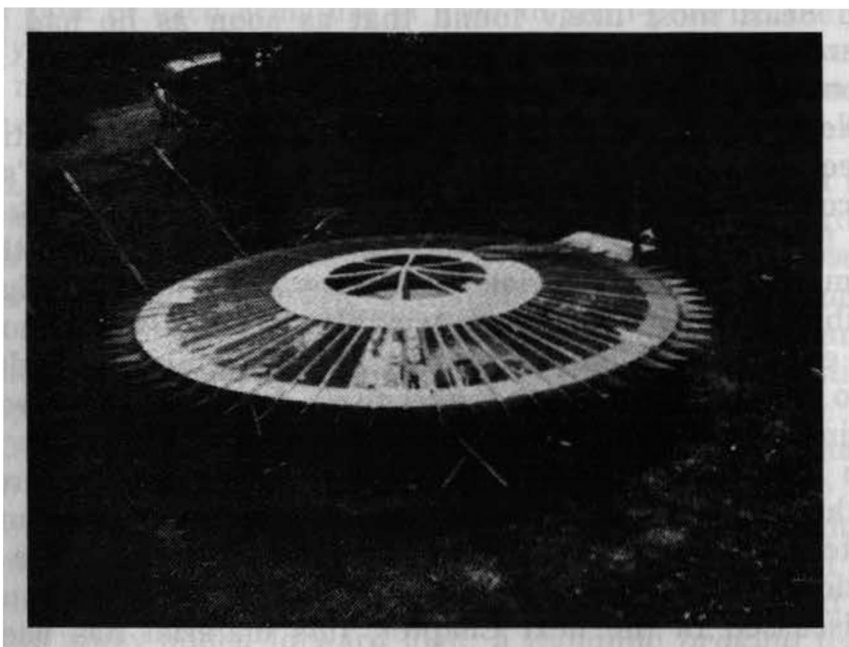


Fig. 6: *A purported Searl levity disc rotor assembly.*

A disturbing thing about the disc "rotor" as depicted in the photograph is that **64 metal segments** of the thickness indicated could not possibly carry sufficient field envelope current *to develop more than 1g of thrust* (and thereby achieve net lift), at least in the manner we will examine later on, without effecting a nearly 2-to-1 reduction in the total vessel weight as compared to the EDF Generator. Interestingly enough, one Searl-related paper I studied did stress an 'ultra-light' mode of construction although the design as proposed would not be suitable for operation in the vacuum of space.

Also, no structural insulators are shown between the segments and, at the levels of rotor speed required for full-power Drive Unit operation, these structural ceramic pieces, or **segment separators**, will be an absolute necessity to stiffen the entire rotor assembly and *to provide a non-conductive base for the mounting of all other rotating components.* However, what we are actually being shown here is

a levity disc superstructure made of wood, not a real rotor assembly!!

Be that as it may, in the StarDrive device a total of 180 copper rotor segments will be employed, in a manner similar to that implied in Fig. 6, with 180 ceramic insulators between them. The segments are to be cut from flat stock and the segment separators will thus be slightly wedge-shaped in radial width. Segments and separators will be equal in their inner end width, or about 1° each of inner rotor circumference, and will be bonded together with a refractory adhesive.

Finally, it would appear from the photograph that an integral tapered portion of each segment projected beyond the outer electrode ring into the peripheral space charge chamber. This is also misleading, for in reality these segment 'tips' would erode drastically if composed of copper, in their role of distributing field current to the negative housing section. And, any other known metal used (even silver) has relatively reduced conductivity at elevated temperatures. It required a fair amount of research for the EDF Generator's rotor design to determine that these field emitters must actually be separate high-density tungsten-copper composite pieces which are equal in peripheral width to the segment separators.

The specified number, size, and shape of the rotor segments underwent many changes as my understanding grew of how many interrelated factors were involved in selecting these characteristics. Since virtually every aspect of the complete Primary Power System will be affected by the final choice(s), let's take this opportunity to discuss certain key issues central to a determination of the segments' best possible physical specifications.

As the impulse thrust produced will be a function of the field envelope current, it was obvious that maximizing the rotor's safe current conduction capability, or ampacity, was called for to a point. Employing unnecessary conduction mass entails unnecessary weight increase, and therefore wasteful power expenditure. Maximum rotor ampacity and vehicle thrust capability are thus both covariable with the vehicle gross weight!

Since presumably no reference data or technical consultants in this area exist on Earth, I had to rely on my personal experience in electromechanical systems design and construction and make an educated best-guess estimate of weight for a particular size prototype model before I could proceed with rotor design. I already had a strong notion that a four foot diameter device would probably be the very smallest that could be built (due to the tinyness of the parts required), and so after a great deal of careful thought and scratching of the head I decided a gross weight of 75 kg or 165 lbs. was appropriate for the 4ft. model: the Badlander, which later became the basis of most further design calculations.

Later and much more accurate computations of estimated device weight revealed that the figure was actually nearer 90 kg. However, once this had been decided, it was necessary to develop a reasonable maximum thrust capability, as a limiting factor of rotor ampacity, in terms of acceleration in g 's or multiples of Earth's force of gravity. After numerous sample calculations, I selected $1.67g$'s as the approximate base design thrust limit (and the actual peak thrust of the 4ft. model is $1.877g$) for three important reasons: [1] this level of acceleration is readily tolerable to any large-model crewmember in relatively good physical

condition; [2] it allows for fairly responsive maneuvering; and [3] it enables the craft to achieve lift-off on an alien world whose gravity is substantially greater than that of Earth.

Finally, the vertical thickness of the rotor (or height of the rotor segments) is of fundamental import in determining the greatest space available for attached components within the narrow confines of the vessel's tapered peripheral "wing". I therefore endeavored to minimize segment height without sacrificing ampacity (by reducing the number of segments). The significance of this criterion cannot be exaggerated for, as we'll see, the size and positioning of rotor assembly components in very small devices must be specified to the thousandth or ten-thousandth of an inch with little margin for change whatsoever!

In any event, the calculation of prototype rotor ampacity is outlined in WorkSheet II(b), and the method used may be applied with reasonable accuracy to any vessel up to 100ft. in diameter. The design of the field emitters as specified in SpecSheet II {Rotor Segment Dimensions} ensures that they will safely pass full rotor current at any feasible operating temperature.

The Hooper Effect and Inertiomotive Force: The purpose of the tapered segment ends was quite apparent from the outset given a good working knowledge of electrostatics. The applicable axiom involved is that a negatively charged object, or a polarized object wherein positive and negative charges have been separated, will much more readily leak or discharge electrons from sharp or pointed projections than from smoother and flatter surfaces. Thus, the *tapered segment tips enhance the Hooper effect*.

The valence electrons in copper are very mobile, hence its excellent conductivity, and in fact only silver's valence electrons are more loosely held. Therefore, if we spin a segmented rotor fast enough, electrons located on the outer surfaces of the segment tips need only be given the equivalent of 4 electron-volts (the 'work function' of copper) in kinetic energy as a result of centrifugal force to exit the metal *even without an applied voltage* on the rotor!

This inertiomotive force behaves as if it were an applied voltage, in that it can create and/or boost an electric field within the rotor segments, by the physical displacement of valence electrons. If we offset the resultant electrocentripetal (inward-pulling) force by supplying the rotor's two inner primary anode rings with additional electrons, they will continue to be centrifuged from the segment tips. These centrifuged electrons are, of course, used to charge the peripheral negative section of the vessel's hull.

This is not quite, however, the whole story. The Hooper effect provides an outward inertial 'bias' or drift which promotes the electron starvation of the rotor. Centrifugal force in this case acts as a sort of 'check valve' to ensure that *the rotor is maintained at an over-all net positive charge* and therefore has a positive external electrostatic field.

If this positive static field is induced into the two axially-central hull sections, these now positive hull sections will tend to *strip and absorb ambient electrons* from the atmosphere and general surroundings when the field envelope voltage reaches ionizing energy levels. Thus, the Hooper effect actually serves to initiate

the device's capacitive electrostatic induction capability, enabling the net storage of tremendous quantities of ambient charge! In ground-based Thermal Power Units, excess ambient charge (from operation in air) above and beyond the limited amount required for field voltage control purposes must be grounded off. In Impulse Drive Units, however, a bank of from 4 to 7 centrally-located *superconducting current storage rings* would allow the accumulation of millions of coulombs of locally-borrowed static charge, and the saturation limit of these storage rings ultimately determines the vessel's range of operation in space.*

As we will learn more about shortly, the sectional vessel hull itself is actually capacitive to a certain extent within two small regions of the field envelope (near the two neutral hull sections which separate the charged electrical sections already identified). It is the Hooper effect which also allows us to deduce that the polarity of the charge stored in the *hull static capacitance* is actually positive, and that an equal and opposite negative space charge will tend to accumulate in these two envelope *power field* regions. You may want to take a look at Fig. 11 on pg. 65, and don't worry: this will become clearer as we go . . .

Toroidal Generator Coils: Conventional generators today are designed and built much as they were a century ago by Edison and Tesla. To be sure, many refinements and improvements have been made down through the years, but dc and AC generators alike still produce power at an efficiency below 100%. It has always been assumed, at least until very recently, that no machine could break this 'efficiency limit'.

One fundamental reason why ordinary methods of generating electricity fail to achieve over-unity operation is the characteristic of coil windings called *inductance*. The phenomenon of inductance is a result of Lenz's Law, which states, "A current set up by an *electromotive force* [emf, or voltage] induced due to the motion of a closed-circuit conductor will be in such a direction that its magnetic field will oppose the motion causing the emf".

So, when a coil is rotated in an external magnetic field (the basis of almost all current methods of power production), its inductance causes the magnetic field established by the current thus created to interact with the external field in a way which resists the coil's rotational motion. The magnitude of this resistive force (or magnetic "drag", if you will) is proportional to the coil's inductance as a dual function of the coil's geometry and the permeability of the material upon which it is wound.

Etude

When a generating coil's radius or cross-sectional area is large compared to its thickness or axial length, it will have severe leakage and "fringing" losses indicating that its magnetic field is inadequately contained. This type of coil geometry requires the use of an iron or steel core to offset its inherent inefficiency in harnessing the applied magnetic field's energy because it has large open ends or sides.

A generating coil's efficiency can be maximized, and its inductance losses simulta-

* **Note:** Considerations related to the capacitive *powered electrostatic induction* of ambient charge and the EDF Generator's Field Voltage Control System are discussed in SpecSheet IX.

neously minimized, when it is helically wound in the shape of a doughnut, or toroid. This is accomplished by minimizing its cross-sectional area and the permeability of its core and maximizing its radius. The toroid coil thus has no fringing losses, as it has no open end(s), and exhibits virtually no leakage as current flowing in a toroid coil produces a magnetic field which is entirely confined to the core. It is the most efficient, yet seldom-used, generator winding geometry known.*

These concepts are reflected in the formula for toroidal coil inductance:

$$L = \frac{\mu N^2 A}{2\pi r} \quad , \quad \text{where } L = \text{inductance in henries,}$$

μ = core permeability (air is $4\pi \times 10^{-7}$, and
iron is $8000 \times$ air),

N = number of turns,

A = cross-sectional area in m^2 , and

r = mean coil radius in m.

The next modification to the Faraday dynamo necessary to adapt it for use in the StarDrive system is to eliminate the inefficient use of permanent magnets about the periphery of the rotor, which induced voltage directly within the rotor material, and instead mount three (3) nonmagnetically-cored toroid coils each on the upper and lower faces of the rotor assembly between the inner and outer *induction* electrode ring pairs. These rotating **field coils** (that's right, Trekkers!) incorporate a large number of turns of very fine wire for induction by two sets of three formidable concentric arrays of stationary permanent **magnetic rings**.

In operation this creates a very high dc voltage which can then be impressed across the rotor, in series with (or added to) the Hooper effect inertiomotive electric field, via the induction electrode ring pairs. The relative positioning of all these components, as well as the central *transfer electrode ring arrays* which connect the field coils of each set in series, are shown in Fig. 7 on the next page.

I have been asked more than once why I elected to go to the extra 'trouble' of using these additional transfer triode arrays to series-connect the field coils instead of just "twisting the wires together". While it is true that there is a great deal more engineering involved in doing so, I have done this for a very good reason. As has been stated (in Chapter 3), the Primary Power System must be biased nearly to the point of current cutoff: a control-grid-produced condition whereby the dc current passed across a triode tube or electrode array is virtually (but not quite) reduced to zero. Thus, series cutoff-biased triodes should maximize the probability that the final level of series group current can actually be maintained within winding wire ampacity.

Ordinarily, triodes are connected in parallel "stages", with a common primary (plate) dc voltage supply, and each stage will amplify an input AC signal control grid voltage from a previous stage or antenna. It is postulated that a 'three-stage' rotor circuit which utilizes the transfer arrays may be similarly designed to detect and amplify a resonant frequency unidirectional or alternating electromagnetic signal *with the external field acting as an antenna!*

Just as important as this intriguing theoretical challenge is the ability to actively modulate the drive field's electrodynamic properties by impressing varying degrees of AC voltage on the rotor current and on the variable inductor power supply current as well, allowing for what might be thought of as a *variable cross-polarization of the drive field*. These rather technical considerations will be discussed in better detail in the appropriate later Chapters.

* **Note:** It should be noted that while a toroid coil of the type described above is ideal for purposes of the StarDrive Primary Power System (where very high voltage and negligible current are desired), it is not necessarily conducive per se to commercial power production. Considerations of that nature will be examined in Chapter 10.

DRAWING NOT TO SCALE

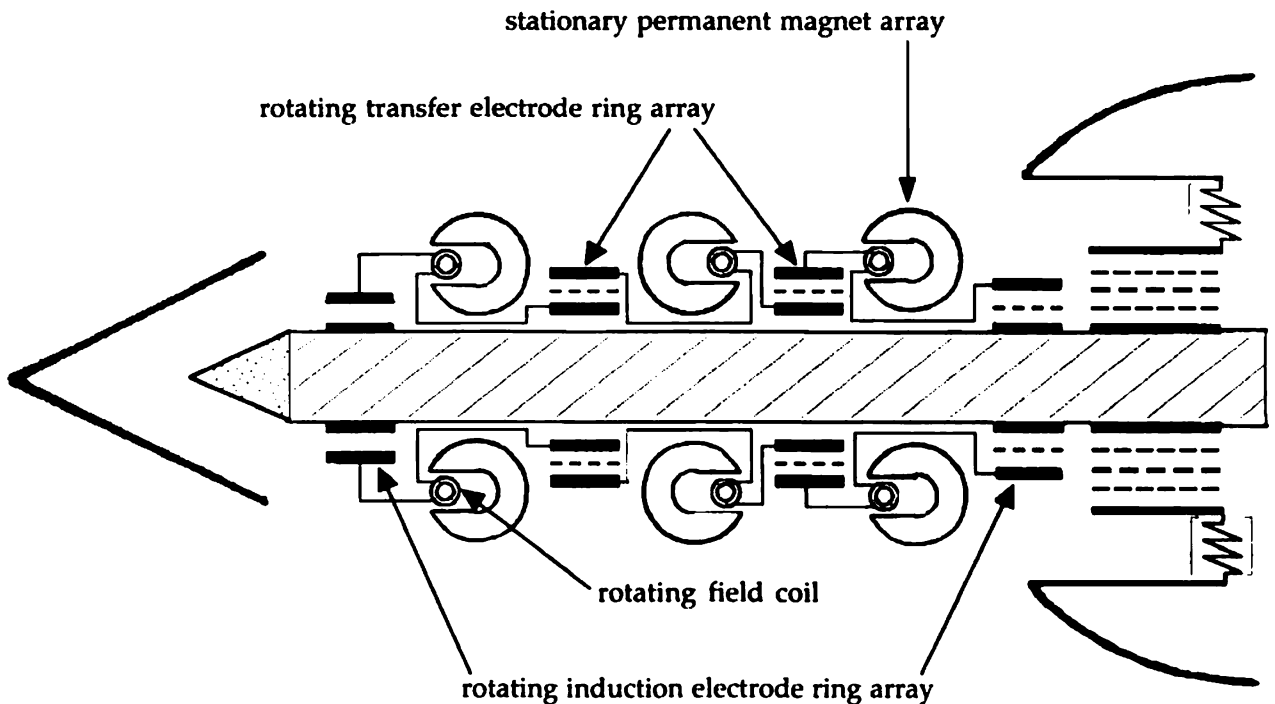


Fig. 7: simplified *Primary Power System* diagram.

The above diagram is a simplified general schematic representation, in that the true relative *sizes* of the various components are not strictly depicted, and the stationary electromagnetic armatures (or variable inductors) are not shown for the sake of clarity. It must be understood that all of the structures mounted on the rotor, as well as those interacting with the rotor which are stationary, are either continuous or repeating in placement around the device in the plane of the rotor segments. A Primary Power System component layout diagram is given on pg.123 in SpecSheet III which is true-to-scale except for the relative spacing of the various electrode rings. A side cross section view of the complete hull *Drive Ring*, which shows the entire Primary Power System including carrier assembly, is provided at the end of Chapter 7.

At any rate, we now have a basic field envelope circuit generator design which thus far, in accordance with Faraday's and Lenz's Laws, can produce maximized dc voltage with minimized inductance losses. This Primary Power System voltage is not made available, however, for purposes of normally-usable electrical output. The problem in extracting any portion of this primary voltage for 'outside' use might not be obvious at first: how do we attach power lines to a rapidly rotating source?! The solution is, of course, to once again use brushless electrode rings.

In this case, the Primary Power System electrical schematic shown in SpecSheet IX on pg. 182 best illustrates the use of two additional *stationary* electrode rings, one suspended immediately adjacent to each inner induction array cathode ring, which will allow us to 'pick off' a high electrostatically-induced positive voltage. Only this positive voltage can be used as a source of power within an external circuit (having a negative ground), and is intended for limited auxiliary *onboard* usage only (as any current drawn thereby must be minimized in practice).

Interlude: Charge

One of the unfortunate side-effects of society's continuing technological advance, as the body of what is not known *appears* ever to be shrinking, seems to be a corresponding diminution of the impetus for young people to indulge in experi-

mental tinkering. The late 1940's, when my father was a teenager, saw perhaps the last great heyday of this fine art, and any talent I have in this marvelous genre no doubt owes to him. He was, and remains, a master of improvisational engineering.

One of his first major acquisitions as a young man was a monolithic old Lincoln welder, which we still use to this day, and he taught himself to be expert in this field. Before he got his driver's license, he and a cousin of similar bent would construct 'doodlebugs' (or jerry-rigged field cars of various designs) which were put together entirely from scratch out of pieces for purposes of "off-road" bombing around. His ingenuity in creating things with his hands was in some ways rivalled only by his capacity for inspired devilry, and thence arises the story of the world's first *real* 'electric car'.

It seems that as his fascination and experience with electrical gadgets grew, he one day had the rather bizarre but original idea to wire a spare Model T coil (an early ignition capacitor) into his latest car's electrical system with one terminal connected *to the body itself!* With this condenser charged (to its rather substantial capacity), the idea was to deter any unsuspecting malefactor from tampering with his vehicle: when they touched it, they'd be "zapped". He could, of course, disable this feature with a hidden switch.

Now this was fine, in theory, but he found this early car anti-theft device had very little effect in practice, as both the car and the person touching it were relatively ungrounded. Neither had a fixed ground reference with respect to the other, so both instantly acquired *the same potential*, and thus no zap. To obviate this problem, he cut a hole in the car's floorboard and connected the opposite condenser terminal to a piece of log chain he could lower at will through the hole. With one side of the condenser thus grounded, the unfortunate victim touching the car body was now at a decided potential difference with respect thereto, and could hence receive a walloping jolt.

Looking for an opportunity to test this new improved equipment, he chanced upon my great-grandfather Albert's car parked at the local general store. While great-Gramps was inside, no doubt buying a plug of chew, my father rolled up and parked with the two vehicles' bumpers touching and dropped his log chain. Sure enough, when great-Gramps went to get in his car - *Zap!!* Upon returning to ground after a brief period of levitation, he stood there just *fulminating* in multiple expletives as my dad beat a hasty retreat.

It is this childhood story, forgotten for many years, which may have provided a subliminal cue prompting me to in fact make the hull of my developing StarDrive device a true active part of the electrical circuit. Although wonderfully apropos, the real instructional beauty of this anecdote is just this: to establish and maintain the necessary potential difference between parts of the *vessel 'body'* itself, the StarDrive Primary Power System *must* run entirely ungrounded *inside* (like the *outside* of my dad's electric car). In this case, all we have to do is pull up the log chain . . .

Prelude

Permanent magnets are similar to [electric] motors in that their capabilities are determined by factors that are part of their design. However, the “load”. . . determine[s] the final performance within the limits of inherent capabilities. It is evident that the “systems” approach is necessary to effectively apply permanent magnets . . .

Lester Moskowitz, C.M.E.

*Permanent Magnet Design
and Application Handbook*

Chapter 5

Magnetics: Rings & Coils

The use of permanent magnets in present-day industry and technology, encompassing dozens of different applications and products, is far more pervasive than most people realize. Perhaps more accurately stated, their usage in general tends to be largely taken for granted because there are few practical common objects in our society which are less well-understood *in principle* by the masses. However, permanent magnets in one form or another enter into a huge number of things we all use virtually every day of our lives.

They are utilized in almost every aspect of the all-important steel industry, from basic manufacturing to material handling and end-product fabrication. They are incorporated in DC electric motors and generators of all types and sizes, and in the starters, alternators, and small motors used in all conventional automobiles. Indeed, they can be found in everyday items from many household appliances and entertainment devices to the watt-hour meters which measure the distributed power to run them. And (of course) computers, while they do not incorporate individual permanent magnets per se, are in many cases still reliant on the principles of permanent magnetism for their data storage capability.

Most people are probably aware that the ancient Greeks knew of permanent magnets, as far back as about 600 B.C.E., in the form of naturally-occurring lodestone. Little was done to expand the knowledge of magnetism until 1600 C.E. when Sir William Gilbert performed the first known systematic studies into the properties of permanent magnets, still formed of lodestone in that day. Since then, scientists and engineers have been fascinated with this phenomenon by means of which work may be performed *without mechanical contact* or connection and *with specificity of direction* (unlike the force of gravity).

The rapid development of electromagnetism in the early 19th century, wherein the strength of the magnetic field produced could be easily rendered variable, led to a corresponding decline of interest in permanent magnets. However, the discovery and development of the powerful, versatile, and economical *Alnico family of magnetic alloys* beginning in 1939 (by G.B. Jonas et al.) – and the metallurgic predictions arising from *studies of magnetism at the atomic level* (by theoretical physicists in the 1950's) – led to a great and continuing expansion in materials and applications development.

The number of individual permanent magnets in use today is estimated at nearly 2 billion units, yet there is remarkably little organized *practical* information about magnets available to students, engineers, and inventors. This point was immediately brought home during the course of research for this book, and if not for a copy of the *solitary* landmark text I was most fortunate to acquire (Permanent Magnet Design and Application Handbook, by Lester R. Moskowitz) I would have been at a considerable impasse with regard to the proper designing of the EDF Generator's magnetic rings. I suppose it was also to be expected that this exceptional work was out-of-print within a few years of its publication.

I found that few (if any) other public library-accessible reference works actually presented essential magnetic concepts and useful 'basic' equations, including those which are generally applicable to both permanent magnets and electromagnets, in a logical and comprehensive fashion. In fact, many small inconsistencies and discrepancies (as well as occasional outright errors) were discovered in otherwise reputable technical manuals, when it comes to relating magnetic theory and practice to the serious reader. Even electrical engineering textbooks many times give permanent magnets hardly more than an honorable mention, yielding the false impression that they are relatively unimportant in modern technology. Sadly, the limited number of published treatises written by the even fewer *real* experts in this field tend to be either far too general or too unintelligibly complex to be of sound practical assistance.

As a good starting point (for our purposes), magnetism and magnetic circuits are fundamentally analogous to electric fields and electrical circuits. Thus, there are direct magnetic analogs to both Coulomb's and Ohm's Laws for electricity. In the application contemplated here, however, we are concerned primarily with magnetism as it relates to *induction* (as of a voltage in a conductor, or of a certain *flux density* at a relative point in free space) and not the production of linear force or angular torque on a current-carrying conductor or other magnetic poles. Thus, we will confine our study to concepts and equations which are pertinent to the *strength and direction* of magnetic fields, as produced by either individual or multiple like-strength permanent magnets or wound electromagnets.

It is strongly recommended that the definitions of specific magnetic terminology first be reviewed by the lay reader, in the Magnetics section of the Special Glossary. Next, the last paragraph of DataSheet #4 will expand somewhat the concepts of magnetic flux and flux density. Before the magnetic DataSheets #5, #6, and #7 are attempted, which are specifically related to C-shaped permanent ring magnets and the induction of voltage thereby, the first page-and-a-half of DataSheet #16 should then be studied. This material discusses what the author feels are the three (3) most important general equations which are applicable to both permanent magnets and electromagnets.

Equation M1 relates the field intensity (H) produced by a single magnetic pole to the *strength* (Φ_p) of that pole and its vector distance (r) from a given point. It must be emphasized here that pole strength is sometimes confused with flux density, but this is not the case, and Equation M2 gives the correct interpretation: where pole strength equals the product of the pole's gross flux density (generally B , or more specifically, B_g as used throughout in this book) and the pole's area A in the direction of its primary magnetic field orientation. Equation M3 then gives the net flux density (B_n) at such a relative spatial point in terms of the field intensity and the absolute *permeability* of the medium.

Before we move on, it is important that the difference between *absolute* and *relative* permeability be clearly understood, as this is also a sometimes-major point of confusion in certain references which may loosely use just the term 'permeability' without proper clarification. It is also most important to note that computations related to *electromagnets* should always be performed exclusively in *MKS units* as used in DataSheet #16 (unless temporary conversion to cgs units

will be expedient in special situations). To avoid potential confusion, problems, and errors, *all calculations related to permanent magnets* should be done in the appropriate *cgs units* (i.e., centimeters, oersteds, and gauss) as has been done in this book. This applies to all work done on the design and development of the magnetic ring configuration employed in EDF Generators regardless of size.

Although the discussion of inductance in the preceding Chapter was hopefully a good parallel introduction to magnetic terms and concepts, we should now examine a related engineering consideration of more practical importance. Hopefully, many of you readers without an engineering background will still be interested in observing how a seemingly simple design question can have a surprising answer. For example, because the Primary Power System's basic 'magneto' design is really so simple, about the toughest decision to make about it is whether all those individual magnetic rings comprising its 6 all-important permanent magnet arrays should be formed of round or square stock. On the surface, this would seem to be an inquiry with a ridiculously obvious result: since the square stock has much more volume per unit length at a given diameter, we should use it and not the round stock. [This volume per length ratio actually reflects the difference in axial surface area, where a 1" diameter round bar magnet would have $\pi/4$ times (or 78.54% of) the end surface area of a 1" square bar magnet.] The round stock will therefore have a smaller *total flux*.

However, an analysis of the comparative *flux density* measured in round and square Alnico bar magnets (of the same diameter) shows that a consistently higher flux density is obtained in the round stock of a given size magnet (see DataSheet #2): about 10% higher on the average for very small sizes and rising slightly with increases in diameter. Since total flux Φ_t is equal to flux density B_g times area A , a round magnet having 78.54% of the volume of the same size square magnet will have a total flux which is at least 86.39% of that of the square magnet. The reason is that the corners of the square magnet cause it to have greatly increased *leakage losses* compared to the round magnet.

Therefore, in the sizes necessary for use in larger models of Electrodynamic Field Generator and even in the smallest prototypes, round stock is more suitable for our purposes once the 21+% weight savings, the far simpler leakage flux computations and smaller leakage losses, and easier mounting arrangements are taken into account. I realize it's probably somewhat less than thrilling, but aren't you glad we figured *that out*?! . . .

Unlike the magnetic subtleties involved in the external field (which we'll look at in Chapter 9), the flux mechanics within the Primary Power System are really quite straightforward. For those of you interested in learning more about working with permanent magnets, and the methods used to design the EDF Generator's magnetic rings, reference should be made to SpecSheets V and VI as well as the previously-mentioned supporting DataSheets. Given this inclination, it really does make for fascinating study.

The next magnetic engineering aspect we need be concerned with is the variant of Faraday's law of magnetic induction required to properly calculate Field Coil output voltage. More traditional methods of voltage production would use an axial rotation of the coil with respect to the magnetic field, and the rate of

change of flux in Faraday's law is then a function of angular velocity ω according to the formula $V = \omega NBA \sin \theta$. Here, as usual, $BA = \Phi$, or total flux per each of N turns of a coil of area A . Thus, the induced emf varies with time in a sinusoidal manner and produces alternating current of a certain power factor.

In our application, the coil rotates in a uniform longitudinal (circumferential) manner perpendicular to the magnetic field (where $\sin \theta = 1$) and the change of flux is then a function of the coil's linear speed of rotation as the length per unit time of the area factor involved, and the 'width' of that area is the individual circumference of each turn of wire in the coil. Therefore, the induced emf is a pure (flat) dc output as we want and expect, and the actual voltage formula becomes: $V = N\bar{B}\pi dCr$ (see DataSheet #7).

The most important term of this expression for us to define at this point is \bar{B} , which reflects the ratio of actual total flux gap area to total coil "silhouette" area times individual ring gap flux density. This yields the average flux density experienced by each of N coil-turns over time. The width of the flux change area is obviously πd and the area length per unit time is Cr , where C is the mean coil circumference and r is coil revolutions per second. As I said, quite straightforward. I never claimed it was all that simple. Nevertheless, we are now armed and ready to accurately make a calculation of Field Coil output voltage, once we know the individual B values for the three slightly different sizes of Magnetic Rings used and the three different sets of Coil specifications! Oh, brother . . .

It is of some mechanical engineering interest at this point to wonder just how we're going to array literally thousands of small individual Magnetic Rings in the exactly tight rotational clearance necessary with respect to the rotor's Field Coils. I decided fairly early on that *the superstructure of the EDF Generator should be divided into 36 equal radial sections*, and it would therefore perhaps be much easier structurally to divide each of the six magnetic arrays into 36 equal (and relatively massive) arc-shaped pieces as well. However, it is for the very reasons related to the selection of round stock over square stock that this has not been done, although each array is to be divided into 36 sections.

Provided the apparent mounting difficulties can be overcome, it is felt that the use of individual Magnetic Rings as depicted in Fig. 25 of SpecSheet V promotes not only the optimal magnetic efficiency of the Primary Power System and the mathematical accuracy of B -value calculations, but the over-all cost effectiveness of the Generator design as well. With regard to computational accuracy, firm reliance has been made upon the Rotor method of computing magnetic leakage and fringing flux permeances (see Bibliography, Electromagnetic Devices). Herbert C. Rotor devised a system of simple equations for estimating the effective magnetic permeances of various spatial configurations (in all three planes) as they occur in air or vacuum, *near and around an air gap*. Traditional magnetic field intensity formulas related to the magnet's physical geometry are of course also used, as can be seen in the various magnetic WorkSheets in Chapter 8.

As it turns out, the dreaded mounting arrangements are in fact quite simple: because round stock is used to form the Magnetic Rings, a total of 216 round sectional 'stringers' whose OD is the same as the Rings' ID may be used to suspend

them in the same manner as when they were magnetized – strung like beads on an abacus wire! [Note: see Section 1 of Material SpecSheet F.] These curved nonmagnetic stringers may then be supported from the superstructure by means of an appropriate number of sheet stainless steel hangers whose thickness is related to the calculated weight of each array section and the average shoulder-to-shoulder Ring clearance therein. If the maximum number of Rings composing each array is used, as in ΔSpecSheet VI {Magnetic Ring Arrays}, it is envisioned that 6 such hangers per array section would have sufficient rigidity to accomplish the easy structural mounting of the Magnetic Rings especially if each of the 216 (or 6 x 36) array sections is ‘potted’ with an epoxy sealant. These structural parts are also depicted in the said Fig. 25.

The most elusive (and certainly the least understood) magnetic engineering concept in the collected Searl literature concerns the nature of iron “field pieces” which were alleged key parts of the levity disc. No other aspect of the device’s design is mentioned less often in the more believable writer accounts. Few analysts seemed able to grasp the critical importance of these disk components, perhaps because they aren’t technically a part of the Primary Power System.

It was never made clear whether or not these armatures should actually be wound, as electromagnets, as they are in the Electrodynamic Field Generator. Most people seemed to think they were passive flux-directing slugs of iron which magnetically linked the field envelope to the rotor *and* to the center field coils. In some accounts, they are even rotating components of the rotor itself. However, they were always positioned somewhere in the hull Neutral Ring (housing the Primary Power System), between the negative and positive hull sections.

They were moreover somehow responsible for the simultaneous generation of torque *and* usable power, once again to account for the levity disc’s self-operation without stored onboard energy. And, in a roundabout way, this does lead one to realize that the Field Coils may in fact be *compound-wound**, since a portion of each center Coil would then have to become part of a separate output circuit!

Therefore, the **Variable Inductor Arrays**, as the two circular groups of stationary electromagnetic armatures are called, are a decisive factor in developing the proper wiring logic and general schematic diagram with respect to the StarDrive Primary Power System and auxiliary output circuits.

The majority of Searl writers were apparently lured by the prospect of using the field envelope to polarize the iron and not *the other way around*, as must actually be done. What they were trying to do is utilize the polar component of the small magnetic field produced by Drive Field current, which in reality tends to be self-randomizing anyway (because of the Field’s arc-discharge nature), and draw usable power from it. This is a beautiful premise and smacks at once of over-unity (hence its fatal attraction), but it is just not tenable as a working theory. I should know: I invested a lot of effort trying to make it work.

For the time being, however, the following question comes to mind: is there a simple way to empirically *know* whether the armatures should be wound? In all truth, there is, but it eluded me for quite some time as I became lost searching for

* A compound-wound coil is one which is comprised of two or more separate windings.

the Grail of over-unity. I won't even reveal the full extent of my optimistic misconceptions, before I discovered the answer. The bulk of the useful knowledge I gained in the process is discussed in Chapter 9, and is related to estimating what level of iron armature-induced flux density near the "epicenters" of the field envelope should be maintained for optimum performance.

With the benefit of hindsight, this performance criteria provides the key to answering the to-wind-or-not-to-wind question. In short, once a decision is made that a *controllable* level of torque should be applied to the rotor, and that an *independently variable* level of flux density should also be imparted into the field envelope (to optimize its as yet unknown performance characteristics), a concomitant position has to be taken that the armatures must in fact be wound. Otherwise, both secondary rotor torque and field flux density are variable only in direct proportion to rotor speed. I suppose we could say, "it's *that* simple".

So that we may proceed to a magnetic engineering consideration of further significance with respect to device performance, a brief crash course in basic magnetic theory will probably be valuable to all but certain trade professionals. After all, magnetics is almost certainly one of the least understood of human sciences: for instance, as of 1980, there was only *one* known college-level text and course in applied magnetics yet offered in the United States!

It is said that when Einstein was a boy of five and confined to bed with an illness, his father brought him a magnetic compass to help keep the lad amused. The young Einstein was fascinated by the mystery of the needle which always pointed north - no matter how he tried to hide or turn the compass case. Thus, the 'simple' mystery of magnetism is perhaps what first drew him toward the studies that would later revolutionize our conception of the Universe.

For our purposes at present, let's first concentrate on a basic look at the source of all ordinarily-useful magnetic effects: the electron. The most fundamental magnetic axiom of all states that "a charged object in motion exhibits a magnetic field which encloses it". In this case, the negatively-charged electron's rotation about its own axis causes it to have an axial magnetic field with fixed north and south poles like a small bar magnet (see Fig. 8a below).

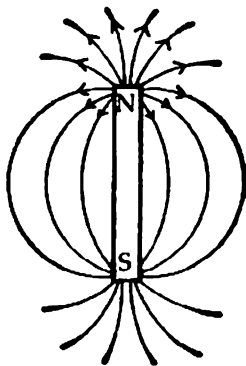


Fig. 8a: axial magnetic field of rotating electron is the same as that of bar magnet.

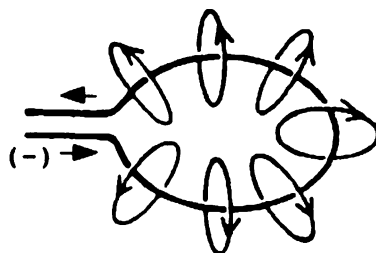


Fig. 8b: radial magnetic field of orbiting electron is the same as that of the current in a single loop of wire.

What is generally less well known is that the electron's orbit within the atom also constitutes the type of motion required to produce a magnetic field. This field, however, has only a very weak axial polarity and instead produces the type of field associated with a large single loop of wire: a toroidal ring of flux lines (formed into 'loops') with an unfixed radial *polar tendency* (Fig. 8b). This type of field is ordinarily not observed in nature as the electron traverses innumerable random orbits within the atom at tremendous speed.

When current flows in a conductor, an observable magnetic field is established because an impressed voltage "orients" the motion of virtually all free (valence) electrons in an orderly way analogous to the way a magnetic field is produced about a permanent magnet by the oriented axial spins of huge numbers of electrons (in "domains") within the magnet material.

When we rotate the segmented rotor and its attached Field Coils, the very high dc voltage impressed across it (via the affixed electrode rings) causes a huge current to flow outward on all of the copper segments given the proper polarity assignment. A tubular flux loop system (of unfixed radial polar tendency) arises about each segment and together they constitute the *primary rotor magnetic field*, which rotates with the motion of the rotor. It is this primary rotor field which allows a rotational torque to be imparted to the rotor by the application of a stationary external uniform polar magnetic field (with fixed north and south poles on opposite sides of the rotor).

Now, we know that the rotor has an over-all net positive charge because of the Hooper effect, and as it spins, this net static charge constitutes a rotational current flow similar to electron orbital motion *but limited to one thin plane*. Thus, the rotation of net static charge on the rotor will induce a fairly weak but useful **secondary rotor magnetic field** which does *not* rotate in that it obeys a second fundamental magnetic axiom, stating "such a field tends to be stationary with respect to the motion of the charge which induces it". Therefore, this net charge rotation produces a toroidal field similar to that which surrounds the electron flow in a single large stationary loop of wire (but of opposite polar tendency)!

Two additional basic magnetic axioms now come into play to explain why this secondary rotor field *must be split into two separate parts*: a half-density toroid field both above and below the plane of the rotor. To wit: (1) "magnetic field lines never cross" and thus the secondary field must completely enclose *the positively-charged portion* of the rotor without 'cutting' its plane or the primary rotor field; and (2) "magnetic flux systems always tend to exert their influence over the easiest pathways available within the smallest work-dependent spatial volume".

Fig. 9a on the following page illustrates how this secondary rotor field might look, given the operation of the first of the criteria just cited, without the presence of the iron 'field pieces' or armatures. Note the attenuated toroidal cross section fading at about the rotor's vertical centerline, where we wish to locate the armatures. Fig. 9b shows how the split secondary field would look with the armatures added, in light of the second such criterion. The region near mean segment length was initially chosen for the location of the Variable Inductor Arrays as being near a true rotor neutral or "ground" potential.

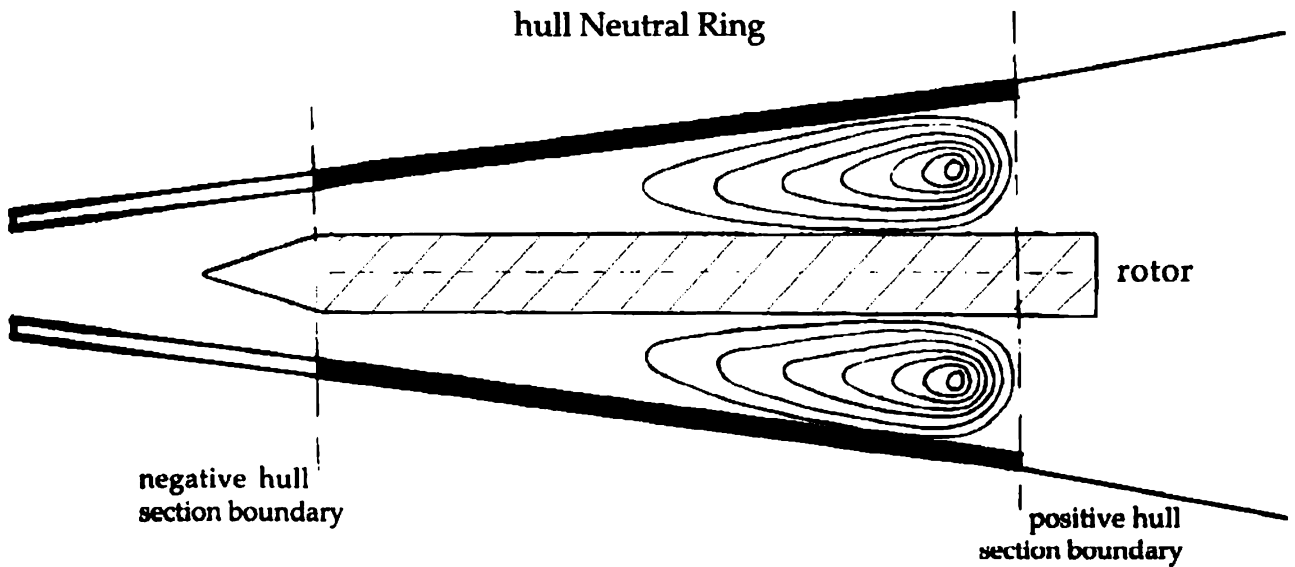


Fig. 9a: secondary rotor magnetic field

This field must enclose the positive portion of the rotor without cutting its plane.

Although the appropriateness of the first just-cited axiom (1) to our contention of a split secondary rotor field is rather self-evident, that of the second (2) may be somewhat more oblique. In the simplest sense, the field pieces or armatures act as a magnetic 'sink' of very high permeability allowing us to attract and capture the secondary rotor field into its most desirable location(s). In this way, its full energy potential can be most effectively harnessed and any otherwise disruptive effects (on the primary induction ring arrays!) are simultaneously minimized.

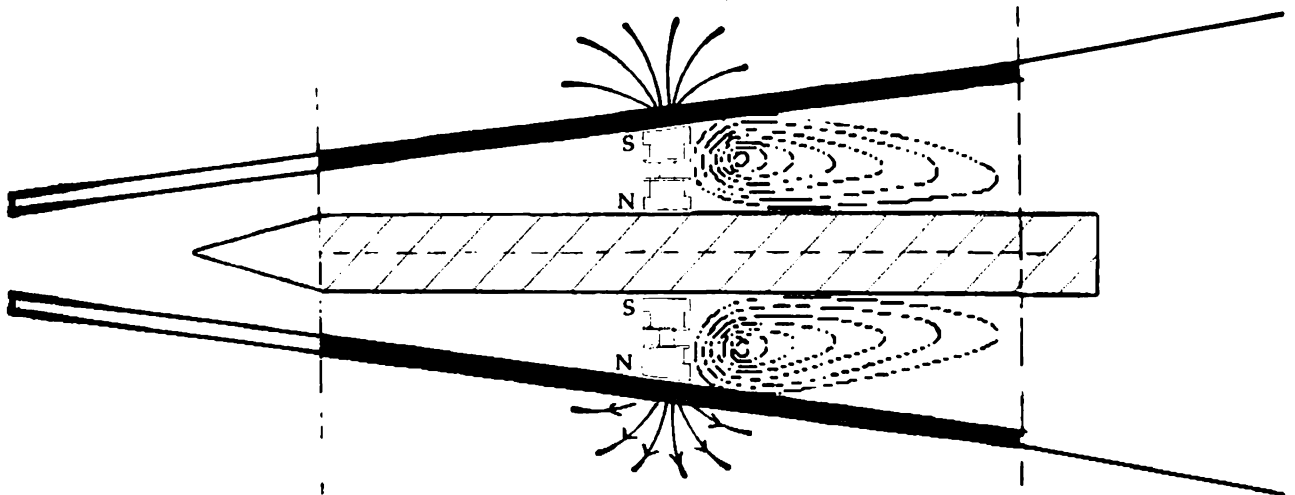


Fig. 9b: 'field piece' induction

The secondary rotor magnetic field will be pulled away from the electric induction ring arrays and polarized by the *variable inductors* which in turn semi-polarize the two halves of the field. The inductor cores only are shown here, and the **core polarities indicated** are those which would **result in clockwise rotation** of the rotor (as viewed from above). Two separate windings will be installed on each core.

Thus, the rotor's net static charge due to the Hooper effect becomes a source of magnetic field intensity with which to energize these field pieces or inductors! We know, however, that the split secondary field of its own accord has only an unfixed radial polar tendency and as such cannot act *directly* to induce a strong polar flux in the inductors. Therefore, a small electromagnetic winding will be installed on the inner section of each inductor (that nearest the rotor) to force the suitable polarization of the secondary rotor magnetic field, and for this reason these windings are known collectively as **flux initiator coils**.

Because of their proximity to the rotor, these identical windings also act as a group to allow a substantial uniform rotational torque to be transmitted to the rotor. And, if the flux initiator coils are parallel-connected, they may be made independently controllable and used to *locally alter the angular acceleration of the rotor*, enabling a small directional force of horizontal thrust to be indirectly imparted to the hull (in Impulse Drive Units) for lateral maneuvering!

It is perhaps not possible or necessary (at least within the scope of our work here) to accurately pre-calculate the magnitude of the magnetic field intensity that the secondary rotor field will exhibit in response to the Hooper effect. While it is anticipated that the initial strength of this field will be very small near the center of the rotor where the inductors are located (due to the attenuation illustrated in Fig. 9a), it is important to remember that the permeability of iron is thousands of times that of air. Thus, whatever portion of the field remains at that point will be "scavenged" and magnified enormously *within the iron*!

This kind of magnetic 'waste' energy reclaiming and amplification at last then constitutes and exemplifies the type of techniques which must be employed in any device which hopes to demonstrate over-unity operation. In essence, the polarized secondary rotor field *effectively doubles* the 'initialization potential' or magnetizing capability of the flux initiator coils with respect to the iron inductors. The reason why this is so has to do with the observed magnetic characteristics of toroid fields.

Etude

Two important magnetic axioms related to toroid fields are essential not only to a full understanding and appreciation of the secondary rotor field's over-unity implications but to a proper performance study of the external electrodynamic field produced by the present invention as well. These axioms are as follows: (1) a toroidal magnetic field will polarize only to the extent necessary, either on a need-to-do-work basis or in response to an applied external field; and (2) interactive toroidal flux systems are always mutually self-reinforcing (attractive) and tend to establish symmetrical and/or balanced relative arrangements.

Therefore, from the first axiom (1) just-cited, we can see that the *maximum* effect the polarized secondary rotor field can have on field piece induction would be to increase flux initiator coil response by 100%. Thus, we may treat the secondary field flux as an effective increase in the initiator coil current with an unknown *augmentation factor* between 1 and 2. This will enable us to establish a reduced input power range due to the augmentation of the flux initiator coils, given desired minimum and maximum inductor output flux density values (traditionally calculated).

The resultant applicable formula for individual variable inductor flux density is:

$$B = \frac{\mu N I f}{2r}, \text{ where } B = \text{flux density in wb/m}^2,$$

μ = core absolute permeability,
 N = number of winding turns,
 r = mean coil radius in meters,
 I = coil current in amps, and
 f = augmentation factor *between 1 and 2.*

From this initial inductor core flux density, we may then calculate the magnitude of the torque on each segment of the rotor, given its amperage (I) and length, according to the traditional formula $F = BIL$, where L is the length of the segment in meters.

The relative complexity of much of this Chapter's material may be a bit intimidating to those readers with a limited math/science background. It is, after all, the result of years of research into a specific and obscure engineering area which has been an enigma to the vast majority of engineers and science writers who even dared to speculate on it publicly. For those who desire a fuller knowledge and understanding of the principles of magnetism, some excellent reference works are given in the bibliography.

As "magnetic" as the preceding revelations about our unfolding StarDrive system may be, especially to real Searl enthusiasts, there is more. Until now, we haven't really looked at the *outer* section of the variable inductors we've worked so hard to understand. As you may recall, they must be used to *semi-polarize* the external field envelope (because we're using only one pole of each inductor). What makes the Electrodynamic Field Generator unique in respect to other corona discharge devices is the application of uniformly distributed and superimposed magnetic fields "to impart a rotational magnetic vector moment upon the external discharge current . . . which subsequently aids in rendering such current quasi-coherent" (in the language of my Patent Application).

Now, this magnetic rotational force acts perpendicular to the electric field applied radially across the hull: the electric acceleration of field envelope electrons takes place *only* in the 'vertical' plane. This "transverse deflection" of field envelope electrons (against the drive field voltage gradient) is proportional to the square of the distance from the inductor pole faces. Therefore, its rotational influence is greatest near the centers of the two hull Neutral Ring surfaces. As was mentioned in the preceding Chapter (in the section on the Hooper effect), a negative space charge tends to accumulate in these two regions as a function of the vessel hull's *static capacitance* which we'll study further in the next Chapter.

In these two portions of the field envelope, the applied magnetic fields are strong enough to 'bend' the electron trajectories into a stable horizontal circular "gyro-orbit", similar to that produced in a cyclotron, which rotates at a particular harmonic velocity. These two electron gyro-orbits therefore constitute *twin* rotational current elements exactly analogous to the net positive charge on the rotor, and together comprise the StarDrive **annular power field**. To attain our desired independently-variable level of flux density within the field envelope, and therefore control the rotational velocity of the space charge in the

power field, we'll need to install another group of parallel-connected windings, or **transflection coils**, on the available outer sections of the variable inductors.

Each transflection coil is separated from its adjacent flux initiator coil by a reduced cross-section connecting portion of the inductor core, as can be seen in Fig. 9b, called a **flux reductor**. These flux reducers are designed to magnetically saturate when either end section of the core is at approximately half of its maximum operating flux density. Although a more complete description of these now identified and named electromagnetic components is given in αSpecSheet XII, suffice it to say here that these reducers allow either of the two sets of core-installed windings to be operated at a broad range of flux densities between 0 and 100% capacity without disrupting the operation of the other. And, at times either the flux initiator coils or the transflection coils may actually be reverse-powered (applying a temporary *counter*-magnetomotive force or -mmf) with respect to the other, always with controllable mutual flux density compensation.

Of course, the rotating power field space charge has a toroidal magnetic field just like the secondary rotor field. This field, however, may not be tapped for power by the variable inductor arrays because Lenz's Law (and conservation of energy) tells us that this field must oppose that which causes it, and therefore the weak axial polarity it exhibits will be the same as that of the inductors. *Unlike* the secondary rotor field, the magnitude of the power field magnetic induction can readily be calculated with excellent precision using the Biot-Savart law for the flux density at a given point near a single currented loop of wire.

Calculating the magnetic flux density produced at points within the electrodynamic field, which is of special concern in investigating its performance characteristics with respect to the production of thrust, is a much more difficult proposition. Specifically, the degree to which the individual fields of the many separate inductors of both arrays 'overlap' or are superimposed must actually be calculated. To do this, a series of equations is developed in DataSheet #16 which allows these computations of *flux superposition ratio* to be made. The actual net *transflection flux density* required to produce a stable power field electron gyro-orbit, which determines the *displacement current* represented by space charge rotation, is computed in WorkSheet XII(b) {Axial Field Flux Balance}.

* * *

Review

Before we move on to an examination of StarDrive design elements which are related to developing a proper capacitive hull shape, we'll conclude our basic analysis of the device's Primary Power System and this study of its principal magnetic features with a brief but somewhat elaborative over-all review.

At the outset, we endeavored to design a workable electromagnetic propulsion system with space travel capability. Because of the enormous distances involved, we know that we need to travel as fast as possible: near light speed *or faster*, if we can. To the best of our knowledge, no one on Earth has ever both claimed they knew how to do this *and* held a successful public demonstration.

Therefore, it was necessary to make at least a few assumptions from which to logically proceed. We began by making the most basic assumption of all: that this is indeed possible. If so, we know our craft or vessel must have a hull capable of protecting the instrumentation, payload, and (hopefully) the crew. To protect the hull itself from catastrophic collisions with even an occasional interstellar hydrogen particle, we've made a further assumption that we must entirely enclose this hull in an impenetrable bubble of electric arc.

Should this arc field fail to charge and/or repel such a particle or very small object, its energy density must be sufficient to totally obliterate the mass before the hull is breached. If such an object is too massive for this shielding to be effective, our vessel must be maneuverable enough to avoid such a collision. Thus, we'll assume that taking advantage of the strongest mechanically-useful force in nature, the electric field, will help us to achieve both of the above objectives and so the hull of our StarDrive craft will be exceedingly charged.

The basic principles of electricity tell us that a flow of current takes place from negative to positive, so our hull must have metallic conductive sections of opposite polarity. Since we want to develop a flow of current which fills the air or space immediately surrounding the hull, we logically must also have a section of the hull between the negative (emitter) and positive (collector) sections which is electrically neutral and insulative. This will force the current to leave the negative hull section and arc across the neutral section provided the driving voltage is high enough. Therefore, our field envelope will be comprised of extremely high dc voltage and very heavy current.

From the commonplace 20th century technology of arc-welding, we know that concentrated arcs of very heavy current will 'burn' through metal. So, we will need to distribute the arc field's energy about the surface of the positive hull section(s) as evenly as possible to avoid damage. The best way to do this happens to be the only way: we must impart a magnetic rotational aspect to the field envelope itself. This will help to ensure a uniform distribution of the inevitable heat generated as the field's current impacts the collector hull sections.

Two principles from high energy particle physics now come into play given the foregoing criteria for the StarDrive system's hull and field envelope. The first is: electrons can very readily be accelerated to near-light speed by the application of a high-voltage electric field. And the second: electrons accelerated to near-light speed have greatly increased relativistic mass, and give up all of their gained kinetic energy upon striking a target. Therefore, our proposed field envelope becomes a viable source of thrust with which to propel the vessel.

To reiterate, then, our fundamental StarDrive assumptions and their related premises:

- (1) electromagnetic space propulsion is possible and achievable *at this time*;
- (2) the proposed vessel's outer hull is to be densely charged and divided into emitter, neutral, and collector electrical sections;
- (3) the vessel's hull is to be encased in an electric arc field which is semi-polarized and rendered quasi-coherent by the application of magnetic fields;
- (4) the external field envelope can be maintained at a sufficient energy density

to protect the vessel from high-speed particle or wave-energy collisions without thermal hull damage; and

(5) the relativistic kinetic energy of the field envelope is a source of sufficient thrust to accelerate the vessel to extremely high velocity.

From these few deductive assumptions, we've now tried to derive the necessary *hardware* inside such a vessel hull that will enable us to achieve our goal. A great many fascinating (yet exasperatingly vague) clues have been carefully weighed so that we may proceed, with an absolute minimum of further assumptions, to develop a complete final design which may be substantiated with proven scientific theory and engineering methods.

Our first and most important hardware component is a segmented copper rotor assembly whose primary function is to develop and carry the enormous energy inherent in the arc field. We know that for the vessel to have an extended operating range in the vacuum of space, tremendous quantities of electrons must be stored in at least one superconducting storage ring onboard (to gradually replace that lost due to inevitable field envelope leakage). Also, if the field is to allow us strip and store atmospheric negative charge in preparation for flight, it must be inductively linked to an onboard conductor which has a net positive electrostatic charge. Hence, the rotor is maintained in a modest state of electron starvation, by its centrifuging of electrons (via the Hooper effect).

To generate the initial or primary voltage from which the field envelope will be produced, two sets of three rotating toroidal field coils are mounted on the rotor faces for electromagnetic induction by six separate arrays of stationary permanent magnets. This *primary power system* impresses its induced voltage across the rotor via two sets of electrode rings which are adjacent to the inner and outer rings attached directly to the copper segments.

The primary power system voltage is then boosted, and its own separate operating current simultaneously minimized, by the action of these electrode rings and their associated control grids. The rotor is thereby caused to negatively charge a proximal section of the evacuated vessel hull in a manner very much like a Van de Graaff generator, and we know all of the net static charge must reside on the outer hull surface due to the Faraday shielding principle.

Another two sets of electrode rings with grid elements inductively couples the maximum positive rotor voltage to two separate positive hull sections. When this positive voltage reaches ionizing energy levels, electrons will be stripped from the surroundings and conducted to the rotor, where the level of current rises in proportion to rotor speed until field 'ignition' occurs.

Two groups of wound ferromagnetic armatures are employed to produce torque on the rotor as well as on the field current itself. Near the center of the hull neutral regions this applied field torque causes a proportional amount of negative space charge to rotate in a manner which is intimately connected with the performance characteristics of the field envelope as a whole. By controlling this space charge's rotational velocity, the level and (to a certain extent) the direction of field-developed thrust may be modulated. This thrust is asymptotic and 'reactionless' in nature and, although its efficiency is under unity, the machine's *overall apparent efficiency* will be in the *millions* of percent . . .

Interlude: Spin

Many readers will remain unconvinced (I'm sure) that the modified disk dynamo described can achieve over-unity operation, just as the notion of faster-than-light travel will be unacceptable to some. After all, we've all been told for a very long time that these two things, in particular, just aren't possible.

Lest the negative appellations 'perpetual motion' and 'free energy' return to haunt us, all you serious StarDrive enthusiasts should be reminded that God himself has already invented the universe's ultimate workhorse and quasi perpetuum mobile: the immortal electron. In fact, I believe the electron to exist in *virtual null time*.

As anyone who has played with a spinning top knows, when an outside force turns or twists the top's axis of rotation, some of its rotational speed is lost. Even neglecting friction, repeated such losses cause the top to de-spin. However, the electron has the inherent capacity, unlike a top, to self-maintain its own gyroscopic momentum: it is able to absorb quanta of ambient electromagnetic energy such that its natural self-decay is *never observed*. The electron converts absorbed photonic radiation as necessary into energy of spin, on a need-to-do-work basis.

"All" we have to do to create a device which is over 100% in *apparent efficiency* is build an electromagnetic circuit which taps the angular momentum of trillions of constituent electrons for energy, *by electric and/or magnetic induction means*, and let natural quantum mechanics fill in the balance! This is the distinctive legacy of New Age magnetic engineer and Patent-holding over-unity pioneer John Ecklin.

A marvelous practical demonstration of this principle ("**conservative electron no-work force**") that Mr. Ecklin taught my research group is the "ball and paper clip trick". In this experiment, which is really not a trick at all, the only items required are a short piece of string, a common paper clip, a small steel ball (not stainless), and a flat 'button' magnet. One ties the string to the paper clip and grips the loose end of the string between the 4th and 5th fingertips and palm of one hand. Holding the clip between the thumb and index finger, one then also carefully grasps the ball with thumb and forefinger such that the end of the clip contacts the surface of the ball.

With the entire hand-held arrangement about 8" above the button magnet (on a horizontal surface), one then quickly lowers the ball-and-clip combination to the surface of the magnet (thereby inducing a *keepered magnetic pulse* in this simple magnetic circuit) and raises it back in one smooth motion. If done properly, the many-times more massive steel ball will then hang magnetically from the paper clip indefinitely, or until shaken loose. That, my friends, reveals one key to over-unity.

My friend Joe Suda was able to perfect this difficult maneuver and performed it repeatedly at a downstate regional science fair to the delight and amazement of school age kids. *Although no work is technically being done*, who are we to say that the electrons in that paper clip are not continually absorbing just a little *extra ambient* electromagnetic energy all the time to pay the cost of supporting that ball?!

It is intriguing to note, and probably beyond the scope of this book to pursue, that the answers to some of the universe's last great mysteries might be found by probing some odd and surely interrelated observations involving the electron. For instance, the magnetic moment (or rotational force vector) of the electron is about the most accurately measured constant in all of science, yet is strangely greater than can be explained by either classical or quantum physics as yet.

A curiously fascinating Maxwellian equation, which may be of special interest to those readers who have a background in math and theoretical physics, has also (in my opinion) never been adequately explored or explained. This simple (?) formula may in fact underlie a key quantum relationship between photonic radiation and the magnetic moment and deBroglie frequency of the electron: the electric permittivity of free space ϵ_0 (8.854×10^{-12} coul²/nt-m²) times the magnetic permeability of free space μ_0 ($4\pi \times 10^{-7}$ Wb/amp-m) equals $1/c^2$. I think that it's possible there's a Nobel Prize somewhere in seeing if this innocuous equation contributes to the derivation of an "essential algebraic" solution to quantum gravity.

As we enter the 21st century, it is distressing to observe how little apparent progress is being made to achieve Tesla's electric millenium or Mitchell's global change of consciousness. If anything, we seem more likely to sooner arrive at some profligate and ignominious fate. The various forms of mass media which engulf us day-to-day seem inclined to dangerously glorify the mundane, the *mediocre*, and even the downright ignorant aspects of modern life, which are certainly many and pervasive. At its worst, the news itself is obdurately filled with apocalyptic and demoralizing messages of doom.

In an effort to stay abreast of our *alleged* techno-social advance, and make the scope of my research well-rounded, I used to subscribe to a plethora of science-based magazines including OMNI, Discover, and Popular Science. Month after month, I found interesting articles containing a great deal of *information* but an amazing lack of real breakthrough solutions to our many world problems. As I see it, the solutions to most of these problems relate directly to both Tesla's vision and Mitchell's message. Regarding our need for a new source of clean power, we've found in the late 90's that sustained nuclear fusion as a practical source of electricity is still at least 50 years away. Our energy problem is likely to become so critical before then that scientists are seriously investigating such stop-gap technologies as solar power and "clean coal". The cost of building nuclear power plants is totally ridiculous and in the United States we aren't even bright enough to make the ones we do build of the 'fast breeder' (free-energy) type.

Each year-end issue of Popular Science usually reviews the top 100 technological achievements of that year. Virtually all of the developments cited of late are directly related to cars, computers, and entertainment. It's not that these things aren't good or valuable, but there seem to be few new milestones in energy production or good old-fashioned electromagnetic engineering in general. In short, we just don't seem to know how to make new "hardware" anymore.

As a proponent of a new hardware-based technology with much more than just the potential to help us solve our energy problems, I find it fitting in a dark sort of way that one of the major recent scientific developments was a decision *not* to build new hardware. The cancellation of the superconducting supercollider project, after more than a billion dollars was spent on it, represents a wise choice not to spend too much money to achieve too few *new* results.

My own belief is that the StarDrive device, in addition to being a power plant and propulsion system in one, would also serve as a far more effective quantum physics laboratory to assist our scientists in developing a new cosmology which includes a quantum gravity and/or unified field theory. God willing, maybe time will prove me right.



Archer Energy Systems, Inc.

Geneva, NY 14456 USA

an Archer Enterprises affiliate

Supplementary Technical Overview of the *StarDrive Dynamo's* Method of Operation

rev.1-101306

The only part of the EDF Generator (“StarDrive”) technology that we are developing which is truly complex is: how to produce an external DC Field voltage across the device’s housing which is much greater than that produced by its internal field coils and magnetic rings. In short, this difficult objective must be achieved using certain ‘classical’ vacuum tube design and operating principles. Without going into greater detail than necessary, the following list of key points will hopefully illuminate the methodology adequately for present purposes:

1) The positive axial collector housing sections of an EDF Generator or *StarDrive Dynamo* must be stripped of electrons much faster than the corresponding negative charge can be replaced by corona or arc discharge from the device’s peripheral negative emitter-ring housing section. This creates a huge cumulative voltage imbalance across the housing, by an electronic principle called ‘*instantaneous charge differential*’, which can be up to many thousands of times larger than the Primary Array voltage used to charge the housing’s positive collectors.

2) Accomplishing this fundamental objective first requires that the collectors be connected to hot tungsten cathodes whose characteristic electron emission is greatly enhanced by impregnating them with any of a number of special alkali-metal compounds, as compared to the emission rate of the much cooler rotor-mounted field emitters that charge the negative housing section.

3) To sustain a corresponding *much-elevated housing-to-rotor voltage differential* at a desired equilibrium value, the electrons stripped from the collectors must then fall into a potential well created by rotor-mounted “field ballast capacitors”, the total storage value of which is figured according to a classically-derived electrostatic formula that relates the desired Field voltage to the equal areas of the negative and positive housing sections and to the given field coil voltage.

4) Finally, the dimensions of the ballast capacitors must be such that the electric field intensity within their dielectrics is equal to or greater than the desired Field intensity across the housing, which (assuming the charge stored therein is equal and opposite that on the housing) thereby provides an ‘equal and opposite force*’ which supports the “*primary voltage expansion ratio*” defined by the primary-cathode to field-emitter electron emissivity ratio. *[$E = V/d$, and $E = F/q$; so, $F = Vq/d$]

For safety reasons, the Field voltage utilized in all *air-cooled StarDrive Generators* will be limited by design to 850 VDC, and to 1,400 VDC in the larger *liquid-cooled StarDrive Dynamos*. With regard to the 24-kW Generator prototype model, such units will operate with a net field coil potential difference of 540–640 volts applied to the stator circuit’s main HV busses. In part due to the odd dual-capacitive geometry of the ‘primary power system’, the peak theoretical induced rotor voltage should be about 1/3 of the HV buss voltage, or +213 VDC (max.), and the corresponding “start” (or no-load) portion of this ‘ideal’ induced rotor voltage that will be impressed on the primary anode rings is projected from strike-voltage analyses *and* recent experimentation to be +77.5 to 90 volts (or ~1/7 of the HV buss voltage). With the primary cathodes at ground potential, or zero volts, this will also be the ‘driving’ Primary Array voltage, the “run” (load-current) value of which is likewise projected at +47.5 to 77.5 volts. [It should be noted that the potential difference across the vacuum chamber will tend to equal the Primary Array voltage, with the inner surfaces of the housing’s Emitter Ring at a zero-volt or ‘ground’ potential (due to the Faraday shielding principle).]

Since the potential on the housing collectors must equal one-half of the Field voltage, the voltage drop across our prototype’s power resistors will be 425 VDC – which is equal to the input voltage of the custom solid-state inverter that will provide the Generator’s usable AC power output. The output inverter will therefore be connected (in parallel) between the collector end of the power resistors and the primary cathodes. The *primary voltage expansion ratio*, or the ratio of Field voltage to Primary Array voltage, will be between about 9- and 18-to-1, and the level of primary cathode chemical treatment required to achieve this ratio can readily be determined once the necessary *cathode work function* is calculated using the venerable Richardson-Dushman emission current density equation.

Prelude

And God said unto Noah . . .
make thee an ark, . . .
and this is the fashion
which thou shalt make it of:
the length of the ark shall be
three hundred cubits, the breadth of it
fifty cubits, and the height of it
thirty cubits . . .

Genesis 6:13-15

Chapter 6

Hull Configuration

At this time, a resurgence of interest in UFOs seems to be taking place, and an unusually well done TV special recently suggested that credible sightings lately are more numerous than ever. As a matter of fact, in 1993, 53% of Americans polled believed in the existence of 'real' UFOs. By 1997, this figure had risen to well over 60%. Millions of people everywhere are fascinated with flying saucers and star travel, as is perhaps borne witness by the tremendous popularity of the StarTrek™ series and its spin-offs: the most successful TV dynasty ever.

This same special (among others), as well as a 1994 six-part series in OMNI magazine, also examines the notion that perhaps no other topic of public and scientific interest has ever been the subject of a more intensive and thorough governmental cover-up. It would seem that the politico-military echelons *really* don't want we the people to know anything about StarDrive.

Fortunately, I have the gift/curse of stubbornly following "the less-travelled way" and of not believing much of what I'm directed to unless it fits logically and scientifically acceptable models that *I* can understand. In this respect, when I began to assess the Searl files my friend Joe provided me with (in late '84), I realized that little of what I was reviewing was of any practical significance *as given*. The more I thought about what I was seeing, the clearer it became that a meaningful tapestry could only be woven by reading between the lines of what I came to view as a combination of unwitting and deliberate misinformation.

Early on, I decided that a careful analysis of what was being said about the outer shape of the levity disc, purportedly in Searl's own words, was much more important than all of the unscientific speculation regarding its internal parts. After all, this device's ultimate purpose is StarDrive, and external shape (as in all aircraft) will be of critical consequence. Just what is it about *that shape*?! For countless decades, the vast majority of eye-witness reports and writer accounts (perhaps going back as far as the Bible) ascribe the characteristic saucer shape to UFOs. Something about this shape must be of foremost scientific significance.

In July of '89, Joe and I finally solved the mystery of the levity disc's hull configuration as a function of the only clues given about its proper shape. Only later would I realize that the list of hull design criteria given by Searl was also like a key with which to unlock a proper understanding of the type, size, shape, and positioning of the various parts and hardware inside. Its main impact upon me was in forcing me to acquire a firm working knowledge of electrostatics and its principles: especially that of capacitance.

Following is the original list of eleven hull design parameters, as seen and cross-referenced in numerous sources: this one reference resource had sparked nearly five years of careful thought and mathematical analysis! Because of the importance of these instructions, we'll examine each one in order and the conclusions which were made regarding it. *It is unequivocally assumed here that the propulsive Searl disc generator variant in fact has a segmented copper rotor.*

Hull Configuration

- * 1) The periphery shall be of negative polarity.
- 2) The summits shall be of positive polarity.
- 3) The merging of the outer shells at the periphery shall be an acute absolute.
- 4) The merging of the outer shells at the summits shall not be an acute absolute.
- 5) The merging of the outer shells at the summits shall be spherical in nature.
- 6) The fixed ring of the generator shall hereafter be described as being the ring nearest the summits.
- 7) The distance between the fixed ring and the peripheral rim shall not be greater than one tenth of the vehicle's diameter.
- 8) The distance described in (7) above shall be reserved to accommodate the flight reaction controls.
- 9) The outer shell shall be constructed of non-magnetic materials.
- 10) The materials used in the outer shell construction shall be made electrically conductive.
- 11) The minimum and maximum deflection angles for the outer shells at the periphery shall not be less than six degrees and not greater than eight degrees. "

Negative Ring: The periphery of the hull adjacent to the outer edge of the rotor is the single negatively-charged hull section, which we have also termed the *Emitter Ring*. It orients the disc's negative electric field vectors in the x-plane, and is where electrons are accumulated and then emitted both for rotation in the power field and for the production of relativistic thrust in the *Drive Field*.*

Positive Zones: The summits or positive hull sections orient the disc's positive electric field vectors about the y-axis and are where the Drive Field imparts its thrust. These summits, which we call *Polar Field Zones*, together constitute the **Field Hub** or center of electrostatic acceleration upon field envelope electrons. This is where these electrons are collected for recirculation.

Acute Peripheral Hull Angle: Rule #3 tells us that the two peripheral extensions of the Emitter Ring (also called Zones) merge at an acute angle. Rule #4 is of little practical value in that it only tells us that the Polar Field Zones do not so merge. We eventually took this to mean merely that the edges of the Field Hub must intersect the planes of the adjacent hull portions at an obtuse angle.

Spherical Field Hub Shape: The following Rule specifies (again somewhat ambiguously) that the outer shell sections composing the Polar Field Zones meet

* It should perhaps be clarified at this point that the polarization of the field envelope affects all of its constituent electrons, although not uniformly. For simplicity's sake, the power field is taken here to represent that portion of total field envelope current which is to all intents and purposes fully-polarized and therefore *axially* rotational to the extent that it produces no relativistic thrust. The Drive Field is then that portion which is considered only semi-polarized and non-axially rotational to the extent that it produces essentially all of the relativistic thrust.

in a spherical relationship. Thus, from analytical geometry we now have a hull shape which, in its purest form, is composed of *two truncated right conic sections* and *two one-base spheric zones*. As yet, we still have no indication of the relative sizes of these fundamental volumetric sections and zones.

Central Chamber: The “fixed ring” spoken of in Rule #6 threw us for a while, but we eventually concluded it was referring to the non-rotational **Central Chamber**. This volume, whatever it turns out to be, will include all of the cargo, instrumentation, and crew the vessel is able to carry in the shallow but wide cylindrical portion of the hull between the Polar Field Zones (see Fig.11/pg. 65).

Neutral Ring Radius: Rule #7 was found to be the second most important of the list, and gives not only the maximum separation between the negative and positive hull sections – and we knew that this hull region had to be neutral – but also the relative radii thereof! This Rule begins to address the issue of the relative sizes, and surface areas, of the Emitter Ring Zones and the Polar Field Zones.

Navigational Controls: We know that the field envelope emanates from the Emitter Ring and arcs through space, across the hull *Neutral Ring*, to the Field Hub. Without the influence of an external electric or magnetic field, the Drive Field will produce radially-impinging thrust vectors which are balanced by symmetry and resolve into purely y-axis resultants.

The transflection coils located in the Neutral Ring, however, can each be used to *alter the local angular acceleration of the Drive Field* and therefore its angular momentum. This conceivably allows a secondary precessional force of axial torque to be imparted to the hull and its gyroscopic rotor. This method of providing the disc with additional directional control and maneuvering capability *in the z-axis* will be examined in Chapter 13, and is exactly analogous to the technique mentioned earlier involving the flux initiator coils with respect to the rotor.

Non-Magnetic Hull Materials: This Rule is not elaborated on in any known Searl information, and the logical implication is that to use magnetic materials in the hull itself would interfere with the field envelope and/or the internal parts and circuitry. It would seem to require that no iron, soft steel, or nickel be used on the outer surfaces or in the supporting superstructure, and can only be taken as an absolute directive with respect to the hull's Neutral Ring and Field Hub.

Electrically Conductive Hull Materials: Rule #10 obviously applies to the hull Emitter Ring (or Negative Ring) and the Polar Field Zones, which must be conductive to carry a high static charge until field envelope current flows between them. No mention is made of what material(s) should be used to cover the Neutral Ring, but we know that whatever material is selected, it must be a relative insulator both electrically and thermally to establish and withstand the action of the field envelope. Ceramic compounds like Cordierite and Zirconia will be examined in this capacity and would theoretically experience some finite (but negligible) skin conduction losses.

Peripheral Deflection Angle: The most important Rule of hull construction has been saved until last. It sets up several crucial electrical and volumetric relationships affecting both field electrodynamics and internal hardware. We are told that the Emitter Ring Zones must each have a surface which is deflected 6°

to 8° from the hull's lateral (x-axis) centerline. As no reason for this is explicitly stated, we assumed that an angle approaching 8° would be desirable to maximize the internal volume of the combined Negative and Neutral Rings: the Drive Ring where our magnets, coils, rings, and grids are located. For our original hull configuration computations, we arbitrarily selected 7.5° as the deflection angle and this was not a bad guess, as we'll see.

As Joe and I sketched various possible hull designs, we discussed the probability that the disc's hull was intended to be a huge modified parallel plate capacitor, with a controlled rate of 'leakage' current. By having the negative rim oriented perpendicular to the positive axis, we were very likely helping to inhibit the field envelope leakage across this capacitance to a value where the Drive Ring could be charged faster than it was discharging to the Field Hub.

Although I didn't realize it yet, the corollary to this notion is that the Field Hub must also be positively charged by the rotor faster than its charge can be neutralized by this very field envelope current. This two-fold concept is related to a capacitance principle called *instantaneous charge differential*, which is discussed in detail in DataSheet #13, and is absolutely essential in the Generator's creation of a 'secondary' envelope voltage which is orders of magnitudes larger than the initial Primary Power System voltage applied to the rotor.

At any rate, we therefore set the negative Emitter Ring surface area equal to that of the two Polar Field Zones (or Field Hub), and a very interesting shape began to take form. Because of the Neutral Ring radius specification, we decided to make $1/5$ of the hull radius be the basic unit of hull configuration. To our mutual delight, we at length had our equal charged-surface areas, without resorting to calculus, by using advanced algebra which is not beyond senior high school math students.

For some reason, I wasn't satisfied with the finality of our computations. Tackling a much higher level of complexity, I told Joe that I desired to simultaneously also set the volume of the Drive Ring equal to that of the Field Hub! He wanted to know why, as we had endured seemingly interminable calculations to achieve our equal-area design. I answered with some enthusiasm that I had a hunch it could be done without a great deal of disruption to our existing equations, on the supposition that to do so might enhance the hull's stability in attempting a jump to supra-light speed!

He looked at me somewhat askance and sighed, but didn't complain as we set out on the next leg of an arduous mathematical journey. As I suspected, once again we were able to succeed without the application of calculus directly, although I did have to derive certain algebraic expressions from a study of the problem in terms of calculus.

Our original hull diagram and its accompanying area/volume spreadsheet follow, for the edification of those with a mathematical bent. In final practice, this design and spreadsheet combination must be fine-tuned just a bit to reflect the need for some finite peripheral edge surface area. Also, in our refined design, we'll wish to make the linear extension of the Emitter Ring deflection angles meet the center points of the Polar Field Zone surfaces for electrostatic force

considerations. This will ensure that the theoretical electric field intensity at these points *due to each Emitter Ring Zone considered separately* is minimized.

Staring up from this cross-sectional diagram when we were done was a shape which not only undeniably fit the description 'flying saucer' but which was also amazingly similar to the main saucer section of the "Next Generation" starship Enterprise, familiar to millions of StarTrek™ enthusiasts around the world! I like to think that this is more than just a coincidence.

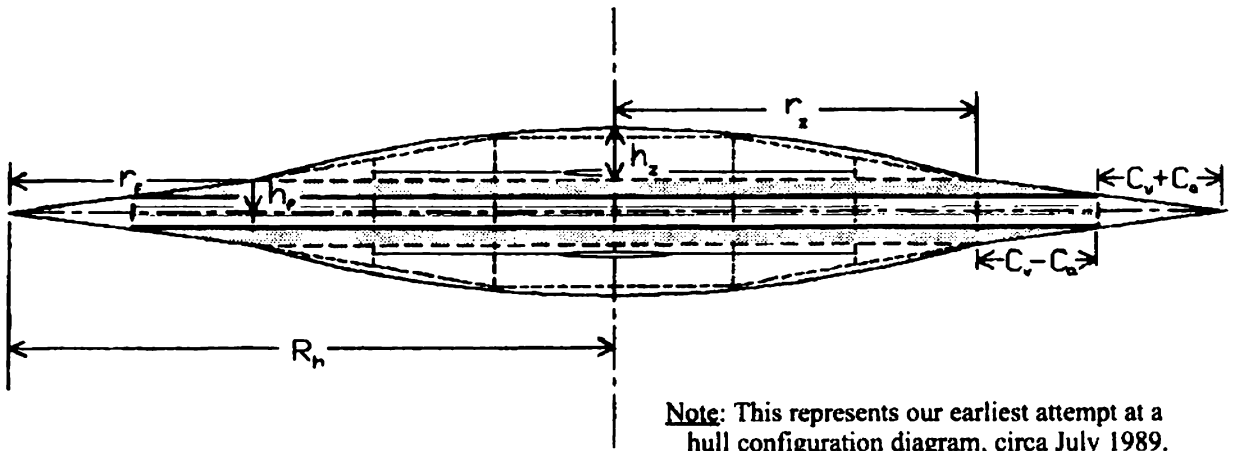


Fig. 10: schematic cross section of the EDF Generator's *design hull configuration*.

The dimensional variables shown are used in the accompanying spreadsheet to verify the equal-area/equal-volume design, using the sectional hull nomenclature developed in the text. A much easier-to-read version of this spreadsheet is provided at the beginning of Chapter 8 {Basic Specifications}, along with a detailed analysis of its derivation. The only material changes made in the upgraded version are the error percentage figures given: ironically, in the original version, these error numbers were very slightly in error themselves! They were off a few millionths of a percent . . .

Just as the beginning of the spreadsheet implies, this design may be scaled-up linearly to virtually any size merely by 'plugging in' the desired hull radius. Two important considerations should be noted here, however. As was mentioned near the beginning of Chapter 4, an Electrodynamic Field Generator 100 ft. in diameter is near the upper size limit for this type of StarDrive device due to excessive operating voltage. Also, the ratio of *net* Central Chamber volume to gross vessel displacement is not very large, meaning that a vessel **about 40 ft. in diameter** would be required before *any* crew could actually be accomodated onboard!

In an effort to further influence perhaps a whole generation of young future scientists and engineers to seriously study and expand upon my work, I have developed a rudimentary Manned Vessel Design DataSheet which may be found immediately after the clarified version of the Master Spreadsheet in Chapter 8. I heartily encourage all of you to 'have a go' at designing your own personal StarDrive vessel, based on the simple size and interior volume guidelines given therein, using the complete Basic Specifications as your workshop.

Hull Configuration

S P R E A D S H E E T

Project: Electrodynamic Field Generator

title: Hull Configuration

Date: Sun 2 July 1989

INSERT HULL DIAMETER HERE:	=	48	inches	prototype
HULL RADIUS (R_h)	=	24		
Hull Volume Constant (C_v)	=	4.8000	NOTE:	$C_v = 1/3 R_h$
DRIVE RING RADIUS (r_r)	=	9.6000	NOTE:	$r_r = 2 * C_v$
Hull Area Constant (C_a)	=	.062011	NOTE:	$C_a = 0.012919 * C_v$
Negative Ring Radius ($C_v + C_a$)	=	4.862011		
Neutral Ring Radius ($C_v - C_a$)	=+	4.737989		
Radius (Neg. Ring & Neut. Ring)	=	9.600000		
FIELD HUB RADIUS (r_s)	=	14.4000	NOTE:	$r_s = 3 * C_v$
Drive Ring Radius (r_r)	=+	9.6000		
RADIUS (Field Hub & Drive Ring)	=	24	NOTE:	$r_s + r_r = R_h$
Polar Hull Constant (h_s)	=	2.046593	NOTE:	$h_s = 0.1421245 * r_s$
Polar Volume Differential (X_h)	=+	49.636512	NOTE:	$X_h = (r_s^2 - h_s^2) / 2(h_s)$
Radial Hull Constant (R_s)	=	51.683105	NOTE:	$R_s = 2.153463 * R_h$ and $h_s + X_h = R_s$
AREA OF POLAR FIELD (POS) ZONE	=	664.5993	NOTE:	$A_s = 2\pi R_s h_s$
AREA OF EMITTER RING (NEG) ZONE	=-	664.5992	NOTE:	$A_n = s(C+c)/2$, where:
$A_s - A_n$	=	.0001	$s = \sqrt{[(C_v + C_a)^2 + (.1317 * (C_v + C_a))^2]}$	
			$C = 2\pi R_h$	
			$c = 2\pi[R_h - (C_v + C_a)]$	
Please observe that the outer areas A_s and A_n , respectively, are equal to within an error of			.000019	% **
Drive Ring Displacement Angle	=	74°	NOTE:	$\tan 74^\circ = .1317$
Volume Of Central Section (V_c)	=	823.6294	NOTE:	$V_c = \pi r_s^2(h_r)$, where: $h_r = .1317(r_r)$
VOLUME OF POLAR FIELD ZONE (V_s)	=	671.1053	NOTE:	$V_s = 2/3 \pi R_s^3 - \pi[R_s^2(X_h) - X_h^3/3]$
VOL. OF DRIVE RING SECTION (V_r)	=-	671.1055	NOTE:	$V_r = \pi h_r[R_h^2 + R_h(r_s) + r_s^2] / 3 - \pi r_s^2(h_r)$
$V_s - V_r$	=	-.0002		
Please observe that the inner volumes V_s and V_r , respectively, are equal to within an error of			-.000028	% **
TOTAL DISC VOLUME (DISPLACEMENT)	=	4331.6804	NOTE:	$V_t = 2(V_s + V_r) + 2V_c$

MASTER SPREADSHEET

Project: *Electrodynamic Field Generator*

title: Design Hull Configuration

<u>INSERT HULL DIAMETER HERE:</u>	=	100	feet (designated 'Toltec')
DESIGN HULL RADIUS (R_h)	=	50	
Hull Volume Constant (C_v)	=	10	<u>Note:</u> $C_v = 1/5 R_h$
DRIVE RING RADIUS (r_f)	=	20	<u>Note:</u> $r_f = 2C_v$
Hull Area Constant (C_a)	=	0.12919	<u>Note:</u> $C_a = 0.012919C_v$
Negative Emitter Ring Radius ($C_v + C_a$)	=	10.12919	
Neutral Ring Radius ($C_v - C_a$)	=	+ 9.87081	
Radius (Neg. Ring & Neut. Ring)	=	20.00000	
FIELD HUB RADIUS (r_z)	=	30	<u>Note:</u> $r_z = 3C_v$
Drive Ring Radius (r_f)	=	+ 20	
HULL RADIUS (Field Hub & Drive Ring)	=	50	<u>Note:</u> $r_z + r_f = R_h$
Polar Hull Constant (h_z)	=	4.2637	<u>Note:</u> $h_z = 0.1421245r_z$
Polar Volume Differential (X_h)	=	+ 103.4094	<u>Note:</u> $X_h = (r_z^2 - h_z^2)/2h_z$
Radial Hull Constant (R_s)	=	107.6731	<u>Note:</u> $R_s \approx 2.153463R_h$
AREA of POLAR FIELD (POS) ZONE	=	2884.5458	<u>Note:</u> $A_z = 2\pi R_s h_z$
AREA of EMITTER RING (NEG) ZONE	=	- 2884.5452	<u>Note:</u> $A_n = s(C + c)/2$, where:
$A_z - A_n$	=	.0006	$s = [(C_v + C_a)^2 + (\tan \alpha (C_v + C_a))^2]^{1/2}$, $C = 2\pi R_h$, and $c = 2\pi[R_h - (C_v + C_a)]$.
<p>***Please observe that the outer areas A_z and A_n, respectively, are equal to within an error of:</p>			
		.000021 %	*****
Drive Ring Displacement Angle (α)	=	$7^{1/2}^\circ$	<u>Note:</u> $\tan \alpha = .1317$
Volume of Central Section (V_c)	=	7447.4595	<u>Note:</u> $V_c = \pi r_z^2 h_f$, where: $h_f = (\tan \alpha) r_f$.
VOLUME of POLAR FIELD ZONE (V_z)	=	6068.2987	<u>Note:</u> $V_z = 2/3 \pi R_s^3 - \pi [R_s^2 X_h - X_h^3/3]$;
VOLUME of DRIVE RING SECTION (V_f)	=	- 6068.3004	and $V_f = \pi h_f [R_h^2 + R_h r_z + r_z^2]/3 - \pi r_z^2 h_f$.
$V_z - V_f$	=	-.0017	
<p>***Please observe that the inner volumes V_z and V_f, respectively, are equal to within an error of:</p>			
	=	-.000028 %	*****
TOTAL HULL VOLUME (DISPLACEMENT)	=	39168.1172	<u>Note:</u> $V_h = 2(V_z + V_f) + 2V_c$

The balance of this Chapter will be devoted to a fundamental analysis of the field envelope and its relationship to the hull configuration. We'll therefore study the outer hull capacitance and basic characteristics of the **radial Drive Field**, including its electric field intensity and subsequent current thrust potential.

Before we begin, though, we need to return briefly to the aforementioned fine-tuning of the hull configuration. Our primary concern here is the initially structural consideration of peripheral edge surface area. As is evident from the original hull diagram and spreadsheet, our calculations presupposed an impractical zero-height (razor-sharp) edge. As it turns out, this is extremely undesirable for electrical reasons related to the Field envelope.

As was alluded to earlier, the Drive Field may be thought of as a leakage current across the hull capacitance, in the *traditional* sense. Because of its semi-circular arc-path towards the Field Hub (which we'll look at shortly), Drive Field current may more accurately be viewed, however, as a controlled 'fringing' phenomenon for our purposes.

We already know that the actual leakage of electrons from a charged object toward ground or a positive potential is proportional to the 'sharpness' of its physical contours. Therefore, the disk's true leakage losses occur primarily as a function of its peripheral thinness! The thicker we make this edge, however, the more we effect an undesirable reduction in useful Drive Field emission area!! Obviously, a compromise solution is necessary.

To develop an appropriate peripheral edge surface area, we must first effect a recession, or cutting back, of the disk's design hull radius (R_h). This will allow us to best accomplish our other fine-tuning parameter involving the Emitter Ring deflection (or displacement) angle. The design displacement angle of 7.5° slightly undershoots the Field Hub 'summits', and a new angle closer to 8° must be derived. By recessing the hull radius slightly, instead of just adding edge height at full design radius, we can minimize the volumetric changes associated with expanding the displacement angle.

Even before we can calculate the effective hull recession (r_1) and subsequent "trim" hull radius (R_1), a new edge height or thickness must be selected. The edge height chosen (h_e), to facilitate such computations, should be nearly the same as the thickness of the almost chemically-pure aluminum we'll use as Emitter Ring plate substrate material. This will yield a peripheral edge surface area which comprises *approximately* 1% of the Thrust Ring area total.

These subtle design refinements involve a greatly expanded level of mathematical complexity which requires some use of calculus to resolve. Additional area and volume constants must be derived to achieve our goal of a perfectly balanced hull configuration for this design which necessitates minimal changes in the original parameters. To all intents and purposes, though, the hull diagram and spreadsheet as given will suffice nicely.

We must begin our analysis of the StarDrive **Field envelope configuration** with a careful look at the nature of the electrostatic field between the oppositely charged hull sections before we may accurately assess the relatively dynamic aspects of Drive Field thrust and power field capacitance. I realize that all you

Trekkers out there have probably been waiting impatiently for the actual “meat and potatoes” thrust calculations, but these cannot be made incontrovertibly unless they’re based on a clear picture of the Field envelope’s working structure. Therefore, we’ll go one step at a time so that our claims about reactionless electric drive may be undeniably substantiated.

Our first concern is the shape of the effective outer perimeter of the envelope, or the longest arc-path continuously associated with the Drive Field. One of the most basic of electrostatic principles tells us that an external electric field’s influence theoretically extends to infinity. Thus, any field envelope electron which is accelerated from the Emitter Ring on a trajectory outside this perimeter will probably be lost toward ground potential. This would obviously tend to occur from our newly-developed edge surface area. We’ll assume conceptually (for ease of computation) that all envelope leakage losses occur essentially from this peripheral surface only.

A basic tenet of electron behavior itself that is perhaps not widely known is that electrons must both enter and leave a conductive surface at right angles to the surface. There is then no purely linear trajectory between the Emitter Ring and the Field Hub. In this type of situation, and especially in the presence of a magnetic field, it is known from particle physics that the electrons prefer to take the shortest circular arc-section pathway available. Thus, we’ll take the outer Field envelope perimeter (or electron path of greatest length) to be a pure semicircular arc across the full hull radius, as shown in Fig. 11 below.

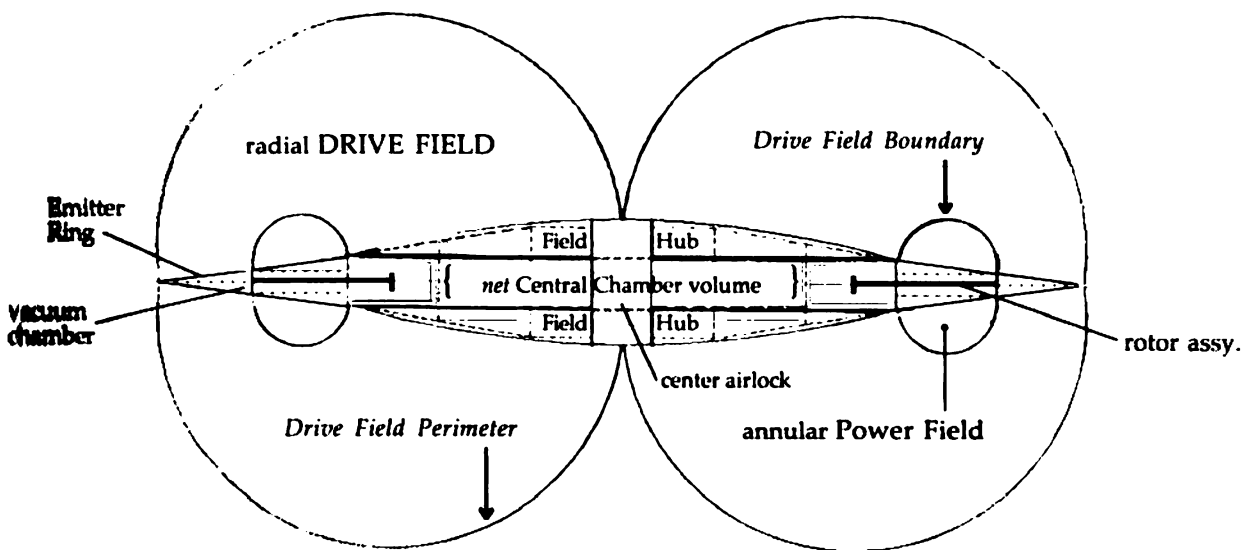


Fig. 11: *idealized field envelope configuration*

In a like manner, we will assign a pure semicircular trajectory across the full Neutral Ring radius as the shortest arc-path continuously associated with the Drive Field *per se* and which therefore represents the inner Drive Field boundary.

That portion of the Field envelope enclosed within these boundaries is taken to represent the power field, where the *field dynamic capacitance* is expressed as a rotating negative space charge and no significant thrust is produced. Thus, the Drive Field boundary also defines the longest arc-path continuously associated with the power field, under the influence of the variable inductor arrays.

Although this neat separation of the Field envelope into two parts is not really accurate in the strictest physical sense, the resultant idealized Field configuration is much easier to visualize and greatly facilitates our required quantitative calculations while remaining fairly accurate mathematically.

Now that we have an adequate basis for perceiving the electric field region about the hull with which we'll be concerned, let's proceed to develop a means of determining its functional capacitance. Concepts, data, and formulae thereby derived will be necessary before we may calculate thrust.

Capacitance is, by definition, the ratio of the charge stored (in coulombs) to a given applied voltage: $C = Q/V$. In an equal-area parallel plate capacitor, C (in farads) is also equal to the area of one plate times dielectric permittivity (ϵ) divided by plate separation distance (d), where A and d are in m^2 and m respectively: $C = \epsilon A/d$. For our purposes, $\epsilon = \epsilon_0 = 8.854 \times 10^{-12} \text{ coul}^2/\text{nt-m}^2$ for air or vacuum.

Were we to assume at this point that our chosen hull configuration would perform (by sheer serendipity) exactly like a parallel plate capacitor, we still cannot use the second equation above to figure its capacitance because the plate separation distance is so non-uniform. We would therefore have to hope that using an *average value* for plate separation would yield accurate results, again by chance. Since the compounding of these assumptions is unacceptable, we need to dig a little deeper and look at electric field intensity.

Field intensity (E) is very much like capacitance in mathematical terms, and is the ratio of voltage or potential difference per unit distance: $E = V/d$. For instance, as we've learned, our base operating envelope field intensity equals the breakdown value for air at 3×10^6 volts per meter. E in a parallel plate capacitor also equals surface charge density (σ) or Q/A divided by ϵ_0 : $E = \sigma/\epsilon_0 = Q/\epsilon_0 A$. Once again, this non-uniform distance factor is a problem in the first intensity equation. Moreover, we can't use the second equation as is because the shape of the Emitter Ring is very apt to cause an extremely non-uniform surface charge density!

Fortunately, the very thing which is causing this computational quandry is the key to its solution: the *combined* shapes of the electrical hull sections. By examining the problem using calculus, it was found that an excellent algebraic approximation of the **hull static capacitance** may be readily formulated by applying simple electrostatic empirical rules. We'll refer to the original hull diagram as a visual aid and use the applicable spreadsheet variables throughout.

We will start with the Polar Field Zones, as they're easier to deal with in respect to an accurate math model. It is known from applied electrostatics that the closer a charged one-base spheric zone approaches being a true hemisphere, the more radial its electric field becomes. Its point of maximum field intensity must then be taken to be the center of the sphere. Conversely, the shallower its height in relation to its radius, the more linear and uniform its field becomes.

Therefore, we can safely treat each positive Zone as a flat circular plate whose centerpoint lies on the Zone's baseline plane and axis of symmetry. The reason we may do so accurately is that the radial declination of each Zone's surface field intensity is vector-linearized through interaction with another electric field of opposite polarity and comparable strength and shape, located *beyond* it, facing its convex side: the field produced by the Emitter Ring!

It can be shown by calculus (using the product rule for differentiation) that the point of maximum electric field intensity E on the vertical centerline of a charged flat ring of inner radius x occurs at a point located at $x/\sqrt{2}$ both above and below the plane of the ring. Each Emitter Ring Zone's vertical declination cancels by mutual symmetry as regards electric field analysis, and the centerpoint of the resultant single flat ring occurs at the intersection of the original x and y axes. Doing the math, these E_{\max} points lie slightly *beyond* each Polar Field Zone!

We may then treat the negative Emitter Ring, also by mutual interaction with the positive Zones, as two flat circular plates of radius r , whose effective separation distance from their respective positive Zones is (from the hull diagram) equal to:

$$d_s = \pm[(r_s + (C_v - C_s))/\sqrt{2} - h_r] .$$

Thus, the approximate hull capacitance of each negative and positive Zone pair, using the second capacitance equation, is equal to $\epsilon_0(\pi r_s^2)$ divided by d_s . The two equal hull capacitances so obtained are additive, as they exist in parallel, and so the formula for total hull capacitance (C_t) becomes:

$$C_t = \epsilon_0 2\pi r_s^2 / |d_s| .$$

Note: r , and d_s must first be converted to meters here!

Referring once again to the hull diagram and spreadsheet from Fig. 10, showing data for a 48" diameter EDF Generator, the prototype's theoretical *peak static* capacitance turns out to be 23.712 mmf (micro-micro-farads). This is in fact extremely small for such a relatively large device, and would perhaps be expected from its rather peculiar 'inside-out' geometry (for a capacitor).

This fact caused me to labor for some time under the erroneous assumption that a tremendous level of net charge must then be stored as the rotating power field space charge we've talked about, to give the disc a large practical flight range (given the inevitable leakage losses). Although we won't study field dynamic capacitance quite yet, this is also not the case: we know that superconductivity must come to our rescue in this respect. As a friend of mine once observed, while we were discussing UFOs hovering over high-tension power lines, "they must be storin' juice on them things *somehow!*".

So, why did we go through 'all of that', you ask? Because therein lies a tale . . . Not only have I thus acquainted the novitiate with certain of the principles of applied electrostatics that will figure so prominently in the pages to come, but I've also thereby shared somewhat the ethos of my own intense struggle to understand how something truly extraordinary works.

Be that as it may, what is essential to realize here is that the electric

acceleration experienced by Field envelope electrons is contingent upon the field intensity between the 'plates', according to the field force relation $a = qE/m_1$, where q is the electron charge and m_1 is its relativistic mass. Thus, if the electric field intensity is non-uniform, the acceleration will be as well, and it becomes extremely difficult to make accurate calculations of over-all Drive Field thrust. But because we know that the vessel hull does at least have a reliable finite capacitance, we can now use our equations to assess its electric field intensity and surface charge density characteristics *prior to Neutral Ring 'flashover' or Field ignition*. Our goal is then to observe **uniform Field intensity** post-ignition.

To keep it simple for now, we'll apply a test voltage of 100,000 to the 48" prototype hull, finding (as we suspected) that the resultant field intensity ranges from a *high* of $E = V/d = 1 \times 10^5 / .1907 \text{ m}$ or $5.244 \times 10^5 \text{ V/m}$ at the inner Drive Field boundary to a *low* of $1 \times 10^5 / .9666 \text{ m}$ or $1.035 \times 10^5 \text{ V/m}$ at the outer Drive Field perimeter. Thus, because the perimeter arc-length is basically 5 times that of the boundary, these intensity values have a *1 to 5 range* (respectively).

Also as we expected, our second field intensity equation tells us that surface charge density σ ranges from $\epsilon_0(5.244 \times 10^5)$ at the boundary to $\epsilon_0(1.035 \times 10^5)$ at the perimeter, thereby yielding the reciprocal ratio of 5 to 1. This situation had me panicked for a bit until I realized that *once the Drive Field becomes a conductor*, and Field current acts to redistribute local hull surface charge densities, its electric field intensity *must* become uniform (by the definition of a conductor) because the equal-area hull sections cause it to have a *uniform cross-sectional area* in the direction of current conduction!

Having achieved this simple empirical revelation, we may now combine our two field intensity equations, which must still apply to a charged conductor *carrying a current*, into one expression which interrelates all of the variables involved as follows:

$$E = V/d = \sigma/\epsilon_0 \text{ and } E^2 = (V/d)(\sigma/\epsilon_0),$$

$$\text{so } E = \sqrt{V\sigma/d\epsilon_0}.$$

A simplified illustration of full-power drive current mechanics will readily demonstrate what happens next. We'll let $E = 3$ (for the $3 \times 10^6 \text{ V/m}$ air breakdown intensity), $V = 3$ (for an applied voltage of 3×10^6), and $d = 1$ for our approximately one meter envelope perimeter. So, $E = V/d$ and $3 = 3/1 = 3$. Right? Next, we'll let $\epsilon_0 = 100$ (for 100% of our only previous constant other than voltage) and solve for an arbitrary but mathematically correct corresponding σ . Thus, $E^2 = 9 = (3/1)(\sigma/100)$, $3\sigma = 900$, and $\sigma = 300$. If we use .20 as the comparable boundary (minimum) arc-length and .60 as the *mean distance*, we find the following (σ) relationships exist:

$$\begin{aligned} \text{perimeter } E &= \sqrt{3 \times (300) / 1.0 \times 100} = \sqrt{900/100} = 3, \\ \text{mean } E &= \sqrt{3 \times (180) / .60 \times 100} = \sqrt{540/60} = 3, \\ \text{and boundary } E &= \sqrt{3 \times (60) / .20 \times 100} = \sqrt{180/20} = 3. \end{aligned}$$

Therefore once the Field ignites, its electric field intensity becomes constant as a function of voltage, and the hull section surface charge densities reverse their minimum and maximum: whereas the maximum σ occurred at the Drive Field boundary and minimum σ at the perimeter, the opposite is now true! And, this would agree with our earlier feeling that the thin peripheral edge should show just this condition!! This situation then allows us to make reasonably accurate thrust calculations as a linear function of voltage *and* uniform field intensity because, in short, the Field envelope now has a *uniform Drive current density!!*

Interlude: Synchronicity

I was once asked by a Cornell physicist to show him my work and briefly describe its nature and purpose. As he is (was) involved in the ongoing particle acceleration studies at Wilson Synchrotron Labs, I felt that perhaps I had found a kindred spirit with whom I could share my total enthusiasm for "reactionless" electric drive. One day in early March of 1998 I drove to Ithaca to see this gentleman and discovered that one's ability to achieve a true meeting of the minds is sometimes directly proportional to the efficacy of one's choice of words and inversely proportional to the classical inertia of the mutual reference frame. As soon as it became apparent to the good professor that the Electrodynamic Field Generator looked like a flying saucer, that I referred to it as reactionless, and that its ultimate purpose was to attempt breaking the time-light barrier, it was all over.

Once he had exclaimed "Recoil!" (with the satisfaction of a miner striking gold) and stated that the machine would produce *no* thrust, I realized my use of the term 'reactionless' had been unfortunate in this situation and could for some be quite misleading. Since this could have decidedly negative consequences in my pursuit of a Patent, the following explanation of how the EDF Generator does in fact produce thrust *in accordance with Newton's laws of motion* is for the die-hard skeptics and the physicists.

Newton's first law (the law of inertia) states that an object will either remain at rest or maintain a uniform velocity unless acted upon by an *unbalanced* force. In effect, this law says that an unbalanced force will always produce a change in velocity – an acceleration – by changing either the object's speed or its direction or both. All forms of propulsion are obviously based on this law.

Newton's second law tells us that when an unbalanced force does act upon an object, the object is accelerated in the direction in which the force acts. This acceleration is directly proportional to the magnitude of the force and inversely proportional to the object's mass: $F = ma$. It is therefore self-evident that *for a given force*, the more massive the object is the less it will be accelerated.

Where I got into trouble at Cornell was in the operation of Newton's third law as it pertains to my machine: whenever one object exerts a force on another object, the second object exerts an equal and opposite force on the first. To wit, the infamous recoil. It is here that I found two subtle but necessary distinctions are involved with which I am intuitively comfortable but which are not entirely self-evident. The first has to do with whether Drive Field electrons are fired (like bullets from a gun) from the Emitter Ring towards the Field Hub. The second pertains to where the *work* required for their passage comes from.

When a radioactive isotope emits an electron through beta decay, the unstable nucleus involved does indeed experience a *repulsive recoil* upon ejection. This happens because the nucleus must provide the work-energy required to effect the electron's passage therefrom against the attractive coulomb force within the Gaussian surface of the atom. This is *not* the case on the EDF Generator's negative Emitter Ring. Here, the accumulated electrons must reside within a Gaussian surface boundary which lies *just outside* the surface of the metal, and have eminent and free mobility to be accelerated or *pulled* toward the positive Zones. In this case, the total positive charge within the Zones does experience an equal and opposite *attractive recoil* force towards the total negative charge emanating from the Ring's surface.

The crucial distinction here is that the positive charge is bound to the material structure of the Polar Field Zones by immutable interatomic forces and the positive recoil force must therefore be imparted to the entire mass of the device. Its resultant recoil velocity is thus microscopically Newtonian by the second law of motion, whereas the acceleration achieved by the comparatively tiny mass of the total free negative charge (comprising Drive Field current) gives it an enormous relativistic velocity. The unbalanced force required to accelerate the Field Generator is then a function of the difference between the *relativistic impulse* imparted to the Drive current and the classically *Newtonian recoil* of the hull. Their respective rates of change in velocity are not, as it were, synchronous.

But, "aha!", you say: with equal amounts of Drive current in each half of the Field envelope, these opposing unbalanced forces are in turn *isometric*. No net thrust. Yes, indeed, we reply, but only until we elect to impose unequal resistances upon each field hemitorus using the primary induction array grids. Then we have a net linear thrust, towards the weaker current, which is equal to the difference between the two now unequal impulse values. Since virtually *no backward exhaust* is produced in the process, and solely to distinguish this propulsion method from rocketry, we elect to call it *reactionless*.

Finally, it is not necessary that we do the work of moving charge *against* a potential gradient. The work may be done by the charge itself in being attracted *along* the potential gradient. In the first case, work is 'performed'; and in the second, it is 'recovered'. Therefore, we (and the disc as our mechanism) provide the work-energy required to establish and maintain the potential gradient, and the negative charge comprising our Drive Field current does the work required to effect its own passage toward the positive Field Hub. The resulting collision is almost completely inelastic, so momentum and kinetic energy are conserved separately, and the Drive current's gained kinetic energy is recovered almost entirely as heat. It's as simple as that . . .

* * *

A neat (but complex) method of deriving the Specification Field Voltage required to produce about $1\frac{2}{3} g$'s of net linear thrust is developed in WorkSheet I(a) {Specific Unit Voltage Values}. Because the radial Drive Field is isometric in nature, producing mutually-opposed y-axis thrust vectors, one *hemitoroidal field envelope half* (or hemitorus) must actually be able to produce twice this much thrust for the *resultant* of the two unequal impulse vector values to equal $\frac{5}{3} g$.

Because I feel that no more than 2/3 of total envelope current should be concentrated in either hemitorus, each Drive Unit's **Field specific impulse** (in this application) is therefore based on 5 times the vessel's weight and the rotor capacity. With a Drive voltage calculated using this specific impulse, and a carefully-estimated average vessel weight of 79.2 lbs. per ft³ regardless of size, the actual peak thrust developed by the Electrodynamic Field Generator is figured in WorkSheet II(c) {Field Power Output}. This maximum net linear thrust value is obtained in overall reliance upon the Uniform Field Intensity equation described above (and elaborated on somewhat in DataSheet #12).

The ability to achieve the requisite tremendous Drive voltage(s) is in turn contingent upon the accuracy of hull static capacitance computation. A pair of **field ballast capacitors** electrically connected to the rotor segments are used to support a *primary voltage expansion ratio*, which is the ratio of the secondary voltage developed across the hull to the voltage across the primary arrays used to charge it. In essence, the value of static capacitance obtained determines the value of these capacitors, as outlined in WorkSheets VIII(d) and (e) for a 4ft. prototype Thermal Unit. In the first of these WorkSheets, the hull capacitance is actually calculated using the standard parallel plate formula, *with a mean plate separation distance*, and using the special alternate method developed earlier in this Chapter. The latter value is just over 80% larger, and is taken to be a theoretical maximum.

As regards my claim that the total *apparent* efficiency of the asymptotic reactionless StarDrive system proposed is *so far over 100%* that it might seem completely ridiculous, please do not be confused by Section C of WorkSheet II(c). Although it is technically precise in showing thermal and drive real efficiencies under 100%, and was purposely written with the Patent examiner in mind, it **does not** relate the EDF Generator's output power to its *actual input torque requirement(s)*. And this is where I've got 'em: as can be seen in WorkSheet II(c), the 4ft. prototype Thermal Unit's theoretical peak power output capability (either thermally or electrically) would be over 60 gigawatts, or the equivalent of millions of horsepower. If I thought for a moment that it would also then take that much torque to turn such a relatively small rotor, would there really be any point at all to this entire exercise?! . . .

Author's Note:

Due to the need for providing college students and engineers with the technical data and validation they deserve, **StarDrive Engineering** is not a book that everyone should feel obliged to read straight through from beginning to end. Therefore, those of you who have had enough for now of all the technical 'stuff' may actually bypass Book II: The Way and resume your reading of this text with Book III: The Stars. [In this case, as John Milton said, "Long is *the way* and hard, that out of hell leads up to light".] The storyline will not be lost to those who take this easier course; you can always go back later to peruse Chapters 7, 8, and 9 once the larger scope of the book has been firmly grasped.

Book II: The Way

"Down here", and Channing began to trace on the tablecloth, "we'll put in a hot cathode . . . Here'll be an accelerator electrode and up near the top we'll put a series of focusing anodes . . ."

"How are you going to make electrodes?"

"We'll use the annular gratings that run around the central well at each level", said Channing. "We'll have a crew of men cut 'em free and insulate the resulting rings with something . . . Then this is where my tablecloth artistry falls flat. The focusing of an electron beam depends upon the electrode spacing and the voltage. Since our voltage is fixed if we take it from the drivers' electrodes, we'll have to do some mighty fine figuring . . ."

George O. Smith

The Complete Venus Equilateral

Chapter 7

Electrostatics: Rings and Grids

I hope by now we've definitely established that the Electrodynamic Field Generator can be made to produce a considerable level of all-electromagnetically-developed thrust, or at the very least an incredible amount of heat, and so we'll go ahead and concentrate in this Chapter on matters directly related to the good old vacuum tube theory which is largely responsible for making it all possible.

Before we get going, though, I would like to return briefly to the characterization of the EDF Generator given way back in Chapter 1: that this machine is essentially a combination (in quite accurate laymen's terms) of a magneto, vacuum tubes, and cyclotron. Quite simply, it is a device which uses permanent magnets and coils of wire to produce a very high dc primary voltage (but with minimized primary current), and vacuum tube constructs to expand and control such voltage for purposes of accelerating huge quantities of electrons to energy levels generally associated only with a particle accelerator.

I believe it might be additionally instructive at this point to view the Generator as also being quite similar to a *huge arc welder*, one whose output is deliberately shorted to its own *chassis*; wherein the electrodes' dc voltage and current are increased to levels usually found only in lightning, but the current density is limited to a value which falls short of literally 'welding' the hull.

Rather than "mess around" studying the by-products of the collision of intermittent 'packets' of electrons with a solid target, however, we are interested in the practical production of great quantities of heat and *variable* thrust within and upon the target(s) as a result of a *continuous* electron stream. Thus, it can be seen that vacuum tube theory forms the crucial intermediary link which unites these disparate technologies to achieve the desired results, because of the vacuum tube's current variability and control characteristics.

Touching briefly upon the magneto aspects of the device, our six separate field coils are each composed of as many turns of fine wire as we can manage. Because of the generating system's bilateral symmetry, they are arranged in two groups of 3 coils each. And, as stated in Chapter 4, the coils of each group are *connected in series* to additively increase the output voltage instead of the current. As was originally shown in Fig. 5 of Chapter 3, each series coil group's output voltage is impressed across the rotor using pairs of **induction electrode arrays** which are rotatably mounted thereon.

Because of severe clearance constraints, each outer induction array has only two electrodes and may thus be viewed as a *diode* vacuum tube construct, which will conduct dc current in one direction only. With more room available, each inner induction array employs a third intermediary electrode or *control grid* to further minimize series coil group dc current (through cutoff bias technique). As we also learned in Chapter 4, the individual outputs of the 3 coils in each group are not necessarily hooked directly end-to-end between these induction electrode arrays, but may be connected using two intermediate **transfer triode arrays**.

These rotating 3-element vacuum tube constructs may be used to amplify any AC signal voltage that is present on the rotor segments but they are (of course) electrically isolated from the rotor segments, unlike the induction arrays.

Each field coil provides the cathode voltage with respect to its adjacent triode array, be that array of the induction or transfer variety. Having studied triodes periodically throughout Chapters 3 and 4, we know that a *separate* source of negative voltage must be applied between the cathode and control grid of each of the Primary Power System's triode arrays to provide the desired plate current bias. But, if each field coil is being used to supply array cathode voltage, what source of control grid voltage are we to use? As was briefly hinted at in Chapter 5 (and as I'm sure many of you have already surmised), the field coils must actually be compound-wound or composed of at least two independent windings. The smaller of these windings will then be used to provide grid bias voltage.

A simplified 3-stage field coil and electrode array schematic, for one of the two identical series coil groups, is shown in Fig. 12 below. You may wish to note both the similarities and differences between this diagram and that of Fig. 13, showing an idealized representation of a type of parallel *resistance-coupled* 3-stage radio amplifier based on Fig. 4 of Chapter 3 (a basic single triode circuit).

DRAWING NOT TO SCALE

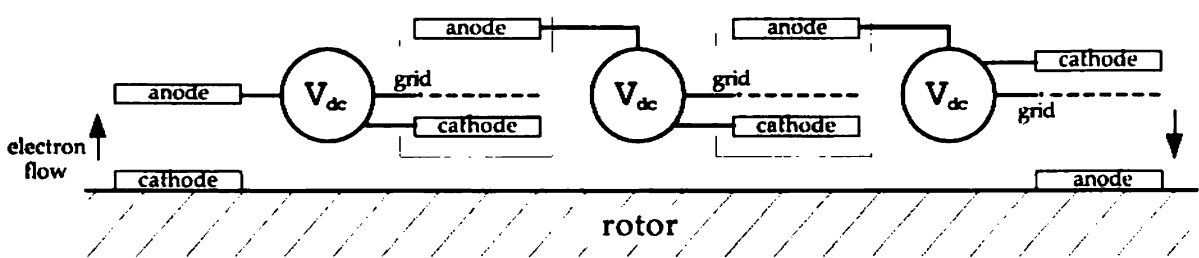


Fig. 12: simplified Primary Power System electrode array schematic

Each field coil (V_{dc}) and its attached electrodes is viewed as one 'stage' of a 3-stage AC signal voltage amplification system. Modest dc voltage amplification ($\approx 40\%$) is also obtained. The two boxed areas enclose the stage-connecting transfer arrays.

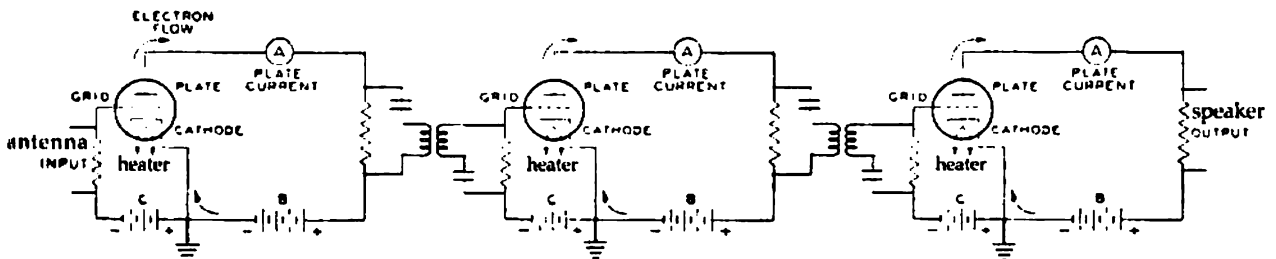


Fig. 13: idealized resistance-coupled 3-stage tube voltage amplifier.

The input voltage of the 2nd and 3rd stages is the voltage drop across the plate resistor of the previous stage. Given an amplification factor of 100 for each triode, net speaker voltage is over 500,000 times the minute antenna AC signal voltage.

An obvious (and very important) difference between the two circuit diagrams above is that in the Primary Power System there is *no ground reference*, whereas in the tube amplifier circuit the cathodes are customarily operated at a common ground potential (due to the fact that they are heated). Not only would it be extremely difficult to provide a good reliable source of ground to the rotor, but we actually do not want one: in this case, we desire the system voltage to “float” such that equal negative and positive voltage values appear at opposite ends of each series coil group! And, due to the significantly capacitive nature of the induction electrode arrays, this is precisely what happens.

As was initially described in Chapter 3 (in association with Fig. 5), biasing a triode to current cutoff causes the potential difference between plate (anode) and cathode to rise above the given source voltage, actually approaching or even slightly exceeding the sum of the source and applied grid voltages, due to what I have referred to as a voltage dam effect. The magnitude of this *cutoff bias voltage rise* is essentially inversely proportional to the triode construct’s amplification factor (μ), this factor representing the amplitude of the maximum control-grid-induced variation(s) in plate voltage in response to a change in grid voltage.

Due to the plate spacing considerations outlined in DataSheet #9 (Electrostatic Load-Line Formula), the three rotating triode arrays of each series coil group shown in Fig. 12 have the very low μ value of 4, and the expected cutoff bias voltage rise across each such array is about 40% (see DataSheet #8 {Bias Voltage Ratio}). Thus, as was stated in Chapter 3, one ancillary (or auxiliary) purpose of the Primary Power System’s triode arrays is to boost the dc voltage impressed across the rotor. Since high voltage is exactly what we want in this application, we’ll gladly accept this handy coincident effect.

The subtext of Figs. 12 & 13 above does not emphasize, however, that highly biased triode constructs may at the same time be used to *de-amplify* or suppress the input current by up to several times, in addition to their much more obvious role in amplifying an AC signal voltage by very-high ratios! Though I’m not aware of any handy formula or method for projecting the cutoff-bias dc current suppression characteristics of a triode of given amplification factor, the suppression ratios which result from this type of ‘Class B/AB,’* operation as compared to unbiased operation average about 3.5:1 in this application. On the other hand, the formula for approximate total AC signal voltage ‘gain’ across a resistance-coupled triode tube amplifier of “n” like stages is $(0.8 \times \mu)^n V_i$, where μ is the common amplification factor and V_i is the 1st stage grid input AC signal voltage.

Such triodes connected in series stages thus *do not* exhibit final dc current suppression ratios which are a product (or even a sum) of the individual stage ratios, in the manner that parallel-connected triodes exhibit AC voltage amplification! The final current suppression capability of the Primary Power System’s 3-stage series coil groups will merely be a function of that of the most completely biased single array. Therefore, the most significant *similarity* between the two circuits shown in Figs. 12 and 13 is that the series-connected stages must be *resistance-coupled* as are those in the tube amplifier circuit, to further limit total AC and dc coil group current to a level within the ampacity of the windings.

* Important concepts of triode operational class are explained in Section C of WorkSheet VIII(b).

These crucial resistors, used to protect both the plate source voltage windings and bias voltage windings of each stage, are not shown in Fig. 12 in the interests of conceptual clarity and due to the limitations imposed by not representing the bias windings separately. Therefore, the Primary Power System semicircuit schematic shown in Fig. 27b of SpecSheet IX best illustrates the complete series 3-stage circuit design for final comparison to the circuit of Fig. 13.

The *communications potential* rationale behind using the two transfer arrays of each coil group to series-connect the field coils in three distinct stages was given in Chapter 4, and is based on the assumption that the Field envelope may serve as a form of antenna given its induced quasi-coherent properties. The principal *ramification* of this decision only became apparent to me upon doing the research required to select the optimum relative values of *stage load resistance* and *applied grid resistance*, such that projected coil group peak dc current would always remain less than about 1/6 of winding ampacity (for reasons related to projected AC load, rotor dc voltage drop, and temperature resistance rise).

The individual stage AC load resistance, which determines the rotor AC power output to the following stage, is equivalent to the *circuit resistance presented* across the resistor shown between each PLATE and its voltage source B in Fig. 13. A simple variant of Ohm's Law is used in DataSheet #9 to determine that the ratio of this anode "ballast" resistor's value in ohms to the attached field winding voltage should in general be *about* 10:1. Because the field winding output voltage of each coil is different, each such load resistor will have a different base value as determined by this method. However, the AC load resistance calculation method developed is as linearly and accurately scalable as the associated vessel hull!

The real problem arose in trying to determine optimal values of the control grid resistance applied to each successive stage. The only guideline I had in this regard was that the typical grid resistor used in each stage (as shown in Fig. 13) was always as 'large' or larger in ohm value than the respective ballast resistor employed, which at least gave me a starting point. [Note: The reason this is done is because the full load resistance of a resistance-coupled amplifier stage is basically equal to the the resistance of its own plate (ballast) resistor in parallel with the grid resistor of the following stage, just as illustrated in Fig. 13.]

What I wanted to do, however, was relate the appropriate size of each applied grid resistor to the magnitude of the *actual potential difference* across its respective triode array! The reason I thought this was necessary is simply that in tube amplifier practice both the plate and grid resistors are indeed selected in this manner, as a result of a graphic analysis of each tube's "static" test electrical characteristics (with dc voltages applied to all electrodes). What I soon realized, though, was that despite the fact I knew the field winding output voltages I had as yet no idea what these specific potential differences would be. Moreover, I therefore couldn't simply calculate the actual voltage impressed across the rotor, and this voltage *must* be correctly predicted to properly design the Primary Induction Ring Arrays. I began to ponder for the first time the all-important concept of **stage voltage balance** and correctly "resolving" the rotor circuit.

In a grounded tube circuit such as that of Fig. 13, the unbiased potential difference across the tube (with no applied grid voltage) is always equal to the 'B'

source voltage. In the *ungrounded* series circuit of Fig. 12, however, the potential difference across each triode array will be *markedly different* than the output voltage of its associated field winding! This complexity-compounding situation results from the very floating-voltage condition we talked of needing earlier: having the potential differences expressed across the inner and outer induction arrays become equal in operation due to equal (and opposite) voltages being applied to one electrode thereof by the series field coil groups.

Fortunately, we can *make* this condition occur, as it is known that two like capacitors whose opposite terminals are connected end-to-end with each other (as are the induction arrays by virtue of the rotor) will redistribute their respective charges until an equal potential difference appears across each. With a degree of foresight, I had indeed decided to make all of the rotor electrode arrays equal in area, and thus the induction arrays are easily made equal in capacitance. Also, should any other capacitor(s) be placed in series in the 'middle' of such a closed loop (as are the transfer arrays), the plate voltages upon *all* of the capacitors in such a loop will similarly redistribute as needed to maintain equality of plate charge! These essential corollary axioms, which I rediscovered in a state of dire need in my most trustworthy physics manual, became the only keys with which to resolve what would otherwise amount to a mathematical puzzle.

Capacitors in series combine in the same way as resistors in parallel. Therefore, the most succinct statement of the combined series capacitance concepts above is as follows: "Capacitors in a simple series circuit or subcircuit loop split the applied voltage inversely proportional to their relative individual capacitances". This rule then governs the principles of *proper circuit resolution* in the Primary Power System {as developed in WorkSheet VIII(d)}, and it thereby becomes possible to accurately calculate what anode and cathode voltages will occur in operation *within all of the rotor electrode arrays* of each series coil group, and therefore the operating rotor voltage becomes known as well. Then, and only then, the proper electrode spacings may be specified as a function of the design amplification factor of the triode arrays.

The foregoing discussion of vacuum-tube-related concepts as they apply to the KDF Generator admittedly constitutes some of the toughest going to be found in *StarDrive Engineering*. In fact, I can heartily recommend its thorough study (even to the technically-oriented reader) mainly as an interesting intellectual challenge and because of its not-inconsiderable relevance to transistor theory, for those interested in solid-state electronics. As I've stated, the art of vacuum tube electronic practice has, with the exception of television, fallen by the wayside.

That I have been able 'work all this out' on my own over the years, with absolutely no specific coaching whatsoever from a living soul, owes far more to the fact that I'm exceptionally stubborn than to any natural gift I might have in this department. My real "saving grace" remains my aptitude in mathematics.

We will return to matters electronic in the latter part of this Chapter, when we study the StarDrive '*field induction system*' and *pentodes*, in relation to the Primary Arrays we know at this point are waiting. For now, however, I feel it's appropriate to take a little break . . .

Interlude: Serendipity

Back in the early 1980's, after I got out of college, I struck up a rather close friendship with a new neighbor who lived around the corner in a house previously owned by a nice old couple for whom I'd mowed the lawn as a boy. This affable young fellow, whose name was Bill, shared my love of reading books – especially technically-oriented science fiction – and was quite intelligent in an offbeat sort of way. He wasn't employed at the time, and was not terribly inclined to be so, and many times after work I could be found in his unearthly cave of a room drinking German beer and discussing various modes of philosophy.

This was for us a favorite arena of repartee, and I was at that time quite passionate about the subject. Since for me the study of philosophy is intimately linked to my fascination with faster-than-light travel, many nights the conversation would (at my instigation) come around to my already-developing ideas for a StarDrive system.

Bill provided an excellent sounding board for these early ruminations, and in many ways guided my insights as much as anyone ever has. He became my constant sidekick and confidant, and for whatever reason I gradually began referring to him as Mr. Bill – probably out of deference to a curiously British sort of dignity he managed to evince.

We came at some point considerably under the influence of the writings of Carlos Casteneda, as was very common at that time for members of our generation. We endlessly debated the rather Machiavellian themes thereof and how Casteneda's ideas might actually be called for and of need applied in 'our' pursuit of StarDrive. From this odd setting therefore springs the tale of Mr. Bill and the Art of the Controlled Bumble.

You see, I knew that I was essentially fumbling in the dark still, wrestling with ideas and concepts which were really quite outside my training. Mr. Bill and I therefore talked about how, in the face of perilous adversity and the Unknown, Casteneda's don Juan would encourage Carlos to exercise the "art of a warrior" and carry on confidently and (above all) in a controlled state of being. Eventually, with patience, perseverance, intuition, and sometimes blind luck, the warrior would ultimately not only survive but succeed triumphantly, often in spite of himself.

The seemingly insoluble problem which was foremost on my mind at that time was the mystery of what I would later learn to perceive as the Searl concept of "bypass current": how could an electrical generating circuit produce an extremely high voltage while remaining isolated from an enormous full load amperage? I played with endless unworkable permutations until, exhausted and disillusioned, I actually gave up on my StarDrive research for over a year.

As it turns out, Mr. Bill's father was an antique dealer and book reseller and he had a small shop at home wherein literally thousands of used books were stored. One day in the summer of '83, I was helping my friend sort through the immense overstock with a view to discarding anything which (according to his father's instructions) was not expected to be saleable. There was so much to dispose of that a small dumpster was placed on-site into which we were hurling all these obscure and in many cases dilapidated old tomes, sometimes with barely a discriminating glance. We were having a fine old time, as we had a goodly supply of Beck's to keep us busy.

Bill said I was welcome to keep anything throwable that caught my eye, but I was finding it to be a fairly miserable lot, at least as far as *my* unorthodox tastes ran. He was maintaining a sort of running commentary on the stuff he was ejecting, and I hadn't selected a thing as yet when he mumbled "Hmm, an old RCA Tube Manual . . .", and I looked up in time to see this large orange and white paperback begin its intended flight towards the dumpster when I shouted "Wait!" and virtually snatched it out of the air. I said, "Let me see that", and we both paused in our labors for a time to study this immediately intriguing volume.

I recall not thinking much of it at the time, possibly because the content was so foreign to the untrained eye, but I did keep it and add it to my small research library. I didn't get around to actually *studying* it a whole lot, though, for about another two years. With the benefit of hindsight, I know now that this was a pivotal event in my life as a research scientist.

In my mind's eye, I see myself at that time to be rather like the man-apes in Clarke's 2001: *A Space Odyssey*, when confronted by that strange rectangular monolith – I didn't know what to make of it, but it sure did change everything! Today, I can safely say that if it were not for this singular event in my past, it is entirely probable that none of you would be reading this outlandish magnum opus now, and the Lord only knows what would have become of me.

* * *

Taking the actual field winding 'source' output voltages calculated in WorkSheet VII(e) and then applying the principles of marginal dc voltage amplification we studied above (as they apply to the series-connected field windings), the final projected *peak* dc rotor voltage of the 4ft. prototype EDF Generator is verified in the epic WorkSheet VIII(a) {Series Electrode Array Capacitance}. It should be noted that throughout the Worksheets related to SpecSheet VIII {Electrode Array Construction}, 'peak' voltage values are always used to derive electrode spacings. Any peak voltage described is based on 110% of a *standard* maximum Specification value, allowing brief periods of operation wherein rotor speed and Drive Field current thrust may of necessity be somewhat higher than the normal full-power level.

For those of you who have already studied SpecSheet I and its associated WorkSheet, it can be seen that this peak rotor voltage (for the 4ft. prototype Thermal Unit) is therefore 110% of the specification 7,732.8 volts – or 8,506.1 volts. The *primary array voltage* is the potential difference between the Primary Induction Ring Array cathodes (at ground) and two unit anode rings at full positive rotor voltage. This primary array voltage is thus always equal to one-half of the rotor voltage, or a Specification value of 3,866.4 volts in the example above. This value is obviously a long way from the corresponding Specification Field Voltage of 2,899,800 which is thereby called for (in the Thermal Unit variety), necessitating a *primary voltage expansion ratio* of 750:1. This high a voltage 'step-up' ratio would be truly hefty even for a primary AC high-line transmission transformer (with a typical secondary voltage of 500,000).

When asked to present the most concise possible description of the EDF Generator (wherein good analogies are very tricky), I lean toward explaining

this device as one example of a dc equivalent (for boosting voltage by *electrostatic* induction means) to the AC transformer (for boosting voltage by *electromagnetic* induction means). [Note: My Patent attorney tended to be rather dubious from the start concerning my efforts at forming such comparisons.]

Up to this point, however, I've said almost nothing about the actual manner in which the 'secondary' voltage across the vessel hull is caused to be orders of magnitude larger than the Primary Power System output voltage impressed across the rotor: the operative mechanism, if you will. You may recall that in Chapter 6 it was intimated that such method is related to the value of the hull static capacitance and to controlling the respective rates at which the electrical hull sections are being both charged *and* discharged. Thus, the voltage developed across the capacitive hull is a function of an Instantaneous Charge Differential or *cumulative voltage imbalance* which is operative upon the hull during the period of time required to bring the rotor up to its full operational speed!

To reach a better understanding of this difficult concept, I must again direct the reader to DataSheet #13 of the same name. This DataSheet describes the way that the *electron emission characteristics* of the cathodes of the Primary Arrays (which regulate the charge upon the Field Hub) and those of the field emitters (which charge the hull's negative Emitter Ring) may be selectively specified to achieve the desired Instantaneous Charge Differential during rotor spin-up.

Thus, the Emitter Ring may be charged by the rotor current faster than it is discharging to the Field Hub, provided these primary arrays impose the proper resistance on the field envelope circuit*. And, the Field Hub may at the same time be positively charged by the primary arrays faster than it is being discharged by Field current! The principal key to accomplishing this set of conditions is 'simply' to use a material for the primary cathodes which exhibits an electron emissivity which is higher than that of the field emitters by *the same ratio* as the required voltage expansion! By adding the radioactive element thorium to the tungsten composing the cathodes, this criterion may easily be achieved.

It is fairly obvious that the notion of modifying a cathode's emission rate came about during the course of the advancement of vacuum tube technology. Without this discovery, the build-up and maintenance of a potential difference across the EDF Generator's hull which is vastly larger than the rotor-induced primary array voltage would not be nearly as feasible. For a further in-depth treatment of this essential topic, the reader may wish to investigate Section 2 of Material SpecSheet C, wherein specific values of primary cathode temperature and *surface work function* are charted against those of the field emitters for a 4ft. Drive Unit. [Note: This work function is the energy cost of each electron exiting a surface.]

But the establishing of a vast differential in the emissivity of the primary cathodes and field emitters really tells only half the story involved in producing a particular primary voltage expansion ratio. In WorkSheet VIII(d) the Uniform Field Intensity Formula we developed in Chapter 6 must be used to calculate just

***Note:** The inherent electrical resistance of a struck arc is a complex logarithmic function of the current conducted, but tends to be *almost* negligible. However, when an arc is included as a component of a circuit, its resistance can assume a much larger value which is dependent on the configuration and characteristics of the circuit as a whole. See section (g) of DataSheet #14!

how much electron charge must be removed from the Field Hub, and *continually withheld upon the rotor* (in operation), to define the point at which the voltage expansion reaches equilibrium and the surface charge densities of the electrical hull sections have the necessary values to maintain the desired Field voltage!

This voltage-stabilizing charge is then stored in two **field ballast capacitors** which are mounted on the outer edge of the rotor, just outside the ballrace assemblies which must be used to center and support the rotor within the vacuum chamber. Fig. 24 of SpecSheet III best illustrates the positioning of these vital components and, although they are not technically a fundamental part of the Primary Power System, they are connected (as shown in Figs. 27 of SpecSheet IX) directly to the outer field winding anode connections.

The outer plates of these ballast capacitors therefore receive a portion of the positive value of their respective series coil group's output voltage which is fixed and determined by the respective series capacitances of that coil group's arrays (as discussed). This is of course exactly what happens across the outer induction arrays as well, and therefore the total potential difference across both these capacitors and induction arrays is equal. But *do their inner 'plates' or rings, which are attached directly to the rotor segments, receive an equal and opposite induced negative voltage??* Although it seems contrary to common sense, the answer here is - No! The dc output voltage of each series coil group is applied in *mutually-opposed electrostatic parallel* across the 'floating' rotor circuit leg common to both groups and, due to a very interesting and simple quirk in electrostatic induction theory, the voltage expressed on each of these rotor-mounted electrodes will *actually approach* twice* that of the respective adjacent electrodes!!

Now, this is an exasperating revelation in a way, and it bears some further explanation and contemplation to apprehend. The applicable electrostatic axiom is as follows: "The electric potential (or voltage) midway between two equal opposed fields created by like charged bodies is twice the potential represented by either charged body considered separately". This potential will be of the same polarity as the two charged bodies at such a midway point in a free-space vacuum, as there is no physical conductor present. In our application, we can see that if we consider these like-charged bodies to be parallel plates with a neutral plate of equal size interposed, the potential induced on the interposed plate will still be twice that of either like-charged plate *but will be of opposite polarity!*

The great thing about this is that the very same condition applies across the inner induction arrays as well (only with reversed polarities) and, even though the two 3-stage coil groups are connected in parallel with respect to the rotor, the actual total potential difference applied across the rotor is *twice* as large as that expressed between opposite 'ends' of each series coil group. Thus, the Primary Power System circuit must be resolved such that the equal induction array and ballast capacitor potential differences are *each 50% larger* than 'expected'!!

***Note:** The net amount by which the Primary Power System output voltage drops below twice either semicircuit's value is proportional to the series coil group current, which has been minimized to the greatest practical extent possible. This unavoidable small voltage drop has been disregarded in the WorkSheets, although it is not negligible, for the sake of simplicity within a descriptive framework which is complex enough for now as it is.

I realize that this particular consequence of the given circuit configuration is a very odd and difficult arrangement to grasp even conceptually at first (it was for me), because it immediately has so many complex logical consequences. It was deciphered with considerable effort from a study of vacuum tube *voltage doubler* circuit design, to which the Primary Power System is in some ways analogous. I fully expect this issue, however, to be the subject of vigorous debate within the electrical engineering community.

Although it is rather against my better judgement to do so, I feel it's important to finally make reference *at this particular point* to the legendary "Searl effect" with which a great many of you readers may already be familiar. This alleged by-product of the levity disc's method of operation is widely believed to represent the production of an inertialess condition within the Field envelope, in order to account for the fantastic claims of enthusiasts associated with the inventor. Because of its "unscientific" premise, this concept *must* be largely ignored. It does symbolize, however, a mysterious unknown 'something' about the levity disc technology which has made it impossible for others to duplicate Mr. Searl's work.

This Searl effect, *the magnetic anomaly I referred to earlier*, represents a specific arcane knowledge which Searl acquired *the hard way* at the expense of a great deal of money and immense personal time and effort. I would like to suggest that the almost bizarre twist in proper circuit resolution discussed in the preceding material, which arises from a simple electrostatic axiom that would be easily overlooked, could *alternatively* explain (with a wicked little pellet of truth) the apocryphal Searl effect: an elusive gremlin factor, a sort of hidden physics-math bugaboo which, left unaccounted for, wrecked all otherwise legitimate spreadsheet calculations. Thus, it would make accurate winding turns ratios and rotor electrode array plate spacings virtually impossible unless planned for *in any brushless Faraday-type levity device*, and a prototype built without this knowledge would inexplicably fail because it *could not* function properly! [The propulsive model levity disc does in fact use brushes; the simple generator variant doesn't!]

Before we move on to an examination of the *Primary Induction Ring Arrays* which constitute the Generator's 'Field Induction System', we need to take a look at the consequences of what I refer to as *zone sector construction*: the segmenting of the Field Hub in a manner analogous to that of the rotor. This is not only directly related to a variety of considerations involving these pentode constructs, but will provide another brief diversion from these terribly-complicated vacuum tube matters as well as an introduction to some other very important "parts".

As it turns out, all of the rotating electrode array elements are constructed as electrically (and physically) continuous rings, since there is no explicit reason not to do so *and* this is probably the easiest method to use. In other words, even though separate thin nickel ring arc-sections would undoubtedly be installed on the rotor and the ends silver-soldered together, the resulting anodes and cathodes are *solid flat rings*. The grids will be in the form of a continuous planar winding.

But more than one good reason exists why this should not (and probably can't) be done in the two stationary *ring-shaped groups* of *electric Primary Arrays*. At the outset, a major and purely structural consideration has to do with the

~~incurring~~ premium on internal space or volume, and allowances which *must* be made for the vessel superstructure. In the same manner that every 6th *potential* ~~variable~~ inductor array position must be 'blank' and the arrays therefore ~~functional~~, to allow for passage of the hull Neutral Ring's primary structural members, these Primary Arrays must be constructed in a *modular* fashion. This means that they are not composed of continuous electrode rings, but are each divided into the same number of individual units (36) as the vessel superstructure to allow for passage of the coolant system's *primary thermal conduits*.

Thus, the thirty-six 5-element modular electrode "stacks" which comprise each Primary Induction Ring Array are called *unit pentode arrays*. They were first depicted in Fig. 5 of Chapter 3, and the basic function of each electrode type was described in the text associated therewith. These unit pentode arrays are of course used to charge the Field Hub, as the heart of the Field Induction System. But now, each hull Positive Zone can also be divided into 36 parallel sectors, whereby each Zone sector may have its own unit pentode array!

As an engineer, I hate to admit it but once in a while the most succinct way of describing a complex thing is the way in which you were forced to try describing it to a lawyer. Hence, the following passage pretty-well outlines a second yet more important reason to sector the Field Hub, and is lifted straight out of the Patent Application:

"One major goal in dividing each of the two (2) hull positive Zones which jointly comprise the Generator's 'Field Hub' into a large number of radial sectors in electrical parallel is to limit the external field current reaching each particular power resistor and unit pentode array combination to a fairly uniform level, while somewhat reducing field current return eddy losses as well. However, each radial sector is thereby also given the capability of effecting a local thrust production differential (in propulsive three-stage rotor devices), by virtue of its electrical isolation, as it is then possible to vary the local resistance presented to the electrodynamic field with respect to any given radial sector so that a substantial measure of navigational control in the z-axis may thus be achieved by varying the proportional field current conducted by that sector."

Now I know that this is really a handful, and that I've given away the name of one type of those important new parts without any warning or explanation. But I feel it's very important to clear up one thing at this juncture: if the StarDrive vessel is to achieve any real measure of maneuverability in the z-axis, the Drive Field must be able to impart a *precessional force of axial torque* upon the hull. And since the primary thrust in Drive Units will be produced only at the Field Hub, this precessional force must be applied just as if we took a huge finger and *preferentially aided* the impinging z-axis *Field current thrust vectors* on one spot (or Zone sector) normal to the surface. Thus, decreasing the resistance of a given aft unit pentode array (so that that sector's share of field current increases) causes a local Field thrust imbalance or differential which results in the vessel's forward trajectory *leaning away* from its prior y-axis toward the stronger force vector!

This is where we can really begin to make powerful use of those vacuum tube current variability and control characteristics referred to at the outset of this

Chapter. Admittedly, this is a rather 'inefficient' way of attaining truly directional thrust, as the amount of force which must be applied to yield a given axial precession is proportional to the hypotenuse of a right force triangle whose shortest side (by far) represents the precessional torque (τ'). However, the Zone sector which is diametrically opposite such single aiding sector, in the *forward* half of the Field Hub, may be used to double this small torque by *reducing* its current; and the sectors immediately-adjacent to both such fore and aft sectors may also be made slightly less or more conductive (and series-aiding with respect to τ').

In conclusion of this brief digression into Drive Unit thrust considerations which are related to Zone sector construction, suffice it to say that z-axis thrust differentials produced in the manner described above may also be aided by either *increasing or reducing transflection coil current* in the variable inductor(s) which are radially-parallel to such fore and aft sector(s) described above. This has the effect of further increasing or reducing respectively the apparent resistance to Field current *along* the radial axis of the desired sector(s), through a proportional change in the local transverse deflectionary force experienced by that portion of the Field current which is being passed in the parallel vertical plane(s). These challenging principles can and will be re-examined later on (in Chapter 13).

Fig. 14 below illustrates the proper sectoring of one Field Hub half, in that an additional *center zone sector* is incorporated, and insulating ceramic *partitions* are indicated between all sectors. The decision to employ a pair of such central sectors is far from arbitrary: they must be used to fully "seal" the Field envelope at the poles and so *maximize its shielding capability* in Drive Units. Since the need for some kind of signal communications is virtually inseparable from any such Drive Unit's very purpose, these special polar sectors may otherwise thus be used almost exclusively as the basis of a specialized resonant frequency *signal detection and transmission methodology*.

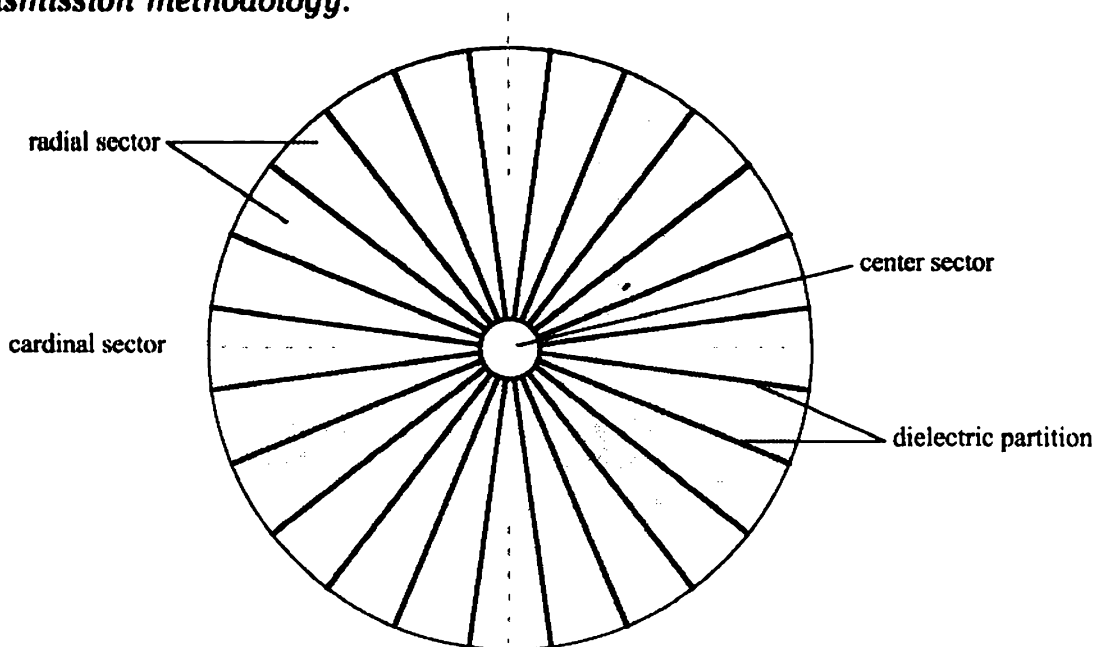


Fig. 14: polar view of sectored Zone

The diameter of each *center zone sector* is equal to 1/10 of the diameter of the Field Hub in Drive Units.

The four (4) equally-spaced radial sectors indicated (with a dashed line) divide each half of the Field Hub into four equal quadrants and mark the cardinal points with respect to the hull's radial centerline plane. The center zone sector together with these cardinal sectors, in each of the two separate Zones, are to be connected in *group parallel* with the rest of the individually-paralleled radial sectors in that Zone. The resulting geometric spatial sector arrangement in effect constitutes a directional antenna system, which can then be largely devoted to exploring various forms of signal communications capability, *including sensors*.

In any event, it can be seen here that the current conducted by any given Zone sector and its unit pentode array may be directly controlled in proportion to an applied *dc control grid bias voltage* (exactly as in a triode). This sector Field current variability next leads us to a discussion of basic guidelines for the active modulation of **Field current bias** in three-stage rotor devices. It should be noted that (for the sake of brevity) the Greek lower-case alphabet symbol 'eta' (η) has been selected to represent "stage" as used pursuant to this application. Thus, the simpler Thermal Units constructed without rotor transfer arrays will be referred to as '1 η ' and the much more complex propulsive Drive Units as '3 η '.

To continue now (just once more *here*) from the Application:

"The external breakdown discharge current once initiated and sustained . . . is generally limited only by the engineered design characteristics of the unit pentode arrays which comprise the Field Induction System. In particular, the negative DC bias voltage applied to the unit pentode array control grids must be sufficient to limit the total primary induction ring array current to a value within the safe operating ampacity of the rotor. For purposes of this text, the term "full-power" as used in relation to the Primary Power System and its incorporating device shall be taken to indicate a corresponding rotor speed wherein a nominal field envelope voltage is achieved, maintained, or exceeded.

In a simple single-stage embodiment of the Generator used as a 'Thermal Unit', no active biasing of the current in either of the two field envelope halves (which are otherwise symmetrical) need take place at the primary arrays, and each such field half's current is essentially equal. In the preferred three-stage embodiment intended for propulsive units, the field current is actively biased or proportionally shunted by the primary arrays between such field envelope halves to render the impulse thrust developed thereby mutually non-isometric along the Generator's vertical centerline.

As a result of the "engineered design characteristics" spoken of above, which are an incredibly specific consequence of relative plate spacings and hence amplification factor, WorkSheet VIII(c) in the next 'Chapter' is able to accurately project standard operating control grid dc voltage levels which are suitable in both single- and three-stage modes of operation. Ideally, as noted therein, basic dc operation at a minimum full-power value of total Field current can be maintained with roughly half of the peak control grid voltage or less. This pertains of course specifically to Thermal Units, and is also not a problem in 3 η operation *provided no AC signal amplification* is required where at the same time *uniform thrust must be maintained!* This follows of course from the observation that broad swings in the Primary Array current are generally expected to accompany such

AC amplification, and therefore wide and certainly disconcerting variations in thrust may ensue.

However, it was discovered in working with tetrodes, which are merely triodes with a positive accelerator grid added, that plate current could thus be made *practically independent* of these control-grid-induced variations without loss of signal amplification. The unit pentode arrays will therefore have a similar 'duplex' signal-handling capability, in that undesirable abrupt changes in sector current (and thrust production) may be compensated by modest changes in accelerator grid voltage. The said half-peak or standard operating level of control grid voltage then constitutes a "zero-signal" level of *dc bias* voltage as defined for Drive Units, and it becomes possible to maintain a uniform or 'smooth' level of Field *dc* current-dependent thrust while simultaneously engaging in Field-enabled AC communications activity. And, the *collective* *dc* biasing of the unit pentode arrays of one Primary Array more than the other (using a higher negative voltage) will cause a non-isometric y-axis force of thrust in the direction of the weaker Field hemitorus current. The *selective* *dc* biasing of specific radial zone sectors can then induce a desired z-axis torque to modify the vessel's base y-axis trajectory, allowing highly accurate navigational computations to be made.

Our present discussion of the electric Primary Arrays must conclude with the **field power resistors**, whose existence was but recently divulged, and two types of special high-temperature support hardware. These final and absolutely crucial Field Induction System components may for now be best understood by observing Fig. 15 on the next page as well as the Fig. 26 'schematic' on page 173 of the next Chapter. Each power resistor is in essence a *solid ceramic resistor block* which must be attached, as indicated, between each radial zone sector and the *cathode* of its corresponding unit pentode array. And, by *ceramic*, I mean not only the ferroelectric insulating encapsulant, but the very *conductive core* itself!

Now, *this* is obviously going to require a crash course in *technical ceramics* to explain, which is best left up to Section 2 of Material SpecSheet D. The specialized engineering covered therein is certainly formidable, as was the design challenge represented, yet it really is fascinating in its, well, audacity. The basic concept, however, is fairly simple: Since a huge primary cathode resistor voltage drop is totally essential (to keep the rotor and Field voltages balanced *with the primary cathodes at ground potential*), and an extremely elevated operating temperature cannot be avoided, a specific ceramic material which is normally a non-conductor may actually be used to provide the necessary voltage drop *when almost no other material has all of the required physical properties*.

Finding a suitable ultra-high-voltage insulating material which *won't* quickly go conductive (by suffering catastrophic breakdown) is an even harder task yet. The *dielectric buffer* or encapsulant which must enclose each power resistor must be able to maintain a minimum dielectric constant *k* of over 750 *while operating at from 620° to 735°C!* Also described in the SpecSheet just-cited is an exotic technical ceramic which is once again almost the only known suitable buffer material. Fig. 15 below illustrates a power resistor, its dielectric buffer and unit pentode array, and the encircling *primary thermal conduit* whose liquid coolant must regulate the resistor temperature, all in relation to the rotor and housing.

Wt. 2:1 for the
4ft. prototype.

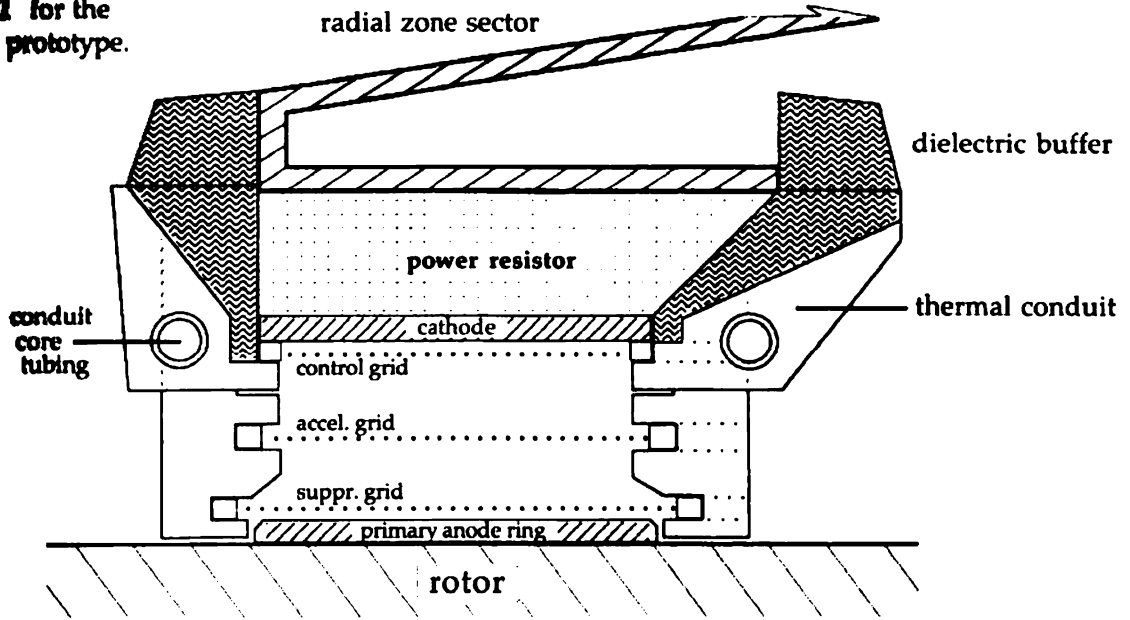
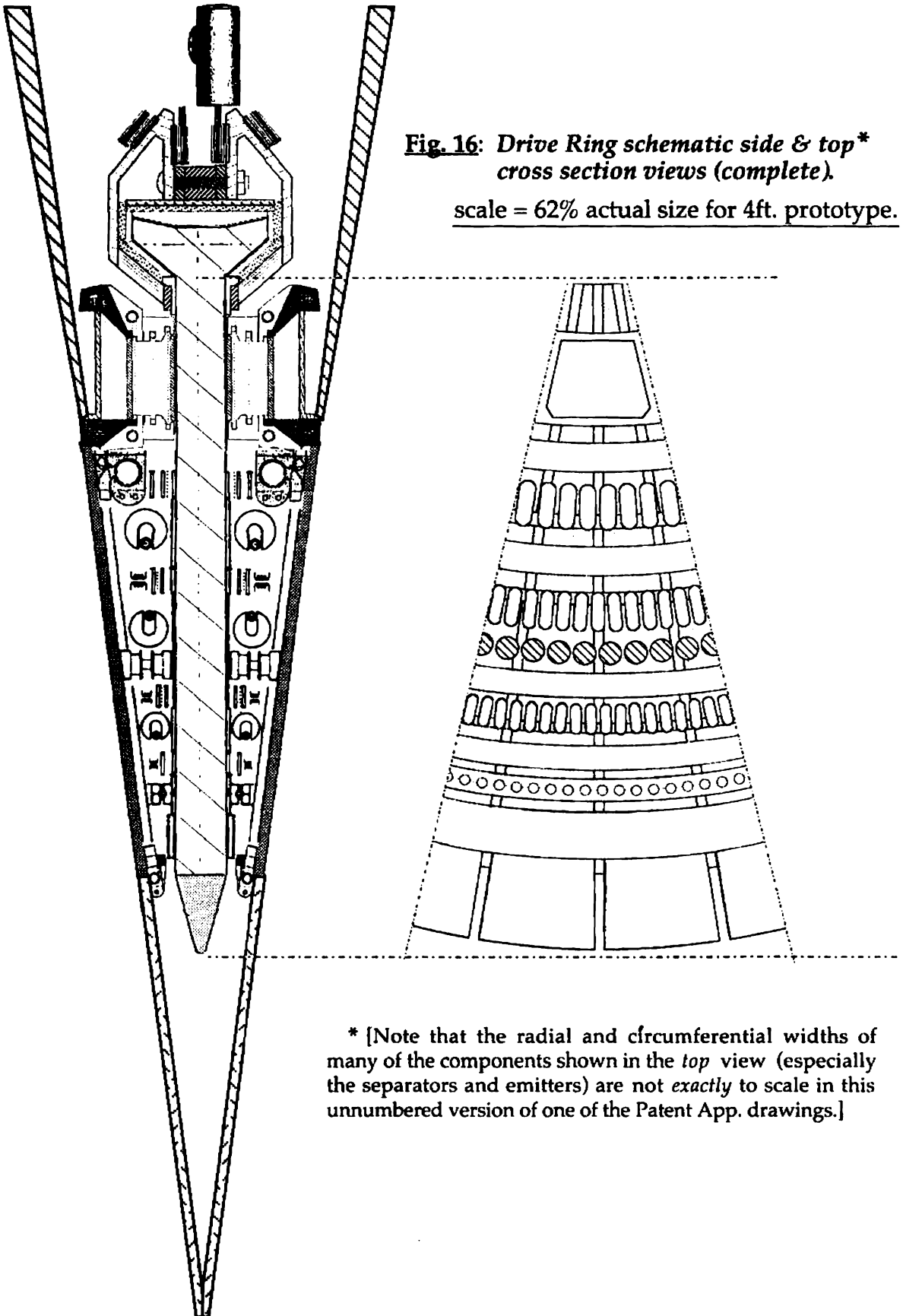


Fig. 15: Power Resistor and Unit Pentode Array assemblies,
including replaceable electrode elements, shown in **radial cross section view.**
[Fig. 53 (Mat. SpecSheet D) is virtually identical, but at a 4 meter dia. unit scale.]

In preparing for the remarkable volume and complexity of the next 'Chapter', some final thoughts which derive from the incredible struggle to Patent this machine should prove valuable. We found that the **Electrodynamic Field Generator** (or **StarDrive** device) must by and large be viewed as an adroit and synergistic combination of five (5) separate and sophisticated primary systems, the two most important of which we've studied in some detail: The *Primary Power System* on the rotor, and the *Field Induction System* (largely encompassed in Fig. 15 above). [A point to note here is that the field ballast capacitors are properly thought of as belonging to both the *Primary Power and Field Induction Systems*.]

The modular *Field Voltage Control System* must be evaluated via SpecSheet IX {Power System Schematics}, and is of particular importance with regard to field ignition and communications activities. The *Structural Intercooler System* {see Material SpecSheet B} has of course a self-explanatory nature and function, and includes the primary thermal conduits in 3η rotor devices. Finally, the *Variable Inductor System* is used principally to modulate the electrodynamic properties of the Field envelope, and is intended to maximize the EDF Generator's performance and efficiency in a variety of important ways.

In many cases, it will be seen that each of these primary systems incorporates some novel and/or theoretical aspect(s), and rigorous algebraic treatment has been given to adequately "prove-out" every such aspect possible. The *Basic Specifications* are quite 'dense', and may prove impenetrable for some. This text has been prepared with the notion in mind that these readers may want to just "meet us on the other side", for Chapter 9 (and *Book III*) of **StarDrive Engineering**. In any event, I believe you engineers and draftsmen will enjoy the next surprise, which is the combined and complete *Drive Ring 'schematic'* top and side cross-section views, on the next page. I think that it's, as the French say, *formidable* . . .



* [Note that the radial and circumferential widths of many of the components shown in the *top* view (especially the separators and emitters) are not *exactly* to scale in this unnumbered version of one of the Patent App. drawings.]

Basic Specifications

for the

*ELECTRODYNAMIC
FIELD GENERATOR*

PROLOGUE

The technical information contained herein constitutes a reasonably complete and accurate account of the methods of design, construction, and operation for an extraordinary new electromagnetic machine and the *primary power system* which enables it to function in the manner claimed. Every effort has been made to present this material in a clear and concise fashion such that any reader fairly acquainted with the general principles of electrical engineering and physics should be able to follow the basic substance of the disclosure.

The content is delivered within the framework of a carefully-constructed matrix of non-calculus *project spreadsheets*, and in several short supporting text articles (contained in the Appendix A). A tri-columnar Directory of these spreadsheets and articles is provided, to allow each reader to investigate the material in their own fashion without necessarily having to proceed linearly through the bulk of it from first to last.

The derivation of the Electrodynamic Field Generator's **design hull configuration** comprises a long and complicated story, as the research and development thereof took place over a roughly five-year period. This should not be taken to imply that the final and rather exacting composite shape selected is the only one that 'works' properly. It merely reflects the preferred embodiment of the author/inventor's conceptualization of a fundamentally mechanical device which happens to entail both tremendous electrical complexity and breath-taking aeronautical implications.

Should the proposed vessel eventually be used to explore the possibility of transcending the time-light barrier, extremely precise calculations regarding its spatial displacement and charge/mass ratio will no doubt become necessary. Therefore, one of the principal reasons for the chosen hull design is that the total vessel displacement may readily be calculated using traditional formulas from analytic geometry for the volumes of the two (2) *truncated right conic sections* and two (2) *one-base spheric zones*, and the volume of the remaining cylindrical Central Chamber.

Using just these formulas, a vessel hull configuration has therefore been developed which may be linearly expanded (as a scalar function of the hull radius) to virtually any size with no significant loss of accuracy. The Master Spreadsheet which follows and its attendant schematic hull diagram, upon which all of the subsequent SpecSheets and WorkSheets are based, illustrates the application of this design technique to a *theoretical* vessel hull only 48" in diameter. It must be emphasized that the construction of an EDF Generator this small might not prove entirely practical in reality, due strictly to mechanical considerations, and the author believes this prototype model to be in fact the smallest such machine that could be built. This original hull size was deliberately selected, however, to encourage the development of the maximum possible accuracy with respect to Specifications for the relative size and positioning of all major internal parts, prior to the actual construction of larger machines.

The *surface areas of the negative and positive hull sections are set equal* to each other, and for two very important reasons: (1) to give the vessel hull some finite theoretical capacitance (despite its unusual geometry); and (2) to render the Drive Field portion of the field envelope uniform in cross section. Considerations related to this fundamental design criteria are fully explained in DataSheet #9 [Uniform Field Intensity Formula].

The decision to simultaneously *also set the volumes of the right conic sections and one-base spheric zones equal* is most assuredly not arbitrary in nature but lies beyond my own ability to elucidate with pure mathematics. In short, it has to do with an intuitive sense that to do so promotes both the structural integrity of the hull in any attempt to establish a stable Kerr metric space warp about the vessel and the gravimetric stability of the Central Chamber in light of the relativistic mass effects involved while doing so. I leave the reader to draw his/her own conclusions on this line of reasoning.

In any event, to achieve this *equal-area/equal-volume design*, I found it necessary to employ two crucial interrelated constants (in addition to the ratio 1/5 used to 'step-off' the interior space): the **Hull Area Constant** and the **Polar Hull Constant**. The first of these, the Area Constant is (as the name implies) necessary to achieve the equal-area part of the overall design solution. In essence, it merely dictates the deviation of the Neutral and Negative ring radii from the interior radial volume increment of $1/5 R_h$. This constant does, however, become an important structural dimension used to specify the thickness of hull plating materials and superstructure load-bearing members.

The other required design factor, the *Polar Hull Constant*, is much more complex in nature. This value specifies the maximum height of the spheric hull zones, and the corresponding contingent Volume Differential is absolutely essential to achieving the equal-volume component of the design. Expert and laymen readers alike who wish to study and verify the mathematical methods and results shown in the Master Spreadsheet should be aware of (and employ) the following calculation instructions:

(i) the Polar Hull Constant h_r must be rounded (as shown) to the sixth decimal place. The Volume Differential X_h (to the sixth decimal place) must be obtained from the formula noted using the unrounded value for h_r , or a value thereof rounded to the *seventh* decimal place;

(ii) R_n must then be calculated as the sum of h_r and X_h , where both factors are obtained as in the step above, and not from the approximation formula noted; and

(iii) subsequent spheric zone volume computations must use the values for h_r and X_h derived per the above instructions.

In conclusion, it should be noted that a *Trim Hull Configuration* is under development which is just slightly different from (but more complex than) the following Master Spreadsheet configuration. The Trim Hull Spreadsheet will accomplish two important modifications: the derivation of an appropriate yet minimized finite peripheral edge thickness (and hence surface area), and the modest expansion of the Drive Ring displacement angle such that the linear extensions of the Negative Ring surface planes exactly intersect the center points of the Positive Zone surfaces (for electrostatic force considerations). These two criteria together will help to maximize the very limited inboard space available due to the geometry of this chosen hull design, and the final Drive Ring angle will be *very* close to 8° . [A manned StarDrive vessel will carry a bank of 4 to 7 nitrogen /ceramic superconducting current storage rings, encircling the airlock, as is indicated (in cross section) by the small green circles.]

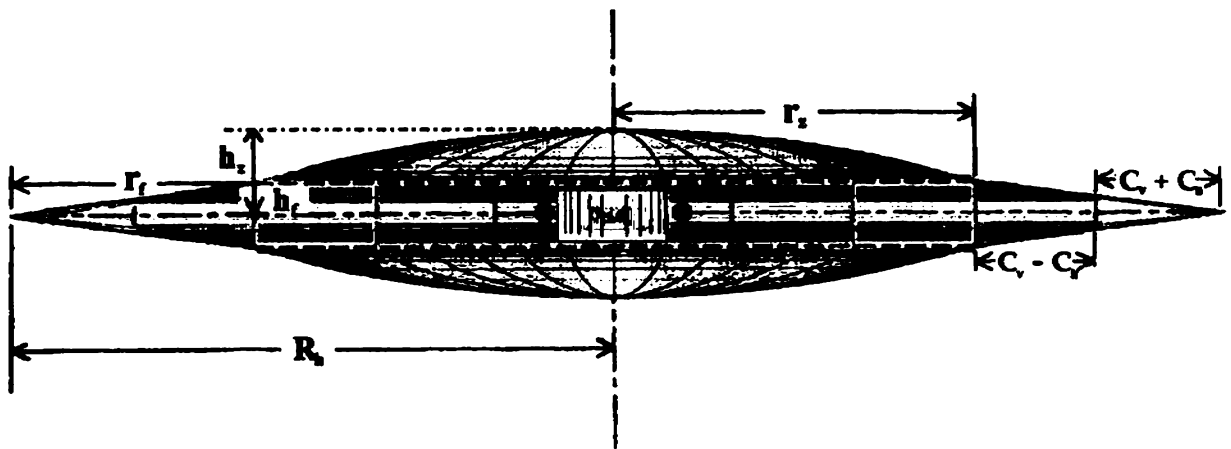


Fig. 17: enhanced side elevation of the StarDrive Generator's design hull configuration.

Notes: It must be emphasized at this point that *all of the Specifications* pertaining to the size and/or positioning of Primary Power System components located within the hull Neutral Ring are given in terms of fractional increments of the hull radius (R_h) and/or the radial width of the Neutral Ring ($C_v - C_r$). This means that these components may be easily scaled in exact proportion to the hull, for any selected radius thereof, with no significant error or modification! The WorkSheets which accompany these Specifications are constructed in spreadsheet format to facilitate the complete *basic design of Primary Power Systems* for any StarDrive device or vessel of from 4 to 100 feet in diameter. Remember, however, that **all of the specific WorkSheet calculations performed herein pertain to the 4ft.-diameter theoretical prototype model.**

The *maximum net* cabin or Central Chamber volume available aboard any size vessel is outlined in yellow in the drawing above. The *gross* volume of **both** of the two (2) Central Sections, as calculated in the following Master Spreadsheet, is therefore reduced by the peripheral center volume required for the rotor carrier assembly (as outlined in white). These indications should be helpful to those who would attempt the design of a personal starship model, as the maximum cabin space may thus be easily calculated using: (1) the term ($r_i - C_v$) instead of r_i in the central section volume formula (in this Spreadsheet); and (2) a projection for a corresponding term equal to *half* of the 'headroom' guideline (given in the *Manned Vessel Design DataSheet* on pg. 107) to be used instead of the original term h_i .

MASTER SPREADSHEET

Project: *Electrodynamic Field Generator*

title: Design Hull Configuration

<u>INSERT HULL DIAMETER HERE:</u>	=	48	inches (prototype model 'Badlander')
DESIGN HULL RADIUS (R_h)	=	24	
Hull Volume Constant (C_v)	=	4.8000	<u>Note:</u> $C_v = 1/5 R_h$
DRIVE RING RADIUS (r_i)	=	9.6000	<u>Note:</u> $r_i = 2C_v$
Hull Area Constant (C_a)	=	.062011	<u>Note:</u> $C_a = 0.012919 C_v$
Negative Emitter Ring Radius ($C_v + C_a$)	=	4.862011	
Neutral Ring Radius ($C_v - C_a$)	= +	<u>4.737989</u>	
Radius (Neg. Ring & Neut. Ring)	=	9.600000	
FIELD HUB RADIUS (r_e)	=	14.4000	<u>Note:</u> $r_e = 3C_v$
Drive Ring Radius (r_i)	= +	<u>9.6000</u>	
HULL RADIUS (Field Hub & Drive Ring)	=	24.0000	<u>Note:</u> $r_e + r_i = R_h$
Polar Hull Constant (h_r)	=	2.046593	<u>Note:</u> $h_r = 0.1421245 r_e$
Polar Volume Differential (X_h)	= +	<u>49.636512</u>	<u>Note:</u> $X_h = (r_e^2 - h_r^2)/2h_r$
Radial Hull Constant (R_c)	=	51.683105	<u>Note:</u> $R_c = 2.153463 R_h$
AREA of POLAR FIELD (POS) ZONE	=	664.5993	<u>Note:</u> $A_r = 2\pi R_c h_r$
AREA of EMITTER RING (NEG) ZONE	= -	<u>664.5992</u>	<u>Note:</u> $A_n = s(C + c)/2$, where:
$A_r - A_n$	=	.0001	$s = [(C_v + C_a)^2 + (\tan \alpha (C_v + C_a))^2]^{1/2}$, $C = 2\pi R_h$, and $c = 2\pi[R_h - (C_v + C_a)]$.
<p>***Please observe that the outer areas A_r and A_n, respectively, are equal to within an error of:</p>			
		.000015 %	*****
Drive Ring Displacement Angle (α)	=	7 ^{1/2} "	<u>Note:</u> $\tan \alpha = .1317$
Volume of Central Section (V_c)	=	823.6294	<u>Note:</u> $V_c = \pi r_i^2 h_i$, where: $h_i = (\tan \alpha) r_i$.
VOLUME of POLAR FIELD ZONE (V_r)	=	671.1053	<u>Note:</u> $V_r = 2/3 \pi R_c^3 - \pi [R_c^2 X_h - X_h^3/3]$;
VOLUME of DRIVE RING SECTION (V_i)	= -	<u>671.1055</u>	and $V_i = \pi h_i [R_h^2 + R_h r_i + r_i^2]/3 - \pi r_i^2 h_i$.
$V_r - V_i$	=	-0.0002	
<p>***Please observe that the inner volumes V_r and V_i, respectively, are equal to within an error of:</p>			
		-0.000030 %	*****
TOTAL HULL VOLUME (DISPLACEMENT)	=	4331.6804	<u>Note:</u> $V_h = 2(V_r + V_i) + 2V_c$

And, now, here's the material I know all of you engineer types have been waiting for: *the Basic Specifications*. These pages represent the crowning achievement of my life thus far, and I hope they will justify the pride I take in their presentation. Although the contents of **StarDrive Engineering** so far reveal no fundamentally brand-new theories in physics, these Specifications do indeed encompass a unique and entirely novel approach to resolving an intimidating physics problem which (until now) has generally been considered unsolvable.

In response to my steadfast enthusiasm for my work, I've countless times heard this old adage: "Well, if it *could* be done, it probably *would* have been done already!". Despite this apparent aspersion upon my abilities, the conclusive proof is offered herein that 'probably' *isn't* necessarily so. Perhaps no one before me has evinced the almost unholy implacability required to unravel such an abstruse Gordian knot. Another ridiculous aphorism is: "the proof is in the pie!". Well, here's the pie, folks. NASA didn't build the first Space Shuttle merely *hoping* it would work: they had a manual from which to proceed, *knowing* it would work.

These StarDrive hardware specifications are, on one hand, as basic as claimed. They are intended only as an initial guiding manual for designing the essential primary systems of *real* starships. By no means do they contain all of the answers to questions that will undoubtedly arise during the development and construction processes. However, a great many aspects of these instructions are virtually immutable, and will apply strictly and uniformly to all feasible sizes or models of this particular design.

Therefore, the SpecSheets which follow are essentially *design-constant* and pertain to models of all sizes as best I can determine at this point, the only notable exception being α SpecSheet XII {Variable Inductor Arrays}. The WorkSheets associated with each such SpecSheet are, on the other hand, *size-contingent* and the particular specifications derived therein must be calculated for each given model (size) vessel. Throughout, the necessary data is included to adequately design either *type* of device (be it a Thermal or Drive Unit).

The several DataSheets in Appendix A should be considered 'required reading' *as a whole* only for advanced students and engineers, and they furnish a great deal of logical and mathematical substantiation underlying the entire spreadsheet matrix. However, the DataSheets specifically related to *Electrode Array Construction* (#9 - #15) would be essential to anyone wishing to fully understand the electrostatic engineering concepts utilized in StarDrive design.

For those of you who are really 'into' illustrations, diagrams, and photos, I realize that this book may have been something of a let-down so far. Many of the really interesting visual aids, however, occur in the Material SpecSheets of Appendix B. This second set of SpecSheets also contains the most specific technical information related to the *actual construction* of StarDrive vessels.

I eventually found it possible to provide individual section page numbers in the Specifications Directory which follows, and the name of each SpecSheet and WorkSheet also appears in a header at the top of each of its pages. Because of the sheer quantity of detailed information presented in Appendix B, its Directory includes page numbers for each major Section of each Material SpecSheet. In any event, may the readers' perusal of all of this data be as exciting and gratifying as was the author's Quest for its proper formulation.

DIRECTORY

SpecSheets

WorkSheets

Appendix A DataSheets

I. Field and Rotor Voltages	100	(a) Specific Unit Voltage Values	103		
II. Rotor Segment Dimensions	109	(a) Spec. Rotor Segment Measurements	113		
		(b) Rotor Ampacity	114	#1 Copper Wire Data	346
		(c) Field Power Output	116		
III. Rotor Component Positioning	121				
IV. Rotor Ballrace Construction	124				
V. Magnetic Ring Dimensions	126	(a) Spec. Magnetic Ring Measurements	128	#2 Sm. Magnet Comp. Graph	348
		(b) Magnetic Ring Gap Flux Density	130	#3 Alnico V B/H Graph	349
		(c) Counterflux Wafers	132	#4 DC Magnetization Curves	351
VI. Magnetic Ring Arrays	133			#5 Mag. Ring Load-Line Formula	352
				#6 Mag. Ring Leakage Factor	352
VII. Field Coil Design	139	(a) Spec. Field Coil Measurements	141	#7 Coil Voltage Formula	353
		(b) Turns Ratio Factors	145		
		(c) Field Coil Output Ratios	146	#8 Bias Voltage Ratio	355
VIII. Electrode Array Construction	149	(a) Series Electrode Array Capacitance	152		
		(b) Triode Potential Differences	160	#9 Electro. Load-Line Formula	357
				#10 Applied Grid Resistances	360
		(c) Pentode Potential Differences	167	#11 Stage Plate Resistances	361
				#12 Uni. Fld. Intensity Formula	362
		(d) Primary Voltage Expansion Ratio	175	#13 Instant. Charge Differential	364
		(e) Field Ballast Capacitors	178		
IX. Power System Schematics	182	(a) Bias Winding Turns Ratios	185	#14 Stage Voltage Balance	367
		(b) Field Coil Voltage Values	187		
		(c) Field Winding Resistances	192		
		(d) Bias Winding Resistances	194		
X. Zone Sector Construction	196	(a) Field Power Resistors	197		
XI. Field Current Bias Values	201			#15 Beam Pentode Character.	378
XII. Variable Inductor Arrays	202	(a) Spec. Armature Measurements	206		
		(b) Axial Field Flux Balance	211	#16 Flux Superposition Ratio	382

Prelude

I miss the Earth so much,
I miss my wife.
It's lonely out in space
on such a timeless flight . . .
And all this Science,
I don't understand:
it's just my job, five days a week.
A rocket man;
a rocket man . . .

Elton John
Honky Château

Before we look at the final method I developed for specifying **Field and rotor voltages** for the StarDrive Field Generator, I should take a little time to describe its evolution so that the student may get a handle on its unavoidable complexity. For a long time, I tried to derive a method of field voltage specification for Impulse Drive Units that simply used an integer multiple of the field voltage for that particular size Thermal Unit. Because as it happens the 4ft. model Drive Unit requires a field voltage almost exactly equal to 12 times that of the 4ft. Thermal Unit, I was hoping to find a fortuitous relationship between hull radius (R_h) and the number 12 or a multiple thereof (in this regard).

At first, as my rough computations began to show me that the magic multiple of 12 formulation could not work for larger StarDrive vessels, I tried 24 as my field voltage multiplier. This seemed to achieve somewhat 'closer' answers (by a country mile or so). Then, as I gradually realized my original vessel weight estimation technique had also been low by about 50%, I started using 36 as my multiplier. Believe it or not, it took my Patent attorney to get me to wake up and derive a far more 'professional' method relating the best possible estimate of a given vessel's weight and its calculated rotor ampacity. Maybe I should have been a Numerologist . . .

It was at about this time that I perfected the *specific impulse* method now used, but a very interesting correlation between the two methods was later pointed out. In the course of impulse research which resulted in the important graph of Fig. 19, it was found that the Spec. Field Voltages for the 20, 40, 60, and 80 ft. diameter Drive Unit models turn out to be respectively 26.64, 36.96, 34.44, and 33.72 times the corresponding Thermal Unit Field Voltages. So, I guess I intuitively did sort of end up 'in the ballpark'.

One of the main reasons the 4ft. diameter model became the mathematical basis for most of the Specifications is that its Drive Field perimeter arc-length turns out to be very nearly 1 meter. As a result, the Spec. Field Voltage for both Thermal Units and Drive Units ends up being .9666 times their respective Nominal Field Voltages. This multiplier is essentially equal to the fraction 29/30, and at one time I rather optimistically used this number throughout the WorkSheets related to electrode array construction to envision the closest possible electrode spacings (short of losing array impedance due to breakdown intensity). In practice, it will probably be wise to limit electrode array field intensity to a smaller percentage of E_{brk} , but only by the absolute minimum amount required to prevent the array from completing the transition to a direct arc discharge condition (see Fig. 36 of DataSheet #15). The fraction 11/12 or .9167 is now used in this respect.

It is very important for engineers to note that the Nominal Rotor Voltage is presently stipulated according to a simple linear proportionality formula based on the device's hull radius, for both Thermal and Drive Units. The Spec. Rotor Voltage is similarly defined, but has also been indexed against the Nominal Rotor Voltage. These relationships constitute only a base *interim method* of roughly assigning rotor voltages, until a precise method of calculating hull static capacitance is developed [see the Section A preamble of WorkSheet VIII(b)]. These formulas must be redefined once optimal 3η rotor speeds (and angular momentums) have been established across the full range of vessel sizes, and the hull capacitance formula has been refined through prototype testing. In the mean time, the Spec. Rotor Voltage for a 100ft. diameter starship turns out to be 144,990 volts, and the necessary design Primary System Voltage is then 289,980: very high values indeed, but not unmanageable.

The only other seemingly arbitrary constant employed in the following SpecSheet is that used (as a divisor) to stipulate the Spec. Field Voltage of a Drive Unit as a percentage of the Nominal Field Voltage. This divisor (equal to .982826) indicates that I would like the Spec. Field Voltage to be just slightly larger than the Nominal value to further ensure the desired thrust performance; it was chosen to match the related *peak* field voltage (used to calculate peak thrust) as closely as was practical at the time to the peak value obtained by the previous method of field voltage specification.

It is important to note that the more logical place for the WorkSheet on Field Power Output [II(c)] would be immediately after WorkSheet I(a) [Specific Unit Voltage Values], instead of its being 'buried' many pages later in the rotor segment section of the Specifications. Because the rotor ampacity of the EDF Generator must be known before its power output may be correctly obtained, this WorkSheet has been placed in what is felt to be its more *proper* location to preserve the linearity of the entire matrix of Specification spreadsheets.

Field and Rotor Voltages**Part A: Model Unit Field Intensity**

[1] The Marginal Envelope Field Intensity for all EDF Generator models regardless of type shall be equal to the breakdown dielectric strength of vacuum at 3×10^6 volts/meter, as measured along a full pure semicircular arc drawn from the center point on the surface of either hull Positive Zone to any exterior point on the vessel's design hull configuration which lies on the horizontal centerline plane thereof (see Fig.18 hereinbelow). This distance shall be referred to as the "Drive Field Perimeter" and is calculated in WorkSheet VIII(d) {Primary Voltage Expansion Ratio}.

[2] For purposes of these Specifications, the "Drive Field Boundary" shall represent the distance measured along a full pure semicircular arc from any point on the peripheral (outer) edge of either hull Positive Zone to the closest point thereto which lies on the innermost edge of the vessel hull's negative Emitter Ring (see Fig.18, on pg.102).

Part B: 1η Thermal Power Units

[1] The Nominal Field Voltage (nom.V_f) shall be numerically equal to 1.5 million (1.5×10^6) times the vessel R_h as measured in feet. This value is also equal to the standard Thermal Unit's design Primary Voltage Expansion Ratio of 750 times its Specification Primary Array Voltage, as a function of the charge stored within the Primary Power System's two (2) Field Ballast Capacitors.

[2] The Specification Field Voltage (spec.V_f) shall be equal to the Marginal Envelope Field Intensity times the distance comprising the Drive Field Perimeter, or (as presently calculated under the above directive) .9666 times the Nominal Field Voltage. This value shall constitute the standard operating value of field envelope voltage.

[3] The Peak (design operating maximum) Field Voltage (max.V_f) shall be equal to 110% of the Specification value thereof.

[4] The Nominal Rotor Voltage (nom.V_r) shall be numerically equal to one-third of the product of 1,000 (1×10^3) times the vessel R_h as measured in inches, as a gauge of the full-power generator value of rotor rotational speed.

[5] The Specification Rotor Voltage (spec.V_r) shall be numerically equal to .25776% of 1.5 million (1.5×10^6) times the vessel R_h as measured in feet, and is also equal to .9666 times the Nominal Rotor Voltage. This value shall constitute the standard operating value of rotor voltage, as a function of Primary Power System output at a nominal design rotor rotational speed.

[6] The Peak (design operating maximum) Rotor Voltage (max.V_r) shall be equal to 110% of the Specification value thereof.

[7] The design Primary System Voltage (spec.V_u) for each single-stage (1η) Thermal Unit rotor shall be equal to three-halves (3/2) of the Spec. Rotor Voltage thereof, based on a projected maximum 40% series array bias voltage rise.

[8] The design Series Coil Group Voltage (spec.V_g) for both Thermal and Drive Unit rotors shall be equal to the design Primary System Voltage divided by 1.4 or to 1.071428 times Specification Rotor Voltage as applies to Thermal Units.

[9] The Specification Primary Array Voltage (spec.ΔV_p) shall be equal to half (1/2) of the Specification Rotor Voltage, with the primary cathodes at ground.

Part C: 3η Impulse Drive Units

Unlike the case with Thermal Power Units, it is not possible to specify in one step a Nominal Field Voltage for Impulse Drive Units which is a linear function of the hull radius R_h . This is, of course, because the Field Voltage which must be produced to achieve the design goal for net unilinear thrust output of five-thirds 'g' is jointly proportional to the rotor ampacity, which rises as a function of the square of increases in R_h , and to the vessel weight which rises as a function of the cube of R_h increases.

Therefore, a "Marginal Field Voltage" is initially to be calculated for Impulse Drive Units which reflects a projected theoretical operating value of Field Voltage required to produce a vessel acceleration approximately equal to 1.67 g outside of a proximal gravity field. This Marginal Field Voltage is to be calculated using the specific impulse of the vessel concerned (in nt-sec), and for purposes of the application contemplated herein this term is hereby defined as being equal to five times the vessel weight (in newtons) divided by the product of the rotor ampacity and the number of electrons per coulomb.

[1] Accordingly, the Marginal Field Voltage shall then be equal to the specific impulse times the speed of light divided by the unit electron charge, as calculated in WorkSheet I(a) {Specific Unit Voltage Values}.

[2] An estimated nominal Field Voltage will also be computed in WorkSheet I(a) in a manner whereby a nominal value for the final electron speed of Drive Field current is assigned which is in fact a linear function of R_h (for vessels of from 4 to 100 ft. in diameter only).

[3] The stipulated Nominal Field Voltage (nom.V_f) shall then be equal to the simple average of the Marginal Field Voltage and the estimated nominal Field Voltage (est.V_{nf}).

[4] The Specification Field Voltage (spec.V_f) shall be equal to the Nominal Field Voltage (nom.V_f) divided by .982826.

[5] The Peak (design operating maximum) Field Voltage (max.V_f) shall be equal to 110% of the Specification value thereof.

[6] The Nominal Rotor Voltage (nom.V_r) shall be numerically equal to one-fourth of the product of 1,000 (1×10^3) times the vessel R_h as measured in inches, as a gauge of the full-power generator value of rotor rotational speed.

[7] The Specification Rotor Voltage (spec.V_r) shall be numerically equal to .19332% of 1.5 million (1.5×10^6) times the vessel R_h as measured in feet, and is also equal to .9666 times the Nominal Rotor Voltage. This value shall constitute the standard operating value of rotor voltage, as a function of Primary Power System output at a nominal design rotor rotational speed.

[8] The Peak (design operating maximum) Rotor Voltage (max.V_r) shall be equal to 110% of the Specification value thereof.

[9] The design Primary System Voltage (spec.V_s) for each three-stage (3η) Drive Unit rotor shall be equal to twice (2x) the Spec. Rotor Voltage thereof, based on a projected maximum 40% series array bias voltage rise.

[10] The design Series Coil Group Voltage (spec.V_g) for both Thermal and Drive Unit rotors shall be equal to the design Primary System Voltage divided by 1.4, or to 1.428571 times Specification Rotor Voltage as applies to Drive Units.

[11] The Specification Primary Array Voltage (spec.ΔV_p) shall be equal to half (1/2) of the Specification Rotor Voltage, with the primary cathodes at ground.

[12] The design Primary Voltage Expansion Ratio for Impulse Drive Units shall be equal to the ratio of Spec. Field Voltage to Spec. Primary Array Voltage.

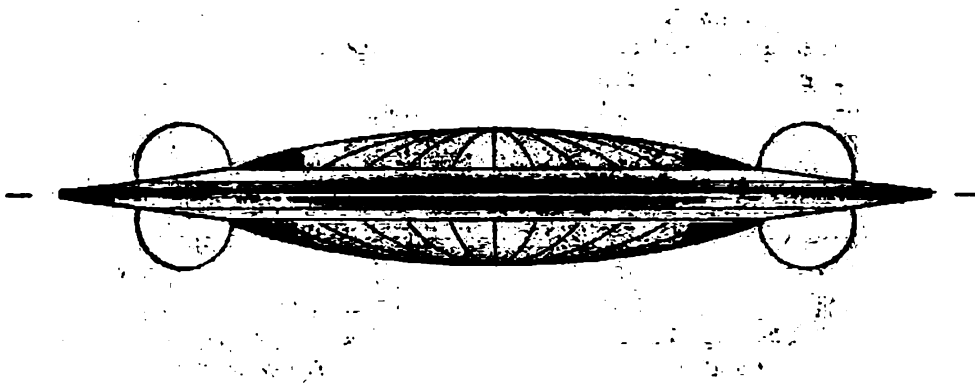


Fig. 18: *StarDrive vessel hull & bihemitoroidal field*

Part D: Rotor Induction Efficiencies

From a careful analysis of the preceding Specifications with regard to the various ratios of Spec. Rotor Voltage (the actual voltage impressed across the rotor) to the net Series Coil Group Voltage or to the gross design Primary System Voltage, it can be seen that the EDF Generator's *Primary Power System* is actually only $46\frac{2}{3}\%$ efficient at best in transmitting the total net coil-generated voltage to the rotor in Thermal Units, and only 35% efficient at doing so in Drive Units. And this is in reliance upon the projected 40% bias voltage rise! Treating this voltage rise as a component of gross total voltage output (Primary System Voltage), these efficiency figures would only be $33\frac{1}{3}\%$ and 25% respectively. [See WorkSheet VIII(a) and SpecSheet IX.]

The principal reason for this low net efficiency is of course that the two *Primary Power System* semicircuits must apply their outputs in parallel across the rotor and not in series. This is a small price to pay, however, for first eliminating any use of brushes and then providing for the possibility of 2-way signal communications capability. As was outlined in Chapters 4 and 7, a third mode of usage to which the EDF Generator may be applied is as an experimental method of sending and receiving specialized AC resonant frequency signals using the field envelope as a form of antenna. This would not be as practical without the transfer array construction employed in 3 η Drive Unit rotors, enabling substantial AC signal voltage pre-amplification (prior to the final stage gain obtained across the *Primary Induction Ring Arrays*).

One type of signal contemplated would couple the electric, magnetic, and gravitic forces to utilize the wave mechanics of *quantum potential vacuum fluctuations* ($|\Delta E_q|/\Delta t$), which are assumed to propagate at c' in order to explain the unified operation of gravity and entropy in two spatial continuums which are coincident but completely out-of-phase. This concept would allow for near real-time communications with a StarDrive vessel's point of origin, and is taken throughout *StarDrive Engineering* to be an integral and inseparable facet of the device's form and function. In fact, the use of different resonant frequencies in each half of the *Primary Power System* to allow the *simultaneous* sending and receiving of information is the principal justification for the other System half's otherwise appreciable redundancy.

Specific Unit Voltage Values

model: Badlander

size: 4ft. dia.

Section A: 1n Thermal Power Unit

Based on the directives of SpecSheet I, a 4ft. diameter EDF Generator constructed for use as a Thermal Power Unit will have specific field and rotor voltages as follows:

- [1] The Nominal Field Voltage (nom.V_f) shall be equal to 3,000,000 .
- [2] The Specification Field Voltage (spec.V_f) shall be equal to 2,899,800 .
- [3] The Nominal Rotor Voltage (nom.V_r) shall be equal to 8,000 .
- [4] The Specification Rotor Voltage (spec.V_r) shall be equal to 7,732.8 .
- [5] The design Primary System Voltage (spec.V_{ps}) shall be equal to 11,599.2 .
- [6] The design Series Coil Group Voltage (spec.V_{scg}) shall be equal to 8,285.14 .
- [7] The Spec. Primary Array Voltage (spec.ΔV_p) shall be equal to 3,866.4 .
- [8] The corresponding design Primary Voltage Expansion Ratio for (this and all) Thermal Power Units is 750:1 .

Section B: 3n Impulse Drive Units

[1] Marginal Field Voltage: The 4ft. Drive Unit's Marginal Field Voltage, which represents the projected theoretical operating value of field envelope voltage, is based on the vessel's specific impulse - given its rotor ampacity of 38,160 [see WSII(b)] and est'd. wt. of 79.2 lbs/ft' - and is figured as follows:

$$F_{dt} = \frac{5(9.8 \text{ m/sec}^2)V_h(79.2 \text{ lbs/ft}')}{(3.816 \times 10^4 \text{ coul/sec})(6.25 \times 10^{18})(2.2 \text{ lbs/kg})'}$$

where $V_h = 2.5068 \text{ ft}^3$ (from Hull Configuration Spreadsheet);

$$\text{so, } F_{dt} = \frac{5(9.8)(90.245)}{23.85 \times 10^{22}} = \boxed{1.8541 \times 10^{-20} \text{ nt-sec}} . *$$

* This impulse is the instantaneous force of thrust produced by each Field current electron's collision with the Field Hub.

Therefore, the Marginal Field Voltage = $F_{dt}c/q$

$$= \frac{(1.8541 \times 10^{-20} \text{ nt-sec})(299.7925 \times 10^6 \text{ m/sec})}{1.6 \times 10^{-19} \text{ coul}}$$

$$= 34.7403 \times 10^6 \text{ volts (nt-m/coul)} .$$

[2] Estimated Nominal Field Voltage: The 4ft. Drive Unit's estimated nominal field voltage, which represents an alternate projection of the minimum standard operating value of field envelope voltage, is based upon an assigned nominal value for the final electron speed of Drive Field current (ΔV_e) which is a linear function of the vessel R_h and is calculated as follows:

$$\Delta V_e = [.999 + (2R_h - 4)(1.03125 \times 10^{-3})]c ,$$

where R_h is in feet, for vessels from 4 to 100 ft. in diameter.

$$\text{Therefore, } \Delta V_e = [.999 + 0(1.03125 \times 10^{-3})]c$$

$$= .999c .$$

Specific Unit Voltage Values

The purpose of this WorkSheet subsection is to verify that a requisite level of Drive Field thrust may be produced by the Unit, at an operating voltage approximately equal to that stated above, within the ampacity of the rotor and at an assigned value of Drive Field velocity (for this model) of .999c. In this manner, it is hoped that unnecessarily high operating Drive Field voltage may be avoided, by virtue of design (due to the finite level of unavoidable uncertainty in the relativistic values involved), without sacrificing device performance.

- (a) The amount of thrust (force) required to produce an acceleration of 1g, thus exactly compensating the weight of the Drive Unit, may be calculated by Newton's Second Law as follows:

$$F = ma, \text{ where } m = \text{est. design mass* of } 90.245 \text{ kg,} \\ \text{and } a = 9.8 \text{ m/sec}^2.$$

Thus, $F = 884.4$ newtons (nt).

*Note: The estimated design weight of any given Drive Unit is 79.2 lbs. per cubic foot. (see Hull Configuration Spreadsheet)

- (b) Since impulse equals change of momentum, the thrust developed by the Drive Field equals the total relativistic mass of Field current times the incident current velocity (as the inelastic final electron velocity equals 0). The amount of thrust equivalent to 1g here is 884.4 nt.

$$\text{Therefore, let } \Sigma M_{\Delta V} = 884.4 \text{ nt.}$$

- (c) The design goal for net linear thrust output of any given Drive Unit is 1.667g (16.333 m/sec') at the minimum standard operating value of Field voltage and rated rotor ampacity. Therefore, given the considerations of SpecSheet XI {Field Current Bias Values}, the total isometric thrust at a Marginal Field Voltage must be equal to 5g. The largest Field current available to effect a Field impulse equivalent to 1g is then equal to I_1 , where:

$$I_1 = I_{\text{max}}/5 = 7,632 \text{ amps.}$$

- (d) Since Σ equals the total number of electrons comprising a Drive current of I_1 , we find:

$$\Sigma = I_1(6.25 \times 10^{18}) = 4.77 \times 10^{22} \text{ electrons/sec.}$$

- (e) Therefore, from [b] above:

$$884.4 \text{ nt}/\Sigma = M_{\Delta V}, \text{ and } M_{\Delta V} = 1.8541 \times 10^{-20} \text{ kg-m/sec.}$$

- (f) Letting $\Delta V_e = .999c$, where $c = 299.7925 \times 10^6 \text{ m/sec}$,

$$\text{we calculate } M_e = \frac{1.8541 \times 10^{-20}}{299.49271 \times 10^6} = 619.08 \times 10^{-31} \text{ kg}, \text{ or } 67.96 m_e.$$

- (g) If m_1 equals the relativistic mass equivalent of the gained kinetic energy of each Drive Field electron,

$$\text{then } M_1 = m_e + m_1, \text{ where } m_e = \text{electron rest mass @ } 9.11 \times 10^{-31} \text{ kg.}$$

Specific Unit Voltage Values

$$\begin{aligned}\text{Therefore, } m_i &= M_i - m_o = 619.08 \times 10^{-31} - 9.11 \times 10^{-31} \\ &= \underline{609.97 \times 10^{-31} \text{ kg}}.\end{aligned}$$

- (h) Each Drive Field electron's gained kinetic energy (E_k) equals $m_i c^2$ Using a precise value of 8.98755×10^{16} for c^2 ,

$$\begin{aligned}\text{we obtain } E_k &= (6.0997 \times 10^{-31})(8.98755 \times 10^{16}) \\ &= \underline{54.8214 \times 10^{-13} \text{ joules}}.\end{aligned}$$

- (1) Here, E_k also equals $W = q(\text{est. } V_{nr})$, where q = electron chg. @ 1.6×10^{-19} coul., and $\text{est. } V_{nr}$ = est. nominal Field Voltage.

$$\begin{aligned}\text{Therefore, } E_k/q &= \text{est. } V_{nr}, \text{ and } \text{est. } V_{nr} = \frac{54.8214 \times 10^{-13} \text{ joules}}{1.6 \times 10^{-19} \text{ coulomb}} \\ &= \underline{34.2633 \times 10^6 \text{ volts}}.\end{aligned}$$

Thus, we find that the estimated nominal Field Voltage required to develop requisite thrust is in fact well within the parameters discussed above, at 98.63% of the projected marginal value.

- [3] The stipulated *Nominal Field Voltage* ($\text{nom. } V_f$) is therefore equal to the simple average of the Marginal Field Voltage and the estimated nominal Field Voltage, at 34.5018×10^6 volts.
- [4] The *Specification Field Voltage* ($\text{spec. } V_f$) shall be equal to $\text{nom. } V_f$ divided by .982826, at 35.1047×10^6 volts.
- [5] The *Nominal Rotor Voltage* ($\text{nom. } V_r$) shall be equal to 6,000.
- [6] The *Specification Rotor Voltage* ($\text{spec. } V_r$) shall be equal to 5,799.6.
- [7] The design *Primary System Voltage* ($\text{spec. } V_{ps}$) shall be equal to 11,599.2.
- [8] The design *Series Coil Group Voltage* ($\text{spec. } V_{cg}$) shall be equal to 8,285.14.
- [9] The *Spec. Primary Array Voltage* ($\text{spec. } \Delta V_p$) shall be equal to 2,899.8.
- [10] The design *Primary Voltage Expansion Ratio* for this model Drive Unit is equal to $35.1044 \times 10^6 / 2,899.8 = 12,106:1$.

The graph on the following page shows the Specification Field Voltage for Drive Units of 20, 40, 60, 80, and 100 ft. in diameter, as calculated using the two-part method developed hereinabove. These figures are based on the actual rotor ampacities and estimated design weights for each of the vessels, and suggest two findings:

- 1) the design methods employed throughout the Basic Specifications seem especially well-matched in the vessel diameter range from 40 to 80 ft., wherein the vessel beam doubles as does the Field Voltage required; and
- 2) It seems that an upper limit of vessel size for this type of drive probably exists at a diameter not greatly above the 100 ft. model, as the required Field Voltages involved would appear to begin climbing tangentially.

Nevertheless, this data is very encouraging with respect to the design goal held throughout - that this device be linearly scalable in size to a level sufficient to accomodate a number of crew and/or passengers. Due to the small net volume of the Central Chamber, however, a StarDrive vessel's payload capacity will be extremely limited.

Specific Unit Voltage Values

max. and min. nominal rotor speeds (in rpm) vs. size (□) *

1025/565
1075/595
1125/620
1175/650
1225/680
1275/705
1325/735
1375/760
1425/790
1475/815
1525/845
1575/870
1625/900
1675/925

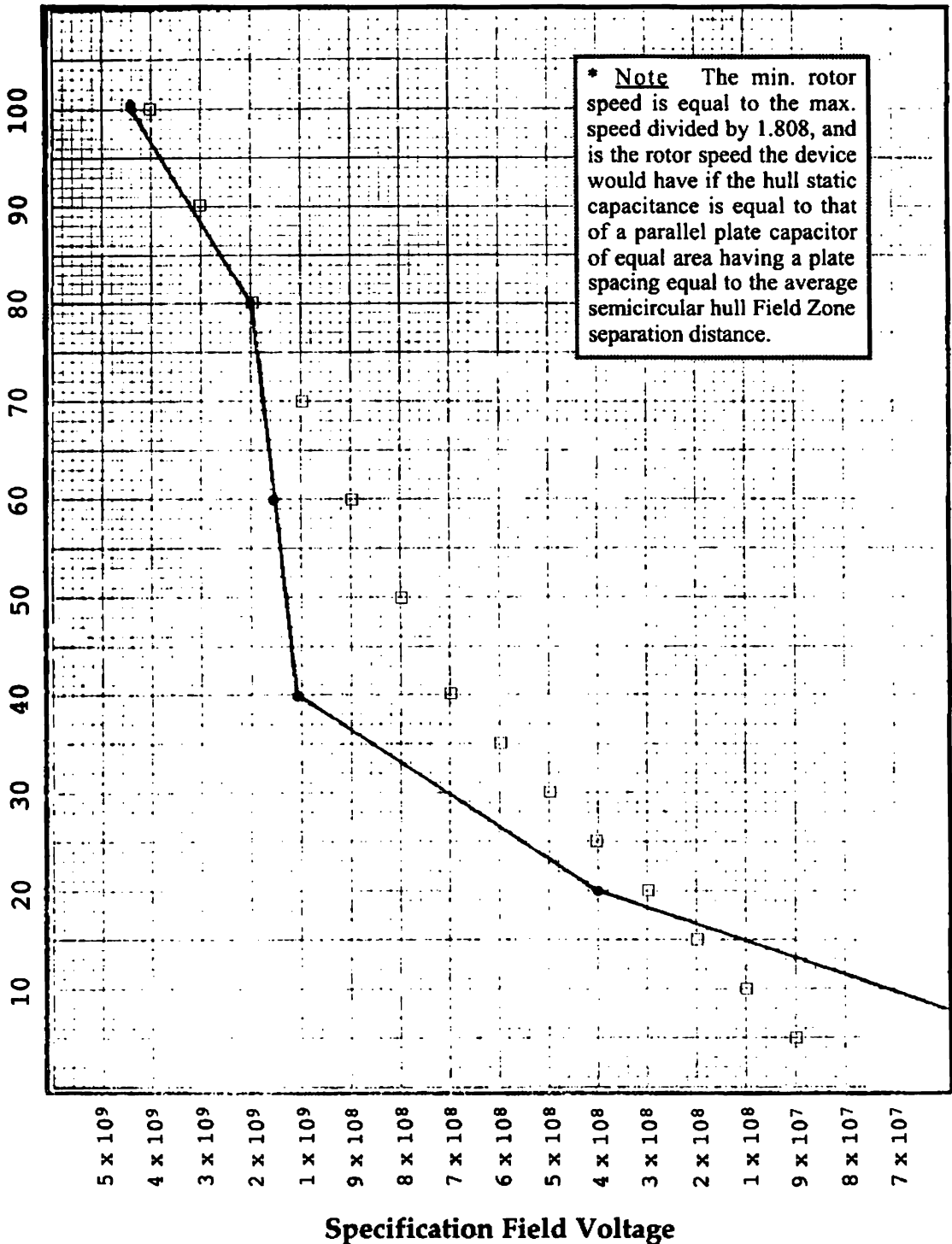


Fig. 19: 3η Drive Unit Hull Diameter (in ft.) vs. Field Voltage req'd. (•)

[The 4ft. Drive Unit's Field Voltage was used to define the slope of the first leg of the graph.]

Propulsive Unit Hull Voltages & Rotor Speeds

- excerpted from 'StarDrive Engineering', copyright ©2001 by Mark R. Tomion - All Rights Reserved.

max. and **min.** nominal rotor speeds (in rpm) vs. size (□) *

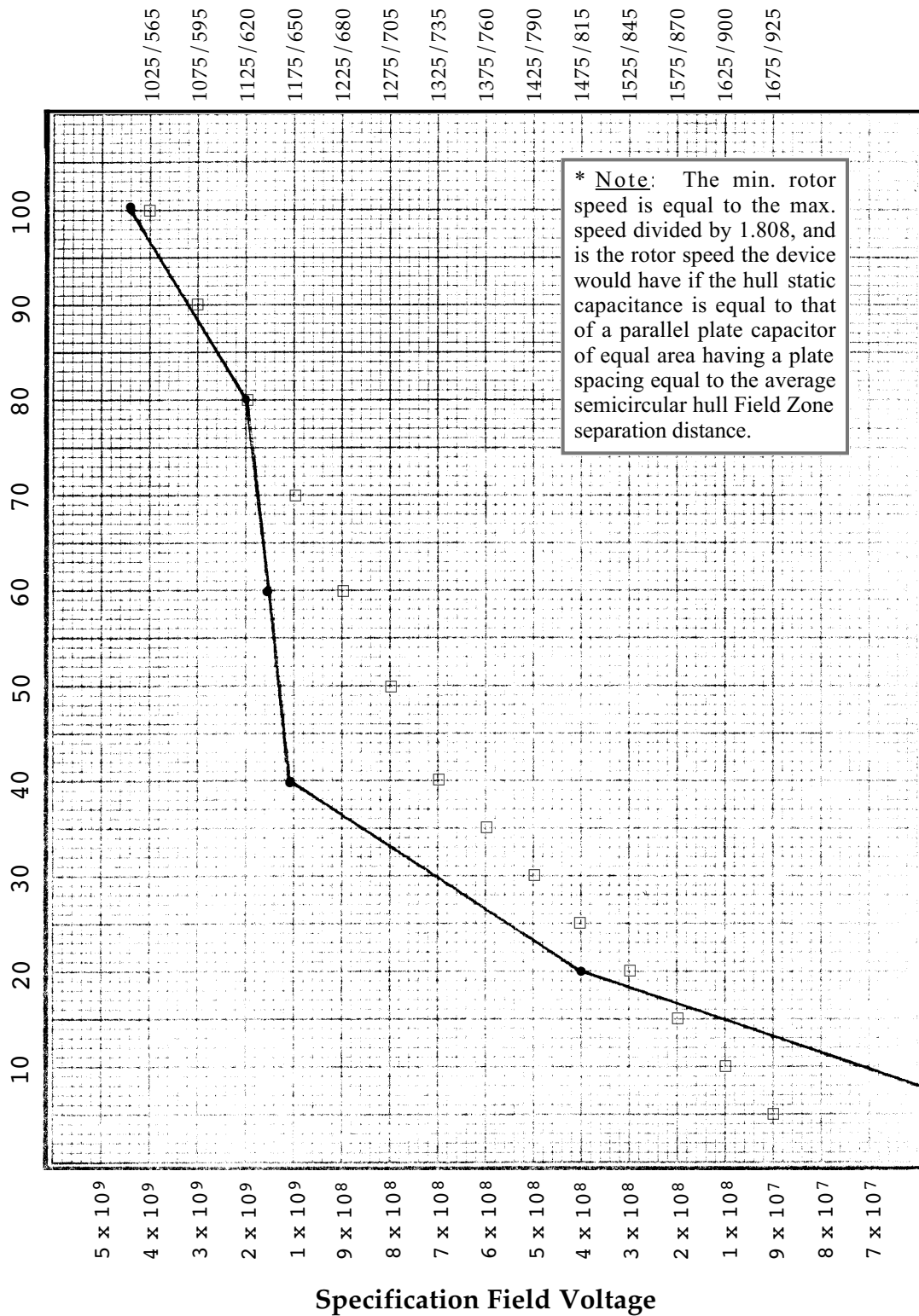


Fig. 19: 3η Drive Unit Hull Diameter (in ft.) vs. Field Voltage req'd. (•)

[The 4ft. Drive Unit's Field Voltage was used to define the slope of the first leg of the graph.]

This excerpt may not be reproduced in whole or in part, by any means except photocopy, without the author's express permission.

Manned Vessel Design DataSheet

As promised, here's what I've come up with to assist real StarDrive enthusiasts in designing their own starship. The standards of 'legroom', 'headroom', and crew capacity outlined below are as accurate as I can manage at this point, although I will no doubt continue my research and offer further insights if I can in any later edition(s) of StarDrive Engineering which might be forthcoming.

For our purposes here, *legroom* is defined as the estimated net radial cabin or bridge area horizontal 'width', between a central airlock bulkhead and the outside circular wall. *Headroom* is then the net floor-to-ceiling height and in this case should be taken as a definite maximum value. As can be seen, this cabin dimension is indeed rather cramped. Maybe this is why star-traveling aliens are usually reputed to be so short . . .

A standard *personnel couch* is taken to be 77 inches long in a fully-reclined position, so legroom is given in terms of this length plus any available radial crawlspace or walkway room. Legroom is also based on a central gross airlock radius (including circular bulkhead). The vessel size stated refers to overall diameter, and *exact* values for each vessel's spec. Field voltage and rotor ampacity are given.

40ft. vessel:		Vega class
legroom:	77 in.	} abs. min. for manned craft
headroom:	2' 3"	
gr. airlock radius:	1.2 ft.	
max. # of crew:	3	
60ft. vessel:		Antares class
legroom:	77 in. plus 1.2 ft.	vol. = 8,460 ft ³ ; wt. = 335 tons
headroom:	3' 6"	spec.V _f = 1.5756 x 10 ⁹
gr. airlock radius:	1.8 ft.	peak I _n = 19.9386 x 10 ⁵
max. # of crew:	5	# of N/YBCO current storage rings: 5
80ft. vessel:		Orion class
legroom:	77 in. plus 2.4 ft.	vol. = 20,054 ft ³ ; wt. = 794 tons
headroom:	4' 9"	spec.V _f = 2.0621 x 10 ⁹
gr. airlock radius:	2.4 ft.	peak I _n = 36.1134 x 10 ⁵
max. # of crew:	8	# of N/YBCO current storage rings: 6
100ft. vessel:		Toltec class
legroom:	77 in. plus 3.6 ft.	vol. = 39,168 ft ³ ; wt. = 1551 tons
headroom:	6' 0"	spec.V _f = 4.4894 x 10 ⁹
gr. airlock radius:	3.0 ft.	peak I _n = 46.9422 x 10 ⁵
max. # of crew:	12	# of N/YBCO current storage rings: 7

As we can see, it requires at least a 100ft. starship before the crew can actually *stand up straight* (and then they'd better not be tall!). Within my small research group, I have for some time referred to the 100ft. model as the *Toltec* class vessel: an acronym for 'total technology'. Although the Basic Specifications were prepared with this vessel in mind as the largest *advisable* size, due to inordinate field voltage considerations, I believe at this point that a *Phoenix* class vessel is possible having a 120ft. diameter. This should relieve the headroom problem, increasing it to 7'3".

I'm extremely uncomfortable with any proposed vessel of *EDF Generator design* which is larger than this. I must leave it up to you future StarDrive engineers to develop a drive method which allows for much larger craft to be built, having the far better payload capacity we will need if we are ever to really explore (and someday colonize) this small corner of our Universe.

Manned Vessel Design DataSheet

- excerpted from '**StarDrive Engineering**', copyright ©2001 by Mark R. Tomion - All Rights Reserved.

As promised, here's what I've come up with to assist real StarDrive enthusiasts in designing their own starship. The standards of 'legroom', 'headroom', and crew capacity outlined below are as accurate as I can manage at this point, although I will no doubt continue my research and offer further insights if I can in any later edition(s) of StarDrive Engineering, which might be forthcoming.

For our purposes here, *legroom* is defined as the estimated net radial cabin or bridge area horizontal 'width', between a central airlock bulkhead and the outside circular wall. *Headroom* is then the net floor-to-ceiling height and in this case should be taken as a definite maximum value. As can be seen, this cabin dimension is indeed rather cramped. Maybe this is why star-traveling aliens are usually reputed to be so short . . .

A standard *personnel couch* is taken to be 77 inches long in a fully-reclined position, so legroom is given in terms of this length plus any available radial crawlspace or walkway room. Legroom is also based on a central gross airlock radius (including circular bulkhead). The vessel size stated refers to overall diameter, and *exact* values for each vessel's spec. Field voltage and rotor ampacity are given.

40ft. vessel:		Vega class	
legroom:	77 in.	} abs. min. for manned craft	vol. = 2,507 ft ³ ; wt. = 99 tons
headroom:	2' 3"		spec.V _f = 1.1298 x 10 ⁹
gr. airlock radius:	1.2 ft.		peak I _{rt} = 11.9394 x 10 ⁵
max. # of crew: 3			# of N/YBCO current storage rings: 4
60ft. vessel:		Antares class	
legroom:	77 in. plus 1.2 ft.	} abs. min. for manned craft	vol. = 8,460 ft ³ ; wt. = 335 tons
headroom:	3' 6"		spec.V _f = 1.5756 x 10 ⁹
gr. airlock radius:	1.8 ft.		peak I _{rt} = 19.9386 x 10 ⁵
max. # of crew: 5			# of N/YBCO current storage rings: 5
80ft. vessel:		Orion class	
legroom:	77 in. plus 2.4 ft.	} abs. min. for manned craft	vol. = 20,054 ft ³ ; wt. = 794 tons
headroom:	4' 9"		spec.V _f = 2.0621 x 10 ⁹
gr. airlock radius:	2.4 ft.		peak I _{rt} = 36.1134 x 10 ⁵
max. # of crew: 8			# of N/YBCO current storage rings: 6
100ft. vessel:		Toltec class	
legroom:	77 in. plus 3.6 ft.	} abs. min. for manned craft	vol. = 39,168 ft ³ ; wt. = 1551 tons
headroom:	6' 0"		spec.V _f = 4.4894 x 10 ⁹
gr. airlock radius:	3.0 ft.		peak I _{rt} = 46.9422 x 10 ⁵
max. # of crew: 12			# of N/YBCO current storage rings: 7

As we can see, it requires at least a 100ft. starship before the crew can actually *stand up straight* (and then they'd better not be tall!). Within my small research group, I have for some time referred to the 100ft. model as the *Toltec* class vessel: an acronym for 'total technology'. Although the Basic Specifications were prepared with this vessel in mind as the largest *advisable* size, due to inordinate field voltage considerations, I believe at this point that a *Phoenix* class vessel is possible having a 120ft. diameter. This should relieve the headroom problem, increasing it to 7'3".

I'm extremely uncomfortable with any proposed vessel of *EDF Generator design* which is larger than this. I must leave it up to you future StarDrive engineers to develop a drive method which allows for much larger craft to be built, having the far better payload capacity we will need if we are ever to really explore (and someday colonize) this small corner of our Universe.

This excerpt may not be reproduced in whole or in part, by any means except photocopy, without the author's express permission.

The actual construction of an Electrodynamic Field Generator of any given size is relatively straightforward, whether it be of a large manned variety or not, and proceeds in fact from the inside out. One of the most practical aspects of the construction process is that the entire instrumentation and payload compartment or *Central Chamber* may be outfitted *first*, using low-density materials wherever possible, before any portion of the Primary Power System is assembled or even necessarily designed!

Construction next proceeds with the unit's ground frame: the metallic structural shell which provides an enclosing framework for the central chamber, to which all inboard electrical equipment may be grounded. This structural framework should be as strong, lightweight, and non-magnetic as possible, preferably being of a welded tubular design using stainless steel or a suitable titanium alloy.

Once the ground frame and enclosed central chamber are completed, including the installation of a preferred total of 32 high-torque dc motor-generator rotor drive units (in four sets of eight), the two rotor mounting frame sections and attached ring gears of the *Carrier Assembly* may be built and dynamically balanced (using a temporary peripheral spacing jig). Then, construction of the *Composite Rotor Assembly* may commence with the laying out of the equal numbers of copper segments, refractory composite field emitters, and ceramic segment separators which are all of *exactly equal weight* by type, the latter components providing the nonconductive base to which other rotating electrical hardware may be attached. The two (2) field ballast capacitors require recessed conductive traces on the segment separators in order to pass the capacitors' operating voltage beneath the rotor ballraces.

When these principal 540 large pieces are bound together with electrode rings silver-soldered to the segments, and clamped between the two halves of the centrifuge-style carrier assembly, the assembly of the *Primary Power System* itself may begin. Once the thin insulative rotor surface facing, ballast capacitor traces, and rotor ballraces have been affixed to the base rotor assembly, and the field coils, electrode arrays, and other rotating components have been added, the fabrication of the vessel's *Structural Intercooler System* may proceed. When this secondary thermal conduit (hull coolant) system is completed and has been pressure-tested, the *Primary and Magnetic Arrays* may be installed - including the 5-armature variable inductor array sections (depicted in Material SpecSheet B). The primary (induction ring) arrays here are comprised of the *field power resistors*, *dielectric buffers*, *primary thermal conduits*, and *unit pentode arrays*.

Finally, once the rotor has satisfied non-energized operational mechanical clearance and dynamic balancing criteria (using a temporary outer rotor bearing support jig) - and a final complete thermal conduit system pressure test has been made - the *Outer Hull Components* may be installed, completing the basic vessel construction in a total of seven distinct steps or stages.

The next set of Specifications and spreadsheets are concerned with the principal components of the base rotor assembly: the segments, separators, and field emitters. These Specifications will determine the exact size, shape, and (ultimately) weight of the rotor itself as the device's most massive single assembly. **Due to the tremendous weight of the finished rotor (copper is denser than stainless steel), an operating characteristic of utmost importance is the actual rotor speed required to maintain Spec. Field Voltage. This will determine the rotor's operating angular momentum, which in 3η Drive Units must be sufficiently large to provide gyroscopic stability against the use of variably-imbalanced isometric thrust (produced by the Drive Field) but not so large that the vessel's navigational and maneuvering characteristics are thereby rendered sluggish.**

The nominal rotor speed for the 4ft. diameter theoretical design prototype turns out to be almost precisely that of a typical small electric motor [see WorkSheet IX(b) {Field Coil Voltage Values}]. However, as the size of device increases, it will be necessary to reduce rotor speed due to the extreme increase in the rotor's 'tip' speed and therefore the centrifugal forces to which it is subjected. Sufficient information is contained in the Basic Specifications to allow engineers to reduce rotor speed as necessary in larger devices *following* the course of an intensive program of small device testing.

Once the rotor's design ampacity is figured [in WorkSheet II(b)], it is possible in the following spreadsheet to calculate the vessel's *field power output* or the peak electrical power inherent to the Field. Although astonishing to contemplate, for the first time in electrical engineering history it is necessary to consider a machine's output not in gigawatts but in *terawatts*. Methods of figuring the heat output of 1η Thermal Units and the thrust output in 3η Drive Units are developed, as is an interesting peak drive efficiency analysis for the 1η rotor device which is classically derived. It would seem to imply that the Generator is non-over-unity in nature, but input torque requirements are not considered.

Rotor Segment Dimensions

This SpecSheet serves to precisely define the relative size and shape of the copper segments, refractory composite field emitters, and ceramic segment separators which comprise the basic construction of the composite rotor assembly for an EDF Generator of any particular given diameter. Reference should be made in all instances to the accompanying diagrams of Figs.20-23.

Section A: Individual Segments

[1] Individual rotor segments for the EDF Generator are to be milled (not stamped) from flat sheet or plate stock, of the most uniform thickness possible, which is composed of metallic copper having a minimum purity 99.95% and which is certified to be oxygen-free.

[2] A total of 180 identical such segments shall be employed in the basic construction of each composite rotor assembly and the two (2) major flat surfaces of each segment shall be medium polished to a finished thickness which is equal to exactly $4/453 R_h$ and designated by the variable T_s .

[3] The design net length of each rotor segment shall be equal to the sum of $1/32 R_h + (C_v - C_s) + 1/18 R_h$, not including the bushing endface shown in Fig.47.

[4] The milled width of each rotor segment with respect to the major portion of its overall length shall be equal to exactly $1/45 R_h$.

[5] The radial width of that portion of the segment length which is denoted in the accompanying diagram as reserved for the primary induction anode ring shall be equal to $3/72 R_h$.

[6] The radial width of that portion of the segment length which is denoted in the accompanying diagram as reserved for the segment lockdown area shall be equal to $1/32 R_h$.

[7] The design radial width of that portion of the segment length which is denoted in the accompanying diagram as reserved for the segment retaining end shall be equal to $1/72 R_h$, not including the bushing endface shown in Fig.47.

[8] The axial length of the segment retaining end with respect to its radial width shall be equal to $2/32 R_h$ as depicted in the accompanying diagram.

[9] The working length of each segment, with regard to the calculation of its resistance in WorkSheet II(b), shall be considered to be equal to the sum of $1/12 R_h + (C_v - C_s)$.

[10] Each segment shall have two (2) holes drilled through its thickness on the radial centerline thereof (in the direction of its length) which are of a size and placement corresponding to the positions of the two (2) field emitter segment locator pins, as described in Section B below.

Section B: Individual Field Emitters

[1] Individual field emitters for the EDF Generator shall be formed of a powdered composite of tungsten and copper which is sintered and pressed to near-net size and then ground to a medium polish on all major flat surfaces.

[2] A total of 180 such field emitters shall be employed in the basic construction of each composite rotor assembly.

Rotor Segment Dimensions

[3] The radial length of the base portion of each such field emitter, which is of rectangular cross section, shall be equal to $\frac{4}{151}R_h + 4C_s$.

[4] The design radial length of the tip portion of each such field emitter (which is triangular in cross section) shall be equal to $\frac{3}{72}R_h$ prior to radiusing, which yields an angular declination of the finished edges thereof with respect to its radial centerline of $14^\circ 56'$.

[5] The design radial length of the tip portion of each field emitter shall be reduced slightly by radiusing to a net length equal to the base portion thereof, and this net tip length is intended to be also equal to approximately $\frac{1}{5}$ of the net distance between the radiused end of the tip and the outermost inside surface of the vacuum chamber (in the hull Negative Ring).

[6] The width of each field emitter shall be equal to the width of the rotor segments at $\frac{1}{45}R_h$.

[7] The thickness of each field emitter at its thinner (inner) end shall be equal to $2.00675 T_s$.

[8] The thickness of each field emitter at its thicker (outer) end shall be equal to $2.29789 T_s$.

[9] Each field emitter shall incorporate two (2) round segment locator pins whose axial centerpoints lie on the emitter's radial centerline (in the direction of its length), and each such locator pin shall be milled to a finished circular diameter equal to $2C_s$ which is perpendicular to the flat face of the emitter from which it extends and shall be ground to an overall length equal to $\frac{1}{120}R_h$.

[10] The net axial distance between each field emitter's two (2) segment locator pins shall be equal to the net axial distance between the emitter's radial centerline and the locator pin nearest thereto, at $1.5 T_s$, as indicated in the accompanying diagrams.

Section C: Segment Separators

[1] A total of 180 identical ceramic structural insulators shall be employed in the construction of each composite rotor assembly to provide a non-conductive base for the mounting of rotating Primary Power System components.

[2] The thickness of each segment separator at its inner (thinner) end shall be equal to the thickness of the rotor segments.

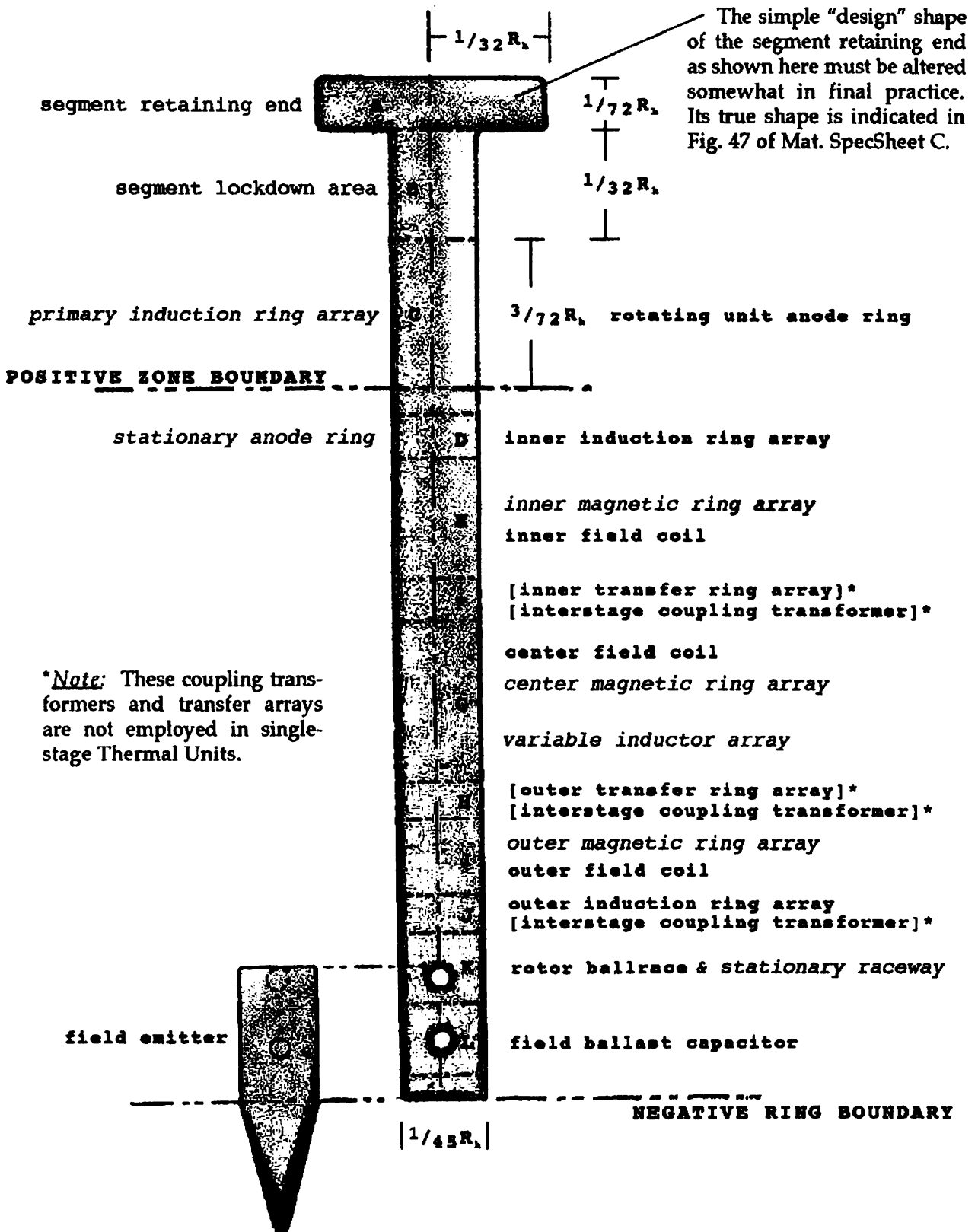
[3] The non-thickness shape of each segment separator shall be exactly the same as that of the rotor segments, except that such separator's over-all length shall be reduced from that of the segments by the length of the base portion of the field emitters.

[4] The separators are to be bonded to the segments with refractory adhesive layers which are limited to $\frac{1}{8000}R_h$ each in thickness.

The diagram on the next page, Fig. 20, shows the rotor segment drawn to a scale of 1:1 for the 4ft. diameter prototype designated by the model name 'Badlander'. Projected lines divide the segment into radial bandwidths within which the indicated parts are located. Rotating components which are attached directly to the rotor segments or segment separators are denoted in bold print. Stationary components which are affixed within the superstructure are denoted in Fig. 20 by *italics*, adjacent to the appropriate bandwidth.

On the following page, Fig. 21 is a sectional plan view of the basic rotor construction, also in 1:1 scale, showing the alternating and interlocking placement of individual rotor segments and field emitters. Figs. 22 and 23 show top and side views, respectively, of an individual field emitter and its defining dimensions which is drawn in 2:1 scale (twice actual size) for the 4ft. prototype. Fig. 24 on pg. 123 shows all named Neutral Ring parts.

Rotor Segment Dimensions



**Note:* These coupling transformers and transfer arrays are not employed in single-stage Thermal Units.

Fig. 20: radial rotor segment bandwidths. The bandwidth indicating characters are the same as those used in SpecSheet III, Fig. 24.

Fig. 22:
top view of
field emitter

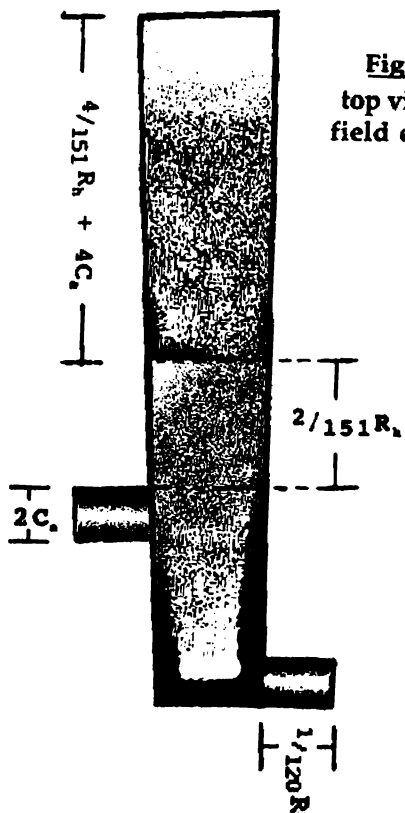


Fig. 23:
side view of
field emitter

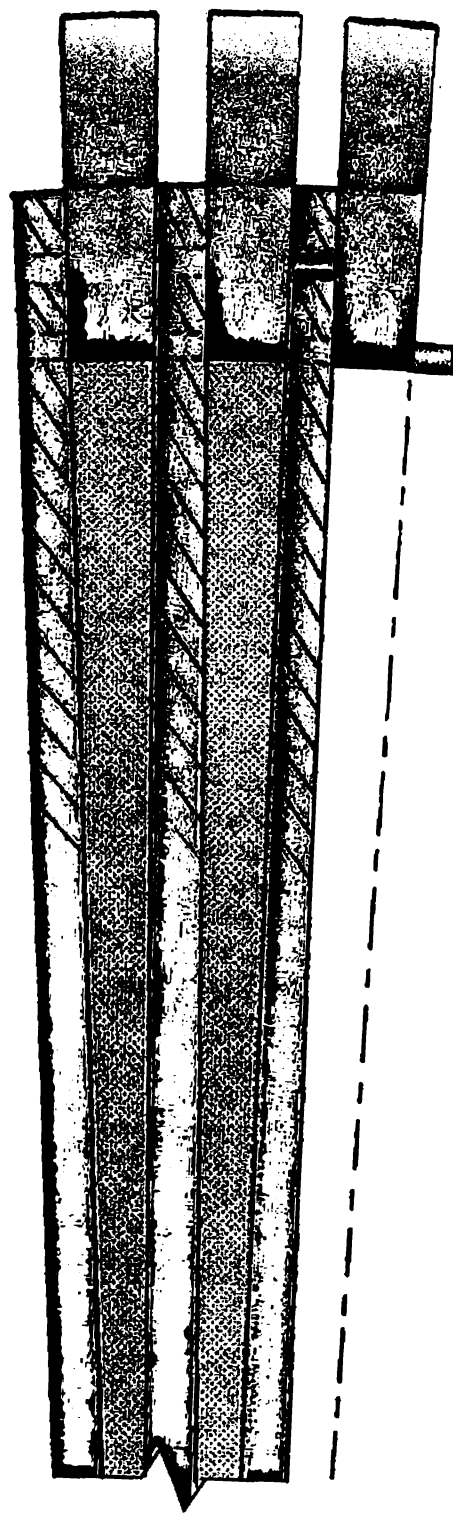
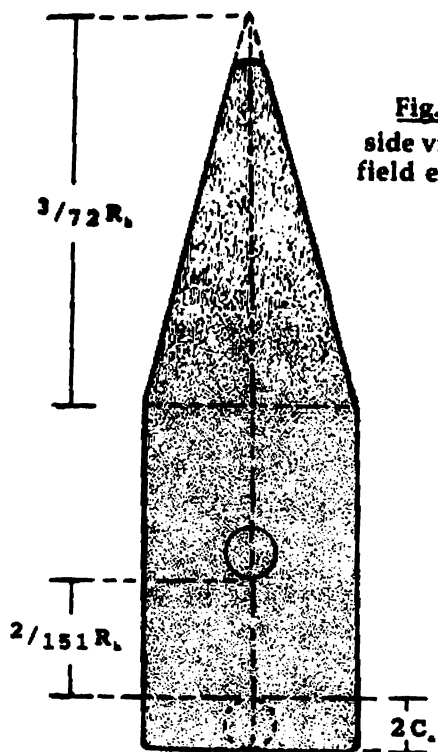


Fig. 21: basic rotor construction

Specific Rotor Segment Measurements

model: Badlander
size: 4ft. dia.

This WorkSheet is used to calculate specific rotor segment and field emitter measurements for a particular size (model) of EDF Generator, per the directives of SpecSheet II {Rotor Segment Dimensions}. To maximize the accuracy of the size-dependent computations, the vessel R_a and Neutral Ring radial width ($C_a - C_r$) from the applicable Hull Configuration Spreadsheet *must first be converted (as necessary) to either inches or centimeters.*

Section A: Rotor Segments

- 1) The *finished thickness* of each rotor segment shall be .21192".
- 2) The *milled width* of each rotor segment (with respect to the major portion of its overall length) shall be .53333".
- 3) The *design net length* of each rotor segment shall be 6.82133", not including the bushing endface shown in Fig.47.
- 4) The radial width of the *primary induction anode ring* shall be 1.00000".
- 5) The radial width of the *segment lockdown area* shall be .75000".
- 6) The design radial width of the *segment retaining end* shall be .33333", not including the bushing endface shown in Fig.47.
- 7) The axial length of the segment retaining end (with respect to its radial width) shall be 1.50000".

Section B: Field Emitters

- 1) The *radial length* of the field emitter base shall be .88380".
- 2) The *design radial length* of the field emitter tip shall be 1.00000".
- 3) The width of each field emitter shall be .53333".
- 4) The thickness of each field emitter at its thinner (inner) end shall be .42527".
- 5) The thickness of each field emitter at its thicker (outer) end shall be .48697".
- 6) The *milled diameter* of the segment locator pins shall be .12402" and the *ground length* thereof shall be .20000".
- 7) The net axial distance between each field emitter's segment locator pins shall be .31788".

Section C: Segment Separators

- 1) The maximum thickness of each segment separator shall be equal to .21192" at its inner (thinner) end, and to .42527" at its outer (thicker) end.
- 2) The maximum over-all length of each segment separator shall be equal to 5.93753", not including the bushing endface shown in Fig.47.
- 3) The maximum thickness of each refractory adhesive layer used to bond rotor segments and segment separators together shall be .003".

Rotor Ampacity

model: Badlander

size: 4ft. dia.

Before the rotor's safe operating ampacity is calculated, a computation should be made of its effective total resistance as a function of the length, cross-sectional area, and number of the individual copper segments.

[1] The resistance of each segment (R_s) may be calculated as follows:

$$R_s = \rho \frac{L}{A}, \text{ where } \rho = \text{the resistivity of copper @ } 1.724 \times 10^{-4} \text{ ohm-cm;}$$

$$L = \text{the working length of the segment in cm;}$$

$$\text{and } A = \text{the cross-sectional area in cm}^2.$$

$$\begin{aligned} \text{Here, } L &= 1/12 R_h + (C_v - C_s) \text{ {from SpecSheet II}} \\ &= 2.00" + 4.738" = 6.738 \text{ in} \\ &= 17.115 \text{ cm,} \end{aligned}$$

$$\begin{aligned} \text{and } A &= 1/45 R_h \times 4/453 R_h \\ &= .53333" \times .21192" = .11302 \text{ in}^2 \\ &= .7292 \text{ cm}^2. \end{aligned}$$

$$\text{Therefore, } R_s = \frac{(1.724 \times 10^{-4})(17.115)}{.7292} = 4.05 \times 10^{-3} \Omega.$$

The rotor's total resistance R_t is then equal to $\frac{R_s}{N_s}$, where N_s is the number of identical segments.

$$\text{Thus, } R_t = \frac{4.05 \times 10^{-3}}{180} = \underline{2.25 \times 10^{-5} \Omega}.$$

[2] To calculate the rotor's total ampacity, we must refer to DataSheet #1 (Part B) and estimate the ampacity of one segment as compared to the known ampacity of a wire gauge of comparable cross-sectional area in square inches.

In developing the ampacity ratings of standard American wire gauges, it was discovered experimentally that the safe ampacity of copper wire doubled when the square area in inches increased by an area-ampacity factor of 2.528.

Because the rotor segment area in in² will be well above the range of values given in Part B of DataSheet #1 in all but the smallest EDF Generator, the following table of powers of the area-ampacity factor allows the relevant segment area (in larger devices) to be reduced to an incremental segment area sector which does lie within the tabular data for wire of known ampacity.

$(2.528)^0 = 1$	$(2.528)^5 = 103.249$
$(2.528)^1 = 2.528$	$(2.528)^6 = 261.013$
$(2.528)^2 = 6.391$	$(2.528)^7 = 659.84$
$(2.528)^3 = 16.156$	$(2.528)^8 = 1668.08$
$(2.528)^4 = 40.842$	$(2.528)^9 = 4216.9$

Rotor Ampacity

Then, the estimated segment sector ampacity is raised to a power of 2 equal to the power to which the factor 2.528 was raised to reduce the segment area (by simple division).

Ex. area of segment (A) = .11302 in² (in the 4ft. dia. model):

(a) This square area must be reduced by the area-ampacity factor to the 0 power, or to $A/(2.528)^0$, to fall between 000 gauge @ .1318 in² and 00 gauge @ .1045 in². This corresponds to an ampacity of 240 amps and 200 amps respectively.

(b) A one amp capacity in the above range corresponds to .0006825 in². Then, .1130 in² - .1045 in² = .0085 in², and .0085/.0006825 corresponds to a 12.45 amp capacity (est.) above the lower bound. Therefore, the ampacity of each segment area sector = 200 + 12.45 = 212.45 amps.

(c) This segment sector ampacity is then multiplied by 2 to the 0 power to yield a total segment ampacity equal to $212.45 \times 2^0 = 212.45$ amps. The design rotor ampacity is thus $212.45 \times 180 = 38,241$ amps.

(d) For purposes of these Specifications and their subsequent Worksheets, the rated rotor ampacity of this model (size) device shall be equal to the integer value of the segment ampacity times the number of rotor segments, or $212 \times 180 = I_r = 38,160$ amps.

Note to Students and Engineers: Although it is not necessary in this case to undertake a determination of the design limit value of field emitter operating temperature, it may be instructive to calculate the temperature at which the peak resistance of each field emitter tip is equal to the resistance of an equal length of copper segment (in terms of solving similar types of problems).

- (a) The finished length of each emitter tip is equal to the radial length of the emitter base, at .8838", or 2.2449 cm [from WorkSheet II(a)].
- (b) The min. emitter tip thickness is equal to $(.42527" + .48697")/2$, or 1.15854 cm [from WorkSheet II(a)]. Likewise, this thickness is also equal to 2.15232 times the thickness of each segment (T_s) [from SpecSheet II].
- (c) The resistivity of the emitter composite is equal to 3.32×10^{-6} ohm-cm [from Mat. SpecSheet C]. The temperature coefficient of resistivity for copper is .00393/°C, and that of the emitter composite is .00452/°C.
- (d) The temperature at which the peak resistance of each emitter tip equals that of an equal length of copper segment, given the tungsten/copper composite specified in Mat. SpecSheet C and a 20°C base of comparison, is calculated as follows (using data from section [1] above):

$$\text{copper } R_t = (1.724 \times 10^{-6})(2.2449)/.7292 = 5.3075 \times 10^{-6} \Omega.$$

$$\text{composite } R_t = (3.32 \times 10^{-6})(2.2449)/(2.15232)(.7292) = 4.7488 \times 10^{-6} \Omega.$$

Using the general temperature-resistance rise formula,

$$R_t = R + R\alpha(t_c - 20^\circ\text{C}), \text{ where } \alpha = \text{temperature coefficient of resistivity} \\ \text{and } t_c = \text{peak operating temperature in } ^\circ\text{C},$$

$$\text{Cu } R_t = 5.3075 + 5.3075(.00393)(t - 20^\circ\text{C}) = W/\text{Cu } R_t = 4.7488 + 4.7488(.00452)(t - 20^\circ\text{C}).$$

$$\text{So, } 5.3075 + .02086(t - 20^\circ\text{C}) = 4.7488 + .02146(t - 20^\circ\text{C}),$$

$$.5587 = .0006(t - 20^\circ\text{C}),$$

$$\text{and } t_c = 951^\circ\text{C} \{132^\circ\text{C below copper's melting point}\}.$$

Field Power Output

model: Badlander

size: 4ft. dia.

Section A: Thermal Unit Peak Inherent Field Electrical Power

[1] The peak (design max.) electrical power (P_f) developed by the Drive Field of the theoretical 4ft. EDF Generator when designed as a 1n Thermal Power Unit is as follows:

$$P_f = (1.1 V_f)(I_{max}) , \quad \text{where } V_f = \text{spec. Field voltage @ } 2.9 \times 10^6 \text{ volts,} \\ \text{and } I_{max} = \text{rated rotor ampacity.}$$

$$\text{Therefore, } P_f = (3.19 \times 10^6)(38,160) \\ = 121,730,400,000 \quad \text{or} \quad 1.217 \times 10^{11} \text{ watts} .$$

This power may also be represented as 121.7 gigawatts.

[2](a) The effective total Field envelope circuit resistance (R_{tf}) which corresponds to the peak Field electrical power of the 4ft. Thermal Unit may also then be calculated as follows:

$$P_f = (I_{max})^2 R_{tf} , \quad \text{and} \quad R_{tf} = P_f / (I_{max})^2 . \\ \text{So, } R_{tf} = \frac{1.217 \times 10^{11}}{1.456 \times 10^9} = .836 \times 10^2 = 83.6 \, \Omega . *$$

* Since network resistance $R_n = 83.6 \, \Omega$ each {per WorkSheet X(a)}, the equivalent parallel resistance is 41.8 Ω . Therefore, the equivalent series vacuum chamber resistance must be 41.8 Ω as well, and the net resistance expressed by either hemichamber current considered separately must equal 83.6 Ω , as the net Field hemitorus arc resistance is all but nonexistent. See section (g) of DataSheet #14 for an important discussion of vacuum chamber resistance.

Section B: Thermal Unit Peak Kinetic Energy Output

The collision of Drive Field current with the Field Hub Zones is treated here as being virtually inelastic, hence momentum and kinetic energy are conserved separately. Drive Field current must give up all of its gained kinetic energy upon collision, and the ratio of the joint kinetic energy of each Field electron and the Field Generator after the collision to the original kinetic energy of the incident electron is in accordance with the following relation:

$$\frac{1/2(m+M)V^2}{1/2mv^2} = \frac{m}{m+M} ,$$

m = the relativistic mass of the incident electron,

M = the mass of the Field Generator,

v = the relativistic impact velocity of the incident electron,

and V = the resultant velocity of the Field Generator-and-electron.

Since $M/(m+M)$ reflects the decimal portion of the incident electron's kinetic energy released as heat, all but a minute percentage of the total gained kinetic energy of Drive Field current will be converted to heat at the nominal Field current velocity calculated in subsection B[4] below.

Field Power Output

- [1] The peak gained kinetic energy of each Drive Field electron (W) is as follows:

$$W = qV, \quad \text{where } q = \text{electron charge @ } 1.6 \times 10^{-19} \text{ coul.}, \\ \text{and } V = \text{peak Field voltage @ } 3.19 \times 10^4 \text{ volts.}$$

$$\text{Therefore, } W = (1.6 \times 10^{-19})(3.19 \times 10^4) = 5.104 \times 10^{-13} \text{ joules}.$$

- [2] The mass equivalent of this gained kinetic energy, letting $W = E_k$, is equal to m_k ,

$$\text{where } m_k = E_k/c^2 = \frac{5.104 \times 10^{-13}}{9 \times 10^{16}} = 56.71 \times 10^{-31} \text{ kg}.$$

- [3] The total relativistic mass of each Drive Field electron is equal to M_k ,

$$\text{where } M_k = m_0 + m_k = 9.11 \times 10^{-31} + 56.71 \times 10^{-31} \\ = 65.82 \times 10^{-31} \text{ kg}, \text{ or } 7.3 m_e.$$

- [4] The relativistic velocity of each incident Field electron (V_e) is as follows:

$$\text{since } M_k = \frac{m_0}{\sqrt{1 - v^2/c^2}}, \quad v/c = \sqrt{1 - (m_0/M_k)^2};$$

$$\text{so, } v/c = \sqrt{1 - (9.11/65.82)^2} = \sqrt{1 - (.1384)^2},$$

$$\text{and } v_e = .99038 c, \text{ or } 2.9711 \times 10^8 \text{ m/sec}.$$

- [5] The total relativistic kinetic energy of each incident Field electron is equal to E_k ,

$$\text{where } E_k = \frac{1}{2} M_k v_e^2 = \frac{1}{2} (65.82 \times 10^{-31}) (2.9711 \times 10^8)^2 \\ = (32.91 \times 10^{-31}) (8.8274 \times 10^{16}) \\ = 2.9051 \times 10^{-13} \text{ joules}.$$

- [6] The peak total thermal power recovered at the Field Hub Zones (P_{dt}) is then equal to the relativistic kinetic energy of each Field electron times the Field current times the electrons per coulomb:

$$P_{dt} = 6.25 \times 10^{18} (E_k I_{ext}) \\ = (6.25 \times 10^{18}) (2.9051 \times 10^{-13}) (3.816 \times 10^4) \\ = 6.93 \times 10^{10} \text{ joules/sec}.$$

This power may also be represented as 69.3 gigawatts. At this Field voltage, the total thermal power recovered equals 56.94% of the peak Field electrical power (P_t).

- [7] The gross peak thermal output (P_{gt}) is the sum of the total peak kinetic thermal power recovered (at the Zones), or P_{dt} , and the peak resistive power expended (P_{rx}):

$$P_{gt} = P_{dt} + P_{rx}, \quad \text{where } P_{rx} = 6.086 \times 10^{10} \text{ joules/sec}.$$

Field Power Output

***Note:** from WorkSheet X(a) {Field Power Resistors}.

$$\begin{aligned}\text{Thus, } P_{at} &= 6.93 \times 10^{10} + 6.086 \times 10^{10} \\ &= 13.02 \times 10^{10} \text{ joules/sec} \end{aligned}$$

Since the peak electrical power developed by the Field of the 4ft. Thermal Unit equals 12.17×10^{10} watts, the *apparent gross peak thermal output exceeds the peak electrical power by $10^{10}(13.02 - 12.17)$ or 8.5×10^9 watts (as 1 joule/sec equals 1 watt).

Section C: Thermal Unit Peak Efficiencies

Apparently, the gross thermal yield equals approximately 107% of the peak electrical power developed, an indication that the device contemplated herein would seem to achieve what some engineers might mistakenly refer to as a "free energy" mode of operation. However, this level of apparent power P_{at} is taken here to reflect the extent to which the collision of Drive Field current with the Field Hub Zones is *not completely inelastic* at the kinetic energies involved. {* see Special Glossary.}

[1] Therefore, the difference between P_{at} and real power P_t is treated rather as a direct power loss with respect to *peak drive power efficiency*, as the thermoelectric efficiency of the field power resistors approaches 100%. Thus, the *peak thermal efficiency* of this model unit is taken as representing the ratio of real to apparent power, or:

$$E_{pt} < P_t/P_{at} < 12.17/13.02 < 93.47\%.$$

[2] The *peak drive power efficiency* is then taken as representing the difference between the drive power equal to P_{at} and the impulse loss $(P_t - P_{at})$ divided by the apparent power:

$$\begin{aligned}E_{dp} &< [(P_t - P_{at}) + P_{at}]/P_{at} \\ &< [(12.17 - 13.02) + 6.93]/13.02 < 46.70\% .\end{aligned}$$

[3] The *peak drive impulse efficiency* is hence taken to be represented by the difference between the drive power and the impulse loss divided by the Field drive power:

$$\begin{aligned}E_{di} &< [(P_t - P_{at}) + P_{at}]/P_{at} \\ &< [(12.17 - 13.02) + 6.93]/6.93 < 87.73\% .\end{aligned}$$

In order to help students and engineers discriminately assess the *relative thrust characteristics* and *drive impulse efficiencies* of various model (size) Impulse Drive Units, as a function of the Field Voltage specification technique developed in WorkSheet I(a) {Specific Unit Voltage Values}, peak thrust calculations for the 4ft. diameter model are included in this WorkSheet below.

Section D: Drive Unit Peak Thrust

The thrust computations which follow are performed according to the premise of DataSheet #12 {Uniform Field Intensity Formula}, wherein it is shown that the acceleration of Drive Field current electrons is essentially uniform throughout the Field composition. Since the acceleration and potential difference are both uniform, these resultant highly-simplified "average transit time" calculations (as in Section B above) should yield sufficiently accurate Drive thrust figures for our purposes here.

Field Power Output

- [1] The peak gained kinetic energy of each Drive Field electron (W) is as follows:

$$W = qV, \quad \text{where } q = \text{electron charge @ } 1.6 \times 10^{-19} \text{ coul.}, \\ \text{and } V = \text{peak Field voltage @ } 1.1 (35.1047 \times 10^4)^*$$

$$\text{Therefore, } W = (1.6 \times 10^{-19})(38.6152 \times 10^4) = \underline{61.7843 \times 10^{-13} \text{ joules}}.$$

*Note: see WorkSheet I(a) {Specific Unit Voltage Values}.

- [2] The mass equivalent of this gained kinetic energy, letting $W = E_e$, is equal to m_e ,

$$\text{where } m_e = E_e/c^2 = \frac{61.7843 \times 10^{-13}}{8.98755 \times 10^{16}} = \underline{687.44 \times 10^{-31} \text{ kg}}.$$

- [3] The total relativistic mass of each Drive Field electron is equal to M_e ,

$$\text{where } M_e = m_0 + m_e = 9.11 \times 10^{-31} + 687.44 \times 10^{-31} \\ = \underline{696.55 \times 10^{-31} \text{ kg}}, \text{ or } \underline{76.46 m_e}.$$

- [4] The peak relativistic velocity of each incident Field electron (V_e) is as follows:

$$\text{since } M_e = \frac{m_0}{\sqrt{1 - v^2/c^2}}, \quad v/c = \sqrt{1 - (m_0/M_e)^2};$$

$$\text{so, } v/c = \sqrt{1 - (9.11/696.55)^2} = \sqrt{1 - (.013079)^2};$$

$$\text{and } v_e = \underline{.999914 c}, \text{ or } \underline{299.7668 \times 10^6 \text{ m/sec}}.$$

- [5] The total number of electrons comprising maximum Drive Field current ($\max.\Sigma$) is as follows:

$$\max.\Sigma = I_{\max} (6.25 \times 10^{18}), \quad \text{where } I_{\max} = \text{rotor ampacity};$$

$$\text{so, } \max.\Sigma = (38,160)(6.25 \times 10^{18}) = \underline{2.385 \times 10^{23} \text{ electrons}}.$$

- [6] The total peak isometric thrust developed by the Drive Field (in newtons) equals the peak change of momentum of Field current, as follows:

$$\max.\Sigma M_e \Delta V_e = (2.385 \times 10^{23})(696.55 \times 10^{-31})(299.7668 \times 10^6) \\ = \underline{4,980 \text{ nt}}.$$

Since the estimated gross weight of this Drive Unit is 884.4 nt, the level of thrust just calculated represents a total of 5.63 g of isometric Field acceleration.

- [7] The total peak unilinear thrust developed by the Field, given the considerations of SpecSheet XI {Field Current Bias Values}, is then equal to 5.63/3 or 1.877 g of net linear acceleration.

Section E: Drive Unit Peak Inherent Field Electrical Power

[1] The peak (design maximum) electrical power (P_t) developed by the Drive Field of the 4ft. EDF Generator when used as an Impulse Drive Unit may be calculated as follows:

$$P_t = (1.1 V_r)(I_{max}), \text{ where } V_r = \text{spec. Field voltage @ } 35.1047 \times 10^6 \text{ volts,} \\ \text{and } I_{max} = \text{rated rotor ampacity.}$$

$$\text{Therefore, } P_t = (38.6152 \times 10^6)(38,160) \\ = 1.474 \times 10^{12} \text{ watts.}$$

This power may also be represented as 1.474 terawatts.

[2](a) The effective total Field envelope circuit resistance (R_{df}) which corresponds to the peak Field electrical power of the 4ft. Drive Unit may also then be calculated:

$$P_t = (I_{max})^2 R_{df}, \text{ and } R_{df} = P_t / (I_{max})^2. \\ \text{So, } R_{df} = \frac{1.474 \times 10^{12}}{1.456 \times 10^9} = 1.012 \times 10^3 = 1,012 \Omega \text{ |.*}$$

* Since network resistance $R_d = 1,012 \Omega$ each {per WorkSheet X(a)}, the equivalent parallel resistance is 506Ω . Therefore, the equivalent series vacuum chamber resistance must be 506Ω as well, and the net resistance expressed by either hemichamber current considered separately must equal $1,012 \Omega$, as the net Field hemitorus arc resistance is all but nonexistent. See section (g) of DataSheet #14 for an important discussion of vacuum chamber resistance.

A Drive Unit energy output study (similar to Section B above) and a peak efficiency analysis (as in Section C) have not been done here, for the sake of brevity. The serious StarDrive student is encouraged to undertake such exercise(s) if they so desire, in which case the Thermal Unit studies will serve as a guide. At this point, I feel that the reader can certainly grasp the rather incredible potential of the EDF Generator without belaboring the issue with numbers which are admittedly difficult to embrace.

In the next SpecSheet, the precise positioning of all major rotating Primary Power System components relative to their principle stationary Neutral Ring counterparts is illustrated (as a complementary extension of Fig. 20 from SpecSheet II). As one might guess, the two component groups which fundamentally affect the positioning of all others are the variable inductor arrays - these being located virtually 'right in the middle' of the available Neutral Ring interior space. Once these are positioned, locating the magnetic ring arrays so that their size may be maximized pretty much dictates where everything else goes. In this respect, the rotating transfer triode arrays (in the 3η rotor device) are then just centered within the remaining spaces.

The vertical centerlines of the rotor ballraces, the magnetic ring arrays, and the variable inductor arrays are given in their respective SpecSheets (IV, VI, and XII). Although I did not have benefit of the use of a computer when I originally laid out the component positioning as shown, I've since been able to assure myself that without the most sophisticated 3D imaging system with which to effect *very small* improvements in specific positioning, I probably wouldn't change a thing.

In SpecSheet V and its attendant spreadsheets, the important and somewhat 'exotic' task of designing the Primary Power System's magnetic rings is undertaken. This will be one of the most interesting aspects of the EDF Generator's design for many readers with a theoretical bent. However, based on the DataSheets related to permanent magnet design and operating characteristics (especially #5 and #6), most of the mystery and potential trial-and-error problems which might be associated with the magnetic engineering required in this application have been dispelled. The resultant concise and practical method developed for magnetic ring design (which is really quite simple yet accurate) is hopefully rendered clearly understandable to all.

Rotor Component Positioning

Section A: Principal Component Layout Parameters

[1] The stationary electromagnetic Armatures comprising the two (2) Variable Inductor Arrays are to be positioned as close as possible to the actual Vertical centerline of the hull Neutral Ring.

Note: Although the stationary Armatures are, of course, not a rotor (or rotating) component, their final position will have a significant effect on the positioning of all other Primary Power System components. It should be noted that the designated Armature centerline given in SpecSheet XII is within approximately 0.11% of the above objective.

[2] Each of the Primary Power System's two (2) center Field Coils are to be positioned as close as possible to the vertical centerline of the "base" length of the rotor segments, such length being defined hereby as the specified design net length thereof plus the design length of the field emitter tip.

Note: It may seem perhaps odd or even arbitrary that the center Magnetic Rings are oriented 'backwards' with respect to the inner and outer Arrays thereof, as a function of the above requirement, especially when their close proximity to the iron-cored Armatures might in fact suggest the use of bismuth shielding to magnetically isolate the two groups from each other (for maximum Armature responsiveness).

As an "alternate embodiment of the present invention", it is entirely possible and acceptable to 'turn around' the center Rings, thereby reversing the relative positioning of the center Rings and Coils (and placing the center Coils next to the Armatures). However, such a reconfiguration of the Primary Power System requires the recalculation of much of the entire SpecSheet and WorkSheet matrix, and is certainly not necessary in the scope of our work here.

One decided advantage of the 'preferred' positioning of the center Rings and Coils illustrated in the accompanying diagram is that by properly assigning the pole positions of the center Rings, the inevitable leakage flux emanating from the outside back surfaces of the Rings is rendered series-aiding (by its very proximity) with respect to the polarity of the Armatures. Thus, it should require somewhat less input current to the Armature windings to achieve a desired output flux density than would otherwise be the case in the alternate positioning scenario.

It should also be noted (in the meantime) that the center Field Coil centerline Specification given below meets the positioning objective stated in subsection [2] above to within approximately 0.063%.

[3] All four (4) of the transfer and induction ring arrays located in the hull Neutral Ring are to have as nearly identical plate surface areas as is practicably possible, given the applicable considerations of Section B below.

Section B: Size and Position Dimensional Increments

[1] All of the fractional increments of the design hull radius R_h which are used to specify the size and/or position of Primary Power System components located in the hull Neutral Ring are to have as their denominator a whole (integer) number which is either a factor or multiple of the numbers 12 and/or 24, excepting certain minor component and adhesive layer thicknesses.

[2] The smallest such fractional increment of the design hull radius R_h that is to be used with respect to vessels of from 4ft. to 100ft. in diameter is

Rotor Component Positioning

1/9600, yielding a minimum increment of relative size and/or position specification equal to .0025" in the 4ft. diameter prototype model (designated 'Badlander') and .0625" (or 1/16") in the 100ft. diameter model to be designated 'Toltec'.

Section C: Component Specifications

Note: The alphabetic characters referred to below are used to denote radial bandwidths around the rotor assembly as illustrated in the accompanying diagram of Fig. 24.

[1] **Field Coils**- The Field Coils which generate the major portion of applied rotor voltage in the EDF Generator shall be positioned as follows:

- (a) the inner Field Coils shall be located upon a vertical radial center-line at $\frac{6166}{9600} R_n$ within rotor bandwidth E;
- (b) the center Field Coils shall be located upon a vertical radial center-line at $\frac{6495}{9600} R_n$ within rotor bandwidth G; and
- (c) the outer Field Coils shall be located upon a vertical radial center-line at $\frac{7045.84}{9600} R_n$ within rotor bandwidth I.

[2] **Transfer Ring Arrays**- The two (2) voltage transfer electrode ring arrays employed in the Primary Power System of 3 η rotor devices to connect the three Field Coils thereof in series combination shall be positioned as follows:

- (a) the inner transfer ring arrays shall be positioned between radial vertical reference lines situated at $\frac{1569}{2400} R_n$ and $\frac{1597}{2400} R_n$, having plate surface area which entirely fills rotor bandwidth F; and
- (b) the outer transfer ring arrays shall be positioned between radial vertical reference lines situated at $\frac{6815}{9600} R_n$ and $\frac{6918}{9600} R_n$, having plate surface area which entirely fills rotor bandwidth H.

[3] **Induction Ring Arrays**- The two (2) induction electrode ring arrays of each major semicircuit of the Primary Power System, which impress the DC voltage generated therein across the rotor assembly, shall be positioned as follows:

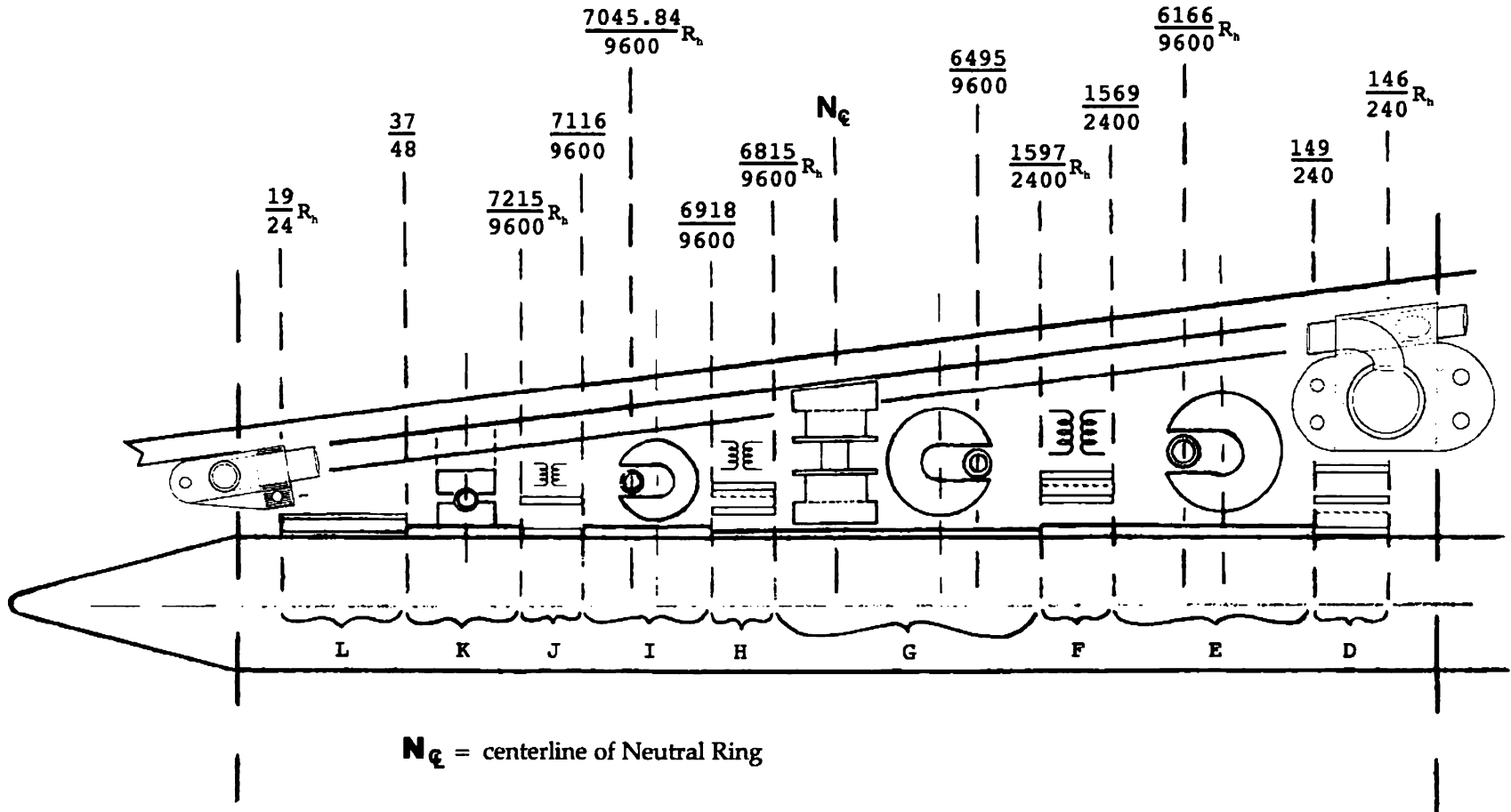
- (a) the inner (triode) induction ring arrays shall be positioned between radial vertical reference lines situated at $\frac{146}{240} R_n$ and $\frac{149}{240} R_n$, having plate surface area which entirely fills rotor bandwidth D; and
- (b) the outer (diode) induction ring arrays shall be positioned between radial vertical reference lines situated at $\frac{7116}{9600} R_n$ and $\frac{7215}{9600} R_n$, having plate surface area which entirely fills rotor bandwidth J.

[4] **Field Ballast Capacitors**- The two (2) field capacitors which store sufficient charge removed from the hull Positive Zones to support the requisite voltage expansion ratio shall be positioned between radial vertical reference lines situated at $\frac{37}{48} R_n$ and $\frac{19}{24} R_n$, having plate surface area which fills no less than 20% of rotor bandwidth L in both 1 η and 3 η rotor devices.

The following diagram exemplifies the Specifications given above, and is accurately drawn to a scale of 1.46:1 for the 4ft. diameter prototype model.

NEUTRAL RING cross section

123



Rotor Component Positioning

Fig. 24: schematic side view showing the relative radial width and placement of major rotor assembly components. A stationary anode ring is shown in zone D, and interstage coupling transformers in zones F, H, & J.

Rotor Ballrace Construction

The construction parameters presented here for the two (2) mechanical bearing assemblies used to center and stabilize the rotor within the vacuum chamber are derived from a thorough analysis of the standard small bore ultra-high-speed steel ball bearing commonly designated R3 within the bearing industry. Because these bearing assemblies must run unlubricated in a very hot electric and magnetic environment, a specialized ceramic compound is utilized for both balls and raceways.

Even with superior hardness (twice that of bearing-grade stainless steel) and centrifugal ball loading characteristics (due to lower material density), these non-magnetic ceramic bearing assemblies would be operating near the very upper limit of ball rotation velocity at nominal rotor speed. Because of the ceramic balls' much greater stiffness compared to steel, and correspondingly increased brittleness, they require a greater ball-to-race conformance to increase the contact pressure ellipse. Thus, the only significant changes to the R3 design parameters employed are a thickening of the raceway channel base and deepening of the raceway channel itself.

Also, instead of a formed metallic ball carrier assembly, a free-floating 'slider' post is used between adjacent balls to provide low-drag uniform positioning of the balls within the raceway. Hexagonal hot-pressed billets having a star-spoked cross-section are formed to near-net length (twice the ball diameter) and are flat and parallel end-face ground only, to produce a sliding ball spacer which takes advantage of the ceramic material's very low coefficient of friction (.17 unlubricated).

The Specifications developed below are deemed suitable for application to EDF Generators of all sizes, and provide a readily feasible mechanical alternative to zero-friction electromagnetic positioning systems (similar to that used in mag-lev train technology) of vastly greater complexity.

[1] The finished diameter of each raceway ball shall be equal to exactly $1/256 R_n$, and a total of 405 such balls shall be used in each raceway.

[2] The finished ground length of each hexagonal sliding ball spacer shall be equal to exactly twice ball diameter at $1/128 R_n$, and a total of 405 such spacers shall be used in each raceway.

[3] The vertical centerline of the raceway channels of each rolling bearing assembly shall be positioned at $73/96 R_n$, near the outer circumference of the rotor, and each such raceway shall completely encircle the rotor and vessel superstructure at that radial distance from the vessel's vertical centerline. As presently contemplated herein, the preceding three (3) Specifications regarding raceway balls, spacers, and channels therefore yield a 'cold' average ball-to-spacer clearance equal to $1\frac{1}{8}$ of ball diameter.

[4] The minimum thickness of the raceway channel base shall be equal to $1/384 R_n$, on the vertical centerline thereof.

[5] The maximum outside thickness of the raceway itself shall be equal to the ball diameter, at $1/256 R_n$.

[6] The raceway channels shall be ground in very close conformance to the specified diameter of the balls to a maximum finished depth equal to $1/768 R_n$, on the vertical centerline thereof, and should be composed of an absolute minimum number of sectional pieces to minimize the number of end-to-end joints.

[7] The overall radial width of each raceway shall be equal to $7/768 R_n$, as shall also be the overall installed height of each rolling bearing assembly, yielding a vertical stationary raceway-to-rotating raceway clearance of $1/768 R_n$ and a raceway horizontal flange width marginally greater than $1/384 R_n$.

SpecSheet IV obviously addresses the issue of *precisely positioning the rotor itself* within the Drive Ring. Meeting this not-inconsiderable but purely mechanical challenge will ultimately determine the Field Generator's basic feasibility, mostly with respect to maintaining the tight Field Coil gap clearances within the Magnetic Rings we'll be studying next. And, although the composite rotor assembly will in larger machines have rolling momentum akin to that of a freight train, it must evidence virtually no axial or radial 'run-out'. I'd therefore like to offer some further thoughts on what I feel represents the Generator's **advanced rotor design**.

The preferred method of eliminating axial run-out at the rotor periphery is still the simple ball-and-raceway method, described in the preceding SpecSheet, which Searl is reputed to have used even in the earliest levity discs. At one time I discussed AC electromagnetic positioning systems with an electrical engineer qualified in this field, but quickly decided they were much more complex and costly, and ultimately less reliable, than the silicon nitride bearing assemblies. The multi-planar ring gear drive system developed for the *carrier assembly* is also contemplated to eliminate inboard axial run-out in the most direct and cost-effective manner, and is the single-best improvement over early Searl design (in eliminating any central axle(s)). This carrier assembly, which minimizes radial run-out, is shown in detail in Section 6 of Mat. SpecSheet C {Rotor Components}.

Unitizing the principal 540 separate large rotor pieces into a tightly-bound composite assembly, to prevent any 'racking' of the segments in the vertical axis or any twisting in the horizontal axis, requires the use of segment locator pins (or 'post-and-hole' construction) as shown in SpecSheet II. This simple but effective technique ensures minimal rotor distortion under dynamic load conditions, when combined with the use of a space-age refractory adhesive to bond the separators to the segments. Once the rotor electrode rings are soldered in place, the resultant assembly should be mechanically strong enough to withstand operation at the tremendous tip speeds that will be evident in large machines.

Another aspect of advanced rotor design in this application would be the use of transfer triode arrays to render a three-stage level of AC signal voltage pre-amplification across the rotor. In the interests of brevity, no Specifications per se for the rotating *interstage coupling transformers* (required in 3η rotor construction) have been included in this book. Transformers are generally not used as rotating components and, were *these* of typical iron-core design, a minor problem could be presented related to dynamic balancing and stability considerations.

It is envisioned that unilayer transformer primary and secondary windings would best be applied to thin toroid air-core forms, or equal and uniformly-spaced arc-sections of such form, to create each of these stage coupling units. The single layer design promotes great accuracy in figuring the coupling coefficient, and the light weight and uniformly-distributed mass of such an arrangement promotes their mounting stability and dynamic balance.

Only one mildly problematic area of rotor design remains: it should be noted that in both 1η and 3η devices, a thin recessed conductive trace along the top of one separator will be needed to connect each outer transfer array anode to its center field coil (similar to the way the ballast capacitors are to be connected). [See Section G of SpecSheet VIII(e).]

Magnetic Ring Dimensions

The primary goal in fixing the dimensional relationships involved in the *Magnetic Ring configuration* is two-fold: to establish a mean magnet length-to-length of flux gap ratio (L_g/L_e) which, when multiplied by the magnet's leakage factor (a function of its end/gap area-to-gap length ratio and minor circumference), yields a working B/H ratio or magnetic load-line which is at or very near the 'knee' of the chosen alloy's demagnetization curve. Attaining this objective will enable the Magnetic Rings to operate at their maximum energy product for optimal efficiency.

In this regard, it must be stressed that the outside diameter of the finished Field Coil must be known precisely before the final general dimensions of its companion Magnetic Rings may be specified. The Coil and Ring sets therefore tended to evolve together under a dynamic (and somewhat tedious) on-going volumetric analysis, and the following Specifications are thus intended to apply to models of all sizes. However, it should be noted that modest improvements in the working flux density of all of the Magnetic Ring shapes may be effected when trim hull configuration improvements are instituted (thereby increasing the net outer volume of the hull Neutral Ring).

[1](a) The *major outside diameter (OD)* of the Magnetic Rings comprising the outer circular arrays thereof shall be equal to $1/72 R_h$.

(b) The major OD of the Magnetic Rings comprising the center circular arrays thereof shall be equal to $1/60 R_h$.

(c) The major OD of the Magnetic Rings comprising the inner circular arrays thereof shall be equal to $1/50 R_h$.

[Therefore, as currently specified above, the major OD of the center Rings shall be 1.2 times that of the outer Rings, and the major OD of the inner Rings shall likewise be 1.2 times that of the center Rings.]

[2](a) The *minor (axial) OD* of each such Magnetic Ring shall be equal to $5/16$ of its major OD.

(b) The *formed inner diameter (ID)* of each such Magnetic Ring shall be equal to $3/8$ of its major OD.

[3] The *rough as-formed flux gap* of each size Magnetic Ring employed in a given size vessel, as currently specified herein, is as follows:

(a) The rough flux gap of each outer Magnetic Ring shall be equal to its formed ID.

(b) The rough flux gap of each center Magnetic Ring shall be equal to its formed ID minus $1/1500 R_h$.

(c) The rough flux gap of each inner Magnetic Ring shall be equal to its minor OD.

(d) The *minimum clearance* between each magnet end/gap face and the finished surface of its companion Field Coil shall be equal to $1/6000 R_h$, or .002" times the vessel R_h as measured in feet. Each such magnet face

Magnetic Ring Dimensions

shall be ground to a smooth finish which yields a uniform flux gap length equal to such Coil's outside diameter plus said clearance.

It should be noted that this gap-to-coil clearance, while both typical and desirable in traditional electromagnetic engineering terms, may not prove entirely practicable in reality. Any increase in this clearance ratio which is found to be necessary in practice should be strictly minimized, and implemented with the trim hull configuration changes which would allow a corresponding increase in L_z and/or the ratio of L_z/L_r for all three (3) sizes of Magnetic Rings used in a given vessel model.

Additional slight increases in the L_z/L_r ratio would then be possible as well for the center and outer Magnetic Rings to effect an increase in their working gap flux density. Ideally, all three (3) Ring sizes should operate as close as possible to a B/H ratio of 18, as calculated prior to the use of counterflux wafers (described elsewhere in material associated with these Specifications), given the current Material Specification of alloy Alnico V-OR1 for the Magnetic Rings of all models.

The side view diagram below shows a center Magnetic Ring and Field Coil cross section drawn according to the Specifications given hereinabove, at a scale of 6.818 to 1 for the 4ft. diameter prototype model. Also shown (at the center of the Ring) is the optional counterflux wafer which may be employed to effect a significant increase in working gap flux density.

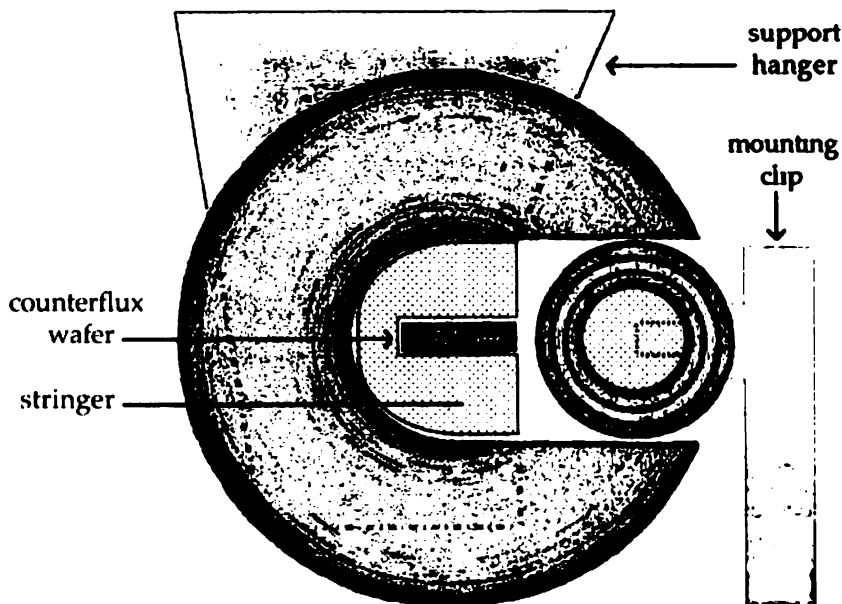


Fig. 25: Magnetic Ring and Field Coil configuration.

Note: An alternate embodiment of the Ring and Coil configuration shown would be to rotate the whole arrangement 90° clockwise, such that the flux gap is perpendicular to (and facing) the rotor surface. This orientation results in somewhat simplified mounting requirements for all three Coil sizes, but involves a significant reduction in the total Coil turns possible for the inner and outer Coils. The stainless steel coil mounting clips are depicted, as are the notched ring array hangers which engage the sectional mounting stringers.

Specific Magnetic Ring Measurements

model: Badlander

size: 4ft. dia.

This WorkSheet is used to calculate the specific Magnetic Ring measurements needed to determine the working gap flux density (in WorkSheet V(b) developed by each of the three sizes of Rings used in a particular size (model) vessel. All these ring measurements must be specified in centimeters, regardless of the units used to indicate the pertinent vessel R_n in the Hull Configuration Spreadsheet.

To avoid confusion and/or error, each of the first four [4] such final measurements for each size Ring should herein be converted to cm as necessary only after all of the underlying computations are completed in the original units used to indicate R_n . This WorkSheet references SpecSheet V {Magnetic Ring Dimensions}.

Section A: Outer Magnetic Rings

$$[1] \text{ major OD} = 1/72 R_n = 24/72" = .3333" = .8466 \text{ cm}$$

$$[2] \text{ minor OD} = (5/16)(24/72)" = .1042" = .2647 \text{ cm}$$

$$[3] \text{ formed ID} = (3/8)(24/72)" = .1250" = .3175 \text{ cm}$$

Note: The specific measurement next to be determined, the flux gap length, is a dual function of the finished Field Coil OD (developed in WorkSheet VII(a)) and the coil-to-magnet clearance (given in SpecSheet V). This consideration of course also applies to the corresponding portions of Sections B and C below.

$$[4] \text{ flux gap length } [L_g] = .1297" + 2(.004") = .1377" = .3498 \text{ cm}$$

$$\begin{aligned} [5] \text{ mean magnet length } [L_m] &= 1/2[\pi(\text{major OD}) + \pi(\text{formed ID}) - 2L_g] \\ &= 1/2[\pi(.8466) + \pi(.3175) - 2L_g] \text{ cm} \\ &= 1/2(2.6597 + .9975 - .6996) \text{ cm} \\ &= 1.4788 \text{ cm} \end{aligned}$$

$$\begin{aligned} [6] \text{ axial circumference } [c_a = c_i] &= \pi(\text{minor OD}) \\ &= .8316 \text{ cm} \end{aligned}$$

$$\begin{aligned} [7] \text{ end/gap area } [A_e = A_i] &= \pi[1/2(\text{minor OD})]^2 \\ &= \pi(.0175) \text{ cm}^2 \\ &= .0550 \text{ cm}^2 \end{aligned}$$

Section B: Center Magnetic Rings

$$[1] \text{ major OD} = 1/60 R_n = 24/60" = .4000" = 1.0160 \text{ cm}$$

$$[2] \text{ minor OD} = (5/16)(24/60)" = .1250" = .3175 \text{ cm}$$

Specific Magnetic Ring Measurements

$$[3] \text{ formed ID} = (3/8)(24/60)" = .1500" = \boxed{.3810 \text{ cm}}$$

$$[4] \text{ flux gap length } [L_g] = .1435" + 2(.004") = .1515" = \boxed{.3848 \text{ cm}}$$

$$\begin{aligned} [5] \text{ mean magnet length } [L_m] &= 1/2[\pi(\text{major OD}) + \pi(\text{formed ID}) - 2L_g] \\ &= 1/2[\pi(1.016) + \pi(.381) - 2L_g] \text{ cm} \\ &= 1/2(3.1919 + 1.19695 - .7696) \text{ cm} \\ &= \boxed{1.8096 \text{ cm}} \end{aligned}$$

$$\begin{aligned} [6] \text{ axial circumference } [c_a = c_g] &= \pi(\text{minor OD}) \\ &= \boxed{.9975 \text{ cm}} \end{aligned}$$

$$\begin{aligned} [7] \text{ end/gap area } [A_a = A_g] &= \pi[1/2(\text{minor OD})]^2 \\ &= \pi(.0252) \text{ cm}^2 \\ &= \boxed{.0792 \text{ cm}^2} \end{aligned}$$

Section C: Inner Magnetic Rings

$$[1] \text{ major OD} = 1/50 R_h = 24/50" = .4800" = \boxed{1.2192 \text{ cm}}$$

$$[2] \text{ minor OD} = (5/16)(24/50)" = .1500" = \boxed{.3810 \text{ cm}}$$

$$[3] \text{ formed ID} = (3/8)(24/50)" = .1800" = \boxed{.4572 \text{ cm}}$$

$$[4] \text{ flux gap length } [L_g] = .1602" + 2(.004") = .1682" = \boxed{.4272 \text{ cm}}$$

$$\begin{aligned} [5] \text{ mean magnet length } [L_m] &= 1/2[\pi(\text{major OD}) + \pi(\text{formed ID}) - 2L_g] \\ &= 1/2[\pi(1.2192) + \pi(.4572) - 2L_g] \text{ cm} \\ &= 1/2(3.8302 + 1.4363 - .8544) \text{ cm} \\ &= \boxed{2.2061 \text{ cm}} \end{aligned}$$

$$\begin{aligned} [6] \text{ axial circumference } [c_a = c_g] &= \pi(\text{minor OD}) \\ &= \boxed{1.1970 \text{ cm}} \end{aligned}$$

$$\begin{aligned} [7] \text{ end/gap area } [A_a = A_g] &= \pi[1/2(\text{minor OD})]^2 \\ &= \pi(.0363) \text{ cm}^2 \\ &= \boxed{.1140 \text{ cm}^2} \end{aligned}$$

As noted in SpecSheet V, the dimensional Specifications for each size of the magnetic rings may be refined slightly from the original fractional values given therein, but this should be attempted only during the course of an ongoing research and development program or (at the least) utilizing a powerful 3D imaging computer. It is also strongly recommended that the fractional format for these Specifications be retained, due to the encouraging success with which it has initially been employed.

In the next WorkSheet, individual magnetic ring flux densities will be computed as operated without counterflux wafers. The average Magnetic Array flux densities calculated in ΔSpecSheet VI assume the use of these components (which are recommended in larger vessels), and the improved individual ring gap flux densities in this size device are between 2.5 and 3.2% higher than if they are not employed.

Magnetic Ring Gap Flux Density

model: Badlander
size: 4ft. dia.

This WorkSheet is used to calculate the working gap flux density (B_g) achieved by each Magnetic Ring associated with the three different size Arrays thereof that are employed in a given size (model) vessel. The various dimensional measurements required are computed in WorkSheet V(a) {Specific Magnetic Ring Measurements}. The resultant flux densities figured herein are used in Design ASpecSheet VI to project the average flux density (\bar{B}) produced by each Ring Array, for purposes of calculating the vessel's rotor voltage output.

The first step involved in finding B_g is to determine the load-line, or B/H ratio, established by the Magnetic Ring configuration as a function of its magnet length-to-gap length ratio (L_m/L_g) and leakage factor (σ). The simple product of these two factors (in this application) yields the slope of the load-line, according to the following formula:

$$B/H = \sigma \frac{L_m}{L_g} . \quad \text{(see DataSheets \#5 \& \#6)}$$

Using a straight-edge, we next draw a line between the 0/0 point at the lower right-hand corner of the *Alnico V demagnetization graph* in DataSheet #3 and the point corresponding to the B/H number (along the left-hand or upper border thereof) as figured above.

Then, if we drop a vertical line from the point where this load-line intersects the OR1 alloy curve to the bottom border of the graph, we locate the point on the H (demagnetizing force) scale corresponding to the actual H_d developed by the Magnetic Ring in question: H_d representing the net field intensity within the magnet.

Finally, we may calculate B_g according to the standard permanent magnet formula $B_g = H_d L_m / L_g$. Therefore, using data from WorkSheet V(a) and the graph in DataSheet #3, the working flux density B_g (in gauss) for each size Magnetic Ring is calculated below.

Section A: Outer Magnetic Rings

- [1] $P_g = A_g / L_g = .0550 / .3498 = .1572$
- [2] $P_i = .26c_m = .26(.8316) = .2162 = P_r = .26c_r$
- [3] $P_t = P_g + P_i + P_r = .1572 + .2162 + .2162 = .5896$
- [4] $\sigma = P_t / P_g = .5896 / .1572 = 3.7506$
- [5] $L_m / L_g = 1.4788 / .3498 = 4.2276$
- [6] $B/H = (3.7506)(4.2276) = 15.86$, where $H_d = 670$ (by graphic analysis)
- [7] $B_g = H_d L_m / L_g = 670 (4.2276) = 2832 \text{ gauss} \mid$.

Due to the design methods employed throughout, the flux densities of the other two sizes of Magnetic Rings are calculated in exactly the same manner.

Section B: Center Magnetic Rings

$$[1] \quad P_i = A_i/L_i = .0792/.3848 = .2058$$

$$[2] \quad P_i = .26c_u = .26(.9975) = .2594 = P_i = .26c_i$$

$$[3] \quad P_t = P_i + P_i + P_i = .2058 + .2594 + .2594 = .7246$$

$$[4] \quad \sigma = P_t/P_i = .7246/.2058 = 3.5209$$

$$[5] \quad L_u/L_i = 1.8096/.3848 = 4.7027$$

$$[6] \quad B/H = (3.5209)(4.7027) = 16.56, \text{ where } H_u = 665 \text{ (by graphic analysis)}$$

$$[7] \quad B_i = H_u L_u/L_i = 665 (4.7027) = 3127 \text{ gauss}.$$

Section C: Inner Magnetic Rings

$$[1] \quad P_i = A_i/L_i = .1140/.4272 = .2669$$

$$[2] \quad P_i = .26c_u = .26(1.1970) = .3112 = P_i = .26c_i$$

$$[3] \quad P_t = P_i + P_i + P_i = .2669 + .3112 + .3112 = .8893$$

$$[4] \quad \sigma = P_t/P_i = .8893/.2669 = 3.3320$$

$$[5] \quad L_u/L_i = 2.2061/.4272 = 5.1641$$

$$[6] \quad B/H = (3.332)(5.1641) = 17.21, \text{ where } H_u = 659 \text{ (by graphic analysis)}$$

$$[7] \quad B_i = H_u L_u/L_i = 659 (5.1641) = 3403 \text{ gauss}.$$

The use of fractional mathematics as a means to facilitate the development *and* refinement of the Field Generator's key design aspects is perhaps nowhere more evident than in the foregoing specifications related to the Magnetic Rings. This is in large part due to the fact that both terms of the expression used to calculate the Rings' load-line (or B/H ratio) are in themselves fractions or ratios.

It was just very handy to gauge the effect of small changes in the physical geometry of the Rings (which change the magnet length-to-gap length and leakage factor ratios) if I envisioned the Rings' dimensions in terms of *fractions of a design constant* like the hull radius. Because of the Rings' simple and elegant geometry, a careful study of these spreadsheets and (more importantly) the several magnetic DataSheets in Appendix A will probably serve as as good an introduction to the *art* of permanent magnet design and circuit analysis as the student is apt to find outside a physics classroom or in any non-specialized literature.

In ΔSpecSheet VI, which serves as its own WorkSheet, the physical geometries of the three different sizes of **magnetic ring arrays** are assessed to determine the average gap flux density achieved by the number of Rings assigned to each. The primary goal here is to "pack 'em in" as tightly as possible while still leaving clearance for 5 or 6 *support hangers* per array section, these being the numbers of hangers per section envisioned as optimal (due to the layout of the Neutral Ring beams from which the hangers must be suspended). In this respect, the number of Rings selected per array section should also be evenly divisible by 4 or 5 (respectively): the extra hanger per section is at the end of the 'string'.

An example of how the numbers in this SpecSheet may be 'juggled' (if need be) would be to slightly decrease the number of Rings per inner array from 576 to 540. This increases the Ring shoulder clearance from a gross average of 14.6 mil to 15.5 mil, while the number of Rings per each of 36 sections goes from 16 to 15. 15 is of course divisible by 5, yielding 3 Rings per each of 5 subsections, with 6 hangers per section. Thus, the array section hangers themselves play a part in setting practical array Ring numbers.

Counterflux Wafers

model: Badlander

size: 4ft. dia.

An analysis of the Magnetic Ring configuration employed in the Primary Power System of the EDF Generator reveals that the rather substantial leakage losses exhibited by each Ring individually may be significantly reduced by the use of *blocking pole technique*. Not only does each Ring act as a blocking pole set with respect to each of its neighbors (once installed in the close-packed Array), and thus acts to reduce side-to-side leakage permeances, but the largest portion of leakage loss in each Ring (that across the formed inside diameter thereof) may be further diminished by installing a *counterflux wafer* in the center of the Ring.

The effective reduction in leakage losses by this method may only be estimated without extensive prototype testing. Applying a not-unrealistic total reduction of 75% in the non-fringing component of leakage losses, given both of the considerations above, the revised leakage factor ($\min.\sigma$) for each of the three sizes of Rings used in the 4ft. diameter model vessel is computed below. All substituted data is from WorkSheets V(a) and V(b).

Section A: Outer Magnetic Rings

$$[1] \quad P_t = P_i + P_s + P_r, \quad \text{where } P_i = .1572 \quad \text{and } P_r = .2162$$

$$[2] \quad \text{let } P_s = .25[.26(c_s)] = .065(.8316) = .0541$$

$$[3] \quad \text{then } P_t = .1572 + .0541 + .2162 = .4275$$

$$[4] \quad \min.\sigma = .4275/.1572 = 2.7195$$

Section B: Center Magnetic Rings

$$[1] \quad P_t = P_i + P_s + P_r, \quad \text{where } P_i = .2058 \quad \text{and } P_r = .2594$$

$$[2] \quad \text{let } P_s = .25[.26(c_s)] = .065(.9975) = .0648$$

$$[3] \quad \text{then } P_t = .2058 + .0648 + .2594 = .5300$$

$$[4] \quad \min.\sigma = .5300/.2058 = 2.5753$$

Section C: Inner Magnetic Rings

$$[1] \quad P_t = P_i + P_s + P_r, \quad \text{where } P_i = .2669 \quad \text{and } P_r = .3112$$

$$[2] \quad \text{let } P_s = .25[.26(c_s)] = .065(1.1970) = .0778$$

$$[3] \quad \text{then } P_t = .2669 + .0778 + .3112 = .6559$$

$$[4] \quad \min.\sigma = .6559/.2669 = 2.4575$$

These revised leakage factors are used in the following Δ SpecSheet to calculate maximum values of average gap flux density (\bar{B}_{\max}) within the Magnetic Arrays. These average Array figures are in turn utilized to calculate the final field winding output voltage/rotor speed ratios {in WorkSheet IX(b)} which ultimately determine the device's nominal rotational speed.

Magnetic Ring Arrays

model: Badlander
size: 4ft. dia.

The primary purpose of this special Design ΔSpecSheet is to establish the number of Magnetic Rings comprising each of the three (3) different size Arrays thereof used in a given size (model) vessel. As a function of this Specification, the individual shoulder-to-shoulder clearance between the Rings of each size Array will also be determined (to verify the mechanical feasibility of the assigned number of Rings) as will the corresponding percentage that the assigned number of Rings represents of the total possible number of Rings (with a mechanical shoulder-to-shoulder clearance which is very close to zero once the array section hangers are added).

A secondary purpose of this ΔSpecSheet is then to calculate the total flux gap area constituted by the assigned number of Rings in each such Array and the corresponding percentage such area represents of the total Field Coil silhouette area located within the flux gap region of that Array. This area percentage will then be used to determine the average (net) gap flux density \bar{B} of each Array as a whole prior to any calculation of rotor output voltage.

Section A: Outer Arrays

[1] Each of the two (2) outer Magnetic Ring Arrays, as currently specified herein, shall be composed of 900 identical stationary C-shaped (ring) magnets attached to the vessel superstructure for purposes of inducing a dc voltage in an adjoining rotating Field Coil.

$$(a) \text{ coil centerline radius} = \frac{7045.84}{9600} R_h \quad \{\text{from SpecSheet III}\}$$

$$= 17.6146"$$

$$(b) \text{ coil mean circumference} = 2\pi(17.6146) = 110.6758"$$

$$[2](a) \text{ ring minor OD} = \left(\frac{5}{16}\right)\left(\frac{1}{72}\right)R_h = .1042" \quad \{\text{from WorkSheet V(a)}\}$$

$$(b) \text{ total ring shoulder thickness} = 900(.1042) = 93.7800"$$

$$(c) \text{ ring centerline radius} = \left(\frac{35}{48}\right)R_h = 17.5000" \quad \{\text{from Section F below}\}$$

$$(d) \text{ ring major OD} = \left(\frac{1}{72}\right)R_h = .3333" \quad \{\text{from WorkSheet V(a)}\}$$

$$(e) \text{ ring shoulder radius} = [2](c) - \frac{[2](d)}{2} + \frac{[2](a)}{2} \text{ in.}$$

$$= 17.5000 - .1667 + .0521 \text{ in.} = 17.3854"$$

$$(f) \text{ ring shoulder circumference} = 2\pi(17.3854) = 109.2357"$$

$$[3] \text{ shoulder-to-shoulder clearance} = \frac{[2](f) - [2](b)}{900} = .0172"$$

Magnetic Ring Arrays

$$[4] \text{ maximum possible number of rings} = [2](f) \div [2](a) = 1,048$$

$$[5] \text{ array area saturation} = \frac{900}{[4]} \times 100\% = \overline{85.88\%}$$

* * *

$$[6](a) \text{ ring end/gap area } (A_r) = .055 \text{ cm}^2 = .00853 \text{ in}^2 \quad \{\text{from WorkSheet V(a)}\}$$

$$(b) \text{ total flux gap area } (\Sigma A_r) = 900 A_r = 7.6770 \text{ in}^2$$

$$[7](a) \text{ outer Field Coil OD} = .1297'' \quad \{\text{from WorkSheet VII(a)}\}$$

$$\begin{aligned} (b) \text{ coil silhouette area} &= \pi(R^2 - r^2) \\ &= \pi[(1a + 7a/2)^2 - (1a - 7a/2)^2] \\ &= \pi[(17.6146 + .06485)^2 - (17.6146 - .06485)^2] \\ &= \pi(312.5630 - 307.9937) \\ &= 14.3549 \text{ in}^2 \end{aligned}$$

$$[8] \text{ flux gap/coil area \%} = \frac{[6](b)}{[7](b)} \times 100\% = \frac{7.6770}{14.3549} \times 100\% = \overline{53.48\%}$$

$$[9](a) \text{ ring gap flux density } B_r = 2832 \text{ gauss} \quad \{\text{from WorkSheet V(b)}\}$$

$$(b) \text{ net array flux density } \bar{B} = [8] \times [9](a) = \overline{1515 \text{ gauss}}$$

Section B: Center Arrays

[1] Each of the two (2) center Magnetic Ring Arrays, as currently specified herein, shall be composed of 720 identical stationary C-shaped (ring) magnets attached to the vessel superstructure for purposes of inducing a dc voltage in an adjoining rotating Field Coil.

$$\begin{aligned} (a) \text{ coil centerline radius} &= \frac{6495}{9600} R_h \quad \{\text{from SpecSheet III}\} \\ &= 16.2375'' \end{aligned}$$

$$(b) \text{ coil mean circumference} = 2\pi(16.2375) = 102.0232''$$

$$[2](a) \text{ ring minor OD} = (5/16)(1/60)R_h = .1250'' \quad \{\text{from WorkSheet V(a)}\}$$

$$(b) \text{ total ring shoulder thickness} = 720(.1250) = 90.0000''$$

$$[3] \text{ shoulder-to-shoulder clearance} = \frac{[1](b) - [2](b)}{720} = \overline{.0167''}$$

$$[4] \text{ maximum possible number of rings} = [1](b) \div [2](a) = 816$$

$$[5] \text{ array area saturation} = \frac{720}{[4]} \times 100\% = \overline{88.24\%}$$

Magnetic Ring Arrays

* * *

$$[6](a) \text{ ring end/gap area } (A_g) = .0792 \text{ cm}^2 = .01228 \text{ in}^2 \quad \{\text{from WorkSheet V(a)}\}$$

$$(b) \text{ total flux gap area } (\Sigma A_g) = 720 A_g = 8.8416 \text{ in}^2$$

$$[7](a) \text{ center Field Coil OD} = .1435'' \quad \{\text{from WorkSheet VII(a)}\}$$

$$\begin{aligned} (b) \text{ coil silhouette area} &= \pi(R^2 - r^2) \\ &= \pi[(1a + 7a/2)^2 - (1a - 7a/2)^2] \\ &= \pi[(16.2375 + .07175)^2 - (16.2375 - .07175)^2] \\ &= \pi(265.9916 - 261.3315) \\ &= 14.6401 \text{ in}^2 \end{aligned}$$

$$[8] \text{ flux gap/coil area } \% = \frac{[6](b)}{[7](b)} \times 100\% = \frac{8.8416}{14.6401} \times 100\% = \boxed{60.39\%}$$

$$[9](a) \text{ ring gap flux density } B_g = 3127 \text{ gauss} \quad \{\text{from WorkSheet V(b)}\}$$

$$(b) \text{ net array flux density } \bar{B} = [8] \times [9](a) = 1888 \text{ gauss}$$

Section C: Inner Arrays

[1] Each of the two (2) inner Magnetic Ring Arrays, as currently specified herein, shall be composed of 576 identical stationary C-shaped (ring) magnets attached to the vessel superstructure for purposes of inducing a dc voltage in an adjoining rotating Field Coil.

$$\begin{aligned} (a) \text{ coil centerline radius} &= \frac{6166}{9600} R_h \quad \{\text{from SpecSheet III}\} \\ &= 15.4150'' \end{aligned}$$

$$(b) \text{ coil mean circumference} = 2\pi(15.4150) = 96.8553''$$

$$[2](a) \text{ ring minor OD} = (5/16)(1/50)R_h = .1500'' \quad \{\text{from WorkSheet V(a)}\}$$

$$(b) \text{ total ring shoulder thickness} = 576(.1500) = 86.4000''$$

$$(c) \text{ ring centerline radius} = (61/96)R_h = 15.2500'' \quad \{\text{from Section F below}\}$$

$$(d) \text{ ring major OD} = (1/50)R_h = .4800'' \quad \{\text{from WorkSheet V(a)}\}$$

$$\begin{aligned} (e) \text{ ring shoulder radius} &= [2](c) - \frac{[2](d)}{2} + \frac{[2](a)}{2} \text{ in.} \\ &= 15.2500 - .2400 + .0750 \text{ in.} = 15.0850'' \end{aligned}$$

$$(f) \text{ ring shoulder circumference} = 2\pi(15.0850) = 94.7819''$$

$$[3] \text{ shoulder-to-shoulder clearance} = \frac{[2](f) - [2](b)}{576} = \boxed{.0146''}$$

$$[4] \text{ maximum possible number of rings} = [2](f) \div [2](a) = 631$$

Magnetic Ring Arrays

$$[5] \text{ array area saturation} = \frac{576}{[4]} \times 100\% = \boxed{91.28\%}$$

* * *

$$[6](a) \text{ ring end/gap area } (A_g) = .1140 \text{ cm}^2 = .01767 \text{ in}^2 \quad \{\text{from WorkSheet V(a)}\}$$

$$(b) \text{ total flux gap area } (\Sigma A_g) = 576 A_g = 10.1779 \text{ in}^2$$

$$[7](a) \text{ inner Field Coil OD} = .1602" \quad \{\text{from WorkSheet VII(a)}\}$$

$$\begin{aligned} (b) \text{ coil silhouette area} &= \pi(R^2 - r^2) \\ &= \pi[(1a + 7a/2)^2 - (1a - 7a/2)^2] \\ &= \pi[(15.4150 + .0801)^2 - (15.4150 - .0801)^2] \\ &= \pi(240.0981 - 235.1592) \\ &= 15.5160 \text{ in}^2 \end{aligned}$$

$$[8] \text{ flux gap/coil area \%} = \frac{[6](b)}{[7](b)} \times 100\% = \frac{10.1779}{15.516} \times 100\% = \boxed{65.60\%}$$

$$[9](a) \text{ ring gap flux density } B_g = 3403 \text{ gauss} \quad \{\text{from WorkSheet V(b)}\}$$

$$(b) \text{ net array flux density } \bar{B} = [8] \times [9](a) = \boxed{2232 \text{ gauss}}$$

Since the Neutral Ring portion of each vessel is structurally divided into 36 equal sections, the outer, center, and inner Magnetic Ring Arrays should each be constructed in 36 equal sections containing 25 (or 5²), 20, and 16 (or 4²) Rings per section respectively. The choice of using these particular numbers of rings per array section is in a way aesthetic in a mathematical sense. An analysis of the data generated hereinabove (and in various alternative ring number studies) reveals, however, that any significant change or increase in these array ring numbers would probably be inadvisable.

Section D: Est'd. Max. Array Flux Density

A significant improvement in array gap flux density may be more reasonably effected by the use of *counterflux wafers*, which reduce the leakage losses exhibited by the individual component Rings. The subsequent decrease in B/H ratio causes a modest increase in H_m (magnet field intensity), as determined by repeating the graphic analysis {in WorkSheet V(b)} of the Magnetic Ring alloy's demagnetization curve. The resultant increased gap flux density is then calculated as follows:

[1] outer arrays

$$(a) \text{ min. } \sigma = 2.7195, \text{ using wafers as blocking poles.} \quad \{\text{from WorkSheet V(c)}\}$$

$$(b) \text{ new B/H} = (2.7195)(4.2276) = 11.50, \text{ where } H_m = 687 \quad \{\text{see WorkSheet V(b)}\}$$

$$(c) \text{ max. } B_g = 687 (4.2276) = \boxed{2904 \text{ gauss}}$$

$$(d) \text{ max. array flux density } (\bar{B}_{\text{max}}) = .5348 (2904) = \boxed{1553 \text{ gauss}}$$

Magnetic Ring Arrays

[2] center arrays

- (a) $\min.\sigma = 2.5753$, using wafers as blocking poles. {from WorkSheet V(c)}
- (b) $\text{new } B/H = (2.5753)(4.7027) = 12.11$, where $H_u = 683$ {see WorkSheet V(b)}
- (c) $\max.B_t = 683 (4.7027) = \boxed{3212 \text{ gauss}}$
- (d) $\max. \text{ array flux density } (\bar{B}_{\max}) = .6039 (3212) = \boxed{1940 \text{ gauss}}$

[3] inner arrays

- (a) $\min.\sigma = 2.4575$, using wafers as blocking poles. {from WorkSheet V(c)}
- (b) $\text{new } B/H = (2.4575)(5.1641) = 12.69$, where $H_u = 680$ {see WorkSheet V(b)}
- (c) $\max.B_t = 680 (5.1641) = \boxed{3512 \text{ gauss}}$
- (d) $\max. \text{ array flux density } (\bar{B}_{\max}) = .6560 (3512) = \boxed{2304 \text{ gauss}}$

Section E: Counterflux Wafers

[1] The counterflux wafer associated with each of the Magnetic Rings composing a given Array thereof shall be square in shape, having length and width equal to $2/3$ of the minor OD of each such Ring, and of a thickness equal to $1/4$ of its length or width.

[2] Such wafer shall be positioned on the horizontal centerline plane of the Ring flux gap in such a manner as to provide sufficient clearance between the outer edge of the wafer and the adjoining Field Coil so that the Coil's free rotation is not impeded.

[3] These counterflux wafers shall be composed of a very highly coercive (demagnetization-resistant) material, such as sintered ferrite, which is also relatively inexpensive and readily available.

[4] Each such wafer shall of course be positioned within the center of its companion Magnetic Ring such that its poles are facing the like poles of the Ring, to reduce flux leakage losses and thereby improve gap flux density.

Section F: Magnetic Ring Positioning

[1] The vertical centerline of each of the Magnetic Rings which make up the two (2) outer Arrays thereof shall lie on a radial vertical reference line located at $35/48 R_h$.

[2] The vertical centerline of each of the Magnetic Rings which make up the two (2) center Arrays thereof shall lie on a radial vertical reference line located at $131/192 R_h$.

[3] The vertical centerline of each of the Magnetic Rings which make up the two (2) inner Arrays thereof shall lie on a radial vertical reference line located at $61/96 R_h$.

It has probably occurred to many of you by now that, up to this point, I've really said very little about the EDF Generator's field coils. In truth, this is not because there's relatively little to say about them or that there's anything secret I don't want to reveal, but because there is *so much* that went into proper **field coil design** that I'm afraid the spreadsheets virtually have to speak for themselves. What I'll try to do here is illuminate certain aspects of the design *process* which might be instructional and not readily apparent within the rather 'dry' treatment of the spreadsheets.

The field coils must obviously relate the net performance of the magnetic ring arrays to the physical geometry of the Primary Power System in the best possible way. This simple criterion immediately suggests the use of *very fine wire*, because the magnets used are so small (compared to the size of the device). Since our objective is essentially to produce as high a voltage as possible, we will therefore want to use as many turns of this fine wire as we can.

Thus, the proper balance between coil core size, number of coil layers, and winding wire size must be struck. If our cores are too small (in an effort to increase the number of winding layers), it is likely to cause insulation stress cracking in the innermost layer(s) during the winding process. If the winding wire is too fine, it will have insufficient ampacity to carry the inevitable Primary Power System current (despite the application of the highest practical level of cutoff bias across the rotating electrode arrays). Fig. 25 of SpecSheet V best illustrates this delicate balancing of coil design criteria.

What makes the EDF Generator's Primary Power System absolutely unique as an electrical generating circuit (as far as I know) is that the field coils conduct only *a tiny portion of the load current*. This attribute speaks directly to the heart of the most difficult design challenge involved in the entire device: how to generate an enormous voltage without having the generating circuit subjected to a proportionally huge current! And, as we already know, this would not be possible without vacuum tube technology. Using cutoff bias technique, we may thus create a dual-output/single-load circuit configuration where the load (or field) current "bypasses" the generating coil (output) subcircuits. In the 4ft. prototype, the ratio of maximum *bypass current* to field coil ampacity is actually almost 49,000:1!

As was disclosed in Chapter 7 of the associated text, the field coils are *compound-wound*, each being composed of two separate windings. One winding comprises the whole of the first two layers of each field coil and constitutes the primary voltage-generating portion thereof, or *field winding*. This voltage is applied between the anode and cathode of adjacent rotor electrode arrays. The bulk of the third coil layer comprises the *bias winding*, which generates the much smaller voltage applied between the cathode and control grid of the *inner* adjacent (triode) electrode array (Figs. 27 in SpecSheet IX will help here). The remaining great challenge in field coil design was then to arrive at the correct bias voltage-to-cathode voltage ratio to achieve near-total current cutoff across these adjacent triode arrays. This Bias Voltage Ratio is developed in DataSheet #8 and is taken to be 40%, which then becomes the *base* bias winding-to-field winding turns ratio.

However, it soon became apparent that not only would the output voltages of each of the three different sizes of field coils be markedly different from one another if wound in the most uniform and efficient manner, but the third layer of each size coil would have a different *magnetic efficiency*. And, since the third layer is right where our bias winding is to be located, this situation required the calculation and use of an appropriate *turns ratio factor*! After zillions of computations, I eventually also realized that the rotating electrode arrays in 3 η rotor devices must share the total applied field winding voltage *unequally*, due to the voltage distribution characteristics of series-connected capacitances. This latter consideration resulted in a 3:1 ratio of induction array-to-transfer array potential difference within each of the two (2) *series coil groups*, given the equal array surface areas.

Thus, to make a very long story shorter, it is actually not possible to accurately determine *final* field coil winding turns ratios without *knowing* these triode potential differences *and therefore the applied bias winding voltage* required. Thus, final Bias Winding Turns Ratios are not developed until WorkSheet IX(a), after the actual applied voltages and required geometry for each rotating electrode array have been determined given the principles of proper Primary Power System circuit resolution as derived in WorkSheet VIII(a) {Series Electrode Array Capacitance}.

In conclusion, these final turns ratios take into account the aforementioned varying field coil performance characteristics (caused by different coil sizes and magnetic efficiencies), and are designed to provide a method of testing the accuracy of the assigned turns ratio factors. With this kind of complexity involved, why would I bother to obfuscate the issue . . .

Field Coil Design

The Specifications set forth herein, related to the construction of each of the three (3) different size Field Coils employed in the Primary Power System, are intended to simplify as much as possible the complex design parameters involved in fixing optimal coil winding measurements and turns composition(s). These parameters therefore relate the size of each winding core to the size of the Magnetic Rings composing its adjoining array, and the size of the wire used (to wind all three Coils) to the size of the smallest such Ring. Specific field coil measurements and bias winding turns ratios are then derived in WorkSheets VII(a) and IX(a) respectively.

- A) *Each Field Coil winding core* (used in the Primary Power System of a given size {model} vessel) shall be nonmagnetic in nature, or of powdered iron, and the outside diameter (OD) thereof shall be equal to $\frac{2}{3}$ of the minor (axial) OD of the Magnetic Rings comprising the adjoining Array thereof.
- B) *The insulated annealed copper magnet wire* used to wind each of the six (6) Field Coils employed in a given size (model) vessel shall be equal in outside diameter to the standard American wire gauge (size) which is closest to $\frac{1}{33}$ of the major OD of the outer Magnetic Rings used in that vessel. This determination is made by referencing DataSheet #1 {Copper Wire Data} under the heavy build OD column.
- C) *Each Field Coil* shall be composed of three (3) toroidal winding layers, each of which is:
 - [1] formed of turns of the appropriate wire tightly-wrapped (shoulder-to-shoulder) about the entire circumference of its respective core; and
 - [2] sealed with a dielectric adhesive bonding agent to form a 'potted' assembly.
- D) The innermost (1st) and middle (2nd) layers of each Field Coil shall be wound of a single piece of magnet wire and as such shall be entirely devoted to the "field" winding, or principal voltage-generating portion of that Coil as a whole.
- E) [1] The third (3rd) layer of each Field Coil shall be largely devoted to the "bias" winding, or secondary voltage-generating portion of that Coil as a whole, which shall be connected either to the full length of that Coil's finished field winding in 3 η rotor devices or in series with one another in 1 η rotor devices.
 - [2] The remaining (minor) portion of each Field Coil's 3rd layer, if any, shall constitute the balance of the field winding thereof and shall be series-connected to the center layer of that Coil.
- F) [1] *The finished field winding* of each Field Coil in 3 η rotor devices shall be connected in series between the anode ring of the larger (outside) adjacent electrode ring array and the cathode ring of the smaller (inside) such adjacent array.
 - [2] *The bias winding* of each Field Coil in 3 η rotor devices shall be connected to the control grid of the smaller (inside) adjacent electrode

ring array, in parallel with the cathode ring thereof (and as otherwise directed in additional material associated with these Specifications).

[3] The field windings in 1η rotor devices shall be connected in series with one another, between the outer induction array anode ring and the inner induction array cathode ring.

[4] The bias windings in 1η rotor devices shall be connected in series between the finished length of the inner field winding and the control grid of the inner induction array, in parallel with the cathode ring thereof.

G) [1] Each layer of the outer Field Coils (of a given vessel) shall be composed of 90% of the maximum possible whole number of turns (of the specified gauge wire) that could be applied to the core thereof as a third layer, rounded to the nearest whole multiple of the number 1,000. This Specification should in every instance yield a total of exactly 10,000 turns per layer regardless of vessel size.

[2] Each layer of the center Field Coils shall then be composed of a number of turns equal to exactly 90% of the number of turns per layer used in the outer Field Coils. This Specification should in every instance yield a total of exactly 9,000 turns per layer regardless of vessel size.

[3] Each layer of the inner Field Coils shall in turn be composed of exactly $\frac{5}{6}$ of the number of turns per layer used in the outer Field Coils, rounded to the nearest whole number. This Specification should in every instance yield a total of exactly 8,333 turns per layer regardless of vessel size, except that the outermost (3rd) layer of said Coil shall contain 8,334 turns.

* * *

Once again, we can see that fractional math has been used to facilitate the careful matching of component sets of different sizes *in a uniform manner*. By doing so, it also becomes possible to achieve an expanded level of precision in making relative performance assessments and in projecting the effects of small changes in the relative dimensional specifications for the components of a given set.

It is for just these very reasons that a great deal of effort was taken (with some providence thrown in) to achieve a general field coil design scenario which allowed the use of a specified number of turns per coil equaling *even multiples of 1,000 turns* in most cases. This precept theoretically allows incremental improvements in prototype device performance to be selectively effected, through the analysis of testing data, with an accuracy approaching four decimal places!

A potential source of some confusion should be pointed out before moving on to the following coil measurement WorkSheet, having to do with the manner in which Specification Field Coil ODs are derived. I originally neglected (during research and development) to use an installed coil winding depth (or height) based on nested layers of *insulated* magnet wire, using instead non-nested layers of a slightly higher ampacity bare wire. In finishing-up this WorkSheet, I of course had to correct this situation.

As it turns out, no damage was done in applying the 'retrofitted' insulated wire specification method to the 4ft. prototype. Using the nested-layer installed height formula given in αWorkSheet XII(a) to check the resulting effect on the field coil ODs, I found (to my relief) that the new coil ODs came in 1.4 mil *under* those shown. This is in fact a desirable outcome, as the coils' specified rotational clearance with respect to their adjoining magnetic ring arrays is very tight. I have not to date ran the spreadsheet for an exhaustive variety of other vessel sizes to verify that this will always be the case, and a few different size devices could conceivably require some slight modification of the format employed.

Specific Field Coil Measurements

model: Badlander
size: 4ft. dia.

The function of this WorkSheet is to develop certain Field Coil measurement with respect to a given size (model) vessel for purposes of: (1) verifying the mechanical feasibility of the underlying Specifications related thereto; (2) assessing characteristics that are related to the performance thereof; and (3) determining dimensional factors affecting each such Coil's voltage output.

The primary determinant in the bulk of the measurement calculations performed below is the wire gauge used to wind all three (3) different size Coils. Therefore, this dimension must be established first, as follows:

- estimated wire size = $(1/33)(24/72)$ in. = $.3333/33 = .01010"$
- from DataSheet #1, #31 gauge wire "heavy build" OD = $.01050"$

Component Specification:

Therefore, all of the Field Coils of the 4ft. model EDF Generator will be wound with #31 gauge heavy build magnet wire, as this size insulated wire is the closest available to the estimated (formula) size required.

It must be stressed that although the Spec. Field Coil OD's derived below are based upon a vertically shoulder-to-shoulder (non-nested) 3-layer winding method using the size and type of magnet wire which is actually the closest in OD to the formula size from above*, it is assumed that a nested (offset shoulder) winding technique using the Specification heavy build wire would result in a Field Coil OD at or within the same Spec. Coil OD.

Section A: Outer Coil Measurements

[1](a) Component Specification:

outer Field Coil core OD = $(\frac{2}{3})(\frac{5}{16})(\frac{24}{72})$ in. = **.0695"**

(b) 1st layer mean diameter = $.06950 + .01003 = .07953$ [gauged @ #30 bare]*
= .202 cm

(c) 2nd " " " = .07953 + .02006 = .09959"
= .253 cm

(d) 3rd " " " = .09959 + .02006 = .11965"
= .304 cm

(e) 3rd layer outside dia. = .11965 + .01003 = .12968"

Specification Field Coil OD = .1297"

[2](a) 1st layer mean circumference = $\pi(.202) = .635 \text{ cm} = 6.35 \times 10^{-3} \text{ m}$

(b) 2nd " " " = $\pi(.253) = .795 \text{ cm} = 7.95 \times 10^{-1} \text{ m}$

(c) 3rd " " " = $\pi(.304) = .955 \text{ cm} = 9.55 \times 10^{-3} \text{ m}$

Specific Field Coil Measurements

- [3](a) major Coil centerline radius (R_c) = $\frac{7045.84}{9600} R_h = 17.6146''$ {SpecSheet III}
 (b) " " " diameter ($2R_c$) = 35.2292"
 (c) mean Coil circumference (C) = $2\pi R_c = 110.676'' = 2.8112 \text{ m}$
- [4](a) fully-wound Coil inner radius = $[3](a) - \frac{[1](e)}{2} = 17.54976''$
 (b) " " " " diameter = 35.0995"
 (c) " " " " circumference = 110.2683"
- [5] maximum 3rd layer number of turns = $[4](c) \div .01050''$ (Spec. wire OD)
 = 10,501
- [6] winding core density = $\frac{10,000}{[5]} \times 100\% = 95.23\%$

Section B: Center Coil Measurements

[1](a) Component Specification:

$$\text{center Field Coil core OD} = (2/3)(5/16)(24/60) \text{ in.} = .0833''$$

- (b) 1st layer mean diameter = $.08330 + .01003 = .09336''$ [gauged @ #30 bare]*
 = .237 cm
 (c) 2nd " " " = $.09336 + .02006 = .11342''$
 = .288 cm
 (d) 3rd " " " = $.11342 + .02006 = .13348''$
 = .339 cm
 (e) 3rd layer outside dia. = $.13348 + .01003 = .14351''$
Specification Field Coil OD = .1435"

- [2](a) 1st layer mean circumference = $\pi(.237) = .745 \text{ cm} = 7.45 \times 10^{-3} \text{ m}$
 (b) 2nd " " " = $\pi(.253) = .905 \text{ cm} = 9.05 \times 10^{-3} \text{ m}$
 (c) 3rd " " " = $\pi(.304) = 1.065 \text{ cm} = 1.065 \times 10^{-2} \text{ m}$

- [3](a) major Coil centerline radius (R_c) = $\frac{6495}{9600} R_h = 16.2375''$ {SpecSheet III}
 (b) " " " diameter ($2R_c$) = 32.475"
 (c) mean Coil circumference (C) = $2\pi R_c = 102.0235'' = 2.5914 \text{ m}$
- [4](a) fully-wound Coil inner radius = $[3](a) - \frac{[1](e)}{2} = 16.16575''$
 (b) " " " " diameter = 32.3315"
 (c) " " " " circumference = 101.5724"

Specific Field Coil Measurements

[5] maximum 3rd layer number of turns = $[4](c) \div .01050"$ (Spec. wire OD)
= 9,673

$$[6] \text{ winding core density} = \frac{9,000}{[5]} \times 100\% = 93.04\%$$

Section C: Inner Coil Measurements

[1](a) Component Specification:

inner Field Coil core OD = $(\frac{2}{3})(\frac{5}{16})(\frac{24}{50})$ in. = .1000"

(b) 1st layer mean diameter = $.10000 + .01003 = .11003$ [gauged @ #30 bare]*
= $.280 \text{ cm}$

(c) 2nd " " " = .11003 + .02006 = .13009"
= .330 cm

(d) 3rd " " " = .13009 + .02006 = .15015"
= .381 cm

(e) 3rd layer outside dia. = $.15015 + .01003 = .16018"$

Specification Field Coil OD = .1602"

[2](a) 1st layer mean circumference = $\pi(.280) = .880 \text{ cm} = 8.80 \times 10^{-3} \text{ m}$

(b) 2nd " " " = $\pi(.330) = 1.037 \text{ cm} = 1.037 \times 10^{-2} \text{ m}$

(c) 3rd " " " = $\pi(.381) = 1.197 \text{ cm} = 1.197 \times 10^{-2} \text{ m}$

[3](a) major Coil centerline radius (R_c) = $\frac{6166}{9600} R_h = 15.415"$ {SpecSheet III}

(b) " " " diameter (2R.) = 30.830"

(c) mean Coil circumference (C) = $2\pi R_c = 96.8555'' = 2.4601 \text{ m}$

$$\begin{aligned} [4](a) \quad \text{fully-wound Coil inner radius} &= [3](a) - \frac{[1](e)}{2} \\ &= 15.3349" \end{aligned}$$

(b) " " " " diameter = 30.6698"

(c) " " " " circumference = 96.3520"

[5] maximum 3rd layer number of turns = $[4](c) \div .01050"$ (Spec. wire OD)
= 9,176

$$[6] \text{ winding core density} = \frac{8,333}{[5]} \times 100\% = 90.81\%$$

Section D: Output Voltage/Rotor Speed Ratios

This WorkSheet Section is devoted to sample calculations of the output voltage-to-rotor speed ratio for each Field Coil as a simple yet effective means of assessing how well the design of each Coil is matched to the size of

Specific Field Coil Measurements

the Magnetic Rings comprising the adjoining Array thereof. Since the center Magnetic Rings are 1.2 times the size of the outer Rings, and the inner Rings are 1.2 times the size of the center Rings, the relative voltage/rotor speed ratios of the center and inner Field Coils should show a very similar relationship respectively if the Magnetic Rings and their adjoining Coils are well-matched. For purposes of these computations, the Coil 2nd layer mean circumference is used as a measure of the mean winding length per turn.**

[1] outer Coil mean output ratio

$$V_o/r = N\bar{B}_{\max}\pi dC, \text{ where } N = 10,000 \text{ turns,} \\ \bar{B}_{\max} = .1553 \text{ Wb/m}^2, \{ \text{see SpecSheet VI, } \Delta D \} \\ \pi d = A[2](b) = 7.95 \times 10^{-3} \text{ m,} \\ C = A[3](c) = 2.8112 \text{ m,} \\ \text{and } r = \text{rev/sec.}$$

$$\begin{aligned} \text{Therefore, } V_o/r &= (1 \times 10^4)(.1553)(7.95 \times 10^{-3})(2.8112) \\ &= (79.5)(.43658) \\ &= \boxed{34.71 \text{ volts/rev/sec.}} \end{aligned}$$

[2] center Coil mean output ratio

$$V_c/r = N\bar{B}_{\max}\pi dC, \text{ where } N = 9,000 \text{ turns,} \\ \bar{B}_{\max} = .1940 \text{ Wb/m}^2, \{ \text{see SpecSheet VI, } \Delta D \} \\ \pi d = B[2](b) = 9.05 \times 10^{-3} \text{ m,} \\ C = B[3](c) = 2.5914 \text{ m,} \\ \text{and } r = \text{rev/sec.}$$

$$\begin{aligned} \text{Therefore, } V_c/r &= (9 \times 10^3)(.1940)(9.05 \times 10^{-3})(2.5914) \\ &= (81.45)(.50273) \\ &= \boxed{40.95 \text{ volts/rev/sec.}}, \end{aligned}$$

and $40.95/34.71 = 1.180$ or 98.33% of the corresponding Magnetic Ring relative size ratio (1.2).

[3] inner Coil mean output ratio

$$V_i/r = N\bar{B}_{\max}\pi dC, \text{ where } N = 8,333 \text{ turns,} \\ \bar{B}_{\max} = .2304 \text{ Wb/m}^2, \{ \text{see SpecSheet VI, } \Delta D \} \\ \pi d = C[2](b) = 1.037 \times 10^{-2} \text{ m,} \\ C = C[3](c) = 2.4601 \text{ m,} \\ \text{and } r = \text{rev/sec.}$$

$$\begin{aligned} \text{Therefore, } V_i/r &= (8.333)(.2304)(1.037 \times 10^{-2})(2.4601) \\ &= (86.41)(.56681) \\ &= \boxed{48.98 \text{ volts/rev/sec.}}, \end{aligned}$$

and $48.98/40.95 = 1.196$ or 99.67% of the corresponding Magnetic Ring relative size ratio (1.2).

****Note:** The derivation of the Coil Voltage Formula is explained in DataSheet #7.

Turns Ratio Factors

model: Badlander

size: 4ft. dia.

An analysis of a given Field Coil's silhouette area relative to the total flux gap area of its adjoining Magnetic Ring Array reveals that a portion of the outer winding layer of each Coil lies outside the true flux gap of the Array, within the fringing field thereof. In the case of the outer Ring Array, a very small portion of the second (middle) winding layer actually extends into the fringing field.

In more traditional electromagnetic engineering designs, this consideration might be of negligible import as the voltage induced in each turn of the Coil would usually be a function of the total flux enclosed by the turn. Thus, the flux density within the very small area of the fringing field involved would be factored with the true gap flux density into the comparatively much-larger total enclosed flux area, and the resultant 'average' flux density would be very close to full gap flux density as the fringing field density must perforce approach gap density at positions very near the perimeter of the gap.

In the specific case of the three different size Field Coil and Magnetic Ring Array sets employed in the Primary Power System, however, the voltage induced in each turn of the Coil is a function of the local flux density which the physical material of the wire intersects. Therefore, the somewhat reduced flux density within the fringing field, even at the close proximity to the true flux gap of the applicable winding layer(s), has a significant effect on the voltage induced within each involved wire turn to the extent that two (2) significant ("side") portions of its overall circumference lie within the fringing field.

Should acceptable operation of the Primary Power System depend upon predicting exactly the value of the induced Coil voltage output at a given rotor speed, a world of mathematical complexity would necessarily be opened up. Within this application, though, we must only provide sufficient 3rd-layer output voltage to ensure the cutoff-bias of Primary Power System current throughout the operating rpm range: in other words, an adequate 3rd-layer field winding-to-bias winding turns ratio [see WorkSheet IX(a)].

If this Bias Winding Turns Ratio is somewhat on the high side, due to a slightly inflated Turns Ratio Factor, an acceptable boosting of rotor output voltage at nominal rotor speed (beyond that predicted) would merely result. Only extensive prototype testing will establish the accuracy of the simple Turns Ratio Factor developed below (for each of the three Field Coil sizes of the 4ft. diameter model), equal to the Field Coil OD-to-Magnetic Ring minor OD ratio:

Section A: Outer Coil/Ring Sets

- [1] outer Field Coil OD = .1297" {from WorkSheet VII(a)}
- [2] Magnetic Ring minor OD = .1042" {from WorkSheet V(a)}
- [3] let Turns Ratio Factor = $.1297 / .1042 = 1.24$

Section B: Center Coil/Ring Sets

- [1] center Field Coil OD = .1435" {from WorkSheet VII(a)}
- [2] Magnetic Ring minor OD = .1250" {from WorkSheet V(a)}
- [3] let Turns Ratio Factor = .1435/.1250 = 1.15

Section C: Inner Coil/Ring Sets

- [1] inner Field Coil OD = .1602" {from WorkSheet VII(a)}
- [2] Magnetic Ring minor OD = .1500" {from WorkSheet V(a)}
- [3] let Turns Ratio Factor = .1602/.1500 = 1.07

The Turns Ratio Factors above are divided into the 3rd layer output ratios first computed in WorkSheet VII(c) for each size Field Coil, to yield an estimated net 3rd layer output ratio reflecting the reduced flux density believed to act upon 3rd layer turns in each case.

It is important to note that the Field Coil vertical centerline radius is taken throughout these WorkSheets (for simplicity's sake) to be equal to that of a theoretical horizontal Ring flux gap of zero length, which therefore has a circular cross section equal in OD to the minor OD of the Ring.

In reality, the parallel ground end/gap faces of each Magnetic Ring have an elliptical cross section, the major axis of which is greater than the minor OD of the Ring, and the actual vertical centerline radius thereof will be very slightly less than the Field Coil centerlines specified.

The effect of matching the Coil centerlines with those of the elliptical end/gap faces may serve to reduce or eliminate the Turns Ratio Factors as developed herein, and should be the subject of further computer modeling and analysis.

WorkSheet VII(c)

Field Coil Output Ratios

model: Badlander
size: 4ft. dia.

This WorkSheet is used to calculate the individual output voltage-to-rotor speed ratio of each layer (as a whole) of the three different size Field Coils employed in a given size (model) vessel. The nominal rotational speed, in revolutions per minute, may then be determined {in WorkSheet IX(b)} although a Specification Rotor Speed cannot be established without the extensive prototype testing required to demonstrate and refine the accuracy of the design methods employed throughout these Specifications.

Section A: Outer Field Coils

- [1](a) 1st layer output ratio = $V_{o1}/r = N\bar{B}_{max}\pi dC$, where $N = 10,000$ turns,
 $\bar{B}_{max} = .1553 \text{ Wb/m}^2$,
 $\pi d = 6.35 \times 10^{-1} \text{ m}$,
and $C = 2.8112 \text{ m}$.

Field Coil Output Ratios

$$\begin{aligned}\text{Thus, } V_{o1}/r &= (1 \times 10^4)(.1553)(6.35 \times 10^{-3})(2.8112) \\ &= (63.5)(.43658) \\ &= \underline{27.72 \text{ volts/rev/sec.}}\end{aligned}$$

(b) 2nd layer output ratio = $V_{o2}/r = N\bar{B}_{\max}\pi dC$, where $N = 10,000$ turns,
 $\bar{B}_{\max} = .1553 \text{ Wb/m}^2$,
 $\pi d = 7.95 \times 10^{-3} \text{ m}$,
and $C = 2.8112 \text{ m}$.

$$\begin{aligned}\text{Thus, } V_{o2}/r &= (1 \times 10^4)(.1553)(7.95 \times 10^{-3})(2.8112) \\ &= (79.5)(.43658) \\ &= \underline{34.71 \text{ volts/rev/sec.}}\end{aligned}$$

(c) 3rd layer output ratio = $V_{o3}/r = N\bar{B}_{\max}\pi dC$, where $N = 10,000$ turns,
 $\bar{B}_{\max} = .1553 \text{ Wb/m}^2$,
 $\pi d = 9.55 \times 10^{-3} \text{ m}$,
and $C = 2.8112 \text{ m}$.

$$\begin{aligned}\text{Thus, } V_{o3}/r &= (1 \times 10^4)(.1553)(9.55 \times 10^{-3})(2.8112) \\ &= (95.5)(.43658) \\ &= \underline{41.69 \text{ volts/rev/sec.}}\end{aligned}$$

- Since the 3rd layer Turns Ratio Factor must be taken into account to reflect the *estimated* reduced flux density acting upon 3rd layer turns:

$$\text{net } V_{o3}/r = 41.69/1.24 = \underline{33.62 \text{ volts/rev/sec.}} \quad \{\text{see WorkSheet VII(b)}\}$$

Section B: Center Field Coils

[1](a) 1st layer output ratio = $V_{c1}/r = N\bar{B}_{\max}\pi dC$, where $N = 9,000$ turns,
 $\bar{B}_{\max} = .1940 \text{ Wb/m}^2$,
 $\pi d = 7.45 \times 10^{-3} \text{ m}$,
and $C = 2.5914 \text{ m}$.

$$\begin{aligned}\text{Thus, } V_{c1}/r &= (9 \times 10^3)(.1940)(7.45 \times 10^{-3})(2.5914) \\ &= (67.05)(.50273) \\ &= \underline{33.71 \text{ volts/rev/sec.}}\end{aligned}$$

(b) 2nd layer output ratio = $V_{c2}/r = N\bar{B}_{\max}\pi dC$, where $N = 9,000$ turns,
 $\bar{B}_{\max} = .1940 \text{ Wb/m}^2$,
 $\pi d = 9.05 \times 10^{-3} \text{ m}$,
and $C = 2.5914 \text{ m}$.

$$\begin{aligned}\text{Thus, } V_{c2}/r &= (9 \times 10^3)(.1940)(9.05 \times 10^{-3})(2.5914) \\ &= (81.45)(.50273) \\ &= \underline{40.95 \text{ volts/rev/sec.}}\end{aligned}$$

Note: Although a very small "slice" of the center Field Coil's 2nd layer does extend into the fringing field on each side of the flux gap, its effect is deemed negligible with respect to this output voltage ratio calculation.

Field Coil Output Ratios

(c) 3rd layer output ratio = $V_{c3}/r = N\bar{B}_{max}\pi dC$, where $N = 9,000$ turns,
 $\bar{B}_{max} = .1940$ Wb/m²,
 $\pi d = 1.065 \times 10^{-2}$ m,
and $C = 2.5914$ m.

$$\begin{aligned}\text{Thus, } V_{c3}/r &= (9 \times 10^3)(.1940)(1.065 \times 10^{-2})(2.5914) \\ &= (95.85)(.50273) \\ &= 48.19 \text{ volts/rev/sec.}\end{aligned}$$

- Since the 3rd layer Turns Ratio Factor must be taken into account to reflect the *estimated* reduced flux density acting upon 3rd layer turns:

$$\text{net } V_{c3}/r = 48.19/1.15 = \boxed{41.90 \text{ volts/rev/sec.}} \{\text{see WorkSheet VII(b)}\}$$

Section C: Inner Field Coils

[1](a) 1st layer output ratio = $V_{i1}/r = N\bar{B}_{max}\pi dC$, where $N = 8,333$ turns,
 $\bar{B}_{max} = .2304$ Wb/m²,
 $\pi d = 8.80 \times 10^{-3}$ m,
and $C = 2.4601$ m.

$$\begin{aligned}\text{Thus, } V_{i1}/r &= (8,333)(.2304)(8.80 \times 10^{-3})(2.4601) \\ &= (73.33)(.56681) \\ &= \boxed{41.56 \text{ volts/rev/sec.}}\end{aligned}$$

(b) 2nd layer output ratio = $V_{i2}/r = N\bar{B}_{max}\pi dC$, where $N = 8,333$ turns,
 $\bar{B}_{max} = .2304$ Wb/m²,
 $\pi d = 1.037 \times 10^{-2}$ m,
and $C = 2.46$ m.

$$\begin{aligned}\text{Thus, } V_{i2}/r &= (8,333)(.2304)(1.037 \times 10^{-2})(2.4601) \\ &= (86.41)(.56681) \\ &= 48.98 \text{ volts/rev/sec.}\end{aligned}$$

(c) 3rd layer output ratio = $V_{i3}/r = N\bar{B}_{max}\pi dC$, where $N = 8,334$ turns,
 $\bar{B}_{max} = .2304$ Wb/m²,
 $\pi d = 1.197 \times 10^{-2}$ m,
and $C = 2.46$ m.

$$\begin{aligned}\text{Thus, } V_{i3}/r &= (8,334)(.2304)(1.197 \times 10^{-2})(2.4601) \\ &= (99.76)(.56681) \\ &= 56.54 \text{ volts/rev/sec.}\end{aligned}$$

- Since the 3rd layer Turns Ratio Factor must be taken into account to reflect the *estimated* reduced flux density acting upon 3rd layer turns:

$$\text{net } V_{i3}/r = 56.54/1.07 = \boxed{52.84 \text{ volts/rev/sec.}} \{\text{see WorkSheet VII(b)}\}$$

Section D: Combined Coil Group Voltage Output Ratio

$$\begin{aligned}V_{tg}/r &= [V_{c1}/r + V_{c2}/r + \text{net } V_{c3}/r] + [V_{i1}/r + V_{i2}/r + \text{net } V_{i3}/r] + [V_{c1}/r + V_{i2}/r + \text{net } V_{i3}/r] \\ &= 96.05 + 116.56 + 143.38 = \boxed{355.99 \text{ volts/rev/sec.}}\end{aligned}$$

Electrode Array Construction

This SpecSheet prescribes certain of the materials, dimensions, and construction techniques to be employed in each of the different types of electrode arrays found in the Primary Power System of the EDF Generator.

Section A: Field Ballast Capacitors

[1] The negative plate of each Field Ballast Capacitor shall be composed of non-magnetic nickel alloy sheet stock measuring $1/768 R_n$ in thickness, and shall be silver-soldered to the rotor segments.

[2] The positive plate of each said Ballast Capacitor shall be composed of non-magnetic nickel alloy sheet stock measuring $1/960 R_n$ in thickness, and shall be bonded to an outside ceramic insulating layer of equal thickness with a high-temperature dielectric adhesive.

[3] The construction of each such Capacitor shall otherwise be subject to the conditions and directions of WorkSheet VIII(e) {Field Ballast Capacitors}, incorporated herein by reference.

Section B: Triode Transfer Arrays

[1] Each rotating anode and cathode* ring comprising the transfer ring arrays employed in the Primary Power System of 3 η rotor devices shall be composed of non-magnetic nickel alloy sheet stock measuring $1/960 R_n$ in thickness, and shall be bonded to an outside ceramic insulating layer of equal thickness with a high-temperature dielectric adhesive. [* see Note in DataSheet #9.]

[2] The control grid electrode of each such transfer array shall be composed of single layer turns of nickel-chromium alloy wire of diameter designated t_1 .

[3] Each such triode transfer array shall be constructed in such a manner that it exhibits a minimum design amplification factor (μ) equal to 4.0, although modest increases in this factor may be effected to improve Primary Power System efficiency after requisite research and development.

[4] The construction of each transfer array shall otherwise be subject to the conditions and directions of WorkSheet VIII(a) {Series Electrode Array Capacitance}, incorporated herein by reference.

Section C: Diode & Triode Induction Arrays

[1] The rotating cathode* ring of each inner (triode) induction ring array and the rotating anode ring of each outer (diode) induction ring array shall be composed of non-magnetic nickel alloy sheet stock measuring $1/960 R_n$ in thickness, *except for the inner induction array cathode ring*, and shall be bonded to an outside ceramic insulating layer of equal thickness with a high-temperature dielectric adhesive. [* see Note in DataSheet #9.]

[2] Each rotating inner induction array cathode ring shall be composed of non-magnetic nickel alloy sheet stock measuring $2/960 R_n$ in thickness, and shall not be bonded to an outside ceramic insulating layer so that it may induce a positive voltage upon an adjacent stationary diode induction ring.

Electrode Array Construction

[3] The stationary diode induction ring adjoining each inner induction ring array shall be composed of non-magnetic nickel alloy sheet stock measuring $1/960 R_h$ in thickness, and shall be bonded to an outside ceramic insulating layer of equal thickness with a high-temperature dielectric adhesive.

[4] The anode of each triode induction ring array and the cathode* of each outer (diode) induction ring array shall be composed of non-magnetic nickel alloy sheet stock measuring $1/768 R_h$ in thickness, and shall be silver-soldered to the rotor segments. [* see Note in DataSheet #9.]

[5] The control grid of each such triode induction ring array shall be composed of nickel-chromium alloy open-mesh wire screen of thickness designated $4t_c$, per the directives of Material SpecSheet D (Section 1[b]).

[6] Each such triode induction array shall be constructed in such a manner that it exhibits a minimum design amplification factor (μ) equal to 4.0, although modest increases in this factor may be effected to improve Primary PowerSystem efficiency after requisite research and development.

[7] The construction of each such induction ring array shall otherwise be subject to the conditions and directions of WorkSheet VIII(a) {Series Electrode Array Capacitance}, incorporated herein by reference.

Section D: Pentode Induction Arrays

[1] The EDF Generator's two (2) Primary Induction Ring Arrays (or "Primary Arrays") shall be divided into 36 separate equal unit pentode arrays, thus forming two (2) ring-shaped groups of such pentode arrays in parallel between the field power resistors and the two (2) rotating unit anode rings mounted on the rotor.

[2] The rotating unit anode ring associated with each of these two (2) ring-shaped groups of 36 unit pentode arrays shall be composed of target-grade tungsten plate measuring $1/384 R_h$ in thickness, and shall be silver-soldered to the rotor segments.

[3] The stationary cathode element of each said pentode array shall be composed of cathode-grade tungsten plate measuring $1/384 R_h$ in thickness, and shall be mechanically affixed to the rotor-facing end surface of its associated field power resistor with high-temperature ceramic retaining pieces. Such cathodes may also be either thoriated (impregnated with thorium oxide) or sub-monolayer thorium metal adsorbed, to achieve the necessary surface work function ϕ and emissivity factor $e^{-\phi/kT}$ with respect to the Field Emitters, depending on the model (size) and unit (type) of device to be constructed (see DataSheet #13 and Section 2 of Material SpecSheet C).

[4] The stationary control, accelerator, and suppressor grids of each said pentode array shall be composed of filament-grade tungsten wire and arranged such that each turn of the accelerator and suppressor grids are shaded from the cathode by a control grid turn, per Material SpecSheet D (Section 1[b]).

[5] Each such unit pentode array shall be constructed in such a manner that it exhibits a minimum design amplification factor (μ) equal to 12.0, although modest increases in this factor may be effected to improve the overall signal voltage gain in 3η rotor devices after the requisite research and development.

[6] The construction of each such unit pentode array shall otherwise be subject to the conditions and directions of WorkSheet VIII(c) {Pentode Potential Differences} incorporated herein by reference.

The previous two major spreadsheet series have dealt (in one way or another) with the geometry and performance of the Field Generator's magnetic arrays. The next such series of spreadsheets defines the geometry of its *electric arrays*, and examines in some detail the performance aspects thereof. These four WorkSheets related to electrode array construction are not only the longest in the Basic Specifications, but are also the most important and complex.

The first WorkSheet of this series {Series Electrode Array Capacitance} is principally concerned with correctly determining the rotor's various **electrode array voltages**. These values must of course be known to the highest accuracy possible before any appropriate electrode spacings may be calculated. Once this has been done, a brief *breakdown intensity analysis* is provided to verify that the specified spacings should not result in any unanticipated arc-discharge conditions during operation.

In WorkSheet VIII(b) {Triode Potential Differences}, peak operating values for these electrode voltages are used to determine appropriate circuit resistor values and current levels, with an emphasis on promoting signal voltage amplification performance in the 3η rotor device. In this respect, DataSheets #9 - #11 should be considered required reading for most before a thorough perusal of this WorkSheet is attempted. Of special interest to electrical engineers might be the incorporated final Section E on *triode array amplification factor*, which deals with theoretical considerations related to increasing such signal amplification capability.

WorkSheet VII(c) {Pentode Potential Differences} performs essentially the same function with respect to the *unit pentode arrays* (comprising the two Primary Induction Ring Arrays) as the previous WorkSheet did with regard to the rotating triode arrays. A highly simplified schematic representation which shows the relative positioning of each unit pentode array's primary electrodes and grids with respect to one another and to the rotor's Primary Power System semicircuits is provided in Fig. 26 of this WorkSheet.

Finally, the next two spreadsheets develop the specifications required for the Field Ballast Capacitors to establish the desired expansion of the external Field voltage relative to the device's rotor voltage. As has hopefully been clearly explained in the associated text, the extent to which the Field voltage is expanded is both defined and achieved through control of the ratio by which the cathodes of the these unit pentode arrays are rendered tremendously more electron-emissive than the rotor field emitters. In reading and assessing these somewhat difficult WorkSheets, reference should often or as necessary be made to the schematics of SpecSheet IX {Power System Schematics}. Taken together with the electrode array WorkSheets, these schematics should provide sufficient illumination of the more technical aspects of the Field Generator's method of operation.

The WorkSheets associated with SpecSheet IX are (at this time) limited to very basic considerations of Primary Power System circuit wiring and related operating characteristics. However, this combined series IX spreadsheet group may easily be expanded in a research lab/shop setting as an active development program proceeds, and bound independently as a separate manual if desired.

WorkSheet IX(a) calculates the final *bias winding turns ratios* for both 1η and 3η rotor variants of a given size (model) device. It is important to note that these ratios as shown are the ratio of each Field Coil's field winding turns-to-bias winding turns, with the latter (bias) turns number being unity. Thus, an increase in the triode array amplification factor used in a given device will cause an increase in the number of field turns available per bias turn and a concomitant but limited increase in Primary Power System efficiency.

Then, the nominal rotor speed of the particular device in question is verified in WorkSheet IX(b) {Field Coil Voltage Values}, as is the dependent design value of *series coil group* voltage. Attention is directed to the interesting Rotor Speed Table of Fig. 29, from which it is evident that the actual operational rotor speed of this machine observed in testing *could be significantly less* than that calculated in the WorkSheet (and shown in the uppermost left corner position of the Table). For instance, were the actual hull static capacitance equal to that figured as if it were a parallel plate capacitor (at a "ballast factor" of 1.00), the actual rotor speed would be a minimum of about 966 rpm.

Thus, it can be seen that engineers working to accurately ensure an acceptable standard operating rotor speed as this device is scaled larger will have already had to perform numerous tests on smaller machines to learn how to *accurately* calculate the hull static capacitance given the design hull configuration and how this static capacitance changes with small changes in that hull configuration.

Series Electrode Array Capacitance

model: Badlander

size: 4ft. dia.

The purpose of this WorkSheet is to calculate the individual primary capacitance and voltage drop of each electrode ring array employed in the Primary Power System of both 1 η and 3 η rotor devices, as well as the collective series capacitance of the either two (2) or four (4) electrode ring arrays used in association with each of its two (2) series Field Coil groups.

The primary capacitance of each electrode array is taken here to represent that which exists between the cathode and anode thereof, and may be used to determine certain Primary Power System resonant frequency characteristics. As a fundamental design criteria, the areas of all of the electrode arrays (figured herein) are as nearly equal as possible.

The secondary capacitance of each triode array, or that which exists between grid and anode, should also be calculated provided a suitable means of estimating the effective grid area is employed. This secondary grid capacitance for each stage would then be added (in parallel) to that of the respective cathode.

Section A: Circuit Resolution

Before either the individual or total capacitance of the electrode ring arrays employed in each of the two (2) series coil groups may be calculated, the final plate spacing of each such array must be known. And, prior to the determination of these plate spacings, the projected peak potential difference across each capacitive array must therefore be calculated. Thus, the relevant series circuit capacitances and voltage drops must be computed in accordance with the following set of empirical principles which reflect traditional rules of proper circuit resolution.

(1) The sum of the voltage drops (potential difference or ΔV) across the capacitive electrode ring pairs within each of the two (2) circuit series loops of the Primary Power System must equal the sum of the generated voltages applied within that loop. Thus, the series capacitances share the total source voltage, splitting it inversely proportional to their individual capacitances.

(2) All capacitive plates within each circuit series loop must exhibit the same induced charge Q , as the current in a series circuit is everywhere the same and hence the total charge is equal to the charge on each such plate.

(3) The absolute value of the voltage expressed upon each rotor induction ring will **approach** twice (2x) that of either of the adjacent plates which are mutually-opposed across the rotor circuit leg common to both series loops.

(4) To obtain equal voltage drops across each induction array, the induction array primary capacitances must be equal. To simplify circuit resolution as much as possible, the transfer array capacitances in 3 η rotor devices should also be equal to one another.

(5) To obtain optimum performance in a 3 η rotor device, the series sum of the final peak potential differences expressed across the field windings of either group should equal the peak voltage impressed across the rotor. Given the operation of principle (4) above, this condition only occurs when the induction array capacitances are equal to 1/3 that of the transfer arrays. Therefore, the peak ΔV across each of the two (2) transfer arrays in each

circuit series loop should equal 1/8 of the projected peak *Primary System Voltage*, and the peak ΔV across each of the two (2) induction arrays in each such loop should equal 3/8 of this same projected peak voltage.

(6) Finally, the actual bias voltage rise experienced by each circuit series loop will be shared by the capacitive ring pairs therein, splitting it inversely proportional to their respective individual capacitances.

Section B: 1 η Thermal Unit

In the 1 η Thermal unit, the peak *Primary System Voltage* of 1.1(11,599.2) or 12,759.12 volts will be split evenly between the two (2) induction arrays of each series coil group, given the operation of principles (1) and (4) above, and the voltage drop across each is therefore 6,379.56 volts. In light of principle (3), the absolute value of the inner induction cathode and outer induction anode voltages will be equal to 2,126.52 (or 1/3 the voltage drop).

The rotor induction ring voltages will then each be twice this value, at 4,253.04 volts, and the peak voltage impressed across the rotor becomes 8,506.08. Thus, it can be seen that the rotor voltage in a 1 η device is equal to 2/3 of the *Primary System Voltage* developed.

[1] Inner Induction Arrays

From DataSheet #8, the peak bias voltage applied to each inner induction array control grid should be equal to 40% of the peak *unbiased* ΔV across the array, or $.40(4,556.83) = 1,822.73$ volts.

Since this represents a negative voltage which is added in series with the cathode voltage, the total negative voltage represented is equal to $(-2,126.52) + (-1,822.73)$, or -3,949.25 volts. With the rotor induction anode ring at +4,253.04 volts, the total peak potential difference between grid and anode equals 8,202.29 volts.

(a) grid-to-anode spacing:

The net separation distance between each inner induction array grid and anode (d_g) must be marginally greater than that which would allow an arc-discharge level of electric field intensity ($\approx 3 \times 10^6$ v/m) to be established between these electrodes at the peak potential difference above. We may calculate the initial nominal value of the grid-to-anode distance d_g as follows:

$$d_g > 8,202.29 / 3 \times 10^6 > 2.734 \times 10^{-3} = .2734 \text{ cm, or } .1076''.$$

Because a marginal buffer distance should in practice be added to d_g , we will divide this nominal distance by the ratio 11/12 (selected for use as a maximum value at this time), or .9167, to calculate the spec. final minimum separation distance d_{gs} as follows:

$$\text{Specification Electrode Spacing } d_{gs} = d_g / .9167 = .2982 \text{ cm, or } .1174''.$$

Note: This same method of computing final minimum electrode spacings is used in each applicable instance below.

(b) cathode-to-anode spacing:

In light of the plate spacing considerations outlined in DataSheet #9 {Electrostatic Load-Line Formula}, the nominal distance between the cathode of each inner induction array and the anode thereof (inner D_i) may be calculated as follows:

$$\begin{aligned} \text{inner } D_k &= \text{inner } d_{gr} + \left(\frac{\text{inner } d_{gr}}{\mu - 1} \right), \text{ where } \mu = 4. \\ &= .2982 \text{ cm} + .0994 \text{ cm} \\ &= .3976 \text{ cm, or } .1565". \end{aligned}$$

Component Specification:

Before a final cathode-to-anode spacing ($\text{inner } D_{kt}$) may be determined, the actual thickness of the grid itself must be taken into account. Assigning a Specification Triode Grid Wire Diameter equal to 1/3.19 times the Field Coil winding wire diameter, or the winding wire gauge plus 10 gauge numbers, the resultant nichrome grid wire size (40 ga.) equals .003145" in diameter. Per SpecSheet VIII, transfer array $t_g = .003145"$.

By using this size grid wire to create a relatively open-mesh screen, the half-thickness of the grid screen closest to the induction array anode will equal $2(.003145")$ or $2t_g = .00629"$.

$$\begin{aligned} \text{Therefore, Spec. Electrode Spacing } \text{inner } D_{kt} &= \text{inner } D_k + 2t_g \\ &= .1565" + .00629" \\ &= \boxed{.1628"}. \end{aligned}$$

Note: The final grid-to-anode spacing of each triode induction array in 3η rotor devices is determined in a manner based on this method of electrode spacing.

(c) cathode-to-anode capacitance:

$$\begin{aligned} \text{[i] area} &= A_{ii} = \pi(R^2 - r^2) \\ &= \pi[(149/240 R_h)^2 - (146/240 R_h)^2] \text{ (from SpecSheet III)} \\ &= \pi[(14.9")^2 - (14.6")^2] \\ &= \pi(222.01 - 213.16) \text{ in}^2 = 27.803 \text{ in}^2 \end{aligned}$$

$$\begin{aligned} \text{Therefore, } A_{ii} &= (27.803 \text{ in}^2)(6.4516 \text{ cm}^2/\text{in}^2) \\ &= 179.37 \text{ cm}^2, \text{ or } 1.794 \times 10^{-2} \text{ m}^2. \end{aligned}$$

$$\text{[ii] capacitance} = C_{ii} = \frac{\epsilon_0 A_{ii}}{\text{inner } D_{kt}}, \text{ where } \text{inner } D_{kt} = .1628", \text{ or } .4135 \text{ cm.}$$

$$\begin{aligned} C_{ii} &= \frac{(8.85 \times 10^{-12})(1.794 \times 10^{-2})}{4.135 \times 10^{-3}} \\ &= 15.877 \times 10^{-14} / 4.135 \times 10^{-3} = \boxed{3.840 \times 10^{-11} \text{ farad}}. \end{aligned}$$

[2] Outer Induction Arrays

(a) cathode-to-anode capacitance:

$$\begin{aligned} \text{[i] area} &= A_{oi} = \pi(R^2 - r^2) \\ &= \pi[(7215/9600 R_h)^2 - (7116/9600 R_h)^2] \text{ (from SpecSheet III)} \\ &= \pi[(18.0375")^2 - (17.79")^2] \\ &= \pi(325.351 - 316.484) \text{ in}^2 = 27.857 \text{ in}^2 \end{aligned}$$

$$\begin{aligned} \text{Therefore, } A_{oi} &= (27.857 \text{ in}^2)(6.4516 \text{ cm}^2/\text{in}^2) \\ &= 179.72 \text{ cm}^2, \text{ or } \boxed{1.797 \times 10^{-2} \text{ m}^2}. \end{aligned}$$

[ii] Because the outer induction array capacitance must be equal to that of the inner induction array, we may provide this value and the area

figured above in the capacitance equation and solve for the necessary plate spacing distance (which will differ only marginally from that of the inner induction array) as follows:

$$\text{capacitance} = C_{oi} = \frac{\epsilon_o A_{oi}}{d_o}, \text{ where } C_{oi} = \boxed{3.840 \times 10^{-11} \text{ farad}}.$$

$$3.840 \times 10^{-11} = \frac{(8.85 \times 10^{-12})(1.797 \times 10^{-2})}{d_o}, \text{ and}$$

$$\text{Spec. Electrode Spacing } d_o = 15.903 \times 10^{-14} / 3.840 \times 10^{-11} = .4141 \text{ cm, or } \boxed{.1630"}.$$

[3] ln Total Series Capacitance

Capacitors in series combine in the same manner as resistors in parallel. Therefore, the total primary series capacitance (C_{st}) associated with each series Field Coil group of this Thermal Unit ln rotor is as follows:

$$1/C_{st} = 1/C_{ii} + 1/C_{oi}$$

$$C_{st} = 1/ (.26042 + .26042) \times 10^{-11}$$

$$C_{st} = 1/.52084 \times 10^{-11} = 1.9200 \times 10^{-11} \text{ farad} = \boxed{19.200 \text{ muf}}.$$

Section C: 3η Drive Unit

In the 3η Drive unit, the peak *Primary System Voltage* of 1.1(11,599.2) or 12,759.12 volts will be split unevenly between the two (2) induction arrays and two (2) transfer arrays of each series coil group, given the operation of principles (1), (4), and (5) above. The voltage drop across each induction array will be equal to 3/8 of this peak voltage or 4,784.67 volts, and the voltage drop across each transfer array will be equal to 1/8 peak voltage or 1,594.89 volts. In light of principle (3), the absolute value of the inner induction cathode and outer induction anode voltages will be equal to 1,594.89 (or 1/3 the voltage drop across the induction arrays).

The rotor induction ring voltages will then each be twice this value, at 3,189.78 volts, and the peak voltage impressed across the rotor becomes 6,379.56. Thus, it can be seen that the rotor voltage in a 3η device is equal to 1/2 of the *Primary System Voltage* developed.

[1] Outer Transfer Arrays

From DataSheet #8, the peak bias voltage applied to each outer transfer Array control grid should be equal to 40% of the peak unbiased ΔV across the array, or .40 (1,139.21) = 455.684 volts.

Since this represents a negative voltage which is added in series with the cathode voltage, and the cathode voltage equals negative one-half of the peak potential difference of 1,594.89, the total negative grid voltage represented is equal to (-797.445) + (-455.684), or -1,253.129 volts. With the transfer anode ring at +797.445 volts, the total peak potential difference between grid and anode equals 2,050.57 volts.

(a) grid-to-anode spacing:

As in subsection B[1](a) above, we may calculate the initial nominal value of the grid-to-anode distance $outer d_g$ as follows:

$$outer d_g > 2,050.57 / 3 \times 10^6 > 6.835 \times 10^{-4} \text{ m} = .06835 \text{ cm, or } .0269".$$

$$\text{Spec. Electrode Spacing } outer d_g = outer d_g / .9167 = .0746 \text{ cm, or } .0294".$$

(b) cathode-to-anode spacing:

As in subsection B[1](b) above, the nominal distance between the cathode of each outer transfer array and the anode thereof (outer D_k) may be calculated as follows:

$$\begin{aligned} \text{outer } D_k &= \text{outer } d_{kr} + \left(\frac{\text{outer } d_{kr}}{\mu - 1} \right), \text{ where } \mu = 4. \\ &= .0746 \text{ cm} + .0249 \text{ cm} \\ &= .0995 \text{ cm}, \text{ or } .0392". \end{aligned}$$

Therefore, Spec. Electrode Spacing $\text{outer } D_{kr} = \text{outer } D_k + t_p^*$

***Note:** Single-layer grid construction is used in the transfer arrays, and the entire wire thickness is added to nominal plate spacing because of the high field intensity.

$$\begin{aligned} &= .0392" + .003145" \\ &= \boxed{.0423"}. \end{aligned}$$

(c) cathode-to-anode capacitance:

$$\begin{aligned} \text{[i] area} &= A_{ot} = \pi(R^2 - r^2) \\ &= \pi[(6918/9600 R_k)^2 - (6918/9600 R_k)^2] \quad \{\text{from SpecSheet III}\} \\ &= \pi[(17.295")^2 - (17.0375")^2] \\ &= \pi(299.117 - 290.276) \text{ in}^2 = 27.775 \text{ in}^2 \end{aligned}$$

$$\begin{aligned} \text{Therefore, } A_{ot} &= (27.775 \text{ in}^2)(6.4516 \text{ cm}^2/\text{in}^2) \\ &= 179.19 \text{ cm}^2, \text{ or } \boxed{1.792 \times 10^{-2} \text{ m}^2}. \end{aligned}$$

$$\text{[ii] capacitance} = C_{ot} = \frac{\epsilon_o A_{ot}}{\text{outer } D_{kr}}, \text{ where outer } D_{kr} = .0423", \text{ or } .1074 \text{ cm.}$$

$$\begin{aligned} C_{ot} &= \frac{(8.85 \times 10^{-12})(1.792 \times 10^{-2})}{1.074 \times 10^{-3}} \\ &= 15.859 \times 10^{-14} / 1.074 \times 10^{-3} = \boxed{14.766 \times 10^{-11} \text{ farad}}. \end{aligned}$$

Note: The outer transfer array grid wire support pins may have to be recessed slightly into the working electrode area itself to provide adequate physical clearance to the Stationary Armatures and/or outer Magnetic Rings. The radial width of the electrode rings should then be expanded as necessary to compensate such that the total area is held equal.

[2] Inner Transfer Arrays

Note: The inner transfer array control grid is herein referred to as the 'center' grid, for purposes of a concise unique nomenclature, as it is the laterally middle one of the three triode control grids in each series Coil group.

The peak bias voltage applied to each inner transfer array is equal to that applied to the outer transfer array control grids, at **455.684 volts**. The peak ΔV between the grid and anode of each inner transfer array is equal to that of the outer transfer arrays, at **2,050.57 volts**.

(a) cathode-to-anode capacitance and electrode spacings:

$$\begin{aligned} \text{[i] area} &= A_{it} = \pi(R^2 - r^2) \\ &= \pi[(1597/2400 R_k)^2 - (1569/2400 R_k)^2] \quad \{\text{from SpecSheet III}\} \\ &= \pi[(15.97")^2 - (15.69")^2] \\ &= \pi(255.041 - 246.176) \text{ in}^2 = 27.850 \text{ in}^2 \end{aligned}$$

$$\begin{aligned} \text{Therefore, } A_{it} &= (27.850 \text{ in}^2)(6.4516 \text{ cm}^2/\text{in}^2) \\ &= 179.69 \text{ cm}^2, \text{ or } \boxed{1.797 \times 10^{-2} \text{ m}^2}. \end{aligned}$$

[ii] Because the inner transfer array capacitance must be equal to that of the outer transfer array, we may provide this value and the area figured above in the capacitance equation and solve for the necessary cathode-to-anode plate spacing distance (which will differ only marginally from that of the outer transfer array) as follows:

$$\text{capacitance} = C_{it} = \frac{\epsilon_o A_{it}}{\text{center } D_{it}}, \text{ where } C_{it} = \boxed{14.766 \times 10^{-11} \text{ farad}}.$$

$$14.766 \times 10^{-11} = \frac{(8.85 \times 10^{-12})(1.797 \times 10^{-2})}{\text{center } D_{it}},$$

$$\text{and center } D_{it} = 15.903 \times 10^{-14} / 14.766 \times 10^{-11} = .1077 \text{ cm, or } \boxed{.0424"}. .$$

Thus, because the discrepancy between the primary plate spacings of each transfer array pair is only about 0.24%, the same values for grid-to-anode and cathode-to-anode spacing as those of the outer transfer arrays may be used (for the inner transfer arrays), with negligible anticipated consequences, in order to facilitate device construction.

[3] Inner Induction Arrays

From DataSheet #8, the peak bias voltage applied to each inner induction array control grid should be equal to 40% of the peak unbiased ΔV across the array, or $.40 (3,417.62) = 1,367.048$ volts.

Since this represents a negative voltage which is added in series with the cathode voltage, and the cathode voltage equals negative one-third of the peak potential difference of 4,784.67, the total negative grid voltage represented is equal to $(-1,594.89) + (-1,367.048)$, or $-2,961.94$ volts. With the rotor induction anode ring at $+3,189.78$ volts, the total peak potential difference between grid and anode equals $6,151.72$ volts.

(a) *cathode-to-anode capacitance and electrode spacings:*

$$\begin{aligned} \text{[i] area} &= A_{it} = \pi(R^2 - r^2) \\ &= \pi[(149/240 R_h)^2 - (146/240 R_h)^2] \quad \{\text{from SpecSheet III}\} \\ &= \pi[(14.9")^2 - (14.6")^2] \\ &= \pi(222.01 - 213.16) \text{ in}^2 = 27.803 \text{ in}^2 \end{aligned}$$

$$\begin{aligned} \text{Therefore, } A_{it} &= (27.803 \text{ in}^2)(6.4516 \text{ cm}^2/\text{in}^2) \\ &= 179.37 \text{ cm}^2, \text{ or } \boxed{1.794 \times 10^{-3} \text{ m}^2}. \end{aligned}$$

[ii] Under the directives of principle (5) from Section A above, the induction arrays in a 3η rotor device must have a capacitance equal to $1/3$ that of the transfer arrays. Therefore, we may provide this value and the area figured above in the capacitance equation and solve for the necessary cathode-to-anode plate spacing distance as follows:

$$\text{capacitance} = C_{it} = \frac{\epsilon_o A_{it}}{\text{inner } D_{it}}, \text{ where } C_{it} = \boxed{4.922 \times 10^{-11} \text{ farad}}.$$

$$4.922 \times 10^{-11} = \frac{(8.85 \times 10^{-12})(1.794 \times 10^{-3})}{\text{inner } D_{it}},$$

$$\text{and inner } D_{it} = 15.877 \times 10^{-14} / 4.922 \times 10^{-11} = .3226 \text{ cm, or } \boxed{.1270"}. .$$

[iii] *grid-to-anode spacing:*

Subtracting half the grid screen thickness (equal to $2t_g$) from $\text{inner } D_{it}$,

the nominal primary plate spacing (inner D_i) is .1207". Therefore:

Spec. Electrode Spacing inner d_e = .1207[(μ -1)/(μ)] = .0905", or .2299 cm.

[4] Outer Induction Arrays

The peak potential difference between the cathode and anode of each outer induction array is equal to that between the cathode and anode of the inner induction arrays, at 4,784.67 volts. There is of course no control grid present, and hence no specified grid-to-anode spacing.

(a) *cathode-to-anode capacitance and electrode spacings:*

$$\begin{aligned} [i] \text{ area} &= A_{oi} = \pi(R^2 - r^2) \\ &= \pi[(7215/9600 R_n)^2 - (7116/9600 R_n)^2] \quad \{\text{from SpecSheet III}\} \\ &= \pi[(18.0375")^2 - (17.79")^2] \\ &= \pi(325.351 - 316.484) \text{ in}^2 = 27.857 \text{ in}^2 \\ \text{Therefore, } A_{oi} &= (27.857 \text{ in}^2)(6.4516 \text{ cm}^2/\text{in}^2) \\ &= 179.72 \text{ cm}^2, \text{ or } 1.797 \times 10^{-2} \text{ m}^2 \end{aligned}$$

[ii] Because the outer induction array capacitance must be equal to that of the inner induction array, we may provide this value and the area figured above in the capacitance equation and solve for the necessary cathode-to-anode plate spacing distance (which will differ only marginally from that of the inner induction array) as follows:

$$\text{capacitance} = C_{oi} = \frac{\epsilon_o A_{oi}}{d_o}, \text{ where } C_{oi} = 4.922 \times 10^{-11} \text{ farad}.$$

$$4.922 \times 10^{-11} = \frac{(8.85 \times 10^{-12})(1.797 \times 10^{-2})}{d_o}, \text{ and}$$

Spec. Electrode Spacing d_o = $15.903 \times 10^{-14} / 4.922 \times 10^{-11}$ = .3231 cm, or .1272".

[5] 3n Total Series Capacitance

Capacitors in series combine in the same manner as resistors in parallel. Therefore, the total primary series capacitance (C_{st}) associated with each series Field Coil group is as follows:

$$1/C_{st} = 1/C_{oi} + 1/C_{ot} + 1/C_{it} + 1/C_{it}$$

$$C_{st} = 1/ (.20317 + .06772 + .06772 + .20317) \times 10^{-11}$$

$$C_{st} = (1/.54178) \times 10^{-11} = 1.8458 \times 10^{-11} \text{ farad} = \boxed{18.458 \text{ mmf}}.$$

Section D: Projected Peak Field Winding Potential Differences

In light of the considerations of principle (5) from Section A above, the final peak potential differences expressed across each of the field windings of either series coil group in a 3n rotor device must be calculated. As a mathematical check of the reasoning which underlies the design principles of proper circuit resolution given in Section A, it will be verified hereinbelow that the series sum of these final peak potential differences across the field windings of either 3n series coil group equals the voltage impressed across the rotor.

(a) 3η Inner Coils

- (i) inner induction array cathode voltage = $-1 (1,594.89)$
 $= -1,594.89$ {from Section C above}
- (ii) inner transfer array anode voltage = $+1/2$ (inner transfer array ΔV)
 $= +1/2 (1,594.89) = +797.445$
- (iii) peak inner field winding $\Delta V = |-1,594.89| + 797.445 = 2,392.335$ volts.

(b) 3η Outer Coils

The peak outer field winding ΔV will be equal to that of the inner field windings (above), at 2,392.335 volts.

(c) 3η Center Coils

- (i) inner transfer array cathode voltage = $-1/2$ (inner transfer array ΔV)
 $= -1/2 (1,594.89) = -797.445$
- (ii) outer transfer array anode voltage = $+1/2$ (outer transfer array ΔV)
 $= +1/2 (1,594.89) = +797.445$
- (iii) peak inner field winding $\Delta V = |-797.445| + 797.445 = 1,594.89$ volts.

Thus, it can be seen that the sum of the peak potential differences calculated above, or 6,379.56, does in fact equal the peak rotor voltage.

Section E: Array Field Intensity Analysis

As an aid to research and development engineers, the percentage of breakdown field intensity existing across each 1η and 3η rotor electrode array as a result of the specified voltages and electrode spacings is calculated below.

[1] 1η Thermal Unit

(a) Induction Arrays

- (i) inner grid-to-anode:
peak $E_{net} = 8.20229 \times 10^3 / 2.982 \times 10^{-3} = 2.75 \times 10^6$; and $2.75/3 = 91.67\% E_{brk}$.
- (ii) outer cathode-to-anode:
peak $E_{net} = 6.37956 \times 10^3 / 4.141 \times 10^{-3} = 1.541 \times 10^6$; and $1.541/3 = 51.37\% E_{brk}$.

[2] 3η Drive Unit

(a) Transfer Arrays

- (i) grid-to-anode:
peak $E_{net} = 2.05057 \times 10^3 / 0.746 \times 10^{-3} = 2.75 \times 10^6$; and $2.75/3 = 91.67\% E_{brk}$.

(b) Induction Arrays

- (i) inner grid-to-anode:
peak $E_{net} = 6.15172 \times 10^3 / 2.299 \times 10^{-3} = 2.68 \times 10^6$; and $2.68/3 = 89.33\% E_{brk}$.
- (ii) outer cathode-to-anode:
peak $E_{net} = 4.78467 \times 10^3 / 3.231 \times 10^{-3} = 1.481 \times 10^6$; and $1.481/3 = 49.37\% E_{brk}$.

Triode Potential Differences

model: Badlander

size: 4ft. dia.

This WorkSheet is used to determine the value of the load resistance which must be applied to each rotor electrode array 'stage', as well as the subsequent required value(s) of ballast (plate) resistance and stage grid resistance per DataSheets #9 and #10 respectively. As a result, it will then be possible to also calculate relevant corresponding maximum values of series coil group current, for both 1 η and 3 η rotor devices.

Section A: Verification of Peak Series Coil Group Voltage

Before commencing these computations, the feasibility of producing peak Series Coil Group Voltage at the assigned maximum nominal rotor speed given in Fig. 19 (on pg. 106) should be confirmed. Actual peak rotor speed in all cases should have the highest value which provides a level of gyroscopic stability in 3 η devices which is not excessive. Given the actual value of hull static capacitance determined in small device testing, the formulas for Rotor Voltage (in SpecSheet I) and the dependent Primary Voltage Expansion Ratio may then be revised accordingly. The nominal rotor speed is verified in WorkSheet IX(b).

Having calculated the combined Rotor Voltage Output Ratio {in Section D of WorkSheet VII(c)}, the estimated nominal value of rotor speed (at Spec.V_r) in 1 η Thermal Units may be figured using the following convenient method given the principles of circuit resolution as presently applied in WorkSheet VIII(a):

$$\text{total Field Winding Voltage Output Ratio } (V_{f,r}) = .8333 V_{f,r};$$

$$V_{f,r} = .8333 (355.99) = 296.65 \text{ volts/rev/sec.}$$

$$\text{design Series Coil Group Voltage}/(V_{f,r}) = \text{std. rotor speed (in rps),}$$

$$\text{and std. rotor speed} = 8,285.14/296.65 \text{ v/r/s} = 27.93 \text{ rps};$$

$$\text{so } 1\eta \text{ Nominal Rotor Speed} = 27.93 \times 60 = 1676 \text{ rpm.}$$

$$\text{peak rotor speed} = 1.1(1676) = 1844 \text{ rpm,}$$

$$\text{and peak Series Coil Group Voltage} = 1.1(8,285.14) = 9,113.654 \text{ volts.}$$

The estimated nominal value of rotor speed (at Spec.V_r) in 3 η Drive Units may be figured using the following convenient method given the principles of circuit resolution as presently applied in WorkSheet VIII(a):

$$V_{f,r} = .8000 (355.99) = 284.79 \text{ volts/rev/sec.}$$

$$\text{design Series Coil Group Voltage}/(V_{f,r}) = \text{std. rotor speed (in rps),}$$

$$\text{and std. rotor speed} = 8,285.14/284.79 \text{ v/r/s} = 29.09 \text{ rps};$$

$$\text{so } 3\eta \text{ Nominal Rotor Speed} = 29.09 \times 60 = 1745 \text{ rpm.}$$

$$\text{peak rotor speed} = 1.1(1745) = 1920 \text{ rpm.}$$

Section B: Stage Load Resistances

The resistance/voltage factor (f_v) used below to calculate triode stage load resistance is taken to be 10 ohms/volt in both 1 η and 3 η rotor devices,

Triode Potential Differences

per DataSheet #9. For purposes of these computations, the applicable stage (source) voltage is equal to the peak unbiased potential difference (ΔV) across the inner induction arrays in 1 η Thermal Units, and is equal to the peak unbiased ΔV across each respective triode array in 3 η Drive Units. All load resistances are rounded to the nearest whole ohm.

[1] 1 η Thermal Unit

(a) In both 1 η and 3 η rotor devices, the inner induction array's load (ballast) resistor is actually connected to the outer induction anode ring (see SpecSheet IX). However, a different approach has been used to determine an appropriate load resistance for the 1 η device than the more traditional method used in 3 η rotor devices. In this case, the single ballast resistor (of value R_{∞}) is first sized such that peak series coil group current cannot exceed one-half of field winding ampacity even under an unexpected zero-resistance arc-discharge condition across each rotor induction array.

Component Specification: $R_{\infty} = 9,113.654 / [(1/2)(.78)] = \boxed{23,368 \Omega}$.

(b) Next, the total load resistance R_L is equal to $f_{\infty} = 10$ times one-half of 9,113.654 (or, the peak unbiased ΔV across the inner induction array).

$$\text{Therefore, } R_L = 10 (4,556.827) = 45,568 \Omega.$$

(c) The net load resistance (net R_L) is taken here to represent the difference between R_L and R_{∞} , and is in turn equal to the resistance of grid resistor R_g in parallel with only the dc or AC plate resistance r_p itself.*

$$\text{Therefore, } \text{net } R_L = R_L - R_{\infty} = 45,568 - 23,368 = 22,200 \Omega.$$

*Note: In a 1 η rotor device, r_p is a static (dc) characteristic when there is not an AC signal voltage component of series coil group current.

(d) By rearranging the terms of the relevant expression from DataSheet #10, we may obtain the following values for the dc or AC plate resistance of each rotor induction array (r_p) and the applied grid resistance R_g :

$$r_p = 22,200 / .825 = 26,909 \Omega \text{ (dc or AC), and}$$

Component Specification: $R_g = 4.7 (26,909) = \boxed{126,472 \Omega}$.

It should also be noted that the value of r_p figured above must be considered a *minimum* operating plate resistance for optimum bias capability. In the unlikely event that the observed value of dc r_p is much less than this figure, and the bias voltage rise is therefore too low, the rotor induction array cathodes may be composed of a suitable metal which has a higher surface work function to compensate as necessary. The actual value of dc r_p may be determined by operating the device with the bias windings "off-line" and measuring the series coil group current with an electronic recording ammeter. [$AC r_p$ represents each rotor array's *apparent dc resistance* at the chosen non-resonant operating frequency, per DataSheet #14, as a function of rotor semicircuit AC reactance.]

(e) The maximum value of the Primary Power System's dc operating current if the bias windings go off-line is equal to peak Series Coil Group Voltage divided by the sum of R_{∞} and $2r_p$ (disregarding field winding resistance):

$$\text{max. } I_{\infty} = \text{peak } V_{\infty} / (R_{\infty} + 2r_p) = 9113.654 / 77,186 = .118 \text{ amps}.$$

This amperage represents 15% of the winding wire ampacity.

[2] 3 η Drive Unit: [Note: Pay careful attention to the resistance position designations used; see pg. 182.]

Before the appropriate values of ballast, grid, and plate resistances may be figured for the 3 η rotor device, the peak unbiased potential difference across each rotor array must be calculated. In this case, the peak Series Coil Group Voltage of 1.1 (8285.14) or 9,113.654 must be split unevenly between these arrays. The peak ΔV across each induction array will be equal to 3/8 of this peak voltage or 3,417.62 volts, and the peak ΔV across each transfer array will be equal to 1/8 of the same peak voltage or 1,139.207 volts.

(a) Inner Induction Arrays:

(i) The required load resistance R_L of each inner induction array is equal to the resistance/voltage factor f_v times the peak ΔV of 3,417.62. With an assigned value of $f_v = 10^*$, R_L is figured as follows:

$$\text{outer } R_L = 10 (3,417.62) = 34,176 \Omega . \text{ *{see DataSheet \#9}}$$

(ii) The corresponding ballast resistance thereof (outer R_p) is equal to the load resistance divided by .825 (per DataSheet #10):

Component Specification: $\text{outer } R_p = 34,176 / .825 = \boxed{41,425 \Omega} .$

(iii) The matching grid resistance of each outer transfer array (outer R_g) is equal to the preceding ballast resistance times 4.7:

Component Specification: $\text{outer } R_g = 4.7 (41,425) = \boxed{194,698 \Omega} .$

(iv) The engineered AC** plate resistance of the inner induction arrays (r_p) must be equal to or moderately less than 1/5 of their load resistance, to optimize both stage voltage gain and over-all device performance (per DataSheet #11). Therefore, the calculated maximum value of inner $r_p = 34,176 / 5 = 6,835 \Omega$. However, it is considered that the plate resistance of the inner induction arrays must be split with the outer induction arrays, as these plate resistances are in direct series relationship.

$$\text{Therefore, max. inner } r_p = (1/2)(6,835) = 3,418 \Omega .$$

**Note: In a 3 η rotor device, r_p is a dynamic characteristic, as there is always an AC signal voltage component of series coil group current.

(b) Outer Induction Arrays:

(i) The engineered AC plate resistance of the outer induction arrays (r_p) must be equal to that of the inner induction arrays, to optimize both stage voltage gain and over-all device performance.

$$\text{Therefore, max. split } r_p = (1/2)(6,835) = 3,418 \Omega .$$

(c) Inner Transfer Arrays:

(i) The required load resistance R_L of each inner transfer array is equal to the resistance/voltage factor f_v times the peak ΔV of 1,139.207. With an assigned value of $f_v = 10^*$, R_L is figured as follows:

$$\text{inner } R_L = 10 (1,139.207) = 11,392 \Omega . \text{ *{see DataSheet \#9}}$$

(ii) The corresponding ballast resistance thereof (inner R_p) is equal to the load resistance divided by .825 (per DataSheet #10):

Component Specification: $\text{inner } R_p = 11,392 / .825 = \boxed{13,808 \Omega} .$

Triode Potential Differences

(iii) The matching grid resistance of each inner induction array (inner R_i) is equal to the preceding ballast resistance times 4.7:

Component Specification: inner $R_i = 4.7 (13,808) = 64,898 \Omega$.

(iv) The engineered AC plate resistance of the inner transfer arrays (r_p) must be equal to or moderately less than 1/5 of their load resistance, to optimize both stage voltage gain and over-all device performance (per DataSheet #11).

Therefore, max. center $r_p = (1/5)(11,392) = 2,278 \Omega$.

(d) Outer Transfer Arrays:

(i) The required load resistance R_L of each outer transfer array is equal to the resistance/voltage factor f_v times the peak ΔV of 1,139.207. With an assigned value of $f_v = 10*$, R_L is figured as follows:

center $R_L = 10 (1,139.207) = 11,392 \Omega$. *(see DataSheet #9)

(ii) The corresponding ballast resistance thereof (center R_p) is equal to the load resistance divided by .825 (per DataSheet #10):

Component Specification: center $R_p = 11,392/.825 = 13,808 \Omega$.

(iii) The matching grid resistance of each inner transfer array (center R_i) is equal to the preceding ballast resistance times 4.7:

Component Specification: center $R_i = 4.7 (13,808) = 64,898 \Omega$.

(iv) The engineered AC plate resistance of the outer transfer arrays (r_p) must be equal to or moderately less than 1/5 of their load resistance, to optimize both stage voltage gain and over-all device performance,

Therefore, max. outer $r_p = (1/5)(11,392) = 2,278 \Omega$.

(e) Maximum Series Coil Group Current Values:

(i) The Primary Power System's peak dc operating current under normal full-signal conditions is equal to the quotient of peak Series Coil Group Voltage divided by the total series resistance (disregarding all winding resistances) times the zero-bias voltage factor (f_{zb}) from DataSheet #14:

$$\begin{aligned} R_{\text{total}} &= \Sigma R_L + \Sigma r_p, \text{ where } \Sigma r_p = \text{the primary load resistance (req'd. @ resonance)} \\ &= [2(11,392) + 34,176] + [2(2,278) + 2(3,418)] \\ &= 56,960 + 11,392 \\ &= 68,352 \Omega. \end{aligned}$$

Thus, peak $I_{s_g} = f_{zb}[\text{peak } V_{s_g}/R_{\text{total}}] = .38[9,113.654/68,352] = .05067 \text{ amps}$.

This amperage represents 6.5% of the winding wire ampacity.

(ii) The maximum value of the Primary Power System's dc operating current assuming a zero-resistance arc-discharge condition across all of the rotating electrode arrays is equal to peak V_{s_g} divided by the sum of the ballast resistances (disregarding all winding resistances):

$$\begin{aligned} \text{Therefore, max. } I_{s_g} &= \text{peak } V_{s_g}/\Sigma R_p = 9,113.654/[2(13,808) + 41,425] \\ &= 9,113.654/69,041 = .1320 \text{ amps} . \end{aligned}$$

This amperage represents 16.9% of the winding wire ampacity.

Section C: Important Operating Considerations

The amplifying action of a triode vacuum tube, which is of great practical concern in 3 η rotor devices, can be used in a number of ways in electronic circuits depending on the results desired. Four classes of amplifier service are recognized by electrical engineers and these classifications depend primarily on the fraction of the input signal cycle during which plate current is expected to flow (under rated full-load conditions). The three such classes of interest with respect to the application contemplated herein are briefly described below, and the term "cutoff bias" used in these definitions is the value of grid bias voltage at which plate current is extremely small (i.e., approaches zero).

A class A amplifier tube is one in which the grid bias and AC signal voltages are such that plate current flows throughout the input electrical cycle, and represents the origin from which the other classes derive.

A class AB amplifier tube is one which utilizes a higher grid bias voltage, and in which plate current therefore flows for more than half but less than the entire input cycle. It is important to note that in subclass AB₁, there is *no flow of grid current*: the peak signal voltage applied to the control grid is limited to a value equal to or less than the negative grid bias voltage. The Generator's AC voltage regulation is to be consistent with this latter criterion.

Finally, a class B amplifier tube is one in which the grid bias is approximately equal to the cutoff value when no AC signal voltage is applied, so that plate current flows for approximately half of the input cycle with the application of an AC signal voltage.

Given equality of amplification factor μ , the value of load resistance for a tube of each class described above will generally be the same. This is an important consideration with regard to the rotor electrode arrays of the 3 η EDF Generator, as the field coils are designed such that each triode array is to be operated as in class B above. Yet, the maximum coil group current values computed at the end of the preceding Section are also predicated upon the operation of each triode array as in class AB₁ (consistent with the prior criterion).

The latter of these two considerations is of particular consequence in the inner induction arrays, where final rotor stage amplification is obtained. The limiting of the peak signal voltage applied to the control grids of the inner induction arrays must be effected by electronic regulation of the input signal voltage resistor shown in the *Field Voltage Control System* schematic (of SpecSheet IX). The value of the AC signal voltage applied to the control grids of the inner induction arrays may be calculated by analyzing the magnitude of the voltage drop across the variable matching (or output signal voltage) resistor, shown in the same schematic.

Finally, it must be emphasized that the output current of the 3 η rotor's AC signal voltage amplification system will have a *pulsed unidirectional waveform*, due to the class B/AB₁ operating characteristics discussed above.

Section D: Stationary Anode Ring Potentials

The marginal, Specification, and peak values of the stationary anode ring voltage must be determined, not only so that the zero-signal value setting of the pentode array bypass resistors may be calculated, but also because these two anode rings constitute the EDF Generator's Field Voltage Control System power source. The marginal anode ring voltage is herein defined as that which would exist if the bias windings go off-line or a zero-resistance arc-discharge condition occurs across the rotor electrode arrays.

Triode Potential Differences

Given the principles of proper circuit resolution as presently applied, these values of stationary anode ring voltage for the applicable 1 η and 3 η rotor device models are figured below.

[1] 1 η Thermal Unit:

The marginal stationary anode ring voltage (marg.V_{..}) will be numerically equal to the *unbiased* inner induction array cathode voltage at nominal rotor speed, or 1/6 of Series Coil Group Voltage (spec.V_{..}).

$$\text{Therefore, } \text{marg.V}_{..} = 8,285.14/6 = +1,381 \text{ volts.}$$

The Specification stationary anode ring voltage (spec.V_{..}) will be numerically equal to the *biased* inner induction array cathode voltage at nominal rotor speed, or 1/6 of the projected Primary System Voltage (spec.V_{..}).

$$\text{Therefore, } \text{spec.V}_{..} = 11,599.2/6 = \boxed{+1,933 \text{ volts}}.$$

The peak stationary anode ring voltage (peak V_{..}) will equal 110% of the Specification value thereof.

$$\text{Therefore, } \text{peak V}_{..} = +2,126 \text{ volts.}$$

[2] 3 η Drive Unit:

The marginal stationary anode ring voltage (marg.V_{..}) will be numerically equal to the *unbiased* inner induction array cathode voltage at nominal rotor speed, or 1/8 of Series Coil Group Voltage (spec.V_{..}).

$$\text{Therefore, } \text{marg.V}_{..} = 8,285.14/8 = +1,036 \text{ volts.}$$

The Specification stationary anode ring voltage (spec.V_{..}) will be numerically equal to the *biased* inner induction array cathode voltage at nominal rotor speed, or 1/8 of the projected Primary System Voltage (spec.V_{..}).

$$\text{Therefore, } \text{spec.V}_{..} = 11,599.2/8 = \boxed{+1,450 \text{ volts}}.$$

The peak stationary anode ring voltage (peak V_{..}) will equal 110% of the Specification value thereof.

$$\text{Therefore, } \text{peak V}_{..} = +1,595 \text{ volts.}$$

Section E: Triode Array Amplification Factor

SpecSheet VIII {Electrode Array Construction} suggests that modest increases in the common design amplification factor of the rotor triode arrays may be effected "to improve Primary Power System efficiency". The nature of such an improvement is two-fold: not only would this allow a corresponding decrease in the nominal rotor speed (due to larger bias winding turns ratios), but the over-all net rotor stage gain in 3 η rotor devices would of course show a substantial increase as well.

It must be stressed that at some point, the increase in winding turns ratios (and decrease in rotor speed) which would result from increasing the amplification factor of the triode arrays will be offset by a decrease in the expected cutoff bias voltage rise associated with the higher μ value. As a possible aid to research and development engineers in exploring the use of higher- μ triode arrays, the following theoretical formulas are given which relate the current cutoff-induced value of plate voltage to the magnitude of the applied grid bias voltage. These two (2) expressions are to be considered

Triode Potential Differences

as working approximations only, which provide a certain basis for instituting a practical program of controlled design modification and improvement.

An extensive analysis of available low-gain triode vacuum tube plate characteristic data reveals a very nearly linear inverse relationship between triode amplification factor and the plate current cutoff value of control grid voltage required to effect a full 40% plate voltage rise. This relationship can be summarized with reasonable accuracy by the following convenient estimation formula:

$$E_{cb} = 1.6E_b/\mu ,$$

where E_{cb} = cutoff bias voltage req'd. to boost E_b by 40% ,

E_b = normal operating source voltage,

and μ = given amplification factor.

Thus, it can be shown that if E_{cb} for a given triode tube (or ring array) of $\mu = 4$ is equal to $1.6E_b/4 = .4E_b$, or 40% of source voltage (as we have relied upon so far with regard to the transfer arrays), the resultant E_{cb} for a tube or array of $\mu = 16$ would be equal to $1.6E_b/16 = .1E_b$, or 10% of applied source voltage. It must be stressed, however, that this expression is acceptably accurate only for low-gain triodes of $\mu = 16$ or less. (Note: Students may wish to check the basic validity of this equation against the examples in DataSheet #8.)

Due to the appreciably linear nature of the cutoff bias grid voltage/low-gain amplification factor relationship described above, it is also possible to develop an expression relating a given level of applied grid voltage and the maximum resultant current cutoff value of plate potential difference strictly as a function of the triode amplification factor. Thus, if a desired peak array potential difference is also supplied, the necessary amplification factor may be accurately solved-for which allows plate current cutoff with a concomitant grid bias voltage rise of less than 40% ! This theoretical expression is as follows:

$$\text{peak } \Delta V_{ic}/|E_g| = \left(\frac{100 - \mu}{100} \right) \mu , *$$

where $\text{peak } \Delta V_{ic}$ = max. plate potential difference at which current cutoff occurs,

E_g = corresponding available grid voltage,

and μ = required amplification factor.

***Note:** This equation must be solved using the quadratic equation discriminant method, the smaller of the two real and unequal roots derived thereby being the answer sought. The easiest alternate approach to use in figuring the cutoff amplification factor here for another size (model) vessel is by direct (trial) substitution. The value(s) obtained will not change significantly from that above due to the design methods employed throughout.

It should also be noted that this equation was derived for optimum accuracy in the middle of the range of μ values from 5 to 25, and it must be "scaled" slightly for increased accuracy at the lowest and highest μ values within this range by either decreasing or increasing respectively the percentage numerator by single digit increments: e.g. 99 or 98/100 (etc.) for very low-gain triodes and 101 or 102/100 (etc.) for high gain units. Access to a broad range of plate characteristics curves graphs in the applicable μ value range would of course be essential for a truly accurate comparative analysis.

Finally, it should be noted that plate spacing limitations will also play a role in determining the maximum practical value of common triode design amplification factor which does not begin to re-increase nominal rotor speed.

Pentode Potential Differences

model: Badlander
size: 4ft. dia.

This WorkSheet is used to determine the peak applied voltages and minimum relative electrode spacings for the primary five-element (pentode) induction ring array associated with each series Field Coil group of the Primary Power System. Reference is made to DataSheet #15 {Beam Pentode Characteristics}, and to WorkSheet VIII(a) {Series Electrode Array Capacitance} and WorkSheet VIII(b) {Triode Potential Differences}.

Section A: Peak Plate Potential Difference**[1] 1η Thermal Unit:**

Based on the reasoning of DataSheet #15 and Section B of WorkSheet VIII(a), the peak potential difference (ΔV_p) between the unit cathodes and plate (anode ring) of each of the two (2) Primary Induction Ring Arrays in 1η rotor devices will approach 1/3 of the peak Primary System Voltage developed.

$$\text{Therefore, peak } \Delta V_p = 1.1(11,599.2)/3 = \boxed{4,253.04 \text{ volts}}.$$

Note: The unit cathodes are assumed to be at ground (0-volt) potential.

[1] 3η Drive Unit:

Based on the reasoning of DataSheet #15 and Section C of WorkSheet VIII(a), the peak potential difference (ΔV_p) between the unit cathodes and plate (anode ring) of each of the two (2) Primary Induction Ring Arrays in 3η rotor devices will approach 1/4 of the peak Primary System Voltage developed.

$$\text{Therefore, peak } \Delta V_p = 1.1(11,599.2)/4 = \boxed{3,189.78 \text{ volts}}.$$

Note: The unit cathodes are assumed to be at ground (0-volt) potential.

Section B: Peak Control Grid Voltage

Component Specification: The source of the negative voltage applied to the stationary control grid of each unit pentode array shall be a variable dc generator or power supply which is common to all of the unit arrays of that given Primary Array thereof, and which is otherwise connected by its positive terminal to ground, as shown in Fig.28 of SpecSheet IX. The peak value of the negative voltage output of said variable dc supply with respect to such control grid(s) (peak E_{cg}) shall be equal to 1/10 of the peak potential difference across the Primary Arrays.

In light of this Specification, the maximum Spec. value of field current bias voltage ($\max.E_{cg}$) applied to the pentode control grids will be equal to 1/11 of the peak potential difference across the Arrays, or $.0909 \times (\text{peak } \Delta V_p)$. The standard (nominal) value of control grid voltage, at zero signal, is then equal to one-half this maximum value, or $\text{std}.E_{cg} = .04545(\text{peak } \Delta V_p)$.

[1] 1η Thermal Unit:

$$\text{Therefore, peak } E_{cg} = 4,253.04/10 = -425.3 \text{ volts,}$$

$$\max.E_{cg} = .0909(4,253.04) = -386.6 \text{ volts,}$$

$$\text{and std}.E_{cg} = .04545(4,253.04) = -193.3 \text{ volts.}$$

[1] 3η Drive Unit:

Therefore, $\text{peak } E_{c_3} = 3,189.78/10 = -319.0 \text{ volts}$,
 $\text{max. } E_{c_3} = .0909(3,189.78) = -290.0 \text{ volts}$,
 and $\text{std. } E_{c_3} = .04545(3,189.78) = \underline{-145.0 \text{ volts}}$.

Section C: Peak Accelerator Grid Voltage

Component Specification: The source of the positive voltage applied to the stationary accelerator grid of each unit pentode array shall be a stationary diode induction ring, located adjacent to the respective inner induction array cathode, which is at an equal and opposite potential (by induction) to the inner induction array cathode relative to ground.

The peak value of this induced stationary anode voltage ($\text{peak } E_{a_3}$) will be equal and opposite to the applied peak cathode voltage of the inner induction array. The standard (nominal) value of accelerator grid voltage, at zero signal, is then equal to 10/11 of this peak value, or $\text{std. } E_{a_3} = \text{peak } \Delta E_{c_3} / 1.10$.

[1] 1η Thermal Unit:

Therefore, $\text{peak } E_{a_1} = +2,126.52 \text{ volts}$,
 and $\text{std. } E_{a_1} = 2,126.52/1.10 = \underline{+1,933.2 \text{ volts}}$.

[1] 3η Drive Unit:

Therefore, $\text{peak } E_{a_3} = +1,594.89 \text{ volts}$,
 and $\text{std. } E_{a_3} = 1,594.89/1.10 = \underline{+1,449.9 \text{ volts}}$.

Section D: Equivalent Load Resistance

The actual load resistance applied to each unit pentode array is of course that of its associated power resistor, whose value must be chosen specifically to fulfill its Field Induction System function and not by using the 'f_v' method outlined in DataSheet #15. The pentode arrays therefore have no load resistance *per se* which is a function of inherent 'plate' resistance, as in traditional amplifier practice, as they are not coupled sequentially to the rotor circuit but rather in what might be termed "group tandem".

It should be noted that the effective median dc plate resistance (r_p) of each unit pentode array will only be in the upper single-digit ohms, in both 1η and 3η rotor devices, and so the individual stage voltage gain obtained thereby will be extremely close to the arrays' actual amplification factor (per the considerations of DataSheet #11). These respective values of r_p are calculated below.

- 1η Thermal Unit: $\text{median } r_{\text{unit}} = \text{peak } \Delta V_p / (I_{\text{max}}/72)$, where I_{max} = rotor ampacity.
 $= 4,253.04/530 = 8.025 \Omega \text{ (dc)}$.
- 3η Drive Unit: $\text{median } r_{\text{unit}} = \text{peak } \Delta V_p / (I_{\text{max}}/72)$, where I_{max} = rotor ampacity.
 $= 3,189.78/530 = 6.018 \Omega \text{ (dc)}$.

As discussed in SpecSheet IX (and in detail in Chap. 12), the accelerator grid (matching) resistor shown in Fig. 28 is analogous to a ballast (plate) resistor on behalf of each 3rd stage inner induction array in 3η rotor devices. This consideration provides the rationale necessary to properly calculate its required "load" resistance in 1η rotor devices as well.

[1] 1η Thermal Unit:

The valid minimum and maximum unit pentode array accelerator grid 'load' resistances ($\text{accel.}R_{L_1}$) are based entirely on the premise that the 1η primary array AC load current should equal 75% of that in the 3η device, in accordance with the rather complex computational considerations of DataSheet #14.

Thus, $\text{min. accel.}R_{L_1} = 64.1 \Omega$; and, $\text{max. accel.}R_{L_1} = 16,842 \Omega$.

Due to the design methods employed, the value of each control grid resistor (R_{C_1}) will be equal to the selected value of $\text{accel.}R_{L_1}$ in the range above divided by the stage coupling transformers' k_{μ} . The corresponding value of each accelerator grid resistor is then $4 \times R_{C_1}$. Base initial setting values are generated below which assume a median value for $\text{accel.}R_{L_1} = 8,453 \Omega$.*

Component Specifications: $\text{median } R_{C_1} = \text{accel.}R_{L_1} / .80 = 10,566 \Omega$,
and $\text{median } R_{A_1} = 4(\text{median } R_{C_1}) = 42,264 \Omega$.

* Corresponding values for the primary load and bypass resistors must be figured per the method in DataSheet #14.

[2] 3η Drive Unit:

In this case, the valid minimum and maximum unit pentode array accelerator grid 'load' resistances ($\text{accel.}R_{L_1}$) are based solely on maximizing the Field envelope circuit AC current and transmit power, in accordance with the computational method of DataSheet #14.

Thus, $\text{min. accel.}R_{L_1} = 97.5 \Omega$; and, $\text{max. accel.}R_{L_1} = 19,604 \Omega$.

Accordingly, the median value for $\text{accel.}R_{L_1} = 9,851 \Omega$ * and the corresponding base initial setting values of control grid resistor R_{C_1} and accelerator grid resistor R_{A_1} are calculated as follows:

Component Specifications: $\text{median } R_{C_1} = \text{accel.}R_{L_1} / .80 = 12,314 \Omega$,
and $\text{median } R_{A_1} = 4(\text{median } R_{C_1}) = 49,256 \Omega$.

* Corresponding values for the secondary load and bypass resistors must be figured per the method in DataSheet #14.

The 1η and 3η grid resistances above merely represent reasonable *trial zero-signal value settings* for the respective variable resistors shown in Fig. 28. As was briefly referred to in Section C of WorkSheet VIII(b), the peak signal feedback voltage applied to the unit pentode array control grids must be regulated (using the control grid resistors) such that the inner induction array control grids are not driven positive and hence draw no current!

Section E: Specification Electrode Spacings

The unit pentode array electrode separation distances figured below are derived in a somewhat different manner than those of the rotor electrode arrays. Whereas the emphasis was toward a *minimum* plate spacing scheme for the rotating arrays, due to their low conduction current, the unit pentode arrays should utilize *maximum* plate spacings because of their very high conduction current.

[1] cathode-to-anode spacing:

Given the present specification regarding the Power Resistor length, the installed pentode total cathode-to-anode spacing ($\text{pentode } D_{kp}$) should be limited to .2913" in this model (size) device, applying to both 1η and 3η rotor units. This figure is derived by subtracting the sum of half the rotor segment width (height), the thickness of the anode and cathode rings, the Power Resistor length, and the "curl" of the Zone sectors (or 4 times their outer thickness)

Pentode Potential Differences

from the hull height value .1317(r_c) [as calculated in the Hull Spreadsheet].

$$\text{pentode } D_{kp} = \underline{.2913''}, \text{ or } .7399 \text{ cm. } \{\text{Specification}\}$$

(a) Breakdown Analysis

(i) Thermal Unit:

$$\text{peak } E_{nat} = 4.25304 \times 10^3 / 7.399 \times 10^{-3} = .5748 \times 10^6; \text{ and } .5748/3 = 19.16\% E_{brk}.$$

(ii) Drive Unit:

$$\text{peak } E_{nat} = 3.18978 \times 10^3 / 7.399 \times 10^{-3} = .4311 \times 10^6; \text{ and } .4311/3 = 14.37\% E_{brk}.$$

[2] control grid-to-cathode spacing:

The cathode-to-anode spacing just figured divided by the design amplification factor yields the pentode arrays' net control grid-to-cathode spacing (pentode d_k), as follows:

$$\text{pentode } D_{kp} = \text{pentode } d_k / \text{design } \mu,$$

$$\text{and pentode } d_k = .2913''/12 = \underline{.0243''}, \text{ or } .0617 \text{ cm. } \{\text{Specification}\}$$

(a) Breakdown Analysis

(i) Thermal Unit:

$$\text{peak } E_{nat} = 4.253 \times 10^3 / .617 \times 10^{-3} = .6893 \times 10^6; \text{ and } .6893/3 = 22.98\% E_{brk}.$$

$$\text{max. } E_{nat} = 3.866 \times 10^3 / .617 \times 10^{-3} = .6266 \times 10^6; \text{ and } .6266/3 = 20.89\% E_{brk}.$$

$$\text{std. } E_{nat} = 1.933 \times 10^3 / .617 \times 10^{-3} = .3133 \times 10^6; \text{ and } .3133/3 = 10.44\% E_{brk}.$$

(ii) Drive Unit:

$$\text{peak } E_{nat} = 3.190 \times 10^3 / .617 \times 10^{-3} = .5170 \times 10^6; \text{ and } .5170/3 = 17.23\% E_{brk}.$$

$$\text{max. } E_{nat} = 2.900 \times 10^3 / .617 \times 10^{-3} = .4700 \times 10^6; \text{ and } .4700/3 = 15.67\% E_{brk}.$$

$$\text{std. } E_{nat} = 1.450 \times 10^3 / .617 \times 10^{-3} = .2350 \times 10^6; \text{ and } .2350/3 = 7.83\% E_{brk}.$$

Component Specification:

Before any further final electrode spacings may be determined, the actual thickness of the control, accelerator, and suppressor grids must be taken into account. Assigning a Specification Pentode Grid Wire Diameter equal to the bare wire diameter which is closest to the formula Field Coil wire diameter {from the preamble of WorkSheet VII(a)}, the resultant grid tungsten wire size (30 ga.) equals .01003" = T_c .

Each remaining electrode spacing is initially computed using the same minimum non-breakdown method employed in the triode arrays. However, ample total separation distance exists in the pentode arrays to allow for the full thickness of each grid screen ($4T_c$) to be subtracted from the net cathode-to-anode spacing before the remaining final electrode spacings are calculated.

Thus, the total thickness of the three (3) grids is subtracted from the difference of the cathode-to-anode and control grid-to-cathode spacings. This figure gives the total net separation distance to be shared by the remaining grid spacings *proportional to their minimum non-breakdown separation distances*.

[3] Interim Grid Separation Distances

(a) suppressor grid-to-anode:

The net separation distance between each unit pentode array suppressor grid and the anode ring of its respective Primary Induction Ring Array must be

Pentode Potential Differences

marginally greater than that which would allow an arc-discharge level of electric field intensity ($\approx 3 \times 10^6$ v/m) to be established between these electrodes at their peak potential difference. Given a peak anode ring voltage of +4,253.04 and a mean suppressor grid voltage of zero, we may calculate the initial nominal value of the grid-to-anode distance d_i , as follows:

$$\text{pentode } d_i > 4,253.04 / 3 \times 10^6 > 1.418 \times 10^{-3} = .1418 \text{ cm, or } .0558''.$$

Because a marginal buffer distance should in practice be added to d_i , we will divide this nominal distance by the ratio 11/12 (selected for use as a maximum value at this time), or .9167, to calculate the interim minimum non-breakdown separation distance d_{si} , as follows:

$$\text{pentode } d_{si} = \text{pentode } d_i / .9167 = .1547 \text{ cm, or } .0609''.$$

Note: This same method of computing interim minimum electrode spacings is used in each applicable instance below.

(b) accelerator grid-to-suppressor grid:

Given a peak accelerator grid voltage of +2,126.52 and a mean suppressor grid voltage of zero, the interim minimum non-breakdown separation distance in this case ($\text{pentode } d_{si}$) is computed as follows:

$$\text{pentode } d_{si} > 2,126.52 / 3 \times 10^6 > .7088 \times 10^{-3} = .0709 \text{ cm, or } .0279''.$$

$$\text{pentode } d_{ssi} = \text{pentode } d_{si} / .9167 = .0773 \text{ cm, or } .0305''.$$

(c) control grid-to-accelerator grid:

Given a peak accelerator grid voltage of +2,126.52 and a peak control grid voltage of -425.3, the interim minimum non-breakdown separation distance in this case ($\text{pentode } d_{si}$) is computed as follows:

$$\text{pentode } d_{si} > 2,551.82 / 3 \times 10^6 > .8506 \times 10^{-3} = .0851 \text{ cm, or } .0335''.$$

$$\text{pentode } d_{ssi} = \text{pentode } d_{si} / .9167 = .0928 \text{ cm, or } .0365''.$$

[4] Separation Distance Multiplier

As outlined in the preceding Section, the interim minimum grid separation distances just calculated must be expanded to fill the remaining net cathode-to-anode spacing. The actual net separation distance is figured as follows:

$$\begin{aligned} \text{net } D_{\text{total}} &= (\text{pentode } D_{kp} - \text{pentode } d_{si}) - 12 T_s \\ &= .2670'' - .1204'' = .1466''. \end{aligned}$$

The sum of the interim distances ($\text{min. } D_{\text{total}}$) is then calculated:

$$\begin{aligned} \text{min. } d_{\text{total}} &= \text{pentode } d_{si} + \text{pentode } d_{ssi} + \text{pentode } d_{gai} \\ &= .0609'' + .0305'' + .0365'' = .1279''. \end{aligned}$$

The separation distance multiplier is then equal to the ratio of $\text{net } D_{\text{total}}$ to $\text{min. } d_{\text{total}}$, or $.1466 / .1279 = 1.1462$. It should be noted that although the sum of the expanded separation distances may not exactly equal $\text{net } D_{\text{total}}$ (due to rounding), the consequences of such a minor deviation are deemed negligible due to the non-extreme breakdown intensity percentage which will be evidenced in each case.

[5] control grid-to-accelerator grid spacing:

$$\text{pentode } d_{gai} = 1.1462 (\text{pentode } d_{ssi}) = |.0418''|, \text{ or } .1062 \text{ cm. } \{\text{Specification}$$

Pentode Potential Differences

(a) Breakdown Analysis

(i) Thermal Unit:

$$\text{peak } E_{\text{net}} = 2.5518 \times 10^3 / 1.062 \times 10^{-3} = 2.403 \times 10^6; \text{ and } 2.403/3 = 80.10\% E_{\text{brk}}.$$

$$\text{std. } E_{\text{net}} = 2.1265 \times 10^3 / 1.062 \times 10^{-3} = 2.002 \times 10^6; \text{ and } 2.002/3 = 66.73\% E_{\text{brk}}.$$

(ii) Drive Unit:

$$\text{peak } E_{\text{net}} = 1.9139 \times 10^3 / 1.062 \times 10^{-3} = 1.802 \times 10^6; \text{ and } 1.802/3 = 60.07\% E_{\text{brk}}.$$

$$\text{std. } E_{\text{net}} = 1.5949 \times 10^3 / 1.062 \times 10^{-3} = 1.502 \times 10^6; \text{ and } 1.502/3 = 50.07\% E_{\text{brk}}.$$

[6] accelerator grid-to-suppressor grid spacing:

$$\text{pentode } d_{s,} = 1.1462 (\text{pentode } d_{s,}) = \boxed{.0350''}, \text{ or } .0889 \text{ cm. } \{\text{Specification}\}$$

(a) Breakdown Analysis

(i) Thermal Unit:

$$\text{peak } E_{\text{net}} = 2.1265 \times 10^3 / .889 \times 10^{-3} = 2.392 \times 10^6; \text{ and } 2.392/3 = 79.73\% E_{\text{brk}}.$$

$$\text{std. } E_{\text{net}} = 1.9332 \times 10^3 / .889 \times 10^{-3} = 2.175 \times 10^6; \text{ and } 2.175/3 = 72.50\% E_{\text{brk}}.$$

(ii) Drive Unit:

$$\text{peak } E_{\text{net}} = 1.5949 \times 10^3 / .889 \times 10^{-3} = 1.794 \times 10^6; \text{ and } 1.794/3 = 59.80\% E_{\text{brk}}.$$

$$\text{std. } E_{\text{net}} = 1.4499 \times 10^3 / .889 \times 10^{-3} = 1.631 \times 10^6; \text{ and } 1.631/3 = 54.37\% E_{\text{brk}}.$$

[7] suppressor grid-to-anode ring spacing:

$$\text{pentode } d_{s,} = 1.1462 (\text{pentode } d_{s,}) = \boxed{.0698''}, \text{ or } .1773 \text{ cm. } \{\text{Specification}\}$$

(a) Breakdown Analysis

(i) Thermal Unit:

$$\text{peak } E_{\text{net}} = 4.2530 \times 10^3 / 1.773 \times 10^{-3} = 2.399 \times 10^6; \text{ and } 2.399/3 = 79.97\% E_{\text{brk}}.$$

$$\text{spec. } E_{\text{net}} = 3.8664 \times 10^3 / 1.773 \times 10^{-3} = 2.181 \times 10^6; \text{ and } 2.181/3 = 72.70\% E_{\text{brk}}.$$

(ii) Drive Unit:

$$\text{peak } E_{\text{net}} = 3.190 \times 10^3 / 1.773 \times 10^{-3} = 1.799 \times 10^6; \text{ and } 1.799/3 = 59.97\% E_{\text{brk}}.$$

$$\text{spec. } E_{\text{net}} = 2.900 \times 10^3 / 1.773 \times 10^{-3} = 1.636 \times 10^6; \text{ and } 1.636/3 = 54.53\% E_{\text{brk}}.$$

[8] induction cathode-to-stationary anode spacing:

The peak potential difference (peak ΔV_i) between each inner induction array cathode ring and its adjacent stationary anode ring is equal to twice (2x) the induced stationary anode ring voltage. This peak ΔV_i is then equal to 4,253.04 volts in the 1 η rotor device, and 3,189.78 volts in the 3 η rotor device.

(a) 1 η Thermal Unit:

The minimum non-breakdown separation distance (diode D_i) between each induction cathode and stationary anode ring pair is computed as follows:

$$\text{diode } D_i > 4,253.04 / 3 \times 10^6 > 1.4177 \times 10^{-3} = .14177 \text{ cm, or } .0558''.$$

$$\text{diode } D_{i,} = \text{diode } D_i / .9167 = .15465 \text{ cm, or } \boxed{.0609''}. \{\text{Specification}\}$$

(b) 3 η Drive Unit:

The minimum non-breakdown separation distance (diode D_i) between each induction cathode and stationary anode ring pair is computed as follows:

diode $D_k > 3,189.78 / 3 \times 10^4 > 1.0633 \times 10^{-3} = .1063 \text{ cm} , \text{ or } .0419'' .$

diode $D_{kr} = \text{diode } D_k / .9167 = .1160 \text{ cm} , \text{ or } .0457'' . \{ \text{Specification} \}$

(c) Breakdown Analysis

(i) Thermal Unit:

$\text{peak } \Delta V_i = 4.2530 \times 10^3 / 1.5465 \times 10^{-3} = 2.750 \times 10^6 ; \text{ and } 2.750 / 3 = 91.67\% E_{brk} .$

$\text{spec. } \Delta V_i = 3.8664 \times 10^3 / 1.5465 \times 10^{-3} = 2.500 \times 10^6 ; \text{ and } 2.500 / 3 = 83.33\% E_{brk} .$

(ii) Drive Unit:

$\text{peak } \Delta V_i = 3.190 \times 10^3 / 1.160 \times 10^{-3} = 2.750 \times 10^6 ; \text{ and } 2.750 / 3 = 91.67\% E_{brk} .$

$\text{spec. } \Delta V_i = 2.900 \times 10^3 / 1.160 \times 10^{-3} = 2.500 \times 10^6 ; \text{ and } 2.500 / 3 = 83.33\% E_{brk} .$

Section F: Est'd. Stage Voltage Gain

As was noted in Section D above, the effective dc plate resistance of the unit pentode arrays will be very low and, although the AC plate resistance in 1η rotor devices will be somewhat higher than the single-digit figures given, the stage voltage gain which would be calculated according to the formula in DataSheet #11 is still well over 99% of the present design μ value of 12. It is contemplated that the actual observed voltage gain 'efficiency' of these pentode arrays will be about 98.5%, and therefore the associated text supposes a net pentode stage voltage gain of 11.82 in calculating the expected total signal voltage pre-amplification possible (in 3η rotor devices).

The side view cross-sectional schematic representation below shows the relationship of each unit pentode array to the rotor and Primary Power System.

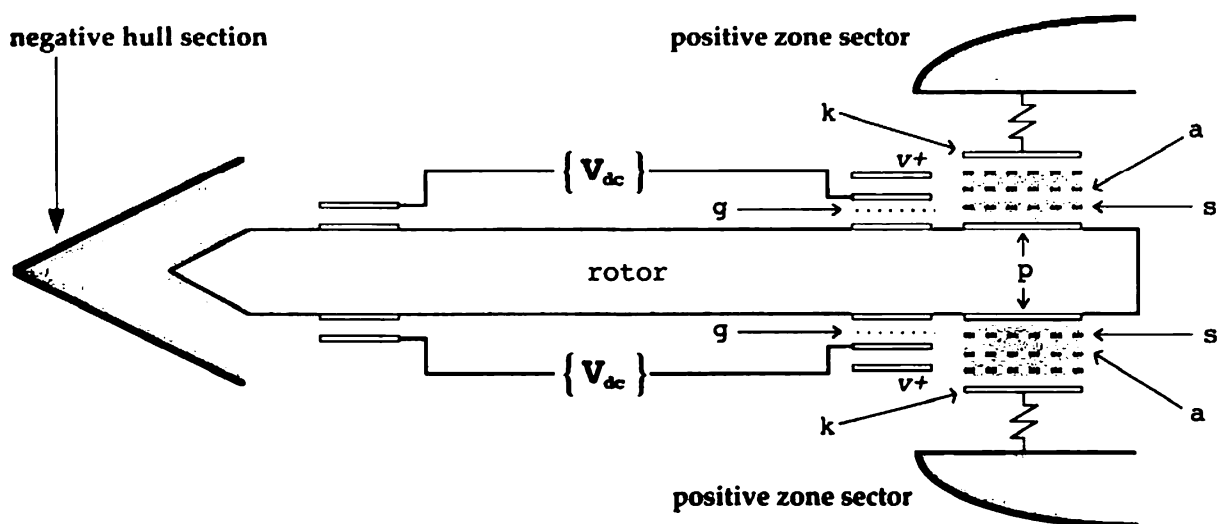


Fig. 26: Primary Induction Ring Arrays (drawing not to scale).

k = stationary cathode

a = stationary accelerator grid

p = rotating unit anode ring

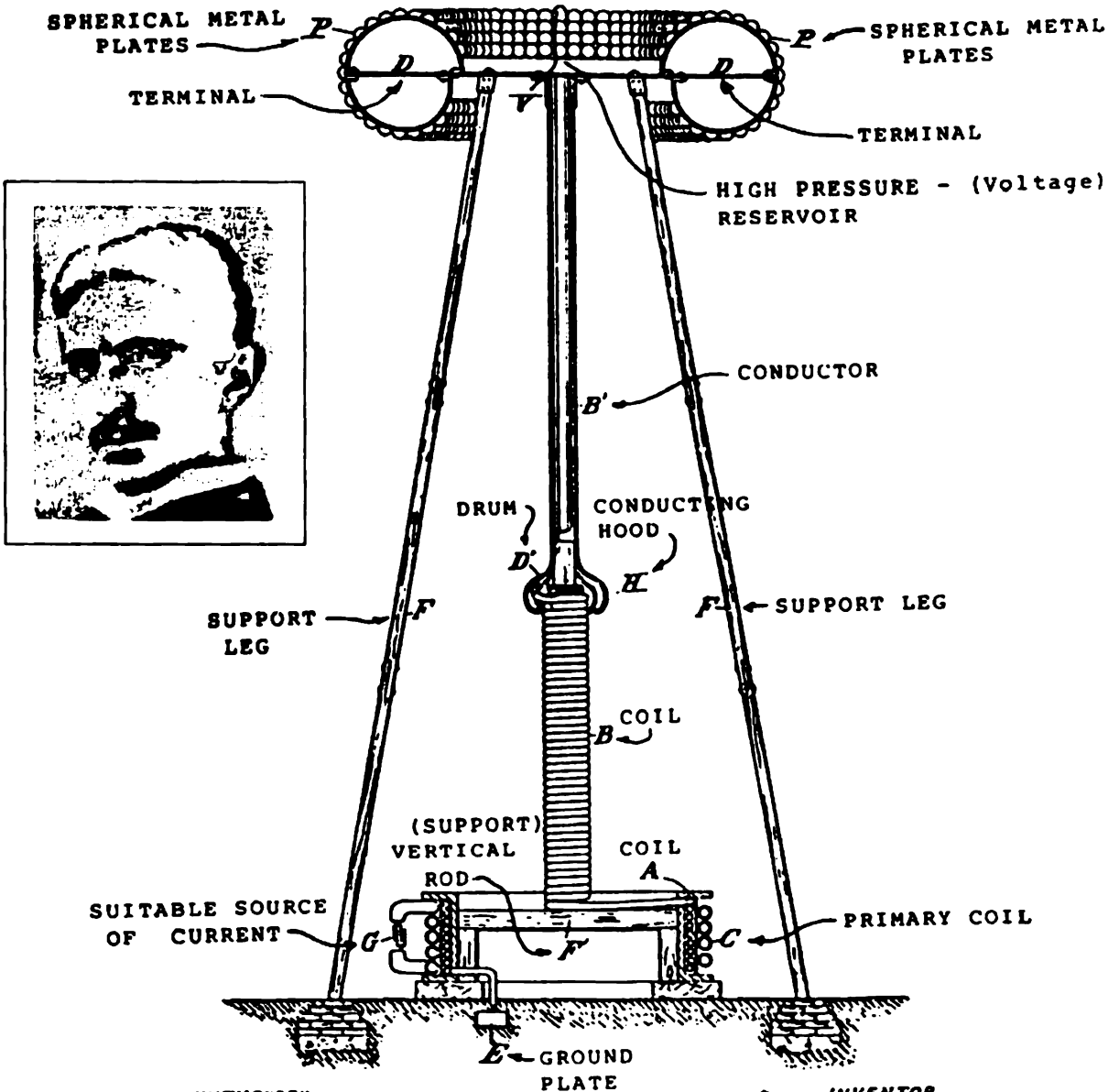
s = stationary suppressor grid

Note: Grids shown between (a) and (k) are control grids, as in (g), but are stationary. A stationary anode ring (v+) is shown next to each rotating induction cathode ring.

N. TESLA
 APPARATUS FOR TRANSMITTING ELECTRICAL ENERGY.
 APPLICATION FILED JAN. 18, 1902. RENEWED MAY 4, 1907.

1,119,732.

Patented Dec. 1, 1914.



WITNESSES

W. Lawson Dyer
Benjamin Miller

Nikola Tesla, INVENTOR,

By *Keen, Page & Cooper*,
 his ATTORNEYS.

Primary Voltage Expansion Ratio

model: Badlander

size: 4ft. dia.

The purpose of this WorkSheet is to calculate the total amount of negative (electron) charge which must be removed and withheld from the hull positive Zones of a given model (size) EDF Generator in operation, in order to achieve the desired expanded potential difference across the vessel hull. This expanded potential difference is required to initiate and maintain a full flow of field envelope current which completely surrounds the vessel. The necessary charge to be removed from the positive Zones will be stored in the two (2) Field Ballast Capacitors mounted on the outer edge of the rotor. Thus, these Ballast Capacitors support the *Primary Voltage Expansion Ratio* that is defined by the vessel's *primary cathode-to-field emitter emissivity ratio*.

Section A: Average Plate Separation Distance

To use the Uniform Field Intensity Formula from DataSheet #12 in calculating a maximum average value for σ , or surface charge density, an average value of d (plate separation distance) must be found. In keeping with the logic of the associated text, d_{av} is taken to be one-half of the sum of the Drive Field Perimeter and the Drive Field Boundary lengths:

$$\begin{aligned}
 [1] \text{ Field Perimeter} &= \pi/2 [R_h + (h_r + h_s)^2]^{1/2} \quad \{\text{per SpecSheet I}\} \\
 &= 1.5708 (586.9621)^{1/2} \\
 &= 1.5708 (24.2273)" \\
 &= 38.056" = .9666 \text{ m}
 \end{aligned}$$

Note: This Drive Field Perimeter length is used in the calculation of Spec. Field Voltage.

$$\begin{aligned}
 [2] \text{ Field Boundary} &= \pi/2 [(C_v - C_s)^2 + ((.1317)(C_v - C_s))^2]^{1/2} \quad \{\text{per SpecSheet I}\} \\
 &= 1.5708 (4.7789)" \\
 &= 7.5067" = .1907 \text{ m}
 \end{aligned}$$

$$\begin{aligned}
 [3] \quad d_{av} &= 1/2 ([1] + [2]) \\
 &= 1/2 (.9666 + .1907) \text{ m} \\
 &= .5787 \text{ m}
 \end{aligned}$$

Section B: Positive Zone Surface Charge Density**[1] 1η Thermal Unit:**

Using a peak field intensity calculated per Parts A and B of SpecSheet I in the UFI Formula, and inserting the corresponding peak field voltage desired, the resultant maximum average surface charge density required (for each field hemitorus) may be solved for as follows:

$$\begin{aligned}
 E' &= \frac{V\sigma}{d\epsilon_0}, \quad \text{where } E = 1.1 (3 \times 10^6 \text{ v/m}) = 3.3 \times 10^6 \text{ v/m}, \\
 V &= 1.1 (2.9 \times 10^6 \text{ v}) = 3.19 \times 10^6 \text{ v}, \\
 d_{av} &= .5787 \text{ m} \quad \{\text{from A[3] above}\}, \\
 \text{and } \epsilon_0 &= 8.85 \times 10^{-12} \text{ coul}^2/\text{nt-m}^2. \quad \{\text{traditional value, used throughout}\}
 \end{aligned}$$

Primary Voltage Expansion Ratio

$$\text{Therefore, } 10.89 \times 10^{12} = \frac{(3.19 \times 10^6) \sigma}{.5787 (8.85 \times 10^{-12})}$$

$$96.3765 (.5787) = (3.19 \times 10^6) \sigma$$

$$\text{max. } \sigma_{av} = 55.7731 / 3.19 \times 10^6$$

$$= \boxed{1.7484 \times 10^{-5} \text{ coul/m}^2} \text{ per hemitorus.}$$

[2] 3η Drive Unit:

Using the peak field voltage desired, as calculated per WorkSheet I(a) and SpecSheet I, in the UFI Formula and inserting the peak field intensity which corresponds to the full Field Perimeter length, the resultant maximum average surface charge density required (for each field hemitorus) may be solved for as follows:

$$E' = \frac{V\sigma}{d\epsilon_0}, \text{ where } V = 1.1 (35.1044 \times 10^6 \text{ v}) = 38.61484 \times 10^6 \text{ v,}$$

$$E = 38.61484 \times 10^6 \text{ v} / .9666 \text{ m} = 39.94914 \times 10^6 \text{ v/m,}$$

$$d_{av} = .5787 \text{ m \{from A[3] above\},}$$

$$\text{and } \epsilon_0 = 8.85 \times 10^{-12} \text{ coul}^2/\text{nt-m}^2. \text{ \{traditional value, used throughout\}}$$

$$\text{Therefore, } 15.95934 \times 10^{14} = \frac{(38.61484 \times 10^6) \sigma}{.5787 (8.85 \times 10^{-12})}$$

$$(141.24016 \times 10^7) (.5787) = (38.61484 \times 10^6) \sigma$$

$$\text{max. } \sigma_{av} = 8.17357 \times 10^7 / 3.861484 \times 10^7$$

$$= \boxed{2.1167 \times 10^{-4} \text{ coul/m}^2} \text{ per hemitorus.}$$

Section C: Hull Static Capacitance

In a standard capacitor, the relationship between the stored charge and operating voltage is governed by the simple equation $Q = CV$, where C equals the capacitance in farads. Thus, the higher the capacitance at a given supplied charge, the lower the resultant induced voltage across the capacitor. Therefore, it must be assumed that the Primary Voltage Expansion Ratio achieved by the EDF Generator is contingent upon (and proportional to) the vessel hull's operative static capacitance.

The first method of estimating the vessel hull's actual total parallel static capacitance (C_h) is by the traditional formula for a parallel-plate capacitor, wherein we must use the average value of d from A[3] above:

$$\begin{aligned} \text{est. } C_h &= 2[(8.85 \times 10^{-12})(.4288)/.5787] \\ &= 2(3.795 \times 10^{-12}/.5787) \\ &= 2(6.558 \times 10^{-12}) \\ &= 13.116 \times 10^{-12} \text{ farad.} \end{aligned}$$

The second method of estimating C_h is described at length in the associated text and yields a much larger value, wherein the plate separation distance d_s is derived from the Hull Spreadsheet:

$$d_s = \pm [(r + (C_s - C_h))/\sqrt{2} - h_s],$$

$$\text{and } \text{max. } C_h = \epsilon_0 2\pi R_s^2 / |d_s| = 23.712 \times 10^{-12} \text{ farad.}$$

This value is taken to be a theoretical maximum; R_s and d_s must be in meters.

Primary Voltage Expansion Ratio

Due to the critical importance of providing sufficient Field ballast, it is deemed desirable to increase the first value of estimated ballast charge Q_b obtained in Section D below (based on the d_{av} method used in the UFI Formula) by an amount corresponding to the ratio of the above-stated higher value of C_b (obtained by a theoretical dual charged ring method) to the lower value thereof. This is done in light of the unavoidable uncertainty involved in both methods used to estimate total capacitance in this unorthodox application, given the direct relationship of hull static capacitance to the required Primary Voltage Expansion Ratio.

Therefore, since $\max.C_b/\text{est. } C_b = 23.712/13.116 = 1.808$,

$$\max.Q_b = 1.808 (\text{est. } Q_b).$$

This value $\max.Q_b$ is used in WorkSheet VIII(e) to design each Field Ballast Capacitor. It must be stressed that any actual operative value of C_b less than the value $\max.C_b$ stated above (as determined in prototype testing) would merely result in a correspondingly higher Primary Voltage Expansion Ratio and lower required nominal rotor speed.

Section C: Estimated Ballast Charge

The Primary Voltage Expansion Ratio sought in both the 1 η and 3 η rotor versions of this model device refers to the ratio of the Specification Field Voltage across the vessel hull to the Specification value of the potential difference across the Primary Induction Ring Arrays, or $\text{spec.}\Delta V_p$. In the 1 η rotor device this Ratio is a constant 750:1 regardless of model (size), per Part B[1] of SpecSheet I. In this particular 3 η rotor device, this Ratio is equal to 12,106:1 as calculated in WorkSheet I(a).

[1] 1 η Thermal Unit:

If we take the maximum average σ calculated in B[1] above and multiply it by the surface area of one plate (per hemitorus), we may now find the estimated total charge (Q_b) that each of the two (2) Field Ballast Capacitors must hold in order to effect a Primary Voltage Expansion Ratio of 750 to 1:

$$Q_b = \max.\sigma_{av}A, \text{ where } A = 664.6 \text{ in}^2 \text{ \{from Hull Configuration Spreadsheet\}}$$

$$\begin{aligned} \text{So, est. } Q_b &= (1.7484 \times 10^{-5})(664.6 \text{ in}^2)(6.4516 \text{ cm}^2/\text{in}^2) \\ &= (1.7484 \times 10^{-5})(.4288 \text{ m}^2) \\ &= 7.4971 \times 10^{-6} \text{ coul., per hemitorus.} \end{aligned}$$

Therefore, $\max.Q_b = 1.808 (7.4971 \times 10^{-6}) = 1.3555 \times 10^{-5} \text{ coul. per hemitorus.}$

[2] 3 η Drive Unit:

If we take the maximum average σ calculated in B[2] above and multiply it by the surface area of one plate (per hemitorus), we may now find the estimated total charge (Q_b) that each of the two (2) Field Ballast Capacitors must hold in order to effect a Primary Voltage Expansion Ratio of 12,106 to 1:

$$Q_b = \max.\sigma_{av}A, \text{ where } A = 664.6 \text{ in}^2 \text{ \{from Hull Configuration Spreadsheet\}}$$

$$\begin{aligned} \text{So, est. } Q_b &= (2.1167 \times 10^{-4})(664.6 \text{ in}^2)(6.4516 \text{ cm}^2/\text{in}^2) \\ &= (2.1167 \times 10^{-4})(.4288 \text{ m}^2) \\ &= 9.0764 \times 10^{-5} \text{ coul., per hemitorus.} \end{aligned}$$

Therefore, $\max.Q_b = 1.808 (9.0764 \times 10^{-5}) = 1.6410 \times 10^{-4} \text{ coul. per hemitorus.}$

Field Ballast Capacitors

model: Badlander
size: 4ft. dia.

This WorkSheet references WorkSheet VIII(d) {Primary Voltage Expansion Ratio} for purposes of developing the dielectric requirements and proper electrode spacing for the Field Ballast Capacitors, in order to effect the requisite Voltage Expansion Ratio of both the 1 η and 3 η rotor versions of this model device.

Component Specification: The source of the applied plate (anode) voltage for each Field Ballast Capacitor shall be the outer Field Coil anode connection within its Primary Power System semicircuit.

The peak potential difference (ΔV) across each Ballast Capacitor, given the Specification above, is equal to that across its respective outer induction array. This voltage is equal to 1/2 of the peak *Primary System Voltage* or 6,379.56 in the 1 η rotor device, and 3/8 of the peak *Primary System Voltage* or 4,784.67 in the 3 η rotor device.

Section A: Maximum Area of Ballast Capacitors

Any unnecessary reduction in the plate area of the Ballast Capacitors from the total area of rotor bandwidth L is to be avoided, especially in 1 η rotor devices, and the net plate area A may represent no less than 20% thereof.

$$A_{\max} = \pi(R^2 - r^2) , \quad \text{where } R = 19'' \\ \text{and } r = 18.5'' \text{ \{from SpecSheet III\};}$$

$$\begin{aligned} \text{thus, } A_{\max} &= \pi(361 - 342.25)'' \\ &= (58.905 \text{ in}^2)(6.4516 \text{ cm}^2/\text{in}^2) \\ &= 380 \text{ cm}^2 = .0380 \text{ m}^2 \text{ per plate, per unit.} \end{aligned}$$

***Note:** The inner plate positioning reference line should remain fixed when area is reduced.

Section B: Per-Unit Ballast Capacitance**[1] 1 η Thermal Unit:**

$$\begin{aligned} \text{design } C_b &= \max.Q_b / \Delta V , \quad \text{where } \max.Q_b = 1.3555 \times 10^{-3} \text{ coul. \{from WorkSheet VIII(d)\}} \\ &\quad \text{and } \Delta V = 6.3796 \times 10^3 \text{ volts . \{from above\}} \end{aligned}$$

$$\text{So, design } C_b = \underline{2.1247 \times 10^{-8} \text{ farad}} .$$

[2] 3 η Drive Unit:

$$\begin{aligned} \text{design } C_b &= \max.Q_b / \Delta V , \quad \text{where } \max.Q_b = 1.6410 \times 10^{-4} \text{ coul. \{from WorkSheet VIII(d)\}} \\ &\quad \text{and } \Delta V = 4.7847 \times 10^3 \text{ volts . \{from above\}} \end{aligned}$$

$$\text{So, design } C_b = \underline{3.4297 \times 10^{-8} \text{ farad}} .$$

Section C: Ballast Capacitor Dielectrics

Since the peak field intensity between the plates of the Ballast Capacitors (E_{\max}) equals the force per unit charge therein, E_{\max} must be equal to or greater than the intensity E, across the vessel hull, to ensure their saturation capability. This places an upper limit on the dielectric constant used and increases any required plate area reduction. The resultant dielectric specifications including the 1 η value k_{\max} and the 3 η value k_{\max} are given below.

Field Ballast Capacitors

Component Specification:

The dielectric material used in the Field Ballast Capacitors of 1 η rotor devices shall be *standard electrical mica*, which should be available (and may therefore be operated) in the range of k values from 5 to 9. The actual grade of mica selected is to be operated at a peak field intensity (E_{bd}) which is a maximum of approximately 33% of its rough breakdown intensity E_{brk} .

[1] (a) 1 η Thermal Unit:

Therefore, $E_{bd} \geq \frac{\max.Q_b}{k\epsilon_0 A} \geq E_t$, where $E_t = 3.30 \times 10^6$ v/m (peak value),
and k = dielectric constant.

$$\text{So, } E_{bd} \geq \frac{1.3555 \times 10^{-5}}{k(8.85 \times 10^{-12})(.0380)} \geq 3.30 \times 10^6,$$

$$\text{and } k_{\max} \leq \frac{1.3555 \times 10^{-5}}{1.1098 \times 10^{-6}} \leq 12.21, \text{ and may require plate area reduction.}$$

Component Specification:

The dielectric material used in the Field Ballast Capacitors of 3 η rotor devices shall be a *calcium titanate composition*, which should be available (and may therefore be operated) in the range of k values from 12 to 24. The actual titanate grade selected is to be operated at a field intensity (E_{bd}) which is a maximum of approximately 83% of its rough breakdown intensity E_{brk} .

(b) 3 η Drive Unit:

Therefore, $E_{bd} \geq \frac{\max.Q_b}{k\epsilon_0 A} \geq E_t$, where $E_t = 39.94914 \times 10^6$ v/m (peak value),
and k = dielectric constant.

$$\text{So, } E_{bd} \geq \frac{1.6410 \times 10^{-4}}{k(8.85 \times 10^{-12})(.0380)} \geq 39.94914 \times 10^6,$$

$$\text{and } k_{\max} \leq \frac{1.6410 \times 10^{-4}}{1.3435 \times 10^{-5}} \leq 12.21; \text{ this represents a reference value only.}$$

It must be pointed out that the value k_{\max} just figured should in every instance actually constitute a value for k which is less than the minimum possible k value which may be used to calculate an acceptable plate spacing (by the method in Section D below) without further reducing plate area.

Section D: Plate Separation Distance

[1] 1 η Thermal Unit:

(a) The first step in finding the distance between the plates, and hence the thickness of the dielectric required, is to select a dielectric k value (to the nearest half unit) that is about midway within the appropriate range. Therefore, let $k = 6.5$ (for medium-grade electrical mica).

(b) Next, E_{bd} and E_{brk} must be calculated:

$$E_{brk} = 6.5 (3 \times 10^6) = 21 \times 10^6,$$

$$\text{and } E_{bd} = .33 (19.5 \times 10^6) = 6.435 \times 10^6. \quad \{\theta E_{bd} = 33\% (E_{brk})\}$$

(c) The acceptable minimum plate separation distance ($\min.d$) may now be computed as follows:

$$\min.d = \Delta V / E_{bd} = \frac{6.3796 \times 10^3}{6.435 \times 10^6} = 0.9914 \times 10^{-3} \text{ m;}$$

$$\text{so, } \min.d = .09914 \text{ cm, or } .03903" \quad @ k = 6.5. \quad \{\text{Specification}\}$$

Field Ballast Capacitors

Note: If the value of $\min.d$ just figured does not lie near the lower end of the range of values between 10/9600 and 20/9600 of the vessel R_v , a higher dielectric k value (to the nearest half unit) should be selected and $\min.d$ recalculated as necessary until this condition exists (but only so long as the concomitant plate area reduction is not deemed excessive)!

[2] 3η Drive Unit:

(a) The first step in finding the distance between the plates, and hence the thickness of the dielectric required, is to select a dielectric k value (to the nearest half unit) that is about midway within the appropriate range. Therefore, let $k = 16.5$ (for medium- k calcium titanate).

(b) Next, E_{bd} and E_{brk} must be calculated:

$$E_{brk} = 16.5 (3 \times 10^6) = 49.5 \times 10^6,$$

$$\text{and } E_{bd} = .83 (49.5 \times 10^6) = 41.09 \times 10^6. \quad \{ @ E_{bd} = 83\% (E_{brk})$$

(c) The acceptable minimum plate separation distance ($\min.d$) may now be computed as follows:

$$\min.d = \Delta V / E_{bd} = \frac{4.7847 \times 10^3}{4.109 \times 10^7} = 1.1644 \times 10^{-4} \text{ m};$$

$$\text{so, } \min.d = .01164 \text{ cm, or } \underline{.00458"} @ k = 16.5. \quad \{ \text{Specification}$$

Section E: Plate Area and Field Intensity

The values for $\min.d$ obtained above must be considered tentative until the corresponding net plate areas are calculated (and verified to be equal to or less than A_{max}), and the resultant peak field intensities are double-checked.

[1] 1η Thermal Unit:

(a) plate area: design $C_b = \frac{k\epsilon_0 A}{d}$, w/d in meters, from above.

$$\text{and } 2.1247 \times 10^{-8} = \frac{(57.525 \times 10^{-12})A}{9.914 \times 10^{-4}};$$

$$\text{net } A = \frac{(21.0643 \times 10^{-11})}{(5.7525 \times 10^{-11})} = \underline{.03662 \text{ m}^2}. \quad \{ \text{Specification}$$

(b) field intensity: $E_{bd} \geq \frac{1.3555 \times 10^{-3}}{6.5(8.85 \times 10^{-12})(.03662)} \geq E_t;$

$$\frac{1.3555 \times 10^{-3}}{2.1066 \times 10^{-12}} \geq 6.432 \times 10^6 \geq 3.30 \times 10^6. \quad \{ \text{check}$$

[2] 3η Drive Unit:

(a) plate area: design $C_b = \frac{k\epsilon_0 A}{d}$, w/d in meters, from above.

$$\text{and } 3.4297 \times 10^{-8} = \frac{(146.03 \times 10^{-12})A}{1.1644 \times 10^{-4}};$$

$$\text{net } A = \frac{(3.9935 \times 10^{-12})}{(146.03 \times 10^{-12})} = \underline{.02735 \text{ m}^2}. \quad \{ \text{Specification}$$

(b) field intensity: $E_{bd} \geq \frac{1.6410 \times 10^{-4}}{16.5(8.85 \times 10^{-12})(.02735)} \geq E_t;$

$$\frac{1.6410 \times 10^{-4}}{3.9938 \times 10^{-12}} \geq 4.11 \times 10^7 \geq 41.09 \times 10^6. \quad \{ \text{check}$$

Note: If the value of E_{bd} just figured is not equal to or greater than E_t , a higher dielectric k value (to the nearest half unit) must be selected and the entire series of calculations in Sections D and E above must be repeated until this condition exists! Also, the lowest such k value which does satisfy this requirement should be used in each instance.

Section F: Vacuum Chamber Transit Time Analysis

The value of field ballast capacitance upon which the above Specifications are based should be considered a nominal value reflecting the maximum theoretical net-hull-charge storage capability required to support the desired Primary Voltage Expansion Ratio. This capacitance determination neglects consideration of the effect that hull Emitter Ring vacuum chamber space charge may have in altering the exterior Field potential difference. The reason why this is so is not necessarily obvious, so a brief elucidation is in order. The crucial role of this chamber space charge in field induction system circuit resistance is also examined at the end of DataSheet #14 {Stage Voltage Balance}.

As was first referred to in SpecSheet I and discussed further in WorkSheet VIII(c) {Pentode Potential Differences}, the plate potential difference across each Primary Induction Ring Array is essentially equal to one-half (1/2) rotor voltage, with the unit cathodes at ground potential as explained in DataSheet #15. Along this line of reasoning, the potential difference across the vacuum chamber will also tend to equal half of the rotor voltage, with the inner surface of the hull Emitter Ring also at ground potential (due to the Faraday shielding principle).

Were the distance between the field emitters and this inner Negative Ring surface uniform and equal to that between the primary unit cathodes and unit anode ring, the transit time of Field current electrons across each would be the same, as would the total amount of in-transit charge represented. However, the over 5 times greater average distance across the vacuum chamber results in a much greater average electron transit time, and a correspondingly greater amount of negative space charge which is in essence stored capacitively.

Contemplating operation of the device as a closed charge system, the amount of this stored negative space charge over and above that of the Primary Induction Ring Arrays must represent either a corresponding intensification of the positive Zones' surface charge density or reduction of the Emitter Ring charge density. This condition perforce must result in either an unbalanced or other-than-expected Field potential difference, if only marginally. Accurately assessing the consequences of this consideration lies within the purview of calculus, and is beyond the scope required of our work here.

Section G: Voltage Supply Traces

One significant design drawback of placing the Ballast Capacitors outside the rotor's rolling bearing assemblies is that their voltage supply must now pass beneath the rotor ballrace. As can be seen in Fig. 24 (on pg. 123), this has been done due to extreme space limitations as well as to take the fullest possible advantage of any Hooper effect voltage rise. Given the right choice of material to use as peripheral rotor facing (or hard insulation covering), this is not anticipated to present that great a difficulty.

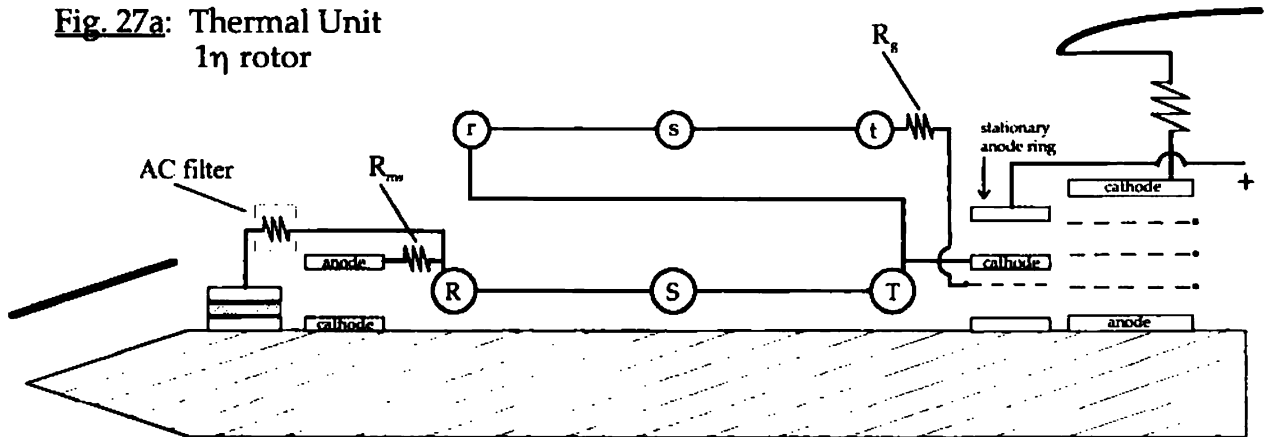
Carefully-considered Specifications are given in Section 4 of Material SpecSheet C for thin conductive traces on a thick-film substrate layer to be used to connect each outer induction array anode directly to the positive plate of its respective Ballast Capacitor in a small and evenly-distributed number of points. A second thin facing layer seals these traces or connection leads against any negative space charge present in that region of the vacuum chamber.

Each outer transfer array anode must be connected to its center field coil in a similar manner, but in this case a groove may be cut in a single segment separator and the trace or lead then laid down and sealed with the silicone elastomer central rotor facing layer.

Power System Schematics

The method of connecting the rotor bias windings of single-stage (1η) and three-stage (3η) devices, while observing appropriate conventions of polarity assignment, is illustrated in the following generalized schematic representation. Providing bias windings which are correctly matched to the potential differences across the various rotating electrode arrays is crucial to maintaining a proper level of series coil group current. Even more important is the **Field Voltage Control System**, and the adjoining schematic for this circuitry which governs all Field Induction System pentode hardware is included on the next page. It should be noted that the *Primary System Voltage* equals the total series voltage of either coil group plus a 40% bias voltage rise, and is the same in 1η and 3η rotor devices.

Fig. 27a: Thermal Unit
 1η rotor

**KEY**

R = outer field winding
S = center field winding
T = inner field winding

r = outer bias winding
s = center bias winding
t = inner bias winding

Fig. 27b: Drive Unit
 3η rotor

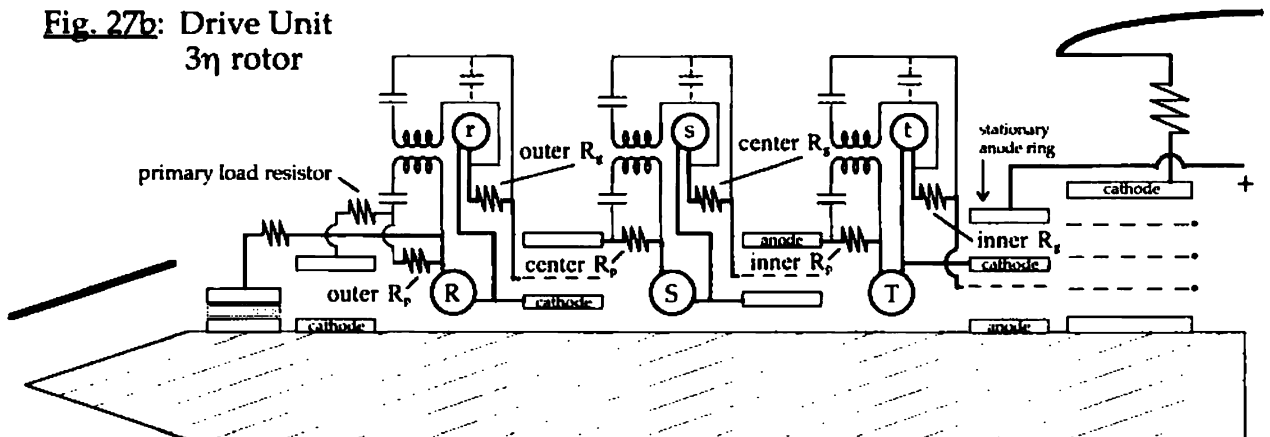


Fig. 27: one-half of symmetrical Primary Power System circuitry.

Rotor voltage approaches $2/3$ Primary System Voltage in the 1η device, and $1/2$ PSV in the 3η device. See Part D of SpecSheet I for a discussion of rotor induction efficiencies.

The control circuit shown below is modular in nature, in that one such unit is provided for each of the 36 unit pentode arrays associated with both of the two Field Induction System semicircuits. All electrode voltage measurements, including positive housing section voltage, are to be made with respect to the model unit's *ground frame*: the metallic structural shell of the device's central chamber to which the rotor carrier assembly is mounted.

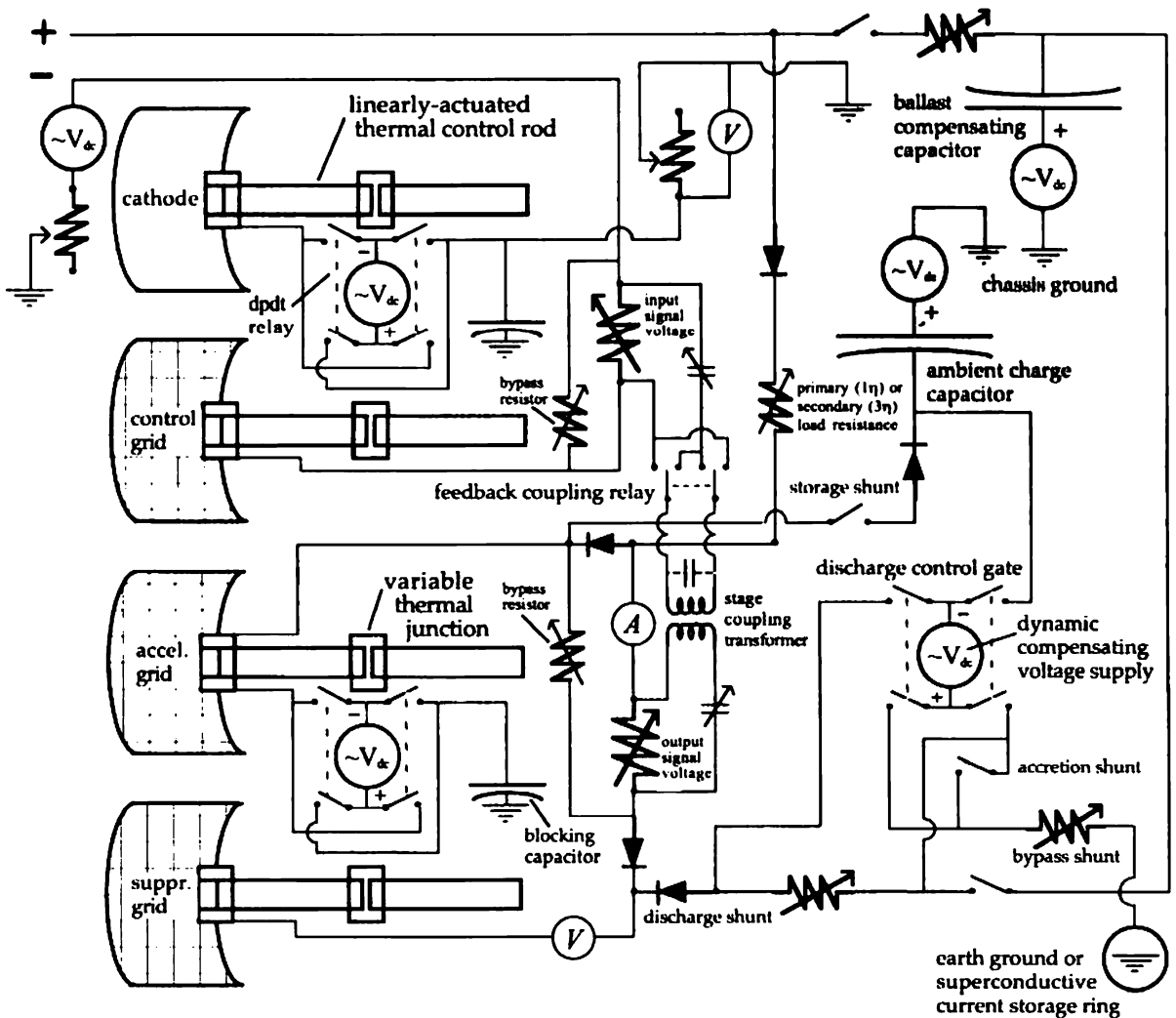


Fig. 28: schematic for the EDF Generator's Field Voltage Control System.

Note: The positive source voltage shown in the top left corner is that shown in the previous Fig.

1) A **thermal control rod** is provided for each unit pentode array electrode which variably engages a cold thermal junction maintained at the reservoir temperature of the principal housing coolant, by means of a linear actuator, to regulate electrode temperature to approximately the same temperature as the associated Power Resistor (at $675^{\circ}\text{C} \pm 55^{\circ}$). In this manner, small adjustments in cathode emissivity may be made as necessary during operation and the various grids may be closely matched in temperature to that of their respective cathode to ensure the accuracy of mutual electrode voltage balance.

2) An independent common variable DC voltage supply is provided for all unit cathodes as a means of ensuring an optimum cathode potential with respect to ground, despite fluctuating Power Resistor temperatures (in 3η devices where field hemitorus current is variably biased). This supply is double-pole shunted to enable either a positive or negative control voltage to be applied to the cathodes in

order to hold their potential as close to ground as possible. Such a voltage supply is also provided for all unit accelerator grids as a means of modulating the level of applied positive voltage and therefore the level of field current bias, independent of the level of applied control grid bias. In both cases, these DC supplies are isolated from ground by blocking capacitors to ensure that a net charge loss or accumulation does not accrue to the ground frame (in model units not connected to true earth ground).

3) **Ballast compensating capacitors** are provided whereby the rotor ballast capacitors' positive-plate outrush charge may be purged from the Primary Power System, via the stationary anode ring associated with each of its two inner induction electrode arrays, to prevent stage electrode array voltage ratings from otherwise being greatly exceeded. Upon rotor de-spin, this ground-restoring charge must be proportionately returned to each stationary anode ring (via the discharge resistor and relay shown) and to the Primary Power System as a whole via the suppressor grid *discharge shunts* after vacuum chamber current (to the hull Negative Ring) has essentially ceased. A dedicated variable DC voltage supply whose negative terminal is connected to the ground frame ensures that the appropriate compensating charge may be stored against the high positive applied potential of the stationary anode rings.

4) The **ambient charge capacitors** absorb ionization charge (arising from operation in air) which perforce must fall into the potential well established by the positive housing sections *at least* until the field current envelope is fully formed, and which would otherwise tend to ground the desired positive housing section voltage. Excess ionization charge above these capacitors' joint storage capability must either be grounded off or deposited in a superconductive current storage ring (in ungrounded Drive units designed for maximum ambient charge storage) via *accretion shunts*. Upon rotor de-spin, this charge may also be dumped across the suppressor grid discharge shunts at a rate sufficient to ensure that the entire Primary Power System returns to a ground potential (by direct rotor-shorting to the outer induction array anode rings).

5) A **variable bypass resistor** is provided between each accelerator grid and its associated suppressor grid which returns the inevitable stationary anode ring and accelerator grid circuit current to the rotor, and which assists in maintaining the suppressor grid at a potential as close to ground as possible. The *output signal resistor* paralleled therewith is analogous to a plate resistor on behalf of each 3rd-stage inner induction array in Drive Units, and the potential difference across it provides the necessary AC signal voltage to be applied to the Primary Array control grids as a further AC voltage amplification or suppression stage. The **stage coupling transformers** ensure voltage reference isolation between stages, and the **feedback coupling relays** are used to apply inverse AC signal feedback to the rotor circuit to provide a requisite level of AC voltage suppression or to de-couple the input and output circuits.

6) The variable output of the **dynamic compensating voltage supply** is to be approximately the same as that of the ambient charge capacitors' positive voltage supply, thereby allowing those capacitors to be gradually saturated during rotor spin-up with electrons collected at the accelerator grids. During the spin-up and 'run' periods, the **discharge control gate relay** is normally closed such that the dynamic compensating supply's negative pole is connected to the negative plates of those same capacitors. The slow 'run' release and distribution of stored negative charge reserves to the rotor from the ambient charge capacitors is accomplished by the gradual synchronized relaxation of the two said supplies' voltages across the discharge control gate.

7) Postulating continuous operation of the device in the vacuum of space, the exhibited field voltage will tend to rise gradually as the total amount of charge contained in the field discharge current is gradually reduced through unavoidable *electron leakage losses* (primarily at the hull Negative Ring peripheral edge). To compensate for this effect, stored ambient charge must therefore be continually released at the suppressor grids into the rotor return current. The rate at which this gradual discharge must be effected is dependent upon the *observed* field leakage rate, as only a rough approximation of the leakage may be pre-calculated. It is for this reason that at least one superconductive storage ring (containing a tremendous quantity of ambient charge in the form of a continuous zero-loss current) must be included in any ungrounded model unit used in space exploration, as the capacity of such storage ring(s) determines the vessel's effective range of operation.

8) Postulating the continuous operation of the device in a gaseous atmosphere, field leakage losses may be compensated by proportionally discharge-shunted charge (with storage and accretion shunt relays closed), should excess ionization charge be found available. If such excess charge is observed to be insufficient for this purpose, due to the external field's *kinetic occlusion* of all or a major portion of otherwise available ambient ionization charge *once the field envelope is fully formed*, the relatively limited capacitively-stored ambient charge would have to be gradually released into the rotor return current and a limited spin-up/run/de-spin *repeating duty cycle* might result unless the dynamic compensating supply is then used to pull bypass-shunted charge from a suitable earth ground connection.

Bias Winding Turns Ratios

model: Badlander

size: 4ft. dia.

This WorkSheet is used to determine the final field winding and bias winding turns Specifications for each of the three different size Field Coils employed in a given size (model) vessel. The subsequent *field winding-to-bias winding turns ratio* for each Field Coil is also calculated, and these ratios will all be different from one another (within each series coil group) because each size Coil is slightly different in magnetic efficiency and total number of turns. As figured in Section D of WorkSheet VII(c), the combined coil group (all winding) voltage output ratio (V_{c}/r) for this model device - whether it be the 1 η or 3 η rotor variant - is equal to 355.99 volts/rev/sec.

Section A: 1 η Thermal Unit**[1] total bias winding voltage output ratio:**

Since only the inner induction array requires an applied bias winding voltage, and the unbiased potential difference across this array will be equal to one-half of the total field winding output voltage, we may derive the following expressions to solve for the total bias winding voltage output ratio (V_{b}/r) which must be jointly produced by the bias windings of all three (3) Field Coils of each series coil group (given a 40% design bias voltage ratio):

let x = total field winding output ratio,
and $.40(.5x)$ = total bias winding output ratio required {per DataSheet #8}.

So, $1.20x = V_{\text{c}}/r = 355.99$ volts/rev/sec.,

and $x = 296.66$ volts/rev/sec.

Therefore, $V_{\text{b}}/r = V_{\text{c}}/r - x = 355.99 - 296.66 = 59.33$ volts/rev/sec.

[2] uniform bias winding voltage output ratio:

To provide a means of assessing the relative accuracy of each Field Coil's assigned Turns Ratio Factor {from WorkSheet VII(b)}, it is desired to split the total bias winding output ratio evenly between the three (3) Coils of each series coil group, thus deriving a uniform bias winding output ratio as follows:

$$V_{\text{b}}/r = (V_{\text{b}}/r)/3 = 19.78 \text{ volts/rev/sec.}$$

If we now divide this uniform bias output ratio by the net 3rd layer output ratio of each Coil {figured in WorkSheet VII(c) and multiply the result by that Coil's 3rd layer number of turns, we may calculate the exact number of turns of which each bias winding must be composed. Then, by simple subtraction, each Coil's total field winding turns may be found.

[3] individual coil turns compositions:

(a) outer Coil net 3rd layer output ratio = net $V_{\text{o}} = 33.62$ volts/rev/sec.

$$[19.78/33.62](10,000) = \boxed{5,883 \text{ bias turns}} \quad \{\text{Specification}$$

$$10,000 - 5,883 = \boxed{4,117 \text{ field turns}} \quad \{\text{Specification}$$

Bias Winding Turns Ratios

(b) center Coil net 3rd layer output ratio = net V_{c3} = 41.90 volts/rev/sec.

$$[19.78/41.90](9,000) = \boxed{4,249 \text{ bias turns}} \quad \{\text{Specification}\}$$

$$9,000 - 4,249 = \boxed{4,751 \text{ field turns}} \quad \{\text{Specification}\}$$

(c) inner Coil net 3rd layer output ratio = net V_{i3} = 52.84 volts/rev/sec.

$$[19.78/52.84](8,334) = \boxed{3,120 \text{ bias turns}} \quad \{\text{Specification}\}$$

$$8,334 - 3,120 = \boxed{5,214 \text{ field turns}} \quad \{\text{Specification}\}$$

[4] final bias winding turns ratios: {reflecting coil field turns per bias turn}

(a) outer Coils- $[2(10,000) + 4,117] \text{ field} \div 5,883 \text{ bias} = 4.10:1$.

(b) center Coils- $[2(9,000) + 4,751] \text{ field} \div 4,249 \text{ bias} = 5.35:1$.

(c) inner Coils- $[2(8,333) + 5,214] \text{ field} \div 3,120 \text{ bias} = 7.01:1$.

Section B: 3 η Drive Unit

[1] total bias winding voltage output ratio:

(a) In the 3 η rotor device, bias winding voltages must be applied to the transfer arrays and inner induction array of each series coil group. Using the logic developed in Sections A and C of WorkSheet VIII(a), the sum of the unbiased potential differences across these arrays will be equal to 5/8 of the total field winding voltage output. Thus, if the design bias voltage ratio is to be 40% in the 3 η rotor device, the total bias winding voltage output ratio would be .40(.625) or 25% of the total coil group voltage output ratio (V_{t3}/r). We may then use the following expressions to easily calculate V_{t3}/r :

let x = total field voltage output ratio,
and $x/4$ = total bias voltage output ratio V_{t3}/r .

Therefore, $1.25x$ = combined coil group voltage output ratio V_{t3}/r .

So, $1.25x = 355.99 \text{ volts/rev/sec,}$

$x = 284.79 \text{ volts/rev/sec,}$

and $V_{t3}/r = 71.20 \text{ volts/rev/sec.}$

[2] individual bias winding voltage output ratios:

In this case, the required inner Coil bias winding voltage output ratio will be equal to .60(V_{t3}/r), or 42.72 volts/rev/sec, and the center and outer bias winding voltage output ratios will each be equal to 1/3 of this value at .20(V_{t3}/r) or 14.24 volts/rev/sec. This condition still provides a means to assess the relative accuracy of each Coil's Turns Ratio Factor, as referred to above.

If we now divide these appropriate individual bias output ratios by the respective net 3rd layer output ratio of each Coil {figured in WorkSheet VII(c)} and multiply the result by that Coil's 3rd layer number of turns, we may calculate the exact number of turns of which each bias winding must be composed. Then, by simple subtraction, each Coil's total field winding turns may be found.

[3] individual coil turns compositions:

(a) outer Coil net 3rd layer output ratio = net V_{o3} = 33.62 volts/rev/sec.

$$[14.24/33.62](10,000) = \boxed{4,236 \text{ bias turns}} \quad \{\text{Specification}\}$$

Bias Winding Turns Ratios

$$10,000 - 4,236 = 5,764 \text{ field turns } \{\text{Specification}\}$$

(b) center Coil net 3rd layer output ratio = net V_{c1} = 41.90 volts/rev/sec.

$$[14.24/41.90](9,000) = 3,059 \text{ bias turns } \{\text{Specification}\}$$

$$9,000 - 3,059 = 5,941 \text{ field turns } \{\text{Specification}\}$$

(c) inner Coil net 3rd layer output ratio = net V_{i1} = 52.84 volts/rev/sec.

$$[42.72/52.84](8,334) = 6,738 \text{ bias turns } \{\text{Specification}\}$$

$$8,334 - 6,738 = 1,596 \text{ field turns } \{\text{Specification}\}$$

[4] final bias winding turns ratios: {reflecting coil field turns per bias turn}

(a) outer Coils- $[2(10,000) + 5,764] \text{ field} \div 4,236 \text{ bias} = 6.08:1$.

(b) center Coils- $[2(9,000) + 5,941] \text{ field} \div 3,059 \text{ bias} = 7.83:1$.

(c) inner Coils- $[2(8,333) + 1,596] \text{ field} \div 6,738 \text{ bias} = 2.71:1$.

WorkSheet IX(b)

Field Coil Voltage Values

model: Badlander
size: 4ft. dia.

This WorkSheet is used to compute specific values of field winding and bias winding output voltages for purposes of determining the nominal rotor speed of both the 1 η and 3 η rotor variants of this model (size) device. Reference is made to data from WorkSheet VII(c) {Field Coil Output Ratios} and WorkSheet IX(a) {Bias Winding Turns Ratios}.

Note: Any peak values shown are considered design operating maximums.

Section A: 3rd Layer Voltage Output Ratios

[1] 1 η Thermal Unit

(a) final outer field winding 3rd layer output ratio: = V_{of}/r ,

$$\text{and } V_{of}/r = (4,117/10,000)(33.62 \text{ volts/rev/sec}) = 13.84 \text{ volts/rev/sec.}$$

final outer bias winding 3rd layer output ratio: = V_{ob}/r ,

$$\text{and } V_{ob}/r = (5,883/10,000)(33.62 \text{ volts/rev/sec}) = 19.78 \text{ volts/rev/sec.}$$

(b) final center field winding 3rd layer output ratio: = V_{cf}/r ,

$$\text{and } V_{cf}/r = (4,751/9,000)(41.90 \text{ volts/rev/sec}) = 22.12 \text{ volts/rev/sec.}$$

final center bias winding 3rd layer output ratio: = V_{cb}/r ,

$$\text{and } V_{cb}/r = (4,249/9,000)(41.90 \text{ volts/rev/sec}) = 19.78 \text{ volts/rev/sec.}$$

(c) final inner field winding 3rd layer output ratio: = V_{if}/r ,

$$\text{and } V_{if}/r = (5,214/8,334)(52.84 \text{ volts/rev/sec}) = 33.06 \text{ volts/rev/sec.}$$

final inner bias winding 3rd layer output ratio: = V_{ib}/r ,

$$\text{and } V_{ib}/r = (3,120/8,334)(52.84 \text{ volts/rev/sec}) = 19.78 \text{ volts/rev/sec.}$$

Field Coil Voltage Values

[2] 3 η Drive Unit

(a) final outer field winding 3rd layer output ratio: = V_{of}/r ,

$$\text{and } V_{of}/r = (5,764/10,000)(33.62 \text{ volts/rev/sec}) = 19.38 \text{ volts/rev/sec.}$$

final outer bias winding 3rd layer output ratio: = V_{ob}/r ,

$$\text{and } V_{ob}/r = (4,236/10,000)(33.62 \text{ volts/rev/sec}) = 14.24 \text{ volts/rev/sec.}$$

(b) final center field winding 3rd layer output ratio: = V_{cf}/r ,

$$\text{and } V_{cf}/r = (5,941/9,000)(41.90 \text{ volts/rev/sec}) = 27.66 \text{ volts/rev/sec.}$$

final center bias winding 3rd layer output ratio: = V_{cb}/r ,

$$\text{and } V_{cb}/r = (3,059/9,000)(41.90 \text{ volts/rev/sec}) = 14.24 \text{ volts/rev/sec.}$$

(c) final inner field winding 3rd layer output ratio: = V_{if}/r ,

$$\text{and } V_{if}/r = (1,596/8,334)(52.84 \text{ volts/rev/sec}) = 10.12 \text{ volts/rev/sec.}$$

final inner bias winding 3rd layer output ratio: = V_{ib}/r ,

$$\text{and } V_{ib}/r = (6,738/8,334)(52.84 \text{ volts/rev/sec}) = 42.72 \text{ volts/rev/sec.}$$

Section B: 1 η Nominal Rotor Speed

[1](a) total outer field winding output ratio: = V_{to}/r ,

$$\begin{aligned} \text{where } V_{to}/r &= (V_{oi}/r + V_{of}/r + V_{or}/r) \\ &= (27.72 + 34.71 + 13.84) \\ &= 76.27 \text{ volts/rev/sec.} \end{aligned}$$

(b) total center field winding output ratio: = V_{tc}/r ,

$$\begin{aligned} \text{where } V_{tc}/r &= (V_{ci}/r + V_{cf}/r + V_{cr}/r) \\ &= (33.71 + 40.95 + 22.12) \\ &= 96.78 \text{ volts/rev/sec.} \end{aligned}$$

(c) total inner field winding output ratio: = V_{ti}/r ,

$$\begin{aligned} \text{where } V_{ti}/r &= (V_{ii}/r + V_{if}/r + V_{ir}/r) \\ &= (41.56 + 48.98 + 33.06) \\ &= 123.60 \text{ volts/rev/sec.} \end{aligned}$$

[2](a) total rotor field winding voltage output ratio:

$$\begin{aligned} V_{tf}/r &= V_{to}/r + V_{tc}/r + V_{ti}/r \\ &= 76.27 + 96.78 + 123.60 \\ &= 296.65 \text{ volts/rev/sec.} \end{aligned}$$

(b) total rotor bias winding voltage output ratio:

$$\begin{aligned} V_{tb}/r &= V_{ob}/r + V_{cb}/r + V_{ib}/r \\ &= 19.78 + 19.78 + 19.78 \\ &= 59.34 \text{ volts/rev/sec.} \end{aligned}$$

The sum of V_{tf}/r and V_{tb}/r calculated below must be essentially equal to the combined coil group voltage output ratio V_g/r originally derived in Section D of WorkSheet VII(c), at 355.99 volts/rev/sec., with any discrepancy being entirely due to rounding.

Field Coil Voltage Values

$$\begin{aligned}\text{Thus, net } V_{tg}/r &= V_{tr}/r + V_{tb}/r = 296.65 + 59.34 \\ &= \boxed{355.99 \text{ volts/rev/sec.}} \quad \{\text{check}\}\end{aligned}$$

[3] If we divide the design Series Coil Group Voltage (spec. V_{tg}) by the total rotor field winding output ratio above, we may confirm the required standard operating rotor speed in revolutions per second as follows:

$$\begin{aligned}\text{standard rotor speed } r &= \text{spec.}V_{tg}/(V_{tr}/r) \\ &= 8,285.14/296.65 = 27.929 \text{ rev/sec.}\end{aligned}$$

$$\begin{aligned}\text{Therefore, } 1\eta \text{ Nominal Rotor Speed} &= \boxed{1676 \text{ rpm}}, \\ \text{and peak rotor speed} &= 110\%(1676) = 1844 \text{ rpm.}\end{aligned}$$

[4] Since the cutoff-induced voltage rise across each of the Primary Power System's electrode ring arrays is assumed to be 40%, the design Primary System Voltage is basically equal to 1.4 (V_{tr}/r) times the standard rotor speed, r :

$$\text{spec.}V_{tg} = 1.4 (296.65) (27.929) \approx \boxed{11,599.2 \text{ volts}} \quad \{\text{check}\}$$

Note: Any disparity between this value and that figured in WorkSheet I(a) is due to rounding.

Section C: 3η Nominal Rotor Speed

$$\begin{aligned}[1](a) \text{ total outer field winding output ratio:} &= V_{to}/r, \\ \text{where } V_{to}/r &= (V_{o1}/r + V_{o2}/r + V_{o3t}/r) \\ &= (27.72 + 34.71 + 19.38) \\ &= \boxed{81.81 \text{ volts/rev/sec.}}\end{aligned}$$

$$\begin{aligned}(b) \text{ total center field winding output ratio:} &= V_{tc}/r, \\ \text{where } V_{tc}/r &= (V_{c1}/r + V_{c2}/r + V_{c3t}/r) \\ &= (33.71 + 40.95 + 27.66) \\ &= \boxed{102.32 \text{ volts/rev/sec.}}\end{aligned}$$

$$\begin{aligned}(c) \text{ total inner field winding output ratio:} &= V_{ti}/r, \\ \text{where } V_{ti}/r &= (V_{i1}/r + V_{i2}/r + V_{i3t}/r) \\ &= (41.56 + 48.98 + 10.12) \\ &= \boxed{100.66 \text{ volts/rev/sec.}}\end{aligned}$$

[2](a) total rotor field winding voltage output ratio:

$$\begin{aligned}V_{tr}/r &= V_{to}/r + V_{tc}/r + V_{ti}/r \\ &= 81.81 + 102.32 + 100.66 \\ &= \boxed{284.79 \text{ volts/rev/sec.}}\end{aligned}$$

(b) total rotor bias winding voltage output ratio:

$$\begin{aligned}V_{tb}/r &= V_{o3b}/r + V_{c3b}/r + V_{i3b}/r \\ &= 14.24 + 14.24 + 42.72 \\ &= \boxed{71.20 \text{ volts/rev/sec.}}\end{aligned}$$

The sum of V_{tr}/r and V_{tb}/r calculated below must be essentially equal to the combined coil group voltage output ratio V_{tg}/r originally derived in Section D of WorkSheet VII(c), at 355.99 volts/rev/sec., with any discrepancy being entirely due to rounding.

Field Coil Voltage Values

$$\begin{aligned}\text{Thus, net } V_{\text{cr}}/r &= V_{\text{cr}}/r + V_{\text{cb}}/r = 284.79 + 71.20 \\ &= \underline{355.99 \text{ volts/rev/sec.}} \quad \{\text{check}\}\end{aligned}$$

[3] If we divide the design Series Coil Group Voltage (spec. V_{cg}) by the total rotor field winding output ratio above, we may confirm the required standard operating rotor speed in revolutions per second as follows:

$$\begin{aligned}\text{standard rotor speed } r &= \text{spec.}V_{\text{cg}}/(V_{\text{cr}}/r) \\ &= 8,285.14/284.79 = \underline{29.092 \text{ rev/sec.}}\end{aligned}$$

Therefore, 3 η Nominal Rotor Speed = 1746 rpm ,
and peak rotor speed = 110%(1746) = 1921 rpm.

[4] Since the cutoff-induced voltage rise across each of the Primary Power System's electrode ring arrays is assumed to be 40%, the design Primary System Voltage is basically equal to 1.4 (V_{cr}/r) times the standard rotor speed, r :

$$\text{spec.}V_{\text{ps}} = 1.4(284.79)(29.092) = \underline{11,599.2 \text{ volts}} \quad \{\text{check}\}$$

Note: Any disparity between this value and that figured in WorkSheet I(a) is due to rounding.

Section D: Verification of System Rotor Voltages

It must be emphasized that the actual operating rotor speed in both 1 η and 3 η rotor devices must in practice be close to the minimum nominal speeds given in Fig. 19 (on pg. 106), due to centrifugal loading considerations [see Section A of WorkSheet VIII(b)]. Fortunately, this will probably be the case, as it is actually unlikely that hull capacitance will exceed parallel-plate efficiency.

Upon verifying that the total rotor field winding output does indeed yield the design Series Coil Group Voltage (spec. V_{cg}) at the theoretical maximum rotational speeds above, for both the 1 η and 3 η variants, it must be assumed that the projected Primary System Voltage (spec. V_{ps}) proportional to that Group Voltage will in fact be developed in each said type of device before the corresponding interim Specification values of rotor voltage may be verified (for each case).

In turn, this supposition is of course predicated upon the presumption that the device's magnetic and electric arrays perform exactly as anticipated, although some deviation from the projections based on their combined theoretical modeling systems (as developed in these Specifications) is unavoidable.

[1] 1 η Thermal Unit:

Based on the logic of the Section B preamble from WorkSheet VIII(a), the peak rotor voltage resulting from peak Primary System Voltage production (at 110% of the confirmed nominal rotor speed) will approach 8,506.08 volts. Thus, the value of rotor voltage at 100% rotor speed will be 8,506.08/1.1 = 7,732.8 volts, which should exactly match the 1 η Spec. Rotor Voltage from WorkSheet I(a). This observation also confirms Spec. Primary Array Voltage, in that spec. ΔV_{p} is equal to one-half Spec. Rotor Voltage.

[2] 3 η Drive Unit:

Based on the logic of the Section C preamble from WorkSheet VIII(a), the peak rotor voltage resulting from peak Primary System Voltage production (at 110% of the confirmed nominal rotor speed) will approach 6,379.56 volts. Thus, the value of rotor voltage at 100% rotor speed will be 6,379.56/1.1 = 5,799.6 volts, which should exactly match the 3 η Spec. Rotor Voltage from WorkSheet I(a). This observation also confirms Spec. Primary Array Voltage, in that spec. ΔV_{p} is equal to one-half Spec. Rotor Voltage.

Basic Specifications

The Basic Specifications which are directly related to the Primary Power System *design* circuit characteristics of the 3η rotor device are all developed in light of the following presumption: that the actual voltage impressed across the rotor will theoretically be equal to half of either coil group's series field winding voltage *and* bias voltage rise, due to the action of the rotor induction arrays of both coil groups taken together *in opposed series-parallel*. In this respect, it can be shown that the 3η Primary Power System as a whole is only 35% efficient *at best* in transmitting generated voltage to the rotor.

The true voltage impressed across the rotor will actually *approach* half of this *Primary System Voltage* due to the voltage drop associated with coil group current, as was described in Chapter 7 of the associated text. Under the simplified design methods employed throughout, the above assumption also does not take into account the possible impact of vacuum chamber space charge in slightly modifying the exhibited rotor voltage. The actual percentage by which rotor voltage might thereby change is extremely difficult to project mathematically (at least for me). Nevertheless, assuming this '1/2 rule' interpretation of 3η circuit resolution is essentially correct, as developed in Section A of WorkSheet VIII(a), one of the only other attributes of this device which could significantly affect its *operational rotor speed* is the actual value of the hull static capacitance [as figured in WorkSheet VIII(d)].

Thus, the Table below has been created to assist development engineers in deriving a reasonably exact formula for the EDF Generator's hull static capacitance, as a function of the observed rotor speed upon achieving Specification Field Voltage *during actual device testing*. [The Table must be refigured for the given size device.] In doing so, the described conundrums may then be resolved such that truly accurate figures for the peak potential difference across the Field Ballast Capacitors (and rotor induction arrays) as well as the most appropriate net ballast capacitance may thereby also be derived.

Thus, this simple Table shows (in the uppermost row) the highest or "worst case" nominal rotor speeds to be expected, including the speed calculated in WorkSheet IX(b), in using a maximum required ballast capacitance which represents 1.808 times a 1.00-base ballast capacitance value that's a function of the estimated *minimum* hull static capacitance derived from a modified parallel plate formula [see WorkSheet VIII(d)]. The *Apparent Induction Efficiency* is then equal to the actual total voltage impressed across the rotor divided by half of the combined potential differences across all of the electrode arrays of either series coil group. In both cases, these numbers are unadjusted for either the aforementioned small net rotor voltage drop anticipated (as a result of the combined series coil group currents) or the effect of chamber space charge. However, the logical course of research is indicated.

3η Nominal Rotor Speed (rpm) for 4ft. dia. model

1.808	1746	1791	1838	1888	1940	1995	2054	2116	2183	2253	2328
1.75	1690	1733	1779	1827	1878	1931	1988	2048	2113	2181	2253
1.60	1545	1585	1626	1670	1717	1766	1818	1873	1931	1994	2060
1.45	1400	1436	1474	1514	1556	1600	1647	1697	1750	1806	1867
1.30	1255	1287	1321	1357	1394	1434	1476	1521	1569	1619	1673
1.15	1111	1139	1169	1201	1234	1270	1307	1347	1389	1434	1481
1.00	965.7	990.5	1017	1044	1073	1104	1136	1171	1207	1246	1288
0.85	820.9	841.9	864.1	887.5	912.1	938.2	965.8	995.0	1026	1059	1095
0.75	724.3	742.9	762.4	783.0	804.8	827.8	852.1	877.9	905.4	934.6	965.7
0.60	579.4	594.3	609.9	626.4	643.8	662.2	681.6	702.3	724.3	747.6	772.5
0.50	482.9	495.3	508.3	522.1	536.6	551.9	568.1	585.3	603.6	623.1	643.9
	100	97.5	95	92.5	90	87.5	85	82.5	80	77.5	75
	Apparent Induction Efficiency (%)										

Fig. 29: Field Ballast & Rotor Induction Performance to Rotor Speed Table*

*Note: This Table further presupposes that the actual Primary Voltage Expansion Ratio during operation equals the specification cathode-to-Field Emitter emissivity ratio.

Field Winding Resistances

model: Badlander
size: 4ft. dia.

This WorkSheet references WorkSheets VII(a) {Specific Field Coil Measurements} and IX(b) {Bias Winding Turns Ratios} for purposes of calculating the resistance of each field winding comprising the three different size Field Coils used in a given size (model) vessel. The values obtained may be used in one or more other WorkSheets to determine peak Primary Power System AC and dc line current(s) and associated resonant frequency circuit characteristics.

The formula used to calculate each winding's resistance is as follows:

$$R = N\pi df_c, \text{ where } R = \text{resistance in ohms,}$$

$$N = \text{number of turns,}$$

$$\pi d = \text{turn mean circumference,}$$

and f_c = the resistance per unit length conversion factor
 = (3.2808 ft./m)(.16075 ohms/ft.*), or .5274
 for the #31 gauge wire used in all windings.

*Note: This value represents the reciprocal of the ft/ohm @80°C rating.

Section A: 1η Thermal Unit**[1] Outer Field Windings:**

$$\begin{aligned} \text{(a) 1st layer turns: } R_{of1} &= (1 \times 10^4)(6.35 \times 10^{-3})(.5274) \\ &= (63.5)(.5274) \\ &= 33.49 \Omega . \end{aligned}$$

$$\begin{aligned} \text{(b) 2nd layer turns: } R_{of2} &= (1 \times 10^4)(7.95 \times 10^{-3})(.5274) \\ &= (79.5)(.5274) \\ &= 41.93 \Omega . \end{aligned}$$

$$\begin{aligned} \text{(c) 3rd layer turns: } R_{of3} &= (4,117)(9.55 \times 10^{-3})(.5274) \\ &= (39.32)(.5274) \\ &= 20.74 \Omega . \end{aligned}$$

$$\begin{aligned} \text{(d) total winding resistance: } R_{of1} &= R_{of1} + R_{of2} + R_{of3} \\ &= 33.49 + 41.93 + 20.74 = \underline{96.16 \Omega} . \end{aligned}$$

[2] Center Field Windings:

$$\begin{aligned} \text{(a) 1st layer turns: } R_{cf1} &= (9 \times 10^3)(7.45 \times 10^{-3})(.5274) \\ &= (67.05)(.5274) \\ &= 35.36 \Omega . \end{aligned}$$

$$\begin{aligned} \text{(b) 2nd layer turns: } R_{cf2} &= (9 \times 10^3)(9.05 \times 10^{-3})(.5274) \\ &= (81.45)(.5274) \\ &= 42.96 \Omega . \end{aligned}$$

$$\text{(c) 3rd layer turns: } R_{cf3} = (4,751)(1.065 \times 10^{-2})(.5274)$$

Field Winding Resistances

$$\begin{aligned} &= (50.60)(.5274) \\ &= 26.69 \Omega . \end{aligned}$$

$$\begin{aligned} \text{(d) total winding resistance: } R_{ctt} &= R_{ct1} + R_{ct2} + R_{ct3} \\ &= 35.36 + 42.96 + 26.69 = \underline{105.01 \Omega} . \end{aligned}$$

[3] Inner Field Windings:

$$\begin{aligned} \text{(a) 1st layer turns: } R_{it1} &= (8,333)(8.80 \times 10^{-3})(.5274) \\ &= (73.33)(.5274) \\ &= 38.67 \Omega . \end{aligned}$$

$$\begin{aligned} \text{(b) 2nd layer turns: } R_{it2} &= (8,333)(1.037 \times 10^{-2})(.5274) \\ &= (86.41)(.5274) \\ &= 45.57 \Omega . \end{aligned}$$

$$\begin{aligned} \text{(c) 3rd layer turns: } R_{it3} &= (5,214)(1.197 \times 10^{-2})(.5274) \\ &= (62.41)(.5274) \\ &= 32.92 \Omega . \end{aligned}$$

$$\begin{aligned} \text{(d) total winding resistance: } R_{itt} &= R_{it1} + R_{it2} + R_{it3} \\ &= 38.67 + 45.57 + 32.92 = \underline{117.16 \Omega} . \end{aligned}$$

$$\begin{aligned} \text{[4] Total 1}\eta \text{ Field Winding Resistance: } R_{ft} &= R_{ot} + R_{ct} + R_{it} \\ &= 96.16 + 105.01 + 117.16 \\ &= 318.33 \Omega . \text{ (per series coil group)} \end{aligned}$$

Section B: 3 η Drive Unit

[1] Outer Field Windings:

$$\begin{aligned} \text{(a) 1st layer turns: } R_{of1} &= (1 \times 10^4)(6.35 \times 10^{-3})(.5274) \\ &= (63.5)(.5274) \\ &= 33.49 \Omega . \end{aligned}$$

$$\begin{aligned} \text{(b) 2nd layer turns: } R_{of2} &= (1 \times 10^4)(7.95 \times 10^{-3})(.5274) \\ &= (79.5)(.5274) \\ &= 41.93 \Omega . \end{aligned}$$

$$\begin{aligned} \text{(c) 3rd layer turns: } R_{of3} &= (5,764)(9.55 \times 10^{-3})(.5274) \\ &= (55.05)(.5274) \\ &= 29.03 \Omega . \end{aligned}$$

$$\begin{aligned} \text{(d) total winding resistance: } R_{oft} &= R_{of1} + R_{of2} + R_{of3} \\ &= 33.49 + 41.93 + 29.03 = \underline{104.45 \Omega} . \end{aligned}$$

[2] Center Field Windings:

$$\begin{aligned} \text{(a) 1st layer turns: } R_{ct1} &= (9 \times 10^3)(7.45 \times 10^{-3})(.5274) \\ &= (67.05)(.5274) \\ &= 35.36 \Omega . \end{aligned}$$

Field Winding Resistances

$$\begin{aligned} \text{(b) 2nd layer turns: } R_{ct2} &= (9 \times 10^3)(9.05 \times 10^{-3})(.5274) \\ &= (81.45)(.5274) \\ &= 42.96 \Omega . \end{aligned}$$

$$\begin{aligned} \text{(c) 3rd layer turns: } R_{ct3} &= (5,941)(1.065 \times 10^{-2})(.5274) \\ &= (63.27)(.5274) \\ &= 33.37 \Omega . \end{aligned}$$

$$\begin{aligned} \text{(d) total winding resistance: } R_{ctt} &= R_{ct1} + R_{ct2} + R_{ct3} \\ &= 35.36 + 42.96 + 33.37 = \underline{111.69 \Omega} . \end{aligned}$$

[3] Inner Field Windings:

$$\begin{aligned} \text{(a) 1st layer turns: } R_{it1} &= (8,333)(8.80 \times 10^{-3})(.5274) \\ &= (73.33)(.5274) \\ &= 38.67 \Omega . \end{aligned}$$

$$\begin{aligned} \text{(b) 2nd layer turns: } R_{it2} &= (8,333)(1.037 \times 10^{-2})(.5274) \\ &= (86.41)(.5274) \\ &= 45.57 \Omega . \end{aligned}$$

$$\begin{aligned} \text{(c) 3rd layer turns: } R_{it3} &= (1,596)(1.197 \times 10^{-2})(.5274) \\ &= (19.10)(.5274) \\ &= 10.07 \Omega . \end{aligned}$$

$$\begin{aligned} \text{(d) total winding resistance: } R_{itt} &= R_{it1} + R_{it2} + R_{it3} \\ &= 38.67 + 45.57 + 10.07 = \underline{94.31 \Omega} . \end{aligned}$$

$$\begin{aligned} \text{[4] Total } 3\eta \text{ Field Winding Resistance: } R_{tt} &= R_{ctt} + R_{itt} + R_{it} \\ &= 104.45 + 111.69 + 94.31 \\ &= \underline{310.45 \Omega} . \text{ (per series coil group)} \end{aligned}$$

WorkSheet IX(d)

Bias Winding Resistances

model: Badlander
size: 4ft. dia.

This WorkSheet also references WorkSheets VII(a) and IX(b) for purposes of calculating the resistance of each bias winding used in a given size (model) vessel. As with the field winding resistances, the values obtained may be used in one or more other WorkSheets to determine peak Primary Power System AC and dc current(s) and associated resonant frequency circuit characteristics.

The formula used to calculate each winding's resistance is as follows:

$$R = N\pi df_c , \quad \text{where } R = \text{resistance in ohms,} \\ N = \text{number of turns,} \\ \pi d = \text{turn mean circumference,}$$

$$\begin{aligned} \text{and } f_c &= \text{the resistance per unit length conversion factor} \\ &= (3.2808 \text{ ft./m})(.16075 \text{ ohms/ft.}), \text{ or } .5274 \\ &\text{for the \#31 gauge wire used in all windings.} \end{aligned}$$

*Note: This value represents the reciprocal of the ft/ohm @80°C rating.

Bias Winding Resistances

Section A: 1η Thermal Unit

[1] Outer Bias Windings:

$$\begin{aligned} \text{(a) 3rd layer turns: } R_{ob} &= (5,883)(9.55 \times 10^{-3})(.5274) \\ &= (56.18)(.5274) \\ &= 29.63 \Omega . \end{aligned}$$

[2] Center Bias Windings:

$$\begin{aligned} \text{(a) 3rd layer turns: } R_{cb} &= (4,249)(1.065 \times 10^{-3})(.5274) \\ &= (45.25)(.5274) \\ &= 23.86 \Omega . \end{aligned}$$

[3] Inner Bias Windings:

$$\begin{aligned} \text{(a) 3rd layer turns: } R_{ib} &= (3,120)(1.197 \times 10^{-3})(.5274) \\ &= (37.35)(.5274) \\ &= 19.70 \Omega . \end{aligned}$$

$$\begin{aligned} \text{[4] Total 1}\eta \text{ Bias Winding Resistance: } R_{bt} &= R_{ob} + R_{cb} + R_{ib} \\ &= 29.63 + 23.86 + 19.70 \\ &= \underline{73.19 \Omega} . \text{ {per series coil group}} \end{aligned}$$

Section B: 3η Drive Unit

[1] Outer Bias Windings:

$$\begin{aligned} \text{(a) 3rd layer turns: } R_{ob} &= (4,236)(9.55 \times 10^{-3})(.5274) \\ &= (40.45)(.5274) \\ &= 21.33 \Omega . \end{aligned}$$

[2] Center Bias Windings:

$$\begin{aligned} \text{(a) 3rd layer turns: } R_{cb} &= (3,059)(1.065 \times 10^{-3})(.5274) \\ &= (32.58)(.5274) \\ &= 17.18 \Omega . \end{aligned}$$

[3] Inner Bias Windings:

$$\begin{aligned} \text{(a) 3rd layer turns: } R_{ib} &= (6,738)(1.197 \times 10^{-3})(.5274) \\ &= (80.65)(.5274) \\ &= 42.53 \Omega . \end{aligned}$$

$$\begin{aligned} \text{[4] Total 3}\eta \text{ Bias Winding Resistance: } R_{bt} &= R_{ob} + R_{cb} + R_{ib} \\ &= 21.33 + 17.18 + 42.53 \\ &= \underline{81.04 \Omega} . \text{ {per series coil group}} \end{aligned}$$

It should be noted that neither these bias winding resistances nor the field winding resistances calculated above have been incorporated into the rough determination of maximum dc operating current, for 1η or 3η rotor devices, as carried out (for the sake of brevity) in the important WorkSheet VIII(b).

Zone Sector Construction

The primary goal in dividing each hull Positive Zone into a large number of parallel sectors is to limit the Field current reaching each particular Power Resistor and unit pentode array combination to a fairly uniform level, while reducing Field current return eddy losses. At the same time, each Field Hub Zone is given local thrust differential production capability in 3η rotor devices, by virtue of its electrical isolation.

Because the resistance of each sector will be negligible even at an extremely elevated operating temperature, in part due to the very low temperature coefficient of resistivity of the hull plating material, the voltage drop across the radial length of each sector will also be negligible. Thus, the determination of an appropriate sector thickness becomes an entirely structural consideration. A secondary design goal is therefore to select a uniform cross-sectional area for the radial Zone sectors which yields a total Field Hub conduction mass approaching that of the device's rotor segments.

[1] The stainless steel hull plating which forms each Positive Zone of the EDF Generator's Field Hub shall be divided into **thirty-six (36)** equal-area wedge-shaped radial Zone sectors and a circular center Zone sector of just less than 1% of the total area of that Zone.

[2] The gross length of each radial Zone sector shall be equal to 90% of the radius of the Field Hub, or $^{27}/_{50} R_h$, and the radius of each center Zone sector shall be equal to 10% of the radius of the Field Hub, or $^{3}/_{50} R_h$.

[3] The Specification minimum thickness of each radial Zone sector, as measured at the major (outer) design* arc width thereof, shall be equal to the Hull Area Constant (C_r) from the applicable Hull Configuration Spreadsheet.

[4] The Specification maximum thickness of each radial Zone sector, as measured at the minor (inner) design* arc width thereof, shall be equal to ten times (10x) the Hull Area Constant from the Hull Configuration Spreadsheet.

[5] Each radial Zone sector shall be formed of a single piece of the hull plating material in such a manner that its cross-sectional area in the direction of its radial length is maintained at a very uniform value.

[6] The uniform thickness of each center Zone sector shall be equal to that of the radial Zone sectors as measured at the minor (inner) design* arc width thereof, and the radial sectors shall be insulated from the respective center sector where they meet that center sector's periphery.

[7] The uniform flat thickness of the suitable ceramic insulating partition which must be installed between each adjacent pair of radial Zone sectors and around each center Zone sector shall be equal to the radial sector's minor (inner) design* arc width minus the rotor's segment thickness (or $^{4}/_{453} R_h$).

[8] For purposes of this SpecSheet, the design* arc width of each radial Zone sector at a given point on its radial length is that which it would have if no insulating ceramic strip were installed between adjacent such sectors, or $^{1}/_{36}$ of the total Zone circumference at that point.

[9] Four (4) radial sectors of each Positive Zone which are separated from each other by 90 arc-degrees of the incorporating device's circumference, and which divide the Field Hub as a whole into four (4) equal quadrants, are to be connected in parallel with the center sector of that Positive Zone at the positive voltage end of their respective Power Resistors.

Field Power Resistors

model: Badlander

size: 4ft. dia.

The calculations contained in this WorkSheet are based on the premise that the gross intrinsic positive voltage upon the Field Hub of the Electro-dynamic Field Generator in question must, in the floating-ground Primary Power System thereof, be numerically equal to one-half (1/2) the total Field potential difference across the vessel hull due to the hull's capacitive nature.

Section A: Required Voltage Drop and Resistance

[1](a) The gross peak operating potential difference (ΔV_{ts}) across each of the two Field Power Resistor Networks of the 4ft. Thermal Unit, given the considerations of DataSheet #15 {Beam Pentode Characteristics}, may be calculated as follows:

$$\Delta V_{ts} = 1/2(1.1 V_t) , \text{ w/primary cathodes @ ground potential,}$$

where V_t = Spec. Field Voltage @ 2.8998×10^4 volts,

and spec. ΔV_p = Spec. Primary Array Voltage @ 3,866.4 volts.

$$\text{Therefore, } \Delta V_{ts} = 1/2(3,189,780) = 1,594,890 \text{ volts} .$$

(b) In like manner, the gross peak operating potential difference (ΔV_{ds}) across the Field Power Resistors of the 4ft. Drive Unit equals:

$$\Delta V_{ds} = 1/2(1.1 V_t) , \text{ w/primary cathodes @ ground potential,}$$

where V_t = Spec. Field Voltage @ 35.1044×10^4 volts,

and spec. ΔV_p = Spec. Primary Array Voltage @ 2,899.8 volts.

$$\text{Therefore, } \Delta V_{ds} = 1/2(38.6148 \times 10^4 \text{ volts}) = 19.3074 \times 10^4 \text{ volts} .$$

[2](a) By Ohm's Law, the total group resistance of each of the two Field Power Resistor Networks used in the 4ft. Thermal Unit equals:

$$R_{ts} = \frac{\Delta V_{ts}}{1/2 I_{max}} , \text{ where } I_{max} = \text{rated rotor ampacity.}$$

$$\text{So, } R_{ts} = 1,594,890/19,080 = 83.59 \Omega .$$

The individual parallel resistance of each of the 36 Field Power Resistors per Network used in the 4ft. Thermal Unit (to the nearest ohm) therefore equals:

$$r_{ts} = 36 R_{ts} = 3,009 \Omega .$$

Note: Because no bias of hemitorus Field current occurs in a Thermal Unit, the above resistance values are relatively fixed or non-variable.

(b) By Ohm's Law, the median* total group resistance of each of the two Field Power Resistor Networks used in the 4ft. Drive Unit equals:

$$R_{ds} = \frac{\Delta V_{ds}}{1/2 I_{max}} , \text{ where } I_{max} = \text{rated rotor ampacity.}$$

$$\text{So, } R_{ds} = 19.3074 \times 10^4 / 19.08 \times 10^3 = 1,011.9 \Omega . \text{ {see *Note on next pg.}}$$

Field Power Resistors

The individual median* parallel resistance of each of the 36 Field Power Resistors per Network used in the 4ft. Drive Unit (to the nearest ohm) therefore equals:

$$r_{ds} = 36 R_{ds} = \underline{36,428 \Omega}.$$

***Note:** Based on the considerations of SpecSheet XI {Field Current Bias Values}, the actual operating value of R_{ds} above must be rendered variable in the range from $3/4 R_{ds}$ (at a maximum Network current of 25,440 amps) to $3/2 R_{ds}$ (at a minimum Network current of 12,720 amps). This is accomplished by incremental adjustment(s) of the Network operating temperature, given the relatively linear nature of Resistor volume resistivity changes per °C (see subsection B[5] below), as necessary to hold the Network voltage drop constant with varying hemitorus current levels.

{3}(a) The total peak resistive power expended as heat (P_{ts}) in the 4ft. Thermal Unit is as follows:

$$\begin{aligned} P_{ts} &= \Delta V_{ts} I_{max} = 2(1/2 I_{max})^2 R_{ts} \\ &= 2[(19,080)^2 (83.59)] \\ &= \underline{6.086 \times 10^{10} \text{ joules/sec}}. \end{aligned}$$

(b) The median* total peak resistive power expended as heat (P_{ds}) in the 4ft. Drive Unit is as follows:

$$\begin{aligned} P_{ds} &= \Delta V_{ds} I_{max} = 2(1/2 I_{max})^2 R_{ds} \\ &= 2[(19,080)^2 (1,011.9)] \\ &= \underline{7.368 \times 10^{11} \text{ joules/sec}}. \end{aligned}$$

Section B: Cross-Sectional Area and Length

[1] The total available primary electrode ring surface area of each major semicircuit of the Primary Power System is equal to:

$$\begin{aligned} A_{ts} &= \pi(R^2 - r^2), \text{ where } R = 3/5 R_n, \text{ or } 14.4", \\ &\text{and } r = 67/120 R_n, \text{ or } 13.4". \text{ (SpecSheet III)} \end{aligned}$$

$$\text{Therefore, } A_{ts} = \pi(207.36 - 179.56) = 87.336 \text{ in}^2 = 563.46 \text{ cm}^2.$$

[2] The maximum unit pentode array area, given 36 individual (identical) parallel arrays per Network, is thus equal to $563.46/36$ or 15.65 cm^2 .

[3](a) Component Specification: The assigned net cross-sectional area of each Field Power Resistor (A_{tr}) shall be equal to 90% of the maximum unit pentode array area (figured above).

$$\text{Therefore, } A_{tr} = .90(15.65) = \underline{14.09 \text{ cm}^2}.$$

Note: This net area is then equal to that of each primary cathode element.

(b) The median* full-power unit pentode array current density (J_{tr}), applicable to both Thermal and Drive Units, may be calculated as follows:

$$J_{tr} = 1/2 I_{max} / 36 A_{tr}, \text{ where } I_{max} = 38,160 \text{ amps.}$$

$$\text{So, } J_{tr} = 530/14.09 = \underline{37.62 \text{ amps/cm}^2}.$$

(c) The peak* unit pentode array current density (J_{tr}), applicable to Drive Units only, may also be calculated as follows:

Field Power Resistors

$$J_{ir} = 2/3 I_{max}/36 A_{ir}, \text{ where } I_{max} = 38,160 \text{ amps.}$$

$$\text{So, } J_{ir} = 706.67/14.09 = \boxed{50.15 \text{ amps/cm}^2}.$$

[4] Component Specification: The assigned length of each Field Power Resistor (L_r) shall be equal to $1/72 R_b$.

$$\text{Therefore, } L_r = .3333" = \boxed{.8466 \text{ cm}}.$$

[5] Component Volume Resistivities and Operating Temperatures:

The Field Power Resistors used in the 4ft. *Thermal Unit* are to be composed of Steatite 357 ($MgO \cdot SiO_2$) and those of the 4ft. *Drive Unit* must be composed of Cordierite 547 ($2MgO \cdot 2Al_2O_3 \cdot 5SiO_2$). The volume resistivities and estimated operating temperatures thereof are figured below.

(a) Thermal Power Unit:

$$r_{ir} = \rho_o \frac{L_r}{A_{ir}}, \text{ where } \rho_o = \text{operating resistivity.}$$

Making the appropriate substitutions:

$$3,009 = \rho_o (.8466/14.09),$$

$$\text{and } \rho_o = 50,079 \approx \boxed{5 \times 10^4 \text{ ohm-cm}}.$$

Therefore, from Material SpecSheet D(2)[b], we find the estimated operating temperature required to be approximately 645°C, a "dark-red" heat.

(b) Impulse Drive Unit:

$$r_{dr} = \rho \frac{L_r}{A_{ir}}, \text{ where } \rho = \text{operating resistivity.}$$

Making the appropriate substitutions:

$$(i) \text{ median } r_{dr} = 36,428 = \rho (.8466/14.09),$$

$$\text{and } \rho = 606,273 \approx \boxed{6.06 \times 10^5 \text{ ohm-cm}}.$$

Therefore, from Material SpecSheet D(2)[b], we find that the estimated median operating temperature required is approximately 655°C.

$$(ii) \text{ } 3/4 r_{dr} = 27,321 = \rho (.8466/14.09),$$

$$\text{and } \rho = 454,705 \approx \boxed{4.55 \times 10^5 \text{ ohm-cm}}.$$

Therefore, from Material SpecSheet D(2)[b], we find that the estimated minimum operating temperature required is approximately 620°C.

$$(iii) \text{ } 3/2 r_{dr} = 54,642 = \rho (.8466/14.09),$$

$$\text{and } \rho = 909,409 \approx \boxed{9.09 \times 10^5 \text{ ohm-cm}}.$$

Therefore, from Material SpecSheet D(2)[b], we find that the estimated peak operating temperature required is approximately 735°C.

From the above data, it is apparent that precise control of the EDF Generator's Power Resistor operating temperature must be effected at all times to ensure a proper Field Voltage. Both heating and cooling systems (for cold-start and normal load operation, respectively) must therefore be maintained. The primary thermal conduit and structural intercooler systems anticipate the use of both high-temperature and cryogenic liquid thermal transfer media.

Once I arrived at the conclusion that the Field Hub Zones should be divided into sectors, for reasons adequately delineated so far in the preceding SpecSheet, it quickly simplified a number of troublesome considerations plaguing me. For instance, if the Primary Induction Arrays were constructed as solid rings, like the rotating electrode arrays, how could I pass any *non-electrified* supporting structural members through to the Drive Ring? This was a big problem, but an even more important issue was: if the Primary Arrays were one-piece, how could I vary the *local* resistance presented across the Drive Field so that navigational control in the z-axis (for Drive Units) could be achieved??

Basically, the only real concern I had regarding *zone sector construction* was that it entailed a significant reduction in Power Resistor cross-section. To begin with, the whole idea of heating a ceramic insulator until you forced it to become conductive – and then using it as a very high-value resistor – was disturbing enough. But I was used to thinking of a conductor as something metallic which had a definite working ampacity and which suddenly evaporated if that ampacity was exceeded! And who knew what the ampacity of a *ceramic* might be? Eventually, I just concluded (through sheer faith in the ‘rightness’ of my intentions) that so long as you provided *adequate cooling means*, you could to a point just keep cranking the power through it. Hopefully, we’ll find out soon enough.

As we know, these Field Power Resistors have the formidable task of reducing the half-value of Field voltage to zero (and not disintegrating in the process). The next really major problem was how to ever insulate the Resistor itself, and this one was (believe it or not) one of the greatest challenges of all in the EDF Generator’s design. If not for *one* special ceramic compound, I do believe this obstacle would have been insurmountable (and it sort of reminded me of John Searl).

What I eventually conceived of were conical **dielectric buffers**, one of which encapsulated each Resistor in a sharply tapering manner so as to only provide just the minimum necessary surface resistance to keep it from flashing over to something conductive nearby. The peculiar thing about the exotic buffer material is that it exhibits a relatively low dielectric strength *until* it is very hot. Its peak dielectric capability occurs at 655°C, and this then becomes the mean operating temperature of the Power Resistors. The story behind the dielectric buffers, composed of a ferroelectric substance called Sodium Bismuth Titanate, makes for fascinating study (for you materials engineers) and it is recommended that those having the inclination investigate Section 2 of Material SpecSheet D in this regard.

The adequate cooling means was a snap after all these Resistor troubles, and here again zone sector construction is indispensable. My idea was to form a loop of molybdenum tubing, which was thinly coated with a high thermal conductivity ceramic and tightly wrapped about the encapsulated Resistor, and pump liquid sodium through it – in the manner normally associated with nuclear reactors. These thermal loops or primary **thermal conduits** should be able to pull off the absolutely tremendous quantities of heat generated within the Resistors. They constitute the principal means by which a Thermal Unit may be used to generate commercial electric power: this heat may be used to produce steam for turning a conventional turbine generator.

Secondary thermal conduits of a very similar nature would then be used to pump liquid air or nitrogen coolant through the Drive Ring, to maintain the interior temperature thereof at a level well below the maximum 180°C rating of the magnet wire used to wind the field coils and variable inductors. Also, and very importantly, these cryogenic secondary conduits would be used to cool the inner edge of the aluminum negative hull plates by being structurally attached thereto.

In fact, I decided along the way that these secondary conduits, having great physical strength, could actually serve as the principal load-bearing structural members supporting the Drive Ring and its heavy negative plates. They therefore constitute the EDF Generator’s **Structural Intercooler System**: rather like the tubular chassis of a dune buggy and a refrigerator coil in one! For further information about this interesting design conception, attention is directed to Material SpecSheet B.

It is my sincere hope that a Drive Unit operated in the vacuum of space would be able to dump its excess heat by actually circulating the primary conduit liquid sodium through the secondary intercooler system! Since thermodynamics is definitely *not* an area of expertise for me, I leave that concept up to better qualified engineers to pursue. One thing about this I do know: unless this idea does actually work, I can envision no other existing means of liberating the StarDrive device from permanent ground-based support to achieve free-ranging operation in space.

Field Current Bias Values

This Specification Sheet serves to delineate certain key operational levels of *Drive Field* current as a function of the relative value of Primary Induction Ring Array control grid bias. Reference should be made to DataSheet #15 {Beam Pentode Characteristics}.

For purposes of this SpecSheet, and the textual material associated herewith, the term "full power" used in relation to the Primary Power System and its incorporating device shall be taken to mean a corresponding rotor speed wherein Nominal Field Voltage is achieved, maintained, or exceeded.

[1] Maximum full power total Field current shall be equal to the rated ampacity of the System rotor.

[2] Minimum full power total Field current shall be equal to either $\frac{1}{2}$ of rated rotor ampacity or a level of total rotor current sufficient to allow the System's incorporating device to accelerate at $1g$ (9.8 m/sec^2), whichever is the lesser, in an EDF Generator used as an Impulse Drive Unit.

Note: Given the engineered triodic amplification factor of the Primary Induction Ring Arrays, this minimum level of total Field current may in all likelihood be maintained with an average value of applied Array control grid bias voltage less than or equal to about one-half ($\frac{1}{2}$) of the maximum value thereof. (see WorkSheet VIII(c) {Pentode Potential Differences})

[3] Maximum Field hemitorus current at any given value of operating rotor current shall at all times be limited to a value less than or equal to two-thirds ($\frac{2}{3}$) of that operating rotor current.

Note: Given the considerations set forth above, this maximum authorized level of 'unshunted' hemitorus current may in all likelihood be maintained with a value of applied Array control grid bias voltage equal to approximately one-third ($\frac{1}{3}$) of the maximum value thereof. Due to the lag time in heating the Field Power Resistor Network through which an increasing Field hemitorus current must return, the associated Array bias voltage may be briefly reduced to $\frac{1}{6}$ of the maximum value thereof as a standard *minimum* operating level.

[4] Minimum Field hemitorus current at any given value of operating rotor current shall at all times be maintained at a value equal to or greater than one-third ($\frac{1}{3}$) of that operating rotor current.

Note: Given the considerations set forth above, this minimum qualifying level of 'shunted' hemitorus current may in all likelihood be maintained with a value of applied Array control grid bias voltage equal to approximately two-thirds ($\frac{2}{3}$) of the maximum value thereof. Due to the lag time in cooling the Field Power Resistor Network through which a decreasing Field hemitorus current must return, the associated Array bias voltage may be briefly increased to $\frac{5}{6}$ of the maximum value thereof as a standard *maximum* operating level.

[5] The parallel resistance of the four (4) conductors which connect each center Zone sector to its respective Power Resistor Network should be such that that sector's per unit surface area level of Field current conduction is slightly higher on the average (under uniform zero-signal Field bias conditions) than that of its adjacent radial sectors.

[6] The four (4) unit pentode arrays of each Primary Induction Ring Array which correspond to the Power Resistors connected to that Primary Array's center Zone sector are generally not to be utilized individually in the active Field current bias modulation related to the production of local thrust differentials in 3η rotor devices, being instead reserved primarily for potential involvement in signal communications transmission and/or reception.

Variable Inductor Arrays

Design Synopsis: The purpose of the Variable Inductor Arrays, the two (2) ring-shaped groups of *stationary electromagnetic armatures* located around the vertical centerline of the hull Neutral Ring of the device, is to create and independently control a variable level of both rotor torque and field current rotational force. Therefore, each Armature comprises two (2) separate wound core sections joined by an unwound connecting center section of the core called a *flux reductor*, which is of a *significantly reduced cross-sectional area*. These Armature sections are shown in Fig.40 of WorkSheet XII(a).

This connecting center section or flux reductor is designed to saturate magnetically when either the inner (torque) section of the core or the outer (transflection) section thereof is at a flux density equal to or greater than approximately one-half ($1/2$) of the Specification Core Flux Density derived hereinbelow.

The flux initiator coils on the inner sections of the Armatures are then normally powered to half Spec. Core Density and the corresponding level of Armature-applied torque may be independently increased by a factor approaching 100% or more, for Drive Unit navigation and maneuvering purposes, without affecting the relative flux density of the transflection section of the core(s).

The outer sections of the Armature cores must then be maintained at the proper variable level of net polarization flux density to sustain an optimal power field (electron gyroradius) "displacement" current. To achieve this end, a counter-polarity magnetomotive force (mmf) may at times be applied (by reversing the polarity of the transflection coils). As necessary or desired, the net level of mmf or counter-mmf applied to the transflection section(s) of the Core(s) may then be decreased or increased (respectively), for purposes of optimizing Field magnetic properties, without substantially affecting the relative flux density of the torque section(s) thereof.

* * *

The purpose of this provisional αSpecSheet is to define the largest mechanically-practicable size and shape for the Stationary Electromagnetic Armatures employed in any size (model) of Electrodynamic Field Generator. The general design parameters thereby developed may then be employed to produce final construction specifications in a like-named ΩSpecSheet for a given size (model) vessel once certain of its external field magnetic effect requirements have been derived by mathematical analysis and dynamic testing techniques.

Section A: General Non-Provisional Specifications

[1] The metallic core of each such Armature shall be composed of pure annealed iron in square stock form (prior to machining).

[2] The axial centerline of each such Armature shall lie very nearly on the vertical radial centerline of the vessel's hull Neutral Ring at $\frac{6715}{9600} R_h$, and all of the Armatures shall be uniformly positioned between radial vertical reference lines at $\frac{6781}{9600} R_h$ and at $\frac{6649}{9600} R_h$.

[3] A ring-shaped (circular) array composed of 180 such Armatures shall be so-located in both the upper and lower halves of the symmetrical vessel hull, above and below its horizontal centerline, for a total of 360 Armatures per vessel.

[4] Five (5) such Armatures shall be uniformly so-positioned within each of the Drive Ring superstructure's 36 major sections, or between any adjacent pair of said superstructure's 36 primary load-bearing members, both above and below the vessel hull's horizontal centerline.

[5] The outer section of each Armature core shall be slightly undercut by machining (as hereinafter directed) and installed with a "transflection coil" or electromagnetic winding for purposes of imparting a variable transverse deflectionary force upon field envelope current.

[6] The inner section of each Armature core shall likewise be slightly undercut and installed with a "flux initiator coil" or electromagnetic winding for purposes of imparting a variable force of rotational torque upon the vessel's rotor.

[7] The overall installed length of each such coil or winding shall be limited to a maximum value of $43/9600 R_n$, as relates to the particular size vessel in question (per the Hull Configuration SpreadSheet).

[8] The Armatures should be designed to achieve a Spec. Core Flux Density which falls between 1.8 and 2.0 Wb/m², due to the sharp drop in core permeability at higher output, as core efficiency rises proportional to increases in core size and the winding wire size decreases slightly in proportion thereto.

[9] The flux reductor or center connecting section of each Armature core shall be machined to a significantly reduced cross-sectional area compared to the inner and outer sections thereof, so that the magnetic saturation of the reductor allows the unsaturated inner and outer sections of the core to be operated at different relative flux densities.

[10] The mechanical clearance between the end-face of each Armature core's outer section and the inner surface of the Neutral Ring's outer hull layer shall be the same as that specified for the clearance between the Field Coils and their adjacent Magnetic Rings, as shall also be the clearance between the end-face of each Armature core's inner section and the adjacent outer surface of the rotor assembly. This Specification thus defines the Armature's overall finished (cut and polished) length, when taken with the further general Specifications above.

Section B: Structural Dimension Specifications

It is very difficult to specify certain final Armature dimensions prior to the development of a final trim hull configuration, wherein the Drive Ring displacement angle is expanded slightly and the Negative Ring peripheral edge is slightly truncated to provide finite edge surface area not accounted for in the design hull configuration.

Therefore, 'hard' Specifications are given below for all key Armature dimensions except the flux reductor, which is given a minimum specified length. Any significant increase found to be available in the gross Armature length (as a result of trim hull changes) should be applied to the reductor, to diminish any tendency extant toward flux leakage between the reductor flanges.

It is important to note that the thickness of the proximal central rotor

facing layer, or mid-rotor surface insulation applied between Armatures and rotor segments, is .75 mil per foot R_h or .0015" in the 4ft. diameter model.

[1] The minor thickness of the canted outer end/face of each Armature shall be equal to $29/9600 R_h$.

[2] The uniform thickness of the inner end/face of each Armature shall also be equal to $29/9600 R_h$.

[3] The axial length of the undercutting performed on each wound Armature section shall be equal to $43/9600 R_h$.

[4] The flux reductor section of each Armature shall be milled to a circular cross section having a maximum diameter of approximately $41/9600 R_h$ and a minimum axial length of $45/9600 R_h$.

[5] The two (2) thin flanges of core material located at the immediate ends of each Armature's flux reductor section shall each have an axial thickness equal to $7/9600 R_h$.

Section C: Provisional Core Specifications

[1] The fundamental design parameter of the stationary electromagnetic Armatures, which also constitutes the principal determinant of their mechanical clearance with respect to certain rotor components, shall be the gross radial width. This dimension shall be equal to $\frac{132}{9600} R_h$ and designated w_{gr} .

This assigned maximum Armature width results in an inner and outer radial rotor component clearance of between approximately $\frac{17}{9600} R_h$ and $\frac{19}{9600} R_h$, given certain applicable considerations of SpecSheet III {Rotor Component Positioning}, for vessels of from 4ft. to 100ft. in diameter respectively. All other core dimension Specifications, with the exception of the radial clearance undercut (described hereinbelow) are then given in terms of w_{gr} .

[2] The Armature core's net circumferential length, or L_{nc} , shall be equal to $1.065 w_{gr}$ and determines the mutual (side-to-side) wound Armature clearance. This assigned maximum Armature length (in the horizontal plane) results in a mutual wound Armature clearance approximately equal to or very slightly greater than $1/768 R_h$.

[3] The Armature core's design corner radius shall be equal to $.2177 w_{gr}$ and designated as r_c . The ratio of this dimensional Specification to w_{gr} should not be reduced unless deemed absolutely necessary.

[4] The Armature core's minor rectangular length shall represent the linear portion of the gross radial width between the circular corner quadrants specified by r_c . This dimension shall be equal to $.5645 w_{gr}$ and designated as l_m .

[5] The Armature core's major rectangular length shall represent the linear portion of the net circumferential length between the circular corner quadrants delineated by r_c . This dimension shall be equal to $.6296 w_{gr}$ and designated as L_m .

[6] The inner and outer radial faces of both the transflection and torque sections of the Armature core shall be undercut to a depth equal to $19/9600 R_h$ (or just greater than the core's rotor component clearance) and to an axial length sufficient to accomodate each of the installed coils (or $43/9600 R_h$).

This depth shall be designated by u and the ends of the resultant radial clearance undercut shall be re-radiused as in subsection [3] above.

[7] The radial clearance undercut described above serves to reduce dimension l_o by $2u$, and the resultant net minor rectangular length shall then be designated by l_u (where $l_u = l_o - 2u$).

[8] The minor armature circumference (that of the wound undercut area of its inner and outer core portions) may now be calculated by the following formula:

$$C = 2\pi r_c + 2l_u + 2L_u.$$

[9] The Armature's minor average coil radius (for purposes of calculating its coil-induced core flux densities) shall be designated as r_c and may then be calculated as follows:

$$r_c = C/2\pi.$$

[10] The flux reductor of each Armature core shall be machined to a reduced cross-sectional area representing a maximum of 29.65% of the area of either the inner or outer core section's end face (non-undercut) portions. The actual such net percentage reductor area used in practice (to achieve saturation of the reductor when either undercut core section is at or above half Spec. Core Density), as determined by dynamic testing, may need to be somewhat reduced to compensate for flux leakage between the reductor flanges.

Section D: Provisional Winding Specifications

[1] The transflection coil installed on the outer section of each Armature core and the flux initiator coil installed on the inner section thereof shall be of identical construction but powered in parallel (by variable low-voltage dc current) such that they are rendered independently controllable.

[2] Each such coil or winding shall be composed of twelve (12) identical nested layers, formed of a single piece of magnet wire, the outside layer of which is bonded to the core with a high-temperature dielectric adhesive.

[3] Each such coil or winding layer shall comprise a projected minimum of twenty-one (21) offset-shoulder turns of said magnet wire.

[4] The single build insulated annealed copper magnet wire which shall be used to form each such coil or winding shall be no larger than one (1) std. American wire gauge smaller than the gauge which is closest in bare diameter to 2/9600 R_u . The selected wire diameter shall be designated as d_u .

Section E: Primary Design Goal Parameter

The Variable Inductor (or armature assembly) Arrays employed in any given EDF Generator used as a Thermal Power Unit should, as described hereinabove, be capable of producing a Specification Core Flux Density approaching as closely as possible that required to effect a stable full-power field electron gyroradius (at Nominal Field Voltage) which lies on the vessel hull's annular power field centerline at full selector plane velocity.

The calculations necessary to verify this consideration are performed in WorkSheet XII(b) {Axial Field Flux Balance}. In achieving this goal, it is postulated that field erosive effects upon the hull may be minimized at the high temperatures associated with operation in air.

It should be noted that the above relation as stated will not be applicable to the operation of Impulse Drive Units, due to the extreme increase in the relativistic velocity and mass of field envelope electrons. In the latter case, the objective is mainly to optimize the quasi-coherent aspects of the field envelope current at a much-reduced selector plane velocity despite the extraordinary field voltages employed, in reliance upon the temperature of space for adequate hull thermal protection.

Specific Armature Measurements

model: Badlander
size: 4ft. dia.

This αWorkSheet develops various specific component measurements with regard to the wound stationary electromagnetic armatures or *Variable Inductors* (used to create variable magnetic fields) which are employed in the operation of the Electrodynamic Field Generator.

It must be stressed that the measurements figured herein, as a function of αSpecSheet XII {Variable Inductor Arrays}, are provisional in nature. They may therefore be revised as a result of calculations performed in WorkSheet XII(b) {Axial Field Flux Balance} and/or those used to figure the marginal field flux balance as described in the associated text. Such revised dimensions should then be specified in a like-named revised βWorkSheet and, if found suitable for final action, a similar final αWorkSheet.

Section A: Principal Core Dimensions

- [1] gross radial width:

$$\begin{aligned}W_{gr} &= 132/9600 R_h \\&= 132(.0025") = .33", \text{ or } .8382 \text{ cm} .\end{aligned}$$

- [2] net circumferential length:

$$L_{nc} = 1.065 W_{gr} = .8927 \text{ cm} \text{ {see subsection [6] below}}.$$

- [3] design corner radius:

$$r_d = .2177 W_{gr} = .1825 \text{ cm} .$$

- [4] minor rectangular length:

$$l_o = .5645 W_{gr} = .4732 \text{ cm} .$$

Note: The figure calculated here should also equal $W_{gr} - 2r_d$, as follows:

$$l_o = .8382 - 2(.1825) = .4732 \text{ cm} .$$

- [5] major rectangular length:

$$L_s = .6296 W_{gr} = .5277 \text{ cm} .$$

- [6] As a further check of the dimension L_{nc} , the figure calculated in [2] above should also equal $2r_d + L_s$, as follows:

$$L_{nc} = 2(.1825) + .5277 = .8927 \text{ cm} .$$

If these two figures do not agree exactly, that calculated by the equation immediately above should be used in all applicable instances.

Section B: Secondary Core Dimensions

- [1] radial clearance undercut:

$$\begin{aligned}u &= 19/9600 R_h \\&= 19(.0025") = .0475", \text{ or } .1207 \text{ cm} .\end{aligned}$$

Specific Armature Measurements

- [2] net minor rectangular length:

$$\begin{aligned}l_u &= l_o - 2u \\&= .4732 - 2(.1207) = \boxed{.2318 \text{ cm}}.\end{aligned}$$

- [3] minor armature circumference:

$$\begin{aligned}C &= 2\pi r_d + 2l_u + 2L_s \\&= \pi(.3650) + 2(.2318) + 2(.5277) \\&= 1.1467 + .4636 + 1.0554 \\&= \boxed{2.6657 \text{ cm}}.\end{aligned}$$

- [4] minor average coil radius:

$$r_c = C/2\pi = \boxed{.4243 \text{ cm}}.$$

Section C: Gross Core End Area

- [1] area of the four (4) corners (A_1):

$$A_1 = \pi r_d^2 = 3.1416(.3331) = \boxed{.1046 \text{ cm}^2}.$$

- [2] area of center band (A_2):

$$\begin{aligned}A_2 &= l_o (2r_d + L_s) \\&= .4732(.8927) = \boxed{.4224 \text{ cm}^2}.\end{aligned}$$

- [3] area of outside centers (A_3):

$$\begin{aligned}A_3 &= 2r_d L_s \\&= .3650(.5277) = \boxed{.1926 \text{ cm}^2}.\end{aligned}$$

- [4] gross end cross-sectional area (A_{gt}):

$$\begin{aligned}A_{gt} &= A_1 + A_2 + A_3 \\&= .1046 + .4224 + .1926 \\&= \boxed{.7196 \text{ cm}^2}.\end{aligned}$$

Section D: Net Core End Area

- [1] reduced area of center band (A_{2n}):

$$\begin{aligned}A_{2n} &= l_u (2r_d + L_s) \\&= .2318(.8927) = \boxed{.2069 \text{ cm}^2}.\end{aligned}$$

- [2] net end cross-sectional area (A_{nt}):

$$\begin{aligned}A_{nt} &= A_1 + A_{2n} + A_3 \\&= .1046 + .2069 + .1926 \\&= \boxed{.5041 \text{ cm}^2}.\end{aligned}$$

- [3] The ratio of the net core end area to gross end area, expressed as a percentage, is then equal to:

$$\begin{aligned}A_{nt}/A_{gt} &= .5041/.7196 \\&= \boxed{70.05\%}.\end{aligned}$$

[4] *flux reductor area (A_{r}):*

The cross-sectional area of the unwound connecting center section of each Armature is as follows:

$$A_{\text{r}} = .2965 A_{\text{g}} = .2965(.7196) = \underline{.21336 \text{ cm}^2}.$$

Section E: Wound Armature Operating Characteristics

[1] *magnet wire diameter (d_{w}):*

The standard American wire gauge (size) used to form the transflection and flux initiator coils installed on each Armature core is, according to Specification, #37 at d_{w} equal to .0050", or .0127 cm {see DataSheet #1 Part C}.

[2] *wound armature circumference:*

Were the coils installed on the two wound Armature sections composed of non-nested layers, each winding layer would add one (1) wire diameter (d_{w}) to core dimension r_{c} . Before the wound Armature circumference may be figured in this application, the installed height (h) of the nested turns layers must be calculated. An extremely accurate manner of doing so, provided the base layer is wound virtually shoulder-to-shoulder, is to use the following formula:

$$h = \left[\frac{\sqrt{3}(\#1 - 1) + 2}{2} \right] d_{\text{w}}, \text{ where } \#1 = \text{the number of coil layers.}$$

Therefore, the wound Armature circumference (C_{w}), for purposes of calculating the coil-induced core section flux densities, may be figured as follows (with a Specification #1 of 12 coil layers, having 21 turns each):

$$\begin{aligned} C_{\text{w}} &= 2\pi[r_{\text{c}} + h] + 2L_{\text{w}} + 2L_{\text{c}} \\ &= 6.2832[.1825 + .1337] + 2(.2318) + 2(.5277) \\ &= 1.9867 + .4636 + 1.0554 \\ &= \underline{3.5057 \text{ cm}}. \end{aligned}$$

[3] *major average coil radius (R_{c}):*

$$R_{\text{c}} = C_{\text{w}}/2\pi = \underline{.5579 \text{ cm}}.$$

[4] *mean coil radius:*

The Armature's mean coil radius (r_{m}), for purposes of calculating its coil-induced core section flux densities, may now be figured as follows:

$$\begin{aligned} r_{\text{m}} &= 1/2(R_{\text{c}} + r_{\text{c}}) \\ &= 1/2(.5579 + .4243) = \underline{.4911 \text{ cm}}. \end{aligned}$$

[5] The Armature's Specification Core Field Intensity (H_{cu}), at the center of the wound (undercut) section(s) thereof, may be obtained as follows:

$$H_{\text{cu}} = \frac{NI}{2r_{\text{m}}}, \text{ where } I = 90\% \text{ of rated winding ampacity.}$$

$$\text{Thus, } H_{\text{cu}} = \frac{(252)(.252)}{2(.4911 \text{ cm})} = \frac{63.504}{9.822 \times 10^{-3} \text{ m}} = \underline{6465 \text{ amp-turns/m}}.$$

[6] Specification Core Flux Density:

From a graphic analysis of the DC magnetization curves graph in the

Appendix A [see DataSheet #4], it may be ascertained that the Field Intensity above corresponds to a Specification Core Flux Density (B_{cu}) of approximately 18,350 gauss at a Core relative permeability (k_{μ}) of 227.

This determination can be verified to a high degree of accuracy as follows:

$$\text{absolute permeability} = \mu = k_{\mu}(\mu_0)$$

$$= 227 (4\pi \times 10^{-7}) = 2.853 \times 10^{-4} \text{ nt/amp}^2;$$

$$\text{Since } B = \mu H, H_{cu} = B_{cu}/\mu = (1.835 \text{ wb/m}^2)/2.853 \times 10^{-4} = 6432 \text{ amp/m.}$$

This figure is within 0.5% of that calculated in subsection [5] above.

The following side view diagram shows the Stationary Electromagnetic Armature core configuration drawn according to the directives of SpecSheet XII, at a scale of 4.545 to 1 for the 4ft. diameter prototype model.

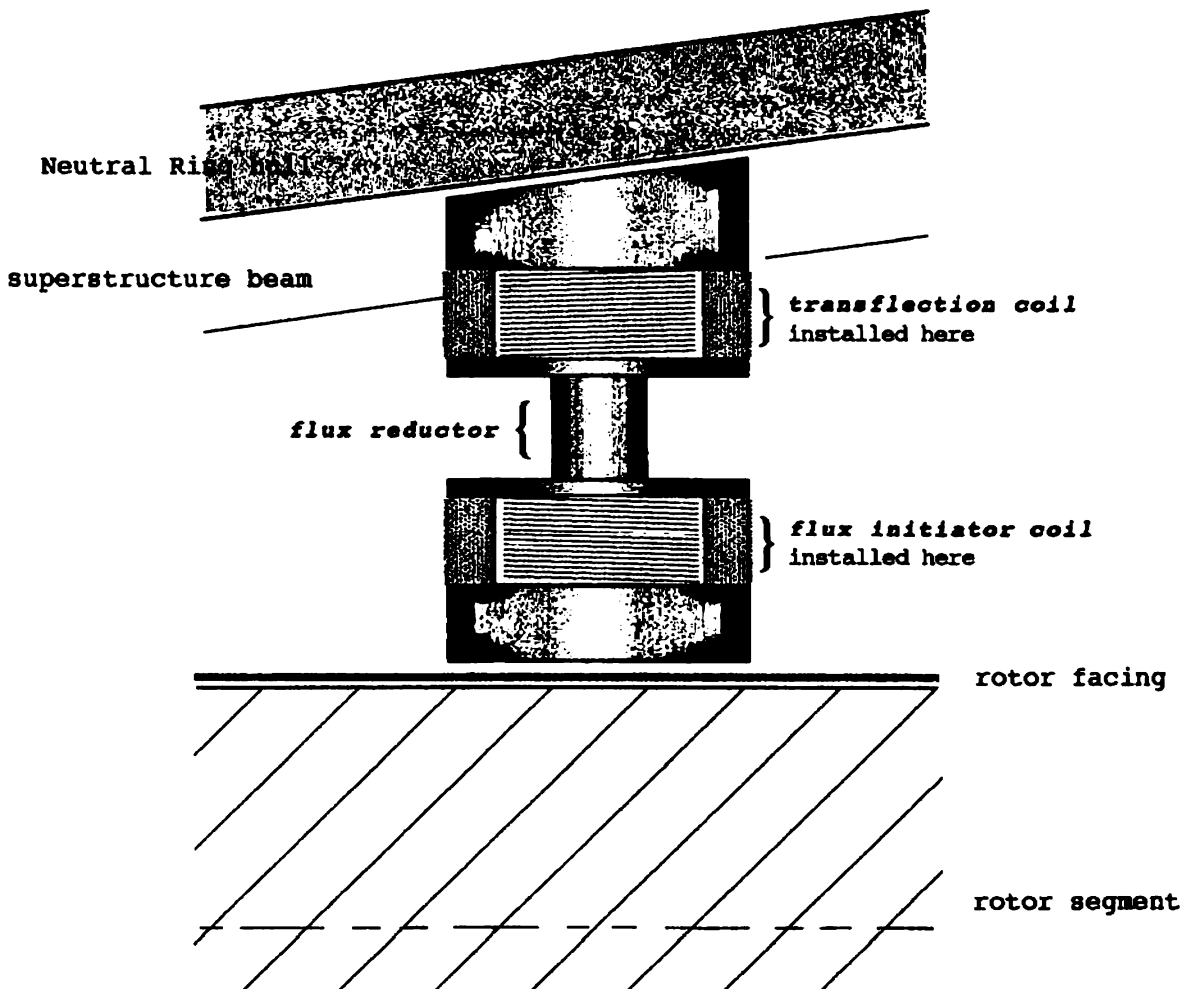


Fig. 40: Armature core configuration (windings represented).

A maximum of 252 turns (21 in each of 12 layers) could be used in a 4ft. prototype.

Basic Variable Inductor Array Wiring

The magnetic polarities indicated in the diagram below are those which would result in *clockwise rotation of the rotor* as viewed from above; counterclockwise rotation is just as easily accomplished.

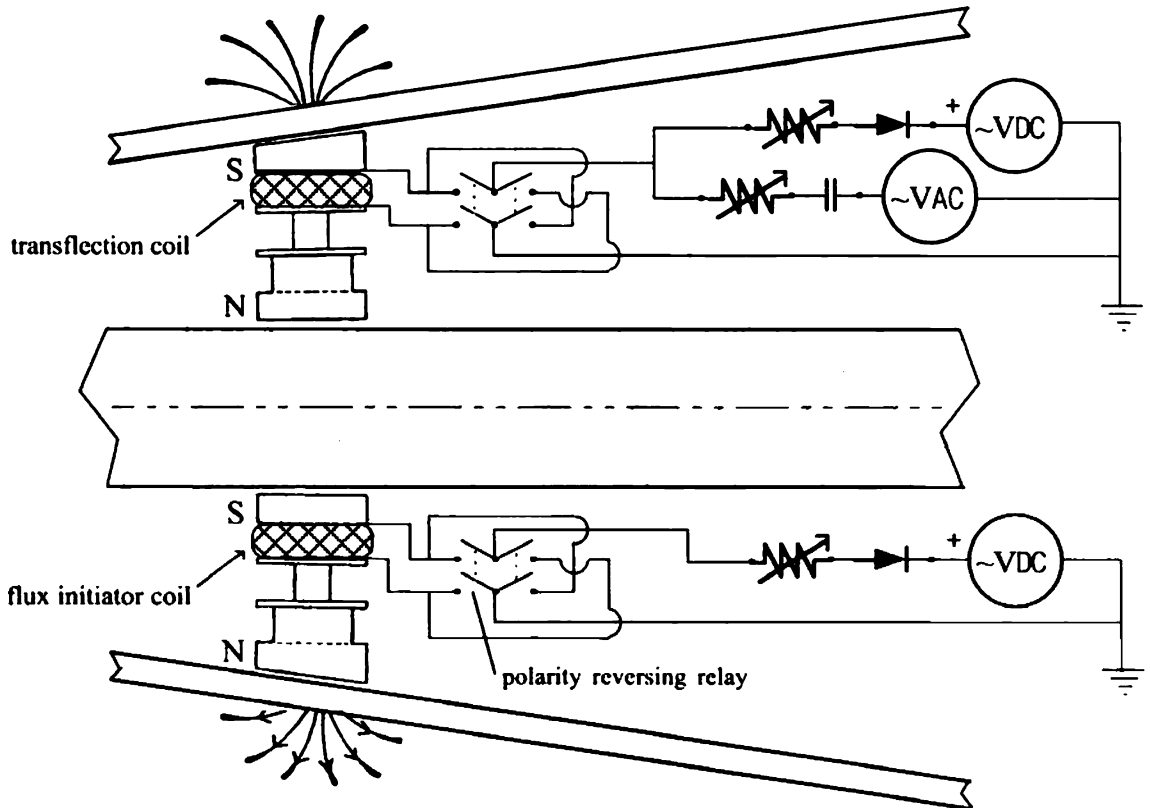


Fig. 41: armature power distribution system

The flux initiator coils are so-named because their required as-wound polarity relative to the fixed outward direction of the primary dc rotor current establishes both the direction of rotor rotation and the contingent winding direction and polarity of the transflexion coils.

The transflexion coils are so-named because they impart a *transverse deflectionary force* upon field current electrons. In the power field region of the field envelope, this force may be large enough to establish a continuous annular flow of 'displacement charge' current.

The *isolation capacitor* shown on the ungrounded pole of the transflexion coils' AC voltage source(s) blocks dc current from crossing the AC source(s). The *filter diode* shown on the positive pole of both armature coils' dc voltage source(s) blocks positive AC half-cycles from crossing the negatively-grounded dc source(s). However, each such dc voltage source must be sufficiently rated to carry the resultant unidirectional negative current impulses to ground. Any or all of these voltage supplies may be of a solid-state or rotary induction type.

This basic parallel-bussed *armature power distribution system* anticipates the use of a computer-controlled servo-system of conventional nature to render its functions manually-interactive. Such ancillary subcircuitry may be connected to any *non-buss* open circuit junction(s) indicated (by a dot).

Axial Field Flux Balance

model: Badlander

size: 4ft. dia.

This WorkSheet is used to figure the level of Armature-applied flux density required to effect a peak displacement current gyro-orbit on the power field centerline, due to the transverse deflection of field envelope electrons, during full-power operation of the EDF Generator as a Thermal Power Unit.

Section A: Full-Power Selector Plane Velocity

Because the Variable Inductor (armature) Arrays function as a velocity selector with regard to the gyroradius of the displacement current, the vertical centerline of the Arrays is herein referred to as the **selector plane**. The velocity and relativistic mass of field envelope electrons as they cross the selector plane must therefore be known before the Power Field flux density required to achieve the desired gyro-orbit may be calculated.

It is assumed here that the voltage gradient across the Power Field is uniform and that the potential difference between the innermost edge of the hull Negative Ring and the selector plane is therefore equal to one-half (1/2) the applied field envelope voltage, because the selector plane is located virtually on the hull Neutral Ring's vertical centerline.

- [1] The gained kinetic energy of each Power Field electron at the selector plane (W) is as follows:

$$W = qV, \text{ where } V = \text{one-half Nom. Field Voltage } (@ 1.5 \times 10^6 \text{ volts}), \\ \text{and } q = \text{the electron charge } @ 1.6 \times 10^{-19} \text{ coulomb.}$$

$$\text{Therefore, } W = (1.6 \times 10^{-19})(1.5 \times 10^6) = \boxed{2.4 \times 10^{-13} \text{ joules}}.$$

- [2] The relativistic mass increase represented (m_i) is equal to E/c^2 , where $E = W$:

$$m_i = W/c^2 = 2.4 \times 10^{-13} / 8.98755 \times 10^{16} = \boxed{26.70 \times 10^{-31} \text{ kg}}.$$

- [3] The total relativistic mass (M_i) of each Power Field electron equals the rest mass (m_o) plus the mass increase (m_i):

$$M_i = m_o + m_i = 9.11 \times 10^{-31} + 26.70 \times 10^{-31} \\ = \boxed{35.81 \times 10^{-31} \text{ kg}}.$$

- [4] electron selector plane velocity:

$$v/c = \sqrt{1 - (m_o/M_i)^2} = \sqrt{1 - (9.11/35.81)^2} = \sqrt{1 - .0647} \\ \text{and } v = .9671c, \text{ or } \boxed{2.8993 \times 10^8 \text{ m/sec}}.$$

Section B: Gyroradius Flux Density

- [1] The desired gyroradius of the displacement current (r_{dc}), near the center of the Power Field region* of the field envelope, is calculated as follows:

$$r_{dc} = \frac{6715}{9600} R_h = \boxed{.4264 \text{ m}}. \text{ {see aSpecSheet XII}}$$

*The Neutral Ring's exact vertical centerline is located at $[r_i + .5(C_o - C_i)]$, or .426 m.

Axial Field Flux Balance

[2] The net transfection flux density (B_{tr}) required to achieve this electron gyroradius on the selector plane is calculated using the cyclotron formula:

$$B_{tr} = \frac{M_e v}{qr_{dc}}, \text{ with values from above.}$$

$$\text{So, } B_{tr} = \frac{(35.81 \times 10^{-11})(2.8993 \times 10^8)}{(1.6 \times 10^{-19})(.4264)} = \frac{10.382 \times 10^{-22}}{6.822 \times 10^{-20}}$$

$$= 1.522 \times 10^{-2} \text{ Wb/m}^2, \text{ or } \boxed{152.2 \text{ gauss}}.$$

Section C: Armature Flux Density

According to Specifications, each Stationary Electromagnetic Armature must produce an inherent core flux density approaching as closely as possible the output flux density (B_i) calculated as follows (see Section E of aSpecSheet XII):

$$B_i = \frac{4\pi r^2 B_{tr}}{f A},$$

where A = spec. core end (face) area @ $7.196 \times 10^{-3} \text{ m}^2$,*

r = the linear core-to-gyro-orbit distance of 3.324 cm ,**

and f = 2.2672 , the calculated flux superposition ratio.***

* see WorkSheet XII(a) {Specific Armature Measurements}.

** This distance represents the thickness of the Neutral Ring hull (appr. $2C_r$ @ $.124"$, or $.315 \text{ cm}$) plus one-fourth ($1/4$) of the Neutral Ring diameter ($((C_v - C_r)/4$, or 3.009 cm) or half the distance from the hull surface to the Power Field apex. This point on the selector plane is taken to be the center of the Power Field (and disregards the virtually negligible core face-to-inner hull surface clearance).

*** see DataSheet #16 {Flux Superposition Ratio}.

Note: It is interesting to note that this same flux superposition ratio (2.2672) was originally calculated for a different gyro-orbit also lying on the selector plane but at a linear distance from the core faces corresponding to the apex of the Power Field region! It is thus presumed that this ratio will probably apply to any such selector plane gyro-orbit.

$$\text{So, } B_i = \frac{(12.5664)(11.05 \times 10^{-4})(1.522 \times 10^{-2} \text{ Wb/m}^2)}{(2.2672)(7.196 \times 10^{-3} \text{ m}^2)}$$

$$= \frac{211.343 \times 10^{-6}}{16.3148 \times 10^{-3}} = 1.2954 \text{ Wb/m}^2, \text{ or } \underline{12,954 \text{ gauss}}.$$

The value of B_i calculated above represents the net flux density of each Armature end (face) cross section. However, the reduced cross-section of the undercut wound sections of the core means that these parts of the core must actually produce a proportionally higher gross input flux density in operation. The applicable cross-sectional transition formula is as follows:

$$B_1 A_1 = B_2 A_2,$$

where B_1 = net core end flux density @ $12,954 \text{ gauss}$,

A_1 = core end cross section @ $.7196 \text{ cm}^2$,

B_2 = the unknown higher gross flux density,

and A_2 = reduced wound core cross section @ $.5041 \text{ cm}^2$.

$$\text{Therefore, } B_2 = 12,954(.7196/.5041) = \boxed{18,492 \text{ gauss}}.$$

The core flux density figured in aWorkSheet XII(a) is **99.2%** of this value.

Section D: Estimated Displacement Current

The value of the displacement current induced within the Power Field region of the field envelope (by the action of the Variable Inductor Arrays) is arrived at by the following chain of logic:

- i) the charge stored in the vessel hull's static capacitance is assumed to be positive, in response to the Hooper effect acting upon the rotor;
- ii) an equal and opposite (negative) *space charge* is assumed to occur within the relatively neutral Power Field region between the charged sections of the hull; and
- iii) this negative space charge will tend to rotate at the highest speed allowed by the available (net*) transfection flux density existing at the center of the Power Field on the selector plane (per the cyclotron formula).

[1] Power Field Space Charge:

By the reasoning above, the max. value of the negative space charge (Q_s) at full-power (Nominal) Field Voltage for a Thermal Unit is as follows:

$$Q_s = C_h V, \quad \text{where } C_h = \text{hull static capacitance @ } 28.652 \times 10^{-12} \text{ farad**}, \\ \text{and } V = \text{Nominal Field Voltage (nom. } V_f) \text{ @ } 3 \times 10^4 \text{ volts.}$$

** from the associated text.

$$\text{So, } Q_s = (28.652 \times 10^{-12})(3 \times 10^4) \\ = \boxed{8.596 \times 10^{-5} \text{ coul}} \quad (1\eta \text{ Thermal Unit only}).$$

[2] Space Charge Rotation:

The approximate revolutions per second accomplished by the space charge captured within the Power Field gyro-orbit may be found by dividing the net* selector plane transit velocity by the gyro-orbit circumference (C_o):

$$\text{space charge rps} = v/C_o, \quad \text{where } C_o = 2\pi r_{dc} \text{ @ } 2.677 \text{ m.}$$

$$\text{Thus, space charge rps} = (.992*)(2.8993 \times 10^8)/2.677 = \boxed{1.0744 \times 10^8}.$$

[3] Displacement Current Equivalence-Amps:

The maximum equivalent amperage of the displacement current (I_{dc}) which results from the rotation of Power Field space charge may now be calculated as follows:

$$I_{dc} = Q_s (\text{rps}) = (8.596 \times 10^{-5})(1.0744 \times 10^8) \\ = 9.236 \times 10^3, \text{ or } 9,236 \text{ amps,}$$

$$\text{and max. hemitorus displacement current } (1/2 I_{dc}) = 9,236/2 = \boxed{4,618 \text{ amps}}.$$

Section E: Displacement Current Flux Density

The maximum full-power value of the magnetic field due to space charge rotation within each field hemitorus, as calculated at the hull's vertical centerline, is as follows:

$$\text{max. hemi } B_{dc} = \mu_o (1/2 I_{dc})/2r, \quad \text{where } r = \text{displacement gyroradius @ } .4264 \text{ m.}$$

$$\text{So, max. hemi } B_{dc} = (4\pi \times 10^{-7})(4.618 \times 10^3)/.8528 = 58.031 \times 10^{-4}/.8528 \\ = 68.05 \times 10^{-4} \text{ Wb/m}^2 = \boxed{68.05 \text{ gauss}} \quad (1\eta \text{ Thermal Unit only}).$$

It should be noted that although these two hemitorus fields are of an axially-polarized nature, they are mutually opposed (due to opposite current rotation) and tend to cancel.

As the diligent reader has discovered in reaching the preceding material on stationary armature and field flux density considerations, which in many ways represents the most sophisticated and elegant aspects of Generator operation, the really crucial hardware has now all been defined and expanded-upon in what is felt to be the best possible order – that of increasing complexity.

Perhaps this would be a good place and time, therefore, to take a look at some **closing hardware considerations**, before returning in Chapter 9 directly to further theoretical discussion of the Variable Inductor Arrays and the nature of *field flux dynamics*. At any point in the remaining pages of **StarDrive Engineering**, one can of course return to the Basic Specifications or Appendices as necessary to reinforce certain technical knowledge which must underlie a true *intellectual conviction* that the StarDrive system as a whole is sound.

What should be almost striking by this time is the *sheer simplicity* of most of the StarDrive components. It is the manner in which the five primary systems interrelate, each composed of simple parts, which is extraordinarily complex. This beautiful simplicity is most evident in the level of mathematics required to model the principal design characteristics of these parts *with admirable accuracy*, and in this respect the math required is elegantly direct.

For instance, the magnetic rings are perhaps the most key fundamental component type inherent to the Generator's overall design, yet both physically and mathematically they each constitute the simplest variant of the simplest magnetic circuit possible! Likewise, their associated field coils are marvelously simple and efficient magnetically, extending the *ring* motif to include ring (or helical toroid) windings. And, each of the various electrode arrays*, which of course utilize a flat ring or ring section configuration, constitutes both capacitor and vacuum tube in one and functions in a manner which is eminently suited to traditional analysis.

In fact, a great many Patents have been awarded for inventions which faded into obscurity simply because the suitably novel claims involved could not be *achieved or substantiated using traditional methods*. Thus, industry's rapid acceptance of a brand-new technology, presaging its coming assimilation into society, is the greatest validation of his work an inventor can hope for (and may be all the remuneration he will enjoy for it). It signifies that present-day experts are satisfied the innovation represents an *acceptable risk of resources*, and sometimes comes about only through the foresight and artful maneuvering of the originator.

I feel quite confident in this respect about the 1η Thermal Unit EDF Generator: it is a 'physical plant' of tremendous potential value, for generating electricity or desalinating seawater. It's the 3η device we'll worry about from here on out . . .

* In assessing "related or prior art" to prepare for filing a Patent Application, I found right away that there really *was* no prior art per se in my case. A fair number of Patents have been issued for devices which incorporate one or more *electrode arrays* and endeavor to use various forms of "electric wind" to achieve propulsion. However, in most cases the engineering involved was either too purely theoretical to allow satisfactory mathematical modeling or too mechanically and expensively complex to encourage development. Or both; to wit, one may wish to study the U.S. Patent #3,464,207; Quasi-corona Aerodynamic Vehicle, by E. C. Okress; Sept. 2, 1969.

Chapter 9

Field Electrodynamics

Having arrived at this juncture by diverse but more or less difficult paths, you true aficionados are heartily congratulated. Those of you who journeyed via the entire Specifications have now seen pretty solid proof that this machine can be successfully built and operated, and that the Way was found only through the application of an impeccably-reasoned and lean yet *holistic* design method, or 'systems approach'. And for the less-inclined to obsession with *hardware* who took but a sampling expedition in Chapter 8, your good faith will still see you through the largely-conceptual part of our story remaining with no penalty incurred.

In this Chapter, it will however be assumed that everyone is basically familiar with all of the special *nomenclature* that has been carefully developed. As you can see, many of the component names have a decidedly StarTrek™ 'feel' about them, and this is neither surprising nor accidental. It was decided early on, though, that the name of each of the really crucial components should directly reflect both the traditional aspects of its design or form and the innovative nature of its usage *in this application*, if possible.

We will now proceed beyond basic hardware considerations and take a much closer look at the Variable Inductor System and its complex yet controllable influence on the StarDrive electrodynamic field, as well as the relationship of the Field envelope's *induced magnetic properties* to its desired performance on all levels. Since the EDF Generator operates within a number of modes of usage, a study may then be made of how specific Field magnetics can be developed to: (1) maximize a Thermal Unit's output potential without it burning up!; and (2) optimize long-range communications and sensor capability in 3η rotor devices without unduly constraining net thrust.

In order to apprehend these challenging but fascinating magnetic subtleties in the most direct fashion, we must begin with a minimum number of *axiomatic observations* which will apply equally to both Thermal and Drive Units. This understanding of the fundamental magnetic rules which must apply to the conditions evident in the Field envelope will allow us to assess and develop basic *operational guidelines* governing the Generator's 'start' and 'run' behavior.

Beginning at the simplest level (but quickly becoming more complicated), it is self-evident that Drive Field dc current will develop an associated unidirectional magnetic field. But, because of its dual hemitoroidal configuration, what will be the nature and 'shape' of the two resultant Drive-current-hemitorus magnetic fields? By virtue of the same line of reasoning used with respect to the secondary rotor field (discussed in Chapter 5), we may safely assume that that portion of such hemitorus current-induced flux with which we need be concerned must assume a toroidal configuration within each of the two defined power field regions. [Two equivalent flux system portions must lie outside the field envelope, to finish enclosing the current, and theoretically attenuate indefinitely.]

Also, we've learned that the outer inductor (armature) sections and their transflection coils are used to cause *an annular rotation of space charge* in these

power field regions which is radially perpendicular to Drive Field current. Once again, these two annular current elements will each have a magnetic field, but in this case one which is exactly analogous to that around a single loop of wire. Thus, these two fields are wholly *contained* within the power field, and also have a toroidal configuration, so that the Drive current hemitorus fields are in part superimposed upon them. The corresponding annular current elements are then thought of as comprising the Field envelope's flow of **displacement current**.

Now, a moment must be taken here to see this latter term in the proper context. Displacement current is a traditional capacitance concept deriving from the work of James Clerk Maxwell, and denotes the brief plate inrush or outrush current which takes place during 'charging'. However, technically, a capacitor stores *energy* in the form of the electric field between its plates. A capacitor only stores electric charge *per se* via the displacement current of one plate with the other plate at ground potential! In an ungrounded dc capacitance exhibiting high leakage current *between* the plates (like the hull), the instantaneous storage of charge itself is essentially ZERO.

We can now see that the vessel hull's true **field dynamic capacitance** (the only kind it can exhibit) must be a function of the variable inductors' ability to supply a sufficient magnetic rotational force on power field electrons to establish a *continuous* flow of displacement current despite the intense radial Drive Field voltage gradient. Therefore, in this respect the Generator's Field stores *power*, not energy! And yet, the maximum value of this stored power will indeed be a function of the hull static capacitance (and Field voltage), as it is dependent on the total amount and velocity of this rotational space charge given the pertinent considerations of WorkSheet XII(b) {Section D}.

In any event, the annular power field constitutes a spatial realm where three magnetic field systems are most interactive: those produced by the stationary armatures, hemitorus Drive currents, and displacement current(s). The armatures or variable inductors have of course a fixed axial polarity, but both other flux systems only have inherently-unfixed radial polar tendency (due to the toroid field rules that have previously been studied). These two toroid field systems will thus polarize only to a certain extent, but it may be necessary to know the correct relative polarities they will acquire by induction before important *field flux balance* calculations are attempted.

Therefore, the first key field flux axioms, which govern the *net level of polarization* within the power field, must be carefully deduced and stated as follows:

(1) the *Drive current's magnetic fields* will polarize attractively to the transflection fields applied by the variable inductors, and such consecutive fields of like direction (having unlike facing poles or *equal polarity*) will thus be series-aiding; and

(2) the *displacement current's magnetic fields* will then polarize attractively to the Drive current fields, satisfying the toroid field rule(s) in that such coincident fields of unlike direction will be parallel-opposed, while these same fields also oppose the applied transflection fields in satisfaction of Lenz's law (having like facing poles or *opposite polarity*).

These fundamental relationships provide the proper basis for evaluating the net flux balance or density at certain points within the Field envelope, with regard to Field ignition mechanics and the accuracy of net thrust calculations. Fig. 55 on the next page visually illustrates these principles in fairly good form.

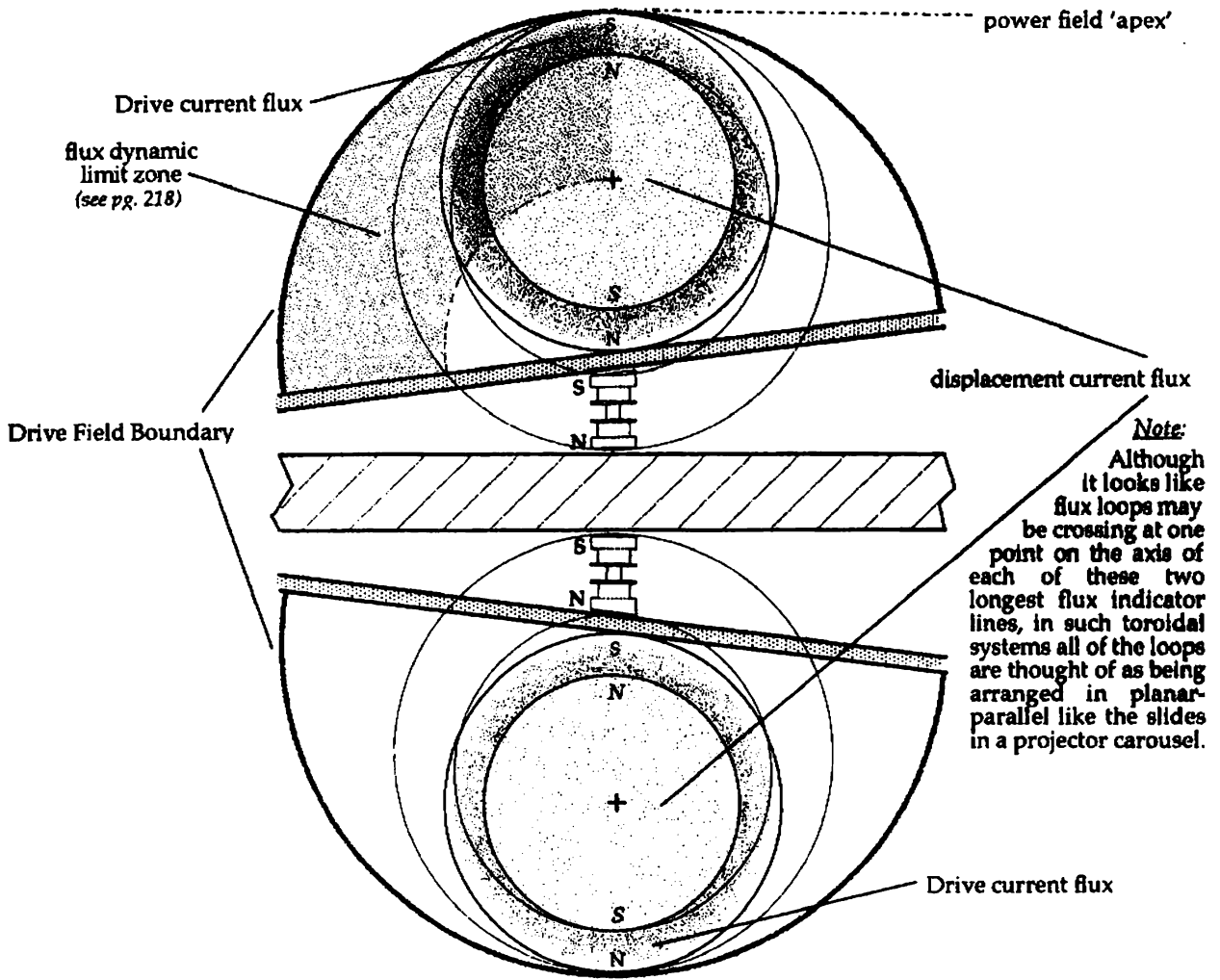


Fig. 55: power field flux polarity diagram (in cross-section).

The armature polarities indicated will result in clockwise rotation of the rotor, as viewed from above, like those in Figs. 9 on pg. 49 (of Chapter 5). More accurately, the chosen polarity of the flux initiator coils determines the rotational direction of both the rotor and the power field space charge.

The electron experiences a force in a magnetic field which is mutually perpendicular to the field and to its own velocity. In a *uniform* field of induction, this force is equal to its charge (q) times its velocity (v) times the flux density denoted of course as B : $F = qvB$. Equating this force with the centripetal force required to keep power field electrons moving in a circle of radius r , we obtain: $F = mv^2/r = qvB$, and so $B = mv/qr$. This simple equation is sometimes referred to as the "cyclotron formula", and will be used later in this Chapter to perform important power field "gyro-orbit" calculations in relation to two basic 'start' and 'run' axioms of Field mechanics.

Thus, perhaps an easier and more insightful way to remember this important equation is: the radius of curvature of an electron's trajectory in a uniform magnetic field is equal to its momentum divided by the charge-flux product. The simple alternate form of the formula is then $r = mv/qB$.

An initial observation which arises from the cyclotron formula as used in this application is that since the electron's charge q is constant and its relativistic mass m , is a function of a given velocity, the gyro-radius it will tend to assume in a *non-uniform* magnetic field is inversely proportional to the flux density in evidence at the particular point *where the given velocity was measured*. And, since flux density is inversely proportional to the square of the distance from the magnetic field source, there will then be a huge variation in the trajectory modification experienced by Field envelope electrons nearing the inductor arrays even within the narrow volume of the defined power field. Depending on the flux density, in other words, there are as many theoretical stable gyro-orbits within the power field as there are points of velocity measurement!

Obviously, one preferred point of velocity assessment must be selected where optimal accuracy is assured and which also preferably lies *on the desired gyro-orbit*. Due to the displacement current magnetic field considerations discussed earlier above, the most reasonable power field gyro-orbit to use as a benchmark for Field performance calculations and analysis is one which is centered within the power field volume. Therefore, we'll assume for conceptual clarity that all displacement current actually occurs on the *power field annular centerline(s)*, and the corresponding points of velocity measurement are indicated in Fig. 55 as $+$.

As outlined in WorkSheet XII(b), it is possible to make a highly accurate assessment of a power field electron's velocity as it crosses the Neutral Ring vertical centerline because the voltage gradient across the Field is essentially uniform (as we've learned): this means that such an electron has at that point been accelerated through exactly half the total Field voltage!* This also means that another small concession to simplification may be made: we may eliminate the $\sin\theta$ factor usually associated with B in the cyclotron formula (just as in the coil voltage formulas), because all power field electron trajectories are at that point perpendicular to the axial plane of the variable inductor array(s).

The most important thing to realize about this axial magnetic plane is that it acts as a true electron *velocity selector* with respect to the stipulated gyro-radius: any electron traveling slower than the one co-dependent B -function velocity as it crosses this **selector plane** is side-deflected but rapidly reintegrated with Drive current; and if moving faster than this specific velocity, it will actually be back-scattered but with the same end result. Thus, the cyclotron formula allows us to use a variable level of armature flux density to select the *containment velocity*, or $v_c = qBr/m$, at which Field envelope electrons are confined to the power field.

We can now visualize and state the first simple precept of Generator 'run' field flux dynamics: The operating power field gyro-radius for all devices must be greater than the selector plane radius for all points that lie farther from the armatures in the outer half of the power field than the specified gyro-orbit. [see Fig. 55] All Field electrons at such points must pursue modified arc trajectories which complete the Field envelope circuit but are quasi-coherent without undue impedance. And, due to the armatures' output limit, this will be the case even in Thermal Units (provided armature current is *evenly* proportional to rotor speed).

* Although the stationary armatures are not located *precisely* on the Neutral Ring vertical centerline, the difference in positioning is so small that any discrepancy in the calculated value of electron velocity is deemed negligible for present purposes.

It's also important to point out that the rate at which Field-generated heat is distributed to the hull Neutral Ring surfaces is postulated to display an inverse bell-curve relationship to *the displacement-to-Drive current ratio*, and thus field-induced heating effects on a Thermal Unit's hull may be minimized during high-temperature operation in air by somehow determining the optimal value of 'run' displacement current. [Direct experimentation may be the only way to do this, but half of the peak value is the proposed initial 'setting'.] The effects that *active magnetic modulation of Field electrical dynamics* will have on AC signal activity or dc thrust output in the 3η rotor Drive Unit need not be considered just yet.

For now, using the same armatures defined in α SpecSheet XII in the 3η rotor device, it is expected to observe higher levels of peak 'run' displacement current than in same-size Thermal Units despite the greatly-reduced tranflection flux density proportional to Field voltage. In fact, refiguring WorkSheet XII(b) for the 4ft. diameter Drive Unit, it can be seen using the space charge rotation approximation method in Section D that peak displacement current I_{dc} will rise to about 12,125 amps or just over 130% of the value calculated for the Thermal Unit.* Reliance must then be made upon the extremely low temperature of space itself for adequate hull thermal protection in Drive Units, given the vastly higher Field voltages (and heat) developed and reduced proportional electron deflection.

Nevertheless, if we view the proper local armature-induced magnetic effects on space charge drift across the power field as corresponding to an increase in the thermal 'efficiency' of the hull materials, we must logically also then treat these *magnetomotive* modifications on Field envelope electron trajectories as a direct *Field thermal efficiency loss!* Thus, in keeping with the overall efficiency analysis developed for the 4ft. Thermal Unit in WorkSheet II(c) {Field Power Output}, the *apparent power equivalent* of the field dynamic capacitance will be added to Field apparent power (P_{gt}). This will have the effect of not only reducing peak thermal efficiency but *peak drive impulse efficiency* as well, giving us the ability to readily calculate how the peak displacement current levels described above will affect net thrust production in the 3η StarDrive vessel.

Using data from WorkSheet XII(b), we may calculate the angular gained kinetic energy W of each displacement current electron as equal to one-half the mass times the square of the instantaneous rotational velocity v . This value turns out to be 1.481×10^{-13} joules for the 4ft. diameter Thermal Unit. However, this gained kinetic energy is also electrodynamically equal to electron charge q times a theoretical applied potential difference V . Therefore, the displacement current is held in containment at a valid equivalent voltage equal to W/q (in that $W = qV$), or 9.256×10^5 volts, and the *apparent dc power represented* (P_{dc}) is equal to the equivalent voltage times the equivalent displacement current (9.236×10^3 amps) at 8.55×10^8 watts.

Comparing this power with a value for full nominal inherent Field electrical power P_f , equal to 3 million volts at rated rotor amperage or 1.1448×10^{11} watts, we now find that P_{dc} represents only 0.75% of the total Field power. And, the Unit's

* Ideally, the net containment velocity should be recalculated from the third given form of the cyclotron equation, where v_c is dependent on the other known co-variables. However, the quick estimation method used in the said WorkSheet yields a displacement current value *in this example* within 1% of that obtained by the longer method.

peak thermal efficiency will still be reduced by less than 1%! When these calculations are repeated for the 4ft. Drive Unit, interestingly enough it is found that the full 'run' level of displacement current apparent power P_{dc} increases by only about 15% while total Field power rises of course by over 12 times. Thus, it can finally be seen that field dynamic capacitance will have a virtually negligible effect on the overall average Drive Unit net thrust output, and full attention can be paid to 'tuning' the Field envelope's AC signal characteristics!

In order to further develop our understanding of Field dc current magnetic effects, we must now attempt to make use of the two initial field flux axioms associated with Fig. 55. These axioms will allow us to accurately calculate what may be termed the *residual induction* in this application: the net polarized 'run' flux density at any point within the power field *which lies on the selector plane*, as this is the spatial axis for which we've verified the variable inductors' flux superposition ratio. Since it is now known that this residual induction or field flux balance will have little effect on Drive dc current mechanics, we can try to assess its value at a certain point along the selector plane which will yield the most meaningful data with regard to Field AC signal current dynamics. The question then becomes: what point constitutes the basis of the best resolution of power field flux balance which is representative of the *entire Field envelope*?

Logically, this question almost answers itself by empirical deduction, and the solution will become evident conceptually from another look at Fig. 55. For instance, while we may easily discuss the flux density on the power field gyro-orbit with respect to that of the armatures and Drive current, it is not meaningful to talk about the flux density there which is attributable to the displacement current (as this is taken to be that current's very axis of flow). Realizing that such a point of optimal flux resolution (on the selector plane) should be common to both the idealized Drive and power field regions *as we view them*, the most suitable flux balance point(s) might appear to be those located on the Drive Field boundary at the indicated *power field apex*. Hence, electrons on the intersecting trajectories at these points could be relied upon to exhibit magnetic attributes representative of both Drive and power field currents, or what may appropriately be thought of as **the StarDrive integral Field**.

This field apex might seem a bit inappropriate as our resolution point due to its perceived inclusion within the Drive current, but we may properly take an algebraic flux density 'reading' at a point an infinitesimal distance beneath the apex on the selector plane - once it can be determined where the axial centerline of the hemitorus Drive current(s) is located! Given the precisely-defined configuration of the hull and Field envelope, it can be shown by highly accurate graphic analysis that the middle of the hemitorus current 'thickness' along the selector plane will be located very nearly 1.5 times the Neutral Ring's radial width from its surface. Therefore, the selector plane distance from this Drive current axial centerline to the Neutral Ring surface shall be equal to $1.475(C_v - C_a)$, and the resultant selector plane distance from the *apex to the Drive current axial centerline* is equal to this said distance minus one-half of $(C_v - C_a)$; or $.975(C_v - C_a)$. This latter distance is then referred to as the *field harmonic radius*.

As stated earlier on, we may easily use the traditional Biot-Savart formula for

the flux density near a single currented loop of wire to find the unpolarized total displacement current flux density at the power field apex (B_{dc}). The induction is then: $B_{dc} = \mu_0 I / 2r$, where I is current in amps and r is the selector plane distance from the power field centerline to the apex [or $(C_v - C_s)/4$] in meters. But what about the hemitorus Drive current – what is the nature of the magnetic field associated *with half a loop of wire*??

Fortunately, it can be shown using basic calculus that a semicircular conductor lying in a plane perpendicular to a uniform magnetic field will experience the same force as a straight conductor placed along the connecting diameter. It may therefore be cautiously inferred that the magnetic flux density at a given point in space near the surface of a uniformly semicircular conductor will be equal to that occurring at the same distance from the surface of a straight conductor. Now, we may readily use the corresponding Biot-Savart expression for the flux density near a single straight conductor, which is basically the same as the other but reduced by a factor of π , to calculate the unpolarized total Drive current flux density at the power field apex (B_{df}): so that $B_{df} = \mu_0 I / 2\pi r$, where in this case r is the field harmonic radius (plus that infinitesimal increment).

We are now in the admirable position of being able to compute not only the flux density at the power field apex which is attributable to all three flux sources, since the appropriate method of figuring the total polar flux density developed by each inductor array (B_{tr}) is given in WorkSheet XII(b), but also then the residual polar induction exhibited at the apex – by virtue of the two key field flux balance axioms derived on pg. 216. This will still be somewhat tricky going, however, so we will work it through using the 4ft. Thermal Unit prototype as an example.

Given a Specification core flux density of 18,350 gauss and the method shown in Section C of WorkSheet XII(b), we may calculate the value of transflection flux density at the apex (apex. B_{tr}) as equal to 41.6 gauss. Applying the two single-conductor formulas from above, it turns out that either of the two displacement current's unpolarized flux density $B_{dc} = 965.3$ gauss and the unpolarized Drive hemitorus current $B_{df} = 317.1$ gauss (respectively) at that same point.

Applying the logic of the field flux axioms in order (and above all keeping in mind the two toroid field rules from Chapter 5 on pg. 50), we can see that even though B_{df} is over 7.6 times larger than the modest apex. B_{tr} of 41.6 gauss, the only effect it will have is to add another 41.6 gauss of like-direction polar flux density at that point in the combined field(s)! And, it is now apparent that the opposed displacement current B_{dc} can only reduce the total polar induction by this same 41.6 gauss, so the residual induction is still just the transflection flux density we had originally!! [This outcome results from the operation of Equations M1-M3 from DataSheet #16; toroid fields in a vacuum will seek to match local polar flux densities.]

Such an anticlimactic yet disturbing outcome, like others that we've seen manifested during our studies, seems especially vexing due to the trouble we went to in obtaining it. But *now* it is crystal clear that the net polar induction anywhere in the Field envelope will merely be that in evidence due solely to the variable inductor arrays. Moreover, it will now make sense that our real point of interest magnetically must be the farthest point out on the selector plane which lies right on the Field perimeter: this point is called the *harmonic polar margin*.

Due to the mutually-compensating effects of the displacement and Drive current magnetic fields just demonstrated, the residual induction at the polar margin(s) will still accomplish the aim of being representative of the magnetic attributes of all Field envelope electrons – as such electrons must technically all be constituents of *both* of these two types of Field current. Furthermore, the residual induction in evidence at the polar margin will be more plainly indicative (than that at the apex) of the *minimum level* of ‘unitizing’ magnetic effects on Drive Field current to be expected, as such effects (to a point) promote the desired quasi-coherent properties within the integral Field.

To calculate the residual induction at the margin(s), or *marginal field flux balance*, we must know the accurate distance from there to the armature outer pole faces. By means of the same graphic analysis that was used to determine the field harmonic radius, it can be shown that this distance is equal to $2.4(C_v - C_a)$ plus the Neutral hull thickness (appr. $2C_a$). Applying the appropriate B_a formula from DataSheet #16, we find that the maximum marginal polar flux density for both Thermal and Drive Units of the 4ft. model will be 1.96 gauss.

While this indeed represents a very small level of induction, there would be little point in having a large polar margin ‘B’ as only the quasi-coherence within the defined Field envelope is of practical concern. Not only that, but as αSpec-Sheet XII implies, the variable inductors would customarily be operated at a mean value of *half* their Specification core flux density (due to the function of the flux reductor): so the maximum normal ‘run’ margin flux density in this example drops to essentially a single gauss! Nevertheless, this extant residual B-value now gives us a meaningful scale against which observed Field AC signal performance characteristics may be correlated and assessed.

Perhaps more importantly, the *exo-envelope gyro-radius* associated with this harmonic margin flux density begins to address the issue of a minimum safe proximity to a StarDrive Generator in full-power operation. Without delving into the inevitable high-energy radiation hazard presented by this device (which we’ll examine in the next Chapter), this exo-envelope gyro-radius suggests a physical approach-distance limit for Thermal Units operated in air which should be observed so that potentially harmful beta (electron) radiation associated with the movement of *entrained static charge* may be avoided.

The exo-envelope gyro-radius for a 4ft. Thermal Unit turns out to be 28.41 m (or 93.2 ft.)* which gives us a measure of the physical ‘sphere of influence’ of the full integral Field. This minimum proximity for the Drive Unit will of course be many times greater, due to the vastly increased envelope electric field intensity. It remains to be seen, however, whether a Drive Unit can actually be operated at anything approaching full power within the atmosphere, or how long it would have before it *must* attain the ultra-cold environment of space (or burn up).

* * *

Sometimes the most relevant yet confounding discoveries can occur due to the simplest observations. In this regard, I feel it’s important now to discuss what was

* To calculate the exo-envelope gyro-radius, one must first know that the arc-length from the Emitter Ring to the harmonic margin corresponds to 74° of the 180° Drive Field perimeter, and thus the approximate accelerating Field potential difference is assumed to be $74/180$ of a nominal 3 million volts, or 1.2333×10^6 volts (for the 4ft. Thermal Unit).

learned as a result of the “stunning” realization that the integral Field – and particularly the displacement current – could perhaps be thought of as *a flow of ion plasma*. To understand the implications of this simple but dangerously misleading intuitive leap, we will need to take a brief yet interesting look at the *magnetohydrodynamic formula* or what has been called “the Tokamak equation”.

It has been established from high-energy plasma physics experiments that a continuous pressurized ionized plasma stream similar to our said displacement current actually *cannot* be dealt with (in an electromagnetic sense) ideally as a current loop of negligible conductive diameter (or “wire” size, if you will), but must be treated as a hydrodynamic fluid column of consequential radius r_c . Because of its internal kinetic pressure, such a plasma stream will actively seek to fill its available *containment corridor* to capacity. In short, as our displacement current increases, it *might* be thought of as assuming a circular conductive path with a minor radius approaching that of the power field (as depicted in Fig. 55).

Now this disclosure in no way obviates or negates our hard-won analysis of the displacement current’s magnetic characteristics, as its flux density was calculated entirely in keeping with traditional method. What this does mean is that it is not really meaningful to consider this flux density at *any* point within the defined power field region(s), as we quickly concluded in principle on our own. What we were mainly not taking into account at that time is the tremendous temperature involved in such a huge *volumetric energy flow density*.

The full magnetohydrodynamic formula (which has been substantiated through Russian Tokamak nuclear fusion research) equates the plasma stream’s internal kinetic pressure as a function of its charge density per unit volume (n) and temperature in °K to its magnetic energy density, and is stated as follows:

$$nkT = \frac{\mu_0 i^2}{8\pi^2 r_c^2} \quad , \quad \text{where } k = \text{Boltzmann's constant } (1.38 \times 10^{-23} \text{ joules/}^\circ\text{K}) \\ \text{and } i = \text{containment current in amps.}$$

Etude

A simpler derivative of the Tokamak or magnetohydrodynamic formula could also be of practical use to StarDrive engineers later on. This expression relates the internal kinetic pressure as a function of its temperature and charge density per unit *length* (N) solely to the known containment current, and in alternate form allows the minimum plasma temperature to be estimated on this basis: $NkT = \mu_c i^2 / 8\pi$, or solving for temperature, $T = \mu_c i^2 / 8\pi Nk$. The self-generated magnetic energy density developed by the plasma current actually provides the surface containment thereof against its rising internal kinetic pressure, and this magnetic energy density is equal to $B^2 / 2\mu_0$, where B is measured at the containment corridor surface.

A crucial observation with regard to the attempted use of these equations in this application is that the charge density n refers to the number of *positive ions only*, and must equal about 10^{20} to yield meaningful solutions. It may also be of interest to note that the axial electrostatic energy density is equal to $\epsilon_0 E^2 / 2$. In the full form of the Tokamak formula, the volume of the toroidal containment field is factored in, and the *collapse of the corridor will occur when the magnetic energy density exceeds the kinetic pressure* nkT (where $n = N / \pi r_c^2$). [The toroidal containment volume is most easily calculated here as equal to πr_c^2 times the gyro-orbit circumference C_0 .]

I had originally hoped that this equation would provide future StarDrive engineers with a powerful mathematical tool which could be used to accurately model and assess the tremendously complex working physics involved in the StarDrive integral Field. However, it is imperative to stress that great caution must be exercised in endeavoring to apply the Tokamak equation to the operation of StarDrive Generators! During the course of incredible quantities of calculations in this regard (somewhat reminiscent of hull configuration days), I discovered that sometimes theoretical validation based on someone else's work just can't be had even by the truly persistent. Otherwise, I might still be at it . . .

The first and perhaps determinant observation which must be made here is that plasma per se is generally considered to be a mixture of electrons and much-heavier gaseous atomic ions in roughly equal numbers which is therefore *electrically neutral overall*. So, unless atmospheric positive ions are entrapped in the power field region(s) in roughly equal numbers to the displacement current electrons, it's probable that the Tokamak equation *as is* may be of no use at all in helping us select that optimum value of 'run' displacement current we desire.

Another empirical observation which should be made is that in any usual working solution to this equation the actual operating temperature of the plasma *must always be almost ten times higher* than the minimum estimated temperature found by the derivative formula, or containment corridor collapse cannot be avoided! This situation has almost certainly been the primary reason why no Tokamak fusion reactor to date could be made to produce more energy in operation than it consumed. One *might* think this fact in itself would not present any great problem in the StarDrive Generator, however, due to the plausible concept of ancillary heating from the much-larger proximal Drive current.

My initial interest in finding a solution for the Tokamak equation which worked for the 4ft. theoretical prototype was in fact related to predicting the temperature of the power field as a sort of feasibility study. If I derived no meaningful solutions *at less than sun-like heat* (~6,000°K), I was afraid that my whole beloved project could remain no more than an interesting yet aberrant intellectual conundrum. This state of mind persisted until I finally understood that the concept of 'temperature' *within a virtual vacuum* is essentially a null issue: as we'll see in a bit, the absolute kinetic energy associated with the molecules of a highly-attenuated gas is actually the key concept, and there can be no integral Field temperature per se at anything close to the *relatively cool* surface of the sun! The real issue is whether the Drive Field is self-evacuating!!

Note for Theorists and Magnetic Engineers: At the risk of briefly losing half my readers, I feel that we should nevertheless digress for a moment to wrap up my findings regarding the Tokamak equation for the benefit of all you hard-core technical types. I hate to "waste" a rather fascinating solution I found to the aforementioned excess magnetic energy density (and containment corridor collapse) difficulty as it might relate to the StarDrive device, and this challenging little resolution is actually inherent in its power field magnetic configuration (as shown in Fig. 55).

Were we to reasonably consider the superpositioned parallel-opposed displacement and Drive current field reluctances as being magnetic analogs to electrical resistances in parallel, thereby mutually reducing the available magnetic force of containment, the *effective* value of containment flux density for purposes of figuring the relevant magnetic energy density ($B^2/2\mu_0$)

should be equal to the reciprocal of the the sum of the reciprocals of the said two superimposed field flux densities. This would be expressed as $1/\text{apex } B_{dc} + 1/\text{apex } B_{dr} = 1/\text{net } B_c$. So, using data in Wb/m² for the 4ft. model, $\text{net } B_c = 1/(1/.09653 + 1/.03171) = .02387$ Wb/m², and B^2 then becomes 5.7×10^{-4} instead of 9.3×10^{-5} . This would reduce the corresponding plasma temperature needed to avoid corridor collapse by a factor of over 16 to 1.

Also, if we let B_o represent $\text{max. } B_r$ and I_o represent $\text{max. } (I_{dc}/2)$, the value of the net hemitorus displacement current i would be calculated according to the simple relation $B_r/B_o = i/I_o$, *if the applied transfection field were uniform*. Since this is not the case in this application, a modest correction factor would have to be developed whereby the adjusted hemitorus displacement current ($\text{net. } i_{dc}$) as a function of the net transfection flux density B_r is always *somewhat less than* its otherwise linear proportional value. The 'empirical' correction factor I developed which seems appropriate (but which is at best an approximation) is as follows:

$$[1 - \cos(B_r/B_o \cdot 90^\circ)] I_o = \text{net. } i_{dc},$$

where B_r is in fact calculated using current i in the linear proportionality above.

Although this entire Tokamak-related discussion may actually seem almost counterproductive, there can be little doubt that this now-classical physics knowledge will have *some* bearing on the project at hand (and I'll refer to it again later). For example, an empirical observation arising from the application of this esoteric formula is that the plasma stream current can generally be expected to start becoming unstable at levels from 10^4 to 10^5 amps. Disruptive perturbations called "kinks" and "pinches" can result which eventually cause the destructive collapse of the containment corridor. This knowledge might be of considerable interest to us at this point because this is *precisely the level of displacement current* projected for the larger Impulse Drive Unit models!

As shown in WorkSheet XII(b), the maximum hemitorus displacement current ($I_{dc}/2$) will be about 4.623×10^3 amps for the 4ft. model, and its standard operating value would be roughly half this figure. Thus, the entire range of containment current values is comfortably below that where instability may occur. However, we may safely assume that the net transfection flux density (at the power field annular centerline) for the 100ft. diameter Drive Unit will be the same as for the 4ft. model, and the maximum value of $I_{dc}/2$ can then be expected to range from 3.5 to 7×10^6 amps! This level of displacement current now exceeds the upper end of the customary instability range *by a factor of up to 100 times!*

The ramifications of this observation with respect to the largest StarDrive Generators, and indeed the very applicability of the Tokamak equation to their operation *in its stated form*, constitute far too complex an issue to be fully resolved *here*. My own conviction is that the Tokamak equation will only be of seminal assistance in mathematically modeling the StarDrive integral Field, for it must be remembered that in reality the displacement current is not strictly constrained within the theoretical power field we've defined, but is an attenuating component of the entire integral Field. I *was* able to obtain a working solution to the equation using the parallel magnetic reluctance method described (which probably baffled just about everyone except magnetic engineers). The numbers I derived, however, had little real-world significance; they described a working

solution, but not a very meaningful one.

This solution would lead us to believe that the real purpose of the outer armature sections must be to almost totally *degauss* the Field envelope, in order to prevent a horrific temperature rise within the power field, and this I believe is completely contrary to common sense at this point. [To limit field temperature to 25,000 °K, current i had to be 1.91 *micro*-amps, and the gyro-orbit flux density B_r was 6.24 *micro*-gauss!] So for now, we'll just have to have a small extra measure of faith, and leave these intriguing ruminations to the experts in plasma physics. Oh, and by the way, when I tried using the Tokamak equation 'by the books' to figure the power field temperature at full displacement current *for the 4ft. device*, it turned out to be over 1.4×10^{24} °K . . .

* * *

Perhaps the most haunting allegation of all regarding the Searl levity disc is that the machine was able to draw a "virtual" vacuum around the hull as it powered up, thereby allowing the Drive Field current to generate net thrust (without impeding collision with the atmosphere). In fact, I boldly stated in my Patent Application that such an operational state was not only presumed but was "essential to the successful atmospheric ground launch" of a StarDrive device. While this pronouncement is absolutely true, the inherent risk was that the Examiner would ask me prove this theory of *kinetic occlusion*. I was actually not able to do so until about a week before the Application was filed, and the following theoretical validation constitutes some of the most interesting and *accessible* original work I've revealed thus far. At least, I *believe* it might be original, as I've never encountered its like anywhere else . . .

This crucial concept and how to prove it had obviously bothered me for a long time, because no one is going to spend the tremendous sums of money required to build and test a large Drive Unit without an indubitable assurance that kinetic occlusion will occur. I investigated a number of different potential methods of solving this problem, without success, but I always came back to the strong hunch that the answer had to lie within the realm of **the electrophysics of lightning**. Specifically, I was convinced that the solution was intimately connected not only with the assertion that the field envelope of Searl's original levity disc turned from pink to blue just before it disappeared, but with the real fact that some strokes of lightning, and even some different known forms thereof, are in fact pink or red while others are blue!

It is well known, at least among certain investigators of electrical phenomena, that a corona discharge in a nitrogen/oxygen atmosphere will be pink or pale violet in color, while an arc discharge in vacuum will be a bright whitish-blue. This naturally leads one to the supposition that some lightning strokes have sufficient energy density to be *self-evacuating*, while others do not. Finding out the actual reason why became for me an unavoidable challenge. I was unable to achieve any real breakthrough, however, until I realized that the Tokamak equation was in essence a highly-modified form of the *ideal gas law*. To wit, the volumetric temperature and pressure of any gas is generally related according to the formula: $NkT = PV$, where N is the number of molecules in a volume V , T is temperature in °K, P is of course pressure, and k is Boltzmann's constant.

The insight I eventually achieved was this: the main reason I couldn't get meaningful solutions to the Tokamak equation for the StarDrive Field was that it had no actual containment corridor or vessel and so was *unpressurized* at least in the fashion of a fusion reactor. It was open to the atmosphere - and hence its internal pressure, despite its theoretical 'temperature', would still be 14.7 lbs/in² or about 1×10^6 dyne/cm²! The next step would be to see at what temperature a virtual vacuum within the integral Field could be produced which still exhibited atmospheric pressure (as a function of an extremely elevated absolute kinetic energy). This would initially require a reasonable approximation of the volume of one Field hemitorus. By the simplest method of estimation, which will be only modestly on the low side, this volume is 2.486×10^6 cm³ for the 4ft. device.

Then, it becomes necessary to know that the hardest vacuum which may be drawn in the laboratory, at 10^{-10} Torr (dyne/cm²), corresponds to about 2,500 air molecules per cm² at room temperature. Selecting a slightly more feasible and convenient 1×10^4 molecules per cm², we may then solve the ideal gas formula for $T = PV/Nk = 724,600^\circ\text{K}$, where k is equal to 1.38×10^{-16} dyne-cm/^oK. Now, this temperature might seem outrageously high - enough so that the hull would be quickly vaporized - but with so few molecules present to impart their kinetic energy to the hull, the actual heat transmitted should be readily tolerable.

The next step in the procedure begins with the simple formula for the average absolute kinetic energy of the molecules comprising *any* gas. This absolute kinetic energy is independent of such a molecule's mass; the molecules of all gases have the same absolute kinetic energy at a given temperature. Thus, we may write: $\overline{KE} = 3kT/2$, wherein the variables have their stated units. Since kinetic energy is also equal to half the mass times the velocity squared, a more useful derivation of this latter formula equates the *mean square speed* of each gas molecule ($\overline{v^2}$) with the term $3RT/M$, where R is a gas constant equaling 8.313 joule/^oK-mole, and M is the mass of one *mole* of the gas. To simplify matters, we will use the molar mass for pure nitrogen (at 28 g per mole) divided by 2, because we'll assume that all of the gas will become ionized. Substituting our data (including that outrageous temperature), we find the *root-mean-square speed* of the ionized (atomic) nitrogen to be $v_{rms} = 3.593 \times 10^4$ m/sec.

We must now do a bit of inductive reasoning to infer that, for the Field envelope to be self-evacuating, its Drive current electrons at a velocity corresponding to *half* the Field voltage must be able to raise free nitrogen ions from rest to *at least* the v_{rms} we just calculated by colliding therewith. Only half Field voltage is used here because such ions will inevitably be drawn into the outer half of the integral Field by electrostatic force. By conservation of momentum, we may calculate the required ion change of momentum at 8.336×10^{-22} kg-m/sec. Using data computed in exactly the same manner as in Section A of WorkSheet XII(b), whereby the corresponding electron-ion collision impulse for a 4ft. Drive Unit may be obtained by multiplying the incident electron's total relativistic mass by its selector plane velocity, the available per-collision impulse is equivalent to 9.363×10^{-21} kg-m/sec. So, this particular device's Drive current will have *over 11 times* the kinetic energy necessary to evacuate its Field!

Repeating the calculations for a 4ft. Thermal Unit, we find that even the integral Field of this lower-voltage model will be self-evacuating - at something

like 80% of its full nominal Field voltage. Rather amazingly, this would seem to lend significant credence to the original Searl legend I spoke of earlier! Moreover, to bring this portion of our discussion of field electrodynamics full circle, I'd like to recount what I feel is an intriguing correlation between the color of lightning and the Field evacuation mechanics described above.

While it generally takes a 3 million volt/meter potential gradient to strike an arc in vacuum, a lightning stroke in air may initiate at any field intensity over 1 million v/m. This situation results from the active participation of atmospheric ions, particulate matter, and indeed water vapor in stroke 'ignition'. Using the discharge kinetic occlusion analysis technique we just studied, it can be shown that any lightning stroke which occurs at a field intensity not much greater than the said base "flashover" or ignition gradient, at 1.13 million v/m, will have sufficient energy density to be self-evacuating. Hence, lightning strokes of between 1 and 1.13 megavolts per meter intensity will be pink, and any of higher intensity will be blue. "Fascinating, Captain" . . .

Having taken such a trip into the theoretical stratosphere of Field dynamics, wherein we have been able to gain a pretty fair understanding not only of what we're really dealing with here but also of the extent to which there's more to learn about it, perhaps the best thing we can do at this point is take a deep breath and boldly "light that baby up!". Therefore, I feel that we should conclude this portion of ***StarDrive Engineering*** with a fairly detailed look at the fundamentals of **Field ignition**, under the assumption that those persons who build and test the world's first Electrodynamic Field Generator will be able to control its operational characteristics and behavior (!) in accordance with the specifications and general instructions provided in this book.

Most levity disc writers adopted the graphic yet accurate term "flashover" to describe what happens when the secondary hull voltage exceeds air or vacuum breakdown intensity. I have no objection to this term, and will use it myself in this regard for the sake of convenience. However, if we are to examine all of the relevant aspects of a true Generator 'cold-start', we must also consider *vacuum chamber flashover* (and at what rotor speed it will occur) because this rotor-to-Emitter Ring current must first be established before Field ignition may ensue.

Going 'upstream' one step further, it becomes obvious that Primary Array current must already be initiated in order to charge the Field Hub *and ballast capacitors* before any rotor bypass current will be available with which to charge the Emitter Ring! Moreover, since the primary cathodes and field emitters are emissivity-matched for the requisite voltage expansion ratio only at their *final* operating temperatures, and no emitter heating at all will occur until vacuum chamber flashover happens, it can now be seen that the preliminary heating of the power resistor networks must be carefully coordinated with the lowest rotor speed at which flashover of both the vacuum chamber and hull may be achieved.

The most important observation to make at this point is that the Field Voltage Control System (and primary coolant) must be utilized to regulate Field current post-flashover, such that its observed rate of rise is roughly in linear proportion to the rise in rotor speed during spin-up, as the only available means of ensuring that the exhibited Field voltage rises *in the same linear fashion!*

Although the Primary Power System output voltage itself will rise as linearly as the rotor speed, it can be shown that vacuum chamber flashover will not occur until the *effective* rotor voltage rises to about 64% of Spec. value in Thermal Units and 85% thereof in Drive Units (strictly as a function of breakdown intensity). This is due to the present specifications for the thickness of the heat transfer channel on each negative hull plate, which “latches” the vacuum chamber (or bypass) current as a function of its distance from the field emitter surface. Consequently, it will be necessary for the resistor networks to be heated in such a way that they achieve an operational conduction temperature *far in advance* of reaching these same respective percentages of rotor speed.

We may therefore take a vital cue from standard vacuum tube operation, and minimize the incorporating device’s “warm-up” time, by applying the primary voltage and cathode heating simultaneously. In other words, rotor rotation and power resistor heating may be initiated at the same time, but the rotor speed must be held at the spin-up level where hull flashover *should* occur (given a linear Field voltage rise as a function of rotor speed) until resistor temperature has been raised to the point where hull flashover *does* in fact take place. The early onset of bypass current – as compared to the above-stated rotor speed percentages – will hopefully avoid the otherwise explosive initialization of Field envelope current, and can be considered the first ‘stage’ of Field ignition.

This ‘forced’ chamber flashover happens because such a temporary ‘excess’ level of primary cathode emissivity will cause the polarized rotor’s periphery to acquire a far heavier negative charge than it would ordinarily have with the field emitters still at a low ambient temperature! This condition elevates the *apparent* negative rotor voltage: yet the resultant bypass current will always seek to reduce the charged state of the rotor to a radial potential difference which represents only the *true* net voltage applied by the Primary Power System, so that rotor electrode array voltage ratings should not be exceeded during the start-up process. Then, standard Primary Array *cooling* procedures may be implemented as necessary during the extended interim period remaining (until nominal rotor speed is reached) so that primary cathode current, final rotor speed, and effective Field voltage may be tailored for proper temperature equilibrium. This represents the second and final stage of Field ignition.

It is at this point that we must consider a first simple axiom of ‘start’ field flux dynamics, for we must now know at what hull potential difference flashover should occur in both Thermal and Drive Units if we are to choose the appropriate interim rotor ‘idle’ speed from which to linearize the rate at which Field voltage rises. And, the variable inductors may be used to influence if not determine the Field voltage at which hull flashover will occur! All we need to do first is select the power field trajectory along which we wish flashover to take place.

As one might guess, it will be most expedient if hull flashover occurs along a circular arc-sectional path which passes through the power field annular center-line. To keep it simple, the easiest way to figure the length of such an arc section is merely to take the average of the Field boundary length and Neutral Ring radial width. Using data for the 4ft. prototype, this arc length is .1555 m, and the resultant breakdown voltage V_n (according to the formula $E = V/d$) will be equal to 466,500 volts for both Thermal and Drive Units. The linear proportion of

nominal rotor speed represented is then equal to the ratio $V_n/\text{spec.}V_r$, or 16.09% for the Thermal Unit and only 1.33% for the Drive Unit. These values determine our interim *maximum** idle speeds: 270 rpm and 23.22 rpm respectively.

Now, our simple Generator 'start' axiom may be stated as follows: At the first stage of Field ignition, the standard transfection gyro-orbit radius must be *larger than one-half the Neutral Ring radial width*, so that flashover electrons are then able to reach the Field Hub. Using the cyclotron formula and the flashover voltage V_n , we may now calculate the exact value of transfection flux density B_r , which will satisfy this condition, reasonably assuming that at 'lower' trajectories (closer to the armature cores) flashover will be effectively suppressed. This maximum value for B_r equals a mere 4.6 gauss in this example, at an armature output flux density of 391.5 gauss and input core density of 558.9 gauss, and actually defines a rough initial setting for variable inductor system current which should be valid for any size device of this design (proportionally).

To recapitulate the Field Generator's effective 'ignition sequence' in general terms: Rotation of the massive rotor assembly is initiated and the primary thermal transfer medium heaters are activated. Unlike a typical electric motor, the Generator's rotor speed is gradually increased to a predetermined idle setting and the transfer medium (or 'coolant') is circulated until flashover occurs. Rotor acceleration is then resumed for an extended period, during which the field emitter temperature gradually rises due to bypass current heating.

At any given level of Field envelope circuit current, heat will be generated within the power resistor networks (and their attached primary cathodes) enormously faster than in the field emitters due to the vastly lower resistance of the latter. [The reason why this is so is most evident from the simple power formula for conductor heating: $W_h = Pt = I^2Rt$.] Therefore, the Field Voltage Control System must continually adjust not only the primary accelerator and control grid voltages during this second stage of Field ignition but also the primary coolant flow rate and cathode thermal control rod engagement, to prevent radical changes in the exhibited Field current (and voltage) due to the exponential nature of primary cathode emissivity.

This method of Field envelope expansion allows a Thermal Unit to be operated at fractional output, as it's virtually certain that catastrophic failure cannot be prevented during prolonged atmospheric full-power operation at ambient temperatures. When a Drive Unit Generator's rotor has reached nominal rotor speed, and the Field voltage has been stabilized at the design Primary Voltage Expansion Ratio, its Field envelope should be fully self-evacuated (by kinetic occlusion) and therefore in a state of operational readiness for purposes of developing sufficient thrust to effect its rapid withdrawal to the coldness of space.

* * *

In the final 'book' of **StarDrive Engineering**, we're going to assume that (for the first time) humans thereby have the very real capability to travel at what to all

* As noted in the Rotor Speed Table on pg. 191, the nominal rotor speeds calculated in WorkSheet IX(b) are taken to be theoretical maximums. Lesser rotor speeds will be observed should the value of hull static capacitance be less than the maximum theoretical value assumed in projecting these highest or 'worst-case' rotations.

intents and purposes is light speed: to rise up off the ground of our original home and journey at large into the limitless expanse of the Deep. In genuine sincerity, and with what may be interpreted as a notable lack of modesty, I submit that the only foreseeable way we are going to do this is with the Electrodynamic Field Generator that I have strived to create.

In approaching the time-light barrier, we must also presume that an effective means will eventually be found to break it. As we'll see in pages to come, I can further envision no other way for this to be achieved. And failure to do so means that we can still *never* arrive at any truly worthwhile destination in space, let alone one where we can comfortably dwell for a time *under a different sun*.

But for now, I feel that the obvious place to start in this imperative and noble enterprise is in building a modestly large but practical-size Thermal Unit, say one of 20ft. in diameter, for experimental use in the generation of incredible amounts of steam and therefore electric power and/or desalinated water. From WorkSheet II(c), it can be shown that the EDF Generator's peak thermal output efficiency will essentially be the same as its 'peak drive power efficiency' at 46.7%. With a calculated rotor ampacity of 414,720 amps and a peak Field voltage of 15.9489 million, the *theoretical* peak thermal net output of a 20ft. Thermal Unit would approach 3.1×10^{12} watts – or over 3 million megawatts!

In the next Chapter, we are going to take a serious look at the StarDrive Generator's awesome potential for commercial power production. Naturally we'll discuss aspects of its operating efficiency and over-unity (heaven forbid!), so its rotor input torque requirements will be carefully assessed. Perhaps more importantly, however, the magnitude of the actual *electric binding force* on the rotor will also be examined, to take the teeth out of the first argument certain non-trade opponents are apt to make against the Generator's very feasibility.

It would be Promethean indeed if, at the advent of a StarDrive Age, we found that the greatest source of power for our planet merely involved the clever use of natural forces like those which produce lightning, which we've always known and feared (and which likely led to our very discovery of fire). Later on in this century, when it's quite probable we'll have pumped most of the accessible oil out of the ground and *still* failed to achieve cost-effective controlled fusion, I think we're really going to need such a clean and economical-to-build power source: even if it does have to run at only a fraction of its true output capability.

During the process of developing and building such a physical plant, there is little doubt that sufficient knowledge would be gained to enable the construction of the much more complicated 3η device. Faster-than-light communications should theoretically then be possible because the EDF Generator is the only object known so far which would be able to exhibit *oscillatory apparent mass*. While the 'simple' experimentation with such a machine as a novel means of effecting two-way communications would be exciting enough in itself, such efforts may in fact be able to reveal the secrets of trans-light velocity. The practical utilization of relativistic mass effects to produce thrust at heretofore impossible velocity would just be the next logical step to take on the way to the stars.

Book III: The Stars

Prelude

"This is Major Tom to Ground Control;
I'm stepping thro' the door,
And I'm floating in a most peculiar way.
And the stars look very different today . . .
For here am I sitting in a tin can
Far above the world;
Planet Earth is blue and there's nothing I can do" . .

David Bowie

Space Oddity

Exceeding the Limits

Have you ever really wondered who will build the world's first starship: one that is capable of even *sublight* relativistic drive speeds? What country or aerospace agency or corporation will someday (and hopefully soon) announce to the global community that "we have that capability!"? Well, I have considered and researched such questions nearly all my life and, for most of that time, I can safely say that I found very little evidence to suggest that the world's engineers are doing much more than just marking time in an almost haphazard pursuit of such a prospect.

However, a few years back (in Dec. 1997), NASA unveiled a startling and microscopically-funded new program called: *Breakthrough Propulsion Physics*. Headquartered at its Lewis Research Center in Cleveland, Ohio, this program is devoted to soliciting and assessing, from all would-be contributors, advanced aerospace propulsion concepts of a specifically non-rocket nature which encompass the potential for exceeding the speed of light in manned vessels! They, of all people, know how fantastically far it really is to *anywhere else*. And they know we're *not* going to get there without a trans-light drive.

The stated objective and *raison d'être* of this new 'StarDrive' division is to find "a method . . . where a vehicle can create and control an external asymmetric force on itself without expelling a reaction mass and the method must satisfy conservation laws in the process". Well, the first part of this fascinating challenge was an unexpected and instant hit with both the trade-professional and fringe area crowds, and the program's website attracted over 50,000 'hits' in its first month alone! Since then, a virtual flood of response has occurred from all over the world, and teams of graduate students had to be recruited merely to process let alone critique the many submissions. {see: www.lerc.nasa.gov/www/pao/warp.htm}

It is in this clause's second criterion, the area of feasibility and practicality, that the proposals received have fallen woefully short. Of the roughly half-dozen disclosed strategies which even have any *theoretical* significance, none have more than the slightest similarity to the StarDrive Generator or any alternate *workable hardware* designs. Perhaps this is one reason why Lawrence Krauss, who wrote *The Physics of Star Trek*TM, has publically criticized the whole operation.

The main law of conservation which everyone's so concerned about (especially the Patent Office) is, of course, that of energy. Such a device as postulated by NASA must be able operate on its own power for very extended periods of time, while simultaneously performing a task which appears to require near-infinite *work*, and no one seems to know where all that energy is going to come from. And, without an understanding of the Ecklin principle of conservative no-work electron force, which we'll study further in a bit, a workable *electromagnetic* solution is apt to prove extremely difficult to find. So, perhaps a good place to start in putting this whole venture into perspective is with our present global production and use of *energy*.

Energy is of course the driving force and life-blood of our industrialized civilization, and without it the type of modern living to which we've become accustomed would disappear. In the last two centuries, the obvious favorite as energy's global 'medium of exchange' has been the natural but nonrenewable hydrocarbons: oil, natural gas, and coal. The standard of living we enjoy in the world's developed countries is determined far more by the cost of this energy than by any other single factor, and sudden shortages in supply or dramatic price increases have been known to precipitate world-wide recessions.

The industrial revolution of the 19th century was of course fueled by coal. And although the world still possesses enormous reserves thereof, the well-documented hazards to the health of our planetary ecosystem which are inevitably associated with its intensive use have greatly curtailed that use today *except* in the commercial generation of electricity. We may end up polluting everything around us, but the lights will at least stay burning into the indefinite future: the world's coal reserves are at least 5 times as vast as the proven oil reserves, and in the U.S. we have enough coal to last for at least 1,000 years.

In the 20th century post-WWII, of course, the oil industry's hold on energy production has been unbreakable, and oil and natural gas still provide about 53% of the world's primary energy consumption today. This is strictly a marriage of convenience, however, as it's important to note that a typical fossil fuel electric power plant's best efficiency is about 40% or less; so we're in no danger of perpetual motion there! It is also less than surprising that nuclear-generated power accounts for only about 6% of world energy production at the present time, as it is decidedly inconvenient and costly by comparison and has proven to be almost as environmentally-unsound as coal.

What I'm sure would be mighty disheartening to Nikola Tesla is the very secondary role hydroelectric power has come to play in the energy industry. He must've thought that by now most of our energy needs, at least in this country, could be met *if need be* by this absolute cleanest present-day source of power. Here again, however, environmental concerns not obvious in his day have had their constraining effect on dam building in ours. Otherwise, as an Army Corps of Engineers study indicated years ago, hydroelectric plants could be built on many of the almost 10,000 North American river sites potentially suitable for this purpose.

In any event, annual world electric power production and consumption rose from around 1 trillion kwh in 1950 to over 11.5 trillion kwh by 1990. In 1950, roughly 2/3 of our electricity was generated in thermal stations (fired steam plants) and virtually the entire balance from hydroelectric sources. In 1990, the only notable difference was that hydro-power had dropped to under 19% of total production, with nuclear power having already achieved its zenith share of 15% of the world market and then begun a slow but steady decline. In the U.S., nuclear plants today produce about 20% of our electric power, or over 3 times the current world average. France alone is the remarkable exception to this nuclear decline, producing almost 75% of its electricity by nuclear means.

Looking ahead a mere 25 years or so, the world's population will likely grow by about 2 billion people (or 33%), yet electric power consumption can reasonably

be expected to reach *double* its 1990 level. On closer inspection, it can be seen that the vast bulk of this increase in the *number* of consumers will take place in the developing nations roughly referred to as 'third-world', and that they are very unlikely to share per capita in the fruits of this energy expansion. The projected cost of this energy will surely be outside their economic reach, especially when citizens of the developed countries are already paying record prices for energy amid renewed concerns over the possible recessionary ramifications.

So, where is all this energy going to come from, even if we do live in North America or Europe? These continents, together with Japan and the Russian republics, use about 2/3 of the world's energy total. Are our third-world cousins doomed to a life of ever-deepening poverty, perhaps representing a standard of living below that of their ancestors?? If we are to assume responsibility for *all* the people in our now-global community, at least in ensuring them a humane standard of living, we must somehow achieve an electric power source which is *renewable* (or better yet, omnipresent) with a *very-low uniform per-capita cost* regardless of the relative wealth of the country who wishes to build it. Since the French seem to have a somewhat better handle on this difficult objective, I'd like to return briefly to the topic of nuclear power plants.

The first point I'd like to make is that I am *not* a nuclear power advocate per se. Nuclear energy lobbyists would generally have us believe that there is no workable alternative to increased reliance on nuclear power, at least in the foreseeable future. In this view, they may *in principle* be partially correct. I think most civilized people understand that, if we are to protect and enjoy our small world ecosystem, we *must* stop burning wood and fossil fuels.

What the French people seem to have realized some time ago is that fast-breeder reactors actually constitute a *partially* renewable energy source, albeit one which is still staggeringly expensive to build. Although financially inaccessible to most of the undeveloped nations, this type of nuclear plant produces about 20% more fuel than it consumes – and so it might appear to be an *over-unity* device, but really isn't. And yet, while you traditionalists obviously can't scream "perpetual motion", a case could be made (but isn't) for shouting "free energy"!

Hundreds of nuclear plants have been built, in at least 40 countries, in the latter half of the 20th century. What most of us informed world citizens realize is that severe problems regarding primary fuel scarcity (and nonrenewability), plant and regional safety, and hazardous radioactive waste disposal are not likely to find truly satisfactory solutions any time soon. When coupled with grave doubts about its very fiscal propriety, these concerns have greatly curtailed the growth of the nuclear power industry especially in the United States.

This country's first full-scale commercial nuclear power plant opened at Shippingport, PA on December 18, 1957, and was capable of producing a modest 60 megawatts of electrical output. Like the great majority of U.S. nuclear plants, its fuel was uranium oxide isotopically enriched to about 3% U-235 content. Ordinary water serves as both neutron moderator and coolant in this type of plant, called an LWR (light water reactor) system. It is known that the fission of 1kg. of U-235 is capable of releasing about 18.7 million kwh of power as heat. But in LWR plants, only about 1% of the uranium fuel's energy potential is

recovered; yet ironically the U.S. actually pioneered the development of fast-breeder reactors which are able to recover up to 75% of the fuel's energy content!

The most famous U.S. nuclear plant is of course Three Mile Island, located on the Susquehanna River in Pennsylvania southeast of Harrisburg. On March 28, 1979, its core suffered a partial meltdown (the very first such) and forced the evacuation of thousands of area residents. Understandably, the nuclear industry soon became mired in controversy in the industrial nations, and by the late 1980's there were few orders being placed for new plants and many cancellations of plants already under construction. By the mid-90's, there were no new nuclear plants either under construction or in planning in the United States.

The event which basically clinched this general nuclear decline was, of course, the Chernobyl meltdown. The Chernobyl Power Station was one of the largest in the Soviet Union, and with all four of its 1 GW (gigawatt) reactors running it was able to meet around 10% of the Ukrainian republic's electricity needs. While a typical such plant operates at 75 to 85% capacity nearly all the time, the design employed in these reactors unfortunately made them tend to be unstable during very low-power operation. On the day of the accident, April 26, 1986, reactor #4 was operating at about 7% during a planned shutdown, to test changeover procedures from the standard power source to a back-up system. The technicians were apparently careless about certain safety precautions, and an unanticipated power surge caused two explosions which destroyed the reactor core and building. *Without a containment building*, the ensuing fire and updraft then spread a tremendous quantity of radioactive debris into the atmosphere.

Due to prevailing winds, over 20% of the republic of Belorussia (renamed Belarus after 1991) was contaminated by high-level radioactive fallout and soon about 200,000 people had to be evacuated. Raw clouds of irradiated material were swept as far westward as Sweden, and a National Geographic study revealed that this material eventually settled over a fair portion of the whole Atlantic region. The Ukrainian parliament finally declared a moratorium on nuclear power plant construction in 1990, but ironically it was repealed in 1993 because of severe regional energy shortages.

Many of us are quite familiar with the basic facts concerning this terrible disaster, but I feel obliged to state that there may yet be more to the story than is generally known. I'm afraid to have to say it, but it appears to me that this incident could in fact be *a literal fulfillment of Biblical prophecy*, and that mankind might be wise to perceive it in this way. Therefore, please consider the following passage from Revelation 8: 10-11: "And the angel sounded, and there fell a great star from heaven, burning as it were a lamp, and it fell upon the third part of the rivers, and upon the fountains of waters; And the name of the star is called Wormwood: and the third part of the waters became wormwood; and many men died of the waters, because they were made bitter." The literal translation of the Russian word 'Chernobyl', my friends, is Wormwood.

* * *

It should be apparent at this point that I feel it's my duty to advocate the StarDrive Generator as a means of satisfying our rapidly-expanding global

energy needs, and of doing so in a manner which does in fact meet the dual new power source criteria stated above. The *omnipresence* of ambient static charge as a 'fuel' source and the relatively *low fixed cost* of building Thermal Units of this design would make this power source uniformly available to virtually every nation on Earth. And, such Thermal Units could conceivably lower the per-kwh cost of energy to the point where the commercial desalinization of water becomes practical for the first time ever. Although not widely understood, it is entirely possible in certain world regions that the availability of potable water will become critical in the not-so-distant future, and some political analysts have expressed the opinion that the next major war could be fought over *water*!

Be that as it may, it can be seen that the EDF Generator bears a stronger resemblance to liquid metal fast breeder reactor (LMFBR) systems than to any other major electrical power generation method. In fact, a friend of mine once called the Generator "a sort of electronic reactor", and I feel this is a not-inaccurate comparison. Since we've already characterized such LMFBR systems as a type of free energy device, I would like to now discuss certain aspects of **power and over-unity** which are pertinent to the EDF Generator.

The preferred primary coolant in fast breeder reactors has always been liquid sodium, which has excellent thermal transfer properties and is actually lighter than water.* Thus, it can be pumped at very high speed and volume to maximize heat extraction from the reactor core, typically leaving the reactor at around 500°C. However, LMFBR systems share a significant difficulty with the far less efficient light- or pressurized-water systems in that the primary coolant is radioactive, and intermediary heat exchangers must be employed to produce non-radioactive steam for turning the turbines (which likewise lowers such a plant's overall efficiency). Of course, this is *not* the case with the EDF Generator.

In a typical LMFBR plant, the entire core assembly is cylindrical in shape and measures about 3 meters in height by 5 meters in diameter. This core is then surrounded by a vessel containing the liquid sodium. Although the core itself is extremely complex in design and difficult to construct, huge amounts of heat can thereby be extracted. One drawback inherent in the EDF Generator's design is that a very much smaller volume of primary coolant may be passed through the rather restrictive primary thermal conduits and, though the coolant would leave the Primary Arrays at a much higher temperature (~675°C), a much lower percentage of the device's *potential* heat output can be extracted. Thus, it is almost certain that a Thermal Unit can only be operated at fractional output.

Even so, such a Thermal Unit would certainly be able to operate continuously for a period of many years before the magnetic rings would have to be replaced. Not only will the cost of replacing these rings be incredibly lower than that of replacing the fuel rods in a reactor, the magnetic rings are *100% recyclable* and pose no waste or material handling hazard. However, the EDF Generator could indeed pose a significant radiation hazard, albeit in a manner quite different from a nuclear reactor, which will likely incite some environmentalists

* Our old friend (and Faraday's teacher) Sir Humphry Davy discovered sodium in 1807 and developed a cell for producing the pure metal, which melts at 98°C and boils at around 890°C. It is interesting to note that he is also credited with the discovery of the controlled electric arc!

to wail like banshees. So, we must finally address the inevitable production of X-rays within the Field Hub and envelope, for most of us realize from familiarity with television picture tubes that high-speed electrons produce X-rays.

Inside a normal vacuum tube, X-rays are produced in the target material at all times during operation, although the bulk of the incident electrons' kinetic energy is released as heat. The relative intensity of this radiation is proportional to the product of the current, the *square* of the accelerating voltage, and the atomic number of the target material. Due to the selective filtering of the special glass envelope and the low applied voltage in a TV picture tube, this radiation is readily limited to acceptable levels. It can be seen, however, that tremendous quantities of hard X radiation will be produced at the Field Hub of the EDF Generator which can actually overlap the gamma ray energy spectrum. This radiation is called *brehmsstrahlung* (German for braking radiation) and occurs across a broad range of wavelengths beginning with the near-ultraviolet.

More alarming yet for some will be the fact that even the smaller such Generators will operate above the *pair creation threshold*: where the incident electrons have sufficient energy to penetrate the electron shells of iron atoms in the positive Zones and whose trajectories are bent so much that electron and positron pairs can be produced from the change of momentum. These pairs tend to be instantly self-annihilating, releasing bursts of pure radiant energy which once again may be of very short wavelength. X-rays of much lower energy will **also** be produced in the envelope itself as *synchrotron radiation*, caused by the intense centripetal acceleration of Drive current electrons in a magnetic field!

So, am I saying that the development of a StarDrive Generator industry would be a wonderful thing, but that we just can't risk it because of dangerous radiative emissions? Fortunately, I believe emphatically that the answer to this question is - No! Although it is certain that a form of open-air containment "pavilion" will be needed to block all line-of-sight radiative emissions from such a Generator (which must be operated essentially out-of-doors), I believe I can explain why the Generator's Field envelope must be *almost opaque* to these emissions in order to illustrate how its output energy debit is accounted-for!!

Under the Ecklin concept of conservative no-work electron force, the Drive Field electrons pay their own "freight bill" from Emitter Ring to Field Hub, and must reabsorb an equivalent amount of quantum energy to maintain their spin. Thus, it is believed that *the majority of all the Generator's radiative emissions energy* will be preferentially reabsorbed by the Drive Field through continuous Compton effect interactions, which return to them a large share of the energy they expended in-transit! Specifically, the energy equivalent to that which we recover from the power resistors as heat output *and more* may be reabsorbed!!

Now, some people will think that this is a truly outrageous claim, I'm sure, but I think many theorists will see the essential logic in this assertion. If I'm right, this operational characteristic would remove the only serious objection anyone could raise to the much-needed development of this technology. Moreover, I'm fairly certain that the 'efficiency' of this emissions absorption can be optimized through the proper tuning of the AC Field characteristics: to wit, the armatures can be used to induce an AC Field polarization which is variably in- or

out-of-phase with an applied AC signal voltage in a broad range of frequencies. Experimentation with this type of variable Field “cross-polarization”, which was mentioned near the end of Chapter 4, should reveal the means to achieving this goal even if theoretical methods cannot be developed to “prove” it first!

To wrap up our power and over-unity considerations with regard to the StarDrive Generator, we must address what for some may be the critical issue here: how much *input rotor torque* is required? If we answer this question correctly, we’ ll then be able to determine a number of important consequences: (1) what *real* net output can we expect from a given Thermal Unit; (2) what minimum apparent efficiency does that Thermal Unit then exhibit; and (3) how long will a full cold-start take for a large Drive Unit (which I’m sure all of you Trekkers want to know!). We’ll therefore generate some applicable numbers for the 4ft. and 20ft. Thermal Units, as well as for the 100ft. Drive Unit, which is surprisingly easy to do while maintaining good accuracy.

To calculate a given Generator’s input torque requirement, one must first know what nominal rotor speed that machine will have. We know that the larger the device, the slower its rotor must turn because of the drastic increase in tip speed as the scale increases. As can be seen from the 3η Rotor Speed Table on pg. 191, the nominal rotor speed of a 4ft. Drive Unit could be anywhere from 1746 rpm to about half that: with perhaps no way of knowing without actually building one! Therefore, the suggested *maximum* 1η and 3η rotor speeds are given in the Table below and these same Drive Unit nominal speeds are also plotted in Fig. 19 on pg. 106. These speeds seem to correlate well with the field voltages.

Thermal Unit	hull dia.	Drive Unit	Thermal Unit	hull dia.	Drive Unit
1625	5 ft.	1675	–	40	1325
1575	10	1625	–	50	1275
1525	15	1575	–	60	1225
1475	20	1525	–	70	1175
1425	25	1475	–	80	1125
1375	30	1425	–	90	1075
1325	35	1375	–	100	1025

Fig. 56: Combined Maximum Rotor Speed Table (in rpm)

A couple of observations should be made about this Table before we move on. As indicated, it is deemed unnecessary to build any Thermal Unit above 35ft. in diameter: as we’ve seen, a 20ft. machine is already incredibly large as regards its power yield. A 40ft. device is probably the smallest manned vessel advisable, as shown in the *Manned Vessel Design DataSheet* on pg. 107, and so it is assumed that any Field Generator this large or larger would be used exclusively as a starship due to the steeply rising cost of construction at these sizes.

In order to achieve these gradually-lessening rotor speeds (as size increases), it will be necessary to implement not only certain magnetic array refinements as have been discussed but also a program of strategic increases in the amplification

factors of both rotating and primary arrays. I feel that ample 'leeway' exists in the scalable specifications for the Generator to refine and increase the device's output capability and keep the rotor speed at or well below these given numbers, *without unduly increasing the primary voltage expansion ratio*. It should be pointed out that the rotor tip speed in a 100ft. Drive Unit* at the maximum 1025 rpm would be 4,477 ft/sec, or over 4 times the speed of sound! It is obviously hoped that its actual rpm would be nearer the 50% level stated above, due mainly to a hull capacitance that in reality is much lower than the theoretical maximum. [* The rotor drive hp we'll soon figure will support a rotor tip speed of 2,300 ft/sec.]

The next important fact which must be known about the particular size Generator in question is the total mass of the rotor assembly. In carefully developing this figure for the 4ft. prototype, and disregarding the weight of the carrier assembly for now in the interests of simplicity, we will also begin to get a feel for how accurate my stated estimate was of the machine's total weight (198.54 lbs.). Using the data provided in the various Material SpecSheets, the 4ft. Badlander's finished rotor assembly would weigh about 98.14 lbs. and this figure is broken down as follows: the segments at 46.81 lbs., the separators at 13.63 lbs., the field emitters at 33.03 lbs., and an adjustment factor of 5% of the sum of these three principal weights (~4.67 lbs.) to allow for the installed weight of all other rotor components (including field coils, electrode rings, etc.).

The first step in computing the input torque requirement is to calculate the rotor's *moment of inertia*. For a disk-shaped flywheel, the inertial moment I is equal to $mr^2/2$, or 5.770 kg-m^2 . The work required to bring the rotor up to speed is equal to the kinetic energy stored therein at that speed. This kinetic energy E_k is in turn equal to $I\omega^2/2$, where ω equals the rotor's angular speed in radians/sec. Thus, $\omega = (1676 \times 2\pi)/60 = 55.87\pi$, and $E_k = 88,880 \text{ joules}$. Since power is the time rate of doing work, and the input torque divided by time (or p) is power in watts, it can now be seen that the selection of drive motor output horsepower will determine how fast the Generator reaches its nominal rotor speed. We also know as previously discussed that an extended start time is not only acceptable but in fact desired, so we can select a modest standard horsepower for the 32 separate drive motors which will yield an acceptable figure for the extended start time.

Since one horsepower is equal to 746 watts, and the total start time t_w is equal to E_k/p , we will select our standard low-volt dc motor size at 1/16 hp (for a total of 2 hp of input torque *in this size device*) and therefore a 4ft. Generator's minimum start time $t_w = 88,880/1,492 = 59.57 \text{ seconds}$, or basically 1 minute. This to me seems a thoroughly appropriate figure, and the reason it's a minimum estimate is because at very low initial rotor speeds the drive motors will not be quite as efficient as they will be nearer their rated design rotation.

Taking the estimation of component weights a step further, the 4ft. prototype would have about 43 lbs. of stainless steel in the Field Hub, about 18 lbs. of clad aluminum plates in the Emitter Ring, and 13 lbs. of magnetic rings. This yields a total weight *so far* for this device of 172.1 lbs., or over 86% the stated estimate of total device weight, and we haven't yet added the weight of the drive motors, Primary Arrays, or Central Chamber! So, I'm afraid my earlier figures for Drive Unit net thrust may have been just a little on the high side, and thus *every effort*

will obviously have to be made to minimize the weights of all vessel components. I am fairly certain that engineers more qualified than myself (hopefully at NASA) will be able to trim a Drive Unit's total weight such that its net thrust may still approach the stated and greatly-desired 1.67g goal.

With no good reason not to just take this potential disappointment in stride, we're now going to take a shot at figuring the minimum start time for the 100ft. Drive Unit. The easiest and fastest way to do this is to realize that the volume of the finished rotor assembly will 'blow-up' proportional to the cube of increases in the vessel R_n . Therefore, since the 'Toltec' beam is 25 times that of the Badlander, the weight of the rotor should be 15,625 times that we figured for the 4ft. device. This gives us a rotor weight of 766.7 tons (wow!), or 697,016 kg. The inertial moment I is now equal to 5.63×10^7 kg-m² and $E_k = 3.25 \times 10^{11}$ J. Choosing a hefty 1,000 hp rating for each of 32 drive motors, torque quotient p becomes 2.387×10^7 watts and the minimum start time t_w is then 13,594 seconds or 226.58 minutes, or 3.78 hours. I feel that this is also a very reasonable figure, because it clearly indicates that we do *not* just jump in this thing, fire it up, and take off!*

Before we calculate the real net output and apparent efficiency of a typical Thermal Unit, we have to take a look at the magnitude of the electric binding force that will be manifested across the Primary Arrays. This electrostatic load or drag will have the effect of increasing the rotational inertia of the rotor assembly, and is the only retarding force on the rotor other than simple friction.

Once again, the method for figuring this binding force is quite straightforward. First, we must compute the electric field intensity E across the Primary Arrays, and in the 4ft. Thermal Unit this intensity's peak value is equal to 574,730 v/m [using data from WorkSheet VIII(c)]. For capacitive parallel plates, this intensity is also equal to $q/\epsilon_0 A$ where q is the charge on one plate of area A . Each primary cathode's area is 14.09 cm², so each Array's total A equals .057 m², and $q = 2.58 \times 10^{-7}$ coul. Here, the binding force F caused by each Array is thus equal to $Eq = .1483$ nt and the total force equals .2966 nt. This translates as an inertial increase in the rotor's weight of .0666 lbs. or *only* 0.068%.

Repeating these calculations for the 100ft. Drive Unit, we find that although the total retarding force rises to 23.41 nt, the percentage inertial increase falls to 0.0015% (due to the cubic nature of the rise in rotor mass). Therefore, we can now say with a certainty that the electric binding force on the rotor is entirely negligible, and that to calculate a Thermal Unit's apparent efficiency all we have to do is compare the input motor power to the net thermal output in watts!

Returning to the proposed 20ft. Thermal Unit as a good basis for this efficiency calculation, we saw that the peak thermal output would be 3.1×10^{12} watts if 100% of the heat developed in the power resistors could be recovered. The corresponding Specification output value is thus 2.8 million megawatts. We also determined near the end of the last Chapter, however, that the lowest feasible fractional output of such a device would be about 16%. Therefore, if we were to operate this Unit at its *flashover idle speed only*, we could still expect to produce a maximum of about 450 gigawatts of recoverable power.

* All preceding start time computations assume that the *estimated 0.5% rolling friction losses* are negligible.

Were the Unit's efficiency at extracting recoverable power comparable to that of a coal-fired steam plant (at 40%), with the balance lost let's say to necessary cryogenic cooling, this means that the actual yield power at idle speed would *only* be something like 180 gigawatts! Even if a 20ft. Thermal Unit's extraction efficiency were merely comparable to that of a typical LWR nuclear plant (at 1%), the net yield power would still be *4.5 gigawatts*; and to my knowledge this is far higher than that of any single power plant (nuclear or otherwise) in the world!!

The rotor assembly in such a 20ft. plant would weigh about 5,576 kg. and its rotational kinetic energy (at 1475 rpm) would equal 2.151×10^8 joules. Assuming we utilize 4 hp drive motors in this Unit, its cold-start time would be 37.54 minutes at an input torque equal to $(4 \times 746 \times 32)$ or 95,488 watts. So, if we now divide the latter said *absolute minimal yield power output* by the total input motor power just figured, we can calculate the minimal over-unity ratio which when multiplied by 100% gives the minimal apparent efficiency (in percent). Thus, the resultant over-unity power ratio is over 47,125 to 1, and the apparent efficiency exceeds **4.7 million percent!** More shocking still, I intend that all 32 drive motors in any StarDrive device or *vessel* may be switched-over from battery-bank power to run entirely off special low-voltage taps in the power resistors at some point during rotor spin-up . . .

* * *

It's time for us now to return to matters which are more related to locomotion and the production of thrust. Specifically, we should begin by discussing the search for a form of reactionless drive or, more properly speaking, a form of locomotion which entails *no net or apparent* reaction. This subtle distinction is necessary because, like the concept of inertialess drive, no means of obviating Newton's Third Law (action and reaction) is known to exist.

The most fundamental type of propulsion is what may be referred to as *traction drive*, because this is what happens when we walk or use a car. This type of locomotion depends on friction against a contacted physical medium to generate any movement, and thus is nearly always horizontal or perpendicular to gravity. A second and less obvious source of motion is the *displacement drive*, which depends on a density imbalance between a vessel and a surrounding material medium (as in zeppelins or submarines) to achieve a useful propulsive effect which is vertical or parallel to gravity. Both these forms of propulsion are reactionary in nature, although this is a bit harder to see in the latter case.

The third and most important type of reaction drive, especially in terms of man's pursuit of aeronautical misadventures, is of course the *rocket principle*. The greatest advantage this type of propulsion has in this respect is that it is not reliant upon the presence of any physical surrounding medium and may in fact operate at peak efficiency in space. Thus, it can be seen that under ordinary conditions a jet aircraft uses both the displacement and rocket drive principles.

A fourth and more obscure form of propulsion does exist, however, which is also not dependent on the presence of a reactionary medium: that of *rectified centrifugal force*. This largely-theoretical propulsion principle bears the strongest resemblance to the EDF Generator's method of thrust production, but the mechanical problems associated with it have been hard indeed to overcome.

A rock which is whirled on a string and then released, at the instant when the string is *perpendicular* to the intended ballistic trajectory, illustrates this concept to a degree. But the trick here is to continually demonstrate this type of thrust without breaking or releasing the "string", thus converting rotary motion into a constant unidirectional force. Many engineers and inventors have tried their hand at constructing or proposing a practical device of this type, but few if any have really met with much success (at least in any commercial sense).

Before we examine any real or proposed centrifugal drives, a quick clarification of applicable terms and concepts is in order. To wit, every object which exhibits uniform circular or rotary motion possesses two basic properties: *gyroscopic inertia* and *precession*. Gyroscopic inertia is a natural consequence of Newton's First Law, and so a spinning object tends to maintain one original or given plane of rotation. Precession is the motion which results when a force is applied to a gyroscopic object which tends to change the orientation of its axis of rotation. Such an object's axis of rotation will then move in a direction which is at right angles to the applied force.*

Centrifugal force is often mistaken for centripetal or inward-pulling force, but it is actually an *apparent* force only. Centripetal force is the only real force acting during uniform circular motion, and a real force is always attributable to a moving object or a field. An apparent force only acts upon an object or observer from *within* an accelerated frame of reference. Thus, a person riding a carousel feels an outward or radial pull yet, at the point of release from the real centripetal acceleration (upon jumping off the ride), an observer on the ground notes that the person's trajectory is actually perpendicular or tangent to the ride's radius at the point of departure.

Perhaps the most notable of the centrifugal drive experimenters is Prof. Eric Laithwaite, a British engineer who was involved in the development of mag-lev trains. His experimental gyroscopic drive, which to me resembles the flyweight governors on old steam trains, utilized the principle of precession to produce a force of levity during one half-cycle of each rotation. Its principle drawbacks are shared by almost all known centrifugal 'engines': its mechanical complexity and susceptibility to catastrophic failure pretty much preclude its practicality.

An American inventor named Hans Schnebel developed a weighted planetary gear arrangement that my friend Joe and I studied, which has the apparent advantage of greater simplicity and smoothness of operation. This wheel-within-a-wheel system causes a large centrifugal mass to describe a highly eccentric orbit around the central drive shaft, wherein its centrifugal acceleration is continually concentrated to one side. The main drawback with this device is that it is quite heavy and bulky for the net unidirectional thrust output obtained.

So, let's take a closer look at a couple of those inspired tinkerers and armchair engineers who were in fact somewhat **on the right track**. The first gentleman whose work will be instructive is Calvin Cuff, of Brooklyn, NY. He holds three U.S. Patents for variants of the centrifugal drive, and his earliest and fundamental invention is illustrated (using the original Patent drawings) on the next page.

* It is important to point out here that the electron is presumed to be forced to apply a conservative no-work force when it is precessed by magnetic (or electric) induction means.

During the time of our collaboration, Joe actually endeavored to build a working model of the "Cuff Drive" while I supplied what help I could in the form of basic engineering and mathematical analysis. In the course of this project, we gained some fine empirical knowledge which I was later able to apply to the StarDrive Generator. But, while centrifugal drives do illustrate the concept of action without apparent reaction, they remain largely an abstract proposition.

U.S. Patent 3,968,700
Calvin I. Cuff, July 13, 1976

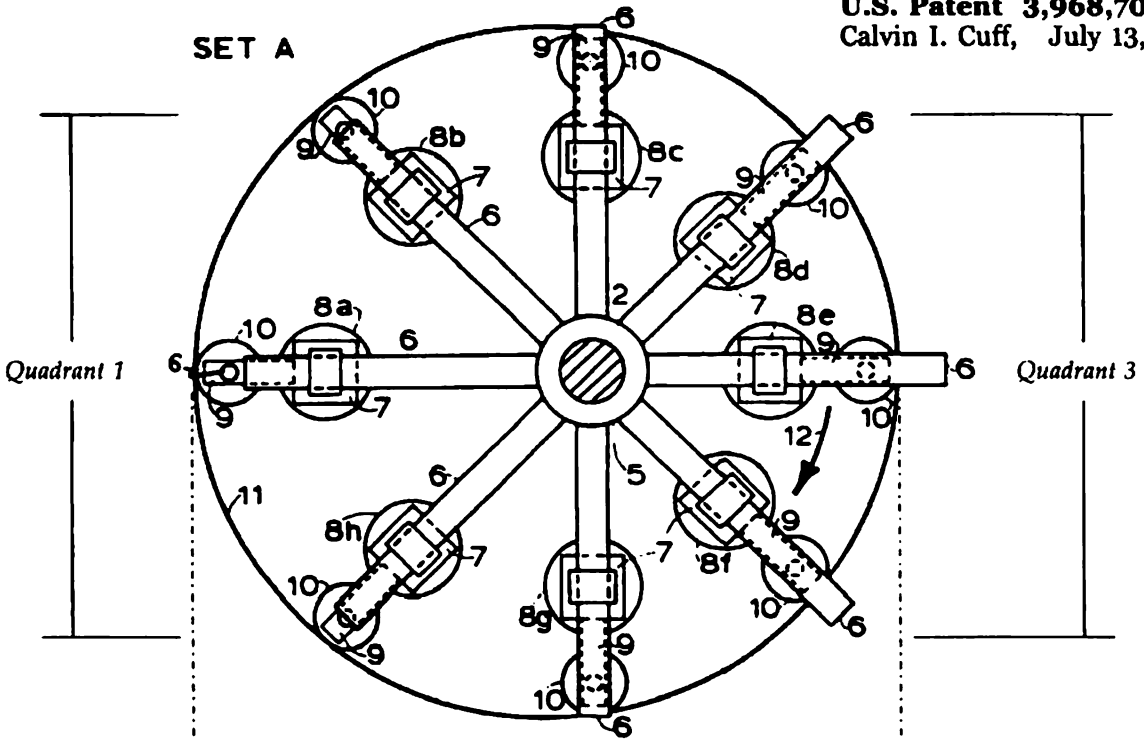


Fig. 57a: Cuff centrifugal drive (top view)

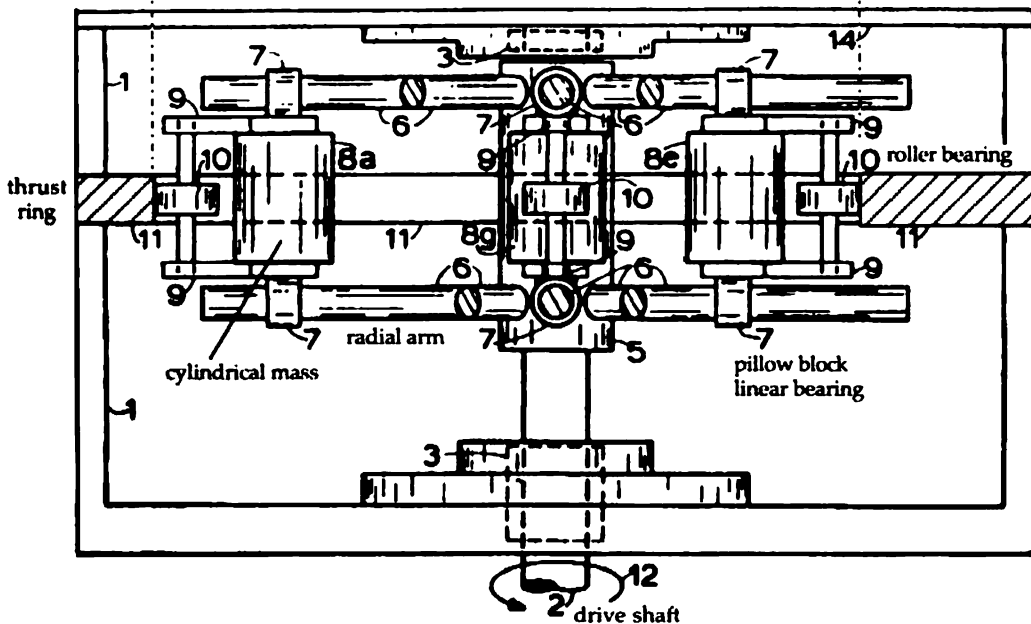


Fig. 57b: Cuff centrifugal drive (side view)

The Patent title of this invention is “device for converting rotary motion into a unidirectional linear motion” and, as can best be seen in the preceding Fig. 57a, it is intended to achieve a net imbalance of centrifugal force components of gyrating masses at successive incremental rotational positions by varying the radius of gyration. A beautiful aspect of this odd machine is that the necessary centripetal force is supplied by the outside thrust ring, which keeps the ‘string’ from breaking, and so the ‘output’ force components are indeed a function of the square of the positional mass velocities. Accordingly, any net thrust produced will actually represent the difference between centripetal force components in the circular sector of greatest radius of gyration (Quadrant 1) and those in the opposite such sector of minimal radius of gyration (Quadrant 3).

What is not apparent from the drawings is that a single such drive unit will *not* produce significant linear thrust, but will in fact exhibit a violent side-to-side or oscillatory motion! Thus, the language of the Patent makes provision for the coupling of two *counterrotating* drives, which will tend to mutually cancel or dampen any such oscillatory forces. Joe’s attempts to measure the level of net thrust produced by a single unit (by placing it upright on a scale!) were unfortunately inconclusive due to these mad oscillations. We tried this of course to determine if the device’s underlying logic and feasibility warranted the cost of building a second unit and the required counterrotational coupling means.

Complex and painstaking vector analysis per degree of rotation in both of the principal Quadrants eventually convinced us that the dual-drive machine would *still* produce a less-than-practical level of net thrust as long as the thrust rings were purely circular in shape! Our calculations revealed that a complex egg-shaped thrust ring would be needed in order to produce any significant linear thrust, and that due to the escalating costs the project probably did not merit further investigations.

What *can* be derived from studying the preceding material and drawings related to applied gyroscopics is a feel for how I eventually deduced the concept of *counterrotating fields* which each utilize only mutually-opposed half-cycles of rotation, and which may therefore be rendered variably non-isometric and unidirectional in their combined net thrust output! Moreover, in studying the principle of *precessionary forces*, a clearer understanding was gained of how to take greatest advantage of the electron’s ability to exert a naturally-conservative force which results in its absorption of quantum energy (to defray its travel expenses) and which is coincidentally no-work *on our part* in the process.

In light of all these centrifugal drive considerations, I feel obliged to give a special honorable mention to the reknowned Canadian inventor and science writer, T.B. Pawlicki. He may already be familiar to many of you for his now-famous cult classic How to Build a Flying Saucer (©1981). This wonderfully thought-provoking little book became an early addition to my professional library, and I must say it has probably influenced my own work in a significant way. I still feel, after all these years, that Mr. Pawlicki deserves some recognition for having in my opinion come closer than anyone else to the truth about the StarDrive device and its eminent suitability in the pursuit of light speed.

Not only does he intelligently discuss the concepts and difficulties involved in

trying to perfect a working centrifugal drive, but he actually proposes the use of *modified betatrons* (electron centrifuges) mounted on gimbals in an annular disk arrangement to propel a saucer-shaped vessel to relativistic near-light speeds! In a simple "Mark I" version of this concept, the outboard annular ring of betatrons would itself be fixed in relation to the superstructure. He further postulates, however, a "Mark II" variant in which this annular disk itself becomes a rotating element or rotor, about which a gravitational energy vortex would be established for increased performance, control, and stability(!)(?).

While these ideas are rather fascinating, and are implicit in his original drawing below, he does not specifically address the issue of exactly how the rectification of the betatron output is to be achieved. And, from what we have learned so far of mechanical centrifugal drive devices, this would likely be a very difficult technological challenge. I myself am going to resist the distinct urge to speculate thereon, and at this point I feel that credit has been given where credit is due. One thing I can say about this proposed design is that it *could* be easier and cheaper to build than mine, although it would not provide any comparable means of protection against interstellar particles and radiation!

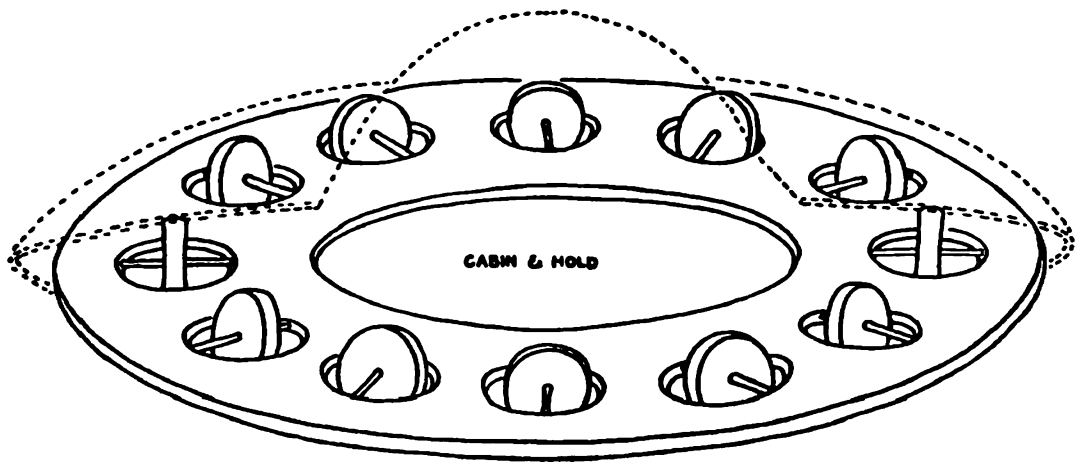


Fig. 58: simplified schematic representation of Pawlicki betatron drive

In recent years, various types of *linear ion drives* have generated a great deal of interest among space scientists, particularly at NASA. While still a reactionary propulsion method like the rocket, ion drives would nevertheless allow top vessel speeds approaching that of light. Perhaps the single greatest problem that will be encountered by *any* type of space vessel which manages even a fair fraction of light speed is the inevitable collisions with interstellar hydrogen molecules. Thus, one interesting and feasible ion drive would use a magnetic ram-scoop to collect and focus the onrushing hydrogen in the ship's trajectory into a long hollow central shaft, wherein it could be fused into alpha particles and electrically ejected at tremendous speed.

It is estimated that our region of the galaxy has about one hydrogen molecule per cubic centimeter of space. Although this sounds like almost nothing at all, at even half of the speed of light every square centimeter of the forward surface of a

starship which did not possess such technology or other *electromagnetic shielding* (like the StarDrive Generator's) will suffer billions of atomic collisions per second, and the crew could be subjected to millions of roentgens of radiation per hour! And, while the magnetic scoop would afford protection from this radiation by displacing and controlling its creation, it would be of little value in protecting the ship from the micrometeoroids which are not that uncommon in the void. So, the search for the ultimate in velocity will truly be a risky and dangerous business, and requires a very special kind of bravery: just like that of each astronaut (and especially Jim) in the 2000 movie "*Mission to Mars*"...

We could use an old Navy test pilot expression to describe this level of daring, wherein the combined limits of man and machine are ultimately tested and redefined, and that is - **pushing the envelope**. In all of aviation history, very few tales are as inspiring or even compare in exemplifying this kind of courage to that of now-retired General Charles (Chuck) Yeager's legendary breaking of the sound barrier. The following account of this pivotal historic event is based on writer Tom Wolfe's version of the story from The Right Stuff:

The Bell Aircraft Corp. had built a projectile-like rocket plane under contract to the Army, called the X-1. During the course of a testing program encompassing some 20 flights, Bell's civilian test pilot Chalmers "Slick" Goodlin had carefully nudged the bright orange X-1 toward the transonic zone and had reached a speed of .80 Mach (or 80% of the speed of sound).

But as any conventional jet-powered aircraft neared Mach 1, shock waves would wildly buffet the wings and tail. The pilots would lose control, and sometimes the aircraft would actually disintegrate. By the time the famous British pilot Geoffrey de Havilland was killed at .94 Mach, many engineers and aviators had concluded that attempting to break through this "wall of air" or sound barrier was virtually as suicidal as a kamikaze mission. And Bell wasn't paying Goodlin enough to risk it...

However, Army testing director Col. Albert Boyd at Wright-Patterson thought that the sound barrier was merely an engineering problem that could be solved with sufficient science, determination, and daring. He selected a cocky young test pilot named Chuck Yeager for the final assault on Mach 1, set for October 14, 1947. Yeager wasn't an engineer and didn't believe the barrier existed. *He* predicted that as the X-1 went beyond Mach 1, the stability of the aircraft would return to normal. Yet when he pushed the plane to .94 Mach, the air compression patterns over the tail caused a total loss of elevator control, and a moving stabilizer system had to be developed.

On the momentous day of the official transonic attempt, Yeager and his rocket plane were flown to an altitude of 20,000 feet in the bomb bay of a B-29. They were then released to begin a climb which would ultimately extend beyond 42,000 feet.

Yeager soared ever higher into the clear desert sky as he ignited one after the other of the X-1's four rocket chambers. At .965 Mach, the airspeed indicator went mad and the turbulence was tremendous, but a moment later a sonic boom rolled over what would later be Edwards Air Force Base as Yeager went supersonic. Hearing this, the ground crew was afraid that Chuck had 'bought the farm', but in reality he had reached a maximum airspeed of 1.07 Mach and was at such an altitude that he could see the Sun and the stars at the same time. He had been right: the awful turbulence had subsided as soon as he exceeded the speed of sound. He was flying faster than any human ever had, and had reached the threshold of space itself . . .

Chuck Yeager is a Southern good ol' boy who showed us all that sometimes the seemingly impossible *can* be done. And he did it after having to be helped into the cockpit: he had busted a rib or two the night before after a night of hard partying at his favorite watering hole (near the Muroc Dry Lake Bed) and a subsequent wild ride through the chaparral on his horse during which he failed to stay on it! I rather suspect he's the person that Paramount had in mind as the model for Zephram Cochran in one of the StarTrek™ motion pictures: the inventor of warp drive who was also the first man to break the time-light barrier. I like to think that in reality the world's first starship captain to do so will be a man just like General Yeager. I guess I'm just enamored of this image of **an unlikely hero**.

Assuming that an inertialess or inertia-dampened method of propulsion won't be discovered for a *very* long time, if ever, it will take just about a full year (or 354 days) to reach light speed at a constant 1g acceleration. Were the EDF Generator capable of a sustained 2g's, and as we've seen this is rather doubtful, this endeavor would take 'just' half that time. The converse of this situation also applies, of course, so it will take a corresponding length of time to deaccelerate back to zero velocity for a landing. The expected duration of any trans-light trip onboard a starship will thus always be roughly *at least a year*, and more likely will be a minimum of half again that time.

Postulating that my Field Generator will actually be the first propulsion method used to attempt this level of velocity, in large part due to the dire need for the electromagnetic shielding it would provide, it becomes obvious that a tremendous amount of onboard stored ambient charge will be needed to replace the inevitable leakage of Field envelope electrons during such an extended period of operation. Even huge banks of capacitors could not begin to accumulate the levels of charge which would be needed, despite any fortuitous discovery that the Field leakage rate is extremely low.

This is the reasoning which underlies my proposal to use a number of large-diameter superconducting current storage rings for this purpose, and a moment should be taken here to describe this concept. While it is not possible for us to go into the fascinating field of superconductivity in depth, certain of the most basic information about it will suffice to outline its intended use in this application.

Superconductivity was discovered by Dutch physicist Kamerlingh Onnes in

1911 when he observed zero resistance in frozen mercury below 4.2°K, at the temperature of liquid helium. While most metals are actually superconductive at this temperature, liquid helium is a costly and inefficient refrigerant, and is hard to use because it's superfluid and requires the use of special lines and fittings to prevent its strong tendency to leak from any pressurized system.

Many other materials have been discovered or developed which are superconductive at the temperature of liquid nitrogen (77°K), which is about 20 times more efficient to use than helium. It was also learned that each superconductive material has a critical level of current conduction beyond which normal resistance returns. However, the premier nitrogen-cooled ceramic superconductor Yttrium Barium Cuprate ($\text{YBa}_2\text{Cu}_3\text{O}_7$) will carry as much as 800,000 amps or more in a large circular ring as thin as *a single inch* in cross-sectional diameter!! [Lead Molybdenum Sulfide (PbMo_6S_8) could perhaps also be used.]

The language of my Patent Application makes provision for the development of suitable "charge deposition and retrieval means" with respect to the proposed onboard current storage rings. This means that a system must be derived for not only electrostatically charging and discharging these rings but for making this charge rotate as a continuous dc current in the meantime! I presume this will not be an easy task and cannot say at present how best to accomplish it, although I am investigating a possible solution (using electrodes and wound inductors!): like a super-cold version of the Tokamak with a ceramic core instead of vacuum . . .

In a very similar vein, I am now able to describe the general method by which the EDF Generator may be used to break **the time-light barrier**, if *not* the specific math means or "mechanism" which must be understood and employed to do so. In all my years of research, I have found no other such method proposed. I have no doubt, however, that there are physicists today who will be able to work out the necessary details given the 'basic' suggestions which follow.

Laws of quantum mechanics dictate that deep-space "vacuum fluctuations" must exist: local oscillations in the positive and negative quantum energy balance at various points within the void. This concept has been verified by the indirectly-observable occurrence of spontaneous virtual pair creation as proof of *electromagnetic vacuum fluctuations* (or EM flux) and, more importantly, by the predicted thermodynamic "evaporation" of black holes as evidence of *gravimetric vacuum fluctuations* (or gm flux) in the pioneering work of Stephen Hawking.

The laws of *quantum fields in curved space-time* (derived from the study of black holes) furthermore require that gm flux in close proximity to the event horizon of a black hole must have a negative average energy density. Similarly, the work of physicists Robert Wald and Ulvi Yurtsever suggests that a heavily-gravitating object moving at relativistic velocity can also produce surrounding regions of gm flux with a negative average quantum energy density.

It has been postulated by physicists for some time that such regions of relative space-time instability may in fact provide a "bridge" to hyperspace, and a few sophisticated sci-fi writers have long used the concept of combining these two mechanisms for producing negative gm flux (for lack of a better concise term) in order to generate *a stable open-ended wormhole*. Thus, to open and cross a local space-time warp and therefore achieve travel that is relatively faster-than-light,

a starship moving at (let's say) .99999 *c* would execute a "sling-shot" maneuver very near the event horizon of a black hole.*

At first glance, this technique appears to offer significant merit, for not only do we now have an achievable Impulse Drive (in the form of the EDF Generator) which is capable of this velocity but black holes would seem to be far more common than was once thought. Much more importantly, however, Don Page (a professor at Penn State University and former student of Hawking) has shown conclusively that any wormhole either naturally- or artificially-produced *must* have a uniform distribution of "exotic material" holding it open to avoid instant collapse. And, this exotic material can theoretically only have two forms: antimatter or *concentrated negative gm flux!*

The main problem with this scenario is that famed mathematician Roger Penrose has used topological analysis techniques to prove that *every* black hole must have a singularity at its core. It would then seem that any wormhole produced by the method above would stand a good chance of having this very singularity at its other end! This situation would, of course, completely preclude travel by means of this type of wormhole. Additional insights derived from the work of Prof. Page and from Einstein's famous Field Equations further show that there is in fact no natural way to produce a stable wormhole.

Therefore, the *method* by which this writer proposes to show that the creation of a stable wormhole is achievable arises from the *Reissner-Nordstrum solution* to Einstein's Field Equations. This important work clearly shows that an exploding star forms a temporary wormhole, albeit one of incredibly brief duration, provided it has a sufficiently high electric charge. If such a star's residual core mass is less than 1.4 solar masses, the subsequent *electron degeneracy pressure* resists the collapse of the white dwarf star which results and *prevents a neutron star or a black hole (and therefore a singularity) from forming*. Thus, each white dwarf star we see in the heavens is in fact a stellar remnant whose very atomic structure might have been erased – but wasn't because its excess electric charge prevented its total collapse and, at the instant of its creation, produced a wormhole.

Thus, it is my proposal that the EDF Generator could be driven to a sufficiently extreme velocity that its self-generated negative gm flux at some point causes a stable open-ended wormhole to arise, the collapse of which is resisted by the electric charge in its Field envelope. In this condition, ship-and-field would constitute a mobile *Charged Vacuum Envoldment* (CVE): an artificial black hole without a singularity. This may be one reason for that classic flying saucer shape: the shape of the event horizon and accretion disk of a rapidly rotating black hole.



Fig. 59: theoretical shape of rapidly rotating black hole.

* A black hole's rotation produces a gravimetric vortex effect on local space-time, so it would appear that such a sling-shot maneuver might be most effective if performed tangent to the rotational plane on the receding 'side' of the hole: if such a trajectory could even be determined!

There are strange things in front of us -
how strange we cannot at present even guess.
Doubtless some of the difficult things to
understand, which lie behind the veil, will in
time be shown to us to see and understand.
In the meantime, all we can do is to think
and work patiently, fearlessly, and unselfishly
to an end that we think is right.

Bram Stoker

The Lair of the White Worm

The Quest for Quantum Gravity

So far as we know, the one characteristic of humanity which fundamentally separates us from the rest of the animal kingdom is our ability, and indeed propensity, to question the nature of the world around us. Not only do we actively seek to know *how* the universe is made and how it operates, at both its smallest and largest levels, but also to learn *why* it should do so in the manner(s) we observe. We think, therefore we are mathematicians and scientists.

It is just such intellectual curiosity which caused Sir Isaac Newton to develop the indispensable form of mathematics we now call calculus, which he later used in the formulation of the Universal Law of Gravitation. He published his theory of gravity in the famous Principia Mathematica in 1687 which, in conjunction with the inspired experimental work of Galileo on the same subject, almost inarguably marks the advent of the era of 'modern' science. Today, over three hundred years later, it is therefore rather amazing and ironic that exactly *what* gravity really is constitutes one of the few remaining great mysteries of the ages.

Almost everything we presently know about the elementary particles which constitute matter, and about the various fundamental forces of nature, can be summarized by what physicists now call *the Standard Model*. In the relativistic *quantum field theory* from which the Standard Model arises, all matter consists of real particles called *fermions* (which can be directly observed in particle or mass detectors). Similarly, all of the fundamental forces of nature are thought to be effected through the interaction or "exchange" of other virtual particles called *elementary bosons* (which cannot be observed in particle detectors). The existence of such virtual particles can in most cases, however, be indirectly verified through their effect(s) on local energy transformations.

While the Standard Model does an admirable job of being consistent with the results obtained in all high-energy particle physics experiments so far, it is far from complete and in some ways even unsatisfactory. This Model is built upon 18 arbitrary parameters which in no way contribute to an understanding of *why* the Model describes nature at all: they merely show how the results obtained in such experiments might be explained. The most significant of these parameters is the so-called Higgs particle, a boson of no intrinsic spin or electric charge, whose manifestations are believed to be responsible for the masses of the quarks and leptons (which comprise all ordinary matter) as well as for much of their behavior. But all of the aspects of the Standard Model which are contingent upon this particle are untested, as the Higgs boson to date has never been observed!

Perhaps more importantly, however, the Model is reliant upon the exchange of virtual particles called *gravitons*, having no mass or electric charge and spin-number 2, to explain the force of gravity between all objects large and small. But what no one has made clear (at least to me) is how a *black hole* would therefore be able to exert its tremendous gravitational force if these massless gravitons – like massless photons of light – are equally unable to escape its event horizon!

Furthermore, *real* gravitons would then have to make up the gravity waves that physicists say are predicted by Einstein's theory of relativity: but no one has ever yet observed or detected the type of gravity waves that relativity predicts, *or* any gravitons (virtual or real).

So, as they say, something is definitely "wrong with this picture". Obviously, scientists used Newton's theory of gravity (as an emanative *field* of force) for generations, obtaining accurate results without apparent difficulties. However, as mass, energy, and velocity climb to extreme levels, this theory is also seen to be incomplete. The first major problem in this respect appeared when James Clerk Maxwell showed that the velocity of light always has a constant value he called *c*: in traditional mechanics, *all* speeds had been considered relative. Moreover, in Newtonian mechanics, gravitation was free to propagate at infinite velocity: an exploding star for example would then cause gravitational ripples which could spread throughout space in virtually zero elapsed time!

When Einstein's general theory of relativity proposed in 1916 that gravity should not be viewed as a field of force, and must furthermore propagate at the limiting value of *c*, we learned that it could more properly be viewed as the distortion of a four-dimensional geometry comprising 3 spatial dimensions and time. Thus, space-time is a construct of *geodesic curves*, the contours of which are proportional to relative mass. The power and elegance of this theory cannot be denied, and so far it has measured up under all tests of its validity. But it does *not* include provisions for quantum mechanics (which Einstein didn't really care for much), and theoretical physicists to this day have been unable to successfully formulate *a similar theory which incorporates quantized gravity or gravitons*.

To be fair, Einstein did spend the greater part of the last years of his life trying mightily to reconcile general relativity with quantum mechanics and formulate a unified field theory which accurately described all of nature's forces and their fundamental rules – a theory of *quantum gravity*. Such a "theory of everything" is certainly not required for physicists (and the rest of us mortals) to understand or explain events in the everyday realm. But it is necessary in most physics problems involving *either extreme of scale in size or mass*. Many physicists, like Steven Weinberg (an American), feel that such a theory would probably be "logically isolated" or immutable (unlike the Standard Model), in that it could not be significantly modified without destroying it. It would likely also be far more streamlined mathematically than general relativity, and much easier to apprehend by the general populace.

In the quantum mechanical universe, nearly everything must be viewed as coming in discrete bits of miniscule size or amount, according to relationships governed by Max Planck's constant *h*. In the macroscopic world, this concept presents little problem for the Standard Model and its notion of forces as the exchange of virtual particles. But theories which treat the force of gravity as having a particulate nature run into big trouble on the subatomic scale. While general relativity says that gravity is the very geometry of space-time, the presence of the proposed gravitons in the submicroscopic realm results in impossibly distorted parameters whereby the probability of a certain event could be greater than 100%; or in particles being produced with a negative probability!

Oxford's Roger Penrose and other relativists began to insist that gravity cannot receive the same mathematical treatment that was being given to the other forces under the Standard Model. The relativistic geometry of space-time had to somehow become an active participant in the entire unified quantum field drama, and not merely a passive backdrop when considered within the arena of the ultra-small in order to avoid these unsolvable metaphysical conundrums. As long ago as the mid-50's Princeton's John A. Wheeler suggested that to resolve this issue, it appeared that space might have to be ascribed a flexible cellular nature that he likened to a "space-time foam". Thus, it would seem that, in the final analysis, *space itself must be quantized!* In the words of Max Born, a past professor of theoretical physics at Göttingen and associate of Planck, "space is not merely a background for events, but possesses an autonomous structure"! But, how can this be?! Such a turn of events would seem to indicate a revival of the "aether" (ether) theory, which the Michelson-Morley experiment was supposed to have put to death once and for all in 1887!!

Before the principle of wave/particle duality was firmly established, all of the types of waves with which scientists were familiar needed a substantive medium through which to travel. Since light was able to travel through an interstellar space which was otherwise thought to be utterly empty, they postulated the existence of an invisible aether as the medium which allowed stellar light to reach the earth. Unfortunately, theories concerning the aether (which go back to Aristotle) were built upon one or more erroneous assumption(s), and a plausible model for its operation was never found.

If we consider that radiant energy crosses the void strictly as particulate quanta, there is of course no logical imperative for there to be an aether-like medium. But, if we alternatively consider radiant energy solely from a wave point of view, a logical case *could* be made that space must have a quantized structural nature! As the material above concerning the melding of relativity and quantum mechanics at the microcosmic level implies, the two aspects of wave/particle duality should not be *separately* applied preferentially in certain situations in order to avoid logical or mathematical incongruities: they should both be in a form suitable for application uniformly from quasars to quarks!!

To return for now specifically to the search for a theory of quantum gravity, mathematicians like Penrose soon began a struggle to put relativity's equations into a form compatible with quantum theory *without* the assumption that gravity has to be caused by virtual particle exchange. While some were able to develop systems of equations which seemed to be consistent with how gravity should operate at the quantum level, they were generally unsuccessful at deriving meaningful solutions with existing mathematical techniques.

Then, in 1986, physicist Abhay Ashtekar and associates Lee Smolin and Carlo Rovelli published a paper entitled Weaving a Classical Geometry with Quantum Threads. While this landmark treatise is not a complete unified field or quantum gravity theory, it does make a formidable case for the quantization of space by examining how gravity might act as one considers ever-smaller spatial volumes or sections. It suggests rather brilliantly that the space-time continuum is not quite analogous to a smoothly pliable mat (as described by Einstein's disciples),

but is itself composed of an endless weave of nearly infinitesimal *space-time loops* which are interlinked like three-dimensional chain mail! This is what I hope I may refer to as the theory of **quantum potential loop-space**.

Ashtekar was able to find a method of reformulating Einstein's relativity equations so that the mathematical concepts of *connections* and *frame fields* were incorporated, deriving a set of four original equations of a form very similar to those already employed in quantum mechanics. These equations constituted a fresh geometric language which permitted easier descriptions of the complex relativistic curvatures of space-time, and were at the same time quite similar to those developed by Maxwell to unify electromagnetism!

When Ashtekar's research team combined these equations with classical elements of mathematical knot theory, specifically those related to simple loops, they began to find more and more solutions to quantum problems that were previously considered unsolvable. They were, in effect, writing the first pages of a new quantum gravity manual. Each quantum loop, or discrete unit of space, is very similar in concept to a single circular magnetic field line as envisioned by Faraday to describe the discrete components of which a magnetic field of force is established. Similarly, it is thought that the density of the quantum loops at a given point in space is proportional to the local 'intensity' of the gravitic field, or to the quantity of mass which is present.

Interestingly enough, the estimated diameter of such a space-time loop is essentially equal to the *Planck length* - about 1.6×10^{-35} m - a unit of measure which is related to the smallest conceivable quantum of energy. [The Planck length is calculated according to the expression $(Gh/2\pi c^3)^{1/2}$, wherein each constant has its traditional value.] Physicists for a long time have suspected that nothing in the universe can be smaller than this length, and this notion becomes a virtual certainty in light of the loop-space theory: nothing at all can exist outside of a space-time loop, because the loop becomes the very definition of space. And, if a single quantum of energy were smaller than the loop, there would simply be no 'frame' within which to suspend it . . .

I must state emphatically at this point that the ideas set forth hereinafter in relation to the Ashtekar theory of gravity, which we will return to nearer the end of this Chapter, are entirely my own. In as far as I am not a trained physicist *per se*, I sincerely hope that these ideas are not construed to reflect in any negative way on the outstanding work of a great scholar. They should be taken rather as being indicative of my intense desire to formulate a cosmological model which supports the concept of trans-light velocity. Each of you must judge for yourself how successful I have been in this endeavor.

In Chapter 2, I submitted the view that the universe comprises two completely separate continuums: the space-time continuum in which we ourselves exist, and a complement time-energy continuum which exists 'beyond' the time-light barrier wherein all velocity is hyper-light compared to our inertial reference frame. This abstract logical construct is deemed necessary to explain the fact that all signal- and phase-velocity products equal c^2 , which is highly suggestive that c^2 is in fact the ultimate velocity in *either* continuum relative to the other.

It was also later implied (on page 102) that the two continuums are *coincident*

yet completely out-of-phase. By this, what I mean to say is that they actually occupy *the same physical place at the same time*, yet they never intersect because all of their respective mass and energy waveforms share exactly the same nodal points within the postulated discretely-quantized framework of space. A notion which might immediately suggest itself under these circumstances, and on the surface does not seem that implausible, is that this complementary continuum is composed entirely of antimatter. And, the reason why the near-instantaneous obliteration of everything has never occurred might be that time itself in this other continuum is *negative or opposite* with respect to ours!

Without proceeding any farther than necessary into the almost stultifying complexities of *symmetry theory*, let's just say that it was once thought the laws of nature must always conform to each of three different symmetries known as C, P, and T; and that any true quantum gravity theory must always obey the combination of these same symmetries. To briefly elucidate this, if we change a particle's quantum number (and hence its charge), we effect an operation of symmetry C and the particle becomes its antiparticle. If we take a mirror image of the particle *and* reverse all of the force vectors associated with it (and hence its spin), we effect a reversal of parity or symmetry P. Neither of these operations entails a violation of classical mechanics or electromagnetism. However, it was found in the late '50's that the weak nuclear force did not obey either C or P symmetry separately, yet it did appear to obey the combined symmetry CP. This would seem to imply that a mirror-image universe or continuum composed of antimatter *could* develop similarly to our own, even without symmetry T (time).

The basic validity of *joint CPT symmetry* does *not* imply, however, that an alternate universe or continuum which even obeys this triple symmetry *must* exist, and we now know that it is only approximately true. In this respect, it was demonstrated in 1964 by two American physicists named James Cronin and Val Fitch that even the combination CP symmetry is not always obeyed in space-time (continuum) particle physics. Furthermore, they showed that unless the direction of time *were* reversed, such a mirror-image antimatter universe or continuum *cannot* behave the same as ours. Thus, the laws of physics themselves do not obey the symmetry T, and *must be* different if one reverses the "arrow of time". This is perhaps a difficult way of saying that, if a *coincident* time-energy continuum does in fact exist, it is not composed of antimatter nor is the direction of time reversed with respect to our own space-time continuum! The simplest underlying justification for this conclusion is that scientists do of course observe the universe to be expanding; therefore, any coincident continuum such as that which I postulate, and within which navigation is possible utilizing the Lorentz transformation, must also be "co-expanding" and therefore time-parallel.

The very best way I've found to understand the implications of these ideas is using the British physicist Stephen Hawking's "no-boundary universe" theory. Hawking is, of course, the gentleman whom most educated persons recognize as perhaps the most brilliant theoretical physicist of the late 20th century, who is also sadly confined to a wheelchair with Lou Gehrig's disease. He was appointed Lucasian Professor of Mathematics at the University of Cambridge in 1979, which is the same chair held by Newton himself three centuries ago.

Newton apparently believed that there was only one universe or continuum which was infinite in size and which contained an infinite number of stars, in order to explain why all of creation did not collapse into itself as a result of his own Law of Gravitation. Today, physicists understand that it isn't possible to define an infinite static model of the universe wherein the force of gravity is always attractive in its effect; but Hawking's no-boundary universe proposal suggests that four-dimensional space-time can be interpreted mathematically to form a finite closed surface which has no boundary and therefore no absolute beginning or end. The more important predictions of this theory for our purposes, and which so far as I know have not been disproved, are: 1) that the universe will at some point in *near-infinite* time begin to contract; and 2) that *space-time* entropy will continue to increase throughout such a contractionary phase.

We will examine the no boundary theory in further detail in the final Chapter but, in light of the preceding discussion of symmetry, I believe that it clearly supports a notion which I've long accepted intuitively as fact: that there can be *no backward relative motion in time*, whether in this continuum (if its the only one which exists) or in the time-energy continuum I am certain is also real. In his best-selling book A Brief History of Time, Prof. Hawking seems to agree with my belief that if we are ever to effect real star travel, it must occur in or through one or more dimension(s) which are *separate from* the space-time continuum. It's just not going to be possible to "beat" the light-speed limit by some alternative time-reversal scheme. Instead, a 'modified' or *compound time dilation* effect would result while traversing such dimension(s) or continuum, to make star travel *subjectively* manageable within an all-too-finite human lifetime.

Hawking's work further supports a view that the fundamental laws of physics in two coincident continuums almost have to be very similar, but implies that the *conditions* therein might be very different indeed. He also suggests that by the time a universal contraction period does begin, it is likely that energy will only exist in the form of radiation in our continuum: that even the protons and neutrons of which matter is comprised will have decayed. My own hypothesis based on these suppositions, which is admittedly slanted to the view that trans-light travel through a coincident continuum is possible, is that conditions in the time-energy continuum during the present universal expansionary epoch are those we could expect in *our continuum* during the contractionary epoch! In other words, we would probably find little if any solid matter present there now: only *heavy* radiation. While the fact that good solutions of the Lorentz transformation (as described by Bilaniuk et al.) require that mass in the time-energy continuum be "imaginary" in mathematical treatment, this does not mean that matter per se actually cannot exist there. As we'll see later, the average mass density in either continuum is probably inversely proportional to that in the other . . .

As Stephen Hawking so aptly points out, the scenario of travel through hyperspatial dimensions has long been a common device of science fiction writers. And, as one might guess, this notion received very little acknowledgment within the scientific community prior to the career of Isaac Asimov. In the latter 1980's, however, the emergence of *superstring theory* as one of the best candidates for a unified theory of physics began to lend a fair measure of

respectability to this concept. Before we take a look at why this should be so, I'll try to briefly review as simply as possible the relevant aspects of this current golden-child of theoretical physics - which I find to be unnecessarily abstruse and, well, *convoluted*. String theory has yielded no testable predictions to date.

In string theory, all of the basic particles and forces in the universe are thought to consist of strings of intense quantum energy which exist in a super-spatial realm having *ten dimensions* but which themselves exhibit only the dimension of length. A total of ten dimensions was found to be necessary in mathematical treatment in order to *avoid* the very tachyons that we StarDrive enthusiasts might find encouraging - as well as certain *ghost particles* having the aforementioned negative probability. These superstrings would then vibrate under a fantastic level of tension, with the various elementary particles being regarded as corresponding to different quantized modes of the string's oscillation. The main (and I believe insupportable) problem with this theory is that in each of these extra six dimensions, the strings are curled up into infinitesimally small circles which are thereby rendered virtually unobservable! Not to mention that such dimensions wouldn't seem to allow for the passage of a starship . . .

Of particular interest with regard to our present topic is the string theory concept of how forces between particles and mass bodies would be effected, primarily the force of gravity. Most succinctly put, the force of gravity would behave rather like an exchange of virtual particles, but in this case would correspond to additional quantum energy strings which connect each particle-string in one mass object with those comprising another such object. The total amount of tension in such particle-connecting strings would then represent the magnitude of the force between such mass bodies, as a function of string *elasticity* in a manner exactly analogous to that proposed by Faraday to describe the observed properties of a magnetic field of force. At macroscopic distances, this elasticity would yield just that force predicted by the theory of relativity. On the microcosmic scale required in quantum mechanics, however, the resultant predictions of gravity's influence are contrived to avoid the insufferable incongruities described earlier above.

The one fascinating thing about superstring theory, at least for me, is that the theoretical length of the strings within those extra dimensions *must be equal to the diameter of the quantum space-time loops in the Ashtekar theory of gravity*: the very same Planck length we talked about earlier on! Once again, I suspect that this is more than just a coincidence. I can't help thinking that if those physicists who are active proponents of such an esoteric doctrine as superstrings would only spend half as much time and energy working on a quantum gravity model that *accepted the possibility of tachyons* and eliminated an "extra" *third* continuum - like the Ashtekar-based gravity theory we'll discuss shortly - we would probably be able to break the time-light barrier well before this century's end!!

From this point on, we are going to operate under a small number of assumptions which I believe are in keeping with the train of thought developed hereinabove. It will also then be necessary to define some terminology which I have either contrived myself or borrowed from other sources (who may or may not wish to be acknowledged). I must stress again that the ideas set forth below

are of my own formulation so far as I know, and are the product of a method of derivation which is far more intuitive than demonstrable in nature. I therefore take full responsibility for what some trained scholars may find objectionable.

Accordingly, the principal assumption I'm going to make is that the Ashtekar theory of space-time quantization is the correct model for such a concept. We will therefore choose to view the very "fabric" of the universe's fundamental spatial construction as being composed of an almost limitless number of space-time loops connected after the fashion of three-dimensional chain mail. Thus, energy in all its forms, including matter, must be suspended and conveyed as quanta within a locally-appropriate number of these loops - wherever it occurs in all of creation.

Secondly, it is believed that the causal agent responsible for the force of gravity propagates at c^2 , and that inertial mass is an "inductive" property of matter (probably associated with spin) which limits its velocity to a value less than that of light relative to the spatial continuum within which it is located. I have elected to call gravity's causal agent or operative mechanism **quantum vacuum fluctuations**. [We have already seen that electromagnetic and gravimetric vacuum fluctuations are accepted concepts in today's quantum physics lexicon. Hopefully, this 'new' similar term and its associated principle(s) will not be perceived by the physics community as inappropriate or untenable.]

Finally, we're going to assume that the universe indeed comprises a total of "only" *seven* dimensions, but that they constitute instead two distinct spatial continuums which are *coincident in that they share the temporal dimension*. A metaphysical interpretive basis for this consideration could perhaps be found in the ancient Chinese concept of *yin and yang* and its associated symbol.*

Having thus basically amplified a recurrent theme of **StarDrive Engineering**, let's proceed to the definition of certain special terms which will hopefully support an intelligent discussion of the ramifications of these ideas. The first such term which should be defined is *quantum potential*, which is taken to mean the total level of energy present at any given "point" in the universe and which is deemed to be simultaneously determined by the physical laws of both the space-time and time-energy continuums. The local value of total quantum potential tends everywhere to be **ZERO**, within limits set by the uncertainty principle.

The combination of both continuums, which represents the actual totality of the universe, may then be called the *quantum matrix* and is constituted of the described universal system of quantum potential space-time loops. These theoretical constructs have also been called "quantum potential niches" by various scientists and science fiction writers alike for some time, but I know of no one before Abhay Ashtekar et al. who gave them a better 'material' definition. I leave it up to the mathematical specialists to determine in which situations this matrix 'combination' should be interpreted as a sum or as a product, but "it" represents the absolute stasis energy per unit volume of space itself.

In any event, it can now be seen more clearly (I hope) that quantum vacuum fluctuations which propagate at c^2 could very well be essential if quite different

* Another interesting correlation to this interpretation can be found in the writings of Carlos Castaneda, wherein the protagonist Don Juan reveals that Yaqui Indian medicine men were able to perceive "seven bands of emanations" which comprised everything in the universe.

conditions in two coincident continuums are going to conform to the same or a very similar set of observed physical laws: wherein gravity and total entropy are always positive, *and relativity is uniformly enforced!* These “cosmic signal specifications” or coded sets of patterns for local energy transformations, which would be required to ensure that the proper conditions are manifested at all points *in both reference frames simultaneously*, must arrive at those points *before* those conditions can be expected to occur!! I’m afraid that this is the best way I have to express this idea. And, as I admitted, I’m not able to “prove” it mathematically, even if this book were the proper vehicle in which to try and do so.

Nevertheless, in order to begin tying all of these quantum gravity contemplations together, we’ll start with the notion that the Ashtekar model of space-time in conjunction with the dual-continuum proposition is actually quite similar to superstring theory. *Therefore:*

If we consider the quantum potential loops (or niches) to exhibit the string theory property of *elasticity* (due to an inward-pulling tension), we could say that the size of potential loops larger than those in the unoccupied state is *proportional to the positive energy contained*. Borrowing from superstring theory, we could then assign each space-time loop *a theoretical maximum diameter equal to the Planck length*. Such a largest spatial loop (‘above’ the unoccupied state) would contain a quantum of the highest positive energy; the smallest such loop might then correspond to its containment of a graviton having the lowest positive energy – or to the superposition of such graviton loops, yielding a spatial (quantum potential) *loop density proportional to mass and the force of gravity*. [Gravitons are bosons, and hence may occupy the same space at the same time as they do not obey the Pauli exclusion principle.] All positive energy quanta, including matter and its entire spectrum of particle energies, will then occupy loops of varying sizes between the loops’ maximum and unoccupied diameters.

However, each potential loop must also be able to contain a quantum of *negative* energy and therefore function as a component of the time-energy “phase” or continuum! I postulate that this state may correspond to a range of potential loop diameters from an unoccupied or “median” size to *a theoretical minimum loop circumference equal to the Planck length*, and that in this state the spatial loops actually exhibit the reverse of the ordinary string property of elasticity (due to *outward-stretching* tension). And, such a smallest negative potential loop would correspond to the containment of a graviton-equivalent having the highest negative energy, once again yielding a spatial (quantum potential) *loop density proportional to mass and the force of gravity*. Thus, in the dual-continuum cosmological model that I am proposing, the space-time potential loops which make up the quantum matrix will exhibit the property of reflexive elasticity around a zero-point energy level (in the unoccupied state) which corresponds to a potential loop “surface” area that is midway between the two such areas which correspond to the maximum (positive energy) loop diameter and the minimum (negative energy) loop circumference. The quantum energy contained in any given potential loop may actually be located anywhere in its planar area due to the uncertainty principle, in that *volume per se at this fundamental and irreducible cosmic level does not exist!* Given the operation of reflexive elasticity, I therefore propose that an equal quantized change of area should occur between the maximum (positive) and unoccupied loop sizes as occurs between the unoccupied and minimum (negative) loop sizes, to account for an equal maximum change of quantum loop tension versus energy displacement. The minimum potential

loop diameter *here* will of course be equal to the Planck length divided by π . But, the properties of negative and positive quanta having equal absolute values of wave energy per unit planar “displacement” or *area differential* (from the unoccupied state) may be radically different, due to the difference in scale of the change in energy versus change in area *with respect to an unoccupied potential loop having a median area and zero containment energy*.

To clarify this, we can find the Planck length equal to about 1.6161×10^{-35} m, using the expression given earlier. Using the standard formula for the area of a circle, a smallest possible potential loop with a *circumference* equal to this length will have the infinitesimal area of $.20784 \times 10^{-70}$ m², and a largest loop having a *diameter* equal to the Planck length will have an area which is π^2 (or 9.8696 times) as great. If the size of the potential loops in their unoccupied state is such that there will be an equal change of area between unoccupied loops and those having the stated maximum and minimum occupied diameters, this means that the zero-point loop diameter will correspond to a containment area *equal* to the simple average of the lowest and highest such areas, or in this case 5.4348 times the minimum area calculated above. This theoretical unoccupied (median) diameter would be equal to 1.19925×10^{-35} m. [See Fig. 78, on pg. 339.]

It should be relatively easy for mathematicians and theoretical physicists to check the *conceptual* validity of this simple theory; it nicely supports certain cosmological observations which are either self-evident or seem sound enough in principle. The first such idea is that, in our continuum, *EM energy tends to dissipate and matter tends to accumulate*, and this condition is clearly indicated by the normal elasticity portion of the quantum gravity model presented thus far. And, this model would seem to indicate a plausible mechanism for the present inflationary expansion stage of universal evolution, if we consider that according to this model the average size of the potential loops in our continuum could be rising faster than the average size of the loops in negative time-space is falling *during the present universal epoch!* [More on this in the last Chapter.]

Anyway, the next bit of reasoning based on the reflexive elasticity principle is somewhat tricky, and I hope I’ve done it right. By this, I mean that any proper interpretation of the natural laws and conditions operative in the universe’s negative energy phase must explain the observational considerations which astrophysicists associate with *dark matter*. To wit, it is believed that a source of positive gravitational effect which may be unobservable from our continuum is responsible for the non-dispersal of galactic clusters in the cosmos, as well as certain observed peculiarities in the rotation rates of individual galaxies.

As I’ve intimated earlier, any successful quantum gravity theory which is based on a dual-continuum model must explain the *unified* operation of gravity and entropy in both universal phases. Where it gets tricky is that *this is not the same as saying that entropy must always be positive in both continuums*, even though we’ve established that time will be positive in both and that entropy will probably remain positive in the space-time phase throughout a full universal cycle. If we reverse our observation that energy in our continuum dissipates and matter accumulates, *we might theorize that matter tends to radiate or dissipate in the time-energy continuum and EM energy tends to impinge or accumulate!* Prof. Hawking’s work on black hole evaporation would seem to clearly imply that this

condition holds true if black holes exist in an alternate continuum or **negative quantum time-space**. Such evaporation constitutes *a negative entropy effect* in this 'time-energy phase', entailing a flow of negative energy into the black hole which reduces its entropy; however, this negative entropy is *less than* the rise in entropy which results from a concomitant flow of positive EM energy into *our* continuum (so that the second law of thermodynamics isn't violated *overall*).

We could then postulate in line with the earlier thought that gross 'negative' matter tends not to exist in the expansionary cosmic half-cycle that the dark matter effect could perhaps be explained as the relativistic consequence of impinging negative EM energy in the time-energy phase. To get a handle on this one, we must be aware that the temperature of a black hole (in Hawking's work) is inversely proportional to its mass: *the larger it is, the colder it is*. And, very large black holes such as those believed to inhabit the central regions of most galaxies would have a temperature so close to absolute zero that their matter could exist in a quantum form very similar to Bose-Einstein condensate. [Matter in the Bose-Einstein condensate state (a verified phenomenon I'll refer to again) completely loses its spatial definition, and exists as a standing wave construct.] From this, I can infer that gm vacuum fluctuations which represent impinging negative EM energy, or a local near-absolute loss of thermal kinetic energy, thus constitute the exotic or negative matter we discussed earlier and can be thought of as entailing *further shrinkage* of the quantum matrix in that universal region.

This realization is important as perhaps the only way we laypersons have of making the proper assignment of gravity's "polarity" with respect to the tension of the potential loops in the time-energy phase! Thus, it is my contention that the negative graviton's position within the postulated loop size range for negative energy is *that farthest from the unoccupied state*, and that all other negative quanta will occupy larger potential loop sizes. In this manner, it is possible to explain the further spatial contraction believed to be associated with dark matter, revealing a beautiful symmetry between the operation of relativistic gravity in both continuums, in that the average local size of potential loops in either the space-time or time-energy phase is inversely proportional to mass! At the same time, an inherent asymmetry in the operation of entropy becomes apparent in the cosmic construction which does not necessarily violate the second law of thermodynamics, and is almost certainly a function of *the difference in the area enclosed* by potential loops of the respective spatial phases given quanta of equal frequency but opposite energy 'polarity'. This concept may someday be used to examine and explain: 1) the observed spectrum or "harmonic series" of particle masses; 2) why the universe may be expected to eventually have a contractionary stage; and 3) how and why conditions in a coincident continuum may be very different than in ours yet obey a nearly identical set of physical laws.

It can nevertheless be seen that quantum vacuum fluctuations are essentially changes in the local space-time loop diameters proportional to the nature of the quantum energy they must temporarily contain and properly convey. The 'cosmic signal' referred to above is best understood as the resultant quantum impulse transmitted throughout the interconnected space-time loops, which propagates *in each coincident continuum at c^2 relative to the other* as a function of

the rate of change in tension of reflexive-elasticity! It is for this reason that I have chosen to represent these fluctuations with the term " $|\Delta E_q|/\Delta t$ ", as the time rate of change of quantum potential. The individual quanta of energy are, however, free to move or be displaced from loop to loop in response to that quantum impulse only at $v \leq c$ in either continuum (due to relativity).

An analogy which may be effective in illustrating this principle, although perhaps is somewhat undignified, is one that I call "yanking the blanket". To wit, if we take a two-dimensional or flat piece of cloth (which is itself composed of interlocked fibers) and give it a sharp lateral tug at one end which represents gravity, any up-and-down "shake" imparts a surface wave thereto which has a readily observable transit time and represents inertial mass. But the other end of the cloth *itself* will exhibit a near-instantaneous "pull" whose only lag time will be a function of the very limited "give" or elasticity of its constituent fibers!

Analogies are not necessary, however, to readily see how the quantum loop-space model supports my earlier contention that mass and energy waveforms in two coincident continuums share the same nodal points of oscillation. Such nodal points would merely constitute the actual contact points shared by any given set of interconnected space-time loops! Fig. 60 below is a representation of the three-dimensional model built by Ashtekar's associate Carl Rovelli, entirely of interjoined key chain rings, so that they could more readily envision their own postulated loop-space system. In addition to being exceptionally 'cool', this model nonetheless clearly depicts the described loop contact nodal points.

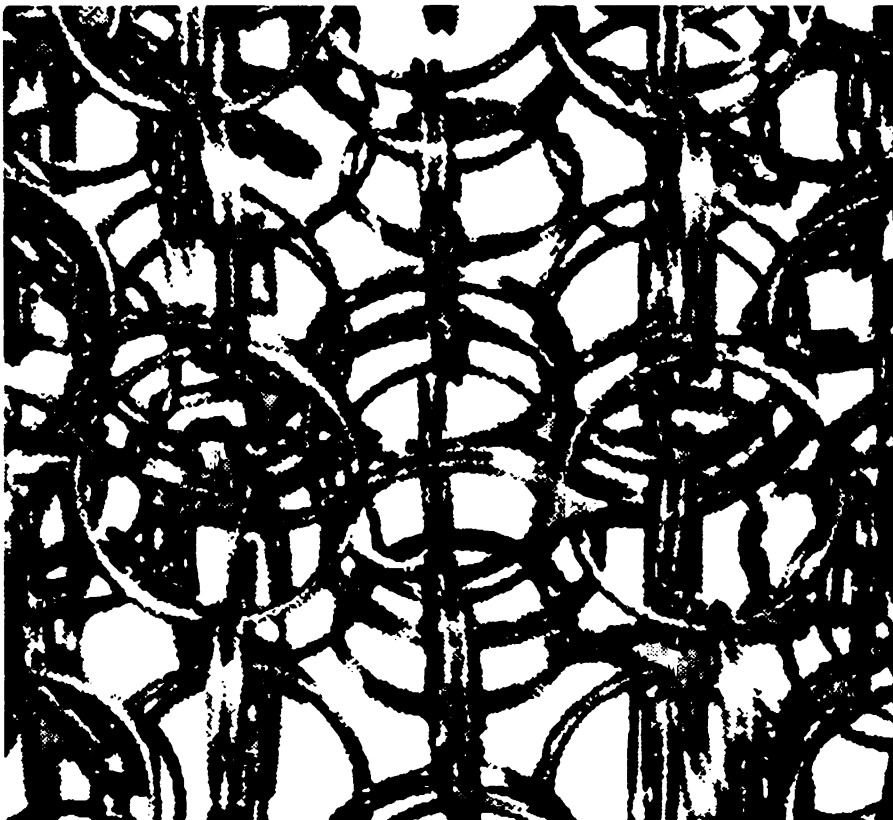


Fig. 60: *A representation of quantum potential loop-space*

To summarize, I believe my proposal for a reflexive-elasticity property of these space-time loops as described reveals that they would actually be *entropic* in nature, while also tending to distribute quantum potential as uniformly as possible. This property would also seem to support the Hawking view regarding the eventual decay of all matter in our own continuum toward the end of an expansionary *half-cycle* of universal evolution, yet at the same time suggests an anti-entropic mechanism which acts to break the equilibrium state represented at the expected contractionary cusp (in a manner which is once again beyond my own ability to further illuminate). This feature of the universe's design and construction might then be intimately related to the ways in which the time-energy continuum's physical laws may only be subtly different than those of our own, the said negative entropy effect being perhaps the only major difference. As I've said before, though, I believe the logical course of research is indicated . . .

* * *

The preceding material will hopefully serve to prepare us for a look at some very basic **trans-light mechanics**, for I acknowledge myself to be conversant with respect to such an abstract and complex concept only in general terms! It should be possible, however, for us to examine certain fundamental principles which would be involved in the workings of a hyperspatial "warp jump" with an application of straightforward logic and a couple of basic relativistic formulas which are actually easy to work with.

The analytical procedure we'll use in this discussion derives from the method of breaking the time-light barrier which was proposed at the end of the last Chapter: whereby a StarDrive Generator will be driven to a speed sufficient to cause its relativistic mass to *very* closely approach a level which would ordinarily correspond to the *Chandrasekhar limit**, in reliance upon its electron degeneracy pressure to prevent the formation of a neutron object or a black hole. In doing so, it is hoped that an open-ended wormhole will arise which is navigable by means of the Lorentz transformation, in accordance with the work of O.M. Bilaniuk.

In order to work with the largest values for starship mass and Field electron velocity (as a function of Field voltage), data will be supplied for a vessel 100 feet in diameter - which as I've said is the largest model advisable using this technology. What we'll do first is calculate such a vessel's total relativistic mass at a velocity which corresponds to its peak Field electron collision speed: the reason being that it will be interesting to see what happens when the starship reaches a velocity which a reactionary ion-thrusted rocket, having the same exhaust speed, *couldn't possibly exceed*.

The next step will be to compute the starship's expected *foreshortening* in the direction of travel, according to the Lorentz contraction which is an inevitable consequence of relativity. This 'shrinking' of the vessel's length along its axis of velocity may be figured according to the most fundamental factor or expression in relativity theory, which is sometimes called the *FitzGerald ratio*. This factor, usually designated as τ (tau), is equal to $\sqrt{1 - v^2/c^2}$, and is used in any calculation of relativistic mass or time dilation.

* In the natural universe this limit is equal to about 1.4 solar masses, or around 2.785×10^{30} kg. The Sun's mass is 1.989×10^{27} metric tons, where one metric ton equals 1,000 kg or 2,204.6 lbs.

Since the computations we'll be making are only intended to constitute the roughest of approximations, being largely illustrative and instructional in nature, a related parameter called the *Schwarzschild radius* will then be calculated. This radius defines the physical size at which a 'cold' *spherical* object can't avoid becoming a black hole. Once again, this expression is actually very simple: the Schwarzschild radius $R_s = 2GM/c^2$, where c is the speed of light, M is the total mass, and G is the universal gravitational constant (at 6.6726×10^{-11} nt-m²/kg²).

Our goal in this endeavor is then simply to observe how closely the ship's foreshortened half-length approaches its Schwarzschild radius! We'll let L_o equal the starship's rest length, while bearing in mind that it will drive upper-face-on during space flight, and this "length" (or hull height) is equal to $2(h_f + h_r)$; then, L_r will be the resultant contracted length. If we assume that one half of L_r will need to approach R_s , as closely as possible in order for a stable wormhole to be induced, we can state our speculative trans-light parameter thusly: $L_r/2 \geq R_s$.

Using the Hull Configuration Spreadsheet, the hull volume or displacement of the 100 ft. "Toltec" is 39,168 ft³ and, at a weight/volume ratio of 79.2 lbs/ft³, the ship's rest mass (m_o) is 1.4071×10^6 kg. And, it turns out that the value for L_o equals 4.205 m. The equations in steps [1] - [4] on pg. 119 (in the *Field Power Output* worksheet) may then be used to calculate the peak Field electron velocity and a corresponding value for τ , but we must first know the value for peak Field voltage. Using the method developed in WorkSheet I(a), this voltage value equals 4.93834×10^9 , or nearly 5 billion volts!

Accordingly, peak Field electron velocity is between "8- & 9-9's light": in other words, $0.999\,999\,995\,c$. [It should be noted that in performing relativistic calculations, you basically can't use *too* many decimal places!] The contingent value for τ is then 7.0711×10^{-5} . The ship's total relativistic mass is equal to $M = m_o/\tau$, at 1.98993×10^{10} kg, and $L_r = L_o(\tau) = 2.9734 \times 10^{-4}$ m. Computing the *rough* value for the starship's Schwarzschild radius, we find $R_s = 2.9536 \times 10^{-17}$ m; and, $L_r/2$ is equal to 1.4867×10^{-4} m. So, we can see that the foreshortened half-length is indeed greater than the absolute minimum safe value, but by many orders of magnitude instead of only marginally: in fact, about *five trillion times* greater!

However, if we calculate the *critical density* of an object of Chandrasekhar limit mass and Schwarzschild radius, this density is equal to 9.4×10^{18} kg/m³. Then, if we compute a relativistic density for the 100 ft. starship, neglecting its non-sphericity and assuming that its hull volume is reduced by the given Lorentz factor τ , we find this relativistic density equal to 2.5374×10^{11} kg/m³. *Now*, the limit critical density exceeds the starship's theoretical relativistic density by "only" 3.7×10^7 or 37 *million* times. To actually reach a Schwarzschild critical density, by which time we know a warp field must be induced, we must 'merely' allow the ship to apply positive reactionless acceleration a bit longer to raise its velocity just slightly above its Field impulse velocity and to lower its factor τ by $(37 \times 10^6)^{1/2}$ or 6,083 times: this will yield $\tau = 1.1624 \times 10^{-8}$ [$1/\tau = 86,028,906\,x$].

So, it would seem the latter trans-light parameter tends to indirectly verify a StarDrive vessel's ability to induce a warp field, although the first such exercise did not. And, I can't presently say *just how close* such a ship must come to equality with either parameter we developed above (the latter being preferred).

Independent Publisher
of
Quality Technical Nonfiction



Archer Enterprises

2938 Ferguson Crs. Rd.
Geneva, NY 14456
585-526-6817 / 526-5936 fax

Custom Engineering Design
and Consultation Services

Date: 3/21/02

Chapter 11 Revision Form Letter

Pages: 1

Dear Book Order Customer:

Thank you very much for your StarDrive Engineering order; I hope you find the book to be both readable and enjoyable. Please be advised that a short time after we unveiled our marketing website, we discovered a simple but significant error had been made in the relativistic math of the brief passage on pg. 267 which outlines the theoretical induction of a localized space warp. It seems that I neglected to square the Field electron velocity (v) and light speed (c) in the process of figuring the value of the FitzGerald ratio! With so much math to double-check elsewhere in the book prior to publication, much of which is actually more complicated, this error was not caught during pre-press proofing.

Many readers might perhaps overlook the difference which now exists between the corrected version of this passage, as shown below and on the StarDrive Engineering website, and the version in the First Edition copies of the book. Fortunately, we elected to produce a very small First Edition print run, and this Chapter 11 Revision Form Letter now accompanies every First Edition copy sold to give each customer the benefit of the corrected math. Unfortunately, this is the worst type of problem a publisher can have, especially when it occurs due to a seemingly inconsequential oversight.

In any event, please feel free to share with us any comments about StarDrive Engineering you may have in the future, and again I thank you for your order.

Sincerely,

Mark Tomlin

Accordingly, peak Field electron velocity is between "8- & 9-9's light": in other words, $0.999\,999\,995\,c$. [It should be noted that in performing relativistic calculations, you basically can't use *too* many decimal places!] The contingent value for τ is then 1.0000×10^{-4} . The ship's total relativistic mass is equal to $M = m_0/\tau$, at 1.4071×10^{10} kg, and $L_r = L_0(\tau) = 4.205 \times 10^{-4}$ m. Computing the rough value for the starship's Schwarzschild radius, we find $R_s = 2.0893 \times 10^{-17}$ m; and, $L_r/2$ is equal to 2.1025×10^{-4} m. So, we can see that the foreshortened half-length is indeed greater than the absolute minimum safe value, but by many orders of magnitude instead of only marginally: in fact, about *ten trillion times* greater!

However, if we calculate the *critical density* of an object of Chandrasekhar limit mass and Schwarzschild radius, this density is equal to 9.4×10^{18} kg/m³. Then, if we compute a relativistic density for the 100 ft. starship, neglecting its non-sphericity and assuming that its hull volume is reduced by the given Lorentz factor τ , we find this relativistic density equal to 3.9845×10^{12} kg/m³. Now, the limit critical density exceeds the starship's theoretical relativistic density by "only" 2.36×10^6 or 2.36 million times. To actually reach a Schwarzschild critical density, by which time we know a warp field must be induced, we must 'merely' allow the ship to apply positive reactionless acceleration a bit longer to raise its velocity just slightly above its Field impulse velocity and to lower its factor τ by $(2.36 \times 10^6)^{1/2}$ or 1,536 times: this will yield $\tau = 6.51 \times 10^{-9}$ [$1/\tau = 15,360,983 \times$].

It also seems reasonable to postulate, however, that a narrow velocity range will exist within which the desired wormhole effect is stable: on the low end of such a “safety zone”, the vessel risks “dropping out of warp” (with a bothersome loss of time and energy), and on the high end its mass risks a *rapid* ascent to certain disaster! This latter effect I feel would be a consequence of the starship’s magnetic field, which so far we have not even considered. And, at the levels of charge and velocity we’re considering, the strength of the magnetic field “corridor” associated with such a vessel will be truly tremendous! Remember what we learned about magnetic energy density in relation to the Tokamak equation?! . . .

By far the most important consideration to bear in mind, however, is that a StarDrive vessel represents an *asymptotic reactionless drive*, and therefore the ship’s ultimate velocity is *not* limited to the velocity of the electrons comprising its isometric Drive Field. Unlike any form of rocket, it is free to accelerate beyond the velocity of its “exhaust” - and to achieve an ultimate velocity *in space-time* which is only infinitesimally less than that of light. Therefore, an unmanned probe Drive Unit could be turned loose to accelerate until its relativistic mass becomes almost astronomical, and it either finds a stable warp corridor within such a safety zone or is destroyed in the process.

For now, we of great faith and dedication in the pursuit of StarDrive must presume that eventually a manned trans-light star vessel will be built and successfully launched, upon what will almost inarguably be the most important journey mankind has ever made. Even more certain will be such a starship’s absolute need for a sophisticated *sensor system* by means of which its crew may effect accurate navigation to their destination. Without the ability to steer by the very stars we seek, unlike our seafaring ancestors, these future astronauts will be utterly reliant upon the artificially-tuned properties of the Field envelope which protects them in the Void. Perhaps just as important on a personal level will be their ability to use those Field properties, which we’ll evaluate as best we can in the next two Chapters, to communicate with those they left behind - whom they won’t see for very long periods of time (and *may* not ever see again).

Assuming that even our first working starships have viewscreens, what would we actually *see* outside as the vessel approaches light speed? After all, it is only human nature to ask such a question, and interestingly enough science is able to provide an answer using traditional methods involving the optical phenomena of *aberration* and *Doppler shift*.

Aberration causes an apparent discrepancy between an object’s perceived position within an observer’s field of vision and the object’s true location. This effect is caused by the vector combination of the observer’s velocity and that of light. Technology exists today with which to measure the minute aberration of a starfield even at large nonrelativistic velocities, but at speeds extremely close to that of light this visual distortion will be enormous. The stars will appear to be heavily concentrated toward the ship’s spatial bow and to slowly slide by the vessel as they become greatly thinned-out behind.

Meanwhile, the Doppler effect will furthermore cause the bulk of the starfield to amass into a *rainbow-colored ring* ahead of the ship. The center of this ring will be totally black, because the light from it will be blue-shifted out of our visual

range of frequencies. Thus, the ring's appearance will run the color spectrum from bluish at the inner edge to reddish at the outer perimeter. Years ago, noted science-fiction writer Frederick Pohl coined the term "starbow" to describe the forward starfield's visual appearance at very-near light speed.

The first trans-light astronaut(s) will therefore probably not be able to navigate using any form of visual input above about .99c, relying instead on tremendous onboard computing power to effect navigation from a *mathematical astrometric model* that is compiled from bulk nonrelativistic data and telemetry. This daunting task is almost certain to require superconducting supercomputers to accomplish, while making a very large number of short practice jumps at first to develop and refine the actual "program" and its dependent algorithms.

In closing, I must say that (to my knowledge) *no one* knows what the actual transition between the two continuums will be like or what we will "see", except that our StarDrive ship must somehow traverse a dimensional boundary beyond the starbow wherein it *must instantaneously exist in the realm which only photons can normally inhabit* and in which time itself is essentially stopped. And this consideration, I feel, is going to take an absolute faith in the wave/particle duality of nature. Our starship is going to have to cross the time-light barrier *as a quantum probabilistic wave function*, or perhaps not at all. In this respect, one thing we *do* know from classical wave theory is that the starship's uniform standing-wave deBroglie frequency will be governed by the relation $f_{ab} = mv^2/h$ throughout such a phase transition, providing one means of assessing the special quantum mechanics involved in the "warp-jump".

It is therefore appropriate to observe that scientists not long ago succeeded in creating in the laboratory a new state of matter which actually exhibits such a standing-wave condition, in a manner which in fact *visually observable!* The temporary production of brightly-shining Bose-Einstein condensate in rubidium gas at an estimated temperature of only 20 nanokelvins, by a team of University of Colorado physicists in 1995, could be taken as a kind of absolute proof that matter may briefly exist as a pure wave function yet return to its normal state without being otherwise altered. [In this case, the standing-wave/particle energies are able to be *seen* according to the relation $E = mc^2$, at virtual absolute zero. It would also be absolutely exhilarating to determine if matter loses its inertial mass in this state!] And so, we StarDrive faithful (or at least I myself) will take this as a portent of controlled warp jumps to come, knowing something very similar *will* then take place, which in the meantime may sustain our certainty that "this too shall come to pass".

Prelude

If a man could be two places at one time,
I'd be with you. Tomorrow and today,
beside you all the way . . .

If the world should stop revolving
spinning slowly down to die,
I'd spend the end with you.

And when the world was through,
then one by one the stars would all go out –
then you and I would simply fly away . . .

David Gates & Bread

Manna

Field Resonance & Communications

Legend has it that after John Searl tested his first levity disc, which promptly disappeared skyward, he and his associates proceeded to lose well over a dozen *more* of these small (but still expensive) machines before they'd successfully "developed a form of remote control". While this might seem like a dubious assertion to many, I can easily understand how such a shocking turn of events could happen. It is really rather logical to believe that no regular radio-control arrangement could punch a reliable signal through the solid wall of "static" which the Field envelope represents *with a purely dc drive current*. A close-up photo I have showing the open central chamber of the under-construction disc seen in Fig. 6 reveals what looks like an elaborate internal electronic control system including a small tape drive, which is presumed to have had a set of pre-programmed operational instructions for device demonstration purposes. But without today's sophisticated and miniaturized digital equipment, such a 'primitive' set-up could also hardly have yielded satisfactory results.

It therefore seems quite likely that the said workable form of remote control actually involved the application of an unorthodox AC signal transmission and detection methodology, comprising the electromagnetic coupling of the field envelopes of *two similar devices* - one of which was ground-based - at a shared resonant frequency. The reason I say that a like device was probably used as a remote control unit is that a more traditional ground-based AC control-signal transmitter/receiver in all likelihood could not be made to adequately match the totally-different *output power characteristics* of the levity disc's Field. And, the fundamental difference between a radio or microwave transceiver and a levity disc or EDF Generator whose Field envelope has an AC signal component is that the latter's drive current will exhibit an **oscillatory apparent mass effect** which is synchronous with the AC electromagnetic alternations. Thus, the Fields of two separate discs or StarDrive devices which are electromagnetically coupled by an AC signal are at the same time gravimetrically-coupled!

Now, no natural macroscopic object has an apparent mass which is anything except constant, or gradually but uniformly increasing or decreasing. However, an EDF Generator's driving dc Field voltage will be *alternately aided and opposed* given the addition of a sizeable AC signal voltage, and thus the relativistic mass achieved by Drive current electrons will oscillate at the AC signal's frequency! These gravitic fluctuations, while quite small in amplitude, should be feasibly detectable even at extreme distances since gravity is the longest-range of all the forces. All we need is a suitable mass detector tuned to the exact frequency of the Drive current's relativistic mass oscillation.

I further believe that this concept explains why the SETI project and others like it have all failed to detect any evidence of extraterrestrial communications: not only are they looking for the wrong type of signal, they're also looking for it at the wrong wave velocity! In support of my contention that gravity-inducing

quantum potential vacuum fluctuations propagate at c^2 , I'd like to say that I've read somewhere in my library research travels that the interchange of energy between magnetic poles is "virtually time-instantaneous by all known methods of measurement". [Could it be that magnetism is the key to unifying gravity with the other forces, because of its intimate relationship to particle spin, and *might not a change in magnetism actually propagate at c^2 ?*]

In any case, I'd like to briefly quote from my Patent Application again if I may, to reiterate that the EDF Generator's Primary Power System may be designed and operated in such a manner that:

"a minor pulsed unidirectional or alternating voltage is superimposed upon the high-energy DC rotor current, and the external discharge current therefore acquires a discrete AC power factor, for purposes of modulating the electrodynamic characteristics of the external field during normal operation and/or for purposes of exploring the invention's potential signal communications capability in relation to intriguing new theories in high-energy quantum physics and relativity.

... It is contemplated that one possible type of communications signal which might be investigated employing the EDF Generator would couple the electric, magnetic, and gravitic forces to utilize the wave mechanics of quantum potential vacuum fluctuations ($\Delta E_q/\Delta t$), which are believed by some theoretical physicists to propagate at c^2 in order to explain the uniform operation of gravity and entropy in two space-time continuums which are coincident but completely out-of-phase. Should this quantum gravity theory prove correct, the transmission delay of a gravimetrically-coupled EM signal at this wave speed would be only .105 seconds per light year."

While the last part of this excerpt may get a little ahead of ourselves, it is still important to note that it would take *only half a second* for a message sent from Earth to reach the nearest stellar system at a c^2 transmission speed! And while this speed of telemetry is not crucial to the testing of "local" unmanned probes of StarDrive design, it will be to the men and women who risk their lives in deep interstellar flight: at times just needing to hear voice messages from home.

But what about the established principle that the electromagnetic patterns which accompany a sub-light energy signal, which can only move faster than light (as we learned in Chapter 2), cannot convey either energy or information? Traditionally, the *changes of wave pattern* which constitute the only way of doing so must always move at light speed or slower! As it turns out, a number of great sci-fi writers (like Poul Anderson) and eminent mathematicians as well have postulated that *a system of pulse-coded signals based on the operation of the Doppler effect* could be devised which obviates the normal restrictions imposed by Special Relativity. In such a manner, changes of wave pattern at phase velocity could be artificially induced to carry information, but would require continuous data decryption. Once again, this would require enormous computing power.

Regardless of whether such a trans-light signal will be amplitude-modulated (AM) or frequency-modulated (FM), it is certain to be effected at a particular AC *resonant frequency* which is a function of the StarDrive device's physical size and rotor circuit configuration. Most people today are aware that electronic devices

for communication can generally be designed to operate within a very broad range of frequencies because their component specifications may be easily tailored to select a particular wavelength band. This will not be the case with an EDF Generator, however, as the two AC circuit characteristics which wholly determine the resonant frequency - inductance and capacitance - are in this case a function of field coil and electrode array specifications which are *quite* rigid. Each size of device will therefore have a different inherent resonant frequency.

The concept of resonance, by way of a quick review, may be illustrated by the empirical awareness we have that all ordinary physical objects have a *natural frequency of vibration* depending on their mass and dimensions. A struck crystal glass or brass bell will ring at this natural frequency. A much better example of resonant frequency for our purposes may be seen in the mechanical oscillating system represented by a weight suspended on a spring which is fixed at its other end. When the weight is pulled down and released, it will oscillate up and down at its natural frequency, which is a function of the magnitude of the weight and the elasticity of the spring. If we give the weight a small tug near the bottom of each oscillation, large and continuous cycles of motion will result which will fade only after the incremental inputs cease (due to frictional resistance).

Electrical circuits which contain both inductance (L) and capacitance (C) are essentially analogous to the described mechanical oscillating system. Just as the spring alternately stores potential energy as tension and releases it as the induced kinetic energy of the moving weight, an L-C circuit alternately stores electric field energy in the capacitor(s) and releases it into the magnetic field which builds up around the coil(s). Thus, when small pulses of energy are fed to either type of oscillating system at its natural frequency, the amplitude of the resulting cycles will be at a maximum and the system is said to be in resonance.

The real reason why this effect occurs in an AC electrical circuit can be most easily explained as follows: The *inductive reactance* of a coil (X_L), or its magnetic resistance to any change in current, increases with frequency, and the *capacitive reactance* of a capacitor (X_C) - its "electric" resistance to a change in current - decreases with frequency. Therefore, a certain frequency exists at which these two reactances cancel each other in a given simple series circuit, and the only *impedance* present (or opposition to AC current flow) is the actual net resistance of that circuit. And thus, at the resonant frequency of a series L-C circuit the impedance is at a minimum and the AC line current is at a maximum.

Resonance can also occur in a parallel circuit having separate inductive and capacitive branches, although its effects are rather different. Simply put, such an "opposed" arrangement places the two branch currents nearly 180° out-of-phase, since current through a capacitance tends to lead the impressed voltage and current through an inductance tends to lag behind the voltage. Therefore, the resonant frequency will once again be that at which the two reactances are equal, but at the resonant frequency of a parallel L-C circuit the impedance is at a maximum and the AC line current is at a minimum!

The most important consequence of resonant electrical operation is that it allows the most efficient possible transfer of energy from a power source to a load, even though in the case of a series circuit the AC line current is maximized and

in a parallel circuit it is minimized. [We will presently examine how each type of resonance will be used *in the StarDrive device.*] And, the amplitude of oscillation drops off so precipitously when the input pulses are off-timed *in either case* that both resonant circuit configurations are highly selective in their frequency sensitivity, and thus are fundamental in communications signal amplifiers.

What we'll do now is figure the inherent resonant frequency for the 4ft. Drive Unit (3η), using data from the WorkSheets. This will hopefully be done in such a way that serious students would then be able to figure the resonant frequency of any size device on their own, although this would of course require generating the necessary revised WorkSheet data. We will calculate the total equivalent AC capacitance of *one Primary Power System semicircuit* first, this being somewhat less involved than the corresponding computation of its total inductance. The simple 4-step procedure which follows takes into account the slightly different method of circuit resolution that must be applied to figure this value properly, compared to the manner in which the dc series array capacitance and resultant array dc potential differences were figured {in WorkSheet VIII(a)}.

Step #1 is to first add the Ballast Capacitance (in parallel) with the outer induction array capacitance, and that of the Stat. Anode Ring to that of the inner induction array. The equivalent resolved capacitances (C_{ac1} and C_{ac2}) will then become components of the combined AC series group capacitance. The reason this is not done in the series electrode array WorkSheet is simply that the Ballast Capacitors do not pass any dc current, and thus have no associated dc circuit voltage drop, and the Stat. Anode Rings pass very little. The Ballast Capacitors and Stat. Anode Rings will readily pass any semicircuit AC line current, however, and therefore must be resolved jointly with the outer and inner induction arrays (respectively). So, from WorkSheets VIII(a), (c), and (e), we find:

$$C_{ac1} = (34,297 + 49.22) \times 10^{-12} \text{ farad} = 34,346 \mu\text{f},$$

$$\text{and } C_{ac2} = (136.87 + 49.22) \times 10^{-12} \text{ farad} = 186 \mu\text{f}.$$

Step #2 is of course to now figure the new AC series group capacitance (C_{ac3}) similar to the way it was calculated for the dc series arrays (on pg. 158), substituting the new induction array capacitance values C_{ac1} and C_{ac2} :

$$1/C_{ac3} = (1/C_{ac1}) + 1/C_{ot} + 1/C_{it} + (1/C_{ac2})$$

$$1/C_{ac3} = (1/3434.6) \times 10^{-11} + 1/C_{ot} + 1/C_{it} + (1/18.6) \times 10^{-11}$$

$$C_{ac3} = 1/(.000291 + .06772 + .06772 + .05376) \times 10^{-11}$$

$$C_{ac3} = (1/.18949) \times 10^{-11} = 5.277 \times 10^{-11} \text{ farad} = 52.77 \mu\text{f}.$$

Step #3 addresses the issue of the AC capacitance of the Field Induction System subcircuit, so we now have to calculate the parallel capacitance of the 36 unit pentode arrays associated with either rotor semicircuit. This capacitance will thankfully be just 36 times that of a single pentode array. Using data from WorkSheet VIII(c), the unit cathode area equals .057 m² and the plate separation

distance is 0.007399 m. Since $C = \epsilon_0 A/d$, $C_{upa} = 68.178 \mu\text{f}$, and C_{PA} (or the parallel capacitance of the 36 unit pentode arrays of either Primary Array) is equal to $2554.4 \mu\text{f}$.

We must now take the equivalent resolved capacitance C_{PA} and add it (in series) to *half of hull static capacitance* (C_h) to find the Field induction subcircuit's total AC capacitance (C_{ac3}) from the Emitter Ring to the rotor.

$$\begin{aligned}\text{Thus, } 1/C_{ac4} &= 1/C_{PA} + 1/C_h \\ &= (1/2454.4 + 1/11.856) \times 10^{-12} \\ C_{ac4} &= [1/((.000407432) + (.084345479))] \times 10^{-12} \\ &= 11.80 \mu\text{f}.\end{aligned}$$

Finally, in Step #4 we add the Field induction subcircuit's total AC capacitance (C_{ac4}) to the Primary Power System's total AC series group capacitance (C_{ac3}), to find the combined total rotor-and-field *hull semicircuit* capacitance C_{semi} :

$$C_{semi} = 52.77 \mu\text{f} + 11.80 \mu\text{f} = 64.57 \mu\text{f}.$$

[It is important to note here that the capacitance of the entire hull circuit, comprising both of the two such semicircuits (added in parallel), is merely *double* the C_{semi} capacitance above.]

The most direct and accurate method of figuring the *field winding inductance* of one Primary Power System semicircuit, since the Field envelope subcircuit has no appreciable inductance, still involves numerous repeated use of the equation (from pg. 38 in Chap. 4) for toroidal coil inductance: $L = \mu N^2 A / 2\pi r$. In this case, a 5-step procedure is followed which has been rendered as straightforward as possible. Two important things about this equation should be noted before we continue: (1) the denominator as given actually represents the coil's mean *length* (or circumference), and hence the length of a partial toroid winding or the axial length of a straight coil may be input instead with no real loss of accuracy; and (2) it is valid as given for single-layer coils only! The main benefit for students in careful study of this system of calculation is that a proper method of figuring the total inductance of a three-layer coil is given, including the inter-layer mutual inductances. [In all my research, I've never found another "formula" for multi-layer toroid coil inductance I thought was truly acceptable, believe it or not!]

Before the actual Steps of the method are undertaken, *the inductance of each separate layer of each size coil must first be figured* and tabulated. The variables I assigned in doing this are as follows: the inductances of each coil's inner, middle, and outer field winding layers are L_1 , L_2 , and L_3 (respectively). The outer coils' total inductance will then be a function of L_{o1} , L_{o2} , and L_{o3} , the center coils' total inductance will be a function of L_{c1} , L_{c2} , and L_{c3} , and so on. *Mutual inductances must also be computed for each distinct pair of layers in a given coil*, so there will be three mutual inductances (M) for each size coil. For the outer coils, these would then be $M_{o(1,2)}$, $M_{o(1,3)}$, and $M_{o(2,3)}$, and so forth, where $M = k_1 \sqrt{L_a + L_b}$. The total inductance of each series-aiding pair of coil layers (L_a and L_b) is equal to $L_a + L_b + 2M_{(a,b)}$.

And so, **Step #1** is to add the three separate L values (in *henries*) for the layers of a given size coil, as calculated using data from WorkSheet VII(a) {Specific Field Coil Measurements}. To get the mean layer radius needed in determining the cross-sectional area enclosed (by each layer), care must be taken to use *half of the layer's mean diameter*, as computed in the appropriate section of the WorkSheet; this measurement must then be *converted to meters*. For example:

For the outer field coil's first (inner) layer, $N = 10,000$, and $N^2 = 1 \times 10^8$;
 $\mu = 4\pi \times 10^{-7}$ (for nonmagnetic core);
 $A = 3.205 \times 10^{-6} \text{ m}^2$;
 and coil mean circumference ($2\pi R_c$) = 2.8112 m.

$$\begin{aligned} \text{Thus, } L_{o1} &= \frac{(12.5664 \times 10^{-7})(1 \times 10^8)(3.205 \times 10^{-6})}{2.8112} \\ &= 14.327 \times 10^{-6} \text{ henry} = 143.3 \mu\text{H}. \end{aligned}$$

Similarly, the value $L_{o2} = 224.7 \mu\text{H}$. However, the 3rd (or outer) coil layer has only a partial field winding, and we must know the total field turns as well as the fractional (circumferential) length of those turns before L_{o3} may be calculated. The number of field turns for each coil's 3rd layer in the 4ft. 3 η device is given in WorkSheet IX(a) {Bias Winding Turns Ratios}. This number *divided by the total number of turns in one whole layer* will yield the fractional multiplier which must then be used in the formula denominator. [All coils will have $\mu = 4\pi \times 10^{-7}$.]

For the outer field coil's third (outer) layer, $N = 5,764$ field turns (out of 10,000),
 $N^2 = 3.322 \times 10^7$,
 $A = 7.258 \times 10^{-6} \text{ m}^2$,
 and coil mean circumference ($2\pi R_c$) = 2.8112 m.

$$\begin{aligned} \text{Thus, } L_{o3} &= \frac{(12.5664 \times 10^{-7})(3.322 \times 10^7)(7.258 \times 10^{-6})}{.5764 (2.8112)} \\ &= 186.99 \times 10^{-6} \text{ henry} = 187.0 \mu\text{H}. \end{aligned}$$

Therefore, the L-value sum from this Step = $(L_{o1} + L_{o2} + L_{o3}) = 555 \mu\text{H}$.

Step #2 is to compute the mutual inductance for the outer coil's inner and middle layers, or $M_{o(1,2)}$. To do this, we will assume a realistic *coefficient of inductive coupling* of $k_i = .95$, since these layers are whole and in the tightest possible coupling relationship. So, $M_{o(1,2)} = .95 \times \sqrt{143.3 \times 224.7}$, or $170.5 \mu\text{H}$.

In **Step #3**, we'll do essentially the same thing with respect to the inner and outer layers, with two small differences: we should lower the value of k_i to .90, since these two layers are not quite so tightly coupled (being separated by the middle layer); and we must remember to *use the same fractional length multiplier* as a measure of the proportional flux interlinkage with the other whole layers of this same coil! Thus, $M_{o(1,3)} = (.90)(.5764) \times \sqrt{143.3 \times 187.0}$, or $84.9 \mu\text{H}$.

In **Step #4**, the mutual inductance of the middle (second) and outer (third) coil layers is calculated, but we'll let the value of $k_i = .95$ in this case (as these layers are once again adjacent). We must also use the partial length multiplier, as in Step #3. So, $M_{o(2,3)} = (.95)(.5764) \times \sqrt{224.7 \times 187.0}$, or $112.2 \mu\text{H}$.

Finally, in **Step #5** the sum of the individual coil layer inductances (from Step #1) will be added to *twice* the mutual inductance computed in each of the following Steps (#2 to #4). This will yield the total inductance of the given coil and, once the entire 5-step procedure is repeated for each of the other two coils, the combined total semicircuit inductance becomes the simple sum of the individual coil total inductances (figured in the three successive Step #5's). To complete the illustration of this procedural example:

$$\begin{aligned} \text{total } L_o &= (L_{o1} + L_{o2} + L_{o3}) + (2M_{o(1,2)} + 2M_{o(1,3)} + 2M_{o(2,3)}) \\ &= 555 \mu\text{H} + (341.0 + 169.8 + 224.4) \mu\text{H} \\ &= 1290.2 \mu\text{H}. \end{aligned}$$

Then, the total semicircuit inductance $L_{\text{semi}} = \text{total } L_o + \text{total } L_c + \text{total } L_i$. When the other two coil total inductances of the 4ft. Drive Unit's rotor semicircuit are computed, $L_{\text{semi}} = 1290.2 + 1609.4 + 1189.2 = 4088.8 \mu\text{H}$. For the sake of being thorough, the pertinent individual and mutual inductances are tabulated below.

outer coil			center coil			inner coil		
L_{o1}	L_{o2}	L_{o3}	L_{c1}	L_{c2}	L_{c3}	L_{i1}	L_{i2}	L_{i3}
143.3	224.7	187.0	173.2	255.9	234.1	218.5	303.4	77.5
$M_{o(1,2)} = 170.5$		$M_{o(1,3)} = 84.9$	$M_{c(1,2)} = 200.0$		$M_{c(1,3)} = 119.6$	$M_{i(1,2)} = 244.6$		$M_{i(1,3)} = 22.4$
		$M_{o(2,3)} = 112.2$			$M_{c(2,3)} = 153.5$			$M_{i(2,3)} = 27.9$

[It is important to note that, in this case, the inductance of the entire hull circuit comprising both of the two such semicircuits (added in parallel) is merely *half* of the L_{semi} inductance above.]

As we can see, this method of figuring total inductance is actually more repetitive than complex, but it yields answers which are as accurate *in this application* as those obtained by any other method I'm aware of. It should be pointed out that traditionally an average value of .80 for k_i is generally used in multi-layer coils having a large number of layers (8 or more). If the student follows the pattern established of dropping k_i by .05 for each successive layer (after the first), the method outlined above *does* yield an average k_i value of .80 at the 8th layer, yet will be much more accurate for coils with a lesser number of layers! {The reason for using an average k_i value in "deeper" coils is that the number of distinct mutual inductance layer-pairs, as used in the preferred method above, goes up according to an *N - 1 factorial sum*, equal to: $(N - 1) + (N - 2) + \dots + (N - N)$, where N = the number of coil layers. Thus, a 4-layer coil will have 6 such pairs, a 5-layer coil will have 10, a 6 layer coil will have 15, and so on. It can therefore be seen that 'my' method quickly becomes rather unwieldy after about 5 layers.}

In any event, we may now calculate the 4ft. Drive Unit's inherent resonant frequency (f_r) according to this simple relation: $f_r = 1/(2\pi\sqrt{LC})$, where f_r is in *Hz* (or cycles per second), L is in *henries*, and C is in *farads (F)*. Given that L_{semi} is equal to 4.0888×10^{-3} H and C_{semi} is equal to 6.457×10^{-11} F, we find:

$$f_r = 1/[2\pi(5.138 \times 10^{-7})] = .03098 \times 10^7 \text{ Hz} = 309.8 \text{ kHz}.$$

The first thing which should be observed about this resonant frequency is that *it is rather on the low side*, falling below the lower end of the AM radio band in the electromagnetic spectrum frequency & wavelength diagram of Fig. 61 below. The corresponding wavelength turns out to be about 968 meters. This wavelength may be computed from the standard formula for wave motion: $v = \lambda f$, where v is the wave velocity and f is the frequency. Thus, $\lambda = c/f$, because in this case (as in most) the velocity is that of light - at least in the conventional remote control transceiver arrangement contemplated earlier!

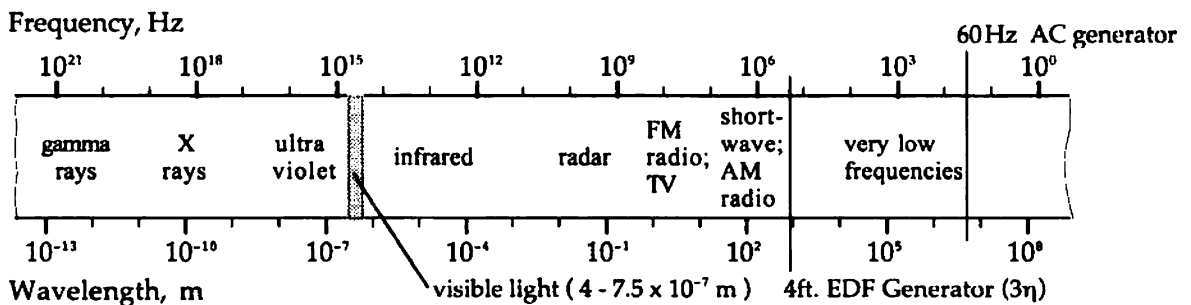


Fig. 61: *the electromagnetic spectrum*

The second observation which must be made is that the resonant frequency of the entire hull circuit, comprising two combined rotor-and-field semicircuits, *will be the same as that of either semicircuit*. This condition happens because the product 'LC' in the resonant frequency formula will remain unchanged when the *doubled* C_{semi} and *halved* L_{semi} full-circuit values (noted at the end of each respective section above) are used.

Finally, it will be instructive to verify that the inductive reactance (X_L) and the capacitive reactance (X_C) are in fact equal at the resonant frequency which we derived. Therefore, the inductive reactance $X_L = 2\pi f_r L$, and in this instance:

$$X_L = 2\pi(3.098 \times 10^5 \text{ Hz})(4.0888 \times 10^{-3} \text{ H}) = 7,959 \text{ ohms } (\Omega).$$

In similar fashion, the capacitive reactance $X_C = 1/(2\pi f_r C)$, and in this instance:

$$X_C = 1/[2\pi(3.098 \times 10^5 \text{ Hz})(6.459 \times 10^{-11} \text{ F})] = 7,959 \text{ ohms } (\Omega).$$

Thus, in a simple series resonant circuit, these reactances are equal and opposite (therefore cancelling), and the total impedance Z is merely equal to the net resistance (R). In a parallel resonant circuit, the impedance may be calculated according to the simple expression $Z = L/CR$. Typically, a series resonant circuit must be ballasted with 'extra' resistance to limit the line current, while line current in a parallel resonant circuit tends to be adequately self-limiting but may only be able to support a very small load. Each circuit type is therefore used in different ways, as we're about to see.

* * *

We must once again turn briefly to a discussion of vacuum tube theory, and especially the principle of amplification factor, as we continue examining the StarDrive Generator's communications potential. However, it is essential at this point for us to realize that the AC voltage (and current) in the Primary Power System circuit is proportional to the total stage gain an outside resonant comm signal would experience, and that the primary rotor circuit is configured for *continuous signal feedback* around each of the two parallel series-coupled loops! Therefore, any AC Field signal *or* internally-applied control voltage will feed back *in a Tesla-style cascade* unless we properly inhibit this effect!!

The most direct way to prepare us for bringing all the pieces of the proposed trans-light signal technology together in light of this unusual situation is for me to quote for a time right from the Generator's Patent Application, in the manner of a recapitulation (and for those who bypassed the Basic Specifications). We'll then be in a good position to talk further about the concept of gravimetric/EM signal coupling, as well as to look at a *basic detector arrangement* for the proposed 'exotic' comm signal and how much initial gm signal pre-amplification to expect.

"Electron vacuum tube design, construction, and operating methods . . . [may be] employed to induce, modulate, and/or amplify a minor pulsed unidirectional or alternating voltage upon the high-energy DC rotor current, and therefore on the field envelope current as well, as a means by which the electrodynamic field produced by the Generator may potentially be used (as a form of antenna) for purposes of transmitting and receiving a variable electromagnetic and/or gravimetric resonant frequency signal either to or from itself or a separate similar device (as the case may be)."

"In a 'single-stage' rotor electrical circuit embodiment of the Generator, as intended for use in an electrical and/or thermal energy output application, any such minor AC voltage present in said rotor circuit receives only a modest and single level of amplification - in a manner generally associated with a single multi-electrode vacuum tube. In a 'three-stage' rotor electrical circuit embodiment of the Generator, as intended for use in a propulsive and/or communications application, any such minor AC voltage may receive a substantial and multiple level of amplification - in a manner generally associated with a multiple number of sequentially-coupled multi-electrode vacuum tubes . . ."

"It is important to observe that both Primary Power System (rotor) field winding circuits as configured in both the single- and three-stage Generator embodiments will have an inherent AC series resonant frequency, and operation at that frequency will maximize the series field winding AC line currents (within given circuit resistor constraints) as well as the dependent stage plate voltage drops . . . which allow stage AC signal reproduction and amplification. As in traditional related practice, the series resonant frequency will be that at which the given circuit's inductive and capacitive reactances are approximately equal and opposite. Thus, the series resonant frequency of either of said Generator rotor-circuit embodiments will be largely

contingent upon the total field winding inductance and coil core permeability, as the various rotor electrode arrays and the plate resistors (92) . . . must have quite specific fixed relative design values of capacitance and resistance (respectively) – as a function of total field winding voltage – for proper overall DC and AC circuit performance.”

“Each Primary Power System control grid winding subcircuit as configured in the three-stage rotor embodiment may then [also] be readily tuned for stage AC parallel resonance at the said inherent series resonant frequency, thereby minimizing stage grid subcircuit line current while maximizing the stage grid voltage drop [across each grid resistor] which determines the level of net stage voltage gain or amplification obtained. As in traditional related practice, the parallel resonant frequency will once again be that at which the given subcircuit’s inductive and capacitive reactances are approximately equal and opposite. This condition may be achieved by connecting an optional capacitor of suitable value if desired across the secondary winding (or control grid resistor side) of each rotor stage coupling transformer (89) as indicated [in Fig. 62 below].”

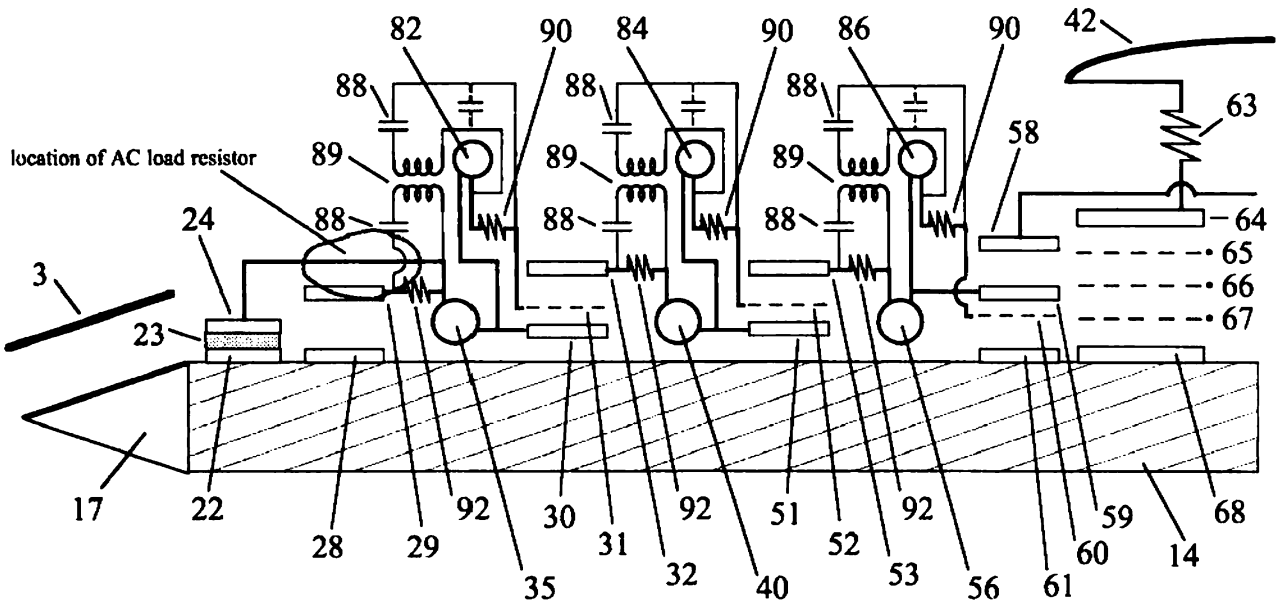


Fig. 62: 3η rotor circuit diagram (per Patent Application)**

“It may be appreciated from [Fig. 62] that each bias winding or series group thereof, its associated triode array, and a corresponding output plate resistor (92) . . . together comprise one stage of amplification of any AC signal voltage which may be present across that triode’s grid resistor (90) as an input. In this way, electromagnetic waves of one form or another from outside the external field created by the Generator may be both detected, from their influence on the waveform(s) of the field envelope current*, and amplified from within the device (when used as an aerospace vessel) . . . ”

* Note: As stated in italics, this applies specifically to local remote control via a conventional EM signal.

** An AC *primary load resistor*, which must in practice be installed in the circled area of this diagram (as in Fig. 27b of SpecSheet IX), was not shown in the Application in the interests of clarity and brevity.

“ . . . It should [also] be noted that the rotor interstage coupling transformers (89) which are depicted [in Fig. 62] . . . would be employed only in a preferred three-stage rotor embodiment, and mounted (one each) immediately above the rotating diode and transfer triode arrays ((28)-(29), (30)-(32), and (51)-(53) respectively). These transformers may preferentially take the form of continuous toroid coils on either powdered iron or nonmagnetic cores (like the field coils), having single-layer primary and secondary windings, or of one or more pairs of balanced toroidal arc-section coils and cores of similar composition which are uniformly distributed above said rotating arrays. Each transformer (89) uses two DC blocking capacitors (88) [one in-line on each winding].”

“Each rotating three-electrode system or triode array [employed in the EDF Generator] should be constructed in such a manner that it exhibits a minimum design amplification factor (μ) equal to 4.0, with reference to any AC voltage or signal present in its electrical circuit and as a function of its engineered relative electrode spacing(s).”

Initially, I selected the amplification factor of 4.0 for each rotor triode array simply because that was about the μ -factor of the example tube used in the early lessons of the RCA Tube Manual that I taught myself tube theory with. This is a very modest amplification factor as triodes go, but I don't foresee being able to make any *substantial* increases in this value, for reasons which are best discussed in Section E of WorkSheet VIII(b) {Triode Potential Differences}. It is important, however, to maximize the triode μ -factor to the extent which is practical in 3η devices. The reason has to do with accumulated distortion in the signal during continuous re-amplification across the rotor circuit. But for now, we can see by using the *stage voltage gain* formula from pg. 77 in Chapter 7 that an AC comm signal would experience a net total amplification of $[.8(4)]^3$ or about 32.8 times in a “single pass” across either series coil group semicircuit. If it is possible to double the μ -factor of each triode to 8.0, the net amplification achieved would be $[.8(8)]^3$ or just over 262 times. I prefer to think of this *single-pass gain* as the total pre-amplification obtained.

In order to understand why signal distortion would be reduced as the triode amplification factor increases, it will be necessary to take a quick look at the two common types of conventional power amplifiers of which the EDF Generator's combined Primary Power and Field Induction Sytems are a *hybrid*. First, a linear amplifier may incorporate almost any number of triode stages coupled in series fashion. The gain in signal amplitude is therefore virtually unlimited, yet the rate at which signal distortion accumulates is also very low compared to the total stage gain. A typical oscillating amplifier, on the other hand, employs continuing feedback of the signal through the same triode stage to achieve a very high total gain, but a significant level of signal distortion may also accrue in the process. In the 3η EDF Generator, the rotor's linear signal gain may not only be further amplified by the Primary Arrays, but may also then be applied as positive feedback to the rotor circuit for re-amplification! Thus, the Generator essentially constitutes a huge ***linear oscillating amplifier!***

It can now be seen that *the lower the ratio of total gain achieved to single-pass gain (or pre-amplification), the lower the total signal distortion will be.* Actually, when the pentode grid resistor values are properly selected in relation to the rotor circuit, the Generator will be able to apply *negative* signal feedback to limit the AC rotor voltage to the proper level while simultaneously maximizing the AC Field operating or transmit power (in 1 η and 3 η devices, respectively). Before the technical treatment of this topic in the last major section of DataSheet #14 is attempted, the following material from the Patent Application will be helpful.

“The bypass resistor (109) provided between each accelerator grid (66) and its associated suppressor grid (67) returns the inevitable stationary anode ring (58) and accelerator grid (66) DC circuit current to the rotor from the suppressor grids (67), and simply assists in maintaining each suppressor grid at a DC potential as close to true ground as possible. [The discharge of stored charge reserves actually takes place from the suppressor grids, which may serve as low-power electron emitters given their proximity to the primary anode rings.] The suppressor grid resistor (111) which is paralleled with said bypass resistor (109), however, is analogous to a plate resistor on behalf of the corresponding inner (rotor) induction array in both the single- and three-stage rotor embodiments, in that any rotor circuit final-stage AC output voltage variations will be reproduced across it once the field envelope current commences. Likewise, any AC signal oscillations from an outside (remote) source which are induced upon the field envelope current will [likewise] . . . be reproduced across the said grid resistor (111).”

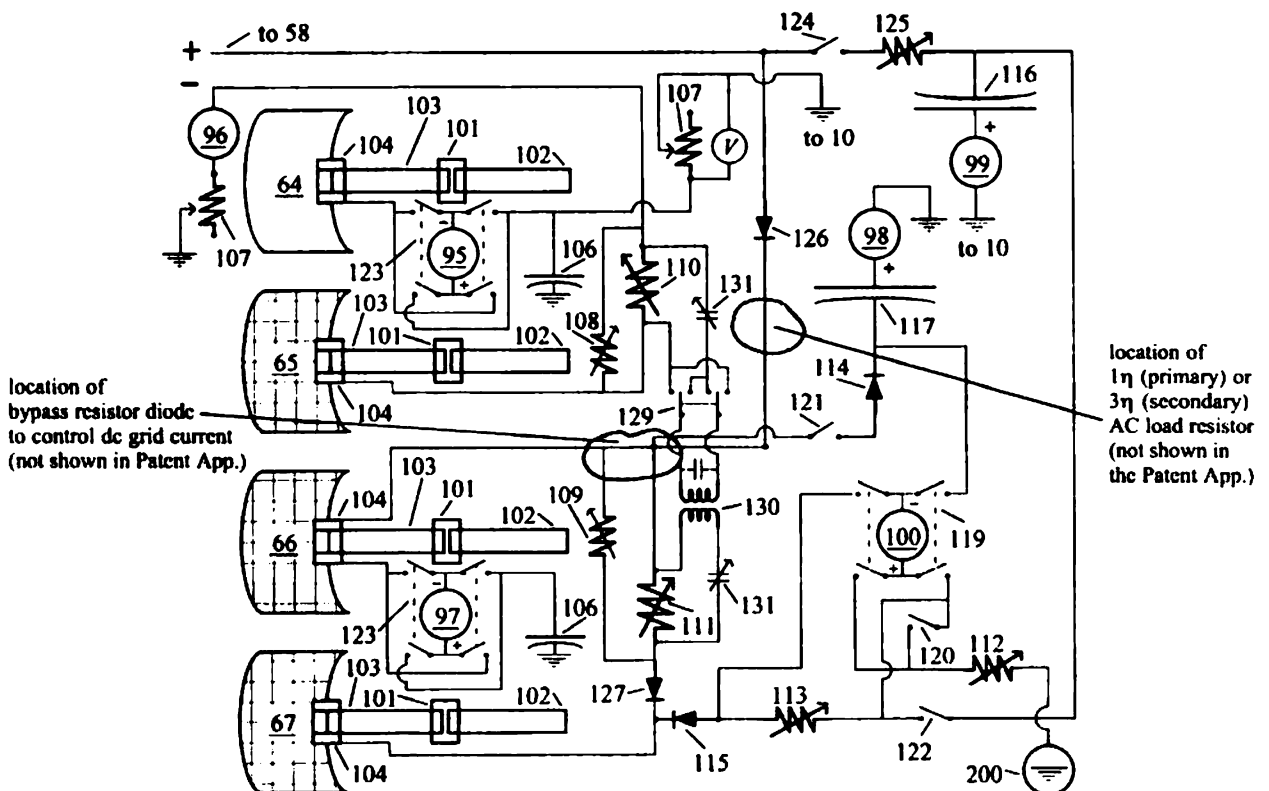


Fig. 63: unit pentode voltage control module (per Patent Application)* {see Note on next pg.}

“Therefore, any rotor or field circuit AC potential difference across this grid resistor (111) provides an output signal voltage that may be: [i] received by an actual communications console or a simple AC control-voltage operating circuit in the Generator’s central cabin; and/or [ii] reapplied either in- or out-of-phase with the voltage across the input signal resistor (110) of the associated control grid (65) as a further AC signal voltage amplification or suppression stage (respectively). An input AC signal or control voltage may also be applied across the control grid resistor (110) from such an onboard communications console or control-voltage operating circuit, as would generally apply to three-stage and single-stage devices, respectively. This grid resistor is variable for circuit tuning purposes related to resonant frequency communications . . . ”

“It can be seen from [Fig. 63], however, that the AC output amplification stage (or inner induction array) of the Primary Power Sytem and its input stage (or outer induction array) are directly coupled by the rotor segments . . . in both single-stage and multi-stage embodiments. Thus, the rotor electrical circuit as configured will be subject to continuous positive (or regenerative) feedback of any AC signal voltage present either in the field current or on the rotor, as described above. To provide a desired or requisite level of signal amplitude suppression or compensation, negative (or inverse) feedback may be applied to the rotor circuit using the feedback coupling relays (129) and stage transformers (130) shown in [Fig. 63].”

“Because plate voltage and grid voltage are typically 180° out of phase in a beam pentode arrangement such as the Generator’s Primary Arrays, inverse feedback is achieved when the voltage fed back to the control grid (65) has the same waveform and phase as the plate or anode (68) voltage. In related traditional practice, an inverse feedback signal applied to the input (control grid) current decreases AC amplifier input impedance and distortion; an inverse feedback signal proportional to the output (plate/anode) current raises the output impedance of such amplifier. Therefore, an inverse feedback AC signal proportional to the current through resistor (111) which is applied in-phase with the AC line current across resistor (110) decreases the rotor input stage impedance yet also reduces the amplitude of the AC output current. A loss of total amplification (through a fractional stage ‘gain’) results, but is accompanied by a decrease in signal distortion.”

“The stage feedback transformers (130) ensure voltage reference isolation between such stationary amplification or suppression stage and the corresponding rotor stages, when AC signal feedback across the control grid resistors (110) is necessary or desired. A double-pole/double-throw switch/relay (129) may be used to decouple each such transformer from the input signal resistor (110) side of its circuit connections, and/or to apply either positive (regenerative) or negative (inverse) feedback to the

* Note: It is important to point out that a *dc grid current control diode*, which must in practice be installed in the lower circled area of this diagram (as in Fig. 28 of SpecSheet IX), was not shown in the Application in the interests of clarity and brevity. Also, the storage shunt connected to the accelerator grid resistor junction in this same area must then be connected to the adjacent bypass resistor junction; a primary (1 η) or secondary (3 η) load resistor required in practice was omitted in the 2nd circled area.

rotor AC amplification stages(s), and tunable blocking capacitors (131) isolate the transformers from circuit DC voltages. The coupling transformers (130), isolation relays (129), and blocking capacitors (131) are therefore only necessary in Generator embodiments not having a central AC control-voltage operating circuit with suitable inverse feedback characteristics and in three-stage Generator embodiments which may be used in a communications capacity. In the latter case, an optional capacitor across the secondary or control grid resistor (110) side of each such transformer (in parallel with the said resistor) may once again be employed in parallel resonance fashion, and is indicated [in Fig. 63].”

“Each . . . “stationary” 5-electrode system or unit pentode array . . . (whose anode element actually rotates) should be constructed in such a manner that it exhibits a minimum design amplification factor (μ) equal to 12.0, again with reference to any AC voltage or signal present in the Field Induction System circuit and as a function of its engineered relative electrode spacing(s).”

Once again, I selected an initial amplification factor of 12.0 for the unit pentode arrays for a rather simplistic reason: since there are three triode arrays in each rotor semicircuit, and each has a μ -value of 4, I figured an amplification factor of 3×4 or 12 would be “about right”. Now, this happened before I learned that total rotor stage gain would *not* be calculated this way, having in mind (at that time) that the pentode gain should equal the total rotor stage gain! As it turns out this was a very fortuitous choice, however, for the grid-to-grid breakdown analyses in WorkSheet VIII(c) {Pentode Potential Differences} reveal that (in this case) it will not be possible to increase the pentode amplification factor much at all: perhaps only to a maximum of about 13.7!

Just as in the case with the triode arrays, it is anticipated that pentode control grid voltages will have to be quite a bit higher than in the data-model tube from which design criteria were derived – *assuming equality of μ -value* – because of the much-higher plate current proportional to plate voltage. Therefore, it is also perhaps fortuitous that the data-model tube (RCA #6AQ5A, per DataSheet #15), which has an amplification factor that is closer to the chosen design value of 12.0 than any tube for which a plate curves graph was included in my trusty Tube Manual, has a μ -value of only 9.5. And so, since the pentode control grid voltage as specified in the above-said WorkSheet is that which would normally be used in the data-model tube (*were plate voltages the same*), the Primary Arrays ended up having a certain amount of additional grid “muscle” built-in.

Due to considerations which arise from DataSheet #11 {Stage Plate Resistances}, the net stage gain which would be achieved by the Primary Arrays, *if used in a positive feedback manner*, is estimated at 11.82. Thus, the actual maximum signal pre-amplification possible when the rotor stages are linearly-coupled to the Primary Arrays would be equal to $32.8 \times 11.82 = 387.7$. Since this is what I have termed a ‘single-pass’ level of amplification, the total stage gain possible – given the oscillating aspect of the Generator’s primary circuit design – is absolutely enormous. Were this total gain limited to a 3-pass level, the AC signal amplification would equal $[.8(387.7)]^3$ or *about 29.8 million times!!*

Some final thoughts from the Patent Application regarding Field-effected AC signal communications in the 3η rotor device, as well as a very important operating consideration which applies to any EDF Generator which utilizes one or more AC Field voltage component(s), should be referenced at this point:

“It is important to note that the current passed by the unit pentode arrays . . . will depend to a great degree on the accelerator grid voltage . . . rather than on the overall primary array potential difference, just as in any standard vacuum tube which employs a screen or accelerator grid whose positive voltage is less than the applied plate voltage. It therefore becomes evident that this positive grid . . . voltage may also be modulated in a manner similar to the negative control grid . . . voltage. This type of ‘duplex’ signal-handling or control voltage response capability allows the unit pentode arrays (of either primary induction ring array) to amplify a resonant frequency communications signal while simultaneously controlling an independent level of current-contingent thrust [in the 3η rotor device].”

While the paragraph above is essentially a complementary recapitulation of text from the end of Chapter 7, the following paragraph states one of the most important StarDrive engineering concepts concisely enough so that technically-oriented readers will hopefully not be too disappointed if the actual operating parameters of *base Field modulation* are regrettably left unspecified at this time.

“ . . . It is postulated that the quasi-coherent aspects of the field envelope may actually be optimized through the proper control of the amplitude, frequency, and/or phase relationships between any minor AC voltage component of the field envelope current and the said minor AC current (if any) supplied by the AC power source . . . to the outer or “transflection” coils . . . (of each variable inductor array). This consideration applies to both single- and three-stage embodiments of the Generator, although it is decidedly more important in the case of the latter, and may also allow the engineered reduction of [undesirable] field radiative emissions . . . by promoting continuous and absorptive Compton effect interactions thereof with the field’s impinging drive current electrons.”

Before moving on to the discussion of EM-coupled gravimetric signal detection, I should point out that the *limit value of AC load current* in the 3η rotor device, as computed in DataSheet #14, represents only 7.36% of winding ampacity and 113.3% of the corresponding peak full-signal dc operating current (equal to .05067 amps) from WorkSheet VIII(b). However, it is also important to note that the peak full-signal dc voltage drop around each series coil group semicircuit, which coincides with full AC transmit power, represents just over 27% of peak Primary Power System voltage output (in the 4ft. prototype example). This in turn reduces not only the net dc rotor voltage available but therefore the Primary Array Voltage *and dependent Field Voltage* as well. It therefore becomes evident that AC communications activity will reduce any 3η rotor device’s available impulse drive thrust, proportional to the concomitant rise in dc rotor circuit operating current!

* * *

It is fairly easy to see how the local remote control of a 3η EDF Generator may be effected, as stated earlier in this Chapter, via the detection of electromagnetic radiation produced by the continuous oscillation of Field current in one device (as a transmitter) from the influence of that radiation on the waveform(s) of the Field envelope current of another such device (as a receiver). But, since a purely EM signal is limited to light speed, this method of communication obviously becomes less and less satisfactory as the distance between two such transceivers increases and the time lag in telemetry becomes greater and greater. This time lag grows to about 1.28 seconds even at lunar distances (3.84×10^8 m).

As I have also stated, however, such a Generator-produced EM signal will be accompanied by a synchronous oscillatory mass effect, a *component* of which is postulated to propagate at c^2 – yielding a signal time lag of only .105265 seconds per light year. This gravimetric signal component, in the form of quantum vacuum fluctuations, is theoretically detectable at huge distances provided we have “a suitable *mass detector* tuned to the exact frequency of . . . oscillation”. The inherent problem with this idea, which is by no means minor, is that no *direct* method of mass detection is known!

Scientists have been indirectly measuring the masses of *charged* particles or bodies for many years. To wit, because the trajectory of a charged particle may be bent by a magnetic field, and the strength of both the charge and magnetic field may be precisely determined, such a particle’s mass may be calculated with great accuracy. But detecting even the *presence* of neutral particles can present a difficult challenge. For example, scientists have devised a method for detecting neutrinos, which are generally considered to be virtually massless, but it is cumbersome indeed. These elementary particles may be detected in huge vats of perchlorethylene (C_2Cl_4), a dry cleaning fluid, in that their passage produces radio-argon nuclei which may be accurately counted. This detection method is used to measure the magnitude of neutrino flux from the Sun at the Earth’s surface (about 70 billion per cm^2 per second).

The only method of actually *measuring* the mass of macroscopic objects at a great distance that I’m aware of is that used by NASA to determine the Moon’s mass during the Apollo program. In this case, tracking stations on Earth beamed a radio signal to the Lunar Orbiter, which then re-transmitted that signal back to the tracking stations. By comparing the two signals using computers, it was possible to get an accurate estimate of the Moon’s mass from the magnitude of its effect on the spacecraft’s position and speed.

In recent years, a certain amount of attention has been given to the detection of gravity waves, which are predicted by Einstein’s general theory of relativity. These waves would be of a quadrature type, having two oscillatory components which would make them somewhat akin to EM waves. The predicted magnitude of these gravity waves, however, is so small as to make their *direct* detection highly unlikely with existing technology. Physicists have used radio astronomy techniques to obtain indirect evidence of gravity waves by measuring the rate of decay in the orbits of binary pulsars, which was found to be consistent with general relativity if these stars are in fact radiating gravity waves. However,

the results are still considered inconclusive due to the tremendous complexity of the calculations required.

If I understand pertinent gravity theory correctly, gravity waves will also be generated by any *rapid* change in an object's mass (Δm), its density ($m/\Delta \text{volume}$), or its momentum ($m \cdot \Delta \text{velocity}$). Thus, it would appear that an object's inherent mass does not necessarily need to change to generate gravity waves, but that such waves may also be produced when that mass's *spatial relationship changes*. This concept would also appear to support the view of quantized spatial structure (investigated in Chapter 11). This type of gravity wave, however, would be of a monopole (or pulse) nature, and the only obvious natural source of such waves as a result of rapid Δm would be an exploding or imploding star! Naturally-occurring rapid changes in an object's volume or velocity *only* would almost never happen, just as regular monopolar changes in its inherent mass do not (as stated earlier).

If we now proceed on the assumption that the synchronous gravimetric fluctuations (gm flux) which will accompany an EDF Generator-produced EM signal will far outstrip that signal in velocity and practical range, we need to devise a gm flux detector which allows the electrical reproduction of the original signal. Once again, I'd have virtually no clue how to do this without a sheer stroke of luck. In this case, serendipity took the form of an old article which appeared in the April 1986 issue of Radio Electronics magazine, by electronics engineer Gregory Hodowanec, which my former research associate Joe S. was good enough to copy for me in the "off-chance that it might be helpful someday".

While I do not exactly subscribe to the specific cosmological theory which the article's author also advocates therein, the method of monopole gravity wave detection proposed is not only fascinating but (in my opinion) quite workable as well. Believe it or not, it is based on the simple fact that a capacitor which is subjected to repeated small gravitational shocks, for instance by dropping it on a hard surface, can develop a significant open-circuit voltage across its plates! This happens because the loosely-bound plate electrons are thereby virtually "jarred" into a mild state of polarization. Therefore, *monopole gm flux which sweeps an isolated capacitor is theoretically capable of causing this same effect*. I probably would have discounted Mr. Hodowanec's claims regarding the rather amazing results obtained if not for the fact that his simple detector was *double Faraday-shielded* during the experiments, being built within an aluminum chassis which was then enclosed in a steel box!

With these considerations in mind, I am going to carefully state the following hypothesis - by means of which the mechanism whereby such a detector may electrically reproduce a gm flux signal may be most clearly understood:

When the orientation, position, or path of an electrically-charged particle is altered by a magnetic field, it could be said that changes are induced in the inertial or gravimetric field associated with such particle - because it must *immediately* move - which are proportional to the strength and duration of the magnetic field. It therefore stands to reason that when the orientation, position, or path of such a particle is altered by a gravimetric field, *a magnetic field is induced which changes proportional to the strength and duration of the gravimetric field*.

The preferred embodiment of the Hodowanec gm flux detecting circuit is illustrated in Fig. 64 below, which when EM-shielded and furnished with resistors of the proper value(s) will function as a **tuned gravity wave cavity detector**. The dual op-amp used is a common 1458 (or dual 741), with the first half acting as the basic detector stage and the second half as a buffer stage which boosts the detector's output by a factor of about 20. Potentiometer R3 merely serves to adjust the output to a desired or requisite level. *Tiny current impulses which are gravito-magnetically induced in capacitor C1 as a sensing element* are coupled to op-amp IC-1a, which is in essence a current-to-voltage converter. This op-amp produces an output voltage which is equal to the product of the input current and the value of resistor R1. The input current in this case may actually be measured in pico-amperes (or *trillionths of an amp*)!

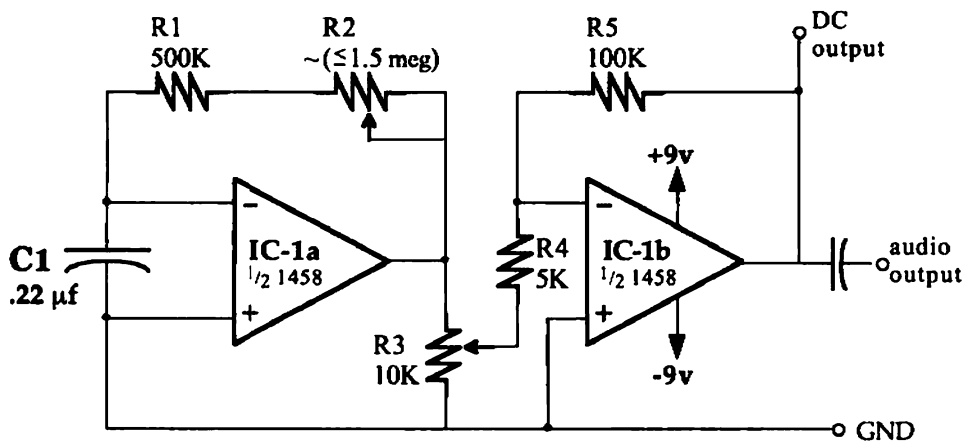


Fig. 64: gm flux cavity detector (variable f_{res} from 300–900 Hz w/resistor values shown)

The following points of observation concerning the detector schematic should be carefully considered, and are given in what I feel is the order of importance:

i) This monopole gravity wave cavity detector circuit is of the “ringing” type, and it therefore has a slowly-decaying output and an adjustable [R2] feedback resonant frequency in the range stated above when the basic resistor values shown in *this example* are used.

ii) Both the 9v power and output terminal connections are to be made through *filter-type feedthrough capacitors*, to provide complete electrical isolation. A possible upgrade of the design shown would be to use op-amps of the low-power CMOS type. Such op-amps are input diode-protected against transient or surge voltages and may allow the detector to operated unshielded.

iii) The output of the cavity detector may be coupled to an oscilloscope and/or high-impedance digital or analog equipment, and to an audio amplifier system for *voice communications*. A chart recorder can be used to plot DC output over time. *Linear input response* may be expected because the unpowered sensing capacitor maintains the detector op-amp's input terminals at virtual ground.

I wish that space permitted a proper discussion concerning the issue of increasing the gm wave detector's frequency response range, but solid-state electronics engineers much more qualified than I will easily be able to accomplish that aim. I'm sure a bit of direct experimentation with the circuit above, as a modular unit, will quickly show the experts *how to adapt and expand this basic design for increased resonant frequency, sensitivity, and power output.** As regards the fact that each size Generator will have its own inherent resonant frequency, I must remind the reader that the larger the device, the *lower* this frequency will be. Therefore, in larger and more practical devices than the 4ft. theoretical prototype, the values of resistors R1-5 proportional to the value of sensing capacitor C1 will not necessarily have to be changed that much.

* A quick thought of my own on the matter would be to try paralleling several of these two-stage units, each of which uses a much-smaller value of capacitor C1, and add a little inductance to cancel or reduce the total capacitive reactance.

Finally, it is both intriguing and disturbing to consider the following chart recorder graph, obtained by Hodowanec himself during the eclipse of May 30, 1984 using a variant of the circuit shown in Fig. 64. It shows what would appear to be a slight gm flux "shadow" which shows up about 8 minutes (!) *before* the optical shadow cast by the Sun. Regardless of the exact reason why the temporary alignment of Sun and moon produced this effect, it would nevertheless seem to lend a certain amount of credence to the notion that *some change in quantum potential* is taking place during this event which has an almost negligible time lag compared to that of light!

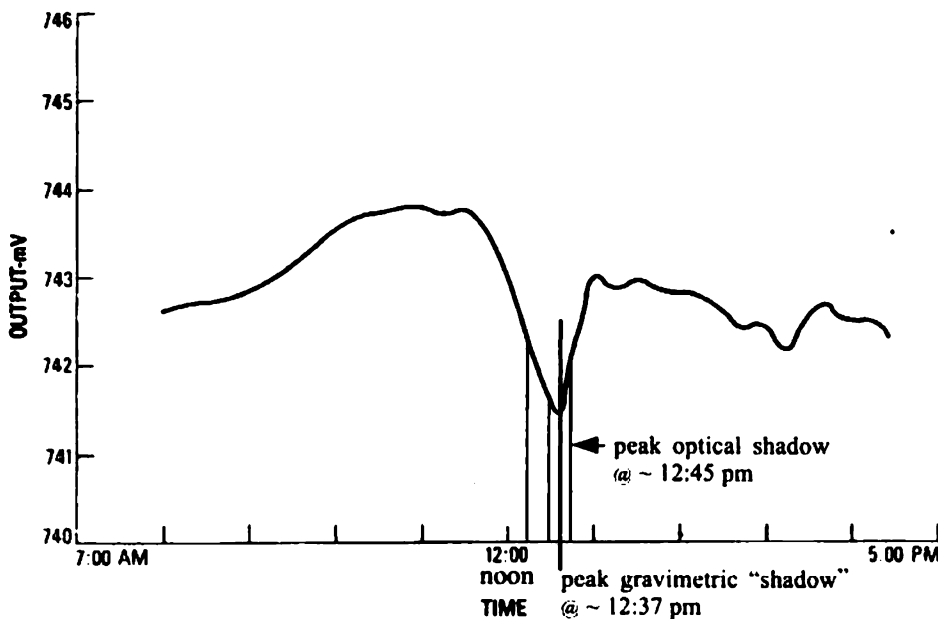


Fig. 65: *gravitic shadow effect recorded using Hodowanec cavity detector*

The field of gravity wave detection, more than quantum gravity theory itself, remains a fascinating yet largely underdeveloped territory. But I believe that the incredibly exciting possibility of demonstrating trans-light communications *is right around the corner . . .*

Prelude

Everybody, listen to me,
and return me my ship.
I'm your Captain, I'm your Captain,
although I'm feeling mighty sick.
I've been lost now, days uncounted,
and it's months since I've seen home.
Can you hear me, can you hear me,
or am I all alone . . .
If you return me to my home port,
I will kiss you, Mother Earth.
Take me back now, take me back now,
to the port of my birth . . .

Grand Funk Railroad
Closer to Home

Chapter 13

Navigation & Sensor Capability

For centuries, mariners have dared the open seas relying on familiar celestial objects to guide them on those longest of earthly journeys. They were aware that while the starmap over their heads seemed to rotate in a uniform way, the stars themselves were also virtually unchanging in their spatial relationships to one another. Especially prominent or distinctive groups of familiar stars were of course arranged into constellations, of which 88 are officially recognized today, that were routinely used in the plotting of courses. But celestial navigation is far from a simple undertaking, requiring the application of spherical trigonometry to accomplish with success. In this day of Global Positioning System satellites, it is hard for us to imagine how difficult a challenge this really was.

To take the base sightings from which a ship's course and position could be determined, the astrolabe and (later) the sextant were developed as essential navigational aids. The *astronomical triangle* is the most important part of celestial navigation, and as such comprises three points which represent the observer's position, the celestial body's position, and the Earth's pole closest to the observer. Solving this mariner's triangle using readings obtained with tools for sighting enables the derivation of a true astronomical line of position. Believe it or not, until the 1960's, submarine navigators still relied on handheld sextants to plot positions by the stars! Now, of course, sophisticated gyrocompasses and digital computers are used which eliminate the need for nighttime surfacings.

The maritime gyrocompass combines a gyroscope and special accelerometers in such a way that the gyroscope's precession always indicates the Earth's true axis of rotation - and therefore the true north pole. In an aerospace application, such an *inertial guidance system* having multiple gyroscopic elements generates signals which are related to the rate, magnitude, and direction of each gyroscope flywheel's precession, and from that data powerful computers continuously calculate the vessel's speed and course heading and any corrections which may be needed. [Advanced quasi-inertial guidance systems are currently under development, including a device which measures changes in counterrotating laser beams as a result of changes in a vessel's speed or direction.] This means of achieving highly accurate navigation without benefit of local landmarks is also eminently suitable for use in any interstellar craft of the EDF Generator design. Like a submarine, a StarDrive ship will have no windows and very limited visual input capability, if any. There just won't be much to see out there that is helpful to deep space navigation, and the vessel's crew will be utterly reliant on instrumentation to that end.

When President John F. Kennedy inaugurated the Apollo Program in May of 1961, both inertial guidance systems and the computers needed to operate them were in an early stage of development. Quite naturally, the foremost concern many scientists and engineers had about trying to land a man on the moon before the end of that decade was that these technologies would jointly not be up

to the daunting challenge presented in trying to precisely hit a remote moving target with a projectile launched from a moving departure point. At one time, this objective was aptly likened to trying to shoot a bumblebee with a BB gun from miles away! The challenge presented in trying to achieve orbit around a star which is *light-years away*, hopefully sometime in the early 21st century, will be many orders of magnitude greater.

The essence of the problem in trying to match the positions of spacecraft and and destination at some future point in time is of course that one must “aim” not at where the moving target appears to be but at where *it will be* at that future time. In the case of the Apollo moon missions, the difference between the objective’s apparent position and its future position is relatively minor and the nearness of the moon makes its true spatial trajectory readily calculable. But the apparent position of an objective stellar system is that which it had some *years* in the past, and its huge distance from the departure point makes for a potentially enormous uncertainty in its future position! An awesome level of attention to detail and computational ability will be required to coordinate the successful solution to each incredibly complex *trans-light* two-moving-body problem.

The success of the Apollo 11 mission, on which Neil Armstrong became the first human to walk another world [late at night on July 20, 1969], may seem small by comparison: but it will forever stand as a triumph of the human spirit. It demonstrated not only Man’s ability *to achieve the seemingly impossible*, as perhaps nothing else has, but also his adaptability to a hostile alien environment and his capacity to carry out practical tasks there. It is believed that 1 out of 4 people on Earth either saw or heard live telecommunications coverage of that historic lunar landing. It has also been said that no one who actually watched Armstrong step off the *Eagle’s* ladder will ever forget it. This I know to be true, for I was one of those who did. I was 11 years old . . .

So, if we’re going to attempt an historic first trans-light voyage to a nearby star system, using (of course) a StarDrive Field Generator, which one would be best to choose? No doubt the folks at NASA have some pretty well-developed mission scenarios, which are ranked according to the most logical and stringent parameters imaginable. I’m also fairly sure that many of these presumed mission profiles involve the very same local stars we’ll be discussing shortly. The reason why this should be so is the same reason why these same stars repeatedly show up in the best science fiction about manned deep space missions: a voyage to the particular stellar objective chosen must involve an optimum balance between *crew safety*, expected *scientific value*, and the potential for *finding life*.

As we look at local stars which may be of interest, we’re actually going to keep the last of the preceding criteria foremost in mind – in that we probably won’t be going to a star system which doesn’t have at least one star *of median size and age*. The reason for this directive is that scientists realize life is most likely to develop on a planet which is located in an “eco-zone” orbit, around a star somewhat like our own Sun, that receives approximately the same intensity of radiation as the Earth. Perhaps the most famous of local Sun-like stars, which may or may not have liveable planets, is Tau Ceti: a class G8V star about 11.9 lt.-yrs. distant. But a virtual twin of the Sun, Alpha Centauri A, is located much closer at hand –

in the very nearest star system to our own! So that we may become familiar not only with stars which are in fact similar to our own (and could perhaps support life), but also with those which are quite different from the Sun yet nevertheless might be of scientific interest, the following star data charts are presented.

Standard Spectral Class	Effective Surface Temp. & Color	Primary Characteristics
O	28,000 to 50,000°K blue	Stars in this group are rare, extremely hot and bright, and emit large quantities of ultraviolet radiation. They are typically the most massive and shortest-lived stars.
B	11,000 to 27,000°K blue-white	Type B stars have higher intensity helium lines in their spectra than lower groups. A typical example of a star in this group is Alpha Eridanus (Achernar).
A	7,400 to 10,400°K white	Hydrogen lines prevail in the spectra of class A stars. Sirius & Fomalhaut are typical stars of this type, which are generally still too young to have planetary bodies.
F	6100 to 7200°K yellow-white	Type F stars show elevated intensity in the calcium lines of their spectra, although hydrogen lines are still dominant. Procyon is a local example of a type F star.
G	5100 to 6000°K yellow	Stars in this group are older and have strong spectral lines of numerous metals and weaker hydrogen lines. The Sun and Alpha Centauri A are both G2V stars.
K	3700 to 5100°K orange	Type K stars have weaker violet light than red light. Spectral lines for metals remain strong. Epsilon Eridani is a near but dim K star; Aldebaran is distant & bright.
M	2600 to 3700°K red	Weak violet light and strong metal oxide lines are characteristic of type M stars, which are generally the least massive and oldest. Wolf 359 is a type M star.

Fig. 66: stellar spectral classes and characteristics

Before moving on to the chart of local stars which may be of interest, we'll take a minute to further clarify this standard spectral class designation system. As can be seen in the type G classification above, each star is also described by an Arabic number denoting its *temperature subclass*. There are ten subclasses for each letter-designated class: these are ordered from 0 through 9, with 0 being the hottest and 9 the coolest (in the appropriate range). [So, the Sun's surface temperature, as a G2 star, is easily figured at 5,800 °K, although textbooks generally just round it off to 6,000 °K.] Then, the subclass is followed by an upper-case Roman numeral denoting the star's *luminosity class*, which actually reflects its relative size. There are six such rankings for all stellar classes:

I = supergiant; II = bright supergiant; III = giant; IV = subgiant; V = dwarf; VI = subdwarf.

This letter/number/numeral system provides a handy means for distinguishing or comparing different stars at a glance: the Sun, for instance, can now be seen as a normal (dwarf) star which is a bit hotter than average for its class. *Relative brightness* is the only other stellar attribute we need discuss for present purposes.

Stellar brightness is ranked on two related scales: *apparent magnitude* and *absolute magnitude*. Apparent magnitude is a measure of how bright a given star appears to be as seen from Earth. Early astronomers devised a logarithmic scale of apparent brightness, for stars visible to the naked eye, having 6 orders of magnitude. Thus, the brightest stars had apparent magnitude = 1, and the faintest had apparent magnitude = 6. Each increase of 1 in apparent magnitude corresponded to a *decrease* in apparent brightness of about 2.5 times, so an increase of 5 magnitudes represented a decrease in brightness of about 100 times. The brightest stars therefore appeared about 100 times as bright as the faintest stars they could see without telescopes. [Each change in magnitude of 1 has since been calibrated to exactly equal the fifth root of 100, or 2.5119. The Hubble Space Telescope can distinguish stars as faint as the 28th magnitude, representing a star which is $(2.5119)^{22}$ or 631 *million* times fainter than can be seen with the naked eye!]

Absolute magnitude, or *intrinsic brightness*, is a measure of a star's actual luminosity, or how bright it would be at a standard distance of 10 parsecs: each parsec equaling 3.264 lt.-yrs. A similar logarithmic scale as above applies to absolute magnitude and, as was found to be the case with apparent magnitude, some stars are so bright they actually require a *negative* magnitude number. Some stars therefore have an intrinsic brightness which is tens of thousands of times less than the Sun's, while the actual luminosity of certain stars may be over a hundred thousand times that of the Sun. [Stars are known whose brightness corresponds to an abs. mag. = -8, while others having an abs. mag. = +16 or fainter have been detected. The nearby star Wolf 359, shown in the chart below, is nearly the faintest star known.]

star name	distance (lt.-yrs.)	abs. mag.	spectral class
Sun (Sol)	-	+4.85	G2V
Alpha Centauri A	<4.40	+4.36	G2V
Alpha Centauri B	<4.40	+5.69	K4V
Proxima Centauri	>4.23	+15.49	M5.5V
Wolf 359	7.80	+16.56	M5.8V
Sirius A	8.61	+1.46	A1V
* Epsilon Eridani	10.50	+6.19	K2V
* Procyon A	11.42	+2.66	F5IV-V
* Tau Ceti	11.90	+5.69	G8V
Altair	16.79	+2.21	A7V
Fomalhaut	25.09	+1.74	A3V
Vega	25.32	+0.58	A0V

Fig. 67: *local stars of interest (in order of increasing distance)*

There are many more known stars within 12 lt.-yrs. of 'home' which are not included in this listing. Nearly *all* of the listed stars, however, have been highly popularized in sci-fi literature. Those marked with an asterisk (*) are the three local stars most touted by UFO groups as the alleged home stars of alien races.

The big question at this point, given our earlier criterion of trying to find life, is just this: Do the real experts in astrophysics feel that *any* of these stars actually have planets which might merit investigation with that objective in mind? We're going to find some pretty surprising answers in just a bit, but first we need to understand the present state of scientific planet detection.

Even using the Hubble Space Telescope, it generally isn't possible to visually confirm the presence of extrasolar planets: they're just not luminous enough. The most successful indirect method of detection to date involves calculating the magnitude of perturbations in a star's motion which are caused by the presence of a planetary mass. Because a planet's orbit is not perfectly circular, it causes the star itself to describe tiny oscillations in its motion relative to Earth. This causes the star's light to exhibit minute Doppler shifts, from which the size and speed of the star's induced 'wobble' may be ascertained. Based on this precession, a *rough* estimate of the size of the planet and the size of its orbit may be obtained.

As of 2000, 30 extrasolar planets had been documented but, not surprisingly, all are at least as large as Saturn and their orbits are far closer to their star than would be considered normal. Thus, not only would their own gravity preclude the presence of life as we know it, but their stellar proximity would likely place them in an inhospitable "torch" orbit (like Mercury or Venus). The analytical detection method presently employed is therefore insufficiently precise to allow confirmation of the presence of smaller planets as yet.

On a more positive note, many astronomers believe that nearly every Sun-like star will have a solar system associated with it at some point in its life cycle. This does *not* mean, however, that it will have solid planetoid bodies in stable orbits: a large percentage of such systems may comprise only clouds of dust and gas, icy comets, and belts of asteroids, as well as the ubiquitous and unlivable gas giants. Nevertheless, let's take a closer look at the four best candidates from our condensed list of nearby stars which might have solar systems, and see which (if any) warrant a manned trans-light mission. These four stars, as one might imagine, are: Alpha Centauri A, Epsilon Eridani, Procyon A, and Tau Ceti.

Alpha Centauri is actually a triple star system, with Proxima Centauri as the third star (alternatively known as Alpha Centauri C). [About half of the 30 stars which are closest to the Earth reside in multiple systems, with the suffixes A, B, and C denoting progressively lesser brightness.] Proxima Centauri – which is actually *the* closest star to the Earth – would almost certainly be interesting enough to merit an *unmanned* trans-light mission, in order to gather data and test the StarDrive technology in much the same way that unmanned Apollo missions 4, 5, and 6 were used to test the launch vehicle and command module systems. This dim red dwarf star has a very high rotation rate and consequently an unusually high magnetic field. It is also a "flare" star, however, and is subject to sporadic bursts of intense radiant energy: suddenly increasing in brightness by up to 100% or more for a few seconds or minutes before settling down! Thus, it is extremely unlikely that this star harbors any life, and there could be a safety hazard involved were such a mission to be manned. With hyperlight telemetry, though, it should be possible to choreograph a safe fly-by of the whole triple system, thereby maximizing the scientific value derived.

Alpha Centauri A is a “main sequence” star like the Sun, meaning it is in the first phase of its nuclear fuel cycle (wherein it fuses only core hydrogen). It is also roughly the same size as the Sun, although it is about 57% brighter, and is approximately the same age. Even so, scientists at one time did not rate it as a likely candidate for harboring life, even if it has one or more planets (which to date has never been established). Their reasoning was that Alpha Centauri A and B orbit each other so closely that the resultant tidal effects on any planet present would be drastic enough to be unfavorable to the formation of life.

It is now believed, though, that life on an eco-zone planet orbiting either star is nearly as likely as it is on Earth! The smallest distance separating these two stars (the “periastron” distance) is 11.43 AU or over 11 times the distance from the Sun to the Earth. By a standard astrophysics axiom, any planet which is closer to either Alpha Centauri A or B than *1/4 of the periastron distance (or 2.86 AU)* would be in a stable orbit. Since 2.86 AU is also greater than the eco-zone orbit radius of either star, an eco-zone orbit around *either* star would be stable! The eco-zone orbit of Alpha Centauri A is 1.252 AU, with an orbital period of 1.34 years. Alpha Centauri B’s eco-zone orbit is .679 AU (or about 94% of the size of the Venus orbit), with an orbital period of about 222 days. Therefore, this closest of all extrasolar star systems could be seen as presenting an almost irresistible allure: as the goal of an historic first manned trans-light mission.

While Epsilon Eridani doesn’t even come close to making the list of brightest stars, it is visible with the naked eye (to the upper right of Orion’s belt). It is also the 9th nearest stellar system, including systems which have only one star. This main sequence star has about 85% of the mass of the Sun and nearly 87% of its diameter, yet is just under 30% as luminous as Sol. Therefore, its eco-zone orbit is a mere .54 AU, with an orbital period of only 157 days. Interestingly enough, Epsilon Eridani recently became *the nearest star confirmed to have any planets*: a supposed gas giant with an estimated mass of about 1.2 times that of Jupiter. This planet resides in a mean orbit of 3.4 AU from the star, with an orbital period of about 6.8 years. [Such an orbit is equivalent to one within the outer portion of our own asteroid belt.] While there is also some indirect evidence of a second planet, it would appear to orbit at an even greater distance from the star.

As was mentioned way back in Chapter 2, Epsilon Eridani has at times been reputed to be the home sun of a star-traveling race. It is also interesting to note that this star is ascribed as the home sun of the planet Vulcan in Star Trek™ lore. However, neither scenario is any more *unlikely* than the other, for Epsilon Eridani is now known to have a protoplanetary debris disk which is quite consistent with models of the very early Sol system. Its age has been shown to be *no more than a billion years*, and so the existence of *any* complex life there is a virtual impossibility – even if another planet exists right in the eco-zone.

Procyon A is the 8th brightest star in Earth’s sky, and may be seen slightly ahead of Sirius, in the constellation Canis Minor. It is the 14th nearest stellar system (inclusive of systems having only one star). Procyon A is somewhat distinctive in that it is unusually bright for its color, and is more massive than average for its spectral class (1.78 solar masses). In fact, spectroscopic analyses

reveal that it is probably at least as rich in heavier elements as the Sun. Its surface temperature of 6700°K makes it about 15% hotter than Sol, and it is generally believed to already be in the process of leaving the main sequence (and beginning to fuse non-core hydrogen). While this would mean that it is slowly expanding toward subgiant status as it grows hotter, hence its dual luminosity class designation in Fig. 67, it does *not* necessarily mean that it is older than the Sun. Nevertheless, thousands of years ago it was almost certainly somewhat cooler and smaller, and a planet much farther from its surface than the Earth is from the Sun could perhaps still have the conditions necessary for harboring life.

To compute the approximate eco-zone orbit distance of any star in terms of astronomical units (AU), we first need to find that star's *relative luminosity in solar units*. This is done by raising the base magnitude increment of 2.5119 to a power which equals the difference in absolute magnitude between the Sun and the object star. Therefore, Procyon A's intrinsic luminosity is 7.5 times that of Sol $[2.5119^{(4.15 - 2.66)}]$.^{*} The rough eco-zone orbit distance in AU is then simply equal to the *square root* of the relative luminosity (in solar units) – since the luminosity falls off with the square of the distance. So, Procyon A's eco-zone planetary orbit would be at about 2.74 AU and would be equivalent to an orbit lying almost 3/4 of the distance from Mars to Jupiter. The orbital period is a little harder to figure; but for an orbit *with negligible eccentricity*, the orbital period $P = (r^3/M)^{1/2}$, where r is the radius of the planet's orbit in AU and M is the star's mass in solar units. Thus, since Procyon A's relative mass is equal to 1.78 x Sol, $P = 3.4$ *Earth years*.

However, a relatively simple analysis of bulk stellar evolution data reveals that Procyon A's probable *main sequence* age is only just over 2 billion years: and unfortunately, this is less than the generally accepted length of time it took on Earth for complex multicellular organisms to arise!

In fact, an equally insuperable problem in this case is that Procyon A is *very* closely orbited by its binary, Procyon B: a star that is probably of about the same age but *which has already collapsed into a white dwarf*. These binaries orbit each other in approximately 41 years, placing Procyon B's orbit just 9.54 AU from Procyon A at periastron. [As it turns out, this orbital distance is exactly equivalent to Saturn's.] In this case, though, such a close relationship *would* greatly disrupt the orbit of a planet in Procyon A's eco-zone: because $1/4$ of $9.54 = 2.385$ (recalling the Alpha Centauri example), and this is significantly *less* than the eco-zone orbit distance of 2.74 AU, the eco-zone orbit around Procyon A would in fact be unstable – and any planet therein would soon drift off into interstellar space! Moreover, any planet which might orbit Procyon B at less than 2.385 AU could not have developed highly-evolved life forms unless for some remote reason it is actually *far older* than Procyon A: and any non-starfaring race that arose there would have been destroyed when the binary entered its red giant phase.

All things considered, it therefore seems entirely unlikely that an advanced civilization could have developed or even based itself in the Procyon system, and a manned trans-light mission thereto would seem justifiably unwarranted.

*** Important Note:** When the object star's abs. mag. is *greater* than the Sun's, the exponent here will have a negative value (as the star's abs. mag. must be subtracted from the Sun's). The base magnitude increment must then be raised to the *absolute value* of this difference-derived exponent, and the reciprocal of the result must then be taken – yielding the correct multiplier.

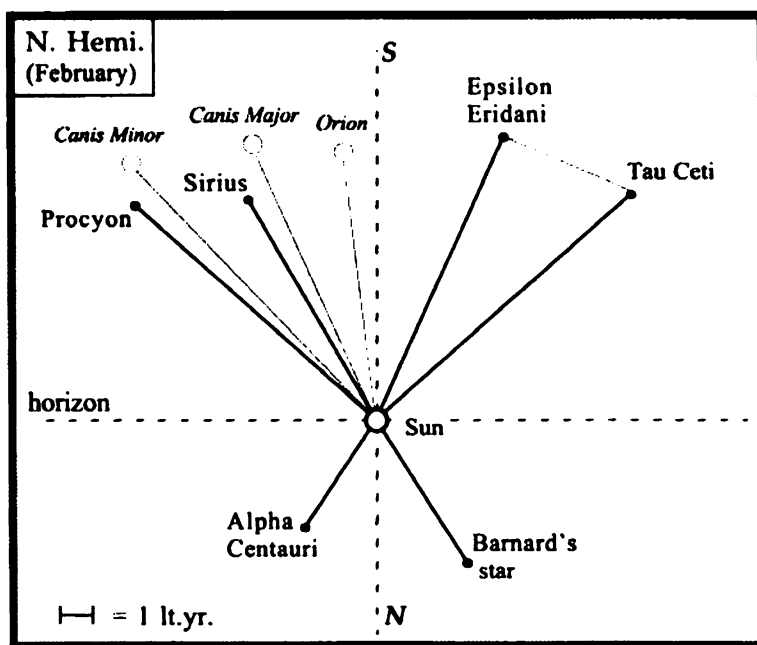


Fig. 68: *skymap of local stars discussed (w/ Orion as reference)*

This local skymap was created especially for *StarDrive Engineering* based on 3D stellar imaging courtesy of www.solstation.com. The distance of each star relative to Sol is to scale, as is that between Epsilon Eridani and Tau Ceti.

Tau Ceti: It's really not hard to say why this otherwise undistinguished G8 star has been the object of so much interest, from science fiction writers and astrophysicists alike, for over 40 years. As one's general knowledge of astronomy grows, one becomes aware of how truly rare Sun-like stars are in our local corner of the galaxy. One fundamental reason for this scarcity is that peripheral portions of the galaxy (like ours) are comprised mostly of old class M red dwarfs, which are generally considered unlikely to harbor life – as are the less common young and hot stars of class A or higher. Astronomers therefore limit their considerations of which systems may have planets with life to stars of class F, G, or K. So, we can see that our two last interstellar mission candidates and Tau Ceti jointly represent each of those preferred classes; but it would seem only the latter star remains a viable choice, and it happens to be the second-closest class G star (after Alpha Centauri A). Other than the local stars on our list (from Fig. 67), there are 8 class K stars within 20 lt.-yrs. of Earth, the closest of which is 61 Cygni (@ 11.44 lt.-yrs.). But, there are only 4 other class G stars within 35 lt.-yrs., the next-closest being Eta Cassiopeiae (@ 19.43 lt.-yrs.).

In fact, Tau Ceti and Epsilon Eridani were the subject of the first SETI experiment, in 1960. This attempt to detect non-random radio signals from what were thought to be the two likeliest nearby sources lasted for four months, but was unsuccessful. Interestingly enough, these two stars are only about 5.5 lt.-yrs. from each other, and are in fact quite similar. With a surface temperature of about 5200°K and a mass = 0.81 x Sol, Tau Ceti is both cooler and smaller than the Sun. It therefore has only about 46% of the Sun's luminosity, and has an eco-zone orbit of .679 AU (or 94.3% that of Venus) with an orbital period of 227 days.

However, its enrichment with heavier elements including the various metals is estimated at only 36% of Sol's, whereas Epsilon Eridani's is 58% and Procyon A's almost double that – and this figure has a bearing not only on the system's ability to develop solid planets suitable for life but also on *the star's projected main sequence age*. As we've seen, a candidate star's age can become a major determining factor in the search for extraterrestrial life, and any error in the star's 'metallicity' percentage or calculated distance will contribute to the uncertainty in its most probable age.

The two best estimates of Tau Ceti's stellar age seem to agree that it is about 3.2 billion years old, or 70% as old as the Sun, and should have 15 billion years remaining in its main sequence lifetime. Happily, the former time span is (at last) enough time for complex life forms to have evolved, even if not to the same degree as here on Earth. Moreover, astronomers have failed to find giant planets *in inner orbits*, which actually improves the chances that smaller and more habitable worlds may occur there. All things considered, the enticing Tau Ceti quite likely constitutes the best candidate for a second and longer warp jump (after that to Alpha Centauri) in any voyage of under 20 lt.-yrs.

The next section of this chapter is going to take a somewhat less prosaic course which I think will be refreshing. So, our story will proceed for a time in the form of a *narrative pre-creation* of an actual trans-light mission to Tau Ceti! This little sketch will hopefully tie together everything we've discussed thus far, while pointing out some important new considerations which are rather fascinating. It presumes that men of vision like former President Kennedy will see to it that a 60 ft. starship is funded and built for this historic trans-light voyage, as part of an ongoing StarDrive program wherein progressively larger ships are built and tested over ever-increasing distances. Perhaps you feel as I do, that such a plan represents the best hope for the dignified long-term survival of our race . . .

The time is T minus 135 minutes, and I am sitting in the StarDrive vessel *Athena*: an Antares-class ship which is the largest such vessel ever built to date. [See the *Manned Vessel Design DataSheet*, on pg. 107.] I'm the science officer aboard for this planned voyage to the Tau Ceti system, and the mission commander is about to initiate powered rotation of the ship's massive rotor assembly. At T minus 132 minutes we'll begin the ship's 2.2 hour pre-launch cold start, here at the NASA Flight Research Center located at Edwards AFB (on Rogers Dry Lake) in California. During this time, I'll be able to provide you with some basic facts about the ship and about the successful first manned trans-light voyage to Alpha Centauri which gave this present mission a "green light".

The *Athena's* displacement is 8,460 cubic feet and her weight is 335 tons. Each of her 32 drive motors is rated at 190 output horsepower, for a total of 6,088 hp to turn the rotor – which weighs almost exactly 50% of the weight of the entire craft. As a good comparison, the largest steam locomotives ever built weighed about 300 tons and developed about 7,000 hp. By the way: the required start time (T_w) for any StarDrive device of 20 ft. in diameter or more is computed from the following formula: $T_w = 141 \text{ seconds} \times (2R_k - 4)$, where R_k is in feet. The total hp required is that which yields this start time, given the rotor's mass.

While an Antares-class vessel is rated to carry a maximum crew of 5, on this mission the *Athena* will carry a crew of only 3 – due to the fact that our cargo capacity is quite limited and the mission profile calls for a total round trip duration of 2.6 years! But before we talk about how this voyage's elapsed time was calculated, it will be necessary to clarify how mass, force, acceleration, and kinetic energy “behave” in negative quantum time-space. Then, I can illustrate these characteristics for you using data from the Centauri mission.

The most curious piece of the trans-light navigational puzzle, believe it or not, can be expressed as simply as this: Do we, or do we not, continue to apply *positive thrust* right on through the supralight velocity transition (to spatial warp), until the exact middle of the entire distance *each way*? If so, we would then need to execute a single “turnaround” maneuver in each half of the entire round trip, to begin *decelerating* for the remaining half of the distance to the destination: thus maintaining a constant apparent onboard gravity throughout the trip.

To answer this seemingly innocuous question, we need to expand on the work of physicist O. M. Bilaniuk which was first described way back in Chapter 2. Bilaniuk found that for relativity to be ‘uniformly’ applied to two coincident continuums, the kinetic energy of an imaginary mass object has to be *inversely proportional to its velocity*. This is, of course, the exact “reverse” of the fact that kinetic energy in our continuum is proportional to velocity. In order to answer the puzzling turnaround question above, care must now be taken to reason correctly from this simple axiom as a starting point.

What he is *first* implying here is that the *faster* an imaginary mass object moves (toward c^2 as a maximum), the *less* negative energy it has; and, that the *slower* such an object travels (toward the value of c as a minimum), the *more* negative energy it has. The trickiest part comes next, in interpreting how an imaginary mass will respond to the application of force – given the reverse kinetic energy property described above. Bilaniuk found, accordingly, that the slower an imaginary mass object moves, the harder it is to force it to move any slower. And, this is a direct corollary to the relativistic increase in positive mass as a normal object approaches the limiting speed at which its kinetic energy has the greatest *absolute value*.

Therefore, an imaginary mass object will go faster when a negative acceleration (or braking force) is applied, and will slow down – thus approaching light speed “from above” – when positive thrust or acceleration is applied. And so, it would appear that our StarDrive vessel must actually execute *a total of 3 turnaround maneuvers* in any given one-way warp jump voyage! The resultant **warp jump turnaround sequence** is illustrated on the next page.

I've found that (for me at least) this interpretation of turnaround sequence may be more clearly understood by means of two simple equations from traditional wave mechanics. The first is: $v = f\lambda$, where v is wave velocity, f is frequency, and λ is wavelength. The only other relation needed to resolve this issue is the de Broglie equation $\lambda = h/Mv$, where h is Planck's constant, M , is the total relativistic mass, and λ is the mass object's wavelength. Thus:

- i) to increase our starship's apparent supralight velocity with respect to the space-time continuum, its wavelength must increase, because its

frequency must remain constant throughout the transition to a “rarer” (higher-velocity) medium [as follows from the first equation];

ii) to increase its λ , the starship must in turn decrease its relativistic imaginary mass (and negative kinetic energy) *as its velocity climbs* [as follows from the second equation]; and therefore

iii) to decrease its relativistic imaginary mass, we must effect the gradual controlled release or decrease of the inherent (positive) kinetic energy the starship *gained during sublight acceleration* (m_i), via the application of reverse thrust or negative acceleration.

To reiterate, we can now see that to gain apparent velocity in hyperspace, we must actually apply braking thrust, and to decelerate therein we must apply ‘forward’ thrust! Moreover, to keep our apparent onboard gravity the same, we should certainly try to follow this “backwards” format while maintaining a constant level of subjective thrust. So, our trans-light ship will have to execute a total of three *180° forward rolls* as follows: 1) once, while accelerating past $v \approx c$; 2) a second time, at the very midpoint of the distance one way; and 3) a third time while decelerating past $v \approx c$.

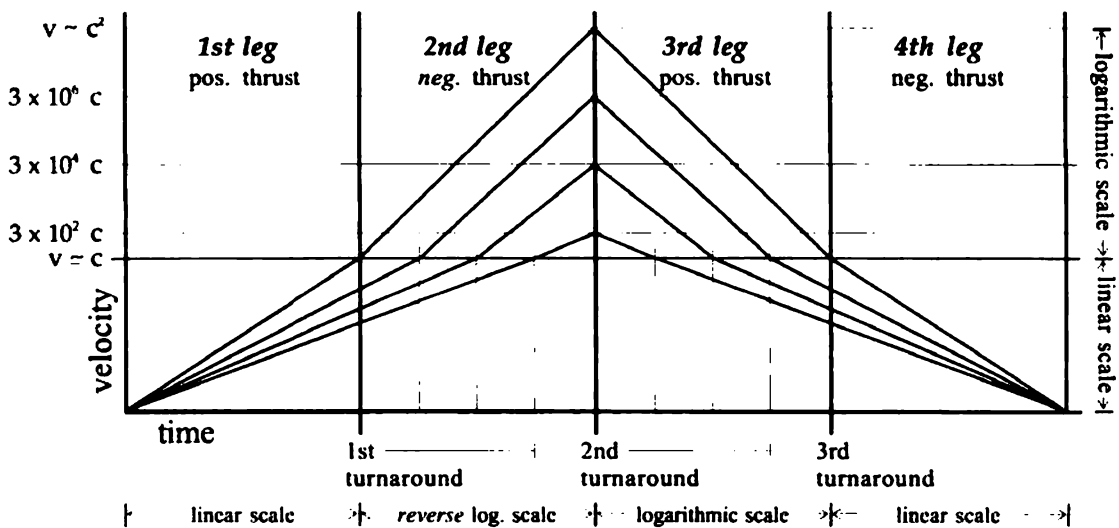


Fig. 69: warp jump turnaround sequence graph

The most important concept to bear in mind as we analyze this graph, which has certain unavoidable limitations, is that the StarDrive vessel’s velocity is assumed to rise as linearly toward light speed as if relativity were not operative! While this may sound like absolute heresy to some, it must be borne in mind that the objective mass of all Field electrons will rise in phase with the relativistic rise in the ship’s mass, yet they must gain a *separate subjective* relativistic velocity across the Field *for which they pay the freight*. Thus, the graph is correct in its rendering of such a ship’s *linearly changing velocity over time*, although I’ve been told that this may only be acceptable for some when it is simply characterized *as an instantaneous consequence of relativistic time dilation*.* Let’s face it: if this weren’t so, the StarDrive vessel would never achieve trans-light speed . . .

* [This linear acceleration phenomenon may be proven with a simple thought

experiment. If we postulate my buddy at Cornell tending his cyclotron, in which a bunch of high-energy electrons are rotating at near light speed, he will *not* observe them to suddenly start slowing down and inexplicably losing all their relativistic kinetic energy if, unbeknownst to him, we accelerate him and his lab to near light speed!]

With the said crucial (and sure to be disputed) observation in mind, we may now state the most important precept of trans-light acceleration (after the Bilaniuk reverse kinetic energy axiom described above). This precept is based (thank God) on the Conservation of Energy principle, although the fact that it is *correlative* with the observation above may still present a problem for some. Nevertheless:

Since the starship's speed will increase on a linear scale from $v = 0$ to $v \simeq c$, we must assume that under exactly the same *subjective* uniform acceleration the ship's speed in the time-energy continuum will increase linearly from $v \simeq c$ to $v \simeq c^2$ during a period of time which is exactly equal to that in which the original sublight acceleration was applied.

What I'm saying here is that we cannot perform more *work* in the time-energy continuum in accelerating our ship and raising its kinetic energy than we did in the space-time continuum. If we spend just a bit longer accelerating in hyperspace at $1g$, let's say, than we did accelerating at $1g$ from rest to light speed, the ship would reach $v = c^2$ and probably erupt like a temporary quasar! Not only can this be seen directly from the graph, but it can also be deduced that extremely long missions may require a period of time under zero thrust (and hence zero gravity), because further acceleration is not possible. I can't conceive of any practical reason why we would need to travel *that* great a distance, because (as we'll see) spending more than *an hour or two* accelerating in hyperspace causes one's velocity and time displacement to mount fantastically.

Now, we can discuss what was learned on that historic first trans-light mission to Alpha Centauri, although any data pertaining to the presence or absence of *life* in that system are still highly classified! Perhaps the gravest concern among the chief engineers at Mission Control was: would the mission's Vega-class vessel *Ariadne II* have enough electron "fuel" to decelerate into a stable system orbit wherein the ship could recharge its superconducting storage rings for the return trip? If the vessel's *Field leakage rate* was too high, it might not be able to do so and could sail right on by into deep space and be lost.

Saturating the ship's storage rings was not a problem. In fact, the best way to do this is actually to orbit the Sun for a time before leaving the solar system, and charge the rings with electrons pulled directly from its outer atmosphere! The key factor involved was the accuracy with which the Field leakage rate was measured, during the innumerable operational tests that were done. After all the numbers-crunching was over, the following scale for the Field leakage rates of manned vessels was adopted (*in parts per million of total operating Field current*):

<u>40 ft.</u> : .07 ppm	<u>50 ft.</u> : .06 ppm	<u>60 ft.</u> : .05 ppm	<u>70 ft.</u> : .04 ppm
<u>80 ft.</u> : .03 ppm	<u>90 ft.</u> : .02 ppm	<u>100 ft.</u> : .01 ppm	

Now, the 40 ft. ship has a peak rotor current $I_{rt} = 11.9394 \times 10^5$ amps. Its standard operating current is 10/11 of this figure, or 10.854×10^5 amps, so the *Ariadne II's* Field leakage turns out to be .076 amps (coul/sec). *This amperage times the total one-way trip length in seconds equals the total coulombs of charge needed.* [This assumes, of course, that one's navigation is sufficiently accurate to allow recharging from the destination star before it becomes a critical problem!] Getting a little ahead of ourselves here for a bit, the outbound mission duration was 472.065 days at 8.64×10^4 sec/day or 40.7864×10^6 seconds. This makes the estimated total electron leakage a staggering 3.1 million coulombs!

This figure actually isn't as terrible as it sounds, for each superconducting storage ring will hold up to 800,000 coulombs in the form of a zero-loss current. Therefore, the total Field leakage anticipated on each half of the round-trip voyage is equal to the capacity of 3.875 storage rings, and so the 40ft. *Ariadne II* was designed to incorporate a total of four current storage rings. It is important to note, however, that to reduce Field leakage to the levels shown in the table above, it was found that the thin outermost edge of the hull's Emitter Ring had to be parabolically faced with a special ceramic material (Titania 193).

At any rate, by now I'm sure you are all impatient to know just how the Alpha Centauri outbound mission duration was calculated. The nice thing about this computation is that, for once, it is actually quite simple: everything is based on a constant (or uniform) acceleration of $1.5g$'s. Knowing this, and the presumed fact that the resultant rise in velocity will be linear, we really only need three basic equations from Newtonian mechanics: $a = \Delta v / \Delta t$, relating acceleration, velocity, and time; $d = \bar{v}t$, where d is the distance traveled and \bar{v} is the average velocity; and $d = \frac{1}{2}at^2$. In this case, where the acceleration is uniform during time t , \bar{v} is equal to half (1/2) of the difference between the final and initial velocities. The third equation may then be used in any instance where the initial velocity is either zero or entirely negligible with respect to the final velocity.

So that this example may be as concise and informative as possible, the *warp jump sequence computation* should be undertaken in the following steps:

Step 1 } the 1st leg elapsed time (to the light barrier) at $1.5g$'s:

$$\begin{aligned}\Delta t_{11} &= \Delta v / a = c / 14.7 \text{ m/sec}^2 \\ &= 20.394 \times 10^6 \text{ seconds} = 236 \text{ days.}^*\end{aligned}$$

* this is also the 4th leg *objective* time to relative rest ($v = 0$).

Step 2 } the resultant 1st leg distance:

$$\begin{aligned}d_{11} &= \bar{v}t = (c/2)(20.394 \times 10^6 \text{ seconds}) \\ &= 3.057 \times 10^{15} \text{ m} = 1.9 \text{ trillion miles.}^*\end{aligned}$$

* this is also the 4th leg distance to relative rest.

Step 3 } the total distance to Alpha Centauri, at 4.31 lt.-yrs. (avg.):

$$\Sigma d = 4.31(5.8786 \times 10^{12} \text{ miles/lt.-yr.}) = 25.3368 \text{ trillion miles.}$$

Step 4 } the 2nd leg and 3rd leg warp corridor distances:

$$\begin{aligned}d_{12} = d_{13} &= .50[25.3368 - 2(1.9)] \text{ trillion miles} \\ &= 10.7684 \text{ trillion miles} = 17.33 \times 10^{15} \text{ m.}\end{aligned}$$

Step 5 } the apparent uniform supralight acceleration (a_ψ) is based on the premise that a StarDrive vessel traveling at light speed would achieve a supralight velocity ψ that is numerically equal to c^2 if negative thrust were applied for exactly the same length of time as positive thrust was applied to reach $v \approx c$ (from rest). Since c is entirely negligible with respect to c^2 :

$$a_\psi = \Delta v / \Delta t = \psi / t_{11} = 8.98755 \times 10^{16} / 236 (8.64 \times 10^4 \text{ sec/day}) \\ = 4.4077 \times 10^9 \text{ m/sec}^2.$$

Step 6 } the 2nd leg and 3rd leg warp corridor elapsed times are found by rearranging terms in the latter distance equation from above:

$$t_{12} = \sqrt{2d/a_\psi}, \text{ where } d \text{ is the 2nd (or 3rd) leg distance in meters.}$$

$$\text{So, } t_{12} = \sqrt{34.66 \times 10^{15} \text{ m} / 4.4077 \times 10^9 \text{ m/sec}^2} \\ = 2.8042 \times 10^3 \text{ sec.} = 46.733 \text{ min.} = .7789 \text{ hrs. (subjective time)}$$

Step 7 } mission one-way duration:

$$\Sigma t_m = 2(236 \text{ days})_{obj.} + 2(.7789 \text{ hrs.})_{subj.} \\ = 472.065 \text{ days} = 1.2924 \text{ years (uncalibrated)}$$

Step 8 } average one-way warp corridor velocity:

$$\psi_{avg} = d_{12} / t_{12} = 6.18 \times 10^{12} \text{ m/sec, or } > 20,000 c; \\ = 3.84 \times 10^9 \text{ miles/sec, or } 13.824 \text{ trillion mi./hr.}$$

Step 9 } peak one-way warp corridor velocity:

$$\text{peak } \psi = 2\psi_{avg} = 27.648 \times 10^{12} \text{ mi./hr.} = 4.7 \text{ lt.-yrs./hr.}$$

The hardest thing to accept about any of the data generated in the preceding *mission profile*, at least for those real StarTrek™ fans like myself, is that without “inertial damping” it always takes most of a year to reach light speed from rest, and vice versa. The time actually spent in the hyperspatial warp corridor is only a fraction of a percent of the 1st and 4th leg elapsed times, even at *kiloparsec distances*. A supralight velocity which is numerically equal to c^2 is equivalent to **34,199 lt.-yrs./hr.**, at which speed we could reach the center of the Milky Way galaxy (in Sagittarius) in about 53 minutes! But, even with zero Field leakage, this fantastic velocity would take nearly 8 months in hyperspace to achieve – at 1.5 *g*’s – and you would have traveled over 96 *million* light years!! [If you really wanted to go to the center of the galaxy, it would take just 20 hours in warp.]

C^2 is also equivalent to **9.5 lt.-yrs./sec.**, so the time lag in telemetry between Alpha Centauri and Earth would be just *half a second*. As you know, the resonant frequency of the StarDrive device goes down as size increases, and *Ariadne II*’s comm frequency was 3097 Hz. While this can just be categorized as a Very Low Frequency, the 60’ *Athena*’s ULF comm frequency is even lower, at only 1376 Hz. [It should be noted that the resonant frequencies of larger starships may be *approximated* by assuming that the inductance and capacitance of the respective primary systems will rise proportional to the square of the increase in vessel hull radius (R_h) above the values determined in Chapter 12 for the 4 ft. prototype.]

Speaking of communications, we've just received one from Mission Control telling me that it's now T minus 5 minutes and we're 'all go' for the launch of our mission to Tau Ceti. All ground personnel have been pulled back beyond the exo-envelope gyro-radius for safety, due to the intense radiative emissions from the vessel's Field. The *Athena's* launch perimeter is over 6.7 miles in radius, because her specification Field electrical power is over 2,800 *terawatts*. Unfortunately, this level of energy is sufficient to kill almost anything alive inside a sizeable portion of the launch perimeter's area, and this is why the Rogers Dry Lake facility or the Bonneville Salt Flats are about the only places around this part of the country where large starships may decently take off and land.

Many people wonder what a starship preparing for take-off *sounds like* from outside, and a rolling freight train would serve as an excellent analogy. Anyone who has stood close to the tracks near a long train runnin' knows that powerful low frequency rumble that you sense in the pit of your stomach. Like a train, the starship is only *loud* in an auditory way when one is very near the motors; once the Field self-evacuates, the ground rumble is all you can hear (and feel) in the lower audible range. A really high frequency whine similar to a jet aircraft engine's is also produced by the shear friction of the atmosphere at the Drive Field perimeter, but much of this noise is beyond the human auditory range. It's a good thing the vessel's crew chamber is completely soundproofed and vibration-dampened, though, or it would be deafening *inside*.

Because of the mission's length, we'll need to carry a total of 5 superconducting current storage rings, which have been saturated during rotor spin-up. Even though we will be lifting off under peak Field power (3,142 *terawatts*), to minimize the heat developed until we reach escape velocity, our *net* acceleration at launch will be equivalent to only about half that of free-fall. We, however, will feel as if we weigh about one-and-a-half times our normal weight, *and will continue to do so* as we pick up net acceleration while Earth's gravity fades away in open space. Once that happens, we'll be about one AU closer to Tau Ceti in under 45 minutes.

It's now T minus 30 seconds as we begin the most delicate part of the launch sequence: the rapid increasing of Field current *by reducing the Primary Array bias from a maximum to minimum operating level*. This will result in a rapid increase in the primary coolant temperature, and unless the *Athena* reaches outer space quickly she'll burn up. [The only way the vessel can survive the extended start time at ambient temperature is by initiating rotation of the rotor when the sodium primary coolant is "frozen" (still solid), and the Primary Arrays are biased as nearly to cutoff as possible during rotor spin-up (so that Field current is reduced by a factor of over 100 times, proportional to its level at standard grid voltages). This reduces the thermal output by at least 10,000 times!]

As our powerful vessel strains skyward, all systems are go "with green lights across the board"; so we may as well take a look at our mission profile. As you can see [on the next page], the outward-bound elapsed time has strangely enough remained almost the same as in the Alpha Centauri mission – even though the corresponding distance has nearly tripled! A 430 lt.-yr. trip to the Pleiades, which (as you'll see) we almost certainly *would not* make, would still only require about 16 hours in warp. It'd just take a larger ship and another storage ring . . .

{1} the 1st leg elapsed time (to the light barrier) at 1.5g's:

$$\Delta t_{11} = 20.394 \times 10^6 \text{ seconds} = 236 \text{ days (objective time)}$$

{2} the resultant 1st and 4th leg distances:

$$d_{11} = 1.9 \text{ trillion miles.}$$

{3} the total distance to Tau Cet, at 11.9 lt.-yrs.:

$$\Sigma d = 11.9(5.8786 \times 10^{12} \text{ miles/lt.-yr.}) = 69.9554 \text{ trillion miles.}$$

{4} the 2nd leg and 3rd leg warp corridor distances:

$$\begin{aligned} d_{12} = d_{13} &= .50[69.9554 - 2(1.9)] \text{ trillion miles} \\ &= 33.0777 \text{ trillion miles} = 53.2336 \times 10^{15} \text{ m.} \end{aligned}$$

{5} the apparent uniform supralight acceleration (a_ψ):

$$\begin{aligned} a_\psi &= \Delta v / \Delta t = \psi / t_{11} = 8.98755 \times 10^{16} / 236 (8.64 \times 10^4 \text{ sec/day}) \\ &= 4.4077 \times 10^9 \text{ m/sec}^2. \end{aligned}$$

{6} the 2nd leg and 3rd leg warp corridor elapsed times:

$$\begin{aligned} t_{12} &= \sqrt{106.4672 \times 10^{15} \text{ m} / 4.4077 \times 10^9 \text{ m/sec}^2} \\ &= 4.915 \times 10^3 \text{ sec.} = 81.917 \text{ min.} = 1.365 \text{ hrs. (subjective time)} \end{aligned}$$

{7} mission one-way duration:

$$\begin{aligned} \Sigma t_m &= 2(236 \text{ days})_{obj.} + 2(1.365 \text{ hrs.})_{subj.} \\ &= 472.114 \text{ days} = 1.2926 \text{ years (uncalibrated)} \end{aligned}$$

{8} average one-way warp corridor velocity:

$$\begin{aligned} \psi_{avg} &= d_{12} / t_{12} = 10.83 \times 10^{12} \text{ m/sec, or } 36,125 \text{ c;} \\ &= 6.73 \times 10^9 \text{ miles/sec, or } 24.23 \text{ trillion mi./hr.} \end{aligned}$$

{9} peak one-way warp corridor velocity:

$$\text{peak } \psi = 2\psi_{avg} = 48.46 \times 10^{12} \text{ mi./hr.} = 8.24 \text{ lt.-yrs./hr.}$$

The mission commander has just informed me that we have achieved escape velocity and are now safely on our way to Tau Ceti. Because our average speed in hyperspace will be over 75% higher than that achieved on the Centauri mission, the one-way elapsed time will only be about 70 *minutes* longer. However, we are still going to be over 15 months getting to Tau Ceti, so we'll have plenty of time to discuss navigation a bit more.

All forms of navigation utilize a three-dimensional coordinate system of some kind, and if we're going to navigate in galactic interstellar space we need to be using **galactic coordinates** [X, Y, Z]. These coordinates define the position of the destination star, in units of light-years, relative to our Sun. The Sun of course represents the point [0, 0, 0] in this coordinate system, and galactic coordinates can then be used to find the distance between any two other stars; but the accuracy of these coordinates is only as good as the accuracy with which astronomers have measured the distances to the stars in question.

The first coordinate (X) points directly from the Sun to the center of the galaxy. The second coordinate (Y) points parallel to the galaxy's rotation in the same plane, perpendicular to the X axis. And, the third coordinate (Z) is perpendicular to both other axes, pointing parallel to the galaxy's axis of rotation. In the case of Tau Ceti, these galactic coordinates are: $[-3.493, 0.373, -11.380]$ (courtesy of www.stellar-database.com). But these coordinates are ever-so-slowly changing all the time, and must be corrected using a corresponding system of *galactic velocity components* (u, v, w). In this case, these incremental "correction factors" describe a *radial velocity vector* that tells how fast and in what direction the entire star system is changing its respective coordinates $[X, Y, Z]$ relative to the Sun. Each component is in units of kilometers/second, and we can use our current destination of Tau Ceti to illustrate this important concept.

Tau Ceti's radial vector velocity is -17 km/sec, which means that this is the speed at which it is spatially *approaching* the Sun (hence the negative sign) *in a direct line-of-sight*. Its galactic velocity components are $(18.81, 29.57, 12.99)$ and the Sun's are once again $(0, 0, 0)$. Since a light-year equals 9.46×10^5 km, the number of seconds it takes a star to change any of its galactic coordinates *by one light-year* is equal to 9.46×10^{12} km/lt.-yr. divided by the corresponding velocity component (u, v , or w). Therefore, to calculate the necessary modification(s) to Tau Ceti's given coordinates that will yield its adjusted coordinates at the end of our voyage (one way), we merely have to plug the given velocity components and the mission one-way duration *in seconds* into the following simple formula:

$$\pm \Delta(X, Y, \text{ or } Z) = \frac{\Sigma t_m [\pm(u, v, \text{ or } w)]}{9.46 \times 10^{12}}$$

Since $\Sigma t_m = 472.114$ days $\times (8.64 \times 10^4 \text{ sec/day}) = 4.079 \times 10^7$ seconds, Tau Ceti will be $(4.079 \times 10^7) \times (-17 \text{ km})$ or almost 431 million miles closer to the Sun than it was when we left, and the change in each of its galactic coordinates (in light-years) that will have occurred by the time we arrive there is as follows:

$$\Delta X = (4.079 \times 10^7)(18.81)/9.46 \times 10^{12} = .0000811$$

$$\Delta Y = (4.079 \times 10^7)(29.57)/9.46 \times 10^{12} = .0001275$$

$$\Delta Z = (4.079 \times 10^7)(12.99)/9.46 \times 10^{12} = .0000560$$

Since even such small changes in galactic coordinates are not really negligible *in our case*, we may convert this change in coordinates into miles if we wish:

$$\Delta X = (.0000811)(9.46 \times 10^{12} \text{ km/lt.-yr.})/1.60935 \text{ km/mile} = 477 \text{ million miles ;}$$

$$\Delta Y = (.0001275)(9.46 \times 10^{12} \text{ km/lt.-yr.})/1.60935 \text{ km/mile} = 749 \text{ million miles ;}$$

$$\Delta Z = (.0000560)(9.46 \times 10^{12} \text{ km/lt.-yr.})/1.60935 \text{ km/mile} = 329 \text{ million miles .}$$

It is essential to understand that the sign of each velocity component will be the sign of any incremental change in the corresponding galactic coordinate, whether that component is negative or positive. For example, if a given star's u, v , or w is -10 , in about 30,000 years it will subtract 1 lt.-yr. from the respective coordinate (X, Y , or Z); and if that same component is $+10$, it will add 1 lt.-yr. in the same period of time. This probably seems easy enough so far, but it will be necessary to clarify how each star's real-time position dictates the sign of its velocity components in order to explain how Tau Ceti can have an approaching

(or impinging) radial velocity with a negative value and yet all of its velocity components have positive values!

To wit: (i) a star whose *X* coordinate is positive lies at an *inbound* position, between the center of the galaxy and the Sun; one whose *X* coordinate is negative lies at an *outbound* position, farther from the galaxy's center than the Sun; (ii) a star whose *Y* coordinate is positive lies ahead of the Sun in the galaxy's general stream of rotation, at an *anterior* position; one whose *Y* coordinate is negative lies behind the Sun in this stellar stream, in a *posterior* position; and (iii) a star whose *Z* coordinate is positive lies above the plane of the Sun's galactic orbit, at an *inclined* position, and one whose *Z* coordinate is negative lies below the Sun's orbital plane in a *declined* position.

And thus, Tau Ceti's coordinates tell us it is located about three-and-a half light years farther from the galactic core than we are, just slightly ahead of us in the galactic stream, and somewhat over 11 light years beneath the plane of the Sun's galactic orbit (which accounts for most of its net distance from us). Since the Sun is considered as being located at the origin of the three coordinate axes, local space can be divided into *eight spatial octants*. The following special starmap shows these local octants as well as three stars of interest which are located in each one, including Tau Ceti. Our view is from behind the Sun, slightly above and outside its orbital plane within the stellar stream, with the galaxy's core to the left and its "north" pole toward the top of the page. The distance of each star relative to Sol is shown as nearly to scale as possible.

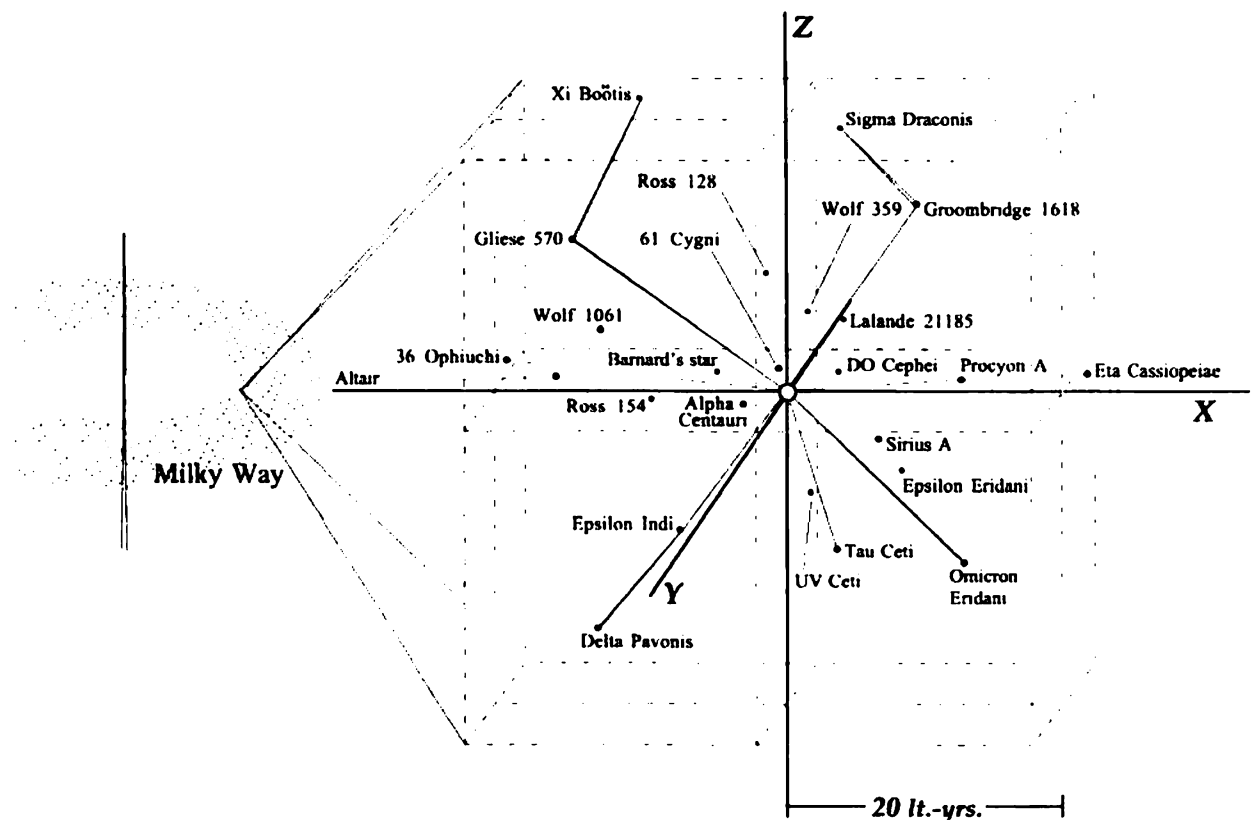


Fig. 70: starmap for local spatial octants and reference stars

Note: The *Y* coordinate appears highly foreshortened from this perspective {see * next page}.

Navigation & Sensor Capability

star name	distance (lt.-yrs.)	color	class/es	age (x 10 ⁹ yrs.)	gal. coord.s @ 2000.0; vel. comp.s (u, v, w)	V _{rad}
Alpha Centauri	4.400	yellow orange	G2V K4V	4.2	[3.169, -3.052, -0.0819] (-32.01, 4.149, 14.16)	-26.2
Barnard's star	5.945	red	M4V	~10	[4.939, 3.003, 1.389] (-141.0, 3.377, 19.03)	-111
Wolf 359	7.803	red	M6V	?- flare	[-1.897, -3.905, 6.483] (-26.94, -44.33, -18.75)	+13
Lalande 21185	8.317	red	M2V	~3-10	[-3.361, -0.321, 7.601] (45.68, -53.62, -74.30)	-84.3
UV Ceti A	8.560	red	M5.5V	?- flare	[-2.103, 0.170, -8.296] (-43.03, -19.20, -19.42)	+29
Sirius A	8.607	white	A1V	.300	[-5.750, -6.279, -1.263] (15.34, 1.105, -11.30)	-9.4
Ross 154	9.700	red	M3.5V	?- flare	[9.328, 1.927, -1.832] (-13.80, -1.30, -7.571)	-12.1
Epsilon Eridani	10.504	orange	K2V	< 1.0	[-6.825, -1.968, -7.739] (-4.145, 6.978, -21.06)	-16.9
Ross 128	10.895	red	M4V	?- flare	[0.149, -5.508, 9.399] (17.46, 5.799, -32.92)	-31.1
Procyon A	11.414	yel/wh	F5IV-V	~2	[-9.186, -6.225, 2.676] (5.234, -8.392, -18.61)	-4
61 Cygni	11.435	orange	K5V	3-5	[1.439, 11.28, -1.189] (-93.16, -54.63, -7.924)	-64.8
Epsilon Indi	11.835	orange	K5V	3-5	[7.164, -3.160, -8.874] (-80.25, -41.40, 3.816)	-40.4
Tau Ceti	11.906	yellow	G8V	~3.2	[-3.493, 0.373, -11.38] (18.81, 29.57, 12.99)	-17
DO Cephei	13.080	red	M3V, M4V	~5-10	[-3.39, 12.60, 0.020] (25.90, -27.50, 1.89)	-33.3
Wolf 1061	13.919	red	M3V	~5-10	[12.78, 0.830, 5.455] (-5.453, -20.08, -17.35)	-13
Groombridge 1618	15.903	orange	K7V	3-5	[-9.344, 2.340, 12.65] (-9.699, -21.03, -35.20)	-25.4
Omicron(2) Eridani	16.466	orange	K1V	~1-2	[-12.20, -4.681, -10.01] (97.06, -12.03, -42.45)	-42.7
Altair	16.785	white	A7V	<1.0	[11.05, 12.34, -2.730] (-28.26, -10.19, -2.350)	-26.1
Sigma Draconis	18.821	orange	K0V	3.3	[-3.454, 17.11, 7.030] (31.08, 44.64, -17.90)	+28.2
Gliese 570	19.278	orange	K5V	3-5	[15.22, -5.909, 10.26] (49.99, -22.58, -32.49)	+29.1
Eta Cassiopeiae	19.429	yellow	G3V	5.8	[-10.55, 16.23, -1.620] (-29.86, -11.09, -15.05)	+8.2
36 Ophiuchi	19.479	orange orange	(2) K1V, (1) K5V	~1	[19.36, -0.459, 2.131] (0.436, -34.30, -6.787)	+0.5
Delta Pavonis	19.933	yellow	G8V	4-6	[14.48, -8.396, -10.83] (-48.78, -14.13, -14.32)	-21.7
Xi Boötis	21.870	yellow	G8V	.060	[9.822, 4.192, 19.08] (5.753, 0.931, -0.643)	+2.2

* With very small negative Z values, Altair, 61 Cygni, and Eta Cassiopeiae actually appear *just above* the X axis.

Electrical Engineering
for the 21st Century



Archer Enterprises

2938 Ferguson Crs. Rd.
Geneva, NY 14456

585-526-6817 / 526-5936 fax

Custom Engineering Design

✱ Energy Systems Integrated
Performance Analysis

Date: 10/03/06
Pages: 12 plus cover

Re: Chapter 13 Excerpt from 'StarDrive Engineering'

Dear Reader:

While my book 'StarDrive Engineering' was published (nearly five years ago now) primarily as a complete basic technical manual and prototyping guide for the EDF Generator technology, I like to think that it has a very good story to tell on a number of other levels as well.

The following text is excerpted from the Chapter 13 material on "Navigation", and postulates a manned *trans-light mission* to the Tau Ceti stellar system about a dozen light years distant, using an as-yet hypothetical 60-ft. diameter StarDrive vessel named *Athena*. As told from a science officer's perspective, the narrative not only points out how comprehensive the specifications methodology is for actual starship systems and hardware, but explains the proper method of '*warp jump sequence computation*' by generating accurate time-and-velocity *mission profiles* for Alpha Centauri as well as Tau Ceti.

Also, included at the end is a brief introduction to the accepted system of *galactic coordinates*, using Tau Ceti as the reference, as well as a 3D starmap and table showing the stellar class and galactic coordinates for two dozen star systems located within about 20 light-years of Earth.

I must say that I still see no other way of truly reaching any of those stars, without the StarDrive technology I've worked so hard to introduce. I hope that you find this Chapter Excerpt stimulating and possibly even inspirational, if you feel as I do that our best - and perhaps only - long-term destiny lies in space.

Yours truly,

Mark Tomion

Inventor

Electrodynamic Field Generator

'StarDrive Engineering' was independently published and
printed in the United States of America by **Archer Enterprises**.

Library of Congress Cataloging-in-Publication data

Tomion, Mark R.

StarDrive Engineering.

Summary: describes development of, and specifications for, a
novel electrodynamic field generator and starship.

Includes special glossary.

1. electrical engineering 2. aerospace propulsion

Library of Congress Control Number (LCCN): 2001118702 [nonfiction]

ISBN 0-9713727-0-5 paperback

All rights reserved.

Copyright ©2001 by Mark R. Tomion

This Chapter Excerpt may not be reproduced in whole or in part, by photocopy
or any other means, without the express written permission of the publisher.

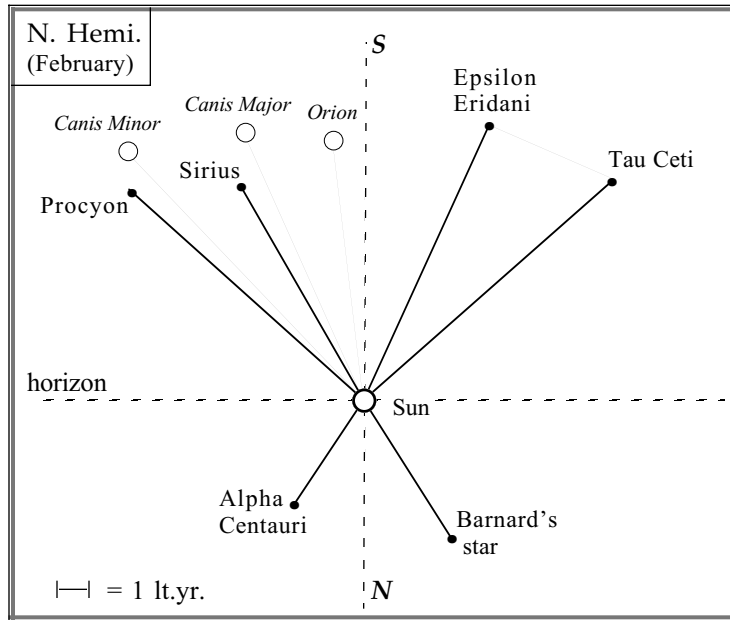


Fig. 68: *skymap of local stars discussed (w/ Orion as reference)*

This local skymap was created especially for *StarDrive Engineering* based on 3D stellar imaging courtesy of www.solstation.com. The distance of each star relative to Sol is to scale, as is that between Epsilon Eridani and Tau Ceti.

Tau Ceti: It's really not hard to say why this otherwise undistinguished G8 star has been the object of so much interest, from science fiction writers and astrophysicists alike, for over 40 years. As one's general knowledge of astronomy grows, one becomes aware of how truly rare Sun-like stars are in our local corner of the galaxy. One fundamental reason for this scarcity is that peripheral portions of the galaxy (like ours) are comprised mostly of old class M red dwarfs, which are generally considered unlikely to harbor life – as are the less common young and hot stars of class A or higher. Astronomers therefore limit their considerations of which systems may have planets with life to stars of class F, G, or K. So, we can see that our two last interstellar mission candidates and Tau Ceti jointly represent each of those preferred classes; but it would seem only the latter star remains a viable choice, and it happens to be the second-closest class G star (after Alpha Centauri A). Other than the local stars on our list (from Fig. 67), there are 8 class K stars within 20 lt.-yrs. of Earth, the closest of which is 61 Cygni (@ 11.44 lt.-yrs.). But, there are only 4 other class G stars within 35 lt.-yrs., the next-closest being Eta Cassiopeiae (@ 19.43 lt.-yrs.).

In fact, Tau Ceti and Epsilon Eridani were the subject of the first SETI experiment, in 1960. This attempt to detect non-random radio signals from what were thought to be the two likeliest nearby sources lasted for four months, but was unsuccessful. Interestingly enough, these two stars are only about 5.5 lt.-yrs. from each other, and are in fact quite similar. With a surface temperature of about 5200°K and a mass = 0.81 x Sol, Tau Ceti is both cooler and smaller than the Sun. It therefore has only about 46% of the Sun's luminosity, and has an eco-zone orbit of .679 AU (or 94.3% that of Venus) with an orbital period of 227 days.

However, its enrichment with heavier elements including the various metals is estimated at only 36% of Sol's, whereas Epsilon Eridani's is 58% and Procyon A's almost double that – and this figure has a bearing not only on the system's ability to develop solid planets suitable for life but also on *the star's projected main sequence age*. As we've seen, a candidate star's age can become a major determining factor in the search for extraterrestrial life, and any error in the star's 'metallicity' percentage or calculated distance will contribute to the uncertainty in its most probable age.

The two best estimates of Tau Ceti's stellar age seem to agree that it is about 3.2 billion years old, or 70% as old as the Sun, and should have 15 billion years remaining in its main sequence lifetime. Happily, the former time span is (at last) enough time for complex life forms to have evolved, even if not to the same degree as here on Earth. Moreover, astronomers have failed to find giant planets *in inner orbits*, which actually improves the chances that smaller and more habitable worlds may occur there. All things considered, the enticing Tau Ceti quite likely constitutes the best candidate for a second and longer warp jump (after that to Alpha Centauri) in any voyage of under 20 lt.-yrs.

The next section of this chapter is going to take a somewhat less prosaic course which I think will be refreshing. So, our story will proceed for a time in the form of a *narrative pre-creation* of an actual trans-light mission to Tau Ceti! This little sketch will hopefully tie together everything we've discussed thus far, while pointing out some important new considerations which are rather fascinating. It presumes that men of vision like former President Kennedy will see to it that a 60 ft. starship is funded and built for this historic trans-light voyage, as part of an ongoing StarDrive program wherein progressively larger ships are built and tested over ever-increasing distances. Perhaps you feel as I do, that such a plan represents the best hope for the dignified long-term survival of our race . . .

The time is T minus 135 minutes, and I am sitting in the StarDrive vessel *Athena*: an Antares-class ship which is the largest such vessel ever built to date. [See the *Manned Vessel Design DataSheet*, on pg. 107.] I'm the science officer aboard for this planned voyage to the Tau Ceti system, and the mission commander is about to initiate powered rotation of the ship's massive rotor assembly. At T minus 132 minutes we'll begin the ship's 2.2 hour pre-launch cold start, here at the NASA Flight Research Center located at Edwards AFB (on Rogers Dry Lake) in California. During this time, I'll be able to provide you with some basic facts about the ship and about the successful first manned trans-light voyage to Alpha Centauri which gave this present mission a "green light".

The *Athena's* displacement is 8,460 cubic feet and her weight is 335 tons. Each of her 32 drive motors is rated at 190 output horsepower, for a total of 6,088 hp to turn the rotor – which weighs almost exactly 50% of the weight of the entire craft. As a good comparison, the largest steam locomotives ever built weighed about 300 tons and developed about 7,000 hp. By the way: the required start time (T_w) for any StarDrive device of 20 ft. in diameter or more is computed from the following formula: $T_w = 141 \text{ seconds} \times (2R_h - 4)$, where R_h is in feet. The total hp required is that which yields this start time, given the rotor's mass.

While an Antares-class vessel is rated to carry a maximum crew of 5, on this mission the *Athena* will carry a crew of only 3 – due to the fact that our cargo capacity is quite limited and the mission profile calls for a total round trip duration of 2.6 years! But before we talk about how this voyage’s elapsed time was calculated, it will be necessary to clarify how mass, force, acceleration, and kinetic energy “behave” in negative quantum time-space. Then, I can illustrate these characteristics for you using data from the Centauri mission.

The most curious piece of the trans-light navigational puzzle, believe it or not, can be expressed as simply as this: Do we, or do we not, continue to apply *positive thrust* right on through the supralight velocity transition (to spatial warp), until the exact middle of the entire distance *each way*? If so, we would then need to execute a single “turnaround” maneuver in each half of the entire round trip, to begin *decelerating* for the remaining half of the distance to the destination: thus maintaining a constant apparent onboard gravity throughout the trip.

To answer this seemingly innocuous question, we need to expand on the work of physicist O. M. Bilaniuk which was first described way back in Chapter 2. Bilaniuk found that for relativity to be ‘uniformly’ applied to two coincident continuums, the kinetic energy of an imaginary mass object has to be inversely proportional to its velocity. This is, of course, the exact “reverse” of the fact that kinetic energy in our continuum is proportional to velocity. In order to answer the puzzling turnaround question above, care must now be taken to reason correctly from this simple axiom as a starting point.

What he is *first* implying here is that the *faster* an imaginary mass object moves (toward c^2 as a maximum), the *less* negative energy it has; and, that the *slower* such an object travels (toward the value of c as a minimum), the *more* negative energy it has. The trickiest part comes next, in interpreting how an imaginary mass will respond to the application of force – given the reverse kinetic energy property described above. Bilaniuk found, accordingly, that the slower an imaginary mass object moves, the harder it is to force it to move any slower. And, this is a direct corollary to the relativistic increase in positive mass as a normal object approaches the limiting speed at which its kinetic energy has the greatest *absolute value*.

Therefore, an imaginary mass object will go faster when a negative acceleration (or braking force) is applied, and will slow down – thus approaching light speed “from above”– when positive thrust or acceleration is applied. And so, it would appear that our StarDrive vessel must actually execute *a total of 3 turnaround maneuvers* in any given one-way warp jump voyage! The resultant **warp jump turnaround sequence** is illustrated on the next page.

I’ve found that (for me at least) this interpretation of turnaround sequence may be more clearly understood by means of two simple equations from traditional wave mechanics. The first is: $v = f\lambda$, where v is wave velocity, f is frequency, and λ is wavelength. The only other relation needed to resolve this issue is the de Broglie equation $\lambda = h/M_t v$, where h is Planck’s constant, M_t is the total relativistic mass, and λ is the mass object’s wavelength. Thus:

- i) to increase our starship’s apparent supralight velocity with respect to the space-time continuum, its wavelength must increase, because its

frequency must remain constant throughout the transition to a “rarer” (higher-velocity) medium [as follows from the first equation];

ii) to increase its λ , the starship must in turn decrease its relativistic imaginary mass (and negative kinetic energy) *as its velocity climbs* [as follows from the second equation]; and therefore

iii) to decrease its relativistic imaginary mass, we must effect the gradual controlled release or decrease of the inherent (positive) kinetic energy the starship *gained during sublight acceleration* (m_i), via the application of reverse thrust or negative acceleration.

To reiterate, we can now see that to gain apparent velocity in hyperspace, we must actually apply braking thrust, and to decelerate therein we must apply ‘forward’ thrust! Moreover, to keep our apparent onboard gravity the same, we should certainly try to follow this “backwards” format while maintaining a constant level of subjective thrust. So, our trans-light ship will have to execute a total of three *180° forward rolls* as follows: 1) once, while accelerating past $v \simeq c$; 2) a second time, at the very midpoint of the distance one way; and 3) a third time while decelerating past $v \simeq c$.

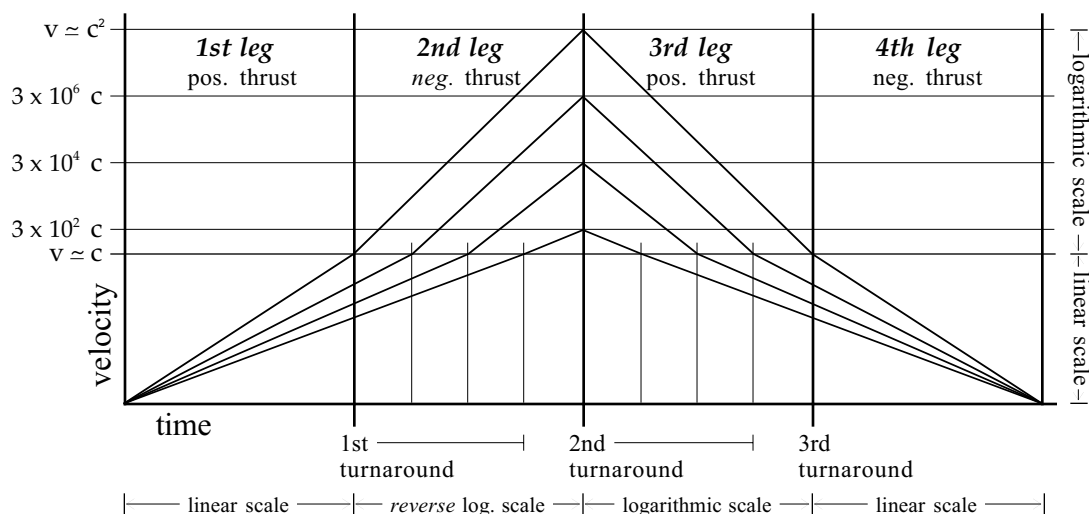


Fig. 69: *warp jump turnaround sequence graph*

The most important concept to bear in mind as we analyze this graph, which has certain unavoidable limitations, is that the StarDrive vessel’s velocity is assumed to rise as linearly toward light speed as if relativity were not operative! While this may sound like absolute heresy to some, it must be borne in mind that the objective mass of all Field electrons will rise in phase with the relativistic rise in the ship’s mass, yet they must gain a *separate subjective* relativistic velocity across the Field *for which they pay the freight*. Thus, the graph is correct in its rendering of such a ship’s *linearly changing velocity over time*, although I’ve been told that this may only be acceptable for some when it is simply characterized *as an instantaneous consequence of relativistic time dilation*.^{*} Let’s face it: if this weren’t so, the StarDrive vessel would never achieve trans-light speed . . .

^{*} [This linear acceleration phenomenon may be proven with a simple thought

experiment. If we postulate my buddy at Cornell tending his cyclotron, in which a bunch of high-energy electrons are rotating at near light speed, he will *not* observe them to suddenly start slowing down and inexplicably losing all their relativistic kinetic energy if, unbeknownst to him, we accelerate him and his lab to near light speed!]

With the said crucial (and sure to be disputed) observation in mind, we may now state the most important precept of trans-light acceleration (after the Bilaniuk reverse kinetic energy axiom described above). This precept is based (thank God) on the Conservation of Energy principle, although the fact that it is *correlative* with the observation above may still present a problem for some. Nevertheless:

Since the starship's speed will increase on a linear scale from $v = 0$ to $v \simeq c$, we must assume that under exactly the same *subjective* uniform acceleration the ship's speed in the time-energy continuum will increase linearly from $v \simeq c$ to $v \simeq c^2$ during a period of time which is exactly equal to that in which the original sublight acceleration was applied.

What I'm saying here is that we cannot perform more *work* in the time-energy continuum in accelerating our ship and raising its kinetic energy than we did in the space-time continuum. If we spend just a bit longer accelerating in hyperspace at $1g$, let's say, than we did accelerating at $1g$ from rest to light speed, the ship would reach $v = c^2$ and probably erupt like a temporary quasar! Not only can this be seen directly from the graph, but it can also be deduced that extremely long missions may require a period of time under zero thrust (and hence zero gravity), because further acceleration is not possible. I can't conceive of any practical reason why we would need to travel *that* great a distance, because (as we'll see) spending more than *an hour or two* accelerating in hyperspace causes one's velocity and time displacement to mount fantastically.

Now, we can discuss what was learned on that historic first trans-light mission to Alpha Centauri, although any data pertaining to the presence or absence of *life* in that system are still highly classified! Perhaps the gravest concern among the chief engineers at Mission Control was: would the mission's Vega-class vessel *Ariadne II* have enough electron "fuel" to decelerate into a stable system orbit wherein the ship could recharge its superconducting storage rings for the return trip? If the vessel's *Field leakage rate* was too high, it might not be able to do so and could sail right on by into deep space and be lost.

Saturating the ship's storage rings was not a problem. In fact, the best way to do this is actually to orbit the Sun for a time before leaving the solar system, and charge the rings with electrons pulled directly from its outer atmosphere! The key factor involved was the accuracy with which the Field leakage rate was measured, during the innumerable operational tests that were done. After all the numbers-crunching was over, the following scale for the Field leakage rates of manned vessels was adopted (*in parts per million of total operating Field current*):

<u>40 ft.:</u> .07 ppm	<u>50 ft.:</u> .06 ppm	<u>60 ft.:</u> .05 ppm	<u>70 ft.:</u> .04 ppm
<u>80 ft.:</u> .03 ppm	<u>90 ft.:</u> .02 ppm	<u>100 ft.:</u> .01 ppm	

Now, the 40 ft. ship has a peak rotor current $I_{rt} = 11.9394 \times 10^5$ amps. Its standard operating current is 10/11 of this figure, or 10.854×10^5 amps, so the *Ariadne II's* Field leakage turns out to be .076 amps (coul/sec). *This amperage times the total one-way trip length in seconds equals the total coulombs of charge needed.* [This assumes, of course, that one's navigation is sufficiently accurate to allow recharging from the destination star before it becomes a critical problem!] Getting a little ahead of ourselves here for a bit, the outbound mission duration was 472.065 days at 8.64×10^4 sec/day or 40.7864×10^6 seconds. This makes the estimated total electron leakage a staggering 3.1 million coulombs!

This figure actually isn't as terrible as it sounds, for each superconducting storage ring will hold up to 800,000 coulombs in the form of a zero-loss current. Therefore, the total Field leakage anticipated on each half of the round-trip voyage is equal to the capacity of 3.875 storage rings, and so the 40ft. *Ariadne II* was designed to incorporate a total of four current storage rings. It is important to note, however, that to reduce Field leakage to the levels shown in the table above, it was found that the thin outermost edge of the hull's Emitter Ring had to be parabolically faced with a special ceramic material (Titania 193).

At any rate, by now I'm sure you are all impatient to know just how the Alpha Centauri outbound mission duration was calculated. The nice thing about this computation is that, for once, it is actually quite simple: everything is based on a constant (or uniform) acceleration of $1.5g$'s. Knowing this, and the presumed fact that the resultant rise in velocity will be linear, we really only need three basic equations from Newtonian mechanics: $a = \Delta v / \Delta t$, relating acceleration, velocity, and time; $d = \bar{v}t$, where d is the distance traveled and \bar{v} is the average velocity; and $d = \frac{1}{2}at^2$. In this case, where the acceleration is uniform during time t , \bar{v} is equal to half (1/2) of the difference between the final and initial velocities. The third equation may then be used in any instance where the initial velocity is either zero or entirely negligible with respect to the final velocity.

So that this example may be as concise and informative as possible, the *warp jump sequence computation* should be undertaken in the following steps:

Step 1 } the 1st leg elapsed time (to the light barrier) at $1.5g$'s:

$$\begin{aligned}\Delta t_{11} &= \Delta v / a = c / 14.7 \text{ m/sec}^2 \\ &= 20.394 \times 10^6 \text{ seconds} = 236 \text{ days.}^*\end{aligned}$$

* this is also the 4th leg *objective* time to relative rest ($v = 0$).

Step 2 } the resultant 1st leg distance:

$$\begin{aligned}d_{11} &= \bar{v}t = (c/2)(20.394 \times 10^6 \text{ seconds}) \\ &= 3.057 \times 10^{15} \text{ m} = 1.9 \text{ trillion miles.}^*\end{aligned}$$

* this is also the 4th leg distance to relative rest.

Step 3 } the total distance to Alpha Centauri, at 4.31 lt.-yrs. (avg.):

$$\Sigma d = 4.31(5.8786 \times 10^{12} \text{ miles/lt.-yr.}) = 25.3368 \text{ trillion miles.}$$

Step 4 } the 2nd leg and 3rd leg warp corridor distances:

$$\begin{aligned}d_{12} &= d_{13} = .50[25.3368 - 2(1.9)] \text{ trillion miles} \\ &= 10.7684 \text{ trillion miles} = 17.33 \times 10^{15} \text{ m.}\end{aligned}$$

Step 5 } the *apparent uniform supralight acceleration* (a_ψ) is based on the premise that a StarDrive vessel traveling at light speed would achieve a supralight velocity ψ that is numerically equal to c^2 if negative thrust were applied for exactly the same length of time as positive thrust was applied to reach $v \simeq c$ (from rest). Since c is entirely negligible with respect to c^2 :

$$a_\psi = \Delta v / \Delta t = \psi / t_{11} = 8.98755 \times 10^{16} / 236 (8.64 \times 10^4 \text{ sec/day}) \\ = 4.4077 \times 10^9 \text{ m/sec}^2.$$

Step 6 } the 2nd leg and 3rd leg warp corridor elapsed times are found by rearranging terms in the latter distance equation from above:

$$t_{12} = \sqrt{2d/a_\psi}, \text{ where } d \text{ is the 2nd (or 3rd) leg distance in meters.}$$

$$\text{So, } t_{12} = \sqrt{34.66 \times 10^{15} \text{ m} / 4.4077 \times 10^9 \text{ m/sec}^2} \\ = 2.8042 \times 10^3 \text{ sec.} = 46.733 \text{ min.} = .7789 \text{ hrs. (subjective time)}$$

Step 7 } mission one-way duration:

$$\Sigma t_m = 2(236 \text{ days})_{obj.} + 2(.7789 \text{ hrs.})_{subj.} \\ = 472.065 \text{ days} = \mathbf{1.2924 \text{ years}} \text{ (uncalibrated)}$$

Step 8 } average one-way warp corridor velocity:

$$\psi_{avg} = d_{12} / t_{12} = 6.18 \times 10^{12} \text{ m/sec}, \text{ or } > 20,000 c; \\ = 3.84 \times 10^9 \text{ miles/sec, or } 13.824 \text{ trillion mi./hr.}$$

Step 9 } peak one-way warp corridor velocity:

$$\text{peak } \psi = 2\psi_{avg} = 27.648 \times 10^{12} \text{ mi./hr.} = \mathbf{4.7 \text{ lt.-yrs./hr.}}$$

The hardest thing to accept about any of the data generated in the preceding *mission profile*, at least for those real StarTrek™ fans like myself, is that without “inertial damping” it always takes most of a year to reach light speed from rest, and vice versa. The time actually spent in the hyperspatial warp corridor is only a fraction of a percent of the 1st and 4th leg elapsed times, even at *kiloparsec distances*. A supralight velocity which is numerically equal to c^2 is equivalent to **34,199 lt.-yrs./hr.**, at which speed we could reach the center of the Milky Way galaxy (in Sagittarius) in about 53 minutes! But, even with zero Field leakage, this fantastic velocity would take nearly 8 months in hyperspace to achieve – at 1.5 *g*’s – and you would have traveled over 96 *million* light years!! [If you really wanted to go to the center of the galaxy, it would take just 20 hours in warp.]

C^2 is also equivalent to **9.5 lt.-yrs./sec.**, so the time lag in telemetry between Alpha Centauri and Earth would be just *half a second*. As you know, the resonant frequency of the StarDrive device goes down as size increases, and *Ariadne II*’s comm frequency was 3097 Hz. While this can just be categorized as a Very Low Frequency, the 60’ *Athena*’s ULF comm frequency is even lower, at only 1376 Hz. [It should be noted that the resonant frequencies of larger starships may be *approximated* by assuming that the inductance and capacitance of the respective primary systems will rise proportional to the square of the increase in vessel hull radius (R_h) above the values determined in Chapter 12 for the 4 ft. prototype.]

Speaking of communications, we've just received one from Mission Control telling me that it's now T minus 5 minutes and we're 'all go' for the launch of our mission to Tau Ceti. All ground personnel have been pulled back beyond the exo-envelope gyro-radius for safety, due to the intense radiative emissions from the vessel's Field. The *Athena's* launch perimeter is over 6.7 *miles* in radius, because her specification Field electrical power is over 2,800 *terawatts*. Unfortunately, this level of energy is sufficient to kill almost anything alive inside a sizeable portion of the launch perimeter's area, and this is why the Rogers Dry Lake facility or the Bonneville Salt Flats are about the only places around this part of the country where large starships may decently take off and land.

Many people wonder what a starship preparing for take-off *sounds like* from outside, and a rolling freight train would serve as an excellent analogy. Anyone who has stood close to the tracks near a long train runnin' knows that powerful low frequency rumble that you sense in the pit of your stomach. Like a train, the starship is only *loud* in an auditory way when one is very near the motors; once the Field self-evacuates, the ground rumble is all you can hear (and feel) in the lower audible range. A really high frequency whine similar to a jet aircraft engine's is also produced by the shear friction of the atmosphere at the Drive Field perimeter, but much of this noise is beyond the human auditory range. It's a good thing the vessel's crew chamber is completely soundproofed and vibration-dampened, though, or it would be deafening *inside*.

Because of the mission's length, we'll need to carry a total of 5 superconducting current storage rings, which have been saturated during rotor spin-up. Even though we will be lifting off under peak Field power (3,142 *terawatts*), to minimize the heat developed until we reach escape velocity, our *net* acceleration at launch will be equivalent to only about half that of free-fall. We, however, will feel as if we weigh about one-and-a-half times our normal weight, *and will continue to do so* as we pick up net acceleration while Earth's gravity fades away in open space. Once that happens, we'll be about one AU closer to Tau Ceti in under 45 minutes.

It's now T minus 30 seconds as we begin the most delicate part of the launch sequence: the rapid increasing of Field current *by reducing the Primary Array bias from a maximum to minimum operating level*. This will result in a rapid increase in the primary coolant temperature, and unless the *Athena* reaches outer space quickly she'll burn up. [The only way the vessel can survive the extended start time at ambient temperature is by initiating rotation of the rotor when the sodium primary coolant is "frozen" (still solid), and the Primary Arrays are biased as nearly to cutoff as possible during rotor spin-up (so that Field current is reduced by a factor of over 100 times, proportional to its level at standard grid voltages). This reduces the thermal output by at least 10,000 times!]

As our powerful vessel strains skyward, all systems are go "with green lights across the board"; so we may as well take a look at our mission profile. As you can see [on the next page], the outward-bound elapsed time has strangely enough remained almost the same as in the Alpha Centauri mission – even though the corresponding distance has nearly tripled! A 430 lt.-yr. trip to the Pleiades, which (as you'll see) we almost certainly *would not* make, would still only require about 16 hours in warp. It'd just take a larger ship and another storage ring . . .

{1} the 1st leg elapsed time (to the light barrier) at 1.5g's:

$$\Delta t_{11} = 20.394 \times 10^6 \text{ seconds} = 236 \text{ days (objective time)}$$

{2} the resultant 1st and 4th leg distances:

$$d_{11} = 1.9 \text{ trillion miles.}$$

{3} the total distance to Tau Cet, at 11.9 lt.-yrs.:

$$\Sigma d = 11.9(5.8786 \times 10^{12} \text{ miles/lt.-yr.}) = 69.9554 \text{ trillion miles.}$$

{4} the 2nd leg and 3rd leg warp corridor distances:

$$\begin{aligned} d_{12} = d_{13} &= .50[69.9554 - 2(1.9)] \text{ trillion miles} \\ &= 33.0777 \text{ trillion miles} = 53.2336 \times 10^{15} \text{ m.} \end{aligned}$$

{5} the apparent uniform supralight acceleration (a_ψ):

$$\begin{aligned} a_\psi &= \Delta v / \Delta t = \psi / t_{11} = 8.98755 \times 10^{16} / 236(8.64 \times 10^4 \text{ sec/day}) \\ &= 4.4077 \times 10^9 \text{ m/sec}^2. \end{aligned}$$

{6} the 2nd leg and 3rd leg warp corridor elapsed times:

$$\begin{aligned} t_{12} &= \sqrt{106.4672 \times 10^{15} \text{ m} / 4.4077 \times 10^9 \text{ m/sec}^2} \\ &= 4.915 \times 10^3 \text{ sec.} = 81.917 \text{ min.} = 1.365 \text{ hrs. (subjective time)} \end{aligned}$$

{7} mission one-way duration:

$$\begin{aligned} \Sigma t_m &= 2(236 \text{ days})_{obj.} + 2(1.365 \text{ hrs.})_{subj.} \\ &= 472.114 \text{ days} = \mathbf{1.2926 \text{ years}} \text{ (uncalibrated)} \end{aligned}$$

{8} average one-way warp corridor velocity:

$$\begin{aligned} \psi_{avg} &= d_{12} / t_{12} = 10.83 \times 10^{12} \text{ m/sec, or } 36,125 \text{ c;} \\ &= 6.73 \times 10^9 \text{ miles/sec, or } 24.23 \text{ trillion mi./hr.} \end{aligned}$$

{9} peak one-way warp corridor velocity:

$$\text{peak } \psi = 2\psi_{avg} = 48.46 \times 10^{12} \text{ mi./hr.} = \mathbf{8.24 \text{ lt.-yrs./hr.}}$$

The mission commander has just informed me that we have achieved escape velocity and are now safely on our way to Tau Ceti. Because our average speed in hyperspace will be over 75% higher than that achieved on the Centauri mission, the one-way elapsed time will only be about 70 *minutes* longer. However, we are still going to be over 15 months getting to Tau Ceti, so we'll have plenty of time to discuss navigation a bit more.

All forms of navigation utilize a three-dimensional coordinate system of some kind, and if we're going to navigate in galactic interstellar space we need to be using **galactic coordinates** $[X, Y, Z]$. These coordinates define the position of the destination star, in units of light-years, relative to our Sun. The Sun of course represents the point $[0, 0, 0]$ in this coordinate system, and galactic coordinates can then be used to find the distance between any two other stars; but the accuracy of these coordinates is only as good as the accuracy with which astronomers have measured the distances to the stars in question.

The first coordinate (X) points directly from the Sun to the center of the galaxy. The second coordinate (Y) points parallel to the galaxy's rotation in the same plane, perpendicular to the X axis. And, the third coordinate (Z) is perpendicular to both other axes, pointing parallel to the galaxy's axis of rotation. In the case of Tau Ceti, these galactic coordinates are: $[-3.493, 0.373, -11.380]$ (courtesy of www.stellar-database.com). But these coordinates are ever-so-slowly changing all the time, and must be corrected using a corresponding system of *galactic velocity components* (u, v, w). In this case, these incremental "correction factors" describe a *radial velocity vector* that tells how fast and in what direction the entire star system is changing its respective coordinates $[X, Y, Z]$ relative to the Sun. Each component is in units of kilometers/second, and we can use our current destination of Tau Ceti to illustrate this important concept.

Tau Ceti's radial vector velocity is -17 km/sec, which means that this is the speed at which it is spatially *approaching* the Sun (hence the negative sign) *in a direct line-of-sight*. Its galactic velocity components are $(18.81, 29.57, 12.99)$ and the Sun's are once again $(0, 0, 0)$. Since a light-year equals 9.46×10^{12} km, the number of seconds it takes a star to change any of its galactic coordinates *by one light-year* is equal to 9.46×10^{12} km/lt.-yr. divided by the corresponding velocity component (u, v , or w). Therefore, to calculate the necessary modification(s) to Tau Ceti's given coordinates that will yield its adjusted coordinates at the end of our voyage (one way), we merely have to plug the given velocity components and the mission one-way duration *in seconds* into the following simple formula:

$$\pm\Delta(X, Y, \text{ or } Z) = \frac{\Sigma t_m [\pm(u, v, \text{ or } w)]}{9.46 \times 10^{12}}$$

Since $\Sigma t_m = 472.114$ days $\times (8.64 \times 10^4 \text{ sec/day}) = 4.079 \times 10^7$ seconds, Tau Ceti will be $(4.079 \times 10^7) \times (-17 \text{ km})$ or almost 431 million miles closer to the Sun than it was when we left, and the change in each of its galactic coordinates (in light-years) that will have occurred by the time we arrive there is as follows:

$$\Delta X = (4.079 \times 10^7)(18.81)/9.46 \times 10^{12} = .0000811$$

$$\Delta Y = (4.079 \times 10^7)(29.57)/9.46 \times 10^{12} = .0001275$$

$$\Delta Z = (4.079 \times 10^7)(12.99)/9.46 \times 10^{12} = .0000560$$

Since even such small changes in galactic coordinates are not really negligible *in our case*, we may convert this change in coordinates into miles if we wish:

$$\Delta X = (.0000811)(9.46 \times 10^{12} \text{ km/lt.-yr.})/1.60935 \text{ km/mile} = 477 \text{ million miles ;}$$

$$\Delta Y = (.0001275)(9.46 \times 10^{12} \text{ km/lt.-yr.})/1.60935 \text{ km/mile} = 749 \text{ million miles ;}$$

$$\Delta Z = (.0000560)(9.46 \times 10^{12} \text{ km/lt.-yr.})/1.60935 \text{ km/mile} = 329 \text{ million miles .}$$

It is essential to understand that the sign of each velocity component will be the sign of any incremental change in the corresponding galactic coordinate, whether that component is negative or positive. For example, if a given star's u, v , or w is -10 , in about 30,000 years it will subtract 1 lt.-yr. from the respective coordinate (X, Y , or Z); and if that same component is $+10$, it will add 1 lt.-yr. in the same period of time. This probably seems easy enough so far, but it will be necessary to clarify how each star's real-time position dictates the sign of its velocity components in order to explain how Tau Ceti can have an approaching

(or impinging) radial velocity with a negative value and yet all of its velocity components have positive values!

To wit: (i) a star whose X coordinate is positive lies at an *inbound* position, between the center of the galaxy and the Sun; one whose X coordinate is negative lies at an *outbound* position, farther from the galaxy's center than the Sun; (ii) a star whose Y coordinate is positive lies ahead of the Sun in the galaxy's general stream of rotation, at an *anterior* position; one whose Y coordinate is negative lies behind the Sun in this stellar stream, in a *posterior* position; and (iii) a star whose Z coordinate is positive lies above the plane of the Sun's galactic orbit, at an *inclined* position, and one whose Z coordinate is negative lies below the Sun's orbital plane in a *declined* position.

And thus, Tau Ceti's coordinates tell us it is located about three-and-a half light years farther from the galactic core than we are, just slightly ahead of us in the galactic stream, and somewhat over 11 light years beneath the plane of the Sun's galactic orbit (which accounts for most of its net distance from us). Since the Sun is considered as being located at the origin of the three coordinate axes, local space can be divided into *eight spatial octants*. The following special starmap shows these local octants as well as three stars of interest which are located in each one, including Tau Ceti. Our view is from behind the Sun, slightly above and outside its orbital plane within the stellar stream, with the galaxy's core to the left and its "north" pole toward the top of the page. The distance of each star relative to Sol is shown as nearly to scale as possible.

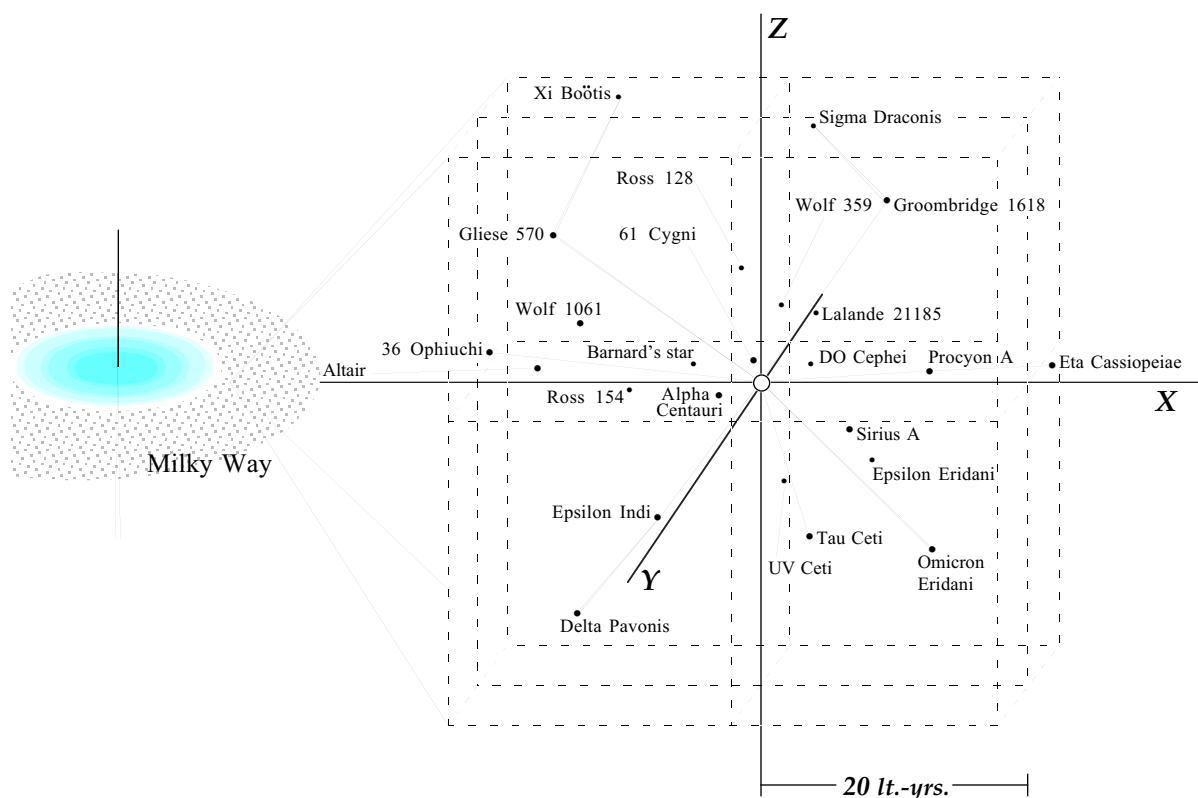


Fig. 70: starmap for local spatial octants and reference stars

Note: The Y coordinate appears highly foreshortened from this perspective {see * next page}.

star name	distance (lt.-yrs.)	color	class/es	age (x 10 ⁹ yrs.)	gal. coord.s @ 2000.0; vel. comp.s (<i>u</i> , <i>v</i> , <i>w</i>)	V _{rad}
Alpha Centauri	4.400	yellow orange	G2V K4V	4.2	[3.169, -3.052, -0.0819] (-32.01, 4.149, 14.16)	-26.2
Barnard's star	5.945	red	M4V	~ 10	[4.939, 3.003, 1.389] (-141.0, 3.377, 19.03)	-111
Wolf 359	7.803	red	M6V	?- flare	[-1.897, -3.905, 6.483] (-26.94, -44.33, -18.75)	+13
Lalande 21185	8.317	red	M2V	~ 3 - 10	[-3.361, -0.321, 7.601] (45.68, -53.62, -74.30)	-84.3
UV Ceti A	8.560	red	M5.5V	?- flare	[-2.103, 0.170, -8.296] (-43.03, -19.20, -19.42)	+29
Sirius A	8.607	white	A1V	.300	[-5.750, -6.279, -1.263] (15.34, 1.105, -11.30)	-9.4
Ross 154	9.700	red	M3.5V	?- flare	[9.328, 1.927, -1.832] (-13.80, -1.30, -7.571)	-12.1
Epsilon Eridani	10.504	orange	K2V	< 1.0	[-6.825, -1.968, -7.739] (-4.145, 6.978, -21.06)	-16.9
Ross 128	10.895	red	M4V	?- flare	[0.149, -5.508, 9.399] (17.46, 5.799, -32.92)	-31.1
Procyon A	11.414	yel/wh	F5IV-V	~ 2	[-9.186, -6.225, 2.676] (5.234, -8.392, -18.61)	-4
61 Cygni	11.435	orange	K5V	3 - 5	[1.439, 11.28, -1.189] (-93.16, -54.63, -7.924)	-64.8
Epsilon Indi	11.835	orange	K5V	3 - 5	[7.164, -3.160, -8.874] (-80.25, -41.40, 3.816)	-40.4
Tau Ceti	11.906	yellow	G8V	~ 3.2	[-3.493, 0.373, -11.38] (18.81, 29.57, 12.99)	-17
DO Cephei	13.080	red	M3V, M4V	~ 5 - 10	[-3.39, 12.60, 0.020] (25.90, -27.50, 1.89)	-33.3
Wolf 1061	13.919	red	M3V	~ 5 - 10	[12.78, 0.830, 5.455] (-5.453, -20.08, -17.35)	-13
Groombridge 1618	15.903	orange	K7V	3 - 5	[-9.344, 2.340, 12.65] (-9.699, -21.03, -35.20)	-25.4
Omicron(2) Eridani	16.466	orange	K1V	~ 1 - 2	[-12.20, -4.681, -10.01] (97.06, -12.03, -42.45)	-42.7
Altair	16.785	white	A7V	< 1.0	[11.05, 12.34, -2.730] (-28.26, -10.19, -2.350)	-26.1
Sigma Draconis	18.821	orange	K0V	3.3	[-3.454, 17.11, 7.030] (31.08, 44.64, -17.90)	+28.2
Gliese 570	19.278	orange	K5V	3 - 5	[15.22, -5.909, 10.26] (49.99, -22.58, -32.49)	+29.1
Eta Cassiopeiae	19.429	yellow	G3V	5.8	[-10.55, 16.23, -1.620] (-29.86, -11.09, -15.05)	+8.2
36 Ophiuchi	19.479	orange orange	(2) K1V, (1) K5V	~ 1	[19.36, -0.459, 2.131] (0.436, -34.30, -6.787)	+0.5
Delta Pavonis	19.933	yellow	G8V	4 - 6	[14.48, -8.396, -10.83] (-48.78, -14.13, -14.32)	-21.7
Xi Boötis	21.870	yellow	G8V	.060	[9.822, 4.192, 19.08] (5.753, 0.931, -0.643)	+2.2

* With very small negative *Z* values, Altair, 61 Cygni, and Eta Cassiopeiae actually appear *just above* the *X* axis.

It becomes clear now that there are actually quite a few interesting stars nearby, if we consider “nearby” in terms of *trans-light* travel, and that some of these stars are definite candidates for harboring life. *All* of these very same stars, though, would probably be forever unreachable without StarDrive. For instance, Epsilon Indi and Groombridge 1618 would appear to be excellent choices as stellar systems which may contain life, given their class and age. And Eta Cassiopeiae is my personal favorite as a worthy possible home sun of a starfaring race, given just the same considerations. However, while we know now that they are really ‘only’ about 15 months away by warp, they are a minimum of about 12, 16, and 20 *years* away (respectively) by any other mode of travel.

Moreover, we now have a workable succinct nomenclature for 8 types of interstellar trajectories which clearly describe the general “direction” that we’d set off in en route to any reference star on the local octant list. For example, the Alpha Centauri mission pursued a course heading which may be referred to as an “*inbound, posterially declining*” trajectory. Similarly, our current Tau Ceti mission is on an “*outbound, anterially declining*” trajectory.

You will note that the galactic coordinates given in the preceding table are referenced at the date 2000.0. What this means is that (roughly speaking) these coordinates *are those measured by telescope* just after the turn of the year, when the visual right ascension and declination were re-specified. Thus, in actuality, the coordinates shown for each star are those it had *at a number of years in the past, from that date*, which is numerically equal to its distance in light-years! Therefore, we must not only correct our destination’s coordinates for our own mission’s elapsed time (one way), but in this case we must *first* correct for 11.906 years of the star’s motion to the present moment: so that we have the real-time coordinates the star will have *when we get there!!*

The change in star-time ΔT_s is therefore the distance in light-years (11.906) times the number of seconds in a year (31.5576×10^6), or 37.5725×10^7 seconds. Multiplying this number times the radial velocity (-17) tells us that Tau Ceti was about 4 billion miles closer to Sol at 2000.0 than it *appeared* to be, given the posted coordinates visually obtained at that time. And, substituting ΔT_s for Σt_m in the three coordinate correction equations on pg. 307, we find:

$$\begin{aligned}\Delta X' &= (37.5725 \times 10^7)(18.81)/9.46 \times 10^{12} = .0007470 \\ \Delta Y' &= (37.5725 \times 10^7)(29.57)/9.46 \times 10^{12} = .0011740 \\ \Delta Z' &= (37.5725 \times 10^7)(12.99)/9.46 \times 10^{12} = .0005160\end{aligned}$$

So, Tau Ceti’s adjusted real-time coordinates on or around our arrival date, considering the present time to be 2000.0, would be:

$$\begin{aligned}X' &= -3.493 + .0007470 + .0000811 = -3.492 \\ Y' &= 0.373 + .0011740 + .0001275 = 0.374 \\ Z' &= -11.380 + .0005160 + .0000560 = -11.379 ;\end{aligned}$$

and we can see that each of its coordinates has changed by only about 5 to 12 ten-thousandths of a light year in the last 11.9 years of real time.

You math nuts will be glad to know that, in each case, the distance of the stars in the Fig. 70 table can be simply verified through two successive applications of the Pythagorean theorem to its posted coordinates. It therefore occurred to me

one day to see if the radial velocity could be verified in much the same manner, since such a determination also constitutes a three-vector resolution problem. However, because 8 different combinations of value signs for X , Y , and Z will be involved, and for u , v , and w as well, it's definitely not as simple as that!

While the radial velocities of local stars are generally determined by telescopic spectral Doppler shift analyses, it theoretically becomes possible to verify the exact radial velocity of any given star whose distance was *accurately* measured using one out of a minimum set of 8×8 or 64 equations. Each of these equations should be in the *general form* of the equation for the length of the line connecting opposite corners of a rectangular volume:

$$D_v = \sqrt{(x_2 - x_1)^2 + (y_2 - y_1)^2 + (z_2 - z_1)^2}$$

I have elected to call the particular one of these 64 or more equations which yields the absolute value of a given star's radial velocity – with no appreciable error – the *equation of motion* for that star, although it really constitutes only an analytical technique for assessing the inherent accuracy of that star's posted velocity components. Finding the best such equation of motion is a challenging affair, but is actually fun and may be done by trial and error. To illustrate the concepts (and problems) involved in this game, consider the following examples:

- 1) the equation of motion for Alpha Centauri A = $\sqrt{(u + v)^2 - w^2 + (w - v)^2}$;
 - the only difference in the signs of *Alpha Centauri B*'s galactic coordinates or velocity components compared to *A*'s is that its value for v is negative. As it happens, the equation of motion for Alpha Centauri B = $\sqrt{(u + v)^2 - w^2 - (w - v)^2}$.
 - In both instances, the variance from the posted value of radial velocity is less than 1%.
- 2) the equation of motion for Epsilon Indi = $\sqrt{(v + w)^2 + v^2 - (u - v)^2}$;
 - in this case, there are no differences in any of the signs for Epsilon Indi's galactic coordinates or velocity components as compared to *Alpha Centauri B*, yet the equation of motion is completely different! Variance from posted value here is entirely negligible.
- 3) the equation of motion for Procyon A = $\sqrt{(u - v)^2 - (u + w^2) + (u + v)^2}$;
 - this equation comes closer to a 'preferred' form, but the variance is just over 2%. In this case, however, we have high values for v and w but a very low net radial velocity, compounding the effect of any inherent error(s) in the posted component values.

These examples should prove sufficient to illustrate this brain-teaser for now, so we'll return shortly to more serious matters. Before we do, though, I must say that, yes, I did find an equation of motion for Tau Ceti. It bothers me a bit that it doesn't quite fit the "usual" format: $|V_{rad}| = \sqrt{u^2 - w^2 + (u - v)^2}$. Oh well . . .

So far, I've said nothing about the effects of *time dilation* in relation to the postulated linear acceleration characteristics of the StarDrive device, either in the sublight legs of this mission or in *warp transit*. I realize, however, that this is where I must make or break my case (as it were), so this Tau Ceti adventure of ours must include a discussion of the Lorentz transformation. Although the standard form of the transformation is generally only useful for *constant velocity* problems, we may safely use it here by entering only an average velocity derived from our given uniform acceleration during any one leg of the journey.

However, it will be much simpler and more instructive for us to talk *first* about the effect of the FitzGerald ratio on time, length, and mass as we approach light speed from either ‘side’ of the light barrier. Then, we will use the Lorentz transformation merely to confirm the conclusion(s) we arrive at this “casier” way.

As you may recall, the FitzGerald ratio is equal to the square root of the term *one minus the ratio of velocity squared to c^2* . By dividing an object’s rest mass by this term (called “tau”) when its velocity is close to that of light, we can find its relativistic mass ($M' = m_0/\tau$). Conversely, it’s possible to find the elapsed transit time or foreshortened length which applies to such an object by multiplying the appropriate value by the FitzGerald ratio, or by dividing that value by the reciprocal of the same ratio, called “gamma” (γ). Thus, $\gamma = 1/\tau$, and $T' = t/\gamma$.

I must reiterate this essential rule of *space-time* relativity, because we’ll also need to understand a *reverse* rule of time-energy relativity! By multiplication, the tau factor or FitzGerald ratio is used to determine relativistic time or length in our continuum, and gamma is similarly used to figure relativistic mass. However, in the time-energy continuum, just the opposite relationship holds: tau’ is used to determine relativistic mass, and gamma’ is used to figure relativistic time or length! Given the Bilaniuk reverse kinetic energy axiom which applies in hyperspace, these two pairs of properties are clearly depicted in the following Table.

velocity	tau	gamma		velocity	tau ’	gamma ’
$v = 0$	1.000	1.000		$v = c$	∞	0
0.01 c	~1	~1		1.01 c	7.0535	.14177
0.10 c	.995	1.005		1.10 c	2.1822	.45826
0.25 c	.968	1.033		1.25 c	1.3333	.75000
0.50 c	.866	1.155		$\sqrt{2} \times c$	1.0000	1.0000
$(1/\sqrt{2}) \times c$.7071	1.4142		1.50 c	.89443	1.11803
0.75 c	.661	1.513		1.75 c	.69631	1.43614
0.90 c	.436	2.294		2 c	.57735	1.73205
0.99 c	.14107	7.0887		5 c	.20412	4.89898
0.9999 c	.014142	70.7114		10 c	.10050	9.94987
0.99999 c	.004472	223.607		1,000 c	.001	999.9995
0.999999 c	.0014142	707.107		10,000 c	.0001	~ 10,000
$v = c$	0	∞		36,125 c	~.000027	~ 36,125

Fig. 71: *dual continuum FitzGerald ratio table*

The first step in “calibrating” the Tau Ceti mission’s elapsed times, in both the objective and subjective senses, is to figure the approximate time dilation during the 1st and 4th legs of the voyage. This is most easily done directly from the Table above: since our *average* velocity during these portions of the trip will be equal to $c/2$ or 0.50 c, our tau factor is .866. So, we will achieve $v \simeq c$ in ‘only’ .866 x 236 days, or 204.4 days of subjective (onboard) time. This makes our calibrated one-way mission duration equal to $2(204.4) + 2(.057) = 408.914$ days.

Now it's time for us to face the grim realities of interstellar flight, by calculating the actual *objective* time that will pass while we are in the warp corridor on our way to Tau Ceti. While we would sincerely like to see an elapsed time which represents a substantial reduction in the 11.9 years traditional science says must ensue, at the same time I'm sure most of us would agree that more than the 2 x 4,915 seconds of subjective time we computed above must certainly pass. I'm also quite sure that many scientists and science fiction buffs alike will be shocked to see the answer we derive (with the easier FitzGerald ratio method) and then confirm, using the Lorentz transformation.

In Chapter 2, I stated that Dr. Isaac Asimov proposed the following concept: that a tachyonic mass object would still travel at a sub-light velocity with respect to any warp corridor whose length was subject to FitzGerald contraction. I further stated that physicist O. M. Bilaniuk had later corroborated this view mathematically. It is much more accurate to say, however, that a trans-light solution found in the manner Dr. Asimov suggests can be verified *correctly* using the Lorentz transformation. This is because, as is evident in the Table, it is actually mass which becomes contracted or diminished with increasing velocity in hyperspace, while time and length become expanded!

Nevertheless, the supralight value for γ' in the present example is essentially equal to 36,125: this is the average one-way warp corridor velocity in units of c , from the mission profile. In Asimov's method, we may divide the 2nd leg warp corridor distance of 53.2236×10^{15} m by this γ' factor to find an equivalent foreshortened distance of 14.733×10^{12} m. [The only reason I have just defied my own earlier rule here is because this will be more accurate than multiplying by the rounded τ' factor from the Table.] Completing this short calculation method requires knowing that *subjective* time during this 2nd leg in the warp corridor will be subject to a FitzGerald *expansion*, which can be seen in the Table. So, if we multiply our subjective 2nd leg elapsed time of 4.915×10^3 seconds by the same value for γ' (or 3.6125×10^4), we find the actual objective time elapsed equal to 17.7554×10^7 seconds or 5.6263 years.

Interestingly enough, if we now take the equivalent foreshortened distance and divide it by our subjective elapsed time in warp, we find that Dr. Asimov is indeed correct: our equivalent velocity is 299.75585×10^6 m/sec, or 99.9878% of the speed of light! But this gratifying insight does nothing to mitigate the awful reality that the *objective* time passed during the first half of our warp jump is still a bit *more than* the very time light would take to cover the same distance!! If only there were something wrong in this easy estimation method that will be discovered in the more difficult (but final) transformation . . .

For those of you who are unfamiliar with the Lorentz transformation, the objective elapsed time $T = (t' - vx/c^2)/\gamma'$, where v in this case is the supralight average velocity and x is the true 2nd leg distance. Since t' (4,915 sec.) is negligible with respect to the following term, the equation reduces to this form:

$$\begin{aligned} T &= [- (10.83 \times 10^{12})(53.2336 \times 10^{15}) / (8.98755 \times 10^{16})] / 3.6125 \times 10^4 i \\ &= - 64.1465 \times 10^{11} / 3.6125 \times 10^4 i = 17.7568 \times 10^7 \text{ sec} / 8.64 \times 10^4 \text{ sec/day} \\ &= 2.055 \times 10^3 \text{ days} = 5.6268 \text{ years.} \end{aligned}$$

Alas, it would seem that our earlier estimate was in fact accurate, because the latter elapsed time differs from that figure by only 0.0005 years. Moreover, because the average supralight velocity in the 3rd leg is the same as that in the 2nd, we can divide the combined distance of 106.4672×10^{15} m by the value 9.4607×10^{15} m per light-year to find the total warp corridor length equal to 11.2536 lt.-yrs. [Amazingly, 11.2536 years is *exactly* twice the latter value of *T* above, although this is actually due to rounding 4,914.7553 seconds up to 4,915.] So, we can finally see (and hopefully accept) that our calibrated *objective* one-way mission duration is equal to 2 (236 days) + 2 (5.6268 years) or **12.5459 years**, and during our warp jump we will *still* only be managing a bit under 99.99% of light speed from the point of view of those back home . . .

As if this realization isn't confounding enough, our starship's huge time expansion factor *gamma*'poses a latent problem in telemetry and communications which is rather unique. Since subjective time (aboard the ship) will be moving an average of 36,125 times slower than objective time, voice messages sent by us to Mission Control will have to be recorded in their entirety and then *speeded-up* by the proper factor before they are transmitted in order to be intelligible at the other end! Otherwise, the data transfer rate of our transmitted telemetry would also be correspondingly slow. Conversely, all voice messages sent by Mission Control to us must be *slowed-down* by the proper factor before being transmitted in order to render them intelligible to us. Despite the fact that the time lag in a c^2 signal going either way would not be more than a second-and-a-quarter on our Tau Ceti voyage, this problem makes true two-way voice communications a bit awkward.

Even though the *Athena* will pursue a course towards Tau Ceti which is fundamentally line-of-sight, it is important to develop a better understanding of just how we are going to steer this thing. I stated earlier [near the end of Chapter 7] that this task is generally accomplished by applying **hull precessional torque**, and the vessel's outer geometry makes that an effective (if rather inefficient) proposition. So, let's take a closer look at the mechanics of this z-axis navigational method to gain a better idea of a StarDrive ship's forward maneuverability.*

If we consider such a vessel in space pursuing a forward trajectory which is purely linear and parallel to the hull's y-axis, we can cause it to veer away from that heading at a desired radial angle if we increase the Field current conducted by the aft Zone sector diametrically opposite that angle. Because the average angle at which Field current impinges on the hull is nearly parallel with its y-axis, the very small net torque applied in this manner must be enhanced by additional similar measures most succinctly described on pgs. 85 and 86. For our present purposes, we will consider the application of hull precessional torque to a single Zone sector. This will give us an idea of *how long* such a minimum force imbalance must be applied to yield a given change in the y-axis course heading.

* **Note:** With respect to the ship's hull, the x-axis is lateral or parallel with the plane of the rotor; the y-axis is parallel with the hull's vertical axis of symmetry; and the z-axis is then considered to be angularly anti-parallel with the other two. Thus, z-axis thrust produced by applying precessional torque causes the ship to pursue a forward trajectory which diverges from the prior y-axis orientation with a minimum lateral inertial force being felt onboard.

As can be seen in the following diagrams, this steerage strategy applies equally to sub-light motion and to motion in hyperspace (wherein the ship's "floor" and aft face are actually pointed in the leading direction). In both cases, applying a force imbalance on one sector of the hull by increasing its Field current causes the vessel to veer in a direction parallel to that force imbalance (or precessional torque).

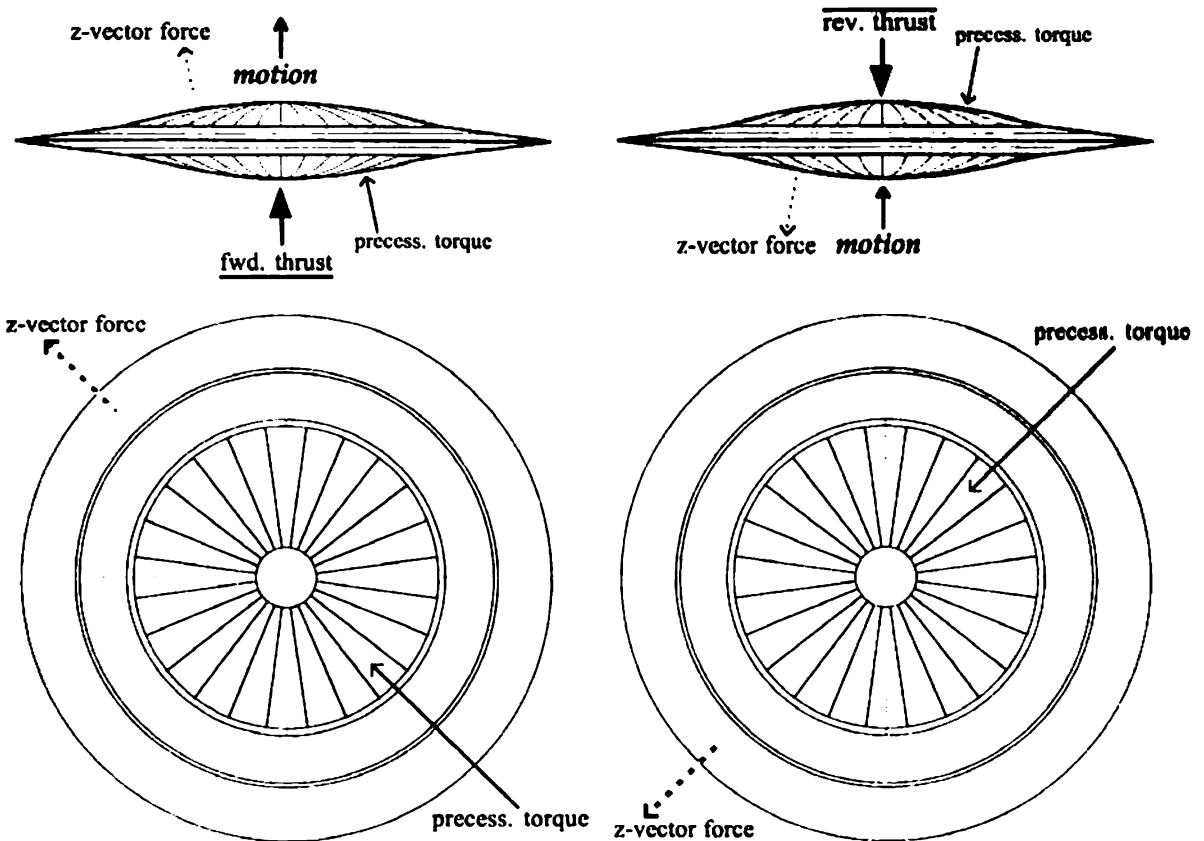


Fig. 72: hull precessional torque vector diagrams

Here, the rotor may be most efficiently precessed when torque is applied to the plane of rotation at 0° (parallel to its axis). To calculate the *average thrust angle*, or the angle at which precessional torque can be applied via an imbalance in the StarDrive vessel's Field current, all we need are two values from the Hull Configuration Spreadsheet. If we divide the Field Hub radius (r_h) by the Polar Volume Differential (X_h), the result is the tangent of *twice* the average thrust angle ϕ . Using data for the 4ft. prototype, ϕ turns out to be only $8^\circ 5'$, as is reflected in Fig. 72 above. So, if torque applied at 0° is considered to be 100% efficient, the *input* torque must be multiplied by the term $[\cos(8^\circ 5')]$, representing the net effective percentage of that torque. Since $\cos(8^\circ 5') = .9900$, any one given sector considered separately is 99% efficient in its production of net precessional torque!

The standard formula by which the torque required to produce a given change of angle per unit time in the rotational axis, *where the rate of precession is low*, is as follows: $\tau' = I\omega(\Delta\phi/\Delta t)$, where I is the rotor's moment of inertia and ω is its angular velocity. [The method by which these values are obtained is given on

pg. 242.] Since the desired change of axial angle will be *given* in ship navigation, and the rate of precession will definitely be low, we may use this formula in the rearranged form that follows to solve for *the time required to effect the new axial course heading*: $\Delta t = I\omega(\Delta\phi_i)/\tau'(\cos\phi_i)$. The torque τ' , in *nt-m*, is the product of the force imbalance and the distance from the rotor's axis to the radial midpoint of the sector where the torque is applied; and the magnitude of this force imbalance is exactly proportional to that sector's Field current imbalance. The value $\Delta\phi_i$ is the fractional rotation of the axis (through a portion of 360°).

Regrettably, the level of mathematics required to illustrate the use of the course change equation above with a specific example lies beyond the allowable scope of this part of our story. So for now, let's just assume that we will continue unimpeded on our present trajectory toward Tau Ceti. With one of the most sophisticated supercomputers ever built to serve as our interstellar autopilot, we should try to relax and enjoy the extensive amount of free time that awaits us on this voyage. Perhaps someday future StarDrive engineers will discover not only inertial damping technology, to eliminate a large part of the long sub-light leg elapsed times, but also a way around that dreadful warp corridor time expansion which (for now) must forever remove us from the temporal stream we knew.

* * *

If we are to avoid an ultra-high-speed collision with a slow-moving mass object which wanders into our flight path, what we really need is a faster-than-light *electronic* method of detecting it: but such a detection method is as yet unknown. The potential for fulfilling just that need, however, may be inherent in the Hodowanec gm flux cavity detector we studied on pgs. 288 and 289. The detector circuit shown in Fig. 64 is configured for audio as well as DC output, and I believe a DC output trace is what is being shown in Fig. 65. One way of explaining this mysterious gravitic shadow effect is that it may depict a temporary local drop in the gross average change of gm flux per unit spatial volume, due to occlusion in the moon-Sun line-of-sight! Since this may be a somewhat difficult concept to grasp, I've come up with an analogy which I think will be quite helpful.

For years I have enjoyed contemplating the wave systems which form on the surface of Keuka Lake, and in just the right semi-becalmed state these seemingly random wave systems acquire a profound orderliness. At one favorite spot near the shoreline, toward which these wavetrains inevitably flow, there is a large submerged rock which extends partially above the surface; and at the right level of "ripple", the normal wavetrains are *occluded* behind the rock (between it and shore) such that a small surface area of almost utter stillness forms.

What I'm saying here is that the complex normal wavetrain pattern on the surface of the water represents the average volumetric Δ gm flux which would ordinarily be evident everywhere in *open* space; and that the small pool of stillness behind the rock is analogous to the drop in the Hodowanec chart recording which was almost certainly caused by the additional local occlusion of gm flux in the direction of the Sun. Thus, should a starship find itself rapidly impinging on an unexpected large mass directly in its flight path, the Hodowanec cavity detector may provide an indirect method of detecting such a mass in time to take adequate evasive action (because of the c^2 speed of these quantum fluctuations)!

Obtaining any type of quality *visual input* from inside the Field envelope would ~~seem~~ to me to present a difficult challenge, and without the relatively recent ~~developments~~ in sophisticated fiber optic and computer imaging systems this would probably be all but impossible. It could be that special high-temperature ~~lens~~ assemblies might be designed and circularly arranged in each Neutral Ring, to gather what radiant photons in the infrared to ultraviolet range are able to penetrate the Field envelope from outside. Two tremendous problems inherent in ~~this~~ endeavor are that the Field envelope current is almost certain to occlude ~~most~~ of this external photonic input – and is in fact an extraordinary source of radiant energy in the same range!

Therefore, the computer imaging system would not only have to filter out the “~~excess~~” Field-produced photons it received from the fiber-optically-connected ~~lens~~ assemblies, but would then have to “descramble” and enormously enhance what little visual data might remain. This is, however, the *only* method I forsee by means of which a starship crew may have benefit of any external visual data. It has been suggested that this method may in fact only be adequate at all if a ~~single~~ lens assembly is located right in the middle of each of the two center Zone ~~sectors~~, where Field envelope occlusion would be at its absolute minimum! While ~~this~~ *might* represent the best approach to the visual input problem, it has its own inherent limitations. The worst (and perhaps insurmountable) difficulty here would be the lens assembly’s direct exposure to the impinging Field current; and a substantial loss of resolution compared to the other arrangement would also be entailed. There is one thing about this challenge, though, in which I have absolute faith: where there’s the will, there’s a way.

Finally, I would like to propose a largely theoretical method of providing a StarDrive vessel with a rudimentary but *direct* sensor capability somewhat akin to that depicted in StarTrek™: whereby the crew may obtain raw data related to the *composition* of external matter, via **induced X-ray emissions detection** which is made possible by the Field’s own radiant energy output! In short, not only do we have an enormous X-ray emission source in the form of the Field envelope, but the energy of Field-emitted X-rays will be sufficient to cause any nearby material irradiated thereby to emit lower-energy X-rays which are uniquely characterisitic of that material!

The type of X-rays generated by Field current electrons is called *synchrotron radiation*, and is emitted as a result of the electrons’ tightly-curved high-speed trajectory in the magnetic field produced by the variable inductor arrays. Since this radiation is emitted tangent to that trajectory, only the X-rays produced in the region(s) of the envelope farthest from the Field Hub will have an outward vector which is useful for sensor capability. But backscattered photons from a “scanned” object will have a very uniform intensity which is directly related to the frequency of the incident X-rays and the square of the range. Before we discuss a method of accurately determining the range of a scanned object from which we might receive an X-ray “echo”, a brief explanation of why such an echo will be characteristic of the elements in that object’s composition must be given.

Field-emitted high-energy X radiation will collide with electrons in the orbital shells of atoms comprising the given material. Many such incident X-rays and

recoil Compton effect electrons with which they have collided will be driven *into* the material (instead of backscattered), some of which will eject electrons located in the *innermost shell orbitals* of the material's atoms. Softer X-rays will then be produced when the atoms' outer electrons drop into these vacated inner orbitals, constituting an internal photoelectric effect, and these soft X-ray emissions will have line spectra which are uniquely characteristic of each element in that material. These secondary emissions must then be processed through an X-ray spectrometer to determine the material's composition, and it would seem that the receiver of this device would have to be located in the center Zone sector(s) based on our earlier reasoning.

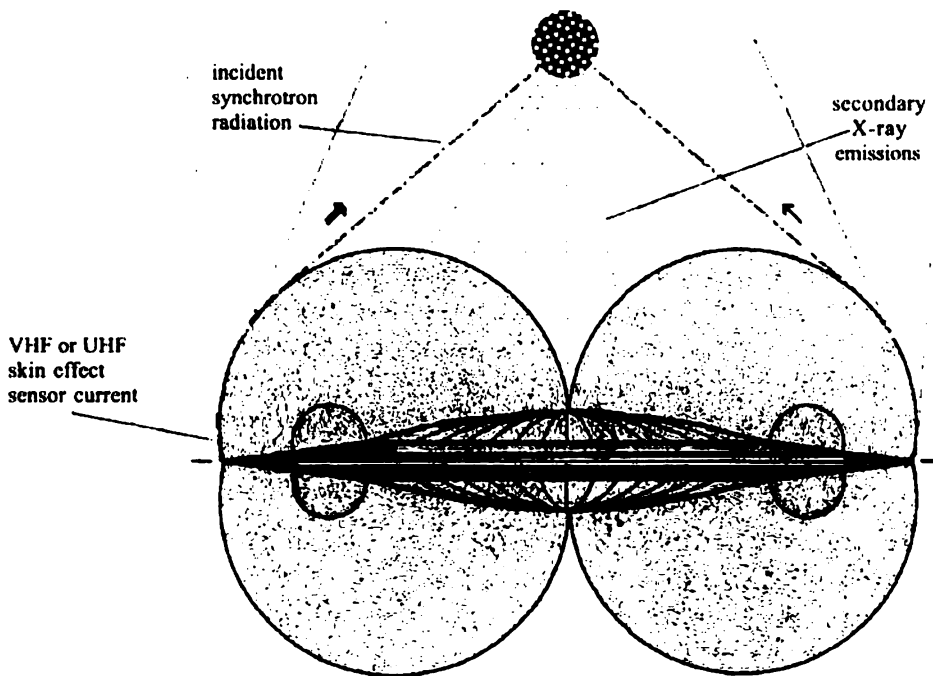


Fig. 73: *induced X-ray emissions detection diagram*

Finding the range at which such an object lies from the vessel, which is actually more important than knowing its composition, is a bit tricky. The only methodology I've developed for this so far is reliant upon the AC "skin effect", whereby an AC current tends to flow only in an *outside tubular cross section* of a conductor at very high frequencies. [This cross section decreases proportional to the square root of the frequency and to increases in the conductor's diameter.] Thus, it is postulated that each vessel should employ a VHF or UHF sensor carrier wave as an AC Field component of an FM nature (distinguishing it from the VLF/AM communications component). A single pulse or a sudden shift in amplitude of this carrier wave would produce a "ping" (as in submarine sonar range-finding) which emanates from the outermost layer of the Field envelope, and whose echo-return elapsed time will yield the object's range. Moreover, should it prove to be that visual and/or X-ray detection devices cannot be located in the center Zone sectors, it is conceivable that the induced emissions from a scanned object might alternatively be detected as harmonic interference in the AC signal generated at the sensor modulation frequency!

Special Section for Students and Engineers:

The following text (from the Patent Application) best completes the description of the geometric spatial sector arrangement, first discussed on pg. 87, which might feasibly serve as a directional sensor (and communications) antenna system. The AC sensor signal may be produced using the accelerator grids of the four cardinal sectors indicated by phantom lines in Fig. 72.

“In three-stage devices, four radial sectors . . . of each positive housing zone which correspond to cardinal points separated by 90 degrees of the hull's circumference, and which divide the Field Hub into four equal quadrants . . . , should be connected in parallel with the center sector of that positive zone at the maximum positive-voltage end of those four sectors' respective power resistors . . .”

“The parallel resistance of the four conductors which therefore connect each center zone sector . . . (in three-stage devices) to its respective network of power resistors should then be such that that sector's per unit surface area level of field current conduction is slightly higher on the average than that of its adjacent radial sectors . . . , under uniform zero-signal [dc] field bias conditions . . .”

“The four unit pentode arrays . . . of each primary induction ring array which correspond to the power resistors so-connected to that primary array's center zone sector . . . would generally not be utilized individually in the active field current bias modulation related to the production of local thrust differentials (in three-stage rotor devices), being instead reserved primarily for potential involvement in signal communications transmission and/or reception activities.”

To conclude this section on sensors, serious students may employ the simple traditional formula below to find the effective AC “skin effect” resistance of any conductor of *uniform circular cross section*, and it will be reasonably accurate for all AC frequencies above 1MHz:

$$R_{ac} = \sqrt{f_{MHz}} (R_{dc}) / d_{in}, \text{ where } f_{MHz} \text{ is the frequency in megahertz,}$$

$$R_{dc} \text{ is the normal dc resistance,}$$

$$\text{and } d_{in} \text{ is the conductor's diameter in inches.}$$

Neglecting the resistance effects associated with the very minor level of current conducted by the center Zone sectors (compared to the radial sectors), this expression in the following modified form may then be used to find the approximate skin-effect resistance of each cardinal sector *considered separately*:

$$R_{df} = 36[\sqrt{f_{MHz}}(2R_{df})/\sqrt{4A_z/\pi}], \text{ where } R_{df} \text{ is the dc Field resistance in } \Omega$$

$$\text{from Section E of WorkSheet II(c),}$$

$$\text{and } A_z \text{ is the total Zone area in sq. inches}$$

$$\text{from the Master Spreadsheet.}$$

It is important to note that the denominator of this modified expression yields an *equivalent flat circular diameter* for each positive Zone, and that the total Zone surface area A_z must in practice be reduced by the ~1% center Zone sector area and by the conduction area that will be lost due to the Zone sector partitions.

* * *

At this point, I feel that we have investigated all of the basic principles of **StarDrive Engineering** necessary to prove that this technology merits the fullest possible development and exploitation. While the total volume and complexity of information presented throughout the book so far has probably exceeded what the average reader initially expected (or perhaps needed!), I am encouraged to believe that it may serve as a valuable *interdisciplinary* reference resource for students and young engineers in many fields of endeavor.

Hopefully, in addition to firmly establishing that we truly now have within our grasp the actual means to travel among the stars, I've also managed to convey to one and all my own conviction that sheer scientific curiosity alone constitutes a sufficiently compelling reason to do so. At least in this particular Chapter we've seen that sufficient navigational means already exist with which to find our way around *Out There* – and to find our way back again!

Perhaps the only really discouraging thing I've been obliged to reveal in this book so far is that *there truly is no breaking the time-light barrier in anything but the subjective sense*. In “bending the rules” (and the fabric of space-time) to exceed light speed from a starship's point of view, its crew merely manages to forever displace themselves into the future. With this realization, those of you who have always been ardent UFO believers (including myself) must now ask yourselves – *why would alien exobiologists ever come here?!* Try as I might, I can only find two plausible reasons: either they're of a nomadic race which has no strong concept of familial ties, or they are extremely long-lived. Even I would find it wrenchingly difficult to say goodbye forever to those I love for the sake of science . . .

And so, in the final Chapter of this challenging and unconventional chronicle, we'll pursue a more philosophical course which will hopefully put everything we've discussed into the best possible perspective. Such an overview, at least for me, entails a profound sense of awe and reverence for this incredible Universe – of which we are a tiny but potent part – that I pray will help encourage us to find a noble yet humble place therein.

Prelude

Things don't have purposes, as if the Universe were a machine, where every part has a useful function. What's the function of a galaxy? I don't know if our life has a purpose and I don't see that it matters. What does matter is that we're a part. Like a thread in a cloth or a grass-blade in a field. It *is* and we *are*. What we do is like wind blowing on the grass.

Ursula K. LeGuin

The Lathe of Heaven

Chapter 14

Dual Continuum Cosmology

If they were asked to briefly describe in simple layman's terms the word "philosophy", many people would probably say something to the effect that it's a discipline concerned with *the search for lasting meaning* in our all-too-short lives as human beings. Some might also add that this is often a difficult and troubling pursuit, because of the dichotomy between the intellectual and emotional parts of our intrinsic awareness. Nevertheless, it could quite accurately be said as well that philosophy at the most personal level involves the contemplation of our origin, evolution, and fate as individual sentient beings. And so it must be that *Cosmology*, as the study of the origin, evolution, and fate of the Universe itself, entails an intimate and unavoidable connection to the discipline of philosophy – and it is certainly one of the most contemplative yet difficult and troubling of all the physical sciences.

The relationship which cosmology bears to philosophy may best be encompassed by comparison to two of the four primary branches into which the latter discipline is usually divided: *metaphysics*, as the systematic study of the fundamental principles which govern existential reality; and *ethics*, or investigation into the concepts and nature of rational judgement, morality, and religion. And while issues of morality per se might not bear directly on the matter at hand, religion certainly does – for it isn't possible to adequately assess the origin or creation of the universe without addressing the possibility of God's existence and His role therein. The inflationary Big Bang theory just barely explains *how* the universe came into being; there is no *scientific* hypothesis whatsoever which even begins to explain *why* it did so.

In any event, philosophical methods of inquiry are generally divided into two types: *analytic*, involving the logical study of concepts within a specific field of endeavor; and *synthetic*, dealing with the organization of diverse concepts into a unified system. Thus, while the scientific study of astrophysics is essentially an analytic philosophy, cosmology could be thought of as a synthetic discipline: a distinction which will be even more evident once it incorporates a proper theory of quantum gravity with which to probe the mysteries of Creation itself.

Western philosophy has its roots (of course) in ancient Greece, and means quite literally "love of wisdom" or the pursuit of knowledge for its own sake. It arose from a remarkable surge of speculation about the fundamental nature of the physical realm, and was initially indistinguishable from natural science. [As we saw in Chapter 3, the study of science was still called natural philosophy in Faraday's time.] Since this initial climate of wonderment provided the impetus for most of what we now consider higher learning, I feel that we should very briefly review the course of philosophical thought which led to the age of modern science and the cosmological inquiries which must someday reconcile metaphysical and 'ethical' considerations.

The Ionian schools of thought in the 6th century B.C.E. first bridged the chasm between the ancient mythological beliefs and a more modern scientific view of the world. One of their principal concerns was identifying an ultimate single form of matter, from which all natural phenomena were thought to derive. The Pythagorean school, while still largely mystical in its scholastic emphasis, made the important contribution of stressing *mathematics* in scientific thought. Later on, while Pluralistic thinkers were preoccupied with their four supposed primary "elements" of earth, air, fire, and water, the 4th century B.C.E. philosophers Leucippus and Democritus actually developed the first *atomic theory of matter*, and believed that all aspects of existence are fundamentally determined by physical laws that could be understood by man.

While Plato was the first to actually use the word 'philosophy', it was his student Aristotle who developed the basic principles of logic, scientific method, and physics itself. He was one of the first to propose the *aether theory of space*, which could be thought of as experiencing something of a revival in our own time (in a highly modified form, of course). Aristotle was undoubtedly the most influential pre-Christian philosopher other than Socrates and, after his death, interest in the natural sciences began a decline which lasted over 1,000 years.

Throughout the Roman, neo-Roman, and Medieval periods, the intellectual emphasis shifted decidedly toward the ethical philosophies and religion. Except for the writings of St. Augustine in the 5th century C.E., who stressed that the metaphysical (scientific) and ethical (religious) schools of thought should in fact be considered complementary, few doctrines of any significance for our present purposes emerged. Not until the 13th century would Aristotelian philosophy regain something of its former influence, in the works of St. Albertus Magnus, his student St. Thomas Aquinas, and the English monk Roger Bacon. Most notably, Aquinas argued for the unification of Aristotelian and Augustinian thinking.

Essentially, the beginning of the scientific age did not occur until the career of the Italian astronomer Galileo in the very early 17th century, who could quite justifiably be thought of as the world's first true physicist. He openly advocated experimentation and the application of mathematics in formulating scientific principles, rather than relying on Aristotelian metaphysical logic and physical theology. He almost singlehandedly created the science of mechanics by applying the principles of geometry to the study of bodies in motion. And, for all of this, he ended up being persecuted by the Roman Catholic Church - which took until the year 1992 to officially recant its position . . .

That the universe began some 10 to 15 billion years ago in a stupendous explosion of radiant energy out of which all matter eventually condensed is almost unilaterally accepted today, and is implicit in the Field Equations of Einstein's general theory of relativity. While Einstein originally believed that the universe was static but finite, somewhat similarly to the earlier Newtonian view, these new equations seemed to imply that it had to be either expanding or contracting. Therefore, he added a "cosmological constant" to his equations which cancelled this apparent non-static condition. Although he later admitted that he felt this had been a serious mistake, astrophysicists now generally believe that a cosmological constant in some form or other must be incorporated

into our present "Big Bang" theory in order to account for the universe being the way we observe it to be in the present epoch; and to provide a missing ingredient in our understanding of a *dynamical gravity*, wherein the gravitational 'constant' itself may be inversely proportional to the distance scale over which it acts! And, as it happens, it's a concept of such key importance that we'll return to it shortly.

Be that as it may, the Russian mathematician Alexander Friedmann proposed in 1922 that the universe is essentially homogenous in its matter distribution or density, and he provided a solution to the Field Equations which furthermore showed that it might necessarily have started at a singular point-like region of infinite density and temperature. When American astronomer Edwin Hubble discovered in 1929 that the farther away all other galaxies were from our own the faster they seemed to be receding from us, such a uniform spatial expansion firmly established the Big Bang theory as the most probable explanation for the manner in which the universe came into being. This view was further supported by the 1965 discovery of the cosmic microwave background radiation, which is not only consistent with Big Bang models in its very-low residual energy and near-isotropy (or almost complete uniformity regardless of direction) but is also now thought to be anisotropic (or non-uniform) only to the extent allowable by quantum uncertainty and to be consistent with a reasonable explanation of the observed non-uniformities in universal structure on the largest of cosmic scales.

But the same relativistic principles which ensure that the universe started with the Big Bang also preclude its present energy uniformity unless it initially underwent a period of *inflationary* expansion, during which it increased in size enormously faster than the speed of light (or even the *square* thereof). Moreover, this inflation can be used to explain why the energy density of the universe is so very close to the value which determines whether it will ever recondense (or collapse) or continue to expand forever. Just as significantly, however, the concept of inflation is about the only way to explain how the universe as it is could have arisen from a variety of different initial states or configurations *without the rate of expansion and most of the physical constants having to be very carefully specified* as part of a Grand Design! Consequently, there is not one but upwards of 50 different inflationary universe models at present, which could be seen as a predictable result of consistent attempts by the scientific community to obviate the possible role of God in creation.

At the most deterministic cosmological level lies the fact that if the rate of expansion of the universe one second after the Big Bang was different by even *one part in millions of millions*, it would have either already collapsed or been too thinly-distributed to even produce the stars themselves. Despite this plethora of universal models in which a great diversity of systems of correlative natural laws is possible, it is also truly stated that the observed values of the key physical constants and the relative strengths of the four fundamental forces in nature are only really critical *to the formation of a universe which includes life* as we could understand it. Not only are physicists confounded as to how the universe could have been created so highly ordered given what we know of statistical probability and the law of entropy, but by the fact that it has a specific configuration which favors and includes life that is by its very nature anti-entropic!

As I intimated near the end of Chapter 5, I personally believe the electron to be the key piece in solving the unified field theory puzzle which in turn would provide the only way for us to complete a true cosmological model. I'd therefore like to point out that if the charge on the electron was only very slightly different, the stars would be unable to fuse hydrogen into helium or to explode in the supernovae which create and distribute the heavier elements out of which living things are made. And if the gravitational constant and the mass of the proton were only the tiniest bit different in relation to the electron's fundamental electric charge, then atomic structure itself would be unstable and life could not appear in *any* form which would be recognizable to us.

Many years ago, Nobel physicist Steven Weinberg expressed the notion that the more comprehensible the universe becomes through the study of cosmology, the more it seems pointless; *particularly if it expands forever to utter emptiness*. One could perhaps cite that old conundrum "if a tree falls in the forest and no one is there to hear it, does it really make a sound?". My answer must of course be "yes, but it wouldn't matter": the universe could only be considered pointless *without* intelligent living observers. Yet it had the very audacity to originate *ex nihilo*, seemingly out of nothing, and it seems to have done so in a fashion that is so fantastically against the odds of chance that sentient beings like ourselves *do* exist and Paul Dirac was moved to utter the following: "One could perhaps describe the situation by saying that God is a mathematician of a very high order, and He used very advanced mathematics in constructing the universe".

Many scientists today are able to find inspiration in theological beliefs, and some New Age physicists feel that studying the mysteries of natural phenomena is essentially an ethical or religious obligation. Scientific research may then be likened to an act of worship, in an Augustinian sense, for science and spirituality have in fact a common goal: the search for the truth. And at some deepest level of quantum mechanics *where the uncertainty principle meets chaos theory*, a number of theologian-scientists have pointed out that God would be free to act in the natural world without violating the laws of physics.

* * *

The problems inherent in attempting any meaningful *non-theological* discussion of the universe's actual origin are as virtually insurmountable today as they always have been. Thus, all of the 20th century cosmological models (even Einstein's) simply assumed that the universe had always existed, from time immemorial as the Bible says, and that it will exist forever or unto time indefinite. This essential feature of the "steady-state" cosmological theory (which the Big Bang hypothesis totally supplanted) was therefore also a basic tenet of the early Big Bang models themselves. Since time itself *for us* to all intents and purposes began with the Creation, as St. Augustine believed, it may not matter all that much just what happened *before* the Big Bang. Such problems, being essentially philosophical in nature, may be judiciously avoided for now through a more practical discussion of the origins of these primary Big Bang models.

So, Einstein assumed in formulating his Field Equations that the curvature of space was independent of time: that the 'shape' of the universe as a whole was

eternally unchanging. In the “spherical” universe that his own solution to these equations yields, space had a positive curvature and was thus “closed” or finite – provided he added a cosmological constant with a negative gravitational effect. The temporal axis, however, was purely linear and this treatment required that *no cosmic event could ever reoccur*. Subsequent astronomical observations soon showed that this type of universe was in fact not valid, and neither was a similar solution found by the Dutch theoretician Willem de Sitter (in which the time axis is also curved but the matter density must be impossibly low).

On the other hand, Friedmann’s later solution to the Field Equations, which did not incorporate the cosmological constant, actually permitted just two kinds of universe: and only one of these involved a Big Bang. In his “hyperbolic” model, space has a negative Lobachevski spatial geometry or curvature (like the surface of a saddle), and such a universe would be “open” and infinite. This model is the exact converse of the Big Bang hypothesis: it shows that the universe could have contracted from an infinitely thin state an indefinite time in the past until it reached a maximum possible level of density, and then it reversed the process to begin a period of expansion which will continue forever. Hence, in this model there is no Big Bang at all, and for reasons which we’ll discuss later on it has also been discarded as invalid.

Thus it is that the only other pre-inflationary-theory Friedmann model, which did not include the cosmological constant yet remains an “available” (or theoretically feasible) candidate, is that of the ‘pulsating’ or *oscillating universe*: such a cosmos would expand to a maximum possible limit and then collapse to a maximum density, only to rebound *in an endlessly recurring cosmic cycle forever*. This closed Riemann spatial geometry remains today one of the only viable alternative universal configurations, and in my own view is entirely more aesthetically pleasing than the ultimately cold, grim, and entropic nothingness that an open universe mandates . . .

However, the prevalent view among today’s astrophysicists *seems* to be that the universe is *either flat or open* and thus will “probably” continue its present expansion indefinitely. And the recent furor over astronomical data which would appear to suggest that the rate of expansion is actually *accelerating* only serves to reinforce this view *by supporting the operation of a large cosmological constant*. But this contention has by no means been firmly established, due to unavoidable covariabilities inherent in the necessary calculations and uncertainties in the observational input data which may in some cases be huge.

The fact is that inflationary theory is fundamentally based on the existence of a cosmological constant, and in general relativity this value remains truly fixed throughout the universe’s expansion. And while the inflationary theory of the universe’s evolution is the *only* way known to account for the degree of homogeneity in its matter and energy distribution, it does not necessarily mean that the universe must be flat or open! It’s just that current *estimates* of the matter density in the cosmos are deemed insufficient to halt the expansion, and a closed oscillating universe would require even more mass yet. But many scientists do support an oscillating universe theory which includes a *small* cosmological constant, and with good reasons (as we’ll soon see). An intriguing

Irony in all this uncertainty is that if new mass estimates do come down in favor of an open universe, inflationary theory itself will have to be radically revised!

Moreover, if we reasonably assume that both matter and energy in our space-time continuum have opposite counterparts in negative quantum time-space, and that gravity in such a coincident continuum is in fact "positive" in effect (as we established earlier), it becomes much more likely that we would then have sufficient total gravitation to ensure that the universe is closed and oscillatory! We'll therefore proceed on this assumption in our discussion of a dual continuum cosmology, and back the dark horse candidate.

The first two questions any child might ask about the universe are still very difficult to answer rightly even at the limits of our present understanding: "how big is the universe?", and "how old is it?". The debate among astrophysicists about the ultimate fate of the cosmos (at least in its present incarnation) can't be satisfactorily answered without somehow achieving more accurate answers to these two simple questions about its evolution. One of the reasons why this has proven so difficult is that Big Bang theory and general relativity can only tell us what happened immediately after the Creation, not what happened during that moment or before (if there was a 'before') . . .

It is possible to model the universe in mathematics with great accuracy back to within an ultra-short time interval of the 'beginning', called *Planck time*. This time interval is the fantastically small span of 5.39×10^{-44} second, but should not be taken to represent or imply that time itself is quantized at this figure. Planck time is simply the time required for light to travel the Planck length, and thus is generally considered to be the smallest interval over which it is possible to derive any meaningful physical measurement. The work of Kip Thorne and Stephen Hawking suggests that if time is quantized, it would have to be at a far smaller interval still. [In Hawking's work on primordial black holes, the *Planck mass* (2.1767×10^{-8} kg) becomes important, obviously not as a smallest unit of mass but as the smallest mass which might exhibit the properties of a black hole.] In any event, only a unified theory of quantum gravity would ever allow us to "see" the Big Bang any more closely than this.

In order to determine the universe's age, both its *size scale* and *expansion rate* must be known. While calculating galactic radial velocities is not that difficult, making accurate estimates of the cosmic distance scale is, because we are limited by light velocity to studying only those parts of the universe we can observe. Thus, due to spatial inflation we cannot accurately know the full measure of the universe's extent. However, it can be shown that that part of the cosmos which is observable is at least 20 billion light-years in diameter, with a radius of over 10^{26} meters. One of the primary motivations for building the Hubble Space Telescope was that it would resolve celestial objects at distances ten times greater than ground-based optical observatories and enhance our estimates of the size scale.

Unfortunately, the age, expansion rate, and *density* of the universe are all covariable, and accurate figures for all three are necessary before astrophysicists will be able to derive a valid model for its geometry and evolution. And it is unlikely we'll be able to obtain an accurate answer as to its ultimate fate without a *best possible estimate of its age*, based on that of the oldest objects we can detect.

Because we are seeing these objects not as they are now but as they were billions of years ago, we are in essence looking far back in time. Therefore, I would like to describe a simple but reasonably accurate method of calculating both the “lookback time” and distance of the oldest and most distant known objects of all – the quasars. Because space-time is *thought to be* extremely close to flat and space itself is so nearly empty, the algebra for an Einstein-de Sitter model may be used not only to derive a rough estimate of the present distance of any quasar given its red-shift but to provide a corresponding estimate of the universe’s size.

The red-shift (z) in an object’s spectrum is the difference between the observed wavelength (λ_o) and the unshifted wavelength (λ_e) divided by λ_e : $z = (\lambda_o - \lambda_e)/\lambda_e$. In this model, the red-shift associated with the Big Bang itself would be infinity; the observed red-shift of the cosmic microwave background is about 1,000, and that of the most remote quasar ever detected as of this writing (in the constellation Cetus) is 5.50. In the Einstein-de Sitter model, lookback time t_l as a decimal fraction of the age of the universe (T_u) is related to red-shift according to the following equation: $t_l = 1 - [1/(1 + z)^{3/2}]$. And so, the lookback time of this quasar is almost 94% of the age of the universe, and T_u has usually been estimated by various methods to be *roughly* 14.5 billion years (as an average); so $t_l \approx 13.6$ Gyr.

The latter figure, however, is *less than* the best estimate we used to have for the mean age of the oldest stars (16.5 Gyr), which are of course known to be far closer to us than quasars. But newer more accurate figures for the distances of the stars comprising globular clusters, some of the first objects to form in the cosmos by standard models of stellar evolution, were made possible by data compiled during the Hipparcos satellite mission. These studies indicate that the most probable estimate of the globular cluster ages is between 10 and 12 billion years, and similar revisions of the several available universe models give the most probable age of the cosmos at between 12 and 13 billion years. So, if we designate 13 Gyr as the upper bound on the age of the universe (T_u), we are seeing the oldest known quasar as it was no more than 12.22 billion years ago: and this ‘age’ is comfortably longer ago than an average globular cluster age of 11 Gyr.

To conclude our cosmological example involving the oldest and most distant known quasar, for an Einstein-deSitter universe we can employ the following relation to find the quasar’s estimated present distance d_p solely in terms of its observed red-shift and the estimated T_u :

$$\begin{aligned} d_p &= T_u (3 \text{ lt-yr/yr}) \left[1 - \frac{1}{(1 + z)^{1/2}} \right] \\ &= 39 \text{ billion lt-yr } (.60777) = 23.7 \text{ billion lt-yr} . \end{aligned}$$

And while this distance is a bit larger than the rough size of the visible universe given earlier, one must remember that the Einstein-deSitter model is suitably accurate only for a very low-density universe. A high-density universe such as that which would be closed and oscillating must necessarily be a younger and smaller universe with a smaller expansion rate, as we’ll see in the coming model.

The expansion rate of the universe, which has of course come to be known as Hubble’s constant (H_o), can be found by ‘simply’ dividing a remote galaxy’s outward radial velocity in kilometers per second by its distance in megaparsecs

(where one *Mpc* equals 3.264 million light-years): $H_0 = v_r/d$. This relationship was discovered by Edwin Hubble, in the study of stars called Cepheid variables located within 1 million light-years of the Milky Way. [I will briefly describe Cepheid variables and their cosmological importance momentarily.] Because this is such a tiny distance on a universal scale, and he was using non-digital photographic methods, the expansion rate he obtained of about 500 km/sec/Mpc was far too high. Despite the factor covariability problem mentioned earlier, the latest estimates of Hubble's constant are now thought to be constrained within the range of values from 40 to 80 km/sec/Mpc. Moreover, the inflationary theory assumption that the universe is essentially flat causes many scientists to feel that the true value must lie toward one end or the other of this same range.

Interestingly enough, some astronomers try to estimate the age of the universe directly from Hubble's constant. They reason that the time it would take for any galaxy to expand away from our own, starting from a contiguous region of space, would be equal to the present distance divided by the average radial velocity: $T = d/v_r$, where v_r is also equal to $H_0 d$. And so, the "Hubble time" T in trillions of years becomes $T_u = d/H_0 d = 1/H_0$. Thus, a value of $H_0 = 40$ would correspond to a universe which is about 0.025 trillion or 25 billion years old, and a value of $H_0 = 80$ would correspond to a universe which is about 0.013 trillion or 13 billion years old. However, because of factor covariability and the great uncertainty in present knowledge of the mass of the universe, this is a highly inaccurate and misleading strategy (as we'll soon discover).

To return to the subject of Cepheid variables, this type of star varies in brightness in a very regular fashion which is intimately linked to its absolute luminosity. Therefore, although quite rare, they have been found to provide the most reliable "standard candle" with which to accurately measure galactic distances. Unfortunately, the most remote Cepheid variables so far detected lie much less than 100 million light-years away, so they must in turn be used to calibrate other 'secondary' methods of measuring distances extending into the billions of light-years. This work has enormous implications in cosmology, as it appears that the larger the distance scale over which data is gathered in order to estimate the Hubble constant, the lower the value thereof that is obtained! The best way to illustrate this important observation is to briefly describe some of these secondary methods of cosmic distance measurement and the corresponding values for Hubble's constant they reveal.

At the root of the problem in getting accurate Hubble values is the fact that galaxies within clusters interact gravitationally with others of that local group, enough so that perturbations in their radial velocity vectors are induced which distort measurements of the main vector associated with a pure Hubble "flow". In fact, in attempting to derive a value for H_0 based on directly measuring Cepheid distances only in the range from 3 to 20 Mpc – without calibrating any secondary indicators – Batra & Willick (Stanford) found that H_0 could appear to be as high as 85, even after correcting for induced "peculiar" motions.

The SBF (Surface Brightness Fluctuation) method of distance measurement developed by Tonry et al. (then of MIT) relies on the fact that the apparent graininess across the photo image of a remote galaxy decreases with increasing

distance, because the resolution of individual stars is ever more reduced. This method is effective in the 50 Mpc range, given Cepheid calibration, and in a 1999 survey of 300 nearby galaxies it resulted in a value for H_0 of ~ 77 . By using the Hubble Space Telescope (HST) to extend this very promising and surprisingly accurate method into the 75 Mpc range, Ferrarese et al. found an implied value for H_0 of ~ 69 .

The Tully-Fisher relation, which can be used to estimate celestial distances approaching 100 Mpc, is based on the correlation of galactic luminosity and rate of rotation - since the more luminous (and massive) a galaxy is, the faster it will rotate. When seen edge-on, a rotating galaxy's light will be slightly more red-shifted on the receding side, proportionally unshifted in the center, and slightly less red-shifted on the approaching side. By complex analytical techniques, this knowledge can be used to find galactic distances with remarkable reliability and accuracy. The important French effort known as the KLUN Project (Kinematics of the Local Universe) found $H_0 \sim 55$ (Theureau et al.) at around 90 Mpc with 'TF'.

The two most significant remaining techniques for estimating galactic distances over much larger portions of the observable universe are the SN1a (type Ia supernovae) and gravitational lensing methods. While SN1a measurements should be accurate over distances approaching 5 billion light-years (or half the radius of the visible universe), the fact that such events are extremely rare severely limits the usefulness of this method. Nevertheless, SN1a studies done by Alan Sandage and associates (a student of Hubble) in the 600 Mpc range indicate a value for H_0 of ~ 50 . This figure tallies well with that derived via gravitational lensing studies, which measure differences in the transit time of light from a very remote source as it bends around an intervening galactic mass in multiple paths on its way to Earth.

In any event, it becomes evident that the speculation regarding an increase in the expansion rate, which may indicate the operation of a cosmological constant, has been stimulated by this apparent decrease in the values of Hubble's constant as measured over increasing distances and thus *over greater lookback times!* Some have said, and perhaps correctly, that Hubble's constant is not so constant but varies over time in such a way that its value beyond our present observational limits becomes very important: having the effect of further reducing the *effective average value* of H_0 sought so desperately today. Thus, it is my belief that any attempt to definitively select the most probable model for the evolution and fate of the universe should always use *the lowest value for Hubble's constant* which is supported by observational data that is developed at the greatest possible distances - using the joint calibration of all suitable techniques.

The preferred HST Key Project methodology for measuring H_0 is: (1) to calibrate primary Cepheid distance indicators in our own local group (e.g., the Milky Way or Magellanic Clouds); (2) measure Cepheid distances for galaxies up to 50 Mpc away and calibrate secondary indicators (like TF, SBF, and SN1a); and (3) then apply these secondary indicators to the remotest galaxies for which observational data is acceptably accurate so that peculiar motions should have negligible effect. I would therefore like to conclude the present discussion with a brief synopsis of findings associated with the KLUN Project. In using two similar

approaches to resolve the distance to the Virgo cluster ('only' about 17.2 Mpc), the research group found the value of H_0 to be about 55. Moreover, a detailed analysis of the various error factors yields a confident value range of $44 < H_0 < 64$ (Tammann et al.), and calibration with SN1a models suggests the further constraint of $H_0 \leq 60$. Gravitational lensing statistics would also seem to imply a lower-end constraint of $H_0 \geq 40$.

As the rough 'Hubble time' relationship described above correctly indicates, a lower value of Hubble's constant suggests an older universe whereas a higher value implies a comparatively young universe. Many astronomers favor a lower value for H_0 because this avoids the globular cluster age concordance problem discussed above. Another reason for favoring a low Hubble constant is that models for large-scale galactic clustering are inconsistent with the observed distribution of galaxies if the Hubble constant is too high and the universe is therefore relatively young. Since a universe with low density, high Hubble constant, and no cosmological constant would be significantly younger than the oldest stars, the following section will describe the cosmological constant and concentrate on comparing three different "valid" (observationally possible) universe models which do incorporate it. These same models also correlate the confident-value range for H_0 given above to the universe's most probable age of 12-13 billion years.

One fundamental assumption of inflationary theory is that the universe has a flat or Euclidean spatial geometry. But when astrophysicists measure the total amount of detectable matter on the galactic cluster scale, they find only about 30% of that needed to make the cosmos geometrically flat. Inflationary theory also considers the positive gravitational effects of a *vacuum energy density*, however, since gravity couples all forms of matter and energy in general relativity. So, quantum vacuum fluctuations such as those we learned are responsible for virtual pair creation can help fill in this 'deficit', irrespective of the effect produced by an as-yet unknown *total* level of dark matter density.

It is apparent from the Field Equations that, strangely enough, a cosmological constant which has a positive value must at the same time act to create a *negative energy pressure* which would correspond to a repulsive gravitational 'force' for which there is no traditional precedent. This odd effect would aid the expansion of the universe, while the positive energy pressure associated with a negative constant (which is possible but unlikely) would oppose that expansion. Either way, the operation of a cosmological constant would seem to imply "new physics" that only a quantum gravity theory could explain, and have profound consequences for the Standard Model of particle physics. Nevertheless, the existence of vacuum energy was experimentally confirmed in 1996 by Steven Lamoreaux, who measured an obscure phenomenon called the Casimir effect.

The Dutch physicist Hendrick Casimir predicted in 1948 that two closely-spaced parallel *uncharged* conductive plates would experience a tiny attractive force due solely to quantum vacuum fluctuations of the electromagnetic field. According to theory, virtual photons whose wavelengths fit evenly into the gap (d) between two plates (of area A) cause the gap volume to have a non-zero potential energy which decreases as the gap is reduced. This vacuum energy

density corresponds to an attractive Casimir force calculated by the following equation: $F = \pi \hbar c A / 480 d^4$, where \hbar is Planck's constant and c is the speed of light. The force that Lamoreaux measured agreed with this equation to within the 5% experimental uncertainty.

Thus, the cosmological constant ('lambda' or λ) remains a physically plausible part of modern cosmology, based on its identification in field theory with the non-zero energy of the vacuum. Its principal attraction for astrophysicists is that it readily improves the agreement between observation and cosmological theory, without having to radically revise that theory as well as the preferred models of stellar evolution in order to resolve the universe 'age problem'.

Of course, therein lies the danger in relying on this kind of "quick fix", without a much more complete understanding of the nature and extent of dark matter. It is entirely possible that a proper theory of quantum gravity may be the only way to determine the true level of dark matter in the cosmos, and that such knowledge may obviate the need for a cosmological constant – in light of certain theoretical evidence which suggests that the net value of all modes of photonic vacuum fluctuation must cause λ to be very small and perhaps zero.

To assess how the Hubble and cosmological constants affect the evolution of the universe, it will be necessary to describe three simple "omega" (Ω) definitions from Friedmann's solution to the Field Equations. The first factor, Ω_{mo} , defines the effect of matter on universal expansion, where G is the gravitational constant and ρ_{mo} is the observed average matter density. This factor does not include the comparatively negligible value of radiative energy density in this epoch (being important only in about the first 300,000 years of cosmic evolution). The second factor, $\Omega_{\lambda o}$, defines the effect of the cosmological constant; and the third, Ω_{ko} , defines the effect of the spatial curvature constant k . The spatial geometry is open or Lobachevskian if $k < 0$, it is flat or Euclidean if $k = 0$, and is closed or Riemannian if $k > 0$. These three definitions are as follows:

$$\Omega_{mo} \equiv \frac{8\pi G}{3H_o^2} \rho_{mo} \quad \Omega_{\lambda o} \equiv \frac{\lambda}{3H_o^2} \quad \Omega_{ko} \equiv -\frac{k}{H_o^2}$$

Friedmann's simplified 'equation of motion' for the universe (shown below) describes the time evolution of the cosmic scale factor a , or the size of the cosmos, which is mathematically normalized to equal one (1) today (so that it drops out of the full relativistic metric form of the equation):

$$\Omega_{mo} + \Omega_{\lambda o} + \Omega_{ko} = 1,$$

where the subscript o indicates values measured at the present time. By simply rearranging the terms of this expression, the factor $\Omega_{total,o}$ can be defined to signify the ratio of the total matter and energy density to the critical density that would result in a flat universe:

$$\Omega_{total,o} \equiv \Omega_{mo} + \Omega_{\lambda o} = 1 - \Omega_{ko}.$$

Like the curvature constant, this factor directly indicates whether the spatial geometry of the universe is open, flat, or closed: in this case, however, it can be seen that if $\Omega_{total,o} < 1$ space is open, if $\Omega_{total,o} = 1$ space is flat, and if $\Omega_{total,o} > 1$ space is closed. The carefully-created Table below and the corresponding graph of

representative available universes will aptly illustrate how the matter density and cosmological constant jointly conspire to determine the configuration and ultimate fate of the universe. Even though the debate still rages over whether the universe is open, flat, or closed, we should be able to use the Table to select the prime candidate for each type of universe, as well as the 'superior' theoretical model overall in light of a logical assessment of all of our best data.

Representative Available Universes

	Ω_{mo}	$\Omega_{\lambda,o}$	$\Omega_{total,o}$	spatial geometry	fate
1	1	-1	0	open	collapses
2	1.5	-.5	1	flat	collapses
3	2	-.5	1.5	closed	collapses
4	.3	0	.3	open	expands
5	1	0	1	flat	expands
6	2	0	2	closed	collapses
7	.3	.3	.6	open	expands
8	.3	.7	1	flat	expands
9	1	1	2	closed	expands
10	.3	1.7	2	closed	expands
11	.3	2	2.3	closed	expands
12	2.5	.05	2.55	closed	collapses

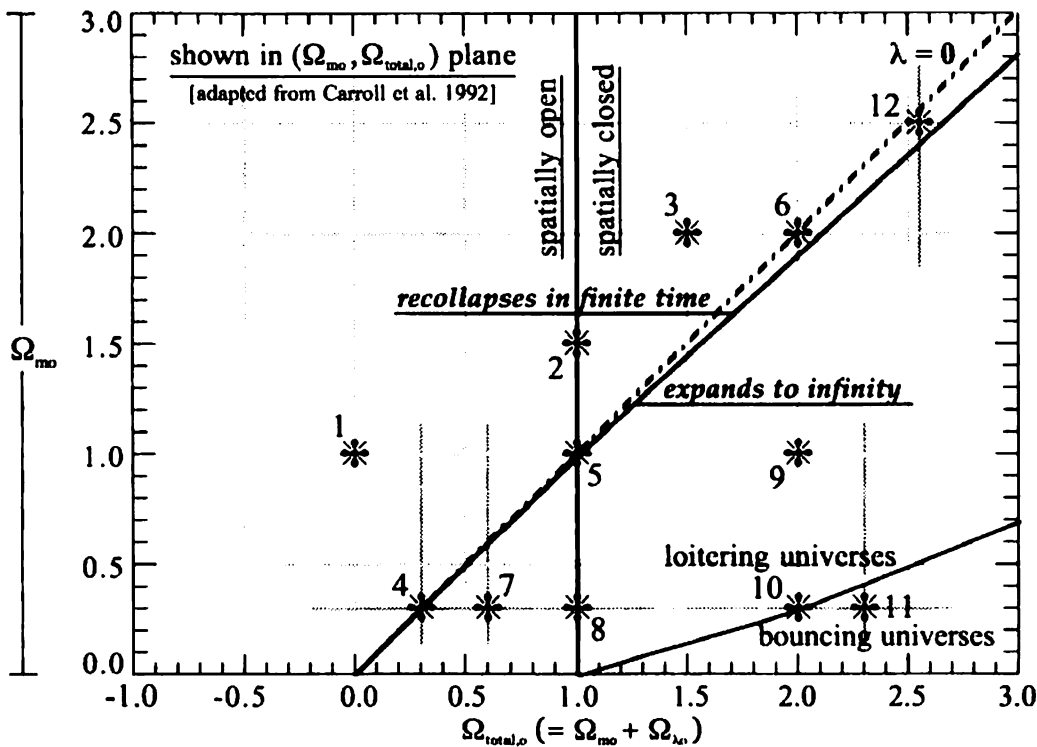


Fig. 74: behavior of representative cosmological models

[The Friedmann equations above and the available universe Table are adapted from the work of Eli Michael of the Dept. of Astrophysical and Planetary Sciences at the University of Colorado in Boulder; the supporting graph beneath the Table is adapted from *The Cosmological Constant* by Sean M. Carroll, William H. Press, and Edwin L. Turner (1992, ARA&A, 30, 499).]

About the graph: the center vertical line divides universes which are open (on the left) from those which are closed (on the right). Thus, models 2, 5, and 8 are flat universes. The diagonal broken (projected) line, indicating $\lambda = 0$, divides universes with a negative cosmological constant (to the left) from those with a positive λ value (on the right). A negative cosmological constant “doubly” adds to gravity’s attractive influence, hence universes with a negative λ value must always recollapse. A positive cosmological constant partially resists gravity because of its negative energy pressure, and would usually drive the universe to expand forever. For a universe model such as 12, with large Ω_{m} and small Ω_{e} , gravity dominates eventually and results in an ‘oscillating’ universe. The dark grey line which runs *almost* parallel with the line for $\lambda = 0$ also separates universes whose fate must be to expand forever from those which must recollapse in some finite time. Universes like model 10 which are located on the grey line in the lower right quadrant of the graph hover for a long time between expansion and collapse, hence they are ‘loitering’ in nature. Universes like model 11 have such a large cosmological constant that they are hyperbolic or ‘bouncing’ (similarly to one of the original Friedmann models described earlier).

Various observational methods may be used to constrain the value of the cosmological constant in any valid universe model, because both the geometry and evolution of the universe would be visibly affected by its operation. We will therefore try to rule out those available universe models listed in the Table which astronomical observation suggests are not valid.

At the outset, loitering universes (like 11) and bouncing universes (like 10) may be excluded due to the fact that the physics in such universes preclude the high red-shifts we know are associated with quasars and the cosmic microwave background radiation.

The universe models which are next most readily eliminated are those having a negative cosmological constant. Based on the highly-reliable SN1a method used by Reiss et al. (1998) and Perlmutter et al. (1999), $\Omega_{\text{e}} > 0$ is reported at 98-99% confidence respectively – without requiring a flat universe. This would not only rule out models 1, 2, and 3 of the Table, but models 4, 5, and 6 as well. The gravitational lensing statistics employed by Myungshin et al. (1997) suggest that the $\Omega_{\text{m}} = 1$ universe can be excluded at a 97% confidence level, which would also seem to exclude models 1 and 5, as well as model 9.

Out of the 12 available universe models shown in the Table, this leaves only models 7, 8, and 12; and these models thus respectively represent the most likely open, flat, and closed universes which we will be able to discuss in the present circumstances. In general, astrophysicists today tend to favor models such as 7 and 8, which show matter and energy density equal to about 30% of that which would result in a flat universe *without* the operation of a cosmological constant. Model 8 is actually preferred in light of the work of Chiba & Yoshii (1999), whose gravitational lensing studies *seem* to indicate that $\Omega_{\text{e}} \sim 0.7$.

Therefore, let's take a look at a plot of *age vs. H_0* for the flat universe of model 8, adapted from Eli Michael's web page (<http://super.colorado.edu/~michaele/lambda.html>), to see how the best figures we developed for those characteristics correlate with such a low mass density and high compensating lambda value. One thing to bear in mind is that this model is easily "corrected" for any awareness we gain of dark matter levels which cause $.3 < \Omega_{mo} < 1$, by a simple corresponding reduction in the value for $\Omega_{\lambda o}$, such that the universe remains flat (with $\Omega_{total,o}$ equal to 1).

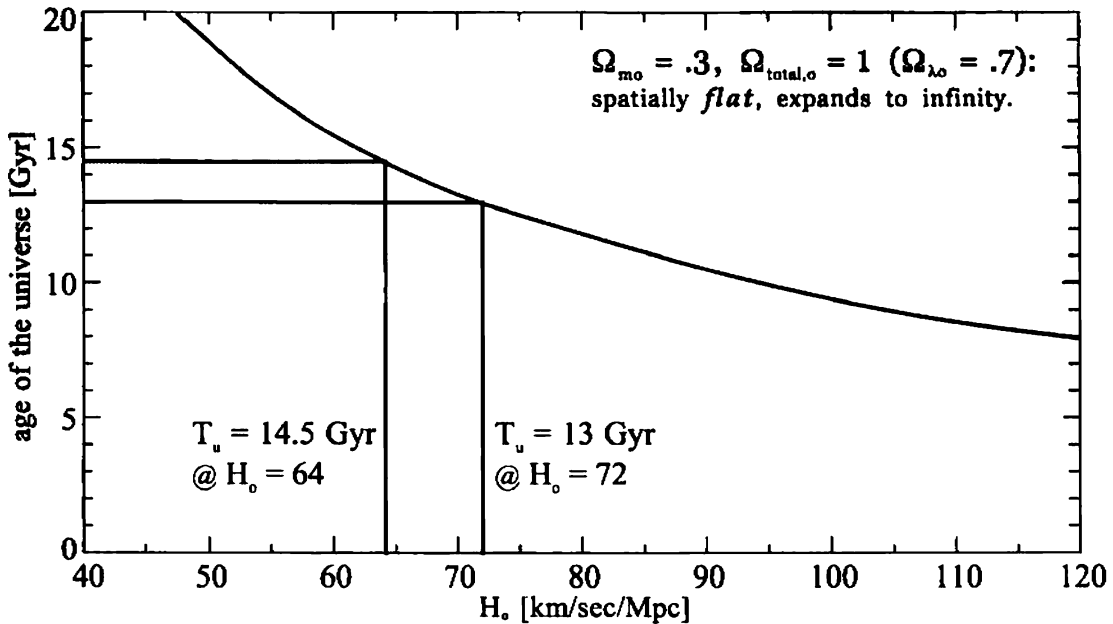


Fig. 75: age vs. H_0 for Flat Universe, model 8.

In this model, we can see that the best age of the universe derived earlier (at 13 billion years) would have to correspond to a Hubble constant of 72. While this value for H_0 is about exactly that preferred by many scientists, the KLUN Project results would seem to favor an older universe having the 'standard' mean age of 14.5 Gyr – wherein the Hubble constant has the peak confidence-range value of 64. Were the value for H_0 equal to 55 as in the preferred KLUN Project finding, the universe would have to be 17 Gyr old and this seems unlikely in light of the Hipparcos data. Furthermore, in this model the universe's age would lie off the chart given a confident lower-end value of $H_0 \sim 44$. With $\Omega_{\lambda o}$ equal to 0.7 in this model, we can find $\lambda = \Omega_{\lambda o}(3H_0^2) = 8602$ with a value for H_0 of 64.

In the open universe of model 7 (on the next page), the plot of *age vs. H_0* reveals an interesting correlation with the model above, in that a value of $H_0 = 64$ yields the preferred age of 13 Gyr. In this model, however, the vacuum energy density factor is only 0.3 and the corresponding value for $\Omega_{total,o}$ of 0.6 is once again insufficient to halt the expansion of the universe given the average matter density we are able to observe today. A preferred Hubble constant value of 55 would indicate that the universe is about 15 Gyr old, or just a bit older than the standard mean age given above. Any significantly lower value for H_0 would imply that the universe is much older than it is likely to be, as in the case above. With $\Omega_{\lambda o}$ equal to 0.3 in this model, we can find $\lambda = \Omega_{\lambda o}(3H_0^2) = 3686$ with a value for H_0 of 64.

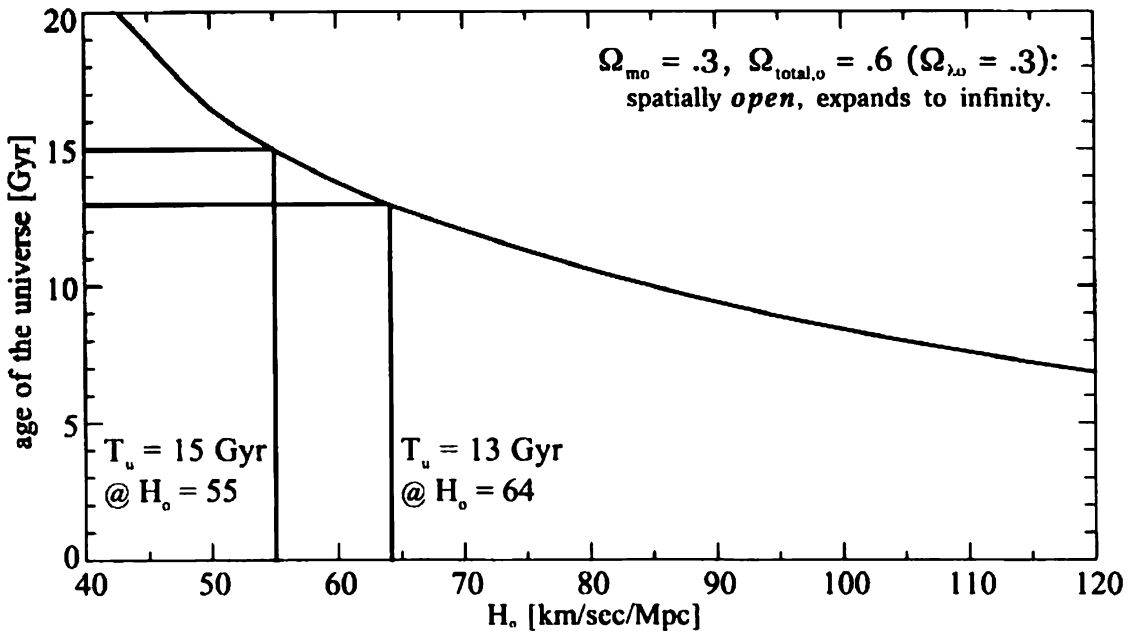


Fig. 76: age vs. H_o for Open Universe, model 7.

One of the reasons for favoring the closed universe model below (12) is that there is significant theoretical support for believing the cosmological constant must be positive but very close to zero. As can be seen in Fig. 74, the less matter there is in the universe, the closer to zero the cosmological constant has to be if the universe is to avoid unlimited expansion. The principal drawback of this model is that it is heavily reliant on high levels of dark matter, to achieve such a high value for Ω_{mo} (2.5). However, dual continuum cosmology provides a logical way to account for a radical increase in the universe's total mass, as mentioned, and astrophysicists are generally convinced that *most* of that mass is dark.

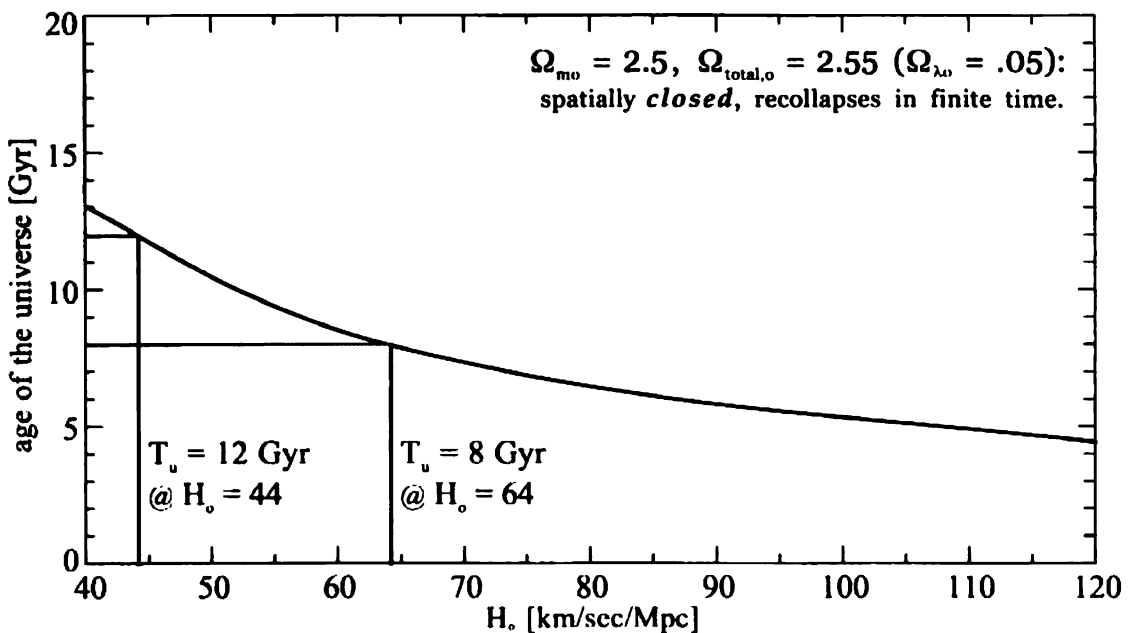


Fig. 77: age vs. H_o for Closed Universe, model 12.

It can also be observed, of course, that there is quite a range of equally valid oscillating universes in the very thin wedge-shaped region (in the upper right quadrant) of Fig. 74, which would be spatially closed without requiring such a high value for Ω_m . For instance, a closed universe with $\Omega_m = 1.5$ and $\Omega_\Lambda \sim .02$ should also be acceptable, which greatly alleviates any dark matter deficit. In fact, as Ω_m approaches 1 at the "nexus" of the graph in the lower center region, the cosmological constant factor Ω_Λ becomes vanishingly small, just as theoretical vacuum energy considerations suggest is preferable. Even so, with Ω_Λ equal to 0.05 in this model 12, we can find $\lambda = \Omega_\Lambda(3H_0^2) = 290$ with a value for H_0 of 44; and for any value of the Hubble constant between the lower constraining bound of 40 and the KLUN Project confident lower bound of 44, the age of the universe falls exactly within a preferred value range which is minimally commensurate with the age of the oldest stars.

The whole concept of dark matter represents perhaps the most important and intractable problem in astrophysics today. Its existence has been accepted for nearly 50 years, but a comprehensive explanation of its nature and extent has never been developed. All we have are observational techniques which give direct evidence of its presence, given the relativistic effect of matter density on the curvature of space. Using radial velocity analysis to measure the pull of gravity on stars in our own galactic halo, for instance, we can tell that the total mass of the Milky Way must be upwards of twice that produced by the visible stars. On this intragalactic scale, however, it is probable that white, brown, and black dwarf stars together comprise the bulk of this missing mass, with the addition of interstellar dust and gas.* On such a small cosmic scale, little truly "exotic" matter may be required to explain the observed level of gravitation; exotic matter being that which would inhabit another dimensional continuum.

However, using radial velocity analyses on the very largest of cosmic scales, that of galactic superclusters, one can trace out the gradient of the dark matter distribution relative to the over-all Hubble flow. In this way, bulk galactic flows have been mapped which seem to indicate that *a level of dark matter nearly equal to the critical density* must be present in order to account for them. It therefore appears that the greater distance over which we measure gravitational effects, the more total mass the universe must possess – and the more 'real' exotic matter may be required to make the universe even flat spatially. It is presently understood from Big Bang nucleosynthesis models that no more than 10% of the matter in the universe could be composed of baryon particles, like all ordinary matter is. In the final analysis, it can be shown that if the universe is in fact near critical density, at least 90% of the matter in the universe must be non-baryonic (but not necessarily exotic, like black holes).

Non-baryonic dark matter is generally divided into two categories: 'hot' dark particles having minute mass but speeds very close to that of light, and 'cold' dark particles with large mass but nonrelativistic velocity. The current favorite

***Note:** A *white dwarf* is the imploded core of a sun-type star, which very slowly cools until it is only a non-luminous cinder-like *black dwarf*. A *brown dwarf* is a massive gaseous object which shines only due to gravitational contraction and not from nuclear fusion.

candidate for cold dark matter is perhaps the Planck mass primordial black hole remnants mentioned earlier, although these will prove to be nearly impossible to detect. Taken together with the enormous black holes which are thought to reside at the heart of nearly every galaxy, such black particles and objects may provide enough exotic matter to explain missing gravitation at the galactic level. The best candidate for hot dark matter, which may explain large-scale cosmic structure, is the background neutrino flux left over from the Big Bang.

At one time, it was thought that neutrinos were essentially massless, and that therefore they could not contribute to a critical level of matter density. These non-baryonic particles are so incredibly numerous, however, that even with the tiniest rest mass they may provide enough gravitation to close the universe. The instantaneous neutrino flux density is about 336 in every cubic centimeter of the cosmos, which translates to about 50 billion neutrinos for every electron! Prof. Ned Wright of the Astronomy Dept. at UCLA has calculated that if the combined rest masses of the three types of neutrinos (or their antiparticles) exceeds about 40 eV, they could provide sufficient gravitation at the supercluster scale to make the universe be closed. Since the rest mass of the electron neutrino (as lightest of the family) is now thought to be constrained within the range of values between 0.07 and 2.2 eV, and the muon and tau neutrinos are far heavier proportionally while being equal in number, it is conceivable that a hierarchy of exotic matter other than galactic and primordial black holes may not be necessary.

In lieu of any working model for a complementary hierarchy of dark matter and dark energy, many cosmologists equate the concept of dark energy with the vacuum energy density itself. However, in the dual continuum model we will discuss from here on, this would be an unnecessary and erroneous assumption. In the author's view, both matter and energy exist in negative quantum time-space as they do in the space-time continuum. Both continuums would contain equal and opposite total quantum energy, although the amounts of matter and energy per se in each are both inversely proportional. Moreover, space-time is believed to express a spherical Riemannian curvature while negative time-space expresses a hyperbolic Lobachevskian curvature, so that the resultant coincident-continuum universe is very nearly flat overall. In this view, a tiny level of vacuum energy density associated with space itself is seen as being responsible for eventually 'tipping the balance' in favor of a closed and oscillating cosmos, by breaking the symmetry inherent in such a system.

I would therefore like to briefly expand on the specific ideas related to the Ashtekar theory of gravity that were set forth in Chapter 11, which I feel represent an excellent model for a balanced (if as yet "uncodified") system of **universal architecture**. As was intimated, if we do in fact assume a closed and oscillating universe comprising two coincident continuums (with a larger set of 'normal' space-time loops and a commingled set of smaller [negative] time-space loops), the *average* size of all positive loops will rise to a maximum at the cosmic cusp and it is only natural to assume that the average size of the negative loops will fall to a minimum over a corresponding time. This observation underlies my hypothesis that the matter and energy balance in negative time-space *now* is similar to what we would observe in space-time during a contractionary epoch.

The diagram below should be most helpful in visualizing this concept as well as certain other attributes of the proposed quantum matrix structure yet to be discussed. It depicts both the maximum and minimum proportional sizes of the potential loops comprising each such coincident continuum in relation to the size of an unoccupied potential loop. The actual loop diameters indicated are not intended to represent 'hard-and-fast' numbers essential to the dual continuum proposal, but to reflect a reasonable starting-point in mathematical investigation which might be consistent with established string theory and the Ashtekar theory of gravity. This Fig.78 should be appraised in conjunction with the foundational material discussed on pages 261 to 266 (of Chapter 11).

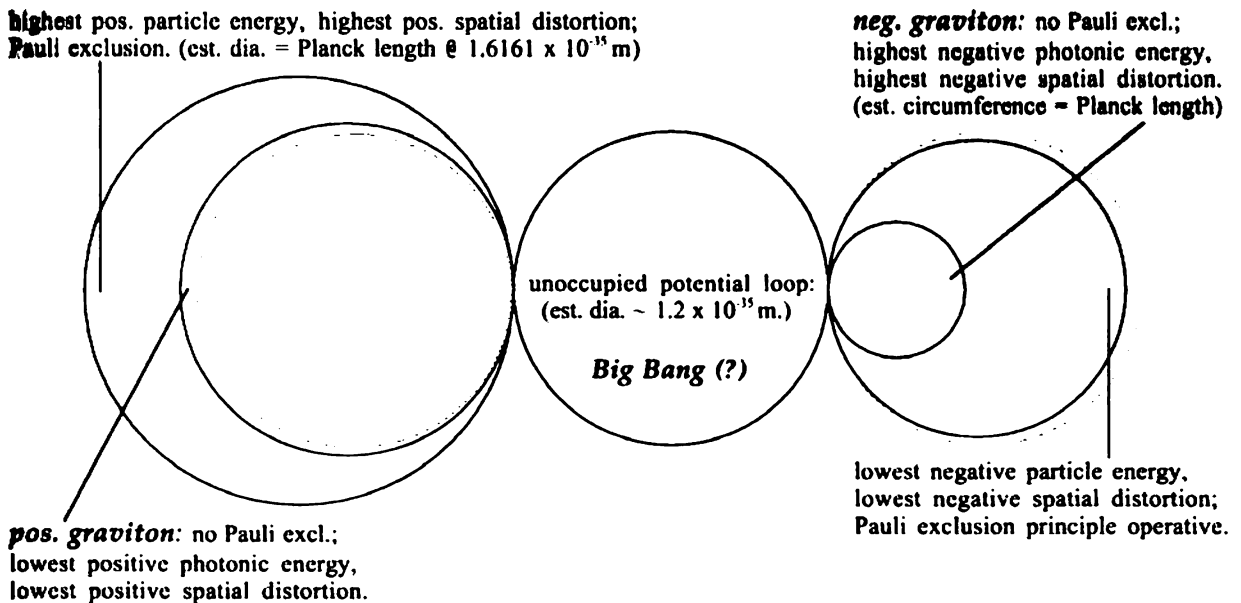


Fig. 78: *simplified proposed quantum matrix structure.*

In using the diagram above simply as a meditative conceptual tool, one of the first observations that comes to mind is that if the total number of quantum potential loops is fixed and finite, the universe *must* be closed and oscillating! In other words, the loop sizes given above are intended to represent absolute minimum values, and it is certainly possible that a larger basic loop-size system may in reality be required. But it also seems reasonable to believe that a change over time in the unoccupied potential loop size does not occur, or the relative properties of all matter and energy would be affected. And 'in the real world', the flat universe (with $\Omega_{\text{total}} = 1$) is unstable and must in the end seek either an open or closed resolution. So, *unless space-time loops are being continually created*, a point in time must come when no more expansion is possible, and the universe must recollapse.

It may be recalled that in *The Quest for Quantum Gravity* I stated (somewhat obliquely) that the appearance of an acceleration in the universal expansion rate today could perhaps be explained by considering that "the average size of the potential loops in our continuum could be rising faster than the average size of the loops in negative time-space is falling during the present universal epoch".

Because gravitons are bosons and not subject to Pauli exclusion, the bulk matter and graviton density ultimately determine the average potential loop size; and the preceding observation could thus be interpreted as indicating that matter is presently being converted into energy in space-time faster than dark energy in negative time-space is coalescing into dark matter!

Such a notion is of course predicated on the earlier proposition that energy, force, and matter in negative quantum time-space behave conversely to those same entities in space-time, according to a rather 'inverse' version of relativity. Hence, my contention that dark matter should tend to radiate or dissipate in the time-energy continuum while negative or dark EM energy tends to impinge or accumulate. Continuing to speculate sheerly from intuition, I might therefore conclude that dark energy can impinge until it *eventually* reaches high enough local levels to coalesce into dark matter, in an exact counterpart of the process in the very early space-time continuum whereby matter condensed out of energy *as soon as* symmetry between the forces was broken and local energy levels had dropped to a low enough level.

Before we take a look at an equally speculative but related format for how the joint evolution of a dual continuum universe might unfold over the course of one complete oscillatory cosmic cycle between successive Big Bangs, I'd like to point out another good example of the fascinating minor asymmetries which seem to be built into the universe (like the vacuum energy). If we consider the FitzGerald ratio table on pg. 312, we can easily see that a 'stationary' black hole in negative quantum time-space could perhaps be thought of as "falling away" from space-time at $v = \sqrt{2} \times c$, whereby it would still possess an imaginary mass exactly equivalent to its 'real' rest mass! I just haven't decided yet what the implications of this simple observation are . . .

Be that as it may, I consider the best *additional* theoretical support for a closed and oscillating cosmos to be Hawking's proposal of **the no-boundary universe**: regardless of whether or not the dual continuum theory is valid. But to see why that is, and what implications this proposal may have for universal evolution in dual continuum cosmology, we must take a moment to outline this facet of Prof. Hawking's work for those who are not that familiar with it.

He begins by assuming (as do many others) that any theory which successfully unifies quantum mechanics and gravity must incorporate the American physicist Richard Feynman's "sum over histories" approach to quantum theory. This mathematical technique involves specifying the wave functions of all possible histories of a given property of space-time and summing those functions in *imaginary time* to find the real probability of that property. Now, we've already seen that Bilaniuk et al. successfully used imaginary mass to describe the behavior of tachyonic objects in negative quantum time-space, so it shouldn't be shocking that the use of imaginary time *as a fourth coordinate which is indistinguishable from the three spatial directions* is a valid and powerful tool for rendering complex space-time calculations more manageable.

By combining this technique with the Einstein concept of the gravitational field as a product of curved space-time, it is possible to show that space-time may be finite in extent yet have no boundary or 'edge' at the Big Bang singularity

which constitutes an *absolute* beginning. Hawking himself describes imaginary time as existing “at right angles” to real time, and in imaginary time the laws of physics would still hold even at the beginning of *our* universe. But in doing the sum over histories for the no-boundary proposal, it would seem that the Big Bang had to *eventually* be followed by a Big Crunch which was likewise not an absolute end. Thus, in order to satisfy the requirement that a finite space-time have no absolute boundary or edge, *it seems to me* there would have to be an endless succession of Big Bangs and Big Crunches. Only with certain non-zero values for the cosmological constant would the universe *appear* to be open and infinite.

Proceeding now on the assumption that entropy is negative in the time-energy continuum to an extent, in line with Prof. Hawking’s earlier work on black hole evaporation, the following dual-continuum evolutionary characteristics could be postulated:

(1) the space-time continuum begins at the Big Bang in a hot, smooth, and highly-ordered energy state but matter quickly forms; an extended inflationary period follows wherein all matter finally decays and space-time becomes a cold and quasi-disordered realm, in which only a near-zero energy density remains by the time a contractionary cusp occurs; and this energy gradually concentrates as space-time collapses until a hot and highly-disordered matter state is attained at the advent of the Big Crunch; and (2) the time-energy continuum also begins at the Big Bang, but in a cold and highly-disordered negative energy state such that matter per se is very slow to form; an extended contractionary period follows wherein the matter lost from expanding space-time gradually accumulates and negative time-space attains a hot and quasi-ordered matter state by the time its expansionary cusp occurs; and this ‘imaginary’ matter finally radiates away as the time-energy continuum expands until a cold and ordered negative energy state is reached, *but wherein matter rapidly recondenses* at the advent of the Big Crunch.

In this view, it can be seen that matter and energy densities are mutually out-of-phase in the two coincident continuums, as was mentioned earlier. The crucial distinction to be made, in light of Hawking’s work, is that any loss of entropy in negative quantum time-space must be more than compensated for by a gain in entropy in space-time (so that the second law of thermodynamics is never violated overall). These postulated relationships can perhaps more clearly be summarized in the simple table below.

<i>space-time</i>		<i>neg. time-space</i>
hot/ordered matter cold/quasi-disordered energy hot/disordered matter	<p style="text-align: center;">Big Bang</p> <p style="text-align: center;">time ↓ cusp ↓ Big Crunch</p>	cold/disordered energy hot/quasi-ordered matter cold/ordered energy

The most common general observation about the no-boundary proposal is that it would seem to obviate the role of God in the universe, if one considers that all of ‘creation’ would then be “completely self-contained” and without true beginning or end. If the universe did in fact have an absolute beginning, it is certainly not inappropriate to believe that it had a Creator as First Cause. And

even if God allows the universe to proceed from such a beginning without intervening to temporarily alter or suspend the operation of physical laws, it is still impossible to know why those laws fit the particular design they do.

To account for this, many cosmologists invoke a version of the *anthropic principle* which essentially says that the universe exhibits just that level of inhomogeneity required for the formation of galaxies which could eventually stand a statistical chance of engendering sentient life. While some scientists (and lay persons) have accused Prof. Hawking of atheism, perhaps because groups like the Scientific Pantheists use his work as a substantiation of their philosophy, he is known by many to find this charge offensively untrue. In an April 1998 lecture entitled "Inflation: An Open and Shut Case", he states his belief that some version of the anthropic principle "is essential in quantum cosmology" to explain why the universe is so very close to flat. What he also says in his marvelous little best-selling book *A Brief History of Time* (if one reads carefully) is that even if the no-boundary proposal is true, God would still have had the option to specify the laws the universe obeys but little freedom to dictate the initial conditions therein *as a result* of those laws: and that there may only be one self-consistent unified theory which allows the existence of life.

And so, this Hawking model of *forever*, in which our own present universe is but one pulse in the never-ending heartbeat of **Eternity**, is not as contrary to religious philosophies like that of St. Thomas Aquinas as some might think. Aquinas argued that without a First Cause there could be no successive and unlimited chain of cause and effect such as we observe in nature, and only God could be that Cause; and that insentient natural artifacts and processes could not conspire to achieve orderly and consistent results, and especially living things, except by the design of an intelligent being whom we call God. Prof. Hawking's no-boundary proposal makes no claims about whether or not God actually exists; only that, if He does, He isn't arbitrary.

Voltaire once said "If God did not exist, it would be necessary to invent Him". I believe the real reason this is true is that humans only seem to exhibit much sense of *conscience* when they choose to believe in a deity whose powers are manifestly greater than their own. God then becomes the mirror of our souls, reminding us that – as divine as our consciousness is – we ourselves are *not* gods. But I don't think, as Stephen Hawking apparently does, that if we find a complete unified theory it would necessarily explain why the universe and we ourselves exist, or allow us to know the mind of God.

It has been said that Albert Einstein believed that what some mathematicians think of as the truest of all Holy Grails – an essential algebraic – could someday be found that revealed *not* the nature of God but the nature of His relationship to all physical Law. This I do, however, believe to be true. But because we live in a universe which is so nearly *flat*, and wherein the difference between right and wrong may sometimes be just as narrow as the vacuum energy band, the way we *know* God must always be the way of our heart.

It has also been said that the most fundamental principle in all physical law is that of uncertainty, so perhaps God is that most Absolute of Uncertainties which

transcends the otherwise ultimate positivity that nothing at all would ever exist. Thus, it could be that God is most properly understood as representing an Infinite Potential which must arise in an infinite time. And because most things in the universe exist in complementary pairs or in a state of duality, I almost can't help but perceive a God of Infinite Potential as the counterpart of the vacuum energy itself. For in light of the best of my cosmological understanding, I believe that only because of this most absolute of dualities is the Universe itself an endlessly repeating cycle of life.

But we mere mortals and our seemingly insignificant yet incredibly special world are delicately poised midway between nothingness and eternity. Even if we somehow manage not to destroy ourselves completely, those leaders who are ultimately responsible for our Earth's global community must have the vision to make whatever long-term investment in science is required to ensure we all have the suitable energy resources we need to live decently on *this* planet for now. With enough time, maybe our presently-unsatisfactory ethics will catch up to our technological potential so that we are actually worthy to live on other green worlds we may one day find.

I would like to believe a good part of that science has been revealed in these very pages. And, to waste the opportunity I believe we now have to go out among *all those stars* and seek answers to the cosmological questions we have, and perhaps find a greater knowledge of our own Creator, would to me represent an unconscionable sin. "For the invisible things of Him from the creation of the world are clearly seen, being understood by the things that are made, even His eternal power . . . (Romans 1:20)". All we really need is that sure and certain faith these things will come to pass.

APPENDIX A

DataSheets #1 to #16

Copper Wire Data

This DataSheet may be used to aid in the design of all of the major coils and windings required in the construction of Electrodynamic Field Generators from 4 to 100 feet in diameter. AWG diameters shown are also applicable to the nichrome and tungsten wire used in the various grid structures. The resistances as given are based on a resistivity for drawn copper equal to 10.371 ohms per circular mil foot @ 20°C. It should be noted that the rated DC ampacity of any given copper wire gauge is one-half that of the fourth lower gauge number and twice that of the fourth higher gauge number.

PART A:

size (gauge)	AWG dia. (mils)	nom. dia. (cm)	ft/lb	ft/ohm @20°C	ft/ohm @80°C	heavy* build OD (in)	heavy nom. OD (cm)	DC ampacity
2	257.6	.6543	4.978	6400	5212	.2617	.6648	120
3	229.4	.5827	6.277	5075	4133	.2335	.5932	100
4	204.3	.5189	7.918	4024	3277	.2084	.5293	80
5	181.9	.4620	9.980	3191	2599	.1859	.4722	70
6	162.0	.4115	12.59	2530	2060	.1659	.4214	60
7	144.3	.3665	15.87	2008	1635	.1481	.3762	50
8	128.5	.3264	20.00	1592	1296	.1322	.3358	40
9	114.4	.2906	25.25	1262	1028	.1177	.2990	35
10	101.9	.2588	31.85	1001	815.1	.1051	.2670	30
11	90.74	.2304	40.16	793.0	648.8	.0938	.2383	25
12	80.81	.2052	50.51	629.3	512.5	.0838	.2129	20.0
13	71.96	.1829	63.69	499.8	407.0	.0749	.1902	17.5
14	64.08	.1628	80.65	396.2	322.6	.0675	.1715	15.0
15	57.07	.1450	101.3	314.4	256.0	.0602	.1529	12.5
16	50.82	.1290	128.0	248.8	202.6	.0539	.1369	10.0
17	45.26	.1151	161.0	197.9	161.2	.0482	.1224	8.75
18	40.30	.1024	203.3	156.6	127.5	.0431	.1095	7.50
19	35.89	.0912	256.4	124.3	101.2	.0386	.0980	6.25
20	31.96	.0813	322.6	98.72	80.39	.0346	.0879	5.00
21	28.46	.0724	406.5	78.31	63.77	.0309	.0785	4.38
22	25.35	.0643	515.5	61.73	50.27	.0276	.0701	3.75
23	22.57	.0574	645.2	49.24	40.10	.0249	.0632	3.13
24	20.10	.0511	819.7	38.96	31.73	.0223	.0566	2.50
25	17.90	.0455	1031	30.89	25.15	.0199	.0505	2.19
26	15.94	.0404	1307	24.38	19.85	.0178	.0452	1.88
27	14.20	.0361	1639	19.44	15.83	.0161	.0409	1.57
28	12.64	.0320	2079	15.31	12.47	.0144	.0366	1.25
29	11.26	.0287	2584	12.31	10.02	.0130	.0330	1.10
30	10.03	.0254	3300	9.643	7.853	.0116	.0295	.94
31	8.928	.0226	4167	7.639	6.221	.0105	.0267	.78

Copper Wire Data

<u>size</u> <u>(gauge)</u>	<u>AWG</u> <u>dia.</u> <u>(mils)</u>	<u>nom.</u> <u>dia.</u> <u>(cm)</u>	<u>ft/lb</u>	<u>ft/ohm</u> <u>@20°C</u>	<u>ft/ohm</u> <u>@80°C</u>	<u>heavy*</u> <u>build</u> <u>OD (in)</u>	<u>heavy</u> <u>nom.</u> <u>OD (cm)</u>	<u>DC</u> <u>ampa-</u> <u>city</u>
32	7.950	.0203	5155	6.173	5.027	.0095	.0241	.63
33	7.080	.0180	6536	4.861	3.958	.0085	.0216	.55
34	6.305	.0160	8333	3.827	3.116	.0075	.0191	.47
35	5.615	.0142	10,537	3.024	2.463	.0067	.0170	.39
36	5.000	.0127	13,210	2.411	1.963	.0060	.0152	.31
37	4.453	.0114	16,313	1.953	1.590	.0055	.0140	.28
38	3.965	.0102	20,661	1.543	1.257	.0049	.0124	.24
39	3.531	.0089	26,954	1.181	.9617	.0043	.0109	.20
40	3.145	.0079	34,364	.9115	.7423	.0038	.0097	.16

* NOTE: The 'heavy build' wire OD is that expected in using magnet wire with a bondable polyester-imide coating and 180°C rating.

PART B:

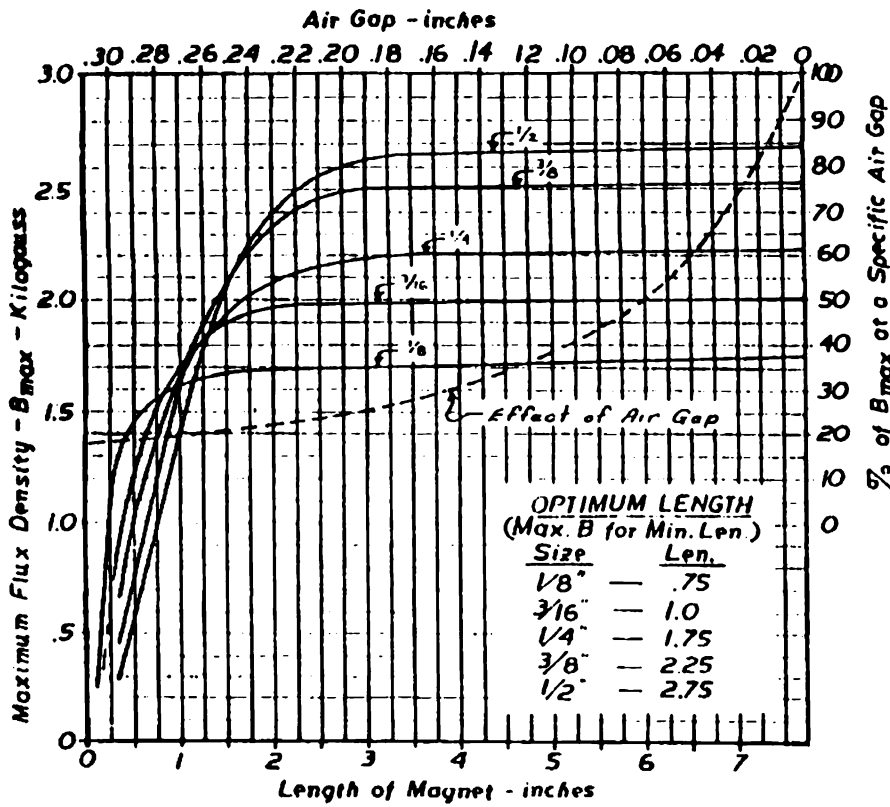
To facilitate the derivation of an accurate estimated ampacity for each rotor segment used in all larger EDF Generators, the following traditional specifications for large gauge standard annealed copper may be referenced per Work Sheet II(b).

<u>size</u> <u>(gauge)</u>	<u>AWG</u> <u>dia.</u> <u>(mils)</u>	<u>nom.</u> <u>dia.</u> <u>(cm)</u>	<u>cross section</u>		<u>ft/lb</u>	<u>ft/ohm</u> <u>@20°C</u>	<u>ft/ohm</u> <u>@80°C</u>	<u>DC</u> <u>ampa-</u> <u>city</u>
			<u>circ.</u> <u>mils</u>	<u>square</u> <u>inches</u>				
0000	460.0	1.1684	211,600	0.1662	1.561	20,400	16,612	280
000	409.6	1.0404	167,800	0.1318	1.968	16,180	13,176	240
00	364.8	.9266	133,100	0.1045	2.482	12,830	10,448	200
0	324.9	.8252	105,500	0.08289	3.130	10,180	8,225	160
1	289.3	.7348	83,690	0.06573	3.947	8,070	6,572	140

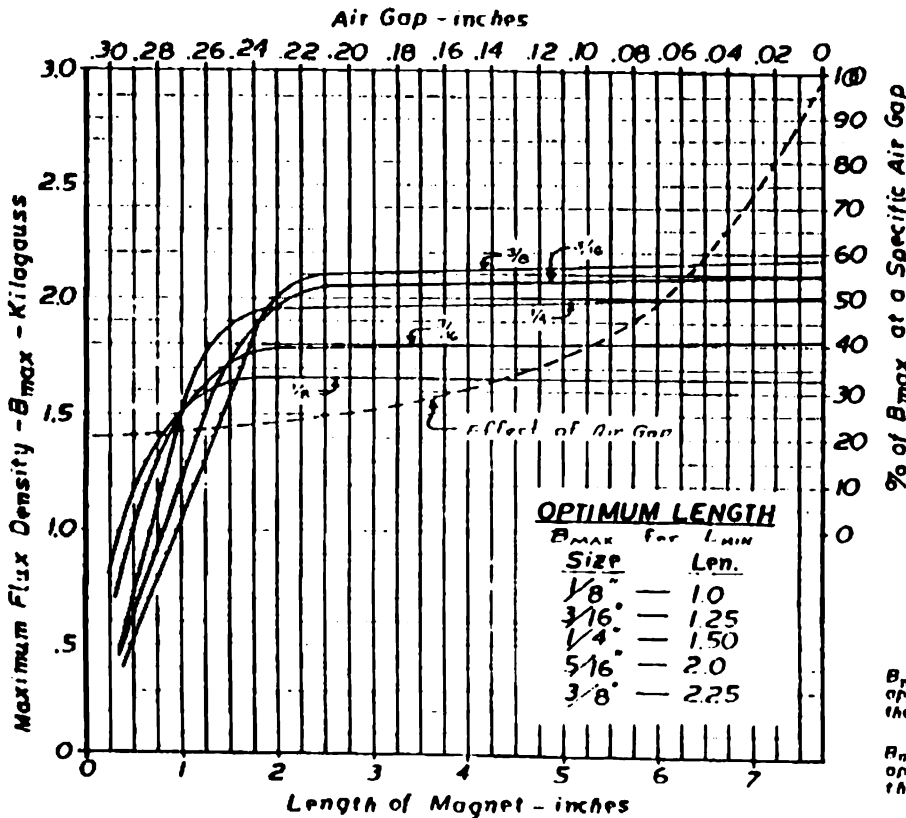
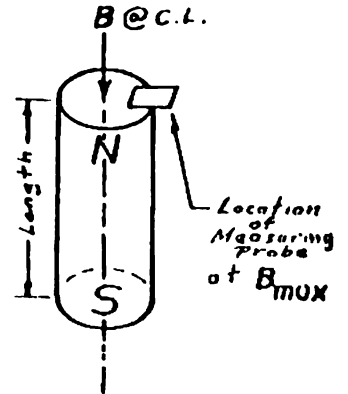
PART C: single build (insulated) nominal outside diameters.

<u>gauge</u>	<u>OD (in)</u>	<u>OD (cm)</u>	<u>gauge</u>	<u>OD (in)</u>	<u>OD (cm)</u>	<u>gauge</u>	<u>OD (in)</u>	<u>OD (cm)</u>
8	.1306	.3317	18	.0418	.1062	28	.0137	.0348
9	.1165	.2959	19	.0373	.0947	29	.0123	.0312
10	.1039	.2639	20	.0334	.0848	30	.0109	.0277
11	.0927	.2355	21	.0298	.0757	31	.0097	.0246
12	.0827	.2101	22	.0266	.0676	32	.0088	.0224
13	.0739	.1877	23	.0239	.0607	33	.0078	.0198
14	.0659	.1674	24	.0213	.0541	34	.0070	.0178
15	.0587	.1491	25	.0190	.0483	35	.0062	.0157
16	.0524	.1331	26	.0170	.0432	36	.0056	.0142
17	.0469	.1191	27	.0153	.0389	37	.0050	.0127

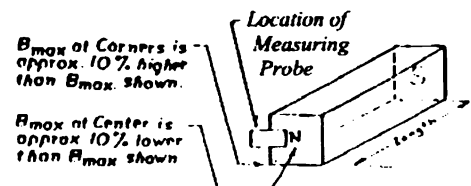
Small Magnet Comparison Graphs

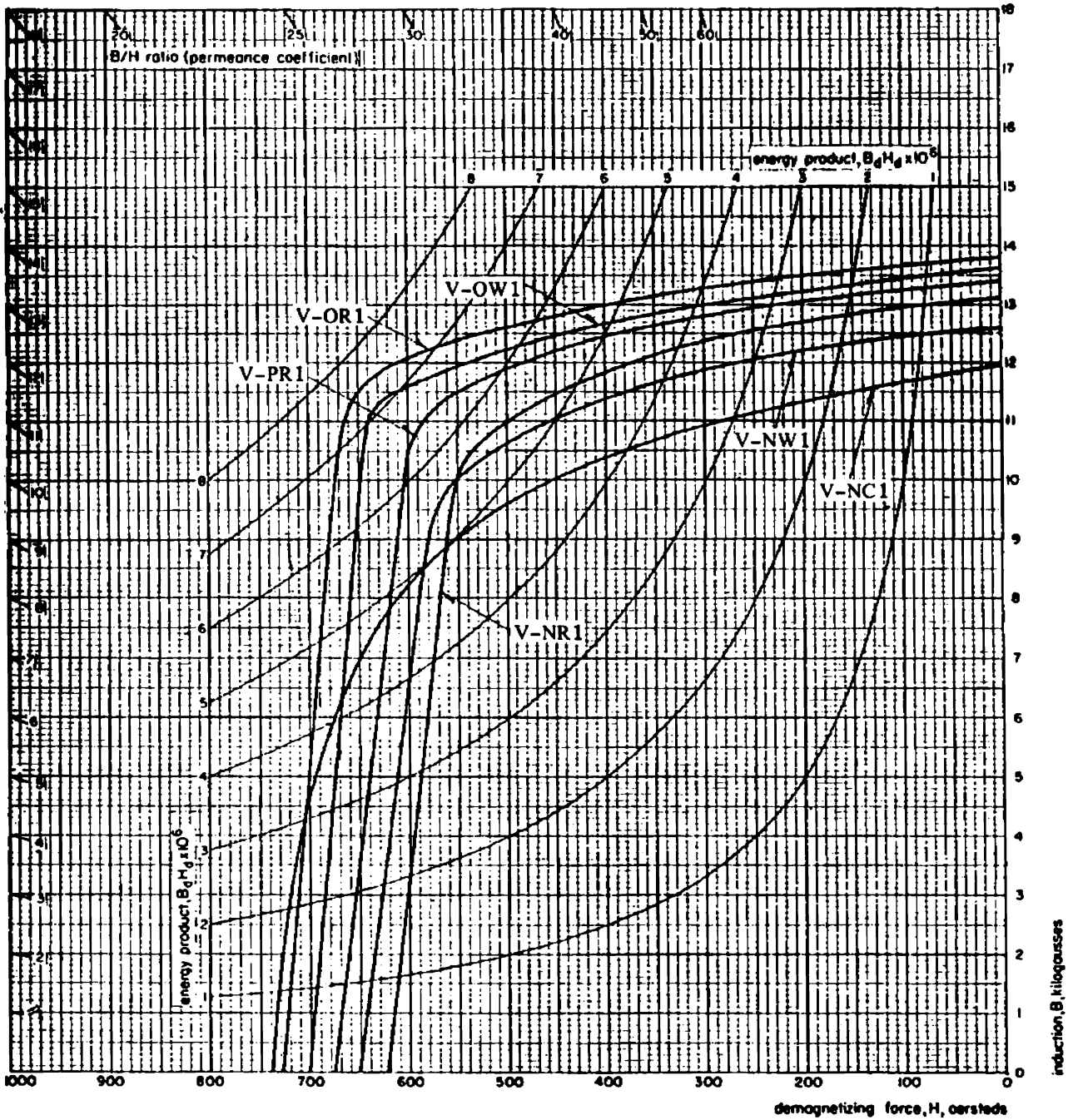


As can be seen clearly in these graphs, round bar magnets achieve a consistently higher gap flux density than square stock of the same size, as a result of significantly reduced leakage losses.



The illustration below reveals that square bar magnets have a higher corner flux density, but in practice much of this flux contributes to leakage losses instead of working gap flux density. In larger sizes, round bar magnets will yield very nearly the same total gap flux, with an over 21% weight savings, compared to square stock.



Alnico V B/H Graph

This DataSheet may be used in conjunction with the method outlined in WorkSheet V(b) to determine the working gap flux density of the Magnetic Rings employed in the Primary Power System. The load-line or B/H ratio established by the Rings is a function of their physical geometry, and must be calculated separately for each different size thereof.

DC Magnetization Curves

This graph presents data showing the magnetic flux density achieved in response to varying levels of magnetizing force (applied by a coil with dc current) for a large number of different magnetic materials. It may be utilized in conjunction with aWorkSheet XII(a) {Specific Armature Measurements} to determine the relative core permeability (k_r) of the Stationary Electromagnetic Armatures employed in the EDF Generator.

Contrary to the conception held by some, relative permeability is a dynamic (not static) characteristic of magnetic materials, and must be determined for each particular flux density achieved by a magnetic component in operation. By way of example, we may take a look at the magnetization curve for the pure annealed iron used as the Stationary Armature core material.

It can be seen here that iron begins to exhibit a magnetic field in response to a very small level of magnetizing force, at or below 0.2 oersteds (in the cgs unit system). The intrinsic induction achieved in kilogauss rises quite linearly and rapidly with increases in applied force through 1.0 oersted, at which point the induction reaches 11,500 gauss. The relative permeability at this point is the ratio of intrinsic induction (in gauss) to the magnetizing force (in oersteds): $11,500/1.0$ equals $k_r = 11,500$.

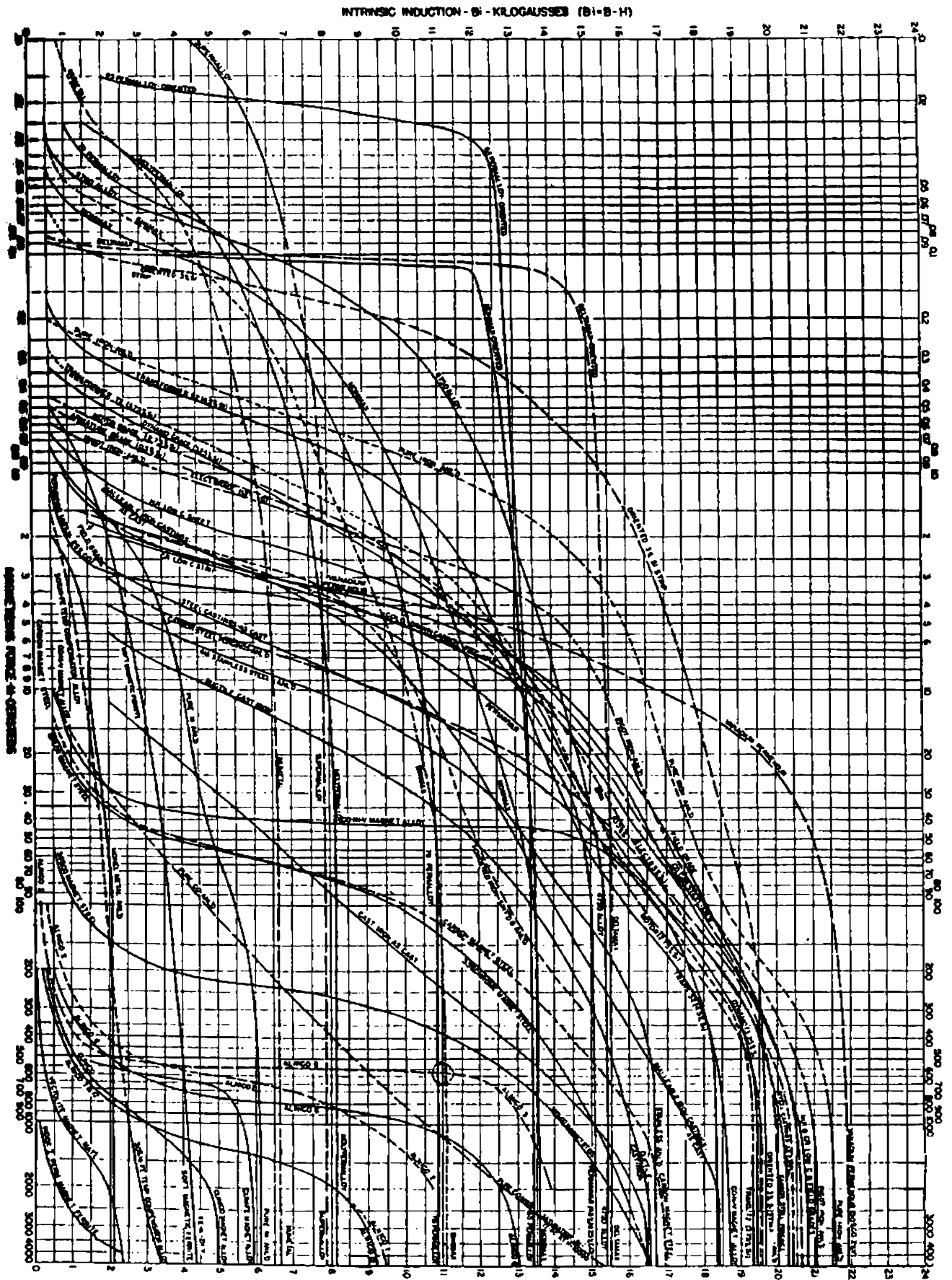
However, the closer a magnetic material is to saturation, where no further increase in applied force will yield a higher induction, the lower its relative permeability. For instance, at an intrinsic induction of 16,500, the magnetizing force required is 10 Oe, and the relative permeability has fallen to $16,500/10$ or 1,650. Finally, at an induction of about 21,500, when iron is to all intents and purposes saturated, the magnetizing force required has risen to 1,000 Oe and the relative permeability has dropped to $21,500/1,000$ or 21.5!

It is therefore obvious that the most efficient usage of a magnetic material must occur at the highest permeability that will allow a sufficiently large intrinsic induction to meet the requirements of the particular application. Ordinarily, this operating permeability would occur at the "knee" of the magnetization curve: the point where the slope of the curve starts becoming more horizontal than vertical.

As it turns out, iron actually has two distinct knees in its induction curve, the first at about 13 kilogauss and the second (reverse) knee at 18.5 kilogauss. Remembering the logarithmic nature of these magnetization curves, iron is normally operated at a point in the second relatively linear portion of its induction curve between these two points.

In working with the DC magnetization curves graph, it is apparent that a certain amount of imprecision is inherent due to the difficulties involved in interpretation of the data. Results should always be checked (whenever possible) in the manner shown in subsection E[6] of aWorkSheet XII(a). It must be stressed that this method of permeability verification requires the conversion of flux density into webers/meter² (Wb/m^2), in the MKS unit system, where one Wb/m^2 equals 10,000 (10^4) gauss. One gauss in turn equals 1 theoretical flux line (or 'maxwell') per cm^2 , so 10^4 gauss equals 10,000 flux lines per cm^2 . Since total flux Φ , equals flux density B times area A , one weber thus equals $10,000 \times 10,000$ or 10^8 magnetic lines of force (10^4 maxwells/ $\text{cm}^2 \times 10^4 \text{ cm}^2$).

DC Demagnetization Curves



Magnetic Ring Load-Line Formula

This DataSheet shows the derivation of the formula used to calculate the load-line established by the magnetic ring configuration employed in the Primary Power System. This calculation is performed within WorkSheet V(b) in conjunction with a simple graphic analysis of DataSheet #3, showing the demagnetization/energy product curves for Alnico V alloys.

The starting point of our derivation is the *standard permanent magnet formula* for B/H ratio in terms of the dimensions and permeance of the magnet:

$$B/H = P_t \frac{L_m}{A_m} \quad , \quad \text{where } P_t = \text{the ring's total permeance,} \\ L_m = \text{the ring's mean length (circumference) in cm,} \\ \text{and } A_m = \text{the ring's axial cross-sectional area in cm}^2.$$

Since $P_t = \sigma P_g$, where σ equals the leakage factor exhibited by the ring and P_g equals the permeance of the working flux gap, we may then show:

$$B/H = \sigma P_g \frac{L_m}{A_m} .$$

In the Rotor method, we may let $P_g = \frac{A_g}{L_g}$, and substitute as follows:

$$B/H = \sigma \frac{A_m L_m}{L_g A_g} \quad , \quad \text{where } A_g = \text{the cross-sectional area of the flux gap in cm}^2, \\ \text{and } L_g = \text{the length of the gap in cm.}$$

In this application (with no pole pieces), $A_m = A_g$, and therefore:

$$B/H = \sigma \frac{L_m}{L_g} \quad , \quad (\text{for C-formed rod}).$$

Magnetic Ring Leakage Factor

This DataSheet shows the derivation of the method used to determine the total flux leakage factor (σ) exhibited by the magnetic ring configuration employed in the Primary Power System. The leakage factor must be known before the magnetic ring's working gap flux density may be accurately calculated, as a function of the ring's actual physical measurements figured in WorkSheet V(a).

The starting point of our derivation is the *standard permanent magnet formula* for the leakage factor:

$$\sigma = P_t/P_g \quad , \quad \text{where } P_t = \text{the ring's total permeance,} \\ \text{and } P_g = \text{the permeance of the flux gap.}$$

Magnetic Ring Leakage Factor

In the Rotor method, P_g is understood to be equal to the area of the gap A_g divided by the length of the gap L_g . Therefore, we may write:

$$\sigma = \frac{P_g}{A_g/L_g} .$$

The value P_g may be calculated according to the formula $P_g = P_1 + P_2 + P_3$, where P_1 equals the permeance due to flux leakage from the magnet itself, and P_2 equals the permeance due to flux which fringes the working flux gap.

In the Rotor method, the fringing flux P_3 for a circular round-stock magnetic ring with a flux-bearing air gap is shown to be equal to .26 times the circumference of the flux gap (c_g), and is thought of as a hollow semicylindrical annulus surrounding the gap.

To develop a formula for the actual leakage flux component of the total flux leakage permeance in such a magnetic ring, for which a standard treatment by precedent is not readily available, we must first think of the ring as a straight rod magnet of circumference c_m equal to c_g . In the Rotor method, a logical basis does exist to then also apply the ratio .26 times the magnet circumference c_m in treating the leakage flux permeance component as a hollow semicylindrical annulus surrounding the magnet itself.

The expanded formula for total magnetic ring leakage factor then becomes:

$$\begin{aligned}\sigma &= \frac{P_1 + P_2 + P_3}{P_g} \\ &= \frac{(A_g/L_g) + .26(c_m + c_g)}{A_g/L_g} , \text{ (for C-formed rod).}\end{aligned}$$

DataSheet #7

Coil Voltage Formula

As it became known in the early 1800's that magnetism was associated with electricity and could be produced by it, many scientists started looking for the reverse effect: the production of electricity from magnetism. Over a roughly seven year period, Michael Faraday conducted a series of painstaking experiments which culminated in the discovery of **electromagnetic induction**. This scientific principle governs the action of all modern-day transformers and generators. This DataSheet should serve to further illuminate the material offered in Chapter 5 regarding electromagnetic induction for those readers desiring a more comprehensive explanation of the concepts discussed.

Faraday's Law of Induction, which is generally stated in two parts to clarify its operation in different situations, may be stated as follows:

(1) an electromotive force (or emf) is induced in a coil of wire whenever the amount of magnetic flux linking the coil is changing, and the magnitude of this emf is proportional to the rate of change of the flux; and

(2) an emf is induced in any conductor that is moving across (or "cutting") magnetic flux lines, and the magnitude of the emf is proportional to the rate at which the flux lines are being cut.

Coil Voltage Formula

At first glance, these two rules would seem to say essentially the same thing. However, the subtle distinction "rate of change" of magnetic flux in the Law's first statement is necessary to explain the manner in which a transformer works, whereby a secondary emf is induced without relative motion between the secondary coil and the source of flux. This first statement is therefore more appropriate for use in AC (alternating current) situations.

As is implicit in the Etude of Chapter 5 in the text, the general form for both these statements for a single conductor is $V = \Delta\phi/\Delta t$, where $\Delta\phi$ is the change of flux (in webers) and Δt is the time interval (in seconds). For a number (N) of multiple conductors, the expression becomes simply $V = N\Delta\phi/\Delta t$. To use the 1st rule with respect to an AC generator, where a coil is angularly rotated in a stationary field, the flux "linking" the coil must more accurately be thought of as the flux enclosed by the coil. This brings to bear the magnetic axiom $\phi = BA$, where the total flux ϕ equals the flux density B times the enclosed area A (in m²). Thus, $V = N\Delta\phi/\Delta t$ becomes $V = N(\Delta BA)/\Delta t$ and, since the coil assumes a relationship with respect to the field which is a function of the sine of its constantly changing angle of rotation, the voltage induced becomes $V = \omega NBA \sin\theta$ where ω is the angular velocity (2 π times the revolutions per second).

In experiments related to the production of a continuous (dc) voltage, Faraday believed it was more efficacious to envision the process of induction as the wire or coil cutting across the flux lines in a linear fashion per the Law of Induction's second statement. The traditional thought experiment of a conductor sliding on a pair of metallic rails perpendicular to a magnetic field perhaps best illustrates this concept. In this case, the rate of flux cutting depends fundamentally upon the flux density, but also on the length L of the conductor (in meters) and the linear speed at which it moves along the rails: $V = BLv$, where v equals the velocity in m/sec. A voltmeter connected between the rails would then form a closed circuit wherein the induced emf can be measured.

If we now replace the single conductor with a coil of N turns, we obtain $L = N\pi d$ as the length of the conductor (between the rails) and the formula becomes $V = NB\pi dv$ where d is the diameter of the turns and the distance between the rails. In the case of the EDF Generator, where a toroidal coil is axially rotated in a stationary field, the linear velocity v is equal to the coil circumference C times the revolutions per second (r), and the final form of the DC coil voltage formula used in this application becomes $V = NB\pi dCr$. In this particular case, an average value of B must be used (\bar{B}), as the magnetic field is not homogenous (or of constant flux density) but is developed by a discreet number of pole sets with breaks in between.

Finally, it should be noted that in a situation calling for the application of the second statement formula from above (or a variant thereof) where the magnetic field is not perpendicular to the motion of the wire or coil, the term $\sin\theta$ may be factored directly into the product of the other terms, in the general form $V = BLv \sin\theta$, provided the angle of incidence θ is known.

Bias Voltage Ratio

This DataSheet presents useful graphic information regarding the static characteristics of a typical low-amplification-factor triode vacuum tube. The values of plate voltage and current shown are therefore plotted against various negative dc potentials applied to the control grid, the successive plate characteristic curves being obtained by varying plate voltage and measuring plate current for different grid bias voltages.

The amplification factor (μ) is the ratio of the change in plate voltage to a change in grid voltage in the opposite direction, under the condition that the plate current and cathode voltage remain constant. The graph shown below is derived from an actual triode tube having an amplification factor of 4.2. Under a certain load, and at a dc source voltage of $E_0 = 250$, the operating current I_0 is .06 amps with a grid voltage of around -44. At a grid voltage = 0, current reaches I_{MAX} at .2 amps and voltage is reduced to 150; at grid voltages above 44 (that at E_0), plate voltage will be elevated above E_0 .

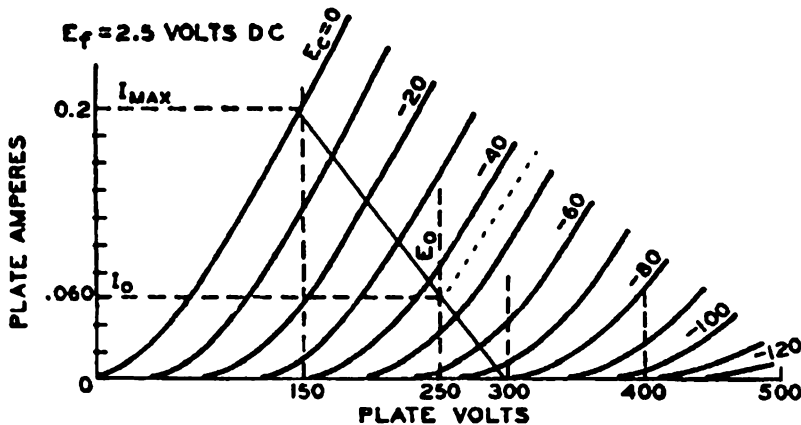


Fig. 30: plate characteristics curves graph
for typical triode of $\mu = 4.2$.

One very important operating characteristic of low- μ triode tubes as a class is that such a triode, if grid-biased to the point where plate current is effectively quenched or cut-off, will exhibit a plate voltage which is elevated to as high as approximately 140% of its regular operating (source) voltage E_0 . The higher the amplification factor, the lower the cutoff bias voltage will be as a percentage of E_0 , and the lower the cutoff bias voltage rise proportional to the source voltage will be as well. At μ values of up to about 12, the maximum value of plate voltage is roughly equal to the sum of the source voltage and the peak grid bias (at current cutoff), and higher factors yet will yield current cutoff-induced values of plate voltage which decreasingly approach this sum.

Since the magnitude of this cutoff bias grid voltage (as a percentage of E_0) is inversely proportional to the amplification factor, and the amplification factor exhibited by the rotating triode ring and grid arrays used in the Primary Power System is approximately equal (by virtue of design) to that of the triode tube depicted by the graph above, the purpose of this DataSheet is

Basic Voltage Ratio

to derive an accurate cutoff bias-to-source voltage ratio for the triode arrays of the Primary Power System through an analysis of said graph. This ratio will then become the design bias voltage ratio used in the derivation of the final field winding-to-bias winding turns ratios for each of the three (3) different Field Coils employed in any given size (model) vessel.

Selecting three separate plate current lines which each meet the 0-current axis at a clearly-interpreted point, we may find three corresponding pairs of cutoff bias voltage (E_c) and $1.4E_0$ values as follows:

- 1) $1.4 E_0$ equals 155 where E_c equals 40 volts;
- 2) $1.4 E_0$ equals 300 where E_c equals 80 volts;
- and 3) $1.4 E_0$ equals 420 where E_c equals 115 volts.

Therefore, E_0 equals 111, 215, and 300 volts respectively in the examples shown above. The resultant cutoff bias-to-source voltage ratios, expressed as a percentage, are then calculated below:

Example 1) $40/111 = 36.04\%$;

Example 2) $80/215 = 37.21\%$;

Example 3) $115/300 = 38.33\%$.

We may then find an average cutoff bias voltage ratio equal to .3719, which when multiplied by the source voltage E_0 yields the projected cutoff bias voltage.

From the pairs of values forming this average bias ratio, we might infer that the higher the source voltage, the higher the grid voltage required (as a percentage of E_0) to effect plate current cutoff. This observation is in fact probably correct. It must be stressed, however, that these plate characteristics obtain from a triode tube with an electrically-heated cathode (dc filament at 2.5 volts). This causes such a cathode to exhibit a far higher electron emissivity (and lower surface work function threshold) compared to the cold-cathode values which will be evidenced in the triode ring arrays of the Primary Power System. [see *Note in DataSheet #9.]

Once again, extensive prototype testing will be required to determine the exact extent to which these factors are mutually-compensating (considering the very high values of E_0 involved), and therefore how accurate the estimated average bias voltage ratio calculated above really would be in practice.

In light of just these considerations, and for simplicity's sake, the actual design bias voltage ratio selected for use at this time - in single-stage (1 η) Thermal Unit models and in three-stage (3 η) Drive Unit models as well - shall be equal to an even 40% of the field winding (source) voltage applied to each of the triode arrays (which is designated hereinabove as E_0). The principal reason for this decision is that this is in fact just that percentage we expect E_0 to be "boosted" as a result of a sufficient level of applied control grid bias voltage to ensure complete plate current cutoff.

NOTE: It is important to point out, before continuing on to DataSheet #9, that the high level of peak current I_{max} compared to operating current I_0 observed in Fig. 30 results from the fact that this graph obtains from the operation of two like tubes in 'push-pull' connection (where their control grids are hooked in series, not parallel). It will also be of some interest to note that the single-tube values for grid voltage E_c and operating current I_0 shown in Fig. 31 on the next page are the same as those in Fig. 30 even under a higher load which results in reduced I_{max} . The proper zero-signal control grid voltage for almost any normal triode in single-tube operation can be calculated according to the following simple relation:

$$\text{std. } E_{c_0} = 46.8\% \text{ of the cutoff bias ratio (as figured above) times the source voltage } E_0 .$$

Electrostatic Load-Line Formula

This DataSheet explains the derivation of the *resistance/voltage factor* used in selecting an appropriate maximum value for the ballast (plate) resistor applied to the anode ring of each triode rotor stage, as well as certain parameters affecting the electrode ring spacing of each inner induction and transfer ring array as a function of its estimated amplification factor, in terms of traditional vacuum tube operational concepts.

Reference is made to a graphic representation below of power triode plate characteristic data from an actual tube having an amplification factor (μ) of 4.2: approximately equal to the minimum design μ value of 4 specified in Spec-Sheet VIII {Electrode Array Construction} for all of the triode arrays.

Ordinarily, a triode tube used as a Class A* amplifier operates with an alternating (AC) signal voltage applied to the grid. A zero-signal bias voltage (E_c) is selected whereby this alternating signal swings the grid voltage from $E_c = 0$ on the positive half-cycle to a value of $2E_c$ on the negative swing. The plate current then assumes corresponding values of I_{max} ($2I_0$) and I_{min} , as shown in Fig.31 below. During these grid voltage swings, plate voltage E_0 also achieves corresponding values E_{min} and E_{max} respectively. The principle underlying the boosting of plate voltage to a value of approximately $1.4 E_0$ at plate current cutoff (with a negative grid voltage just above $2E_c$) is thus clearly illustrated. [* see Section C of WorkSheet VIII(b).]

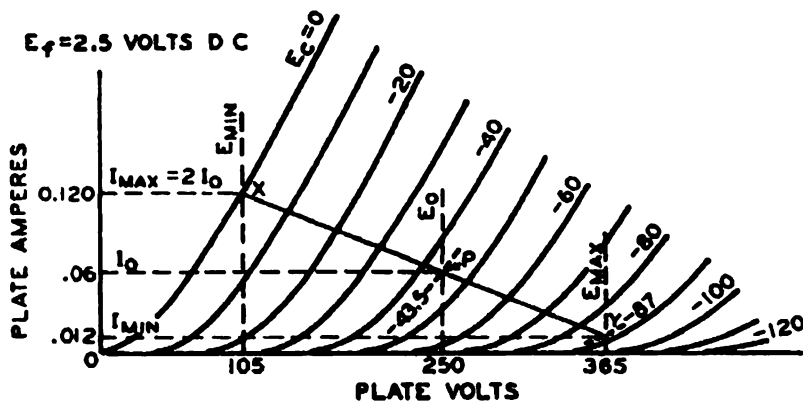


Fig. 31: graphic calculations of load-line
for power triode of $\mu = 4.2$.

In any event, the line drawn through operating point P (where E_c intersects the normal source voltage of 250) which connects points $2I_0$ and I_{min} is known as the *load-line*, and its slope corresponds to the value of the load resistance which should be applied to the plate (in series with the source). The nominal (approximate) value of the load resistance in ohms is then equal to $(E_{max} - E_{min})$ divided by $(I_{max} - I_{min})$, where E is in volts and I is in amperes:

$$R_L = \frac{E_{max} - E_{min}}{I_{max} - I_{min}} .$$

When the appropriate values from Fig.31 above are substituted into this load-line formula, an obvious simple variant of Ohm's Law, the resultant load resistance (R_L) obtained is 2,407 Ω . However, when a load-related consideration known as 'second-harmonic distortion' (in tube amplifier applications) is taken into account, which is not necessarily important in this application, a slightly higher value of 2500 Ω is deemed desirable. Thus, the appropriate R_L is numerically equal to 10 times the value of source voltage (E_0).

Because no actual tube data was found to be available for a power triode of amplification factor = 4 operating at a source voltage in the thousands, the maximum ratio of load resistance to source voltage for the application contemplated herein is taken to be the same as that figured above, or 10:1. A 'resistance/voltage factor' of $f_{rv} = 10$ should remain accurate as an upper bound despite increases in E_0 due to the largely linear nature of the triode plate characteristics shown in the graph above. (See *Note on next page.)

It should be noted that the load-line formula given above is also used for power pentode and beam power tubes, although these tubes are generally operated between current value points I_1 and I_2 on the load-line as illustrated in the generic plate characteristic representation (Fig.32) below. This diagram will be referred to in one or more WorkSheets related to the Primary Induction Ring Arrays employed in the EDF Generator.

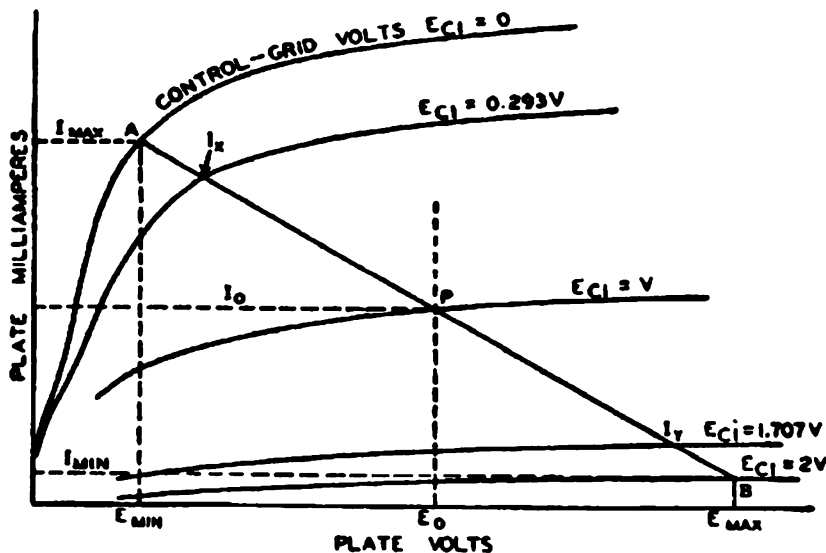


Fig. 32: graphic derivation of load-line for beam power pentode.

The relationship which tube amplification factor has to electrode (ring) spacing is readily understood as a function of the electric field intensity between the grid and cathode. Most traditional electron tubes employ a radial design wherein the cathode is a central post and the anode (plate) is an outer cylindrical envelope (see Fig.33 below). Because the electric field in this configuration is also radial, the force exerted by the grid upon cathode-emitted electrons is a function of Coulomb's Law and is thus proportional to the square of the distance between the electrodes:

$$F = \frac{kQq}{r^2}, \text{ where } r = \text{grid-to-cathode distance.}$$

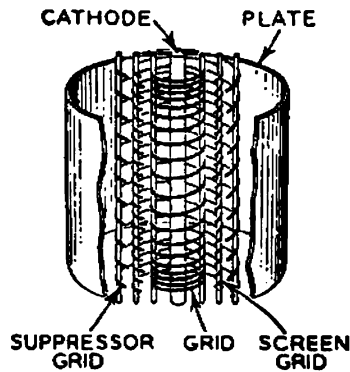


Fig. 33: cutaway showing radial construction of pentode tube.

In the plane-parallel ring array system contemplated herein, where the charge q on each 'plate' is equal (and opposite), this same force F is proportional to the linear distance between the plates (rings):

$$F = \frac{Vq}{d}, \quad \text{where } d = \text{grid-to-cathode spacing.}$$

Therefore, if the grid in a radial design tube is located midway between the plate (anode) and cathode, it may be thought of as having $1/(.5)^2$ or 4 times the force per volt influence upon cathode electrons as the plate itself. This geometry would result in an amplification factor of 4. However, in a linear (plane-parallel) tube or electrode array, the grid would have to be approximately 4 times closer to the cathode than the plate is to have the same effect on amplification factor. It is this line of reasoning which then underlies the Specifications governing electrode ring spacing in the Electrodynamic Field Generator.

***Note:** The dc cathode-to-plate resistance in the 'cold' cathode triode arrays will be substantially higher than that of a similar hot cathode arrangement, and this design resistance/voltage factor $f_v = 10$ may indeed cause the series coil groups to be over-ballasted in 1η rotor devices (excessively restricting the series coil group conduction current). In the same vein, these inherent plate resistances in multi-stage devices are ordinarily not series-additive, as they are in the Primary Power System.

To safeguard stage voltage gain capability, it is probably advisable to reduce this f_v factor only minimally from the maximum value of 10 in practice, as research and development progresses (under a program of extensive device testing). If higher series coil group current is desired in either 1η or 3η rotor devices, each of the rotating array cathodes may be composed of tungsten which is very modestly thoriated or thorium-adsorbed (to raise their emissivity and therefore array conduction current) rather than of the nickel alloy presently specified in SpecSheet VIII. This becomes necessary only to the extent that observed individual plate resistances exceed the maximum design values derived in WorkSheet VIII(b) {Triode Potential Differences}. If lower coil group current is desired in 1η rotor devices, measures may be taken as noted in subsec. B[1](d) thereof.

Applied Grid Resistances

In a normal resistance-coupled tube amplifier application, the load resistance (R_L) of a triode vacuum tube is approximately equal to the ballast (plate) resistor in parallel with the grid resistor of the following stage. Certain traditional formulas and empirical relationships then govern the ratio of the size of the ballast resistor to that of the grid resistor for each such stage, as a joint function of the actual AC cathode-to-plate resistance of that particular tube. In the EDF Generator, the AC plate resistance of each rotor triode array is simply equal to its capacitive reactance at the designated operating frequency.

In the 1 η rotor device contemplated herein, however, the grid resistor must be applied in parallel with only the dc cathode-to-plate resistance itself of the inner induction (triode) array. Since it is perhaps not possible to accurately predict the dc plate resistance for each different electrode ring array in this application, a ballast resistor-to-grid resistor ratio must be selected which effectively limits stage grid emission current to an acceptable level without causing too large a voltage drop across each grid resistor (and a subsequent loss of stage bias capability) in 3 η rotor devices.

This precaution is necessary because all vacuum tubes, and the vessel inner hull chamber contemplated herein, will contain some finite amount of residual gas which allows a minute flow of dc current through the grid resistor because the tube or array primary current heats the grid.

A comprehensive survey of both low- and high-gain triode tubes reveals that three such ballast resistor-to-grid resistor ratios predominate almost exclusively in traditional practice: 1:1, 1:2.2, and 1:4.7. In analyzing the effect upon series coil group current of these three different resistor relationships in 3 η rotor devices, it has been determined that the largest of these ratios is the most appropriate for use in initial experimentation. Substituting representative test values for ballast resistor R_p and grid resistor R_g which correspond to the ratio 1:4.7 into the dual parallel resistance formula below, we may derive the following relationship:

$$R_L = \frac{R_p \times R_g}{R_p + R_g} = \frac{10 \times 47}{10 + 47} = 8.25, \text{ or } .825 R_p.$$

Thus, by rearranging terms, we find that $R_p = R_L / .825$, and this relationship is used in WorkSheet VIII(b) {Triode Potential Differences} to calculate the necessary value for the ballast resistor which must be applied to each induction and transfer array anode ring in 3 η rotor devices as well as the corresponding stage control grid resistor value. It also becomes a relevant factor in the next DataSheet (#11) in defining the ratio of the applied ballast resistance R_p to the maximum design values of cathode-to-plate resistance (r_p) which must be observed in both 1 η and 3 η devices for optimum performance.

To determine the value of the inner induction array grid resistor in 1 η rotor devices, where the grid resistance is applied in parallel with the dc plate resistance r_p only, the relationships expressed in the formula above take the following form in WorkSheet VIII(b):

$$\text{net } R_L = \frac{r_p \times R_g}{r_p + R_g} = \frac{1.0 \times 4.7}{1.0 + 4.7} = .825 r_p.$$

Stage Plate Resistances

As a signal voltage amplifier, a class A* triode tube is used to reproduce grid-voltage variations across a plate resistor. These variations are essentially of the same waveform as the input signal voltage, but their amplitude is increased. Because the voltage variation across the plate resistor is much larger than that required to 'swing' the grid, amplification of the signal is obtained. [* see Section C of WorkSheet VIII(b).]

This does not mean, however, that the ratio of the voltage variation produced in the load resistance to the input signal voltage equals the amplification factor (μ). The ratio of the net plate voltage variation to input signal voltage in each stage actually approaches the amplification factor and represents the stage voltage gain. The voltage gain provided by each stage is expressed in the following formula:

$$\text{Voltage Gain } (V_o) = \frac{\mu \times R_L}{R_L + r_p}, \quad \text{where } R_L = \text{the load resistance,} \\ \text{and } r_p = \text{AC cathode-to-plate resistance.}$$

The graphic diagram below illustrates how the voltage gain approaches the amplification factor ever more closely as the load resistance is increased compared to the inherent AC plate resistance of the tube or electrode array. It can be seen from the graph that above the 'knee' of the voltage gain curve, further increases in load resistance are of little effectiveness in increasing stage gain and in practice should be avoided. Optimal performance is generally obtained when the ratio of R_L to r_p is from 5 to 7.

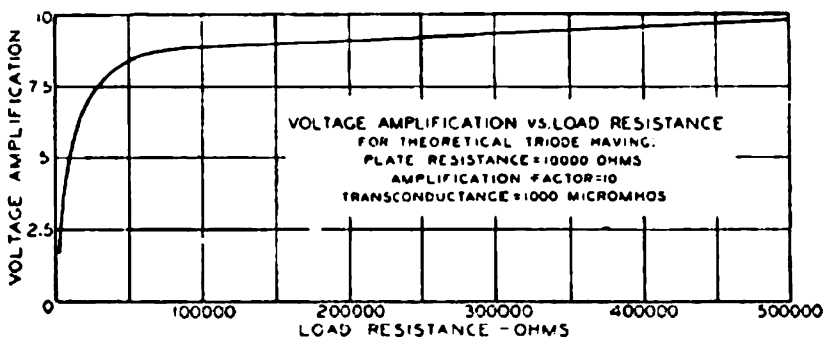


Fig. 34: voltage gain graph.

Applying such a corresponding ratio of 5:1 using representative test values in the formula above, with $\mu = 4$ as in the EDF Generator's rotating electrode arrays, we find:

$$V_o = \frac{4 \times 10,000}{10,000 + 2,000} = \frac{40,000}{12,000} = 3.33, \text{ or } 83.33\% \text{ of } \mu.$$

Thus, to obtain optimized total voltage gain across the 3 η rotor, the AC plate resistance (or capacitive reactance) of each array must fortuitously fall between 1/5 and 1/7 of the load resistance, or must be engineered to do so (by thoriation) as described at the end of DataSheet #9. The ratio 1/5 is therefore used in WorkSheet VIII(b) to determine the maximum design value of r_p , which must be observed in 3 η rotor devices.

Uniform Field Intensity Formula

This DataSheet explains the derivation of the all-important dc capacitance formula which governs the nature of field envelope current, relative to an expanded field voltage that is a joint function of the Field Ballast Capacitor value and the primary cathode-to-field emitter emissivity ratio in relationship to the rotor voltage. Although this formula and its derivation are both quite simple, the consequences thereof are crucial to an understanding of: (1) why the thrust produced in the field envelope is relatively uniform in strength throughout its composition or radial cross section; and (2) how the 'size' (value) of the Field Ballast Capacitors determines the Primary Voltage Expansion Ratio evidenced within the field envelope and the resultant maximum value of the thrust produced.

The first part of the Uniform Field Intensity (UFI) Formula is the standard electrostatic expression for electric field intensity as a function of an applied voltage: $E = V/d$, where d equals the distance in meters. This formula shows that field intensity is actually a simple ratio of volts per meter, or potential gradient. For our purposes, this gradient is roughly equal to or greater than that which allows an arc discharge through air or vacuum, at 3×10^6 volts/meter. This equation is always true as regards ordinary air dielectric capacitors, which are specifically designed to limit field intensity to a value significantly less than 3×10^6 v/m so that essentially no leakage current (between the plates) occurs.

The second part of the UFI formula is also true of all normal parallel-plate (equal-area) capacitors: $E = \sigma/\epsilon_0$, where σ equals the surface charge density of either plate and ϵ_0 is the universal electrostatic constant equal to 8.85×10^{-12} coul²/nt-m'. Thus, a parallel-plate capacitor exhibits a uniform surface charge density because the distance between the plates is uniform. Consequently, the field intensity between the plates is also uniform.

Within the application contemplated herein, however, the vessel hull plates are decidedly non-parallel, although equal in area, and the formation of a continuous leakage current is in fact desired. For purposes of uniform thrust production per unit surface area, we desire a uniform value of plate leakage current (and therefore plate voltage) per unit surface area despite the fact that both plate separation distance and local surface charge density are decidedly non-uniform. To show that this is possible and in fact *must be* true (provided the oppositely-charged plates are equal in area and conducting a continuous symmetrical flow of leakage current), we may combine the two equations above into one expression by taking the simple product of both sides of each as follows:

$$\text{since } E = V/d \text{ and } E = \sigma/\epsilon_0 ,$$

$$\text{then } E \times E = V/d \times \sigma/\epsilon_0 , \text{ and } E^2 = \frac{V\sigma}{d\epsilon_0} .$$

$$\text{Thus, in alternate form: } E = \sqrt{\frac{V\sigma}{d\epsilon_0}} .$$

An analysis of this formula shows that field intensity within the flow of

field envelope current will remain constant throughout a concentric range of semicircular d values (across the hull Neutral Ring) for any given value of voltage (V). The first important observation here is that a capacitor's plates (and hence the vessel hull) can exhibit specific values of extrinsic charge density σ as a function of an applied intrinsic voltage or, conversely, specific values of intrinsic voltage as a function of applied (or induced) extrinsic surface charge densities. The latter of these two situations is what actually occurs in this application, where no "hard-wired" source voltage is provided. Once field envelope current flow commences (as a result of static charge build-up), a redistribution of surface charge density according to the UFI formula causes a uniform (and expanded) intrinsic voltage to appear across the hull given the action of the Field Ballast Capacitors while operating entirely without ground reference in the rotor circuit.

The total amount of negative (electron) charge which must be removed from the Positive Zone sections of the hull, and stored in the Field Ballast Capacitors in order to achieve the required voltage expansion ratio within the field envelope, may be found using the UFI formula and is calculated in Worksheet VIII(d) {Primary Voltage Expansion Ratio}.*

AN IMPORTANT NOTE for Students and Electrical Engineers:

Oddly enough, the issue of *non-uniform* field intensity becomes important when we consider the rotor bypass current's passage across the vacuum chamber. Here, a much-greater space charge impedance is presented to that current than is presented across the primary arrays, as a result of the much-longer average transit time and lower non-uniform field intensity (between plates which are non-parallel and of unequal area! [The mean chamber transit distance should be exactly 5.208 times that in the primary arrays, with their minimum transit distances equal.] Since vacuum chamber current is a direct arc discharge, it is also a virtual conductor; and hence this higher impedance is readily circuit-communicated through it via the infamous Hooper effect's electrocentripetal force component.

Just as important as the accuracy of the UFI formula in this application is the accuracy with which the nominal cathode/emitter emissivity ratio as specified matches the desired ("design") Primary Voltage Expansion Ratio. This is because the actual emissivity ratio expressed determines the net PVE Ratio achieved proportional to the ballast capacitor value. However, the ballast capacitor value is based on the design PVE Ratio, whose net yield is contingent on the value of surface charge density σ from the UFI formula!

Moreover, as complex as this is, the joint accuracy of the UFI-formula-dependent computations described above has an indirect effect on the expressed value of vacuum chamber resistance. As outlined in DataSheet #14 {Stage Voltage Balance}, the space charge current between the rotor field emitters and the Emitter Ring will need to have a quite specific resistance value for the Field Induction System circuit to have the intended "load-line" and voltage values in 3η devices operating far beyond breakdown Field intensity. Thus, errors in assigning the proper value for the ballast capacitors will alter their desired charging rate, affecting the vacuum chamber resistance expressed and the whole System's off-resonance circuit time constant!

* It must be stressed that separate high-capacity charge storage means are required to prevent the 'grounding' of positive hull section potential (by static ionization charge from operation in air) during the start-up period before the field envelope is fully formed. This task is handled by ambient charge capacitors which are connected via diodes to the Primary Induction Ring Arrays as part of a Field Voltage Control System {see Fig. 28 of SpecSheet IX}.

Instantaneous Charge Differential

The purpose of this DataSheet is to clarify the operative mechanism by which a substantial Primary Voltage Expansion Ratio is evidenced across the external vessel hull of the EDF Generator. As delineated in WorkSheet VIII(d) (and pursuant to the considerations of DataSheet #12 {Uniform Field Intensity Formula}), a specific amount of electronic charge must be removed and withheld from the hull positive Zones in order to establish a full flow of field envelope current at the specified operating level(s) of Field Voltage.

As established in WorkSheet VIII(d), the Primary Voltage Expansion Ratio achieved by the EDF Generator is contingent upon the vessel hull's static capacitance. Ordinarily, the voltage across a DC capacitor will rise quickly (according to the circuit time constant) to the intrinsic voltage of an applied source. In this application, however, there is no 'hard-wired' source voltage applied, and the voltage across the hull becomes a function of an extrinsic surface charge density supplied by electrostatic means. Even so, this voltage will conform to a value figured according to the standard relation $V = Q/C$, but the fact that field envelope current constitutes a continuous leakage current (between the capacitive hull plates) must be taken into consideration.

In a DC capacitor which exhibits continuous plate leakage, the operative voltage across the capacitance must be figured using the *Instantaneous Charge Differential*, or Q_{dc} , which represents (in its simplest form) the ratio of the change in charging current (ΔI_c) to the change in the discharge current (ΔI_d) times the time differential in seconds (t_d) until equilibrium is reached (where $I_c = I_d$). Therefore, $Q_{dc} = \Delta I_c t_d / \Delta I_d$, and the capacitive voltage achieved becomes $V = Q_{dc} / C = \Delta I_c t_d / \Delta I_d C$, where (in this case) the expressed voltage is solely a function of electrostatically-supplied plate charge.

Thus, it is evident that to build an extremely high potential difference across the vessel hull, we must be able to charge the positive hull sections much more quickly than the rate at which that charge is neutralized by field envelope current discharge, until the requisite Field Voltage is achieved (at nominal rotor speed). If we assume for simplicity's sake that the transit time of Field current electrons is essentially zero, this effectively means that we must be able to charge the Positive Zones far more rapidly (across the Primary Induction Ring Arrays) than the Negative Ring tends to be charged by the rotor field emitters (across the vacuum chamber). Since we know (as discussed in Section F of WorkSheet VIII(e)) that the potential difference across the Arrays is the same as that across the vacuum chamber, we must therefore somehow achieve a far higher emissivity at the Array cathodes than at the field emitters. This condition will define the Primary Voltage Expansion Ratio to be supported by the Field Ballast Capacitors.

It may be recalled that SpecSheet VIII {Electrode Array Construction} calls for the unit pentode array cathodes to be composed of "thorium-adsorbed" tungsten plate, whereas the field emitters are to be composed of a tungsten-copper sintered composite (per SpecSheet II {Rotor Segment Dimensions}). The fundamental goal here in specifying these different electron-emitting materials is thereby to achieve a vast difference in the amount of electrons that each group of components will tend to emit at a given voltage and temperature. By this mechanism, we may achieve a substantial Instantaneous Charge Differential

and concomitant Primary Voltage Expansion Ratio. A brief technical explanation of the manner in which this goal may be realized follows below.

Mobile conduction electrons within a metallic substance tend to create a surface dipole layer relative to the uniform positive (atomic) background charge distribution which represents its overall structure. This condition causes the electrostatic potential outside the surface to be greater than that within the crystal structure of the metal and, along with short-range Coulomb interactions, acts to keep the electrons 'corralled' within the metal.

The work function of any substance (ϕ) is therefore the minimum energy required to remove an electron from deep within the bulk material, against this resistive effect, to a point some macroscopic distance outside the surface boundary. This characteristic material property was being investigated well before Einstein's famous 1905 paper on the photoelectric effect, and the measured work functions of all the elements were found to be closely-grouped at around $\phi = 3.5 \pm 1.5$ eV.

Pioneering work done by I. Langmuir and K.H. Kingdom (circa 1923) on the electron emissivity characteristics of clean metal surfaces revealed that the current density of electrons 'evaporated' from a hot tungsten filament greatly increased after the filament was exposed to certain metal vapors, whereby foreign metallic atoms were deposited by gaseous adsorption on the surface. Early experiments identified the alkaline rare-earth elements cesium (Cs) and thorium (Th) as being remarkably effective in this respect.

This phenomenon, called *thermionic emission*, therefore involves the somewhat catalytic thermal activation of electrons over the surface energy barrier and into the vacuum, and the greatest increase in emissivity occurs for adsorbates which effect the greatest decrease in substrate work function. It was discovered, however, that the reduction in the work function ϕ 'bottoms out' and actually reverses for pure cesium or thorium adsorption approaching a full atomic monolayer coverage.

The natural work function of tungsten metal is approximately 4.6 eV and, when thorium vapor is adsorbed to a sub-monolayer coverage of about .7 (or 70%), a minimum work function of approximately 1.7 eV is achieved. Thus, a 63% reduction in work function may be accomplished by this technique, which might lead one to assume that a corresponding 270% increase in electron emissivity current density would take place. In reality, though, a complex exponential increase in emissivity occurs across this range of work function values, with corresponding current densities dozens and eventually thousands of times higher than those measured for pure tungsten filaments (co-dependent on operating temperature).

This effect was soon put to practical use in the development of vacuum tubes with far higher power outputs and lower cathode operating temperatures than would otherwise be possible using pure tungsten cathodes. To modify the rather extreme drop in work function associated with pure thorium adsorbate, and therefore control cathode emissivity such that the maximum operating plate current rating of the tube was not exceeded, *thoriated-tungsten* filaments or cathodes were developed. In this case, the tungsten emitter was impregnated with the oxide of thorium applied in a comparatively thick layer.

It was subsequently determined experimentally, however, that in applications calling for operating current densities above around 8 amps/cm², the use of alkaline rare-earth oxide coatings was not practicable (due to destructive disruption of the coating layer). Because the unit pentode array current density in the EDF Generator perforce lies far above this working limit,

selective control of the cathode work function and therefore control of the Instantaneous Charge Differential (exhibited with respect to the charging of the hull capacitance) must be accomplished by very precise control of the relative level of thorium adsorbate coverage. Fortunately, this type of production technique is readily practicable today.

Astute readers will no doubt realize at this point that there are three interrelated factors which ultimately determine the net voltage expansion achieved across the hull:

- (i) the work function of the primary unit cathodes;
- (ii) the 'size' of the field ballast capacitors; and
- (iii) vacuum chamber space charge/transit time considerations.

The optimum joint resolution of these three factors into the working design Specifications for EDF Generators of both Thermal Power and Impulse Drive Unit models will obviously require the extensive use of calculus, computer modeling, and dynamic testing techniques to achieve. More complex than any other single aspect of this proposed new technology, the successful demonstration of the requisite Primary Voltage Expansion Ratio(s) is nevertheless possible with currently available materials, production techniques, and computing capability.

However, a careful mathematical study has been done which reveals that the Primary Voltage Expansion Ratios of Drive Unit vessels of from 20 to 100 feet in diameter range from 28,032:1 to a maximum of 61,928:1 respectively. Not only does this range of values fall nicely within that of known thorium-stimulated emission current density ratios (over clean tungsten cathodes), but this suggests that EDF Generators of these sizes should function properly when the ratios of the respective temperature emissivity factors of their primary unit (Power Resistor) cathodes and rotor field emitters are approximately equal to or greater than their respective Primary Voltage Expansion Ratios!

If the primary cathodes and field emitters happen to operate at the same temperature, this temperature emissivity factor = $e^{-\phi/kT}$, where e is the base of natural logarithms 2.71828..., k is Boltzman's constant, and T is the absolute temperature in °K, derives from the famous Richardson-Dushman equation: a formula for the correct thermionic emission current density J of a clean metal cathode in vacuum. Thus, properly expressed in mathematical terms, the above-stated principle of ratio equivalence is as follows:

$$\text{design Primary Voltage Expansion Ratio} \leq \text{cathode } e^{-\phi/kT} / \text{emitter } e^{-\phi/kT}.$$

It is therefore possible to accurately calculate the exact level of primary cathode thorium adsorption which would be required to effect a specific net rate of cathode emissivity, given the emissivity of the field emitters used, from known vacuum tube test data.

It must be pointed out that when the relative emissivity factors of the primary cathodes and field emitters are calculated using the expression above, the work function ϕ should be specified in electron-volts (eV) and Boltzman's constant therefore in eV/°K at 8.6174×10^{-5} . Alternatively, ϕ may be specified in ergs and the constant in ergs/°K at 1.38×10^{-16} , although the electron-volt-based method is easier to work with. A Table of actual work function values for the primary cathodes of the theoretical 4ft. prototype Drive Unit, which are dependent on an as yet unknown field emitter operating temperature, is provided in Section 2 of Material SpecSheet C. The emissivity factor is equal to the reciprocal of the kT root of e to the power ϕ , but must be multiplied by the term (kT) when the cathodes and emitters operate at different temperatures.

Stage Voltage Balance

The phrase "stage voltage balance" as used in relation to the EDF Generator may be taken to have 4 different meanings, all of which involve important operating considerations. This DataSheet examines each such interpretation, as it relates to both the 1 η and 3 η rotor variants of this device.

(A) The first example of stage voltage balance is the 'automatic' equalization of the respective induction array (and transfer array) potential differences, due to their engineered mutual capacitive relationships, despite the fact that the three independent field winding voltages of each series coil group are all different from one another. If not for this convenient attribute of Primary Power System series-semicircuit design, matching Field Coil voltage outputs to array potential differences in 3 η machines would become a daunting task requiring the creation of secondary bias windings to accomplish.

(B) The remaining stage voltage balance considerations will apply mainly to 3 η rotor devices, and the next most important interpretation to look at involves accurately determining the peak series coil group dc current in order to verify that the level of this current is well within field winding ampacity. Data thereby derived will also be used to project the peak dc voltage swing to be expected across each electrode array and around the rotor circuit.

It will therefore be necessary to return once again to a brief graphic analysis of the same graph depicted in Fig.31 of DataSheet #9 {Electrostatic Load-Line Formula}. This tube data graph (it may be recalled) was used to derive an appropriate resistance/voltage factor (f_v) for use in the Primary Power System, and is taken to be representative of the operating characteristics it would be reasonable to expect within the System triode arrays by virtue of the common design amplification factor ($\mu \approx 4$).

Due to the important operating considerations discussed in Section C of WorkSheet VIII(b) {Triode Potential Differences}, a new load-line must be erected in order to tell (using the data provided) what the maximum dc series current (I_{max}) would be as a function of its level at the normal dc operating voltage E_o given a peak 40% cutoff bias voltage rise. This will allow us to derive a Zero-Bias (full-signal) Voltage Factor (f_{vb}) with which we may calculate the expected full-signal value of series coil group dc current in this application.

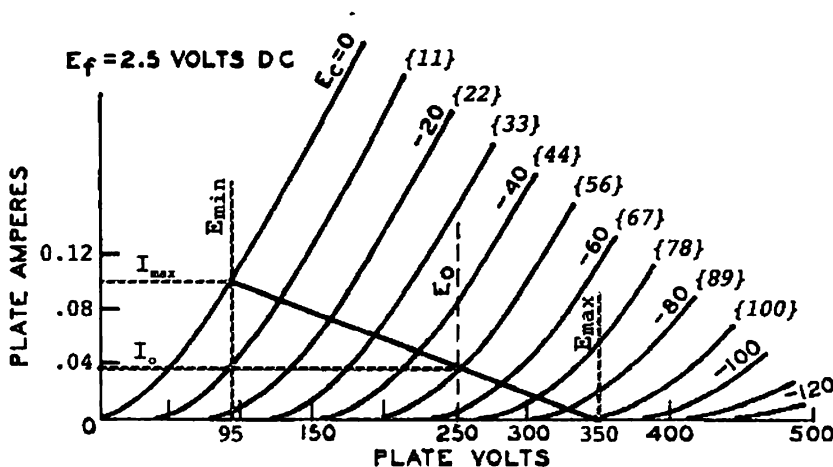


Fig. 35: Determination of Zero-Bias Voltage Factor (f_{vb})

Stage Voltage Balance

One thing which must briefly be pointed out here is that the original grid voltages as shown are not precisely proportional to those which are assumed would be necessary at Primary Power System voltages that are much higher than "normal" (per DataSheet #8), just as they were not in DataSheet #9 when the design load-line and its corresponding resistance/voltage factor were first calculated. Simply explained, the cutoff voltage should equal 1.4 times the source (field winding) voltage if possible, as it does; however, the cutoff voltage should also be equal to the sum of the source and bias voltages with $\mu = 4$, in this application. Thus, the grid line shown intersecting the E_{min} line (at 350) would need to read 100 rather than 90 for this tube data to be truly representative of the rotor triode arrays' anticipated operating conditions. It is therefore possible that the arrays are slightly over-biased as designed (at least at lower rotor voltages), but the refigured grid voltages which would proportionally fit the design tube data-model are shown in brackets.

To continue, the electrostatic load-line formula must be reapplied in interpreting this graph to determine I_{max} and E_{min} , using the final value for load resistance obtained in the original example (from DataSheet #9):

$$R_L = 2500 = \frac{E_{max} - E_{min}}{I_{max} - I_{min}},$$
$$= (350 - 95)/(I_{max} - 0), \text{ where } 95 = \text{est. } E_{min};$$

and $I_{max} = .102 \text{ amps.}$

Thus, the value for I_{max} and the mid-signal current value I_o (at standard source voltage E_o) are interpreted to be .102 and .037 amps respectively to satisfy the operating load-line at the best possible graphic estimate of E_{min} . And, this means that the Zero-Bias Voltage Factor, which we may multiply by the Primary Power System's peak dc series coil group (field winding) voltage to obtain the operative peak low-end coil group voltage under full-signal conditions, should be equal to $f_{lb} = 95/250 = 38\%$ of the peak field winding voltage, or $.38E_o$.

It should be noted that this new revised load-line is virtually parallel to the original in DataSheet #9. By applying the Zero-Bias Voltage Factor to each series coil group semicircuit as a whole, it is possible to calculate a peak full-signal series coil group dc current for 3η rotor devices which can reasonably be expected - given that each coil group's individual triode arrays were designed and ballasted using the original load-line data-model.

[Note: See Section B(2)(e) of WorkSheet VIII(b).]

(C) A third and crucial aspect of stage voltage balance involves using the Zero-Bias Voltage Factor derived above to determine the peak effective AC voltages, line currents, and rms power values expected within each Primary Power System rotor semicircuit, in both 1η and 3η rotor variants. This will be necessary before the rotor triode stages' AC signal output may be properly matched with that of the pentode primary arrays of the Field Induction System. Data for the 4ft. prototype model units will be referenced throughout.

Full-signal AC operation will produce output-stage rotor semicircuit dc voltage swings whose peak magnitude will reflect the difference between the peak Primary System Voltage (at 12,759.12) and 38% of the peak unbiased series coil group voltage (equal to 9,113.654). But the rotor must be viewed as the AC source, and the peak rms rotor voltage represented is calculated as follows:

- i) $.38(9,113.654) = 3,463.19$, and $12,759.12 - 3,463.19 = 9,295.93$ volts.
- ii) $9,295.93/12,759.12 = .72857$, as an "AC rotor voltage multiplier".
- iii) Therefore, peak rms $V_{ac} = .707[(\text{peak rotor voltage}) \times (.72857)]$.

Stage Voltage Balance

Moreover, the corresponding full-signal AC current will flow only "on the half-wave", since its value can only alternate during the positive grid stage input half-cycles. Therefore, the peak values of rms half-wave AC line current attributable to each rotor semicircuit alone may be calculated as follows, given operation at the stated operating or resonant frequency:

$$\begin{aligned}\text{1}\eta \text{ device: peak rms } I_{\text{ac}} &= [\text{peak rms } V_{\text{ac}} / (R_{\text{L}} + 2r_{\text{p}})] \text{ w/r, } = 26,909 \Omega @ 16.24 \text{ kHz.} \\ &= [.707(8,506.08)(.72857)] / [23,368 + 2(26,909)] \Omega \\ &= 4,381.47 / (77,186) = .05677 \text{ amps } |. (\text{half-wave})\end{aligned}$$

$$\text{and peak coil group full-wave AC power} = \text{peak } P_{\text{ac}} = [4,381.47(.05677/2)] = 124 \text{ watts.}$$

$$\text{3}\eta \text{ device: peak rms } I_{\text{ac}} = \text{peak rms } V_{\text{ac}} / (\Sigma R_{\text{L}} + \Sigma r_{\text{p}})^* , \text{ w/r, } = 0 @ 309.8 \text{ kHz.}$$

$$\text{where } \Sigma R_{\text{L}} = 2(11,392) + 34,176 = 56,960 \Omega , \text{ and } \Sigma r_{\text{p}} = 11,392 \Omega **.$$

$$\text{So, peak rms } I_{\text{ac}} = [.707(.72857)(6,379.56)] / (68,352) = .04808 \text{ amps } |. (\text{half-wave})$$

$$\text{and peak coil group full-wave AC power} = \text{peak } P_{\text{ac}} = [3,286.11(.04808/2)] = 79 \text{ watts.}$$

*Note: These denominator resistances presume complete ballast capacitor AC isolation, for simplicity's sake.

**Note: A primary load resistor of 11,392Ω must be used to provide apparent dc plate resistance [see W.S. VIII(b)].

Based on these rms currents, suitable initial or base values for each unit's pentode accelerator and control grid resistors may be derived. The ultimate goal will be to provide for a level of primary array AC output power which would be sufficient to fully quench a resonant frequency signal voltage, as it is amplified across the rotor semicircuit and becomes a component of the Field envelope circuit at a greatly amplified current. However, this aspect of joint primary circuit resolution is extremely involved, and should not be attempted until after discussion of the remaining stage voltage balance consideration.

(D) The fourth and final aspect of stage voltage balance relates to the determination of peak AC grid circuit current in each rotor stage (in the 3η device), which must be limited to a value which yields the correct peak grid signal voltage drop for that stage given the specified grid resistor value(s). This determination will have a fundamental effect on the winding turns ratio and input power rating of each stage coupling transformer employed.

Ordinarily, the total AC line current present in each series coil group semicircuit would represent the vector sum of the branch (stage) currents therein. And, the peak grid circuit load current and the coupling coefficient (k_{ac}) of each air-core coupling transformer will determine the peak permissible transformer primary current, and this in turn will dictate a value for the peak AC line current through each series coil group (and each stage load resistance). [In general, the value of the peak rms AC load current in each rotor semicircuit of the 3η device should only be modestly greater than the corresponding peak dc operating current (figured in WorkSheet VIII(b)).]

But, each series coil group and its associated electrode arrays will have a natural series-resonant AC frequency given its particular R-L-C (resistance-inductance-capacitance) characteristics. If an AC signal voltage at this resonant frequency is present on the 3η rotor, the total AC line current will be at a maximum representing the algebraic sum of the branch (stage) transformer primary currents. The circuit considerations which follow are based upon the Primary Power System's operation under this condition. Also, due to the series stage-coupling, it can be seen that the grid circuit current in each semicircuit rotor stage won't be equal. [Winding resistances are not taken into account, having only a marginal effect on line currents in final practice.]

Stage Voltage Balance

Therefore, to illustrate the proper resolution of this fourth aspect of stage voltage balance, data for the 4ft. diameter 3η theoretical prototype will be used to derive a final rotor semicircuit AC load current limit value. The method of figuring the approximate turns ratio for each stage transformer is also thereby developed. Reference is made to Worksheets VIII(a) {Series Electrode Array Capacitance} and VIII(b) {Triode Potential Differences}.

1) The peak control grid signal voltage for the inner induction arrays must be equal to the peak applied dc grid bias voltage of 1,367.048. Given an inner grid resistor value of 64,898 Ω , the corresponding peak inner grid circuit half-wave current I_{gc} equals $(1,367.048/64,898) = .02106$ amps. [Note: I_{gc} is equal to $(455.684/64,898)$ or .00702 amps for each inner transfer array, and $(455.684/194,698)$ or .00234 amps for each outer transfer array.]

2) The maximum inner grid circuit output power in this case equals peak $P_{out} = E I_{gc}$ (or the product of the rms values for voltage and current respectively). Thus, peak $P_{out} = (.707)^2 [(1,367.048)(.02106)] = 14.4$ watts (half-wave rating).

3) Assuming an air-core transformer with $k_{ut} = .80$ (as is typical), the peak input circuit rms power for the transformer's primary must equal peak P_{out}/k_{ut} , or $14.4/.80 = 18.0$ watts. This gross input power in turn equals peak $P_{in} = I_{bc}^2 R$, where R equals the approximate total load resistance presented at the primary, and inner $R_L = 11,392 \Omega$. So, the rms AC branch current $I_{bc} = (18.0/11,392)^{1/2}$, at .03975 amps. Similarly, the other two I_{bc} values are .01325 and .00441 amps (for the inner and outer transfer arrays, respectively). Therefore, the limit value of rotor semicircuit AC load current = .05741 amps (half-wave, rms).

4) However, it can be seen from (C) above that a rotor semicircuit AC line current deficit exists in the 3η device as compared to the limit value of AC load current just figured (and required for 'full-power' AC operation). But, a corresponding operating level of stationary anode and accelerator grid circuit (primary array) AC current, which must pass through each rotor semicircuit, has not yet been provided for. The accelerator grid resistor value which will allow this small line current deficit to be offset is easily determined, and will be calculated in the remaining major section hereof (below).

5) Given a primary array AC load current of .00933 amps (or .05741 - .04808) which equals the rotor AC line current deficit, the rms voltage drop across the load resistance preceding each inner induction array will be equal to $(.05741 \text{ amp}) \times (11,392 \Omega) = 654.015$ volts. The corresponding peak voltage equals $1.414(654.015)$ or 924.777. Since voltage transformation is customarily equal to the turns ratio despite the coupling coefficient involved, and a peak grid resistor signal voltage drop of 1,367.048 is required, the primary-to-secondary winding step-up turns ratio of the inner stage coupling transformers should be one (1) to $(1,367.048/924.777)$ or 1:1.48. [The center transformers will require a step-down turns ratio of $[(1.414)(654.0)/455.684]$ to one (1), or 2.03:1, and the outer transformers' step-down turns ratio will be $[(1.414)(1,962.0)/455.684]$ to one (1), or 6.09:1.]

* * *

It will now be possible to complete the joint resolution of the Primary Power and Field Induction System circuits for AC operation, allowing the computation of the Field AC signal transmit power and the dependent primary array accelerator and control grid resistor values for both 1η and 3η devices. The first observation which is essential to an understanding of the procedure which must be followed is this:

[i] The main AC conduction current through each primary array, as a stage output which is induced by the stationary anode and accelerator grid circuit(s) 'in tandem' with the output of the rotor's inner induction array(s), will be out-of-phase with the AC current in the corresponding rotor semicircuit. {Thus, when rotor current is dropping, the AC rotor voltage and induced accelerator grid circuit voltage will be rising - and the primary array main current will be rising as well, proportionally.} So, the action of the stationary anode circuit provides an automatic inverse feedback effect with respect to the relationship of the AC current in the field envelope circuit to that in the rotor circuit. But unless regulated, this effect will tend to be far too pronounced (as will be explained shortly).

The primary array control grids should only be used (to the extent possible) for purposes of effecting adequate dc Field current bias in the 3η device, and not to regulate Field envelope semicircuit AC current. The primary control grids must, however, be used to compensate or counteract the negative (or inverse) feedback which must be applied to limit AC rotor circuit voltage, such that a full level of Field signal transmit power is reenabled through induced primary array AC current changes in phase with the original signal. This is because an AC resonant signal allowed to be continuously reamplified across the rotor will become an overly-amplified component of Field current.

Primary array plate current will be largely contingent on accelerator grid voltage, as in any pentode, and modulation of that voltage will only marginally affect the 'plate' voltage. Also, primary pentode plate current will change in almost linear proportion to changes in accelerator grid voltage near its standard value. However, given the levels of induced AC rotor voltage calculated earlier, the magnitude of the accelerator grid voltage swings could approach 73% of the full induced stationary anode AC voltage! This would produce undesirable or unacceptable variations in primary array main current, but no handy formula relating a change in accelerator grid voltage to the resultant change in plate current was found available.

Based on pentode design considerations regarding electrode spacing and voltage, it could be postulated that a 1% drop in accelerator grid voltage (E_a) will cause no more than a one-half percent drop in pentode current. This means that the said 73% stationary anode circuit voltage swings could produce swings in the primary array main current approaching 36% of its peak value, obviously constituting an excessive level of inverse feedback! It can therefore be seen that the accelerator grid voltage supply must be used to regulate the net amount of inverse feedback applied to the rotor circuit current waveform such that the total AC rotor current is limited as nearly as possible to just the sum of the two series coil group AC currents. This is done by applying a level of half-wave positive voltage (directly to the accelerator grids) at the resonant frequency, in-phase with the original AC signal voltage through the accelerator grid resistor, that is sufficient to compensate almost all of the induced stationary anode voltage swing. [The accelerator grids' supply must therefore certainly be solid-state in nature.] The control grids may then be used to re-amplify the original signal within the primary array main current, thus enabling the EDF Generator's full AC transmit power.

[ii] The first step in resolving the primary array AC load circuit is to figure the peak AC transmit power at resonance for a 3η device of the desired model (size), and then compute the 1η device's peak AC Field circuit current when its AC transmit (operating) power is the same - at a non-resonant operating frequency.

Given a total Field envelope circuit resistance (R_{Σ}) of $1,012 \Omega$ {from Work-Sheet II(c)}, and a peak rms $V_{ac} = 3,286.11$ from section (C) above, we find that

Stage Voltage Balance

the 3 η device's total AC Field circuit current $I_{\Sigma} = V/R = 3,286.11/1,012 = 3.247$ amps (rms half-wave); the hemitorus $I_{\Sigma} = 1.6235$ amps (rms); and the unit's corresponding AC full-wave transmit power $= P_{\Sigma} = [3,286.11(3.247/2)] = 5335$ watts.

Similarly, let the 1 η device's $P_{\Sigma} = 5335 - (\text{peak rms } V_{\Sigma})I = 4,381.47(I_{\Sigma})$, where I_{Σ} is the full-wave AC current. Then, the total Field half-wave I_{Σ} is equal to $2(5335/4,381.47) = 2.435$ amps (rms), and the hemitorus $I_{\Sigma} = 1.2175$ amps (rms). [It can be seen here that 1 η AC Field current is exactly 75% of 3 η current.]

The 1 η device's non-resonant operating frequency is the frequency at which the total rotor semicircuit impedance (Z_{Σ}) equals the required apparent dc line resistance ($R_{\Sigma} + 2r_p$), or in this case $77,186\Omega$ [from WorkSheet VIII, section B[1](d)]. It may then be computed using the formula $Z = [R^2 + (X_C - X_L)^2]^{1/2}$, wherein R is the value of the single ballast resistor R_{Σ} , that an operating frequency of 16,240 Hz will yield the necessary net reactance in ohms. [The rotor semicircuit's capacitive reactance (X_C) should be based on the AC series group capacitance C_{Σ} , as calculated by the method in Steps #1-2 on pg. 274.]

For simplicity's sake, all subsequent computations presume that the ballast capacitors are each isolated from passing any AC line current, using suitable filter means only generally indicated by a resistance in the SpecSheet IX schematics. To further simplify the computations which follow concerning the resolution of the primary array circuit in the 1 η device, it is presumed that each stationary anode and inner induction array pair will split the AC series coil group current inversely proportional to their respective individual X_C values (at the non-resonant operating frequency). Thus, the equivalent stationary anode resistance (stat. R_p) can be figured as representing 27.22% of the apparent dc line resistance above, or $21,009\Omega$. This value's calculation method is shown in subsection [iii] below.

Also, it should be noted that the static (dc) plate resistance r_p must still equal the value figured in WorkSheet VIII, section B[1](d), were the 1 η device's Primary Power System to be operated strictly on dc voltage. It is also interesting to observe that the 4ft. 1 η device's resonant frequency of 209.7 kHz is basically 2/3 that of the 3 η device.

[iii] Finally, it is important to realize that all of the rotor array AC plate resistances (ΣR_p) will effectively disappear during 3 η operation at the resonant frequency. It therefore becomes necessary to employ a "primary load resistor" in each 3 η rotor semicircuit, as shown in Fig. 27b of SpecSheet IX. This resistor's value is thus equal to $\Sigma R_p = 11,392\Omega$ for the 4ft. prototype. In the 1 η variant, a similar load resistance may need to be provided within the 36 Voltage Control System modules of each primary array (as shown in Fig. 28). Such a parallel resistance network may also be necessary as a 'secondary load resistance' in the 3 η device. These considerations will be examined below.

It should also be noted here that, whereas large values of array ballast resistance (R_p) and very large control grid resistances (R_g) are required in the rotor arrays, small base values of accelerator grid resistance and very small base values of control grid resistance must be used in the primary array Control System modules! This unorthodox operating condition is necessitated by the fact that the primary control grid voltage swings required to maximize the AC transmit power or Field circuit operating current could be very small indeed, as will be seen. Accordingly, smaller devices could have unit pentode coupling transformers with minimum power ratings measured in micro-watts.

The following multi-step procedure may now be used to complete the resolution of the rotor and primary array circuits for base stage voltage balance:

STEP 1: calculate the peak rms stationary anode voltage swing (peak ΔE_a), and the equivalent stationary anode resistance (stat. R_p) for the 1 η device.

First, we must calculate the peak value of the low-end stationary anode voltage. The simplest way to do so is to multiply peak E_a by the term "one minus the AC rotor voltage multiplier" (from earlier above).

1 η device: stat. $V_{a_{in}} = (.27143)(2,126.52) = 577.2$ volts. From this, we find:

$$\text{peak } \Delta E_a = \text{peak } E_a - \text{stat. } V_{a_{in}} = 2,126.52 - 577.2 = 1,549.32 \text{ volts.}$$

$$\text{However, rms } \Delta E_a = .707(1,549.32) = 1,095.37 \text{ volts.}$$

Stage Voltage Balance

Using data from WorkSheets VIII(a) and (c), each of the stationary anode rings in the 1η device has capacitance $C_s = 10.266 \times 10^{-11}$ farad. At the unit's non-resonant operating frequency of 16.24 kHz, $stat. R_c = 21,009 \Omega$: where $stat. X_c / (stat. X_c + inner X_c) = .2722$; and $stat. R_c = [(V_{ac} / .7278 I_{ac}) \div ((V_{ac} / .7278 I_{ac}) + (V_{ac} / .2722 I_{ac}))] \times (R_{ms} + 2r_p)$.

3η device: $stat. V_{min} = (.27143)(1,594.89) = 432.9$ volts. From this, we find:

$$peak \Delta E_{ag} = peak E_{ag} - stat. V_{min} = 1,594.89 - 432.9 = 1,161.99 \text{ volts.}$$

$$\text{However, } rms \Delta E_{ag} = .707(1,161.99) = \boxed{821.53 \text{ volts}}.$$

STEP 2: figure the total line resistance required to provide a full stationary anode voltage drop in the semicircuit path from the outer rotor induction cathode through the stat. anode ring to the suppressor grid. [In the 3η device, this stationary anode line resistance ($\Sigma R_{s,}$) is based on the primary array AC load current required, which has already been computed.] Once this line resistance is known, the branch accelerator grid circuit current(s) may be determined.

1η device: For simplicity's sake, $\Sigma R_{s,}$ in the 1η device should be exactly the same as the value for total rotor semicircuit resistance (77,186 Ω) calculated in section (C) above. Therefore, the total stationary anode circuit current $I_{s,} = rms \Delta E_{ag} / \Sigma R_{s,} = 1,095.37 / 77,186 = .01419$ amps. So, the branch current unit $I_{u,} = .01419 / 36 = 394 \mu\text{-amps}$.

3η device: In this case, the total stationary anode semicircuit resistance ($\Sigma R_{s,}$) is equal to the 3η value for $rms \Delta E_{ag}$ divided by the primary array AC load current of .00933 amps. So, $\Sigma R_{s,} = 821.53 / .00933 = 88,053 \Omega$, and the branch current unit $I_{u,} = .00933 / 36 = 259 \mu\text{-amps}$. [This current is about 2/3 of that of the respective 1η device.]

STEP 3: calculate the peak primary control grid voltage swing (peak ΔE_{cg}) required to induce a full level of AC Field transmit or operating power. Once this voltage swing is known, the accelerator grid AC load-line may be determined which establishes the ratio of primary array control grid-to-acclerator grid resistance that will be necessary.

This step in the resolution of the primary array circuit must actually be undertaken in a number of separate sections. In the first of these sections, we must derive a suitable expression which relates an induced change in the individual unit pentode plate current to the minimum projected change in control grid voltage required. This becomes possible through a careful analysis of the 'generic' pentode plate characteristic curves graph of Fig. 37 (and its associated text) from DataSheet #15. Thus, in a typical beam power pentode the following relationships may be observed: when control grid voltage E_{cg} changes 70.7%, plate current may be expected to change by 38%. Therefore, in this application it will probably require a minimum of a 1.86% change in E_{cg} to effect a 1% change in unit pentode plate current.

(a) The per-unit decimal change in plate current will be equal to the value for hemitorus $I_{h,}$ (from subsection [ii] above) divided by the term 36 times the peak mean unit pentode current of 530 amps. [530 amps = rotor ampacity/72.] The resultant minimum value of peak ΔE_{cg} will then be equal to this decimal change x 1.86 times 110% of $std. E_{cg}$, and will be the same in both the 1η and 3η variants (of the same size device).

$$\text{Thus, } 1\eta \text{ std. peak } \Delta E_{cg} = [1.2175 / 36(530)] \times 1.86 \times 1.1(-193.3) = -.02524 \text{ volts,}$$

$$\text{and } 3\eta \text{ std. peak } \Delta E_{cg} = [1.6235 / 36(530)] \times 1.86 \times 1.1(-145.0) = -.02524 \text{ volts.}$$

Stage Voltage Balance

(b) 1η device: The accelerator grid AC load-line which corresponds to the minimum control grid voltage swing above is computed as follows:

- 1) $\text{accel.}R_L = \text{min. std. peak } \Delta E_{cg}/\text{unit } I_{cg} = .02524/.000394 = 64.1 \Omega$.
- 2) coupling transformer min. input $P_{cg} = (.000394)^2(64.1) = 10 \mu\text{-watts}$.
- 3) It is desired to establish a base coupling transformer turns ratio of 1:1, assuming $k_{cg} = .80$ (as in section (D) above). Therefore, let control grid branch circuit current $I_{cg} = .8(I_{ag}) = 315 \mu\text{-amps}$.
- 4) So, min. output $P_{cg} = EI = (.02524)(.000315) = 8 \mu\text{-watts}$, and the corresponding control grid resistor value $R_{cg} = E/I = 80.1 \Omega$.
- 5) Since $\text{accel.}R_L = 80\%$ of R_{cg} , it can be verified by the standard equation for the parallel resistance of two resistors that the value of each accelerator grid resistor must be 4 times R_{cg} . Thus, $R_{ag} = 4(80.1) = 320.4 \Omega$.
- 6) As simplified, the equiv. resistance in the stat. anode semicircuit path is equal to $(R_{an} + r_p + \text{stat.}R_L) = 71,286 \Omega$. Subtracting this value from the required total line resistance of $77,186 \Omega$ yields a total line resistance deficit of $5,900 \Omega$. When the value for $\text{accel.}R_L$ above is then subtracted from this resistance deficit, a net total (parallel) primary load resistance of $5,835.9 \Omega$ is obtained. The value of each of the 36 individual load resistors for each primary array is thus equal to $36(5,835.9) = 210,092 \Omega$.
- 7) The corresponding primary load resistor voltage drop will therefore be equal to $IR = (.000394)(210,092) = 82.78 \text{ volts}$, or 7.58% of the peak stationary anode voltage swing of 1,095.37, and only marginally alleviates the excessive negative feedback tendency. The value of the individual bypass resistor (R_{bp}) which must be paralleled with each accelerator grid load resistor to ensure a full stationary anode semicircuit branch voltage drop (to the suppressor grid) = $[1,095.37 - 82.78]/.000394 = 2.57 \text{ megohm}$.

This completes the lowest-power valid resolution of each 1η primary array semicircuit.

(c) 3η device: The accelerator grid AC load-line which corresponds to the minimum control grid voltage swing above is computed as follows:

- 1) $\text{accel.}R_L = \text{min. std. peak } \Delta E_{cg}/\text{unit } I_{cg} = .02524/.000259 = 97.5 \Omega$.
- 2) coupling transformer min. input $P_{cg} = (.000259)^2(97.5) = 6.54 \mu\text{-watts}$.
- 3) It is desired to establish a base coupling transformer turns ratio of 1:1, assuming $k_{cg} = .80$ (as in section (D) above). Therefore, let control grid branch circuit current $I_{cg} = .8(I_{ag}) = 207 \mu\text{-amps}$.
- 4) So, min. output $P_{cg} = EI = (.02524)(.000207) = 5.23 \mu\text{-watts}$, and the corresponding control grid resistor value $R_{cg} = E/I = 121.9 \Omega$.
- 5) Since $\text{accel.}R_L = 80\%$ of R_{cg} , it can be verified by the standard equation for the parallel resistance of two resistors that the value of each accelerator grid resistor must be 4 times R_{cg} . Thus, $R_{ag} = 4(121.9) = 487.6 \Omega$.
- 6) As simplified, the equiv. resistance in the stat. anode semicircuit path is equal to $\Sigma R_L + \Sigma r_p = 68,352 \Omega$. Subtracting this resistance

value from the required total line resistance of $88,053\ \Omega$ yields a total line resistance deficit of $19,701\ \Omega$. When the value for $\text{accel.}R_L$ above is then subtracted from this resistance deficit, a net total (parallel) secondary load resistance of $19,603.5\ \Omega$ is obtained. The value of each of the 36 individual load resistors for each primary array is thus equal to $36(19,603.5) = 705,726\ \Omega$.

- 7) The corresponding secondary load resistor voltage drop will therefore be equal to $IR = (.000259)(705,726) = 182.78$ volts, or 22.25% of the peak stationary anode voltage swing of 821.53, thereby alleviating somewhat the excessive negative feedback tendency. The value of the individual bypass resistor (R_{bp}) which must be paralleled with each accelerator grid load resistor to ensure a full stationary anode semicircuit branch voltage drop (to the suppressor grid) = $[821.53 - 182.78]/.000259 = 2.4662$ megohm.

This completes the lowest-power valid resolution of each 3η primary array semicircuit.

(d) It is virtually certain that as the plate current across a pentode tube or electrode array becomes higher and higher proportional to the applied potential difference, the smaller the magnitude of the induced plate current change will be per volt of the control grid voltage swing. It is therefore very difficult to project exactly how much the minimum primary control grid voltage swing projected above might have to be expanded in actual device operation (to enable full Field AC power).

Data associated with Fig. 38 in DataSheet #15 {Beam Pentode Characteristics} may nonetheless be used to derive an "inverse resistance factor" with which to generate a maximum valid primary array semicircuit load-line resolution. Direct experimentation with the many various viable joint resistor settings which exist 'between' the said minimum and maximum resolutions will readily lead to the optimum base operational settings.

Given a resistance/voltage factor (f_{iv}) of 38 and a source voltage of 250, and knowing that the corresponding load-line resistance of $9500\ \Omega$ will remain essentially constant across the range of operating current, the projected plate current for the design data-model tube (discussed in DataSheet #15) will be equal to $250/9500 = .02632$ amps at that source voltage. We may then say that the base inverse resistance factor f_{iv} is equal to $I/V = .02632/250 = 1.0528 \times 10^{-4}$. Applying the same technique to the unit pentode arrays, we find the unit $f_{iv} = 530/3,866.4 = 1.3708 \times 10^{-1}$ for the 1η device; and unit $f_{iv} = 530/2,899.8 = 1.8277 \times 10^{-1}$ for the 3η device. The resulting ratio of unit f_{iv} to base f_{iv} is equal to 1.302×10^3 (or 1302) for the 1η device, and 1.736×10^3 (or 1736) for the 3η device. Therefore, the maximum control grid voltage swing (max. std. peak ΔE_{cg}) may have to be as much as 1,302 or 1,736 times higher than the respective absolute minimum values calculated above!

(e) 1η device: The accelerator grid AC load-line which corresponds to the maximum control grid voltage swing which is possible with a 1:1 coupling transformer turns ratio is computed as follows:

- 1) Let $\text{accel.}R_L = 5,900\ \Omega$, thus eliminating the need for any primary load resistance. Then,

$$\text{max. std. peak } \Delta E_{cg} = I/R = (.000394)(5,900) = 2.325 \text{ volts.}$$

- 2) coupling transformer max. input $P_{in} = (.000394)^2(5,900) = 915\ \mu\text{-watts.}$

Stage Voltage Balance

- 3) Assuming $k_{\mu} = .80$ (as in section (D) above), let control grid branch circuit current $I_{c_g} = .8(I_{a_g}) = 315 \mu\text{-amps}$.
- 4) So, max. output $P_{c_g} = EI = (2.325)(.000315) = 732 \mu\text{-watts}$, and the corresponding control grid resistor value $R_{c_g} = E/I = 7,381 \Omega$.
- 5) Since $\text{accel.}R_L = 80\%$ of R_{c_g} , it can be verified by the standard equation for the parallel resistance of two resistors that the value of each accelerator grid resistor must be 4 times R_{c_g} . Thus, $R_{a_g} = 4(7,381) = 29,524 \Omega$.
- 6) Since no stationary anode semicircuit line resistance deficit exists, the value of the individual bypass resistor (R_{bp}) which must be paralleled with each accelerator grid load resistor to ensure a full stationary anode semicircuit branch voltage drop to the suppressor grid $= 1,095.37/.000394 = 2.78 \text{ megohm}$.
- 7) The value for max. std. peak $\Delta E_{c_g} = 2.325$ volts employed in this circuit resolution corresponds to 7.076% of the unit f_{1v} -to-base f_{1v} ratio of 1302. Should a higher peak control grid voltage swing be found necessary, the coupling transformer turns ratio may be stepped-up proportionally. Hence, the projected maximum turns ratio $= 1:(1/.07076) = 1:14.13$.

This completes the highest-power valid resolution of each 1η primary array semicircuit.

(f) 3η device: The accelerator grid AC load-line which corresponds to the maximum control grid voltage swing which is possible with a 1:1 coupling transformer turns ratio is computed as follows:

- 1) Let $\text{accel.}R_L = 19,701 \Omega$, thus eliminating the need for any secondary load resistance. Then,
 $\text{max. std. peak } \Delta E_{c_g} = I/R = (.000259)(19,701) = 5.103 \text{ volts}$.
- 2) coupling transformer max. input $P_{a_g} = (.000259)^2(19,604) = 1,320 \mu\text{-watts}$.
- 3) Assuming $k_{\mu} = .80$ (as in section (D) above), let control grid branch circuit current $I_{c_g} = .8(I_{a_g}) = 207 \mu\text{-amps}$.
- 4) So, max. output $P_{c_g} = EI = (5.103)(.000207) = 1,056 \mu\text{-watts}$, and the corresponding control grid resistor value $R_{c_g} = E/I = 24,652 \Omega$.
- 5) Since $\text{accel.}R_L = 80\%$ of R_{c_g} , it can be verified by the standard equation for the parallel resistance of two resistors that the value of each accelerator grid resistor must be 4 times R_{c_g} . Thus, $R_{a_g} = 4(24,652) = 98,608 \Omega$.
- 6) Since no stationary anode semicircuit line resistance deficit exists, the value of the individual bypass resistor (R_{bp}) which must be paralleled with each accelerator grid load resistor to ensure a full stationary anode semicircuit branch voltage drop to the suppressor grid $= 821.53/.000259 = 3.1719 \text{ megohm}$.
- 7) The value for max. std. peak $\Delta E_{c_g} = 5.103$ volts employed in this circuit resolution corresponds to 11.646% of the unit f_{1v} -to-base f_{1v} ratio of 1736. Should a higher peak control grid voltage swing be found necessary, the coupling transformer turns ratio may be stepped-up proportionally. Hence, the projected maximum turns ratio $= 1:(1/.11646) = 1:8.59$.

This completes the highest-power valid resolution of each 3η primary array semicircuit.

(g) IMPORTANT NOTES for Students and Electrical Engineers:

At this point, it should be fairly obvious that a full-wave unidirectional positive pulse signal may be employed, thereby doubling the half-value full-wave AC power as figured in part [ii] of the preceding section. Thus, the AC Field transmit power for the 4ft. diameter 3 η device would then be 10,670 watts, or about the same as that of a typical small local AM radio station. This consideration duly supports the notion that small devices may be successfully deployed as remote-controlled probes.

Of considerably greater importance, however, is that the issue of the "missing" Field envelope circuit resistance be addressed. As many astute and thorough readers will already have realized (from WorkSheet II(c) {Field Power Output}), the circuit resistance provided by the power resistor networks is only half of that which is theoretically required to limit rotor current to the allowable level in light of Ohm's law. However, if the power resistors were to have any higher value, the total thermal power produced would exceed the peak inherent Field electrical power! A proper explanation of where and how this missing resistance must occur may therefore be absolutely essential for some to fully accept the EDF Generator's overall feasibility.

As was stated in the text of Chapter 7, the inherent resistance of a direct arc discharge is generally considered negligible, but it may have a significant circuit resistance. If this were not the case, it might prove difficult to perform continuous controlled arc welding (for example). Even without a circuit per se, natural arc discharges in the form of lightning can be shown to have sizeable inherent resistance. Having made a thorough study of available lightning research, the author found that the median resistance per meter of lightning strokes is about 150 Ω at intensity $E = 2 \times 10^6$ v/m. Since the magnitude of the Field envelope semicircuit resistance in question is 83.6 Ω in the 1 η device, and the average hull plate separation distance is .5787 m, it was intriguing to find that $.5787(150 \Omega) = 86.8 \Omega$ (or only 3.8% higher than necessary)! Thus, in Thermal Units which operate at or below 2/3 of breakdown field intensity (3×10^6 v/m), it might not be necessary to worry further about providing for this deficit in Field envelope semicircuit resistance.

However, a much more reasonable and straightforward method of proving the location and source of the necessary circuit resistance is available, which applies to both types of device with equal validity. This method merely involves calculating the theoretical resistance of the space charge (vacuum) chamber. As given in WorkSheet VIII(c) {Pentode Potential Differences}, the resistance of each 1 η unit pentode array is 8.025 Ω . The net resistance of each Primary Array is therefore equal to $8.025 \Omega / 36 = .2229 \Omega$, and the total circuit resistance of both Primary Arrays equals .11146 Ω . Since the actual effect of the engineered instantaneous charge differential is to make it "easier per volt" for the primary cathodes to emit main current electrons than the field emitters, it may be postulated that the equivalent series resistance of either vacuum chamber half-current should be higher than that of the Primary Arrays by a ratio roughly equal to the primary voltage expansion ratio!

Thus, in this case, with the Thermal Unit's expansion ratio of 750, the mean inherent resistance of either hemichamber current = $750(.11146 \Omega) = 83.6 \Omega$. The parallel resistance of these two hemichamber currents, or the equivalent series resistance of the chamber current as a whole, is therefore equal to 41.8 Ω and the entire Field envelope circuit resistance now resolves correctly even with a Field hemitorus resistance of zero beyond breakdown intensity. [For the 3 η device, the total circuit resistance of both Primary Arrays equals .08358 Ω . With a voltage expansion ratio of 12,106, the series resistance of either hemichamber current = $12,106(.08358 \Omega) = 1,012 \Omega$, as it should.]

Beam Pentode Characteristics

The unit electrode arrays comprising the Electrodynamic Field Generator's two (2) Primary Induction Ring Arrays are designed analogous to pentode vacuum tubes in that they are each composed of a total of five (5) separate electrodes. Because of the extremely high levels of current which they must conduct, this DataSheet will discuss their relationship to "beam power tubes" developed by the vacuum tube industry for purposes related to a substantially increased power handling capability. General operating characteristics will be reviewed as will specific attributes which are directly related to the application contemplated herein.

The principal physical difference between a triode tube or electrode array and a pentode is the presence of a second control grid operating at a positive voltage. This electrode is mounted between the negative control grid and the plate and is usually called a screen grid, as it shields the electrons between itself and the cathode from the electrostatic influence of the plate. Not only does this additional grid effect a desirable reduction in the rather significant control grid-to-plate capacitance found to occur in triodes, but it also makes plate current largely independent of plate voltage over a wide operating range.

In the Primary Induction Ring Arrays, this screen grid is referred to as an "accelerator" grid, to emphasize its role in 'pulling' cathode electrons toward the plate and maintaining a large plate current flow *despite wide variations in negative control grid (and therefore plate) voltage*. The screen or accelerator grid was originally added to triode tubes to form a 4-element tube called a tetrode.

Because of the proximity of this positive grid to the plate, however, it was found that secondary emission electrons from the plate of a tetrode were drawn into the screen grid and caused not only a large grid current but a loss of power output as well. Therefore, the pentode (or 5-element) tube was developed and it incorporated a "suppressor" grid near the plate to which all or a large portion of negative cathode voltage was applied.

This negative *third* grid supplied an electrostatic force which repelled secondary electrons back to the plate, preventing them from returning to the screen or accelerator grid, and thus minimized positive grid circuit current. To maximize the power pentode's current-handling capability, all three grids are placed directly in-line with one another between cathode and plate. Then, cathode-emitted electrons travel in sheets or beams between the turns of the grid wires, giving the beam power pentode the attributes of high power output and efficiency.

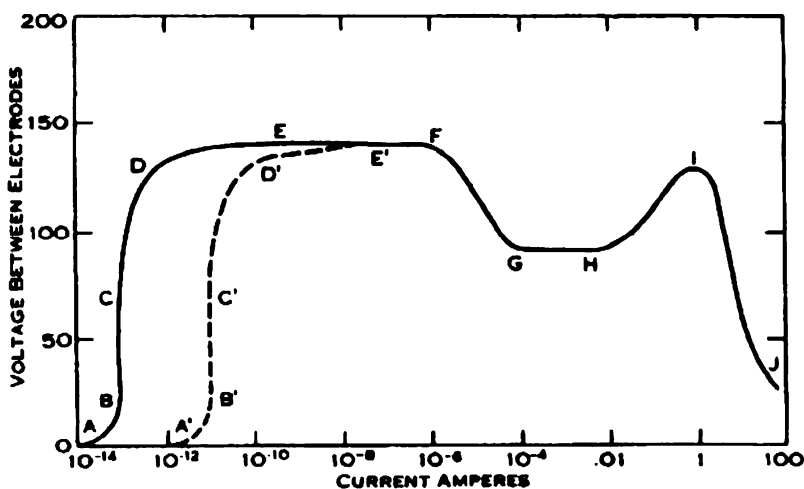
In the Electrodynamic Field Generator, it is in fact not necessary to employ a suppressor grid to minimize secondary emission except at very low rotor speeds. During the development of high-voltage X-ray tubes it became known that the secondary emission of electrons from the plate was effectively quenched at voltages above a few thousand. Also, at the voltage levels used in the Primary Power System, the proximity of the suppressor grid to the plate would result in a direct arc-discharge condition between these two electrodes were any significant portion of actual cathode voltage applied to that grid. Instead, only an extremely small variable negative voltage may at times be

applied to the suppressor grids of the Primary Induction Ring Arrays as part of a Field Voltage Control System.

In determining the functional characteristics of the Primary Induction Ring Array, the total potential difference across it during operation must be known. At first look this total operating voltage would appear to equal full rotor voltage, due to the induction upon the individual array cathodes of a voltage equal and opposite to rotor anode ring voltage. Due to the Faraday shielding principle, however, the primary array cathode voltage must tend to exhibit a ground (0-volt) value because any net charge on the cathodes (due to induction) must reside on the outer surface of the Zone. Thus, the positive voltage across each unit pentode array will tend to equal one-half rotor voltage, or $1/3$ of the Primary System Voltage developed in 1η rotor devices and $1/4$ that in 3η rotor devices. It must be pointed out that the induced negative voltage corresponding to such cathode charge will detract but marginally from the operating voltage that would otherwise be evident on the positive Zone(s), due to the very low effective capacitance of the Primary Arrays.

The effective plate resistance of a pentode is usually between several thousand ohms and several tens of thousands. Because of the extremely heavy current which must be conducted between the positive Zones and the rotor, this cannot be the case in the application contemplated herein. Were the Primary Induction Arrays each constructed as pentodes in unit series between the Zones and the rotor, a total resistance of much less than one ohm would result across each. Since Specifications call for the two Zones to be divided into 36 equal Sectors each, however, an induction ring array which is also divided into 36 equal parallel units yields an individual array unit resistance in the upper single digit ohms ($6-8\ \Omega$).

If we refer to the logarithmic graph in Fig.36 below, which plots plate current versus voltage for a typical low-pressure gas tube*, we see that this level of effective resistance ($R=V/I$) falls well within the abnormal glow-arc transition portion of the example tube's output curve. Accordingly, as long as the control grid retained control over the cathode discharge, and effective resistance was prevented from falling below about $5\ \Omega$, a thyatron-like runaway arc-discharge operating condition could be avoided.**



** It is important to note that while graph portion(s) A-I would be very different for an ordinary evacuated tube, due to its far lower current-handling capability, the std. operating portion I-J for the Generator's Primary Arrays will be very similar to that seen here because the primary cathodes are thoriated to achieve a level of current conduction which is equivalent to that of a gas-filled tube (at a far higher voltage).

Fig.36: tube pre-breakdown phenomena includes BREAKDOWN-GLOW TRANSITION @ F-G, normal glow region @ G-H, abnormal glow @ H-I, and GLOW-ARC TRANSITION @ I-J.

The diagram below shows the general form of the operating plate characteristics for a low amplification factor beam power tube as a function of applied control grid voltage. From an analysis of this diagram, the following tube attributes are evident:

- standard (0-signal) applied control grid voltage (V) corresponds to a plate current value approximately 54% of maximum.
- maximum-signal grid voltage (2V) corresponds to a plate current value equal to 8% of maximum.
- maximum control grid voltage swing points I_1 and I_2 correspond to plate currents of about 8% less than maximum (or 92%) and 8% above minimum (or 16%) respectively, yielding maximum-signal grid-induced swings of 38% of maximum plate current about point P.

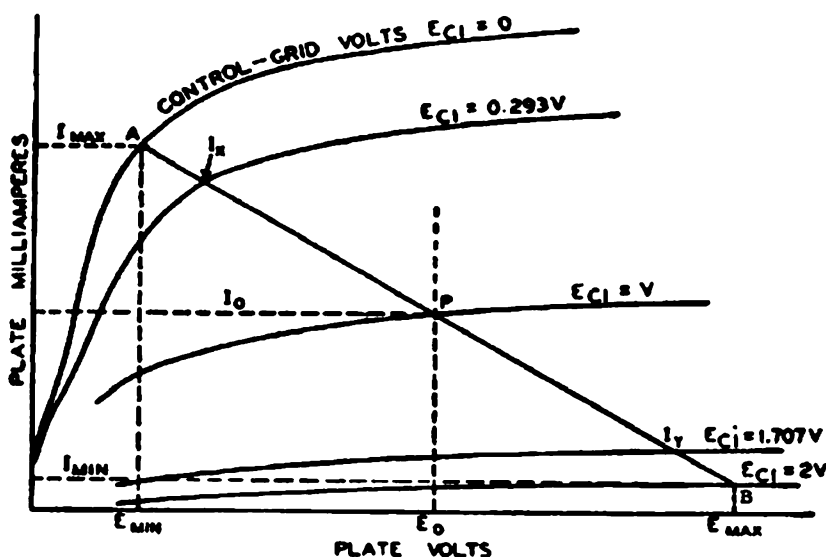


Fig. 37: generic load-line & characteristic curves graph for typical low- μ beam power pentode.

It should be stressed that these plate current values are obtained with the application of a pure dc grid voltage, and are thus a function of the tube's triodic amplification factor. In standard practice the average plate current, with the application of an AC signal to the control grid, may be maintained to within a few percent of 0-signal value due to the action of the screen (accelerator) grid.

The ratio of maximum control grid voltage (2V) to operating source plate voltage (E_0) is, of course, contingent upon the tube (or electrode array) amplification factor. It has been established in other material associated herewith that this voltage ratio, for purposes of the application contemplated herein, is roughly 10% (see WorkSheet VIII(c) {Pentode Potential Differences}). Referring to the plate output graph in Fig.38 below, pertaining to an actual beam power tube whose standard (nominal) grid voltage (V) is 5% of plate voltage, we find the amplification factor to be approximately 10.

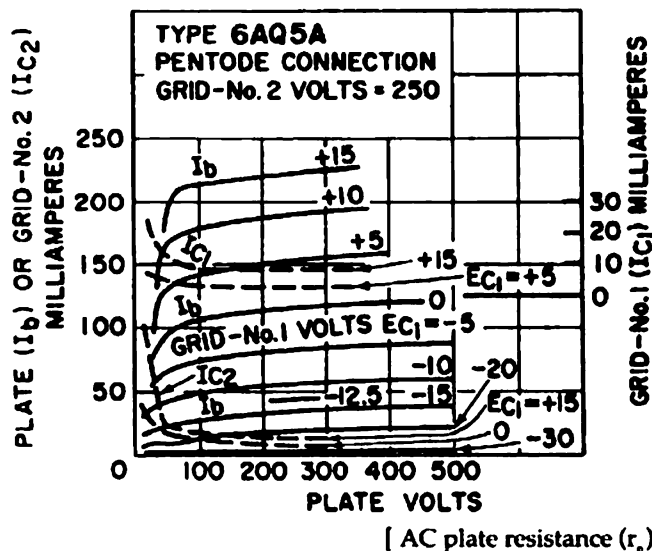


Fig. 38: plate output graph for 250V beam power pentode of $\mu = 9.5$, illustrating current bias effect of grid No.1 negative voltage.

Nominal control grid voltage (V) for this tube is -12.5 volts, and it is apparent from the graph that a grid voltage of -25 volts (2V) will in this case reduce plate current by well over 50%. Since the amplification factor of the inner triode induction array will be equal to or greater than that of the tube represented in the diagram above, the same electrode spacing parameters employed in the rotor triode arrays may be used to construct the unit pentode arrays with the assurance of their capability to achieve the current bias levels required by SpecSheet XI {Field Current Bias Values} as a function of an amplification factor greater than or equal to 10.

It should also be noted that the accelerator grid (positive) voltage, typically either one-half or full applied plate voltage, may be modulated in a manner similar to that of control grid voltage. This type of duplex signal-handling capability allows the unit pentode arrays of both Primary Induction Ring Arrays to amplify a resonant frequency communications signal while simultaneously controlling an independent level of current-contingent thrust.

As mentioned in DataSheet #9, the formula for the load resistance of a sequentially-coupled beam power pentode is the same as that for a triode. However, the relevant values of plate voltage (E) and current (I) which are to be 'plugged' into this formula must be arrived at in the following manner:

"The load-line drawn in Fig.37 from point A (on the knee of the zero-bias voltage curve) through P to point B should be such that the length of line segment AP is equal to that of PB."

Applying this rule and the pertinent data derived thereby from the graph above to the load-line formula, the following load resistance was obtained:

$$R_L = (470 - 30) / (.060 - .012) = 440 / .048 = 9,167 \Omega, \text{ and } f_{\nu} = 9,167 / 250 = 36.67.$$

A good check of this result is the value of 5 times plate resistance (from Fig.38): $5(1,970) = 9,850 \Omega$, or $f_{\nu} = 39.4$. The average of these two figures is 38, and this is the base value of f_{ν} which would be used in this application if the Primary Arrays were in fact sequentially coupled with their respective rotor semicircuits [see Section D of WorkSheet VIII(c)].

Flux Superposition Ratio

The two (2) Variable Inductor Arrays employed in the Electrodynamic Field Generator serve in part to create a transverse deflectionary force upon drive field current. It is desired to accurately supply a specific level of magnetic flux density at a given distance from the Armature cores (i.e. at the center of the power field region of the field envelope), and therefore the degree to which the individual Armature fields "overlap" at any given point on this electron gyro-orbit must be known.

Intensive vector analysis in three dimensions must be undertaken to accomplish this end, and the principal determining factor of the resultant flux "superposition" ratio or *individual-armature flux density multiplier* is of course the radius of the Neutral Ring centerline and power field gyro-orbit. It was found in the course of flux superposition research that the second most important factor in accurately determining this multiplier is the periodicity of the 'holes' or blank positions in the array caused by the necessity of leaving out an Armature due to superstructure (beam) blockage.

In any event, before the flux density at a point in space near a magnetic pole may be calculated, the field intensity at that point must be known. The formula used to calculate the net field intensity H (in amps/m) of a magnetic pole at a given distance is the traditional formula [Equation M1] that follows:

M1. $H = \frac{\Phi_p}{4\pi\mu_0 r^2}$, where Φ_p = total magnetic flux (or pole "strength"),
in webers (Wb), where 1 Wb = 10^8 flux lines (maxwells).
 μ_0 = $4\pi \times 10^{-7}$ Wb/amp-m (the permeability of free space)
and r = the pole-to-point distance, in meters.

Note: The multiplier 4π in the denominator must be used as the flux is thought of as filling a spherical spatial volume.

M2. Since $\Phi_p = B_p A$ [Equation M2], where B_p equals the pole's inherent gross flux density and A equals its primary (working) surface area, we may now write:

$$H = \frac{B_p A}{4\pi\mu_0 r^2} \quad , \text{ in amperes/meter (equivalent to amp-turns/m).}$$

M3. And, because $B_n = \mu_0 H$ [Equation M3], where B_n is the net flux density at a relative point in air or vacuum, we may substitute and simplify as follows:

$$\frac{B_n}{\mu_0} = \frac{B_t A}{4\pi\mu_0 r^2} ; \text{ and } B_n = \frac{B_t A}{4\pi r^2} , \text{ in T (tesla, or Wb/m}^2\text{)}.$$

Should a flux superposition ratio (f) be involved, because of a geometric arrangement of multiple like-strength poles, this expression then becomes:

$$B_n = \frac{f B_s A}{4\pi r^2}, \text{ in T (Wb/m}^2\text{)}.$$

Flux Superposition Ratio

Thus, if we are given a magnetic pole of known strength Φ_p , or an Array of like-strength poles of known superposition ratio f , we may now calculate the total net flux density at a given relative point in space. Conversely, if we need to achieve a certain net flux density B_n at a given point under similar pole positioning criteria, we may calculate the required strength of each pole:

$$\text{since } B_n = \frac{f B_p A}{4\pi r^2} \quad , \quad B_p = \frac{4\pi r^2 B_n}{f A} .$$

$$\text{And thus, } \left[\Phi_p = \frac{4\pi r^2 B_n}{f} \right] ; \text{ or, alternatively, } \left[B_n = \Phi_p / 4\pi r^2 \right] \text{ with } f = 1.$$

The most important thing to remember in making use of the foregoing equations is to remain in the mks system of units throughout a given problem, converting only to gauss and the cgs system at the end if desired to lend a more traditional feel for relative flux density or field intensity. Thus, we should initially be working at all times in webers/m² for flux density, and amps/m or amp-turns/m for field intensity, as has been done in aWorkSheet XII(a) and WorkSheet XII(b). In the cgs system, field intensity is in oersteds, as used in the demagnetization curves graph provided in DataSheet #4.

It is also important to remember that the effect of the opposite pole(s) must be taken into account in determining the flux superposition ratio of the Armatures composing each Array. The calculation of this ratio is then of a two-part nature, as the opposite-pole considerations would be negligible only in Armatures of very great length.

It might seem reasonable to assume that the flux superposition ratio would have to be calculated for each different gyro-orbit in question, although we are primarily concerned only with the power field centerline, as the linear distance from the center of any particular Armature pole face to the nearest point on the given gyro-orbit could have a fundamental effect on the resultant superposition ratio. However, detailed studies of various gyro-obits lying on the selector plane reveal that the same flux superposition ratio will indeed apply! It is then left up to industrious students interested in magnetism to determine if (as is possible) the superposition ratio is not constant among plane-parallel gyro-orbits located at various distances from the Armature faces which do not lie on the vertical centerline of the Armature Arrays.

The actual flux superposition ratio for the 4ft. theoretical prototype EDF Generator, which has been calculated with great care using two different but related methods, turns out to be 2.2672. It should be noted that this figure is actually an average value, since the flux density observed at a point on the desired gyro-orbit which is directly 'above' a blank Array position will reflect a minimum value of 1.8889 times that produced by a single Armature and the corresponding maximum value above the center Armature of each Array section will be 2.6455. Ideally, this average value should be derived from a study of the flux superposition in evidence above each of the five (5) Armatures in any one Array section and above one of the adjacent blank positions (yielding an average of six generated position values).

Although it was found that aiding and opposing poles situated within the semicircular half of both Arrays which is diametrically opposite the particular position being evaluated have a virtually negligible effect on the resultant flux superposition ratio computed, as they tend to completely cancel each

Flux Superposition Ratio

other, the determination of each given Generator's overall superposition ratio still requires a minimum of about 1,860 individual calculations! A straight-forward method considered suitable for figuring this ratio is outlined below, so that students and engineers alike may verify and refine the results obtained by the author (without the use of calculus) and determine if larger sizes of the device exhibit different superposition ratios even though the Array geometry is constant as a function of the vessel's scale.

The following dimensional values will be needed in calculating the flux superposition ratio for the sample 4ft. prototype device:

- 1) the radius r of the Arrays = .4264 m {from WorkSheet XII(b)}; and
- 2) the appr. mean length l of each Armature = $(212/9600)R_n = .01346$ m {given here only}.

In addition to the variables a , b , and r which are self-explanatory from the diagram below, and derive from the equation for a circle, the following variables must also be defined:

c = the 'slant' distance from the Armature or blank position being evaluated to each other Array pole face in a given Quadrant of the Array and in the common plane of the pole face centerpoints;

y = the vertical elevation of the horizontal power field centerline (and gyro-orbit) above these centerpoints (= r from W. S. XII(b) Sec. C); and

d = the linear 3D distance from each given aiding or opposing pole face centerpoint to the Armature or blank position being evaluated.

The only other geometric property of the Array configuration which must be considered prior to commencing work with the superposition ratio calculation method is the uniform angle by which each Armature and blank position is separated from one another. Since there are 180 Armatures and 36 blank positions in each array, this separation angle is $360^\circ/216$ or $1^\circ 40'$. The sine of each integer multiple of this separation angle from #1 through #54 inclusive (90°) is then the only data other than the dimensional values from 1) and 2) above which is needed to compute the flux superposition ratio with great precision.

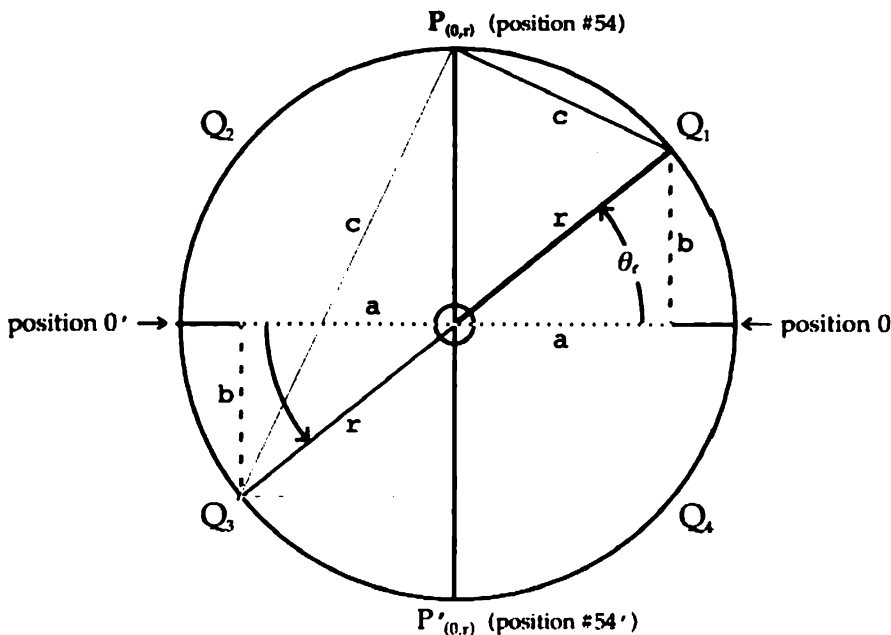


Fig. 39: Armature Array Quadrant & Pole Positioning Diagram

Flux Superposition Ratio

In Fig.39 above, the particular pole or blank position to be evaluated is assigned to point $P_{(0,r)}$ on the vertical axis between Q_1 and Q_2 . The "offset" angle θ_i with respect to the corresponding horizontal axis (and position 0) determines the exact location of each other Armature or blank position on the Array circle, at the point where lines b, r, and c all intersect. Since each successive angle θ_i is precisely known (as a multiple of the incremental separation angle $1^\circ 40'$), the flux density at $P_{(0,r)}$ which is attributable to each such Armature position may readily be determined as a function of the resultant linear 3D distance (d) from $P_{(0,r)}$ to the position in question.

Based on the foregoing definitions and geometric considerations, it can be seen that the flux superposition ratio as calculated at any given position $P_{(0,r)}$ in the Array(s) is basically arrived at through the trigonometric ratio for the sine of angle θ_i (where $\sin \theta_i = b/r$) and three successive applications of the Pythagorean Theorem for each of the 53 other Array positions in a given Quadrant. [The flux density attributable to a blank position is of course 0.] The flux density at point $P_{(0,r)}$ due to the Armatures in Q_1 (B_{01}) is then equal to the difference between the sum of the aiding flux density ($\Sigma B_{aid.}$) and the sum of the opposing flux density ($\Sigma B_{opp.}$). Since B_{02} will of course be equal to B_{01} due to symmetry, both aiding and opposing flux density calculations need only be performed for Q_1 and then doubled. In very small devices (like the 4ft. prototype), the similar computations for Q_2 (and Q_3) may be disregarded without significant error due to the effect of the inverse square law with respect to the distance to point $P_{(0,r)}$. In larger devices reliance should not be made upon this effect, for accuracy's sake, which doubles the minimum total number of calculations required to over 3,700.

Finally, the flux superposition ratio f which is operative at point $P_{(0,r)}$ is equal to the sum of $2B_{01}$ and $2B_{03}$ divided by the flux density B_n attributable to a single outer Armature pole. The total flux density at $P_{(0,r)}$ is then the available transfection flux density B_{tr} referred to in WorkSheet XII(b), Sec. E.

Step 1) determine the gyro-orbit flux density B_n attributable to a single Armature outer pole:

- (a) the Spec. Core Flux Density = 1.835 Wb/m^2 {from α WorkSheet XII(a)};
- (b) using the cross section transition formula from WorkSheet XII(b), and temporarily converting to cgs units for expediency, we calculate the net core end flux density:

$$\begin{aligned} \text{net } B_i &= B_i = B_2 A_2 / A_1 = 18,350 (.5041 \text{ cm}^2) / .7196 \text{ cm}^2 \\ &= 12,855 \text{ gauss} = 1.2855 \text{ Wb/m}^2; \text{ and} \end{aligned}$$

- (c) $B_n = B_i A_1 / 4\pi r^2$, where $B_i = B_i$, and $r = y$ (from preceding definitions);

$$\begin{aligned} \text{so, } B_n &= \frac{(1.2855)(7.196 \times 10^{-3} \text{ m}^2)}{(12.5664)(11.05 \times 10^{-4} \text{ m}^2)} = \frac{9.2505 \times 10^{-3}}{1.3886 \times 10^{-2}} \\ &= 6.6618 \times 10^{-3} \text{ Wb/m}^2 = 66.62 \text{ gauss.} \end{aligned}$$

For each Armature position in the range from #1 to #54, in Q_1 and preferably in Q_2 as well, the Steps below must be followed and the results tabulated for computations to be performed according to the preceding instructions.

Step 2) calculate $b = r(\sin \theta)$; next 3 Steps must be done for both aid. & opp. poles!

Step 3) calculate $a = \sqrt{r^2 - b^2}$;

Step 4) calculate $c = \sqrt{a^2 + (r - b)^2}$; the term $(r + b)^2$ must be used in Q_2 (aid. & opp.);

Step 5) calculate $d = \sqrt{c^2 + y^2}$; the term $(y + 1)^2$ must be used for opp. poles (in Q_1 & Q_2).

Flux Superposition Ratio

Once the numeric data resulting from Steps 2 through 5 have been compiled, the flux superposition ratio (f) which is operative at the particular Array position evaluated may be readily determined from the remaining three simple equations of this calculation method:

Step 6) calculate $B_{Q1} = \Sigma_{Q1} B_{aid.} - \Sigma_{Q1} B_{opp.}$;

Step 7) calculate $B_{Q3} = \Sigma_{Q3} B_{aid.} - \Sigma_{Q3} B_{opp.}$; and

Step 8) calculate $f = (2B_{Q1} + 2B_{Q3})/B_0$. (f @ 1st site = f_1 ; @ 2nd site = f_{11} ; etc.)

As indicated, this entire procedure (with the exception of Steps 1 and 2) must be performed at least twice (using the center Armature of one Array section and one of the two nearest blank positions), and should in larger machines be performed a total of six times (once for each Armature in any one Array section and one adjacent blank position) for optimum accuracy. Researchers will no doubt wish to develop one or more computer spreadsheets to aid in this daunting task, although the author has personally verified that it is possible for students of modest means to accomplish the job 'the hard way' using only a regular calculator (even without trigonometric tables) and still achieve an accuracy of over 97%. Reproductions of basic sample spreadsheets are included below (one for aiding poles in Q_1 and one for opposing poles in Q_3) as a further aid in this respect.

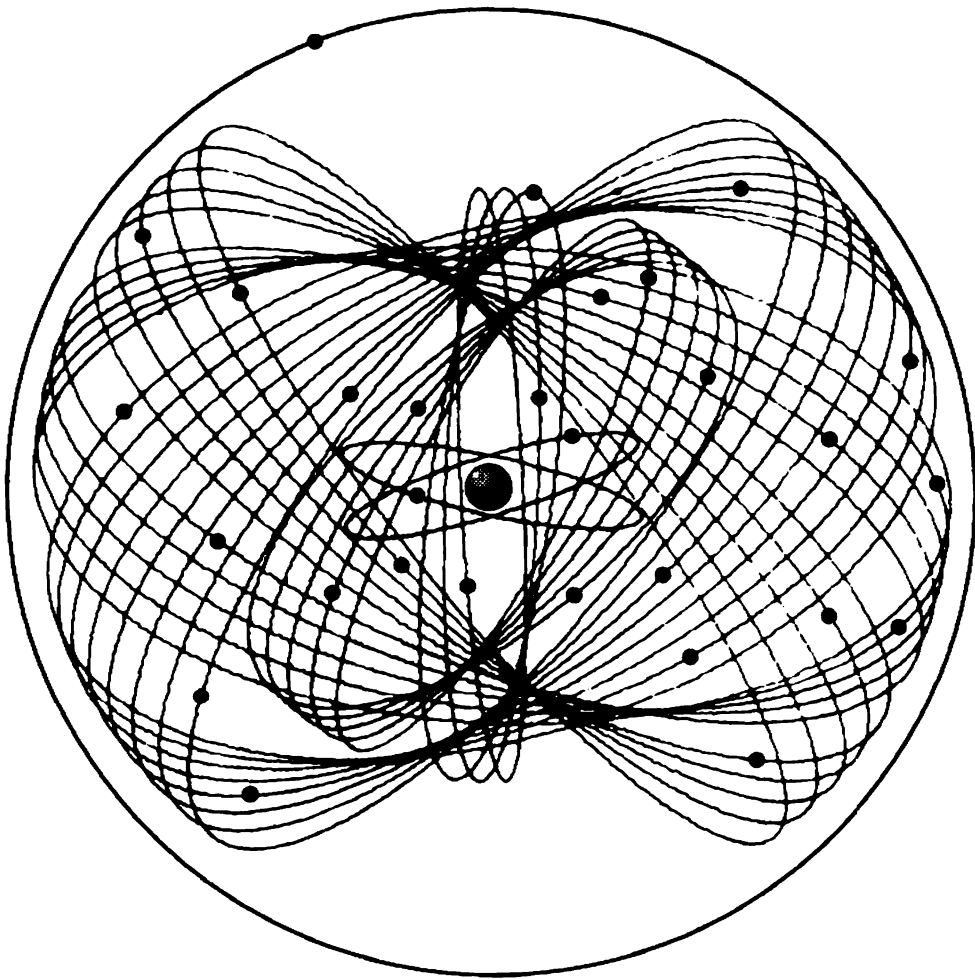
arm. spread. Q1 aid.			
A	B	C	D
1	offset angle @ position #53 = 88 deg. 20 min.		
2	Input: sine of angle = 0.9996		
3			
4	$b = r(\sin\theta): r =$	0.4264	So, $b = 0.42622944$
5			
6	$r^2 =$	0.18181696	$b^2 = 1.8167153e-1$
7	$r^2 - b^2 = 1.4542447e-4$		
8			
9	Thus, $a = 1.2059207e-2$	and $a^2 = 1.4542447e-4$	
10			
11	$r - b =$	0.00017056	$(r-b)^2 = 2.9090713e-8$
12			
13	So, $c^2 = 1.4545356e-4$,	and $c = 1.2060413e-2$	
14			
15	$y =$	0.03324	$y^2 = 1.1048976e-3$
16			
17	$c^2 + y^2 = 1.2503511e-3 = d^2$, and $d = 3.5360304e-2$		
18			
19	arm. B =	1.2855	arm. A = 0.00007196
20			
21	$B^2 A =$	9.250458e-5	$4(\pi) = 12.56637$
22			
23	and $4(\pi)d^2 = 1.5712375e-2$		
24	Therefore,		
25	$5.8873707e-3 = B (w/m^2) = 58.87370789 \text{ gauss}$		
26			

arm. spread. Q3 opp.			
A	B	C	D
1	offset angle @ position #53 = 88 deg. 20 min		
2	Input: sine of angle = 0.9996		
3			
4	$b = r(\sin\theta): r =$	0.4264	So, $b = 0.42622944$
5			
6	$r^2 =$	0.18181696	$b^2 = 1.8167153e-1$
7	$r^2 - b^2 = 1.4542447e-4$		
8			
9	Thus, $a = 1.2059207e-2$	and $a^2 = 1.4542447e-4$	
10			
11	$r + b =$	0.85262944	$(r+b)^2 = 7.2697696e-1$
12			
13	So, $c^2 = 7.2712238e-1$,	and $c = 8.5271471e-1$	
14			
15	$y + l =$	0.0467	$(y + l)^2 = 0.00218089$
16			
17	$c^2 + y^2 = 7.2930327e-1 = d^2$, and $d = 8.5399255e-1$		
18			
19	arm. B =	1.2855	arm. A = 0.00007196
20			
21	$B^2 A =$	9.250458e-5	$4(\pi) = 12.56637$
22			
23	and $4(\pi)d^2 = 9.164694813$		
24	Therefore,		
25	$1.0093579e-5 = B (w/m^2) = 1.0093579e-1 \text{ gauss}$		
26			

Even though these two spreadsheets (of an original set of four) are as rudimentary as can be, they each require that only the sine of each successive offset angle be input in order to instantly generate the exact incremental flux density figure desired. In more sophisticated software this function (and even the rather tedious tabulation procedures) can be rendered automatic. Indeed, all four spreadsheets could ideally be combined into one, and the work above clearly points up the vast time- and labor-saving power of the computer.

APPENDIX B

Material SpecSheets A to F



A computer-generated representation of the **copper** atom.

DIRECTORY

Material SpecSheet A: Hull Components

<u>Section 1:</u>	Negative Ring Hull Plates	391-392
<u>Section 2:</u>	Neutral Ring Composite Hull Construction	392-394
[a]	Deck Layer Sheeting	392
[b]	Substrate Layer Plates	393
[c]	Exolayer Tiles	393-394
<u>Section 3:</u>	Field Hub Construction	394-395
[a]	Positive Zone Sectors	394-395
[b]	Zone Sector Partitions	395

Material SpecSheet B: Superstructure Components

<u>Section 1:</u>	Drive Ring Coolant Conduits & Support Brackets	396-399
<u>Section 2:</u>	Neutral Ring Beams & Struts	399

Material SpecSheet C: Rotor Components

<u>Section 1:</u>	Rotor Segments	400
<u>Section 2:</u>	Field Emitters	400-401
<u>Section 3:</u>	Segment Separators	402
<u>Section 4:</u>	Rotor Facing	402-403
<u>Section 5:</u>	Ballrace Assemblies	404
<u>Section 6:</u>	Carrier Assembly	404-405

Material SpecSheet D: Electrode Array Components

<u>Section 1:</u>	Primary Power System	406-408
[a]	Anodes & Cathodes	406
[b]	Control Grids	406-407
[c]	Electrode Support Pins	407-408
<u>Section 2:</u>	Primary Induction Ring Arrays	408
[a]	Unit Cathodes & Anode Rings	408
[b]	Power Resistors & Dielectric Buffers	408-414
[c]	Primary Thermal Conduits	414-415

Material SpecSheet E: Field Coil Components

<u>Section 1:</u>	Rotating Coil Cores	406
<u>Section 2:</u>	Core Mounting Clips	416

Material SpecSheet F: Magnetic Components

<u>Section 1:</u>	Stationary Field Rings	417
<u>Section 2:</u>	Counterflux Wafers	417
<u>Section 3:</u>	Mounting Stringers & Hangers	419

Hull Components

Section 1: Negative Ring Hull Plates

Because of the large volume of material which must be used to form the Negative Ring hull plates, it is imperative to use a metal which has very high electrical and thermal conductivity yet as low a density or specific gravity as is feasible. In this respect, aluminum is the obvious first choice, as magnesium is much too reactive for serious consideration. Also, a relatively pure grade of aluminum should be used, because its electrical conductivity falls off quickly as the percentage of almost any alloying element(s) rises. However, a major problem which must be overcome in using pure aluminum for the negative hull plates is the tendency of such a relatively soft material to erode badly when used as an electron emitter at high voltage and current levels.

One solution to this problem would be to electroplate the aluminum hull plates with a known stable and hard emitter material like nickel. Unfortunately, aluminum does not cooperate well at all with attempts at direct electroplating, and engineers consulted regarding this approach expressed grave doubts concerning its feasibility. Nevertheless, experts in the field of *metal cladding* (on drawn wire) were able to suggest a viable two-fold resolution which seems eminently satisfactory in this application and which may in fact be the only alternative to using a much heavier metal or alloy.

It is common practice in the wire industry to copper-clad aluminum wire. The process used is to form a tight tubular sleeve of copper around a round aluminum rod, tig-weld the sleeve to the rod, and draw the combination through successive dies to produce an aluminum wire which is tightly clad with a copper coating representing up to about 10% of the total wire volume. And, the clad aluminum wire may then be readily electroplated with nickel. This process should in theory be adaptable to flat plate, by forming a 'sandwich' of aluminum stock between thin tig-welded sheets of copper which is then 'hard-drawn' at the appropriate temperature in somewhat the same manner.

Therefore, high-purity aluminum which is copper-clad and then nickel-plated is specified for the negative hull plates. The particular grade of aluminum to be used is 1350 (electrical conductor purity), and a basic physical properties table is provided below. It is assumed that copper cladding of at least comparable purity will be used, and physical properties for the CDA alloy #110 specified for this purpose may be found in Section 1 of SpecSheet C (Rotor Segments). Also following is a properties table for essentially-pure nickel.

Aluminum (Al)

ALLOY	CHEMICAL COMPOSITION (%)	ULTIMATE TENSILE STRENGTH (PSI)	ELECTRICAL CONDUCTIVITY IACS (20°C)	ELECTRICAL RESISTIVITY (Ohm/Cir mil ft)	DENSITY (lbs/cu in)	SPECIFIC GRAVITY	COEFFICIENT OF THERMAL EXPANSION X 10 ⁻⁶ (20-100°C)	APPROX. MELTING POINT (°C)
1350(EC)	99.5 Al min.	13,000	61.8	17	.098	2.7	23.8	648

Nickel (Ni)

MATERIAL	CHEMICAL COMPOSITION (%)	RESISTIVITY AT 20°C		COEFFICIENT OF LINEAR EXPANSION BETWEEN 20-100°C	TENSILE STRENGTH (PSI AT 20°C)		SPECIFIC GRAVITY	POUNDS PER CUBIC INCH	MAGNETIC ATTRACTION	APPROX. MELTING POINT (°C)
		OHMS/CMF	TCR 0-100°C		MIN.	MAX.				
Nickel 270	99.98 Ni	45	.0067	.000013	48,000	95,000	8.89	.321	Strong	1452

Component Specifications: Surface Layer and Thermal Channel Thicknesses

a) The polished final thickness of each clad and plated Negative Ring hull plate shall be equal to twice (2x) the Hull Area Constant (C_a), with the base and clad layers having also been duly polished.

- b) The maximum proportion of the total volume of the two Negative Ring hull coating layers to the total volume of the coated Negative Ring hull plates shall be 1/11.
- c) The maximum thickness of each of the two Negative Ring hull plate copper cladding layers shall represent 3% of the thickness of the base aluminum hull plate.
- d) The maximum thickness of each of the two Negative Ring hull plate nickel plating layers deposited on the copper cladding shall represent 2% of the thickness of the base aluminum hull plate.
- e) The polished final thickness of the similarly-clad aluminum angle stock used to form each finished Negative Ring hull plate's thermal conduit channel shall be equal to the Hull Area Constant (C). [It should be noted that this last Specification is intended to ensure that the vacuum chamber does not reach breakdown field intensity until at least 64% of Spec. Rotor Voltage has been achieved.]

Section 2: Neutral Ring Composite Hull Construction

[a] Deck Layer Sheeting

Sophisticated carbon composites similar to those found in golf-club shafts and racing-bicycle frames were first developed to make use of their special combination of extreme strength, rigidity, and lightness in aerospace applications. Commonly referred to incorrectly as 'graphite', these materials are generally made from *polyacrylonitrile (PAN)* fibers which have been heated to oxidizing temperature in air under tension and then reheated to between 1200 and 1600°C in the absence of air to drive off the non-carbon portion. Thus, PAN carbon composite is highly anisotropic (or oriented) in nature, and parts with complex (non-unilinear) load patterns may require very careful load analysis and a logically planned fiber-placement strategy. It displays, however, excellent vibration damping characteristics.

The individual fibers are about 7 microns in diameter and approach 300 kpsi in tensile strength. They may then be pulled into a rope-like 'tow' or woven into a fabric-like 'matte' before being coated with either epoxy or polyester resin. Therefore, carbon composites are eminently suited to forming rods, tubes, and sheets, although the final product may still be quite expensive per pound.

To simplify the vast diversity in specialized grades of PAN carbon composite for purposes of this application, this material should be considered as coming in two (2) basic density grades: low-density "deck" grade (at about 35% of the specific gravity of sheet steel), and high-density "beam" grade (at about 65% of the specific gravity of structural steel). It is also available in two (2) standard temperature grades, depending on the bonding agent used: a 350°F rating (lo-temp) epoxy-bonded material and a 750°F rating (hi-temp) polyamide-bonded composition. The high-temperature variety only should be employed in the Neutral Ring, but the lo-temp rating type may be used to build the Central Chamber.

Thus, a low-density/hi-temp grade of carbon composite laminate is to be used as the deck material in construction of the Neutral Ring hull. The table below provides what 'typical' physical properties are to be expected given the very basic average classification system described. The accompanying diagram illustrates the relative thicknesses of the composite decking material, ceramic substrate plates, and exolayer tiles which together comprise the composite Neutral Ring hull. The deck layer itself must first of course be affixed to the vessel superstructure by solvent welding and/or mechanical means.

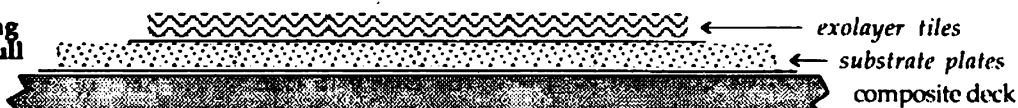
PAN Carbon Composite (deck grade)

Composition (%)		density (lb/in ³)	Max. Use Temp. (°F)	Thermal Expansion Coefficient @200-500°F	Ultimate Tensile Strength (psi)	Flexural Strength (psi)	Electrical Resistivity ohm-cm @200-500°F	Nominal Dielectric Constant
fiber	resin							
carbon	polyamide							
35	65	0.100	750	< 0	60,000	48,000	$> 5.1 \times 10^{-3}$	none

Component Specification: Deck Layer Thickness

The thickness of the carbon composite Neutral Ring deck layer sheeting shall be equal to $20/9600 R_k$.

Fig. 42: Neutral Ring composite hull construction



[b] Substrate Layer Plates

Several factors enter into the selection of an appropriate ceramic material for the substrate layer of the composite Neutral Ring hull section. Of primary concern here is that the material of choice have a very high volume resistivity and extremely low thermal conductivity at temperatures from 300 - 500°C. It is also important that the material have a very low thermal expansion coefficient, as the substrate layer plates must be bonded to the deck layer with a refractory class adhesive. Therefore, the substrate material should also be non-vitreous and have a relatively high porosity to promote adequate adhesion.

This might sound like a tall order to fill, but one of the Cordierite class of compounds, bearing CeramTec designation 447, should work very nicely. Although this material has relatively low hardness and flexural strength, as shown in the table below, it should function admirably in Thermal Units as the center layer of a bonded composite construction given its other highly desirable characteristics. Drive Units may require an alternate plate material per the ****Note in [c] on the next page.**

Cordierite 447 (2MgO·2Al₂O₃·5SiO₂)

Specific Gravity	Hardness Mohs' Scale	Max. Use Temp. (°C)	Thermal Expansion Coefficient @ 25-700°C	Thermal Conductivity W/m-K @ 25°C	Tensile Strength PSI	Flexural Strength PSI	Electrical Resistivity ohm-cm @ 700°C	Dielectric Constant @ 1MHz 20°C
1.8	6.5	1,100	1.5×10^{-4}	1.7	2,500	3,400	4.7×10^6	4.1

Component Specifications: Substrate Plate Dimensions

The thickness of the Neutral Ring substrate layer plates shall be equal to $13/9600 R_n$. These plates shall also be a maximum of $1/11$ of the Neutral Ring radius in radial length and the same in greater radial width, except that the innermost and outermost circular rows* of said plates (on each symmetrical hull half) should be $1/22$ of the Neutral Ring radius in radial length. The plates should be applied to the composite decking with a refractory adhesive layer limited to $2/9600 R_n$ in thickness.

***Note:** Rather than use a solid innermost circular row of plates also equal to $1/22$ of the Neutral Ring radius in radial length (on each hull half), the Dielectric Buffers are extended to the surface of the composite Neutral Ring hull layer (see Fig. 53 in subsection 2[c] of Mat. SpecSheet D).

[c] Exolayer Tiles

The selection of a ceramic material for use as the exolayer dielectric thermal tiles of the EDF Generator is contingent upon the operative Field voltage, and therefore a different material must be specified for Thermal and Drive Units. To prevent substantial skin conduction losses, the minimum dielectric value k for the tile material used in Thermal Units must be calculated, as shown below for the 4ft. diameter prototype model, using the peak Field voltage:

$$\max.V_f = 3.19 \times 10^6, \text{ and } \max.E_n = 3.19 \times 10^6 / .12035m,$$

where .12035m equals the Neutral Ring radius.

$$\text{Therefore, } \min.k = 26.506 \times 10^6 / 3 \times 10^6 = 8.84.$$

Therefore, the material selected is a Zirconia composition bearing CeramTec designation 848, with a minimum (high-frequency) dielectric constant of 28. Even though this material has a comparatively high thermal expansion coefficient, it has very low thermal conductivity and is very dense and hard. Moreover, it exhibits exceptional flexural strength and resistance to fracture.

Zirconia (ZrO₂)

Specific Gravity	Hardness HV 0.5	Max. Use Temp. (°C)	Thermal Expansion Coefficient @ 25-700°C	Thermal Conductivity W/m-K @ 25°C	Tensile Strength PSI	Flexural Strength PSI	Electrical Resistivity ohm-cm @ 700°C	Dielectric Constant @ 1MHz 20°C
6.0	1,150	900	7.7×10^{-4}	2.7	80,000	109,000	NA	28

Mat. SpecSheet A: Hull Components

The minimum dielectric value k for the tile material used in Drive Units must be calculated, as shown below for the 4ft. diameter prototype model, using the peak Field voltage:

$$\max.V_f = 38.6148 \times 10^6, \text{ and } \max.E_k = 38.6148 \times 10^6 / .12035 \text{ m,}$$

where .12035 m = the Neutral Ring radius.

$$\text{Therefore, } \min.k = 3.20854 \times 10^6 / 3 \times 10^6 = 107.$$

Therefore, the material selected is a titanate composition bearing Keramos designation K15. Known chemically as Sodium Bismuth Titanate, this highly unusual compound is technically a piezoelectric material, but is also ferroelectric in that its dielectric constant actually increases on temperature rise to a peak (low frequency) value of about 3,000 at its 655°C curie point. Like most ferroelectrics, its tensile and flexural strengths are quite low yet it is very dense and exceedingly hard. It also exhibits a comparative thermal expansion coefficient which is very high.

****Note:** Should the expected higher flexural stresses upon the Neutral Ring of a Drive Unit (compared to a Thermal Unit) prove sufficient to crack these lower strength tiles, the aforementioned Zirconia compound may be substituted for Cordierite 447 as the substrate plate material. This would likely stiffen the composite Neutral Ring hull adequately to prevent such stress cracking, and effect a much closer match in thermal expansion coefficient to the Titanate tiles.

A basic physical properties table follows, and a much more in-depth discussion of Sodium Bismuth Titanate's special characteristics is provided in subsection 2[b] of Mat. SpecSheet D, as the Dielectric Buffer associated with each Power Resistor is also to be fashioned of this same material.

It should be noted that at least one significant problem exists in forming more complex shapes (like the Dielectric Buffers) of Sodium Bismuth Titanate (NaBiTiO). Like most ceramics, this material must be pressed and sintered in powdered form, and some shrinkage upon firing is to be expected: typically on the order of a percent or so and in some cases a few percent. NaBiTiO, however, generally shrinks about 18% on the average upon firing, with the local shrinkage factor of a given formed object somewhat dependent on the relative thickness at that point.

Thus, there is probably only one way to maintain the type of dimensional control necessary in this application, using NaBiTiO, unless the raw piece is formed purposely-oversized, and is reduced to net size after firing by extensive diamond wheel grinding and/or laser machining. This alternative production method would require the use of a special gravity compaction die, or sectional weighted cavity die made of high temperature metal alloy, which is fired along with the raw piece and continually compresses it to the right size as it shrinks! Therefore, not only is the raw material powder itself quite expensive, but the necessary finishing of each piece of complex shape will also be costly.

Sodium Bismuth Titanate K15 (Na_{0.5}Bi_{1.5}Ti₁O₁₁)

Density (gm/cm ³)	Rockwell Hardness	Max. Use Temp. (°C)	Coefficient of Thermal Expansion per °C x 10 ⁻⁴	Thermal Conductivity W/m-K @ 25°C	Tensile Strength PSI	Flexural Strength PSI	Electrical Resistivity ohm-cm @ 700°C	Nominal Dielectric Constant @ 20°C
7.2	off C	900	9.9	NA	low	low	5 x 10 ⁴	165

Component Specifications: Exolayer Tile Dimensions

The Neutral Ring exolayer tiles shall be equal in size and thickness to the substrate layer plates, except that any 'half' size tiles used should be restricted to the innermost circular row thereof (on each symmetrical hull half). The tiles should be applied over said plates with a refractory adhesive limited to 2/9600 R_n in thickness in a mosaic overlay pattern, such that the edges of each exolayer tile are evenly spaced as far as possible from the underlying edges of the nearest substrate plates.

Section 3: Field Hub Construction

[a] Positive Zone Sectors

Selecting a suitable alloy for the EDF Generator's positive zone sectors requires careful research and analysis. These essentially non-structural but major components will jointly comprise roughly the same volume of conductive material as the rotor segments, and thus the sector material's density must be minimized while meeting a number of other stringent criteria. The most important such criterion is that the sectors be able to operate satisfactorily at a continuous very high temperature, which may

approach an 'orange' heat (or approximately 925 - 975°C).

In further restricting the material selection to non-magnetic alloys which offer superior oxidation and corrosion resistance at these temperatures and are readily available (and therefore affordable), the 309 and 310 series stainless steels emerge as the optimum candidates. They have excellent strength at elevated temperatures and are very ductile, such that *difficult shapes* are easily fabricated or forged. Each provides the desired surface integrity to 1090°C and 1150°C respectively. However, due to its higher chromium content, 310 stainless displays a lower thermal expansion coefficient and therefore tends to warp less at high heat. Also, when intermittent heating and cooling may be involved, type 310 is preferred since it forms a tightly adhering scale. In addition, it is extremely low in sulfur content.

The physical properties given in the table below are based on fully annealed 310 stainless steel, although in this application such large pieces should probably be forged. The data as shown may still be taken as essentially representative, and for best results these truncated wedge-shaped sectors of tapering thickness should be forged at 1125 - 1175°C and then water-quenched at 1125°C. The exterior surface finish specified from the mill should be equivalent to "2BA", or very smooth and glossy.

310 Stainless Steel

MATERIAL	COMPOSITION (%)									Typical Physical Properties				
	C (MAX.)	Mn (MAX.)	Si (MAX.)	P (MAX.)	S (MAX.)	Cr	Ni	Fe	OTHERS	Density (lb/in ³)	Thermal Expans. Coeff. 20-1000°C	Thermal Conduct. W/m-K 20-500°C	Young's Modulus (psi)	Ult. Tens. Strength @816°C (psi)
310 SS	.03	1.75	.75	.020	.002	25	20	bal.		.29	18.9×10^{-6}	10.8	29×10^4	30,300

[b] Zone Sector Partitions

The ceramic composition proposed for use as the Field Hub's *zone sector partitions* is the same material specified for the Neutral Ring hull substrate plates in Thermal Units: Cordierite 447. Although this oxide of magnesium, aluminum, and silicon is chosen for largely the same reasons as those noted in Section 2 above, it additionally offers low weight, excellent thermal shock resistance, and production economy in simple dry-pressed flat stock form.

Ideally, the radial (linear) partitions should be equal in number to the zone sectors, or one-piece in construction and installation. The central (curved) partitions should be fewer in number and installed such that the joints between central partitions are covered by the inner ends of the radial partitions. The diagram below shows the radial partitions in side view, the shape thereof being exactly the same as that of the adjacent stainless steel zone sectors. Reference may be made to the aforementioned Section 2 of this SpecSheet for pertinent physical properties.

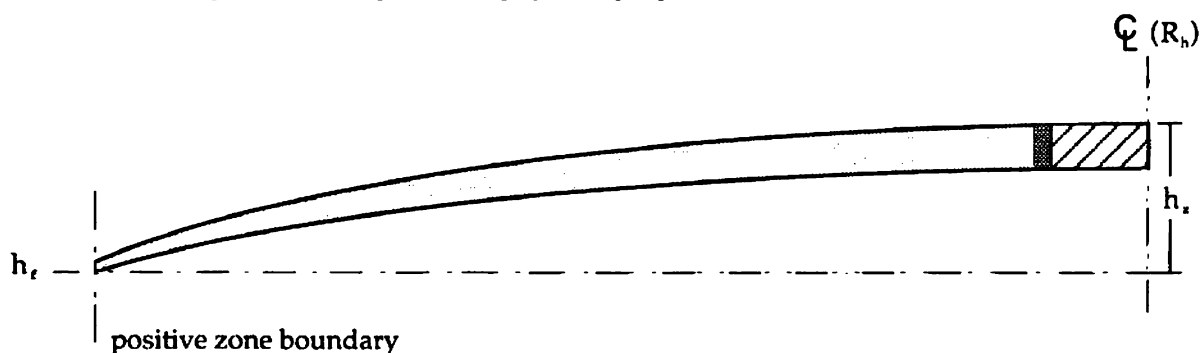


Fig. 43: radial zone sector partition (side view)

The area between the Neutral Ring 'deck' height (h_r) and the inner surface of the zone sectors and sector partitions must be reserved for plumbing associated with the primary thermal conduits and any additional *high-density occluding material* required to adequately prevent hard X-rays from penetrating the Central Chamber. Such radiation **occlusion baffles** should of course be ceramic in nature (to provide a base for mounting the zone sectors) and must be used only where and as absolutely necessary.

Superstructure Components

Section 1: Drive Ring Coolant Conduits & Support Brackets

[a] Secondary Thermal Conduits

The linear secondary thermal conduit sections which carry hull coolant must pass between the Power Resistor assemblies, and so they must conform in outside dimension to the available space within either of the two channels of any given carbon composite tri-beam. The most unusual feature of these secondary conduits is that they also comprise (of necessity) the principle Drive Ring load-bearing members. Together, they form the EDF Generator's structural intercooler system.

As specified in the following Section, the width of each tri-beam conduit channel is equal to $62/96(X) R_h$, and this therefore constitutes the maximum outside square dimension of the secondary conduits. Assigning an *outside* diameter for the molybdenum secondary core tubing which is equal to the *inside* diameter of the primary tubing, we find that the following secondary conduit dimensional relationships result in the 4ft. prototype: the minimum 'skin' thickness of the Alumina core coating is roughly half the wall thickness of the tubing, and the wall thickness is in turn roughly half the inside diameter of the core. As the diameter of the core tubing increases, these relative proportionalities of course change significantly: of primary concern here is that the ratio of wall thickness to inside diameter decreases consistently until at some point (to be determined) extra-heavy (XH) pipe should be specified. Pertinent material properties are provided in subsection 2[c] of Material SpecSheet D.

A primary reason for this choice of proportional tubing size is that in the 4ft. diameter prototype this specification stipulates the standard refrigeration tubing size of 1/8" OD, and in many larger sizes of EDF Generator the use of a standard tubing or pipe size will also be possible. In the 4ft. prototype, this specification also results in a minimum Alumina skin thickness of only about .015", and such a thin layer of ceramic applied to a metallic base could be considered by many as being likely to exhibit serious thermal and/or flexural cracking.

However, below 300°C the thermal expansion coefficients of Alumina and molybdenum are virtually identical, and thus thermal cracking is not expected to be a problem. Flexural cracking is a different matter, and must be controlled by the number of separate ceramic sleeve segments applied to each conduit (which should be strictly minimized). Alumina's flexural strength actually exceeds that of the moly tubing, however, and the resultant secondary thermal conduit sections are expected to exhibit relatively tremendous physical strength.

In actuality, these linear secondary thermal conduit sections will come in four varieties: (i) the initial outbound coolant 'supply' runs, called **headers**; (ii) the circumferential heat transfer sections (to which the Negative Ring hull plates are fastened), called **peripheral shunts**; (iii) the inner and outer intermediary coolant runs, called **transfer links**; and (iv) the radial coolant 'returns' or **recovery lines**. Within the Drive Ring, each of these conduit types are to be fashioned as single units which connect one to another in 'series-parallel' branch systems or **zones**. To wit, one *header* from a reservoir coolant **manifold** connects to one *peripheral shunt* which in turn connects to one *recovery line*. These recovery lines then return through an **exchange manifold**, in a total of 72 individual coolant zones, to a central heat exchanger (in 1η rotor devices). The headers, shunts, transfer links, and recovery lines take advantage of the high thermal conductivity of Alumina to absorb heat from the 1η Drive Ring hull, and in particular the Negative Ring hull plates. A single coolant zone is illustrated in Fig. 44 below.

Just how effective this method of cooling the Drive Ring as a whole will prove to be during operation in air is of course yet to be determined, and is somewhat difficult to project given the as-yet undefined heat transfer characteristics of the Field envelope. It is anticipated, however, that it will be of satisfactory effectiveness during the operation of 3η devices in the vacuum of space, and is principally designed with this mode of usage in mind. The proposed 1η hull coolant to be used is liquid nitrogen, with a reservoir temperature of about 77° K (-196°C), although liquid air might also be considered.

Component Specifications: Secondary Conduit Dimensions

- (i) The secondary Thermal Conduit core tubing (used to circulate liquid coolant through the Drive Ring) shall be equal to $1/192 R_h$ in outside diameter and composed of molybdenum.
- (ii) The ceramic coating applied to each secondary Conduit core section shall be composed of Alumina, except as noted in Section 2[b] of Mat. SpecSheet D, and shall be formed thereon to a final overall square cross section equal to $62/9600 R_h$ on each side.

Scale: appr. 1:1 for the 4ft. prototype.

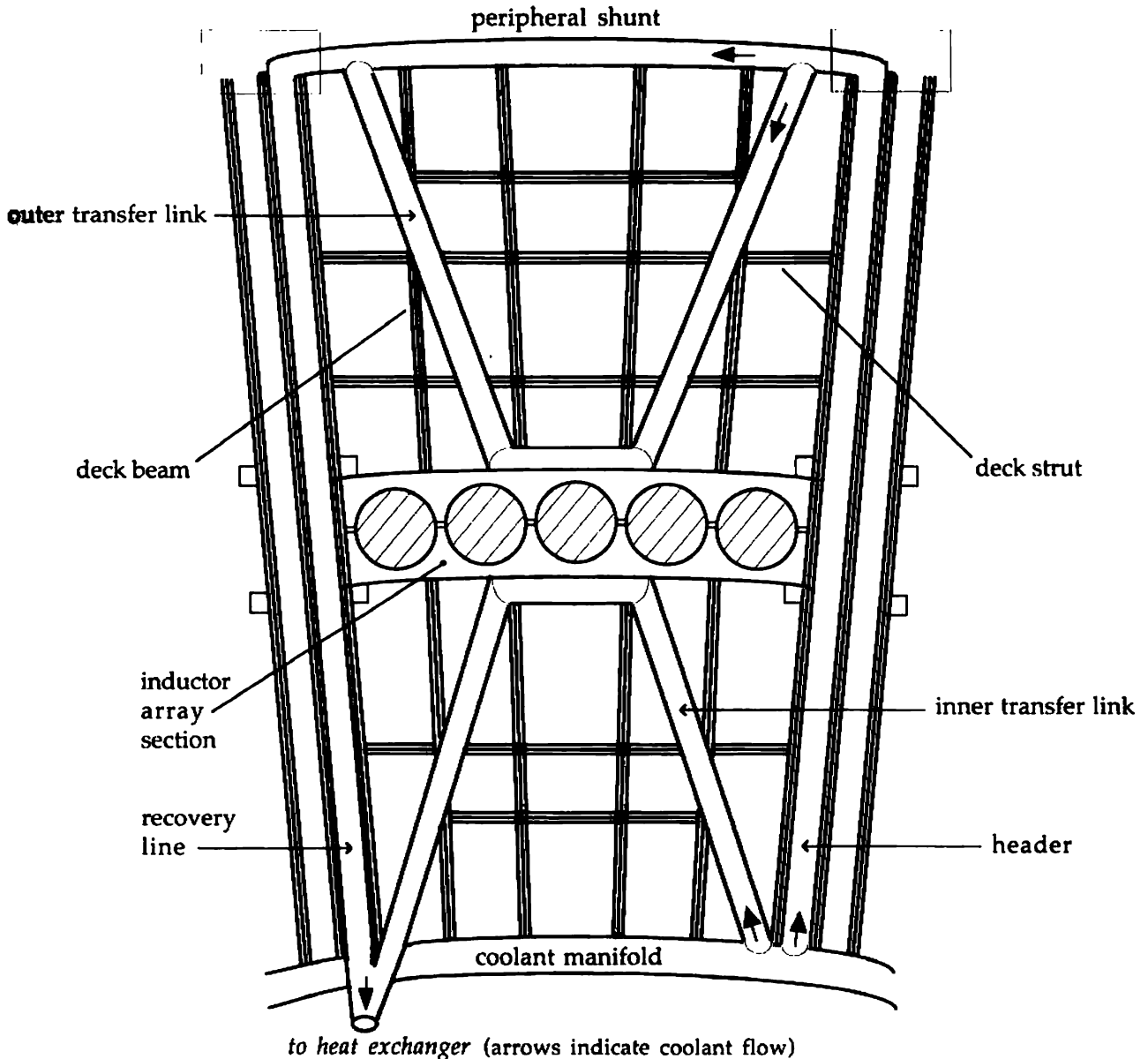


Fig. 44: one (1) Neutral Ring hull section and structural intercooler zone.

The inner and outer Drive Ring support brackets are not shown for the sake of clarity. The outer support brackets are formed as integral units which each contain a pair of weld elbows, and are located in the boxed areas shown at the end of each composite tri-beam. The peripheral shunt fits inside an angle bracket welded to the inner surface edge of each negative hull plate, which thereby forms a heat transfer channel and rotor current shield.

[b] Support Brackets

The outer Drive Ring support brackets not shown in the preceding diagram are all the same in terms of size and shape. In addition to having an opposed pair of 90° weld elbows formed directly within the ceramic material, each one has a set of three (3) molded mounting “knuckles” which secure the inner corners of two adjacent negative hull plates via a matching mounting ring (welded to each plate corner) and a retaining pin. The inner end of each molybdenum elbow protrudes from the bracket, for weldment to the respective header and adjacent recovery line, and this end of the bracket is shaped to fit into the end of the tri-beam just like the conduits. The outer end of each elbow also protrudes for weldment to the respective peripheral shunt.

These outer brackets, like the larger inner variety, are to be cast of Zirconia (zirconium dioxide). A fairly recent development in technical ceramics, Zirconia is the strongest commercially available ceramic material. It exhibits tensile strength *greater* than the yield tensile strength of the moly tubing used in the conduits, and has superior flexural strength, low temperature stability, and resistance to fracture. The reason it is not used for the conduit sleeve material itself, given these otherwise highly desirable characteristics, is that its thermal conductivity is over a dozen times *lower* than that of high-purity Alumina. Physical properties are given at the bottom of pg. 393.

Scale: 3:1 for the 4ft. prototype.

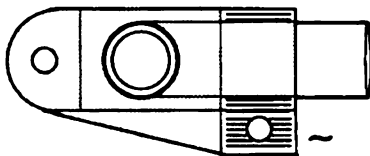


Fig. 45a: *outer support bracket side view:*

The lower bracket portion is extended, so that it may be pinned to the tri-beam.

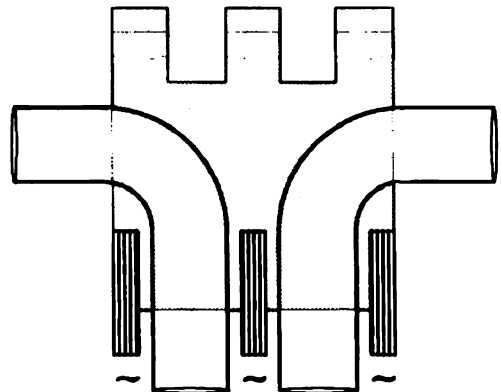


Fig. 45b: *outer support bracket top view*

Component Specifications: *Bracket and Mounting Ring Dimensions*

- (i) The maximum thickness of the negative hull plate mounting rings shall be equal to $\frac{3}{768} R_h$.
- (ii) The maximum thickness of the outer Drive Ring support bracket knuckles shall be equal to $\frac{3}{800} R_h$.

The inner Drive Ring support brackets shown on the following page incorporate an integral 90° elbow for the header coolant inlet, whereas the inner transfer links each have a separate similar take-off directly from their respective coolant manifold section. These inner brackets also incorporate an integral wye which crosses over the manifold core portion.

Each of the two divisions of the hull coolant manifold system is divided into six sections, with each section serving six headers. These manifold sections are actually located in the hull Neutral Ring, immediately ‘above’ the inner induction arrays and their adjacent stationary anode rings. The exchange manifold system carrying heated coolant (in 1η rotor devices) is likewise so divided, but must be located much further inboard ‘behind’ the power resistors and carrier assembly.

Each inner support bracket has a set of two (2) mounting knuckles which secure one tri-beam assembly to the bracket with two retaining pins, and a large single knuckle which in turn attaches the bracket to two matching mounting rings on the central superstructure with a second pair of retaining pins. The base of each inner bracket also incorporates a positioning stud which serves to minimize axial torque stresses on the various conduit sections. Although somewhat unusual, this structural intercooler system (once decked) should readily support a Drive Ring weighing about 275 tons in the 100ft. diameter model!

Scale: 3:1 for the 4ft. prototype.

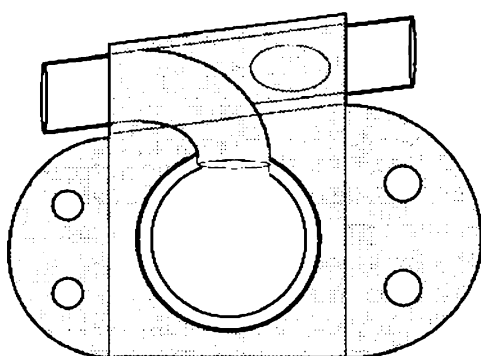


Fig. 46a: *inner support bracket side view:*

The tri-beam section(s) shown in the accompanying Figure are not shown here.

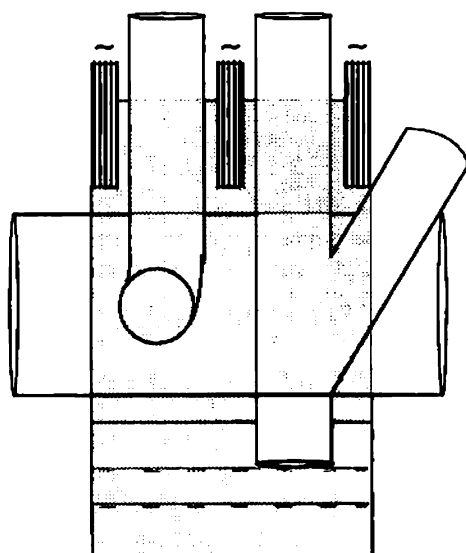


Fig. 46b: *inner support bracket top view*

Component Specification: *Secondary Manifold Diameter*

The hull coolant manifolds shall have an inside diameter which is a maximum of 2.45 times that of the radial header conduit sections, with each manifold section serving six (6) such headers, *except that this specified ID may be revised slightly in light of transfer link flow rate considerations.*

Section 2: *Neutral Ring Beams & Struts*

According to the simplified classification system outlined in Section 2 of Mat. SpecSheet A, the beams and struts which constitute the secondary load-bearing members to which the composite deck material is affixed are to be formed of high-density/hi-temp PAN carbon composite. The primary reason for this material selection is that the radial beams themselves must in places have a very modest 'width', or height in the vertical axis, and must take advantage of the composite's tremendous specific strength (or tensile strength-to-weight ratio). The fact that the deck sheeting may readily be solvent-welded to these beams and struts, to facilitate the sealing of the Drive Ring against the interior vacuum, is also a decided advantage.

A general representation of one layout for these beams and struts is shown in Fig. 44, and anticipates that in certain instances it may not be possible to make the radial single beams (between tri-beams) of one piece across the full radial width of the Neutral Ring. In every instance, it should be possible to make the struts of one piece across each hull section (between tri-beams), being notched to engage the radial beams. The tri-beams which each form two channels in which the zone headers and recovery lines are run must of course be of one-piece construction.

Component Specifications: The minimum width of each Neutral Ring beam (or its height in the vertical axis), including those which comprise each tri-beam, shall be equal to $2C_r$. The thickness of each such beam shall be equal to $16/9600 R_h$. The width of each of the two channels formed by each tri-beam shall be equal to $62/9600 R_h$.

PAN Carbon Composite (beam grade)

Composition (%)		density (lb/in ³)	Max. Use Temp. (°F)	Thermal Expansion Coefficient @200-500°F	Ultimate Tensile Strength (psi)	Flexural Strength (psi)	Electrical Resistivity ohm-cm @200-500°F	Nominal Dielectric Constant
fiber	resin							
carbon	polyamide							
60	40	0.187	750	≤ 0	100,000	80,000	≥ 3.0 × 10 ⁻³	none

Rotor Components

Section 1: Rotor Segments

Specifying the material to be used for the conductive rotor segments is probably easier than for any other EDF Generator component. The goal is, of course, to achieve the maximum ampacity possible within justifiable cost. This consideration virtually eliminates any other material choice. And, because the conductivity of copper alloys drops off dramatically as the percentage of almost any other alloying element(s) increases, the selection of practically-pure metallic copper is almost automatic.

One consideration that is somewhat less obvious is that the actual grade of copper specified should be oxygen-free, as the presence of oxygen radicals released into the vacuum chamber upon substantial heating of the segments would be decidedly deleterious to Primary Power System performance. Therefore, OFHC* (oxygen-free high conductivity) copper of minimum 99.95% purity should always be used. OFHC copper is produced by converting cathodes under closely-controlled conditions, thereby eliminating almost all other elements, and displays the inherent qualities of the metal to the highest degree. In this form, trace silver is counted as copper.

Copper (Cu)

CDA ALLOY NO.	ALLOY NAME	NOMINAL COMPOSITION (%)				DENSITY (LBS. PER CU. IN.)	THERMAL CONDUCT. (BTU/SQ. FT./ FT./HR./°F @ 68 F)	ELEC. CONDUCTIVITY (% IACS @ 68 F SOFT)	ELEC. RESISTIVITY (OHMS (CIRC. MIL/FT.)	MELTING POINT (°F/°C) (DEGREES F)	TYPICAL MECHANICAL PROPERTIES (.08")								
											TENSILE STRENGTH (1000 LBS. PSI)			YIELD STRENGTH @ 0.50% EXTENSION UNDER LOAD (1000 LBS. PSI)			ELONGATION IN 2 IN. (%)		
		Cu	Zn	Sn	OTHER						SPRING	HARD	SOFT .025	SPRING	HARD	SOFT .025	SPRING	HARD	SOFT .075
101	OFHC Copper Cert	99.99 min.	-	-	-	323	226	101	10.3	1981	66	55	34	57	50	11	3	6	54
102	OFHC Copper	99.95 min.	-	-	-	323	226	101	10.3	1981	66	55	34	57	50	11	3	6	53
110	ETP Copper	99.90 min.	-	-	Oxy .04	323	226	101	10.3	1949	66	55	34	57	50	12	3	5	42

* Registered Trademark of AMAX Inc.

Section 2: Field Emitters

In almost no other single aspect of specifying materials for the EDF Generator is extreme care and accuracy more important than in specifying the material to be used for the Field Emitters. The consequences of making an improper selection range from unnecessarily increasing the rotor's overall resistance (and therefore restricting power output) to causing a decidedly undesirable modification of the anticipated Primary Voltage Expansion Ratio. Compounding the difficulties involved is the simple fact that it is extremely unlikely a truly accurate projection of the working Emitter temperature (a most important consideration) can even be made without extensive prototype testing.

In dealing with the latter problem first, it is therefore crucial to select a material which allows the Emitters to be matched in resistance to the rotor segments at an operating temperature above any which is reasonably to be expected, as it is not really possible to provide means for cooling rotor components. Thus, a material which exhibits a certain volume resistivity and temperature coefficient of resistivity, as shown in WorkSheet II(b), will provide for unimpeded rotor current handling capability up to an Emitter operating temperature of over 900°C (or within 150°C of the melting point of the segments). In this respect, it must therefore also be possible to either obtain these material resistivity characteristics from the manufacturer or calculate this data if otherwise not available. In the case of unusual or exotic alloys, this information is usually not documented.

Of particular importance with regard to the Primary Voltage Expansion Ratio and the maintenance of a proper Field voltage is the surface work function ϕ , which must either be known or accurately calculable and which again is very seldom obtainable in the case of metal alloys. Fortunately, the

existence of a broad selection of *refractory composites* enables acceptably accurate estimates of two of these material characteristics to be made as straight proportionalities given the nominal percentage composition. This is in fact what has been done in this application and the necessary resistivity coefficient α and work function ϕ for the material selected, a 68% tungsten and 32% copper powder metallurgy composite, are calculated below. The volume resistivity is available from the supplier.

The natural temperature coefficient of resistivity for tungsten is .0048/°C and for copper is .00393/°C. Using a percentage proportionality, we may then calculate the coefficient for 68/32 tungsten-copper composite as follows:

$$\begin{aligned}\text{composite } \alpha &= .68(.0048) + .32(.00393) \\ &= .003264 + .0012576 \approx .00452/\text{°C}.\end{aligned}$$

In similar fashion, the work function of the tungsten-copper composite may be obtained from the natural work functions for tungsten, which is 4.6ev, and for copper (at 4 ev):

$$\text{composite } \phi = .68(4.6) + .32(4.0) = 3.128 + 1.28 = 4.408 \text{ ev}.$$

The volume resistivity for the composite Emitter material, which is used in WorkSheet II(b) along with the coefficient α to determine the rotor's temperature resistance equivalence point, is figured in the following table of physical properties.

Tungsten-Copper Composite

Nominal Composition % Weight	Rockwell Hardness	Electrical Conductivity % IACS	Ultimate Tensile Strength PSI	Density gms/cc	Thermal Expansion In./In.-°C $\times 10^{-4}$ @ 20°	Thermal Conductivity W/cm-°C 20-400°	Specific Heat J/Kg-°C @ 20°	Electrical Resistivity micro-ohm-cm @ 20°C
32 copper 68 tungsten	88 B	52	75,000	13.93	10.90	2.10	219	3.32

Composites of tungsten and copper are available in which the percentage copper varies from 10 to 45%. The thermal and electrical conductivity increases with the amount of copper and the hardness, strength, and resistance to mechanical wear increase proportional to the amount of tungsten. The manufacturing process is to press the powdered refractory, sinter the pressed compact at high temperature, and infiltrate with copper under closely controlled conditions. The result is a relatively hard non-magnetic material with superior arc erosion resistance. Tungsten-silver and molybdenum-silver composites are also available.

Because the actual equilibrium Emitter operating temperature is not known, the following Table has been created to enable research and development engineers to select an optimal level of primary cathode thoriation, should the Emitter temperature (in all likelihood) fall within the range of values provided, in order to achieve the desired emissivity ratio and reciprocal Primary Voltage Expansion Ratio for the 4ft. diameter Drive Unit. This Table indicates that below the key emitter surface temperature of 510°C, at which no primary cathode thoriation is necessary, the cathodes must be cooled to operate at a temperature *below* a mean Power Resistor operating temperature *as given here**.

Field Emitters		1/emissivity ratio	Primary Cathodes	
ϕ	temperature		ϕ	temperature*
4.408	775°C (1048°K)	1:12,106	3.202	675°C (948°K)
4.408	725°C (998°K)	1:12,106	3.410	675°C (948°K)
4.408	675°C (948°K)	1:12,106	3.639	675°C (948°K)
4.408	625°C (898°K)	1:12,106	3.894	675°C (948°K)
4.408	575°C (848°K)	1:12,106	4.177	675°C (948°K)
4.408	525°C (798°K)	1:12,106	4.496	675°C (948°K)
4.408	510°C (783°K)	1:12,106	4.600	675°C (948°K)

Section 3: Segment Separators

The design of the EDF Generator's composite rotor assembly calls for slightly wedge-shaped ceramic pieces (equal in number to the rotor segments) which are positioned uniformly between the individual segments and which are far more structural than insulative in nature. These segment separators not only stiffen the entire rotor to prevent distortion at elevated temperature and rotational speed but also provide a non-conductive base for mounting all other rotor assembly components.

The two most important criteria for selecting a separator material are that the ceramic compound chosen be readily machinable like steel and provide very high physical strength yet require no firing. As is typical in this particular application, these parameters limit the choice made almost to a solitary substance: magnesium silicate. When suitably formed, this material can be milled, drilled, and tapped like steel (using low-speed tungsten carbide tools) and approaches the physical strength of dry-pressed porcelain. It is ready for use directly after shaping and requires no kiln hardening.

This latter characteristic is very important as it is extremely difficult to produce fired ceramic pieces with the exacting dimensional control necessary in this case, and it eliminates the tendency of thicker fired pieces to develop micro-cracks which may potentially cause destructive failure of the component under high centrifugal loading. Surfacing can be done with abrasive paper or grinding wheels, and it is very important that this material be machined or worked perfectly dry as it is fairly porous and any lubricant used tends to significantly alter its dielectric properties. Magnesium silicate of this type, bearing CeramTec designation 222, will withstand constant working temperature of nearly 2500°F.

Magnesium Silicate (MgSiO₃)

Specific Gravity	Hardness Mohs' Scale	Max. Use Temp. (°C)	Thermal Expansion Coefficient @ 25-600°C	Thermal Conductivity W/m-K @ 300°C	Tensile Strength PSI	Flexural Strength PSI	Electrical Resistivity ohm-cm @ 300°C	Dielectric Constant @ 1MHz, 20°C
2.0	6	1300	10 x 10 ⁻⁶	3.9	2500	5000	6 x 10 ¹¹	5.5

Section 4: Rotor Facing

Because of the close proximity of the various Neutral Ring Primary Power System components to the energized rotor segments, it will be necessary to apply a relatively thin layer of dielectric material to each of the two major flat faces of the rotor assembly. However, in the central region of the rotor (near the vertical centerline of the segments), these dielectric layers must be of an absolutely minimal thickness, as the torque applied to the rotor by the Variable Inductors will decrease by the square of increases in their working clearance with respect to the segments.

This consideration presents a virtually insurmountable problem with regard to the application of any solid dielectric material having a significant *k* value as the central rotor facing. The actual voltage present on the segments near their vertical centerline (with respect to ground) is expected, however, to be normally quite low. Therefore, it is proposed to use a one-component silicone elastomer conformal coating, applied in liquid form by spray or flowcoat method directly to the finished segment and separator composite assembly, which has only a modest dielectric constant but extremely high volume resistivity. The material selected should also have an application viscosity as low as possible, to provide maximum 'wettability' and adhesion to the non-porous segments, and be of a low-temperature cure variety.

Eccocoat* S7003

Specific Gravity	Hardness Mohs' Scale	Tensile Strength PSI	Max. Use Temp. (°C)	Thermal Expansion Coefficient (x 10 ⁻⁶ /°C)	min. cure temp. (°C)	min. cure time (hrs.)	Nominal Dielectric Constant	Dielectric Strength (V/mil)	Electrical Resistivity ohm-cm
0.97	low	125	< 200	410	80	.5	< 3.0	500	3.5 x 10 ¹⁴

* Registered Trademark of Emerson & Cumings, Inc.

Component Specification: Central Facing Thickness

The thickness of the silicone coating used as *central rotor facing* shall be equal to .75 mil (.00075") per foot of hull radius R_h .

It should be noted that the central rotor facing silicone layers must be applied *after* the adjacent **inside and outside facing bands** have been applied, in part due to the large thermal expansion coefficient exhibited by the elastomer coating.

The primary criteria involved in selecting a material for these single-layer rotor facing bands are high k value and very high flexural strength. The chosen ceramic compound should also be of known suitability for use as a 'thick film' substrate. Thus, the inner and outer facing bands are to be composed of high-purity Alumina (bearing CeramTec designation 433), which is also used as the Thermal Conduit sleeve material of choice. It should be formed in partial-ring sections equal in radial width to a whole multiple of the distance between the radial centerlines of the segment separators. These rotor facing sections should also be applied with a refractory adhesive limited to $1/6400 R_h$ in thickness, and should also be pinned to the segment separators in numerous locations.

Alumina 433

Specific Gravity	Hardness Mohs' Scale	Max. Use Temp. (°C)	Thermal Expansion Coefficient @ 25-700°C	Thermal Conductivity W/m-K @ 25°C	Tensile Strength PSI	Flexural Strength PSI	Electrical Resistivity ohm-cm @ 700°C	Dielectric Constant @ 1MHz 20°C
4.0	9.0	1550	7.7×10^{-6}	37.0	35,000	60,000	NA	10.0

An analysis of the minimum peripheral Field Emitter-to-negative hull plate transit distance reveals that the rotor voltage will rise to about 64% of Specification value in 1η rotor devices and 85% thereof in 3η rotor devices before vacuum chamber 'flashover' occurs, as a function of the Negative Ring hull plates' channel thickness specification. Thus, the inside and outside facing need never insulate against more than half of peak rotor voltage. The standard thickness of both these facing bands as specified below is therefore at least 500% above a minimum electrical rating given a value of $k = 10$ for the Alumina composition selected. It can be seen here that these facing sections are clearly as much structural in nature as electrical.

Component Specification: Standard Facing Band Thickness

The standard thickness of the *inside and outside rotor facing* band sections shall be equal to that of the rotating inner and outer induction rings (silver-soldered to the rotor segments) at $1/768 R_h$.

The **peripheral rotor facing** is that which passes the ballast capacitor traces beneath the ballrace assemblies. These facing bands must also be installed in sections similarly to those above but must be divided into two distinct layers, with a small number of *inner* peripheral sections being 'routed' for passage of uniformly distributed nickel alloy traces. Because these traces carry full outer induction anode ring voltage, the inner peripheral facing layers must insulate against 82.5% of rotor voltage. The Specifications below consider that both inner and outer layers of each peripheral rotor facing band are to also be composed of the same Alumina as above, and that the inner layers will not be operated at over 40% of breakdown intensity.

Component Specification: Peripheral Facing Thickness

a) The minimum thickness of each *inner peripheral facing layer* (in its trace locations) shall be equal to $21/9600 R_h$, and such inner layer's adjacent ballrace assembly sections mount directly thereupon.

b) The ballast capacitor plates (rings) as well as the traces which pass voltage to the positive such electrode are to be constructed of the same nickel alloy as the Primary Power System anodes.

c) The thickness of the ballast capacitor traces shall be equal to $1/8000 R_h$.

d) The thickness of each *outer peripheral facing layer*, which must be split into two parts (one on either side of the proximal ballrace), shall be equal to $1/960 R_h$.

Section 5: Ballrace Assemblies

Some basic information is presented in SpecSheet IV on the general properties of ceramic bearing assemblies, although a particular material is not specified therein. The single characteristic which confirms that the final selection should be *Silicon Nitride* is that this ceramic fails by *spalling* (similar to steels) while other ceramics fail catastrophically. Dynamic fatigue tests indicate that silicon nitride bearing balls can be expected to show a service life 10 to 20 times that of conventional stainless steel balls under heavy load conditions, and a nearly unlimited service life under "normal" bearing loads (up to 600 ksi).

Silicon nitride bearing balls are currently available from manufacturer stock in sizes up to 2" in diameter, corresponding to a vessel over 85 ft. in diameter. The light weight, high rigidity, and combined dielectric and non-magnetic properties of all-nitride bearing assemblies make them a very attractive alternative not only to conventional steel rolling bearings (which would barely be suitable) but to electromagnetic positioning hardware of a much greater complexity as well.

Some debate exists, however, as to whether the rotor ballraces themselves may also be composed of silicon nitride (which is greatly to be preferred). Although the density of this material is only 40% that of comparable steel, and thus would impart far less centrifugal load to the rotor, its fracture toughness is only about 1/3 that of bearing stainless. Since it is proposed that integral pins be used to press-fit mount each of numerous raceway segments to their adjoining segment separators, a thin film of refractory adhesive should also be applied between raceway and rotor to minimize any tendency of these underpins to snap if the rotor raceways are in fact ceramic.

Silicon Nitride (Si_3N_4)

Specific Gravity	Rockwell Hardness	Max. Use Temp. (°C)	Thermal Expansion Coefficient @ 20-800°C	Young's Modulus (psi)	Fracture Toughness ($\text{MPa}\cdot\text{m}^{1/2}$)	Bending Strength (MPa) @1000°C	Sphericity/ & Surface Roughness	Dielectric Constant @ 1MHz 20°C
3.2	C80	1,200	1.9×10^{-6}	45×10^6	6	600	$<0.2\mu\text{m}/.005\mu\text{m}$	>8

Section 6: Carrier Assembly

The EDF Generator subsystem referred to and elaborated upon the least in the Basic Specifications is the largely-mechanical rotor carrier assembly, although in a fundamental way the feasibility of the entire device is contingent upon how well it performs its task: to support, center, and stabilize the huge dynamic load presented to the ground frame by the rotor. The carrier assembly must be fabricated in multiple sections, like most of the device's constituent systems, and is constructed in a dual-frame split squirrel-cage fashion somewhat reminiscent of the turntable of a carousel or centrifuge.

This carrier assembly is comprised of three (3) primary component groups: (i) two large ~40° biplanar sectional *ring gears*, each with both major outer surfaces deeply gear-faced; (ii) a total of 32 low-voltage dc dynamic braking gearmotor *drive units*, in four sets of 8 each, with each unit being placed uniformly within a circular configuration (radially-offset 11.25° from each of its neighbors); and (iii) a split sectional *rotor frame* composed of a large number of welded tubular *struts and members*.

Because the rotor is not only electrified but very hot as well at the segment lockdown and retaining end location(s), sets of zirconia thermal spacers and bushings and black nylon load buffers must be employed, which completely enclose this inner portion of the rotor. The thin zirconia spacers (which are to be *completely unadhesed*) provide thermal protection for the nylon buffers, which in turn ensure load shock dampening with respect to the rotor frame. The properties for zirconia are given in Mat. SpecSheet A, and those of the high-temperature nylon are readily available from the manufacturer.

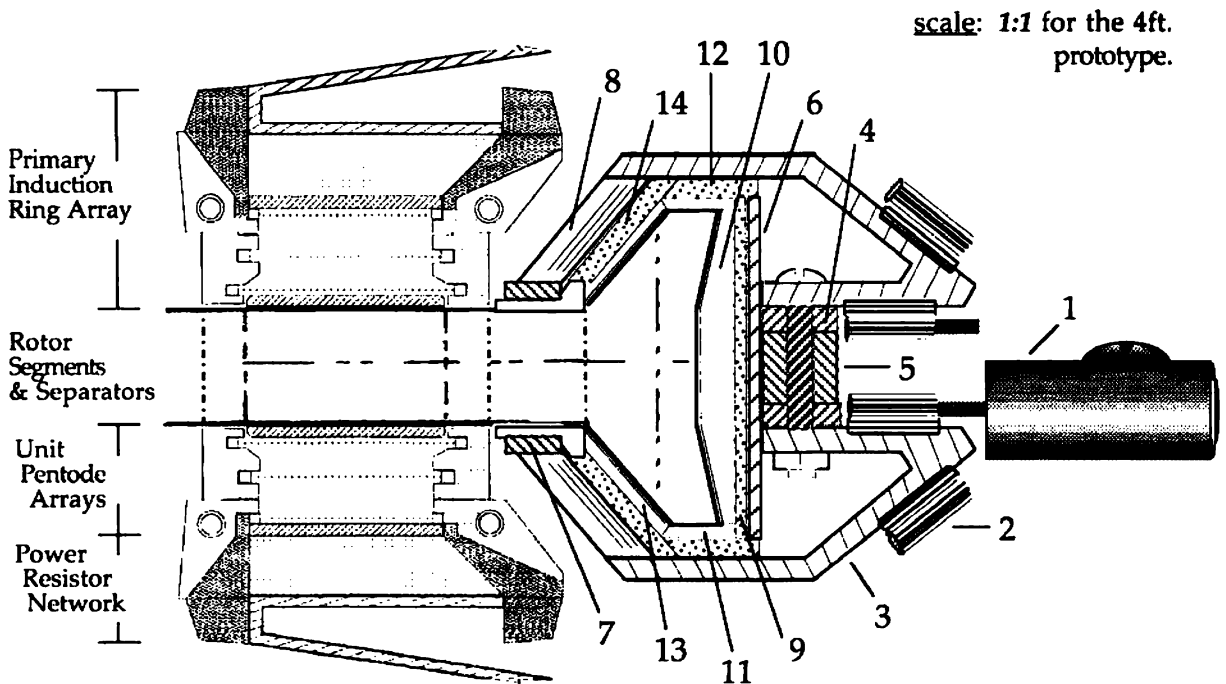
Of greatest importance here is to specify the most suitable structural alloy from which the tubular rotor frame members are to be fabricated. In this respect, type 321 stainless steel is proposed for use at the present time, as is common for heavy welded equipment which can't be annealed. It is stabilized with titanium to prevent carbide precipitation during inert gas welding (and thus minimize intergranular corrosion) and is designed to resolidify with a small amount of ferrite to minimize cracking susceptibility. Its fatigue strength is approximately 35% of its ultimate tensile strength.

321 Stainless Steel (max. nitrogen content = 0.10%)

MATERIAL	COMPOSITION (%)									Typical Physical Properties				
	C (MAX.)	Mn (MAX.)	Si (MAX.)	P (MAX.)	S (MAX.)	Cr	Ni	Fe	OTHERS	Density (g/cm ³)	Thermal Expans. Coeff. 20-600°C	Thermal Conduct. W/m-K 20-500°C	Young's Modulus (psi)	Ult. Tens. Strength @200°C (psi)
321 SS	.08	2.00	0.75	.045	.030	17-19	9-12	bal.	Ti 5x(C+N) min.	7.89	18.9×10 ⁻⁶	21.4	28 × 10 ⁶	66,600

The diagram of Fig. 47 below (in radial cross section view) illustrates the construction of the carrier assembly, and assigns its relevant parts nomenclature. The tubular struts are those frame components which are radially-parallel with the rotor segments, and thus load-bearing in the direction of their length, and the frame members are relatively diagonal tubular cross-braces to prevent twisting between the ring gears and retaining rings. This drawing is done in 1:1 scale (actual size) for the 4ft. prototype.

The numbering system employed in the diagram Key is intended to reflect as nearly as possible the order in which the various parts are used in actual construction. Each component of a particular type must be as exactly equal as possible in weight to one another, to facilitate rotor dynamic balancing. The principal construction parameters are that the two ring gears are first assembled using their respective mounting ring sections, and the retaining ring sections and attached frame struts and members are next welded to the ring gears. These two assemblies are then connected to one another (once all of the thermal spacers, bushings, and buffers are positioned) with the mounting ring spacers. It should be noted that at least two (2) of the latter spacers are to be welded to each flexor plate prior to this step.



KEY:

- | | | |
|---------------------------|----------------------------|----------------------------|
| (1) dc Drive Unit | (6) flexor plates | (11) inner thermal spacers |
| (2) drive pinion gear | (7) retaining ring section | (12) axial load buffers |
| (3) ring gear section | (8) frame struts & members | (13) outer thermal spacers |
| (4) mounting ring section | (9) torsion buffers | (14) radial load buffers |
| (5) mounting ring spacers | (10) displacement bushings | |

Fig. 47: Carrier Assembly Construction

Note: Segment and separator retaining ends must be tapered (with respect to their 'design' shape shown in Fig. 20) to provide adequate clearance to the Primary Induction Ring Arrays.

Electrode Array Components**Section 1: Primary Power System****[a] Anodes & Cathodes**

The material of which the Primary Power System anodes and cathodes are to be composed is **actually** stipulated in SpecSheet VIII (Electrode Array Construction). This is one of the rare instances in **which** this occurs, as the choice would seem to be quite cut-and-dried. The reasons for selecting a nickel **alloy** over tungsten are three: (i) a non-magnetic metal or alloy is preferred whenever possible for **Neutral** Ring components (and tungsten is paramagnetic); (ii) the Power System current is comparatively **low** and the high current-handling capability of tungsten is not needed; and (iii) tungsten is much **more** expensive and difficult to work with.

These considerations would leave only the actual alloy of nickel to be specified, and that chosen **is** Inconel* 600: a nickel, chromium, and iron composition with obviously desirable properties as shown **in** the table below. It is also proposed that the full hardness (spring) variety be used if possible, to further stiffen the rotor assembly especially at the outer induction array location.

Inconel* 600

MATERIAL	COMPOSITION (%)								OTHERS	NOM. TENSILE STRENGTH (PSI) (SIZE RANGE: .002-.032)		MATERIAL CHARACTERISTICS
	C (MAX.)	Mn (MAX.)	Si (MAX.)	P (MAX.)	S (MAX.)	Cr	Ni	Fe		ANNEALED	FULL HARD (SPRING)	
Inconel* 600	15	1	5	—	015	14-17	72 min	6-10	Cu 5 max	90,000 to 130,000	180,000 to 230,000	Resists corrosion and oxidation to 2150°F. Provides springs with high resistance to corrosion and heat up to 750°F. Tough and ductile down to -310°F. is nonmagnetic, easily fabricated and welded. Used for structural parts, cathode ray tube spiders, thyratron grids, sheathing, tube supports, spark plug electrodes.

* Registered Trademark of the Inco family of companies.

As outlined in DataSheet #9 (Electrostatic Load-Line Formula), the rotating cathodes *may* be composed of thoriated tungsten, but only under closely-controlled conditions and as a result of extensive device testing, should a higher level of series coil group current be desired. This would generally be the case only in 3 η rotor devices, to compensate for the greatly increased electrode array impedance resulting from the use of comparatively 'cold' (unheated) cathodes in this application.

[b] Control Grids

The Primary Power System grid wire material is also indicated in SpecSheet VIII, and for largely the same reasons as in subsection [a] above. The actual alloy chosen is commonly known as Nichrome V (bearing MWS designation 650). A further practical incentive for this choice is that this particular nichrome variety has wide commercial availability.

Nichrome V

MATERIAL	CHEMICAL COMPOSITION (%)	RESISTIVITY AT 20°C		COEFFICIENT OF LINEAR EXPANSION BETWEEN 20-100°C	TENSILE STRENGTH (PSI AT 20°C)		SPECIFIC GRAVITY	POUNDS PER CUBIC INCH	MAGNETIC ATTRACTION	APPROX. MELTING POINT (°C)
		OHMS/CMF	TCR 0-100°C		MIN.	MAX.				
MWS-650	80 Ni, 20 Cr	650	00010	0000132	100,000	200,000	8.412	.3039	None	1400

Of considerable importance with regard to device construction is the manner in which the grids are to be 'wound', not only the rotating control grids but also the various stationary grids of the Primary Induction Ring Arrays. Due to the very high field intensity values operative in all of the electrode

arrays, each grid must be wound under extremely high tension of *single pieces of wire*. Otherwise, there is almost no way to assure that grid sagging or drooping will not result given the anticipated operating temperatures: a condition virtually certain to result in the destructive failure of the array(s).

Therefore, the following diagrams illustrate the proposed proper grid winding techniques for both *single-layer* rotating transfer array control grids and for the *screen-type* rotating induction array control grids and all stationary pentode array grids.

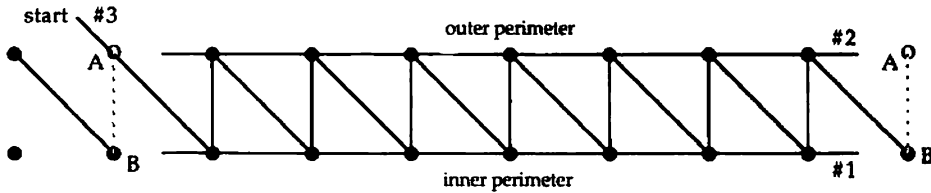


Fig. 48a: Transfer Array Grid Wire Course Pattern

This single-layer grid wire winding method is used for all 3η rotor transfer arrays. Current-confining perimeter wires #1 and #2 must also be employed, and must be installed *in that order* in the cathode-facing end of the electrode support pin undercuts such that they are looped around each pin *with the loops all facing the grid!*

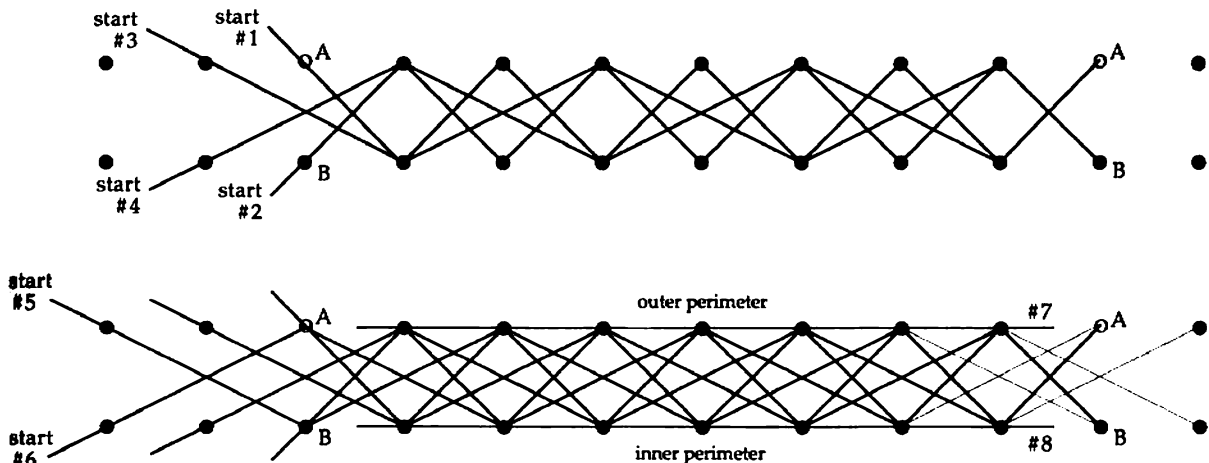


Fig. 48b: Induction Array Grid Wire Course Pattern

This double-layer grid wire winding method is used for all rotor induction arrays and for all of the grids in unit pentode arrays of either 1η or 3η rotor devices, resulting in the shading of the accelerator and suppressor grids (with respect to the control grids) as stipulated in SpecSheet VIII. Current-confining perimeter wires #7 and #8 must also be employed and installed *last but otherwise the same* as in Fig. 48a.

Wires #1 and #2 are of a one-frequency sawtooth configuration, and wires #3, #4, #5, and #6 are installed in a relative half-frequency sawtooth pattern. This yields a *max.* grid thickness equal to four (4) times the nickel grid wire diameter t_g in triode induction arrays and four (4) times the tungsten grid wire diameter T_g in the unit pentode arrays.

[c] Electrode Support Pins

At first thought, it might seem a simple matter to choose a suitable structural ceramic for the electrode support pins used in the Primary Power System, but a number of different factors must enter into the selection process. First, the material should of course have a high k value, as the pins are in contact with electrodes having a high potential difference and relatively close spacing. Secondly, the material must exhibit a high thermal expansion coefficient to match as closely as possible that of the segment separators (into which they are pressed) and that of the metal electrodes themselves. Finally,

the material should be very strong but of somewhat moderate hardness, as grooves must be cut into each pin to hold the electrode edges and grid wire.

Although the ceramic known as Fosterite ($2\text{MgO} \cdot \text{SiO}_2$) would perhaps be the superior choice in consideration of all these factors, it has limited commercial availability today. Therefore, the material specified (at the present time) for these key rotating structural components is a Titania composition bearing CeramTec designation 192. It is very strong and hard, and has good resistance to fracture. It also exhibits superior surface finish, to inhibit static charge effects.

Titania 192 (TiO_2) [Titania 193 is similar in physical properties, but is formulated to actually carry static electricity.]

Specific Gravity	Hardness Mohs' Scale	Max. Use Temp. (°C)	Thermal Expansion Coefficient @ 25-300°C	Thermal Conductivity W/m-K @ 25°C	Tensile Strength PSI	Flexural Strength PSI	Electrical Resistivity* ohm-cm @ 300°C	Dielectric Constant* @ 1MHz 20°C
4.0	8.0	1000	8.3×10^{-6}	11.9	7500	20,000	1×10^9	85

* applies to 192 only.

Section 2: Primary Induction Ring Arrays

[a] Unit Cathodes & Anode Rings

Because of the extremely heavy operating current density of the unit pentode arrays (comprising each of the two Primary Induction Ring Arrays), the choice of essentially pure tungsten for the unit cathodes and anode rings thereof is virtually automatic. In the case of the cathodes, this decision is further confirmed by the fact that these electrode elements will almost certainly require some degree of thoriation or thorium adsorption (in most units), and the bulk of known data with regard to the observed effect upon electrode emissivity of varying thoriation levels will apply to tungsten cathodes. Therefore, both the unit cathodes and unit anode rings (silver-soldered to the rotor segments) are to be composed of tungsten.

It should be noted that although the base conductivity of tungsten is only 30% that of copper, the actual resistance of these cathodes and anode rings will be extremely small compared to that of the rotor segments (as resistance is proportional to conductor length and inversely proportional to area). Thus, no detailed temperature-resistance study is necessary here, as was done for the segments versus the Field Emitters, as the actual net conductivity of the unit cathodes and anode rings will therefore be greatly more than adequate at any feasible operating temperature level(s).

Tungsten (W)

METAL	SYM.	MELT POINT (°C)	BOIL POINT (°C)	DENSITY AT 20°C (gm/cc/cm)	COEFFICIENT OF THERMAL EXPANSION NEAR 20°C ($\times 10^{-5}/^\circ\text{C}$)	SPECIFIC HEAT AT 20°C (cal/g/°C)	THERMAL CONDUCTIVITY NEAR 20°C (cal/sec cm/cm²/°C)	ELECTRICAL RESISTIVITY (microhm/cm)	Rockwell Hardness	Electrical Conductivity %IACS	Ultimate Tensile Strength PSI
Tungsten	W	3410	5930	19.3	4.3	.033	48	5.5 (20°C)	35-50C	30	100,000

[b] Power Resistors & Dielectric Buffers

Ordinarily, one does not think of a ceramic material as being useful as an actual conductor of electricity, and ceramics per se are indeed almost never used in this capacity (unless superconductive). However, in the case of the EDF Generator's Field Power Resistors, where a relatively enormous voltage drop must be achieved, and at very heavy current levels with little axial resistor length, there is almost no other choice. Also, due to the nature of the Dielectric Buffers which must insulate these ceramic pieces in their conductive state (as we'll see), the appropriate resistance must be obtained within a limited fixed range of operating temperature, regardless of model (size) and unit (type).

Therefore, it is crucial to select a ceramic material which has a low enough k value to become conductive at the particular given potential gradient and has the necessary volume resistivity within the fixed temperature range to accomplish the requisite voltage drop. The calculations performed below will illustrate the method which must be used to select a suitable Power Resistor material for both Thermal Unit and Drive Unit types of a given model (size) device, in this case the 4ft. prototype.

The 4ft. diameter prototype *Thermal Unit* has a required peak Resistor voltage drop of 1,582,241 [per WorkSheet X(a)], and the assigned Resistor length is equal to .8466 cm. Therefore, if the Resistor is to be operated at over breakdown intensity, it must have a k value less than that figured as follows:

$$E_{brk} = V/d = 15.9489 \times 10^5 / 8.466 \times 10^{-3} = 1.8839 \times 10^8,$$

$$\text{and } k < E_{brk} / 3 \times 10^6 \text{ v/m} < 62.8.$$

Therefore, we can see that most common ceramic materials should actually work in this capacity, provided that they exhibit a volume resistivity of about 5×10^4 ohm-cm [per WorkSheet X(a)] somewhere in the temperature range from 620 – 735°C. It is also beneficial if the candidate material's projected resistivity plot is fairly linear in this same temperature range, to help ensure the accuracy of the operating temperature estimate made when only a limited number of known values are available.

As we can see from the following (and fairly linear) resistivity plot, the material Steatite 357 seems to work well in this instance, at an estimated operating temperature of 645°C and estimated Dielectric Buffer k value of 2600. [Note: The Power Resistor maximum k value computation above of course yields the Dielectric Buffer minimum k value as well, as does that for Drive Units on the following page.]

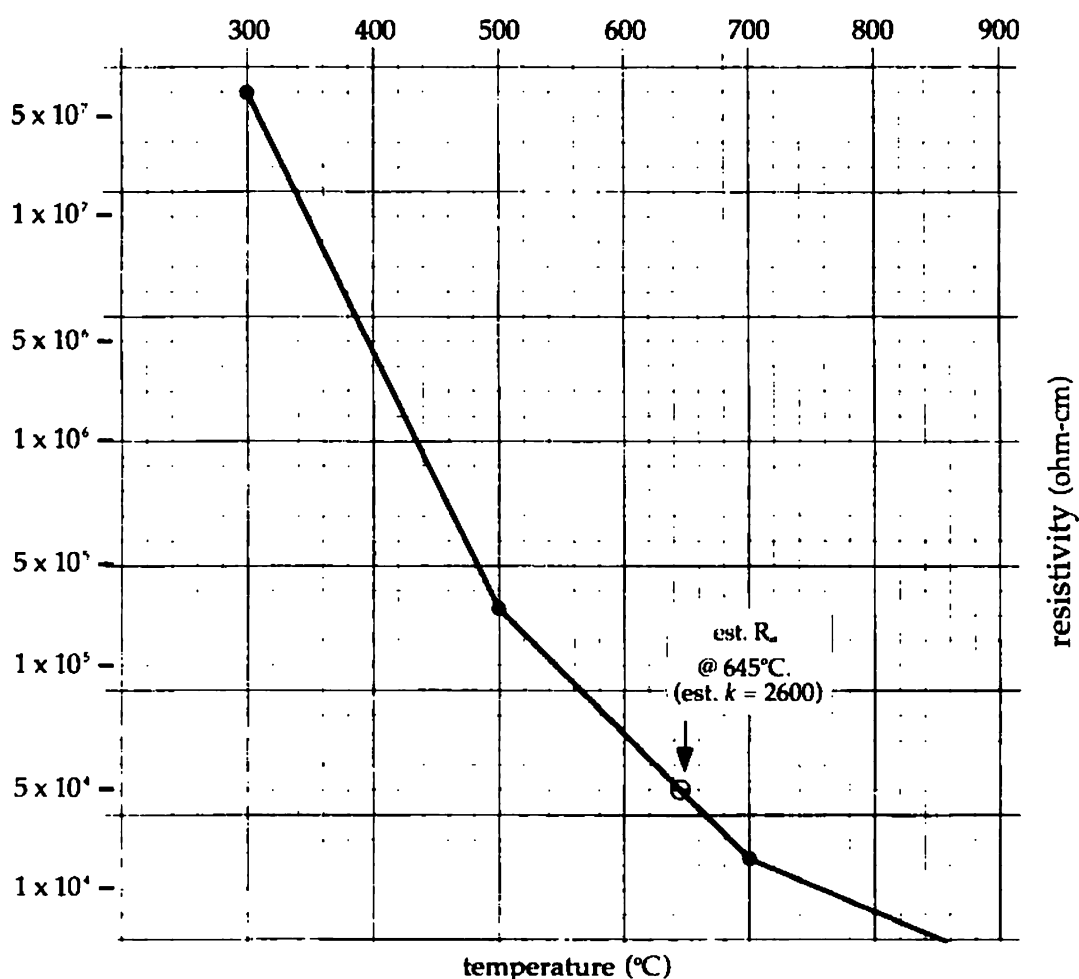


Fig. 49: projected resistivity plot for Steatite 357.

Steatite 357 ($\text{MgO} \cdot \text{SiO}_2$)

Specific Gravity	Hardness Mohs' Scale	Max. Use Temp. (°C)	Thermal Expansion Coefficient @ 25-700°C	Thermal Conductivity W/m-K @ 500°C	Tensile Strength PSI	Flexural Strength PSI	Electrical Resistivity ohm-cm @ 700°C	Dielectric Constant @ 1MHz 20°C
2.5	7.5	1000	8.7×10^{-6}	2.9	8,500	18,000	2.3×10^4	5.8

The 4ft. diameter *Drive Unit* has a required peak voltage drop of 19.3074×10^6 and, if the *Resistor Network* is to be operated at over breakdown intensity, it must have a *k* value less than that figured as follows

$$E_{\text{brk}} = V/d = 19.3074 \times 10^6 / 8.466 \times 10^{-3} = 2.28 \times 10^9,$$

and $k < E_{\text{brk}} / 3 \times 10^6 \text{ V/m} < 760.$

In this case, we can see that almost any common ceramic would seem to be a potential candidate material provided it exhibits a *median* resistivity of about $6 \times 10^5 \text{ ohm-cm}$, as *Resistor Network* resistance must be rendered variable in *Drive Units* at a *median temperature* within the operating temperature range. This consideration adds significant levels of complexity and constraint to the material selection process, and before construction begins the chosen ceramic should be resistivity tested at a number of key temperatures to confirm its suitability (a rather expensive process).

This consideration is clearly indicated in the computer-aided plot below, where a 900°C resistivity figure was not available and an unusual 'switchback' plot portion is involved. Estimated Buffer *k* values are shown at each key resistivity point. The projected 900°C resistivity point shown (x) is based on a detailed trend analysis of a simultaneous plot of four related Cordierite compounds.

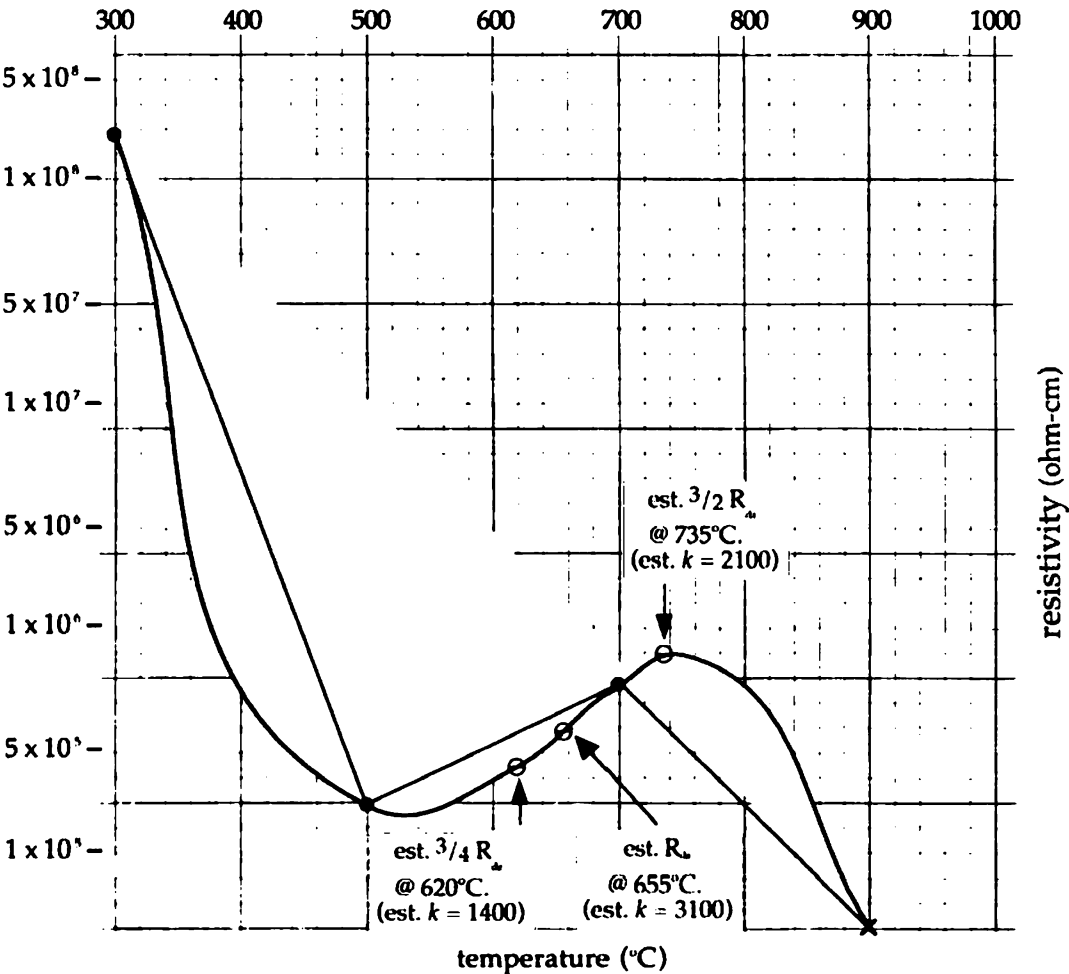


Fig. 50: projected resistivity plot for Cordierite 547.

Cordierite 547 ($2\text{MgO} \cdot 2\text{Al}_2\text{O}_3 \cdot 5\text{SiO}_2$)

Specific Gravity	Hardness Mohs' Scale	Max. Use Temp. (°C)	Thermal Expansion Coefficient @ 25-700°C	Thermal Conductivity W/m-K @ 500°C	Tensile Strength PSI	Flexural Strength PSI	Electrical Resistivity ohm-cm @ 700°C	Dielectric Constant @ 1MHz 20°C
2.53	7.5	1100	3.0×10^{-6}	1.7	3,700	12,000	7.8×10^5	5.2

(i) Although the working temperature resistivity of the Power Resistor material(s) selected is technically more important than the actual k value(s) exhibited, the preceding E_{brk} computations do not tell the whole story involved in the selection process even though the necessary minimum Dielectric Buffer k values (corresponding to Thermal and Drive Unit peak Field voltages) are thereby derived.

Accordingly, the Power Resistors must be in a conductive state at or before the Field voltage level at which the Drive Field boundary reaches breakdown intensity and begins to pass current. Therefore, the actual maximum k value of the Resistors of both Thermal and Drive Units must be calculated as follows (for the 4ft. diameter prototype):

$$\text{boundary } E_{brk} = 3 \times 10^6 = V / .1907 \text{ m, where } .1907 \text{ m} = \text{Field Boundary length} \\ \text{(from WorkSheet VIII(a))}.$$

$$\text{So, } V = 572,100 \text{ volts.}$$

Since the voltage drop across the Resistors is approximately equal to half Field voltage:

$$\text{resistor } E_{brk} = .5V / 8.466 \times 10^{-3} \text{ m, where } 8.466 \times 10^{-3} \text{ m} = \text{Resistor length} \\ \text{(from WorkSheet X(a))}.$$

$$= 28.605 \times 10^4 / 8.466 \times 10^{-3} = 3.379 \times 10^7,$$

$$\text{and } \max.k < 33.79 \times 10^6 / 3 \times 10^6 < 11.26.$$

It must also be understood that the dielectric constant of the candidate material(s) should in reality be minimized (below the above k value), to promote Resistor conductivity as the external Field approaches 'flashover'. In this respect, the two Resistor materials selected for use in the 4ft. prototype are at or below 52% of the above max. k value.

(ii) Because the linear hull coolant (secondary) Thermal Conduit sections which actually support the Drive Ring must pass between the Power Resistor assemblies, the Resistors must assume a complex tapered shape to provide the necessary clearance. They will have a trapezoidal shape at the 'top' (with radial length somewhat greater than circumferential width) and a rectangular shape at the bottom or cathode end (with circumferential width much greater than radial length). In this regard, their engineered shape should still maintain a uniform conduction cross section exactly analogous to the positive Zone sectors.

This situation aggravates an already troublesome difficulty related to the encapsulating Dielectric Buffer material, as discussed near the end of subsection 2[c] of Material SpecSheet A. Nevertheless, the following Resistor Specifications are based on a detailed analysis of this structural requirement, given further Specifications (provided in Mat. SpecSheet B) related to these secondary Thermal Conduits.

Component Specifications: Power Resistor Dimensions

The maximum circumferential width of the Power Resistors shall be equal to $149/2400 R_h$, and the minimum radial length thereof at the outer or Zone end (prior to corner radiusing losses) shall be equal to $162/2400 R_h$.

(iii) An important consideration arising of the Dielectric Buffer min. k computation on the preceding page is that of minimum safe Buffer operating temperature. An analysis of the graph on the following page reveals that at a Buffer $k = 760$, a corresponding minimum safe temperature would be 590°C . Based on this same k value, the following peak voltage Drive Unit maximum Buffer thickness may be figured:

$$E_{brk} = (760)(3 \times 10^6) = 2.28 \times 10^9,$$

$$\text{So, min. } t_k = 19.3074 \times 10^6 / 2.28 \times 10^9 = .8468 \text{ cm} = .3334'' \text{ (for 4ft. prototype).}$$

An exactly similar calculation yields the Thermal Unit and minimum Drive Unit Buffer thickness equal to .0275'', and together these computations lead to the following Dielectric Buffer Specifications.

Component Specifications: Dielectric Buffer Dimensions

The max. thickness of the Dielectric Buffers in a Drive Unit shall be equal to the Power Resistor length, and the min. thickness thereof shall equal the thickness of Thermal Unit Buffers at $11/9600 R_h$.

Dielectric Buffers

Due to the extreme voltage drop across the Field Power Resistors, it is (of course) imperative to electrically insulate them to prevent direct discharge to other nearby structural components from occurring. However, not only is this a problem due to the thickness of insulation which would be required at any 'ordinary' dielectric value, but the Power Resistors' operating temperature range of 600 to 700+°C completely precludes the use of almost *all* known dielectrics. Fortunately, the search for high-temperature dielectrics for use in aerospace electronics applications (particularly multi-layer capacitors) has resulted in the development of a small number of exotic materials potentially suitable for use as a Dielectric Buffer (encapsulant) for the EDF Generator's Power Resistors.

The primary limitation in the development of these stable high-temperature dielectrics was the achievement of both high k (dielectric constant) and high IR (or insulating resistivity). If a candidate material exhibited a very high k value but the IR fell dramatically on temperature rise, conduction losses caused by leakage current between the capacitor plates would lead to destructive *thermal breakdown*. Also, a fair number of complex ceramic Class I (medium k) and Class II (high k) materials exhibit k values of between 200 and 1,000 or more at temperatures approaching 300 °C, yet their k falls precipitously at or beyond 400°C.

In the application contemplated herein, the IR value of the Resistor encapsulant is somewhat secondary to its dielectric constant *at temperature*, because no opposing plate voltage is present (as in a capacitor) to encourage circuit conduction losses within the material. Therefore, the prime consideration is the dielectric's ability to exhibit a very large k value *at over 600 °C*. This places the material squarely in the realm of a very small select group of Class III **high transition temperature ferroelectrics**. These materials, such as Tantalum-modified Lanthanum Titanate and Lead Ytterbium Tantalate, do not begin to demonstrate significant dielectric strength *at less than 300 to 450 °C*. One such compound, **Sodium Bismuth Titanate** ($\text{Na}_{0.5}\text{Bi}_{1.5}\text{Ti}_3\text{O}_{15}$), actually exhibits its *peak* dielectric strength near the beginning of the very operating temperature range of the EDF Generator's Power Resistors: at 655°C (1,202°F).

As the first graph below shows (see Fig. 51), this unique material's k remains at a lowly 200 or so until about 400°C. Then, if we take the 1KHz line as representative of the DC dielectric performance, an astonishing peak k value of 3,100 is reached at the ferroelectric transition temperature (T_c) of 655°C. The k value drops sharply to about 2,100 at 675°C and then oddly enough begins rising again, achieving $k = 2,300$ at 750°C. This would seem to indicate that this compound is eminently suited for use in forming the necessary Dielectric Buffers in this application.

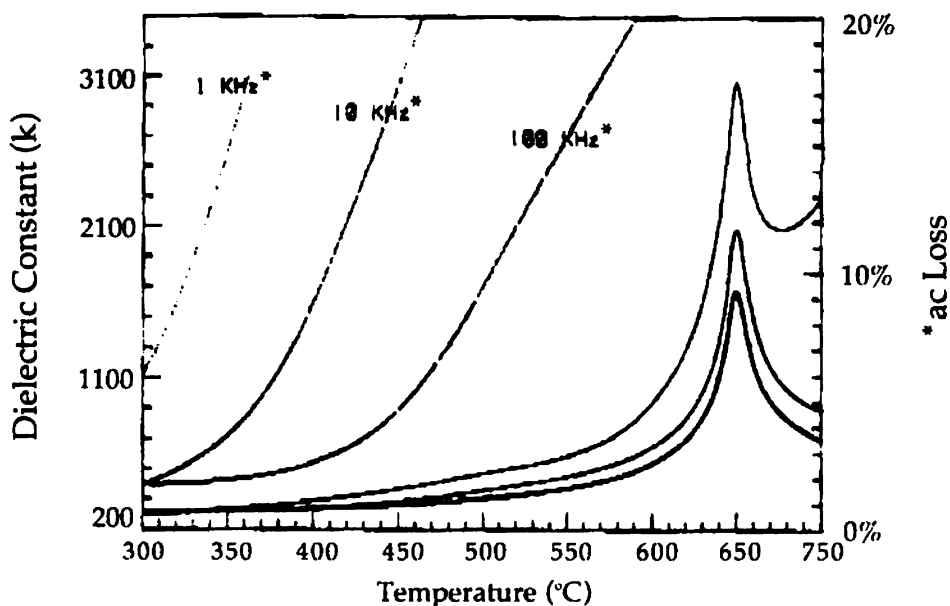


Fig. 51: k and ac loss as a function of temperature for Sodium Bismuth Titanate.

Furthermore, the graph below (Fig. 52), although difficult to analyze, reveals that the volume resistivity of Sodium Bismuth Titanate remains quite high across the Power Resistor operating temperature range, from approximately 1×10^5 ohm-cm at 650°C to 5×10^4 ohm-cm at 700°C . Although relatively commonplace and inexpensive ceramic insulating materials such as the Alumina and Magnesia compounds display IR values 2 to 4 orders of magnitude higher than this at these temperatures, they do so at peak dielectric constants of only 5 to 10. Even the premier standard dielectric Barium Titanate cannot compare to this kind of thermal dielectric performance.

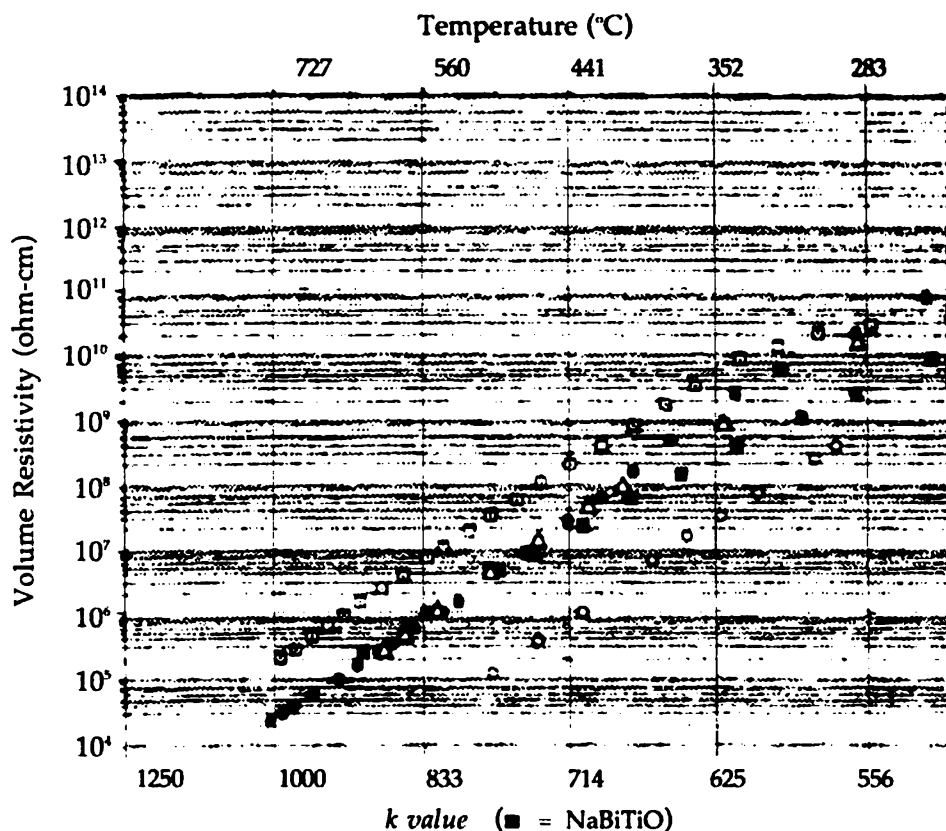


Fig. 52: volume resistivity as a function of temperature for special dielectric materials.

At this point, it should be stressed that the ultimate in quality control must be exercised in formulating and sintering this special compound in the manufacture of the Dielectric Buffer pieces. An absolute minimum of impurities must be assured, the density of the constituent powder maximized, and each piece finally certified as being free of the smallest physical defect prior to use in order to attain the desired operating performance. Physical properties are given in subsection 2[c] of Mat. SpecSheet A.

It is hoped that these crucial components may be compaction die formed and sintered simultaneously with the Power Resistors, and perhaps even also with the Thermal Conduit pieces themselves. All three of these highly-specialized ceramic components are shown in Fig. 53 of the following subsection.

Interestingly enough, considerations related to the selection of the carbon composite deck sheeting over fiberglass (as used in the hull Neutral Ring) led to further important realizations about the dielectric buffers, including the need to incorporate *auxiliary dielectric buffers* in all model Units. As can be seen from the properties table(s) for this highly-engineered material, it is a quite satisfactory conductor and the concern naturally arises over the potential occurrence of a sizable *deck leakage current* between the hull negative plates and the primary dielectric buffer shoulders to which the deck abuts.

Although it might seem that the much-cheaper and nearly-as-strong fiberglass composites available would tend to minimize any such leakage current condition, their use would *not* minimize the

possible build-up of unacceptable levels of static charge within the working Neutral Ring. Therefore the use of a 'technical' conductor as the deck material satisfies an inference, which may be drawn from hull configuration principle #10 (see text Chapter 6), that even the Neutral Ring's "outer shell construction" should be electrically conductive. It also ensures that Faraday shielding protects Neutral Ring components from transient static voltages because the very presence of a deck leakage current means the Neutral shell is a charged conductor (whereupon any net static charge must be external).

Assuming the end of the deck's radial fiber structure is in electrical contact with the buffer shoulders and the negative hull plates, whereby the total buffer/deck contact-zone area of each Primary Array would be about 26.87 cm^2 in the 4ft. prototype, the total leakage current could be over 23,000 amps in a Thermal Unit and over 22,000 amps in the Drive Unit variant were the buffer contact zone at 650°C with no other resistive material in-line! These values drop to maximums of about 33 amps and 32 amps respectively if the said contact zones are maintained at 400°C or less without further buffering.

In both cases the material adjacent to the deck sheeting, which has a maximum safe use temperature of about 400 °C, is expected to be very hot while the primary buffers may be nearly at dark-red heat. In Thermal Units, the use of a secondary cryogenic coolant should keep the deck sheeting near the negative plates at a temperature which is under this limit. In the much-higher-voltage Drive Units, where primary (hot) thermal transfer medium is also circulated through the secondary conduit system, auxiliary thermal conduits which incorporate such cryogenic coolant must be positioned between the inner edge of the hull negative plates and the deck sheeting. A section of such conduit will in all likelihood be required along each primary buffer-deck contact zone in both Thermal and Drive Units, incorporating a high thermal conductivity Alumina coating as described in [c] below.

In a similar vein, it should be noted that the conduit jacket material to be used on the secondary headers, transfer links, and recovery lines in Drive Units may need to possess a low thermal conductivity to minimize the transfer of heat to the adjacent composite tri-beams and structural members. In this case, a Zirconia coating would be indicated, having $k = 28$ and other physical properties as shown in Section 2[c] of Mat. SpecSheet A. Even so, auxiliary thermal conduit sections such as those above may also be required along the tri-beams to maintain their temperature at an acceptable level. Drive Unit secondary peripheral shunts would need of course to retain the Alumina jacket material for maximum transfer of heat to the Emitter Ring, which must be used as the Unit's primary coolant heat sink.

In any event, Specifications for these auxiliary thermal conduits are given below, which are primarily sized to fit into the radial zone width between the outer ballast capacitor reference line and the Emitter Ring boundary (as applies in Drive Units). The requisite material(s) and dimensions for the auxiliary dielectric buffers to be used in all Units is also provided, these being located immediately above this peripheral auxiliary conduit position to maintain the desired buffer/deck temperature. Resistivity data for Zirconia was not available, as this book went to press, with which to project minimum final deck leakage current for a 4ft. Thermal Unit incorporating auxiliary buffers. However, a 4ft. Drive Unit with auxiliary buffers would have a nominal full-power total leakage current of approximately 22.5 amps, which works out to about .42 amps/cm² of the deck's conductive cross-section. This figure is felt to be quite reasonable, and should of course be almost design-constant (for all sizes).

Component Specifications: Auxiliary Thermal Conduit and Dielectric Buffer Dimensions

- (i) The auxiliary dielectric buffers used in all model Units shall be composed of the same material used in that Unit's exolayer tiles, shall be equal in thickness to the composite deck sheeting, and shall be equal in radial width to the auxiliary conduit square cross-section specified below.
- (ii) The auxiliary thermal conduit core tubing (used to circulate cryogenic coolant near the dielectric buffers) shall be equal to $1/216 R_h$ in outside diameter and composed of molybdenum.
- (iii) The ceramic coating applied to each auxiliary conduit core section shall be composed of Alumina, and shall be formed thereon to a final overall square cross section equal to $1/174 R_h$ on each side.

[c] Primary Thermal Conduits

The main concern in 'casting' the ceramic Thermal Conduit associated with each Primary Array power resistor is that the material have superior tensile strength and high (relative) thermal conductivity for an insulator. In this respect, $k = 10$ high-purity (99.9%) Alumina has been selected as the Spec. Primary Conduit jacket to be formed directly onto molybdenum tubing (as the Conduit core). Thus, each Thermal Conduit, whether of this or the secondary housing coolant section variety, becomes an extremely strong structural member as well. Applicable properties tables are included below.

Alumina 433

Specific Gravity	Hardness Mohs' Scale	Max. Use Temp. (°C)	Thermal Expansion Coefficient @ 25-700°C	Thermal Conductivity W/m-K @ 25°C	Tensile Strength PSI	Flexural Strength PSI	Electrical Resistivity ohm-cm @ 700°C	Dielectric Constant @ 1MHz 20°C
4.0	9.0	1550	7.7×10^{-6}	37.0	35,000	60,000	NA	10.0

Molybdenum*

METAL	SYM.	MELT POINT (°C)	BOIL POINT (°C)	DENSITY AT 20°C (gm/ccum)	COEFFICIENT OF THERMAL EXPANSION NEAR 20°C ($\times 10^{-6}/^{\circ}\text{C}$)	SPECIFIC HEAT AT 20°C (cal/g/°C)	THERMAL CONDUCTIVITY NEAR 20°C (cal/sec cm/°C)	ELECTRICAL RESISTIVITY (microhm/cm)	Rockwell Hardness	Electrical Conductivity % IACS	Ultimate Tensile Strength PSI
Molybdenum	Mo	2620	5550	10.22	4.9	.062	.35	5.17 (0°C)	92-98B	33	100,000

***Note:** A number of molybdenum alloys with tungsten and/or rhenium are commercially available, and should be investigated for potential use as a Conduit core tubing material, subject to relative thermal expansion coefficient considerations.

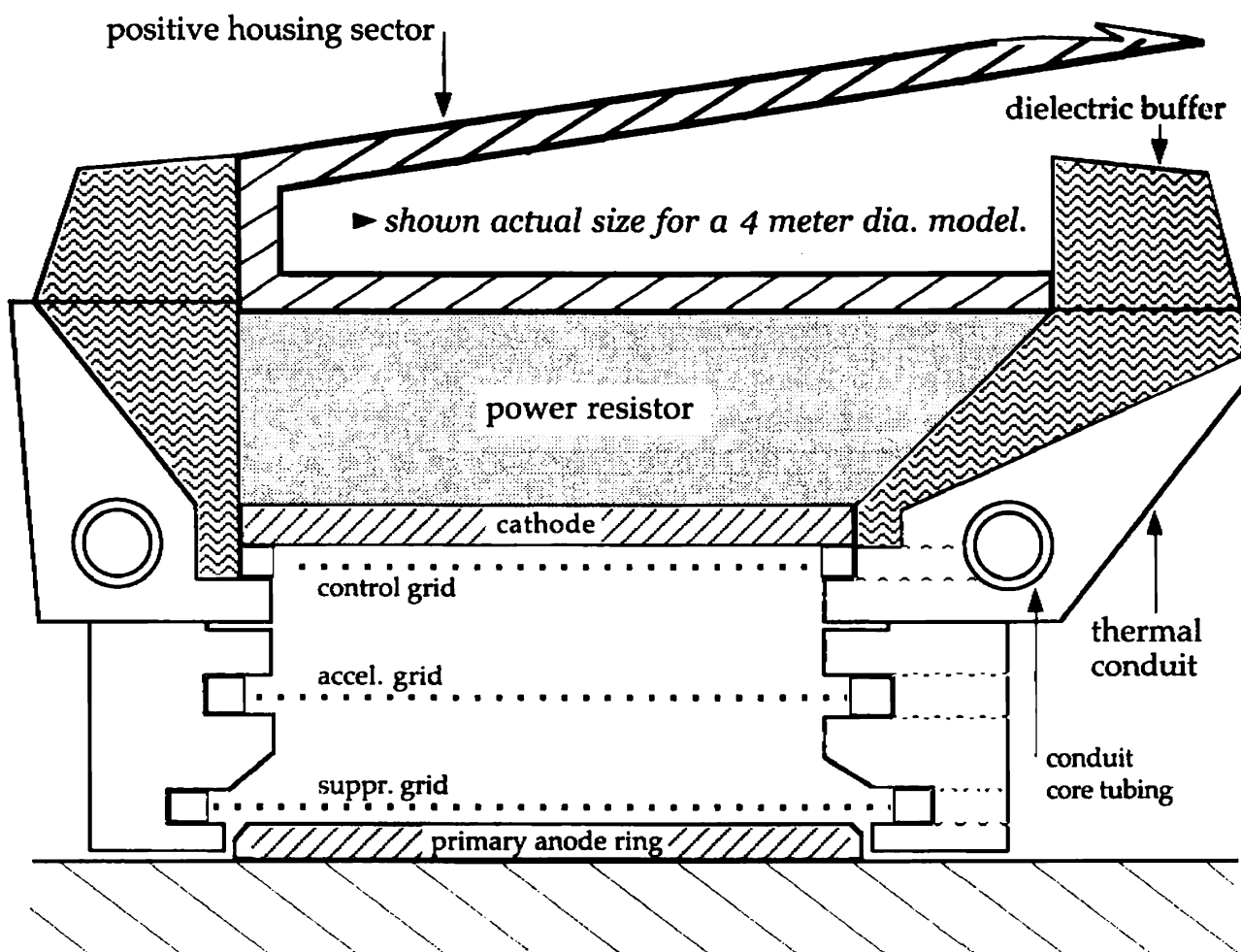


Fig. 53: Power Resistor and Unit Pentode Array assemblies, including replaceable electrode elements, shown in radial cross-section view.

Component Specification: The primary Thermal Conduit core tubing (which surrounds the Power Resistors) shall equal $1/192 R_h$ in inside diameter and be composed of molybdenum.

Field Coil Components

Section 1: Rotating Coil Cores

The nonferrous field coil cores are to be made from filament-wound tube arc-sections of high-density PAN carbon composite, and reference should be made to Section 2 of both Mat. SpecSheets A and B with regard to this material. It is not practicable to form solid rods in arc-section, placing a lower limit on the size of device built in this fashion. The spec. OD must be maintained to the closest possible tolerance and the core section ends should be pinned prior to solvent welding of the joints.

Section 2: Core Mounting Clips

The magnetic ring array and toroidal field coil configuration employed in the Primary Power System presents some interesting challenges in the engineering of a suitable coil mounting arrangement. The first consideration which becomes obvious is that whatever structural bases or members are used to attach the coils to the rotor must be 'narrower' than the magnetic ring gap at the point of attachment to the coil core. If the ring gaps were oriented facing the rotor, as discussed in SpecSheet V, a simple system of press-fit studs or pins could be employed as has been done elsewhere in the Specifications for this device. However, it must also be considered here that large breaches in the shoulder tightness of the toroid coils' turns layers tend to increase coil inductance by promoting core flux leakage.

Therefore, in the preferred magnetic ring orientation format (depicted in Fig. 24 of SpecSheet III), it becomes necessary to use right-angled flat stock "clips" of a high strength non-magnetic alloy which are pressed and adhered into both the coil cores and the segment separators. Once this determination has been made, it is 'merely' required that a suitable mounting clip number, thickness, and material be specified for attaching each size coil to the rotor.

Further study of various coil mounting strategies reveals that only three total numbers of uniformly distributed clips for supporting each coil should be considered as practical and efficient for utilization: 36, 45, and 60. Also, the total thickness of the specified number of mounting clips per coil must represent only a small percentage of the theoretical total shoulder-to-shoulder clearance of that coil's outside layer turns, so that turns "crowding" does not occur during the coil winding process.

In using the same number of clips for each coil, the overall strength of the mounting system may be adjusted by varying the thickness of the individual clips (for a given size coil). It should be noted that the center field coils in the preferred embodiment will have different clip loading characteristics than the inner and outer coils, and somewhat reduced load distribution efficiency, such that the number of center coil clips may need to be marginally increased.

The mounting clips should be stamped or fabricated from type 316 molybdenum-stabilized stainless steel, and all rough edges carefully relieved to prevent turn abrasion. 316 stainless offers high creep and tensile strength at elevated temperatures, as well as excellent corrosion and pitting resistance. It is available in a range of hardness from Rockwell 95B to 45C, and a higher hardness grade should be used for increased rigidity. The mill-specified finish should be "2BA", or very smooth and glossy.

Component Specifications: Mounting Clip Dimensions

The thickness of the sheet stock from which each field coil core mounting clip is stamped shall be equal to 1/3 of that coil's core outside diameter, as shall also be the minor rectangular dimension or height of that clip's core insertion tab. The radial width of such clip's rectangular separator insertion tab shall be equal to 5/6 of its coil's core OD. A total of 45 such clips shall be used to mount each coil.

316 Stainless Steel (fatigue strength is appr. 40% of ultimate tensile strength; max. nitrogen content - 0.10%)

MATERIAL	COMPOSITION (%)									Typical Physical Properties				
	C (MAX.)	Mn (MAX.)	Si (MAX.)	P (MAX.)	S (MAX.)	Cr	Ni	Fe	OTHERS	Density (lb/in ³)	Thermal Expans. Coeff. 20-500°C	Thermal Conduct. W/m-K 20-100°C	Young's Modulus (psi)	Ult. Tens. Strength @200°C (psi)
316 SS	.08	2.00	0.75	.045	.030	16-18	10-14	bal.	Mo 2-3	.29	10.1 x 10 ⁻⁶	14.6	29 x 10 ⁴	75,000

Magnetic Components

Section 1: Stationary Field Rings

The Magnetic (Field) Rings employed in the EDF Generator are probably the only type of component involved wherein commercial availability and relative cost are the principal determining factors in material selection. In this case, choosing a magnetic alloy with optimum performance characteristics is not nearly so important as ready availability in a broad range of sizes. Contrary to the opinion held by some, just because a particular magnetic material functions well in certain sizes and configurations in no way means that it will do so in much larger shapes.

Also, because the performance of the ballast capacitors, field emitters, and primary cathodes have a far more fundamental effect on final Field voltage than the magnitude of the initial dc voltage produced by the Primary Power System, it is not necessary to select an alloy whose energy product is much greater than that of a more convenient common variety if the cost per pound is several or even dozens of times higher. With a maximum total of 4,392 Field Rings used in each vessel, it is of great practical concern to therefore choose an alloy requiring as moderate a capital expenditure as possible – but only to the extent that the material's energy product does not necessitate a higher than manageable rotor speed [as figured in WorkSheet IX(b)].

Taking all of these considerations into account, the magnetic alloy selected for use in this application is oriented cast Alnico 5 (bearing Westinghouse designation Alnico V-OR1) and a demagnetization curve graph for this and other variations of cast Alnico 5 is provided in DataSheet #3. This material represents an excellent compromise between the various factors discussed above, and belongs to a family of a dozen grades of aluminum-nickel-cobalt-iron composition among the most established and widely used of all permanent magnet materials.

In oriented (anisotropic) Alnico grades, elongated crystal growth is first produced during the casting process and the formed magnet is then heat-treated and magnetized as it cools through the curie point. C-shaped magnets of the type used in the EDF Generator are produced in multiple numbers at a time using a water-cooled dc currented rod fixture. The finished magnet is brittle and very hard, such that it must be cut with abrasive wheels and ground or surfaced wet with rubber-bonded oxide wheels.

It should be pointed out that the smallest size ring magnet which may be practicably manufactured at the mill will be determined by the smallest induction coil rod orientation fixture available, and this in turn will fundamentally determine the smallest EDF Generator which may be built.

Alnico 5

Nominal Composition % Weight	Rockwell Hardness	Nominal Tensile Strength PSI	Density lbs./in. ³	Coefficient of Thermal Expansion per °C x10 ⁻⁶	Field Req'd. to Saturate Magnet (Oe)	Max. Energy Product BH _{max} (G-Oe x10 ³)	B/H Ratio (Load-Line) @ BH _{max}	Magnet Flux Density @ BH _{max} (in Gauss)
8 Al, 14 Ni, 24 Co, 3 Cu, bal. Fe	C50	5450	.264	11.6	3000	5.5	18.0	10,000

Section 2: Counterflux Wafers

The technique of using the like poles of a highly coercive (demagnetization-resistant) permanent magnet to reduce the inevitable leakage flux arising from the primary magnetic element in a given assembly or circuit is a fairly recent development. This leakage flux can be particularly large between the legs of smaller horseshoe or C-shaped ring magnets, and can be virtually eliminated through the application of a suitably configured "counter mmf". This is usually called *blocking pole technique*.

These components should, however, be considered somewhat optional in nature due to the relatively

modest increase in Field Ring gap flux density precipitated thereby and the not insignificant installation complications involved. Their use is suggested primarily in larger vessels as a means of providing a higher and more complete level of magnetic engineering and therefore (at least theoretically) of achieving optimum Primary Power System performance and minimum rotor speed.

Once again, cost and availability are the principal criteria in selecting a material for the counterflux wafers figured in SpecSheet V and discussed in SpecSheet VI and its associated WorkSheet. As a result, the material chosen for use in this application is sintered Ferrite 5, a composition of barium and iron oxides commonly known as "ceramic" magnets. This highly oriented or anisotropic material is pressed as a 'wet' brick in cavity dies and then fired, and the resultant basic magnet is so hard that it must be cut or ground with diamond wheels.

In the simple flat shape of the counterflux wafers contemplated herein (like a 'button' magnet), this material is relatively quite inexpensive and readily available, and more importantly is extremely coercive in nature. A physical properties table and demagnetization curve graph are provided below.

Ferrite 5 ($\text{BaO} \cdot 6\text{Fe}_2\text{O}_3$)

Nominal Composition % Weight	Rockwell Hardness	Nominal Tensile Strength PSI	Density lbs./in. ³	Coefficient of Thermal Expansion per °C x 10 ⁻⁶	Field Req'd. to Saturate Magnet (Oe)	Max. Energy Product BH_{max} (G-Oe x 10 ⁶)	Normal Coercive Force (Oersteds)	Magnet Flux Density @ BH_{max} (in Gauss)
Ba 0.6, bal. Fe ₂ O ₃	off C	low	.180	10.3	10,000	3.5	2200	1,900

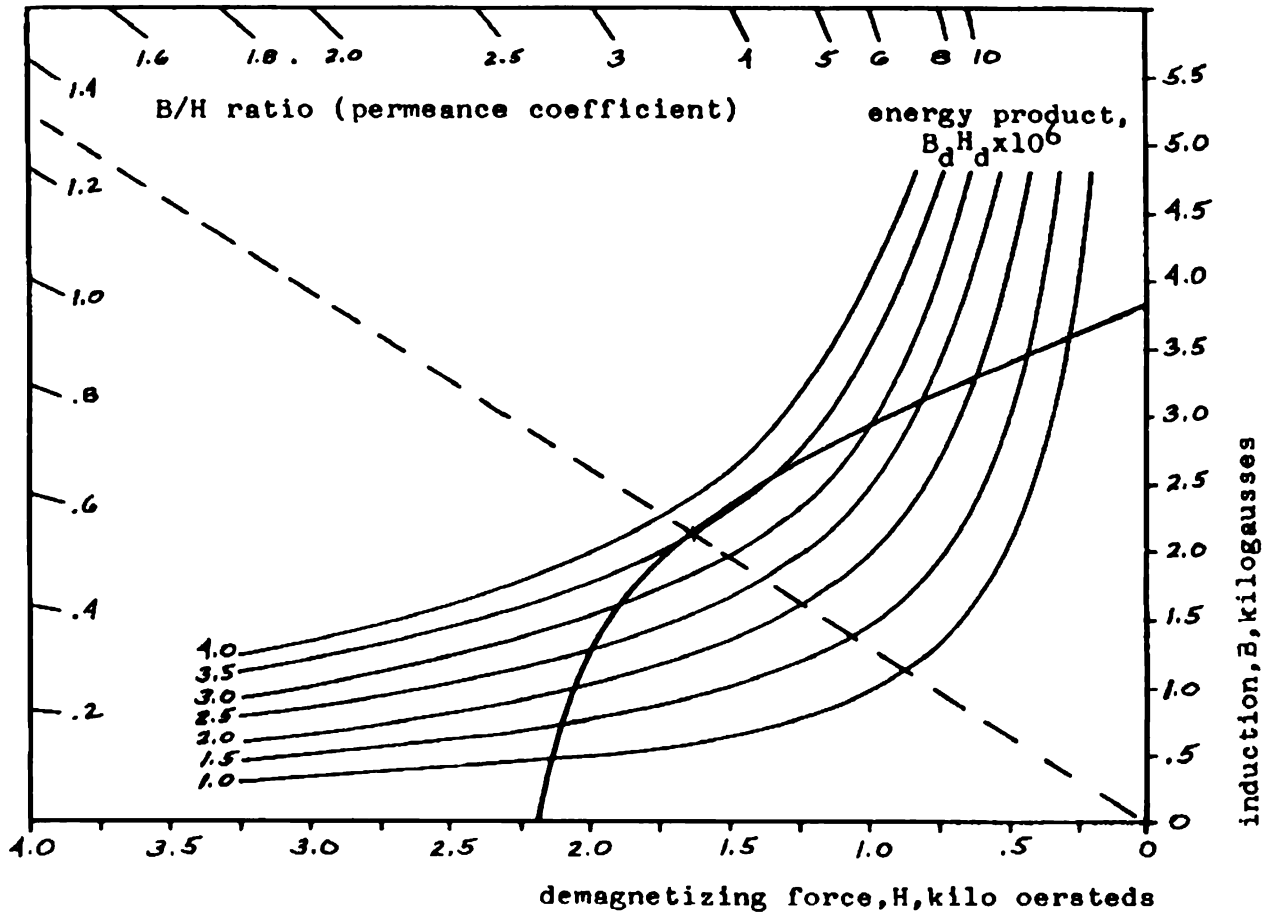


Fig. 54: Ferrite 5 B/H ratio and demagnetization curve graph.

Section 3: Mounting Stringers & Hangers

[a] Mounting Stringers

The magnetic ring stringers are constructed exactly the same as the field coil cores: of high-density carbon composite tubing arc-sections. Because the individual rings which comprise each array section will be strung like beads on an abacus, the OD of the stringer is essentially equal to the ID of the constituent rings. These tubing sections are generally cross-pattern filament-wound on steel mandrels.

Of great concern is the fact that, in order to practicably mount and utilize the counterflux wafer leakage-flux reduction system outlined, the stringers would need to be machined from the finished solid material and peripherally-grooved for wafer insertion. The necessary procedures involved will therefore be considerably more complex and costly than the tubing-construction described.

In either case, these stringers must be cross-scored in numerous places, yielding milled flat strips which press-fit into matching rectangular notches in the array-section support hangers. Therefore, if the stringers are in tube form, all machining should be minimized given wall thickness considerations.

[b] Support Hangers

The magnetic ring array section *support hangers* are very similar to the field coil core mounting clips, in that they are to be stamped (in smaller devices) from 316 stainless steel flat sheet stock, and in that certain construction-related factors must be carefully considered before suitable numbers and thicknesses of these important components may be specified. As was first disclosed in linking text at the end of WorkSheet V(b), it is preferred that each magnetic array section incorporate either five (5) or six (6) support hangers with an equal number of rings between each pair of adjacent hangers if at all possible. This dual criterion greatly constrains the choice of alternate total array ring numbers (from those specified) without a concomitant increase in hanger shape and mounting arrangement complexities.

In the simplest-case scenario, six flat hangers of very narrow trapezoid shape may be used to support each of 36 sections per magnetic ring array by being directly clamped, screwed, or otherwise securely affixed to the radial Neutral Ring beams. The milled flat strips on each stringer section (as described above) then merely press-fit into the matching rectangular notches of its hangers. What remains is thus to determine a simple formula or method by which the most suitable hanger thickness may be derived. Since the magnetic rings in the inner arrays are packed the most tightly on the mounting stringers, the method developed is based on the inner rings' total available shoulder-to-shoulder clearance.

With respect to the hangers' relative load-bearing requirements, a volumetric analysis of the three different sizes of magnetic arrays *as presently specified* reveals that the center arrays will weigh roughly 75% of the weight of the inner arrays, and the outer arrays will in turn weigh approximately 50% thereof. Thus, the respective hanger thicknesses should reflect this same relationship, prior to any further proportional adjustment required for the relative number of hangers used in each array. The hanger Specifications below have been carefully derived with all these criteria in mind, and are based on an inner array hanger thickness which brings the inner arrays to within 79% of complete zero-clearance on the stringers. [See Section 2 of Mat. SpecSheet E for physical properties of 316 stainless.]

Component Specifications: Support Hanger Thicknesses

- a) The thickness of the *outer magnetic array support hangers* shall be equal to $1/1500 R_h$.
- b) The thickness of the *center magnetic array support hangers* shall be equal to $1/1008 R_h$, or approximately 1.486 . . . times the thickness of the outer support hangers.
- c) The thickness of the *inner magnetic array support hangers* shall be equal to $1/652 R_h$, or approximately 1.54 . . . times the thickness of the center support hangers.

It must be pointed out that the hangers as specified provide *at least 250 times* the load-bearing strength required to adequately support the magnetic arrays, even in a 3η Drive Unit accelerating under peak thrust. However, as the device is scaled up, it will become relatively easy to save weight by fabricating these pieces instead of merely stamping them one-piece. It is envisioned that epoxy resin adhesive may be strategically sprayed at the hanger-stringer junctions and across the 'backs' of the magnetic rings in each array section, to further promote unitization of these assemblies.

Bibliography

by title

Non-fiction:

- A Brief History of Time*, by Stephen W. Hawking; Bantam Books, Inc., New York, 1988.
- A Brief Review in Physics*, by Samuel J. Marantz; Cebco/Standard Publishing, New York, 1972.
- Advanced Algebra & Calculus Made Simple*, by Wm. R. Gondin; Doubleday, New York, 1959.
- Analytic Geometry*, by J. H. Tanner and Joseph Allen; from the Cornell University Mathematical Series for Engineering and Architecture; American Book Co. New York, 1898.
- Black Holes and Time Warps*, by Kip S. Thorne; W. W. Norton & Co., Inc, New York, 1994.
- Cosmos*, by Carl Sagan; Random House, Inc., New York, 1980.
- Einstein: The Life and Times*, by Ronald W. Clark; Avon Books printing by arrangement with World Publishing Co., New York, 1971.
- Electricity Made Simple*, by Henry Jacobowitz; Doubleday, New York, 1959.
- Electromagnetic Devices*, by Herbert C. Rotor; John Wiley & Sons, New York, 1941.
- Encarta Encyclopedia Deluxe 2000*, by Microsoft Corporation; Redmond, WA, 1999.
- Encyclopaedia Britannica*, 14th Edition, by Encyclopaedia Britannica, Inc.; Chicago, 1968.
- Ether Technology*, by Rho Sigma; Adventures Unlimited Press; Kempton, IL, 1977.
- How to Build a Flying Saucer*, by T. B. Pawlicki; Prentice Hall, Upper Saddle River, NJ, 1981.
- Permanent Magnet Design and Application Handbook*, by Lester R. Moskowitz; Cahners Books International, Inc., Boston, 1976.
- Physics at Surfaces*, by Andrew Zangwill; Cambridge University Press, 1988.
- RCA Receiving Tube Manual*, by RCA Corporation; Electronic Components Div., 1971.
- Standard Handbook for Electrical Engineers*, by McGraw-Hill Book Co.; New York, 1949.
- The Book of Popular Science*, by The Grolier Society, Inc.; New York, 1958.
- The Physics Problem Solver*, by Research and Education Association; New York, 1976.
- The Right Stuff*, by Tom Wolfe; Bantam Books, Inc., New York, 1979.
- The Systems Approach*, by C. West Churchman; Dell Publishing Co., Inc., New York, 1968.
- Van Nostrand Scientific Encyclopedia*, by Van Nostrand Rheinhold Co., Inc.; New York, 1983.

Fiction:

- Across the Sea of Suns*, by Gregory Benford; Bantam Books, Inc., New York, 1984.
- Cities in Flight*, by James Blish; Avon Books, New York, 1970.
- The Complete Venus Equilateral*, by George O. Smith; Ballantine Books, New York, 1976.
- Faster than Light*, by Jack Dann & George Zebrowski; ACE Books printing by arrangement with Harper & Row, Inc., New York, 1982.
- The Lathe of Heaven*, by Ursula K. LeGuin; Charles Scribner's Sons, New York, 1971.
- Procyon's Promise*, by Michael McCollum; Ballantine Books, New York, 1985.
- Space*, by James A. Michener; Random House, Inc., New York, 1982.
- Time Enough for Love*, by Robert A. Heinlein; Penguin Putnam, Inc, New York, 1973.

Science Magazines:

- Discover*, by Discover Publications, Inc., Burbank, CA; December 1990 issue, Vol. 11, No. 12: "Bolts from the Blue", pgs. 50-56, by David H. Freedman [*on the electrophysics of lightning*]; February 1990 issue, Vol. 14, No. 2: "The Biggest Chill", pgs. 62-70, by David H. Freedman [*on the quest to achieve the laboratory production of Bose-Einstein condensate*]; April 1993 issue, Vol. 14, No. 4: "Loops of Space", pgs. 60-68, by Marcia Bartusiak [*on the Ashtekar model of quantized space-time and the quest for a theory of quantum gravity*].
- OMNI* by Omni Publications International, Ltd, New York; April 1994 issue, Vol. 16, No. 7: "Inside the Military UFO Underground", pgs. 48-59, by A. J. S. Rayl [*interviews with three men in support of a contention that the NATO countries have jointly conspired to cover up an enormous quantity of data about UFOs, during the entire second half of the 20th century*].
- Power Transmission Design*, by Penton Media, Inc., Cleveland, OH; May 1987 issue: "Ceramic Bearings Roll Beyond Convention", pgs. 19-22, by R. A. Hanson [*on silicon nitride bearings*].
- Radio-Electronics*, by Gernsback Publications, Inc., Farmingdale, NY; April 1986 issue: "Gravitational Waves???", pgs. 53-56, by Gregory Hodowanec [*on gravity wave detection*].
- Scientific American*, by Scientific American, Inc., New York; October 1998 issue, Vol. 279, No. 4: "The Asymmetry between Matter and Antimatter", pgs. 76-81, by Helen R. Quinn and Michael S. Witherell [*on concerns regarding the Standard Model of particle physics*].

Author's Note

– regarding John Searl and certain Levity Disc legends:

Regrettably, the Apocryphal sources of information about John Searl and the levity disc would at this time be virtually unobtainable by any but the most persistent and resourceful researcher. Ultimately, these sources were found to be of little real value in deriving practical engineering concepts for a reactionless all-electric aerospace propulsion method, often containing conflicting data and/or plainly unscientific speculations. Therefore, a listing of such sources will not be provided here. An Internet search on "John Searl" will yield far more satisfactory results.

However, the two published reference works below contain some typical information about Searl and the disk generator that is representative of the obscure and questionable writings disseminated in this area. They also offer a fair amount of very interesting (and in some cases entertaining) background material in the related "fields" of free energy theory and anti-gravity. The reader is accordingly urged to adopt an appropriate degree of skepticism with regard thereto.

The Manual of Free Energy Devices and Systems, by D. A. Kelly (1986); 1st printing 1986 by Electrodyne Corp., Clearwater, FL 33516; 2nd printing 1987 published by Cadake Industries & Copple House, Clayton, GA 30525 [*a comprehensive and professionally-assembled compendium, containing a great deal of fascinating technical data that may be of potential value to alternative energy researchers and engineers*].

The Anti-Gravity Handbook Vol. I, by Adventures Unlimited Press (1985), compiled by D. Hatcher Childress; Publisher's Network/Adventures Unlimited Press, Stelle, IL 60919 [*includes an excellent and comprehensive bibliography of books and articles specifically related to UFO research and alternative aerospace propulsion proposals*].

Special Glossary

with separate sections on:

Astrophysics

Ceramics

Electronics

General Physics

Language & Semantics

Magnetics

Mathematics

Mechanics

Special Glossary

This carefully-constructed Glossary is “special” in a number of ways: it will not contain certain words or phrases which may be readily explained in numerous other *general* sources, yet it is structured in a way which *should* facilitate its use by the lay reader. However, seemingly ordinary words or phrases may still be found here if their use in this book involves a special emphasis or connotation. The Glossary is divided into several sections each having a specific category of overall content, so that entries may be rapidly located in what is felt to be their most important context. Therefore, just because an entry is not found under *one* obvious heading does not mean it isn’t included! Terms which have a particular meaning as pertains to dual continuum cosmology or StarDrive devices are in *italics*.

ASTROPHYSICS:

astrometric: having to do with measurements of the positions and changes in position of heavenly bodies.

black hole: a theoretical massive stellar object having enormous mass but zero volume, whose gravitational field is so strong that not even light can escape a spherical boundary region which encloses it (called the *event horizon*). A neutron star (or supergiant ‘cold’ core remnant) of over 1.7 solar masses cannot avoid becoming a black hole.

Chandrasekhar limit: the maximum stellar core mass, remaining after a supernova explosion, that can just avoid becoming a neutron star. This remnant core mass is about 1.4 solar masses. In neutron star matter, the protons and electrons normally present are fused by gravity until only neutrons remain.

continuum: the physical reality associated with three spatial dimensions and the dimension of time, in which any event may be located with four coordinates. The Universe *may* be comprised of more than one continuum.

cosmology: the branch of science and/or philosophy which deals with the study of the form, nature, and evolution of the Universe as a whole physical system.

cusp: the equilibrium midpoint in Universal evolution in any cosmological theory which holds that an extended post-Big-Bang expansionary phase will be followed by a contractionary phase leading up to a “Big Crunch”.

dark energy: some astronomers and physicists maintain that if *dark matter* is presumed to exist, and observational analyses would seem to suggest it must, then it is reasonable to assume that dark energy must exist as well. However, since a good working model regarding the nature and properties of dark matter has yet to be developed, very little speculation about dark energy is available.

dark matter: an inferred mass presence in the Universe that cannot be directly observed because it doesn’t emit or reflect any form of EM radiation but exerts a “positive” gravitational force. At least 90% of all of the mass in the Universe must be dark matter, by most presently accepted cosmological theories; and in fact, the larger the scale of observation and measurement, the more dark matter appears to be required to “balance” large-scale gravitation.

eccentricity: a measure of how much an elliptical or oval-shaped orbit deviates from purely circular. For a planetary orbit around a star, the eccentricity is equal to the distance from the star (or center) to the ‘focus’ of the ellipse divided by the *aphelion* distance (or greatest orbital distance from the center). The closest planetary orbital distance from a star is called *perihelion*. The average of these two distance limits is the *semi-major axis*, which may be substituted for radius in the eco-zone orbital period formula on pg. 297. For binary stellar orbits around a common center of gravity, the greatest orbital distance is called *apastron* and the closest such distance is *periastron*; if such an orbit is stable, the common center of gravity is at the focus. Orbital eccentricity is also equal to this expression: [(the semi-major axis - the closest distance) / the semi-major axis].

electron degeneracy pressure: the *Pauli exclusion principle* dictates that no two *fermions* (having non-integer spin) may occupy the same quantum energy state. When a star explodes and its core collapses, the remnant material is squeezed by gravity into a smaller and smaller volume and the electrons are forced to occupy a larger and larger range of energies. This creates an outward pressure which resists further gravitational collapse, preventing a neutron star from forming if the core charge is high enough. Instead, a white dwarf is produced. The exclusion principle also applies to the free electrons in any electric current caused by the application of a voltage, and so a StarDrive vessel’s Field envelope current would exhibit a tremendous electron degeneracy pressure.

luminosity: the total radiant energy output of a star in watts (joules per second). In general, the more massive a *main sequence* star is, the more luminous it is. By calculating the separation distance and orbital periods for binary star systems, astronomers can accurately compute their individual masses. This direct mass-luminosity relationship then allows the binaries’ intrinsic luminosity to be determined, and from that data an accurate projection of their distance from the Sun can be made. This in turn enables the distances to other stars in the vicinity of such a binary system to be found. By reversing the process above, knowing the distance to a main sequence star allows its luminosity and then its mass to be calculated with a fair degree of accuracy.

main sequence: the phase of a star’s evolution, beginning about a million years after its formation, in which it “burns” or fuses core hydrogen exclusively. The time length of this phase is inversely proportional to the star’s mass, lasting from only 100 million to 10 billion years or more (for giant stars and dwarf stars, respectively).

- negative quantum time-space:** an alternate continuum postulated to coexist within the same spatial volume as our space-time continuum. This "coincident" *time-energy* continuum would share normal space-time's wave energy nodal points, within a universal quantized structural 'fabric' comprised of *quantum potential loops*. To reconcile this concept with relativity, quantum energy in this "hyperspace" must be negative, mass must be 'imaginary', and velocity must always be greater than that of light: although time itself remains ever-positive.
- periastron:** see *eccentricity* above.
- pulsar:** an astronomical pulsating radio frequency source, now believed to be a rapidly rotating neutron star whose intense magnetic field causes it to emit a cone-shaped radio wave "signal" which sweeps across space with each revolution. Pulsars have been found at the center of many supernova-produced nebulae.
- quantum matrix:** the fundamental universal construction which allows relativity to be uniformly applied to two coincident continuums. In quantum matrix theory, this is made possible by *vacuum fluctuations* which propagate at the square of the speed of light and which represent near-instantaneous changes in the relative diameters of potential loops which must carry and locate every *quantum* of matter and energy in the void. These positive and negative fluctuations in local absolute quantum energy or *potential* are believed to occur around a mean potential loop diameter which corresponds to an unoccupied state, in response to a loop property of *reflexive elasticity*.
- quasar:** any one of many remote astronomical objects originally named for "quasi-stellar radio source" by radio astronomers in the late 1950's. Light from quasars is the most highly "red-shifted" known (see *Doppler effect*), indicating that they are probably receding from our relative position at a high velocity. It is now thought that quasars may be vast matter accretion clouds surrounding enormous black holes at the cores of the oldest and largest remaining galactic clusters, which emit incredible quantities of energy as large numbers of whole stars fall into the black hole. Some quasars radiate as much energy as thousands of normal whole galaxies.
- red giant:** the phase of stellar evolution which occurs when a star reaches the end of the main sequence, having burned all available hydrogen in the core. As its thermal output lessens, the core shrinks; but the outer layers of the star expand greatly as hydrogen burning proceeds into layers farther and farther from the core. A red giant can become 100 or more times larger than it was as a main sequence star. Eventually, it will exhaust all its hydrogen fuel, and the core may shrink until its temperature elevates sufficiently to begin fusing helium.
- Schwarzschild radius:** the theoretical radius of a spherical object, having a given macroscopic mass, at which the object can't avoid becoming a black hole. This parameter derives from one solution to Einstein's field equations, found by German physicist Karl Schwarzschild in 1916, which is strictly valid only for "static" black holes having zero spin (angular momentum) and zero net electrical charge. The base formula for the Schwarzschild radius, $R_s = 2GM/c^2$, is closely related to the formula for escape velocity: $V_e = (2GM/r)^{1/2}$.
- SETI project:** the original 'Search for Extraterrestrial Intelligence' experiment was conducted for four months in 1960, using a single-channel receiver, at the National Radio Astronomy Observatory in Green Bank, W. Va. It was, and remains to this day, unsuccessful. Projects of this type are frequently out-of-favor with Congress, and NASA lost its SETI funding for two years in 1981. By the 1990's, NASA had developed equipment capable of monitoring millions of channels simultaneously, and in 1992 initiated a Targeted Search program using the huge Arecibo dish in Puerto Rico. Once again, Congress cancelled funding (a year later). In 1995, the Targeted Search equipment was transferred to a private SETI Institute operating in Australia. At the time of this writing, NASA continues its search operations at the original Green Bank facility.
- space-time [continuum]:** the physical reality we associate with the *observable* Universe, comprising three spatial dimensions and the dimension of time, in which any event may be located with four coordinates.
- space warp:** see *Einstein-Rosen bridge* and *Kerr metric space warp*, under *General Physics*.
- time-energy continuum:** see *negative quantum time-space* above.
- time-light barrier:** the relativistic restriction imposed on any material object such that its mass would reach infinity and the passage of objective time would cease were its velocity allowed to equal that of light. While this consideration remains true even in dual continuum cosmology, it has previously been thought to represent an *absolute* limit in that apparent supralight velocity is also generally assumed to be unattainable. This point of view is exactly analogous to that which was prevalent before Yeager broke the 'sound barrier' (in 1947).
- vacuum fluctuations:** quantum variations in the state of minimum energy represented by the void, which are consistent with the Heisenberg uncertainty principle and are responsible for the observed phenomenon of 'spontaneous virtual pair creation' (or the temporary formation of EM photon particle-antiparticle pairs). It is presently accepted that *gm* vacuum fluctuations also occur, accounting for Hawking black hole evaporation, and that elementary particles having mass like the electron may thereby also be produced.
- white dwarf:** a low- to medium-mass star which has exhausted its nuclear fuel and collapsed under its own gravitational weight. Such a stellar remnant will slowly cool from blue-white to red over billions of years. White dwarfs (and neutron stars) exhibit an inverse mass-to-volume relationship: the larger they are, the less massive. And, the smaller they are, the slower they radiate away their trapped thermal energy; so a white dwarf near the Chandrasekhar limit could take several times the age of the Universe to reach a cold "black dwarf" status.

CERAMICS:

- Alumina:** (Al_2O_3) a multi-purpose family of aluminum oxide ceramics having high density, high physical strength, and excellent dielectric properties. Most grades contain a small percentage of magnesium oxide (MgO).
- Cordierite:** ($2\text{MgO} \cdot 2\text{Al}_2\text{O}_3 \cdot 5\text{SiO}_2$) complex ceramic family having low density, low thermal expansion, and excellent resistance to thermal shock. A semi-vitreous or vitrified material suitable for high-heat applications.
- curie point:** the temperature above which a ferroelectric material begins rapidly losing its dielectric capability.
- ferroelectric:** a dielectric material which can retain its electric polarization indefinitely, in much the same manner as a permanent magnet retains its magnetic polarization. The most practical ferroelectrics typically belong to the perovskite mineral family, having the general formula $A(\text{BO}_3)$. Another unique property of a typical ferroelectric is an inverse temperature/resistance relationship: whereby the material has a fairly normal dielectric constant at standard temperature which rises dramatically upon temperature increase (the reverse of the case with a normal insulator). This relationship peaks at the *curie point* (transition temperature), beyond which the effect reverses.
- magnesium silicate:** (MgSiO_3) a common crust mineral that may be used to form an unfired low-density ceramic which is unusual in that it may be machined like wood or steel yet has good physical strength.
- piezoelectric:** indicates a crystalline substance which develops an electric potential or voltage across certain faces when subjected to mechanical pressure, and which conversely undergoes mechanical deformation when an external electric field is applied. A *transducer* is a device which takes advantage of this "piezoelectric effect" to convert mechanical motion into voltage, or vice versa. Some piezoelectrics are also *ferroelectric*.
- silicon nitride:** (Si_3N_4) a ceramic which is twice as hard as bearing-grade stainless steel but only 40% as dense.
- Steatite:** ($\text{MgO} \cdot \text{SiO}_2$) a medium density ceramic which may be pressed into complicated shapes. May sometimes be substituted for Alumina to reduce component costs, in that it is easier to form and is fired at lower temperatures.
- titanate:** any of a number of ceramic compounds comprised of an active metal and a radical having a titanium atom and three oxygen atoms ($-\text{TiO}_3$). Titanates are generally known for exhibiting outstanding dielectric properties, and Barium Titanate at ordinary temperatures has one of the highest dielectric constants known ($k \Rightarrow 3,000$).
- Titania:** (TiO_2) a ceramic form of titanium dioxide (the white pigment in paint) having good strength, high chemical resistance, and superior surface finishing. In its usual composition, it exhibits a very high dielectric constant ($k = 85$), yet it may also be formulated to actually 'conduct' static (surface) electricity.
- vitreous:** having glass-like nature or properties. Many minerals and ceramics have a glass [silicon dioxide (SiO_2)] "phase" or intergranular component, such as Cordierite and Steatite.
- Zirconia:** (ZrO_2) zirconium dioxide ceramic having very high density and tremendous physical strength.

ELECTRONICS:

- AC (ac):** an alternating electrical current, as opposed to direct (pure) current whose amplitude does not oscillate with time. The corresponding voltage responsible for an alternating current generally has a positive value for one half of each repeating period of oscillation or 'cycle', and an equal (and opposite) negative voltage for the other half-cycle. A less common form of AC is one in which both halves of each cycle are either equal and positive or equal and negative. This is *udac* or unidirectional alternating current, of a *full-wave* variety. In the StarDrive device, pulsed unidirectional current or *half-wave* udac is employed, whereby a negative current flows only during every other voltage half-cycle (due to a current cutoff level of control grid bias on the alternate half-cycle).
- AM:** denotes a method of EM signal generation wherein variations in the *amplitude* of an alternating carrier wave are utilized to transmit information. Commercial AM radio stations may use frequencies between 530 and 1600 kHz.
- ampere (amp):** (coul/sec) the standard MKS unit by which the rate of flow of charge in a conductor is measured. One ampere is equal to a flow of one *coulomb* of charge per second. Named for French scientist André Ampère.
- amplitude:** a measurement of the amount or scale of a quantity, very similar to *magnitude*. Specifically, the widest range of fluctuation of a regularly varying quantity, as measured from the mean or average value to the extreme.
- anode:** the positive electrode or element of an electronic device, also commonly referred to as 'plate'.
- bias:** in general, the use of a minor fixed voltage to divert or control a major level of current in an electronic device or circuit. May also refer to the use of a major fixed resistance to divert or limit a particular circuit current.
- capacitance [static]:** the ratio of charge to voltage anywhere on the surface of an electrically charged conductor, or $C = Q/V$. More generally understood as the ability to store an electrical charge, in units of the *farad*. A *capacitor* technically stores energy in an electric field, however, and only stores a net charge when one plate is grounded.
- capacitance, dynamic:** the ability of a device to store electrical charge in the form of a continuous current. In the StarDrive device, the annular magnetically-induced rotation of *space charge* near the hull's neutral region constitutes a form of dynamic capacitance which is analogous to the operation of an ungrounded capacitor, in that the Field envelope *breakdown* current precludes the hull's capacitive storage of any *net* charge. The induced zero-loss current in a StarDrive vessel's superconducting storage ring(s), constituted of accumulated ambient charge, is analogous to the operation of a capacitor with one plate at ground potential.

- cathode:** the negative electrode or element of an electronic device, also sometimes referred to as 'filament' in cases where such a negative electrode is directly heated to a state of *thermionic emission*.
- discharge, dark:** the induced drift of electrons from the surface of an unheated ('cold') cathode due to the application of a very high electric field; sometimes referred to as "field emission".
- discharge, glow:** generally refers to the complex phenomenon whereby both the ionized gas and the cathode in a gas-filled electron tube are raised to incandescence by the application of an electric field. Thus, technically speaking, the emission of light in a normal evacuated light bulb is not a glow discharge as it is in a neon tube.
- dc (DC):** a flow of electrical current which does not oscillate with time, as produced by a voltage of constant value.
- displacement current:** generally, the brief rush of charge into the negative plate of a capacitor and out of its positive plate when connected to dc voltage; this current and its magnetic field both decay to zero as the capacitor approaches saturation. Denotes the continuous transverse deflection of electrons in a StarDrive device's Field envelope current, causing a rotational "secondary" current effect which produces a magnetic field, as used herein.
- elastomer, silicone:** a rubberlike synthetic polymer often used as a gasket material or insulation, due to its high resistance to water, heat, and electricity. As a polymer, silicone consists of a basic structural unit, each having silicon and oxygen atoms attached to an organic group, which repeats in chain fashion to form giant molecules.
- electrode:** in general, any terminal in an electrical circuit or device which carries current and/or voltage into or away from certain elements or components thereof. Specifically, the main terminals of an electron (vacuum) tube.
- electronic:** dependent on the action and behavior of electrons in vacuum or integrated circuits to perform work.
- farad (f,F):** (coulombs/volt) the fundamental unit of capacitance. A capacitor with a capacitance rating of one farad would hold one coulomb of charge with the application of one volt across its terminals. The farad is a very large unit, so capacitors are typically rated in microfarads (μf) or micro-microfarads ($\mu\mu\text{f}$). Named for Michael Faraday.
- feedback:** the transfer of part of the output of an electrical circuit or device back to the input, either as an undesirable effect or as an intentional operating parameter. Feedback may also be either positive or negative, depending on whether the output is amplified or enhanced or is reduced or suppressed (respectively).
- filament:** the *cathode* or *thermionic* electron emitter of a light bulb or vacuum tube.
- FM:** denotes a method of EM signal generation wherein variations in the *frequency* of an alternating carrier wave are utilized to transmit information. FM transmission is less subject to interference and static than AM, resulting in a higher signal-to-noise ratio and a higher fidelity of signal reproduction. Commercial FM radio stations are assigned frequencies between 88 and 108 MHz, whereas TV stations use two bands between 55 and 88 MHz and two bands between 175 and 890 MHz.
- frequency:** the number of periodic oscillations or waves per unit time, usually in cycles per second (or *hertz*). The prefixes k, M, and G are generally used to denote thousands, millions, and billions of hertz (respectively).
- gain, voltage:** see DataSheet #11.
- grid:** a secondary wire mesh electrode in a vacuum tube, to which a negative or positive voltage may be applied for purposes of controlling the passage of the electrons comprising the main plate current.
- ground:** a large conducting body, most often the earth itself, to which an electrical circuit or device may be connected to obtain a source of zero potential or to bleed off excess charge.
- half-wave:** denotes a manner of electrical operation which is effective or considered only during one-half of each fundamental electrical cycle or current waveform. See *AC (ac)* above.
- henry (H):** (volt-sec/amp) the standard unit of *inductance*, or magnetic opposition to a change in the current carried by a conductor or especially a coil. A coil has a self-inductance of one henry when a change in current of 1 ampere per second produces a counter-voltage (or "back emf") of 1 volt. Named for American physicist Joseph Henry.
- impedance:** the total opposition presented by an electrical circuit to the flow of an alternating current of a particular frequency. The impedance (*Z*) is comprised of the normal dc resistance and the *reactance* of the circuit, and must be figured by different formulas for the many various combinations of resistance, inductance, and capacitance.
- ohm:** the standard MKS unit of resistance or opposition to current flow in an electrical circuit. The resistance of a circuit equals one ohm ($1\ \Omega$) if one volt applied thereto produces a current of one amp. Named for Georg S. Ohm.
- phase:** as applies to a single wave train (system), denotes the relationship between points on successive waves that are displaced by the same amount from their equilibrium (rest) or median positions. If such displacement is changing in the same direction, either increasing or decreasing with the wave's forward motion, the waves are said to be in-phase. Thus, all of the wave crests of a given wave train are in-phase, as are the wave troughs. The x-axis of a sine graph which is measured in angular degrees is most often used to specify the difference in phase relationship between points on a given wave. Thus, a wave train's crests and troughs are 180° out-of-phase. Similarly, two superimposed waveforms may be mutually in- or out-of-phase, and the resultant amplitude of the joint wave system may be determined by vector analysis (as in the case of AC voltage and current in a circuit with reactance).
- plate:** either electrode in a capacitor, specifically a parallel-plate capacitor; or the *positive* electrode in a vacuum tube.
- polarize(d):** may be interpreted as referring either to electrical or magnetic polarization, as used herein. Electrostatic polarization occurs when a charged object is brought near a neutral (uncharged) object, producing a local separation of charges or surface charge imbalance in the neutral object and a corresponding external electric field

- (but no net charge). Magnetic polarization occurs when a magnetizable material is immersed in a magnetic field, whereby that material acquires two distinct opposite poles which are analogous to positive and negative electrical charges. Such a magnetic polarization may be permanent or temporary. The term "phase-polarized" as used in the text regarding the experiments of Nikola Tesla requires a bit of explanation. Tesla was able to create a special kind of 'standing-wave' electrical discharges at enormous AC voltages (once throwing an arc 135 ft. in length through air!) with very little net flow of current, due to the careful balancing of frequency and phase relationships. It is thought that he could also cause a huge net flow of charge in one direction by deliberately imbalancing such relationships. This would result in a phase-polarized arc discharge, as opposed to one which was phase-balanced.
- powered electrostatic induction:** an electrical engineering principle, first developed by Nikola Tesla, whereby a specially configured circuit performs the work necessary to accumulate very high levels of ambient static charge.
- reactance:** the resistance to alternating current which is presented by a capacitance or an inductance in an electrical circuit, as measured in ohms. Since capacitive reactance (X_c) causes the instantaneous current to lead the applied voltage by 90° and inductive reactance (X_L) causes it to lag behind the voltage by 90° , the net reactance in the circuit is simply the arithmetic difference in the magnitudes of the capacitive and inductive reactances.
- resistance, load (R_L):** in the operation of a single vacuum tube, the load resistance is merely the value of the ballast (plate) resistor, in ohms. In the operation of sequentially-coupled tubes, the load resistance is approximately equal to the ballast resistance in parallel with the grid resistance of the following tube (or "stage").
- resistance, plate (r_p):** the resistance (in ohms) of the path between the cathode and plate of an electron tube to the flow of alternating current. This AC resistance is inversely proportional to both the cathode temperature and the finite capacitance which exists between cathode and plate.
- resistor, ballast [plate]:** the resistor (with value $= R_L$) which must be placed in a vacuum tube circuit between the plate and main (B) voltage supply to limit plate current to a level within the operational rating of the tube.
- resonance:** specifically, an operating condition of an electrical circuit wherein the frequency of its input voltage is the same as the design frequency at which its output efficiency is maximized.
- shunt:** a conductive link between two points in an electrical circuit which serves to divert a portion of the current.
- solid-state:** denotes semiconductor technology which is able to control the flow of current in an electrical circuit without vacuum tubes or moving parts.
- space charge:** as applies specifically to vacuum tubes, space charge may be thought of as the total number of electrons in-transit between the cathode and plate at any given instant in time. These electrons set up a negative electric field which moderately impedes cathode emission. The magnitude of this impedance effect is proportional to plate current and cathode-to-plate separation distance and inversely proportional to plate voltage.
- substrate:** specifically, a thin wafer of nonconductive or semiconductor material upon which electrical components are mounted or etched. Computer microprocessor chips (integrated circuits) are produced by the deposition and removal of thin films on an ultra-pure silicon substrate. The fine-grained ceramic *Alumina* is frequently used as a nonconductive substrate in making photoelectric and thermoelectric sensors.
- telemetry:** the signal transmission of data pertinent to or obtained during aerospace vessel operation.
- thermionic:** the stimulated emission of ions and/or electrons from the surface of a heated conductor, specifically from the cathode in a gas-filled or vacuum electron tube. If gas-filled, ion bombardment of the cathode may cause its surface to vaporize slightly during operation, hence the short-range emission of ionized cathode material. Vacuum tubes with very-high-temperature cathodes generally do not exhibit this effect, and therein essentially only electrons are emitted; but at a vastly higher rate than if the cathode were unheated (see *dark discharge* above).
- time constant:** the amount of time required for the charge on a capacitor or the current through a coil to build up to 63.25% of the full value, after a dc voltage has been applied. During the next time constant (T_c), the charge or current builds to a level corresponding to 63.25% of the remaining difference, or 86.494% of full value; and so on for a total of 5 time constants. In a circuit having net capacitance, $T_c = RC$; and in one having net inductance, $T_c = L/R$. At resonance, where a circuit exhibits no net reactance, the time constant approaches zero.
- trace(s):** thin conductive pathways or strips of metal, laminated upon a nonconductive base or printed circuit board, to provide interconnection between electronic components or devices.
- transit time:** specifically, the time required for each plate current electron to travel from the cathode to the plate in a vacuum tube. This transit time may be important in that the inter-electrode *space charge* is proportional thereto.
- UHF:** ultra-high frequency, denoting radio waves of from 300 to 3000 MHz (3 GHz).
- VHF:** very-high frequency, denoting radio waves of from 30 to 300 MHz.
- VLF:** denotes radio waves of from 3 to 30 kHz. The text loosely categorizes the resonant comm frequency of Star-Drive vessels as VLF, when in actuality the comm frequency band for 40ft. to 100ft. starships has been estimated to range from 3097 Hz down to 496 Hz (respectively). This would actually constitute a ULF (ultra-low frequency) band, for which an official designation doesn't yet exist.
- volt:** (joules/coulomb) the standard MKS unit of electromotive force (emf) or *potential difference* between two points in an electric field, such that one joule of work is required to move one coulomb of charge from one point to the other parallel to the lines of force which represent the field.

GENERAL PHYSICS:

- adsorption:** specifically, the process by which a gaseous substance collects in condensed form on a surface.
- antimatter:** matter composed of elementary particles which are essentially mirror images of ordinary matter, having opposite electric charge or *magnetic moment* but equal mass and spin. Massless antiphotons, on the other hand, are identical in all respects with the normal variety. The existence of antimatter was first proposed by British physicist Paul Dirac in 1928, but wasn't confirmed experimentally until 1955.
- arc discharge:** a concentrated flow of electric current in a gaseous medium or vacuum, which exhibits very low or negligible resistance. In a vacuum, an arc discharge will initiate only at *breakdown intensity* (3×10^6 volts/meter).
- attenuate:** to gradually diminish or weaken with increasing distance. Radiant energy and most of the fundamental forces in nature attenuate proportional to the square of the distance.
- boson:** according to the Standard Model of particle physics, there are two fundamental types of bosons: elementary and composite. An elementary boson is a particle having no internal structure and which therefore cannot be subdivided. Elementary bosons are also called mediating bosons in that they are thought to carry the four fundamental forces of nature (electromagnetism, gravity, and the strong and weak nuclear forces). A composite boson is any particle which is itself composed of an even number of quarks equal to or greater than 2, and are also referred to as mesons. Ordinary photons of electromagnetic radiation are examples of composite bosons. All particles have rotations which can be expressed as a whole or half multiple of the term $h/2\pi$, and this multiple is used to signify the particle's intrinsic angular momentum or *spin*. Bosons all have spins that are equal to zero or a multiple of 1 (times the term $h/2\pi$). Elementary bosons do not obey the *Pauli exclusion principle*.
- Bose-Einstein condensate:** an extraordinary form of matter which can only exist at a very small fraction of a degree (kelvin) above absolute zero. A *boson* material such as helium-4 or rubidium gas may be isolated and cooled by a combination of laser and magnetic trapping techniques until the momentum of the constituent atoms becomes highly uniform and their positions become so uncertain (or "fuzzy") that they lose their individual identity and occupy the same space. This phenomenon clearly demonstrates quantum wave-particle duality.
- breakdown intensity [dielectric]:** the highest electric field intensity a material can withstand before it loses its insulating capability and becomes a conductor. The approximate *dc voltage* breakdown intensity of any given dielectric material can be found by multiplying the breakdown intensity of vacuum by that material's dielectric constant: $E_{br} = k (3 \times 10^6 \text{ volts/meter})$.
- bypass current:** that portion of a StarDrive device's rotor current which is equal to the total field envelope current; named as such due to the fact that this part of the rotor current bypasses the rotor-mounted field coils.
- cgs [units]:** the *centimeter, gram, second* system of physical measurement which is used in solving certain types of scientific problems for the sake of expediency, but which is used less often today than the *MKS* system.
- charged vacuum envoidment:** an artificially-generated spatial distortion which resembles a miniature black hole but contains no singularity. Such an 'envoidment' or isolated region of space has finite volume but is much larger internally than externally, and utilizes electron degeneracy pressure to resist gravitational collapse. [The origin of this perfectly valid concept may be traced to the long-running British science-fiction television series *Dr. Who*, wherein the very similar French-derived word "emboitment" is used with a slightly different intended meaning.]
- collision, elastic:** any collision between two particles or mass bodies in which the objects separate immediately after impact and in which both momentum and kinetic energy are conserved.
- collision, inelastic:** any collision between two particles or mass bodies in which the objects remain fixed together after impact, and in which momentum is conserved but a major portion of the total kinetic energy is converted into another form of energy such as heat (or gravitational potential energy).
- constants, fundamental:**
- constant, Avagadro's (N_A): equal to 6.022×10^{23} molecules/mole (of any gas).
 - constant, Bohr magneton (μ_B): equal to 9.274×10^{-24} J/T (amp-m²); represents the theoretical magnitude of the electron magnetic moment (see *moment, magnetic* below).
 - constant, Boltzmann's (k): may be expressed as 1.38×10^{-23} J/K, 1.38×10^{-16} erg/K (cgs), or 8.6174×10^{-5} eV/K.
 - constant, electron magnetic moment: equal to 9.28477×10^{-24} J/T (amp-m²); observed value.
 - constant, electron magnetic moment anomaly (a_e): equal to $0.00116 \mu_B$ (in Bohr magnetons).
 - constant, electron rest mass (m_e): equal to 9.11×10^{-31} kg.
 - constant, electron volt (eV): equal to 1.602×10^{-19} J.
 - constant, elementary charge (q): equal to 1.602×10^{-19} coul.
 - constant, gravitational (G): equal to 6.6726×10^{-11} nt-m²/kg² (or: m³/kg-sec²).
 - constant, light velocity (c): equal to 2.997925×10^8 m/sec. [accepted precise value = 299,792,458 m/sec.]
 - constant, molar gas (R): equal to 8.3145 J/mole-°K [or, Avagadro's constant times Boltzmann's constant (MKS)].
 - constant, Planck's (h): equal to 6.626×10^{-34} J-sec. May also be expressed as 4.13567×10^{-15} eV-sec.
 - constant, vacuum permeability (μ_0): equal to $4\pi \times 10^{-7}$ Wb/amp-m; or 1.25664×10^{-6} H/m (henries/meter) or, nt/amp².
 - constant, vacuum permittivity (ϵ_0): equal to 8.854×10^{-12} F/m (farads/meter) or, coul²/nt-m².

- corona:** a type of short-range electrical discharge with a pinkish or bluish color which may be seen under certain conditions surrounding high-tension power lines, especially during periodic line tests in which the voltage briefly approaches one million. A corona occurs when the electric field intensity at the surface of the conductor exceeds the *breakdown intensity* of air.
- coulomb (coul):** standard MKS unit of electric charge, equal to 6.242×10^{18} electrons or elementary charges. The number of electrons transported through a conductor by a current of one amp flowing for one second is 1 coulomb.
- dielectric:** indicates a material which is a good insulator and conducts little if any electric current, as opposed to materials like metals (which are good electrical conductors). Dielectrics still permit passage of the electric lines of force, and polarize electrically such that the storage value of a capacitor is increased if inserted between the plates.
- dielectric constant (k):** in the MKS unit system, the ratio of the electric permittivity (ϵ) of any given dielectric material to that of vacuum (ϵ_0) (or air, approximately), according to the expression $k = \epsilon/\epsilon_0$ [see *constants* above].
- Doppler effect:** an apparent change in the frequency of sound or electromagnetic waves, which varies with the relative motion of the wave source and an observer or detector. The "red-shift" associated with the spectra of distant celestial objects is a result of the Doppler effect, and indicates that such objects are rapidly receding.
- dyne:** the unit of force in the *cgs* system of measurement, equal to the force that gives a one gram mass an acceleration of one centimeter per second per second.
- Einstein-Rosen bridge:** a type of "wormhole" or space warp produced by a static black hole, or one which does not rotate or have a net electrical charge. Such a wormhole, which connects the black hole with another continuum (or set of dimensions) was found to be necessary to preserve the internal consistency of the Schwarzschild solution to Einstein's Field Equations. A starship can't traverse an E-R bridge because the black hole contains a singularity.
- elasticity, reflexive:** a postulated property of *quantum potential loops*, in the dual continuum cosmology theory presented in the text. Each such potential loop would exhibit both expansionary and contractionary elastic tension about a zero-point energy level representing a state in which the loop is unoccupied by any quantum of energy.
- electrocentripetal:** denotes an inward-pulling positive electric field of force induced within a thin rapidly rotating conductor by the mechanical centrifuging of electrons from its outer edge.
- electrodynamic:** having to do with phenomena produced by electric currents and their associated magnetic forces, especially in a vacuum. As used in this book, this term is taken to have a somewhat more literal meaning referring to the direct use of an electric current to produce a mechanical force of motion.
- electromagnetic [EM]:** specifically, describing the nature of radiation which is constituted of and transmitted as transverse waves in an electric field, or waves which are perpendicular to the direction of motion, and which therefore have an oscillating magnetic component which is mutually perpendicular to both the oscillations of the electric field and the direction of wave motion. Also used to denote the production of a magnetic field by an electric current, as in the operation of an electromagnet.
- electrostatic:** having to do with the type of external electric field which is produced by an object with a net charge, charges at rest, or static electricity. Such a field does not alternate or vary regularly with time.
- elliptical wave:** a type of wave which generally requires transmission through a material medium and which is produced by a combination of transverse and longitudinal oscillations. A transverse wave oscillates perpendicular to the direction of wave motion, and a longitudinal wave oscillates parallel to the direction of motion.
- entrained charge:** ambient or static electrical charge which is produced in a gaseous medium by an ionizing electric field and which is dragged along with the rotation or motion thereof.
- entropy:** a universal property defined by the second law of thermodynamics, which states that in an isolated system which is not at equilibrium (or incapable of undergoing change in the absence of work) the amount of heat or energy that is available to do useful work always decreases with the passage of time as does the orderliness of that system.
- erg (dyne-cm):** the unit of work or energy in the *cgs* system of measurement, equivalent to a force of one dyne acting through a distance of one centimeter. One erg is also equivalent to 1×10^{-7} J (joules).
- exclusion principle, Pauli:** a verified tenet of quantum physics which states that no two like *fermion* particles can exist in the same quantum energy state; that is, they cannot have the same position and the same momentum.
- farad (f, F):** the standard MKS unit of capacitance. [see *capacitance* and *farad* in *Electronics* above.]
- fermion:** according to the Standard Model of particle physics, there are two fundamental types of fermions: elementary and composite. An elementary fermion is a particle having no internal structure and which therefore cannot be subdivided. There are two types of elementary fermions: leptons, which include the electron and neutrino, and quarks. A composite fermion is any particle which is itself composed of an odd number of quarks equal to or greater than 3; the protons and neutrons which comprise atomic nuclei are composite fermions each made up of three quarks (and as such are also referred to as baryons). All particles have rotations which can be expressed as a whole or half multiple of the term $h/2\pi$, and this multiple is used to signify the particle's intrinsic angular momentum or *spin*. Fermions all have spins that are odd multiples of $1/2$ (of the term $h/2\pi$). Fermions must obey the *Pauli exclusion principle*.
- field:** a theoretical means by which any force may be considered to effect action at a distance without resorting to the virtual particle exchange of the Standard Model. The concept of the field of force was first developed by Sir Isaac

Newton to explain gravity, and was later expanded by Michael Faraday to include the electromagnetic forces. The strength and direction of a field can be represented quite reasonably with *lines of force*; in the case of magnetism, Faraday postulated such lines of force to form closed loops that exhibit the property of elasticity.

field intensity: specifically, the magnitude of the electric and magnetic forces utilized in the field of electromagnetic engineering. The electric intensity E in a uniform field, such as that between charged parallel plates, is equal to the voltage divided by the plate separation in meters: $E = V/m$ (volts/meter). Likewise, in the uniform magnetic field produced by a coil or core winding, the field intensity H is equal to the ampere-turns divided by the mean coil diameter in meters: $H = A/m = NI/2r$ (amps/meter) [see pg. 208]. When the physical specifics of the coil are not given but the desired *flux density* B and the core's *relative permeability* k_r can be determined, a gross value for the required field intensity H in A/m can be computed that is entirely equivalent to amp-turns/m [see pg. 209]. Equation M2 in DataSheet #16 gives the magnetic field intensity produced by a permanent magnet, also in A/m.

field strength: specifically, a measure of the full scope of an electric or magnetic field. Electric field strength Φ , is the total electric flux in *nt-m²/coul*, which in a uniform field or parallel plate capacitor is a function only of the net charge Q in *coulombs* and the *permittivity* (ϵ or ϵ_r): according to Gauss's Law, $\Phi_r = Q/\epsilon$ (see *Gaussian surface* below). Magnetic field strength Φ_m is the total magnetic flux in *webers* (or *nt-m/amp*), and is equal to the flux density B times the pole area A (in *m²*).

flux: a measure of the total electric, magnetic, or gravitic energy passing through a plane surface, as *lines of force*, in the interpretation of classical field theory.

free energy [device]: a machine or apparatus, not necessarily having any moving parts, which is more than 100% efficient at converting input energy to potential energy, but whose efficiency at converting potential energy to output power is still less than 100%. A fast breeder reactor is a good example of this type of device: it produces 20% more fuel than it consumes, so it could be thought of as being 120% efficient at converting input energy to potential energy, but is able to extract only 75% of its fuel's inherent potential for power output purposes.

Gaussian surface: a virtual surface used in electrostatic theory to locate the boundary of an electric field and the effective location of the net charge or charge imbalance which causes it. The standard interpretation of this concept may be fully illustrated with the classical Faraday ice-pail experiment, and is evident in parallel-plate capacitors. In the case of such a charged hollow conductor, wherein no *internal* electric field but an *external field only* is observed, one Gaussian surface is drawn enclosing the real inner surface of the conductor and another is drawn which encloses its real outer surface. The adjacent faces of these two rectangular enclosures are thus thought to pass through the middle of the conductor. Gauss's Law states that $\Phi_r = Q/\epsilon_r$, where Φ_r is the electric flux through the Gaussian surface due to the net charge Q within the surface. Since no electric field is observed near the conductor's inner real surface, no electric flux passes through the Gaussian surface ($\Phi_r = 0$) and hence *this* Gaussian surface encloses no net charge. Since an electric field is observed in the space near the outer real surface, the net charge must therefore be located in the outer Gaussian surface. But the potential inside the electrostatically-charged *material* of such a conductor is everywhere the same, since otherwise a current would result, and the net electric field intensity inside the conductor itself must therefore be zero. Thus, the net charge Q must be located in the *outer* portion of the Gaussian surface, and will behave as if it resides *outside* the conductor's real outer surface boundary, because the latter must now be thought of as the *innermost* boundary of the external electric field. By "reversing" this whole logical procedure, it becomes clear why a parallel-plate capacitor exhibits essentially no external electric field.

gradient: the rate of change of electric or magnetic force with distance. If the physical dimensions of two charges or magnetic poles are very small compared to the distance between them, they may be considered point charges or poles and the corresponding gradient (electric or magnetic) diminishes proportional to the square of the distance. If the physical dimensions of such charges or poles are very large compared to their separation distance, and are oriented plane-parallel, the gradient diminishes linearly proportional to the distance. See *field intensity* above.

gram (g): the unit of mass in the cgs system of units. Originally defined as the mass of one cubic centimeter of pure water at the temperature where it has the greatest density (4°C or 277°K), the gram is now defined as 1/1000 of the standard *kilogram* (kg).

gravimetric [gm]: denoting the nature of the unidirectional or monopolar force which is observed to act upon any body having finite mass or momentum. Gravity may be thought of as a field of force, the strength of which can be represented by lines of *gm* flux. The text supposes that all *quantum vacuum fluctuations* have a gravimetric component that propagates at the square of the speed of light, which may allow faster-than-light communications.

Heisenberg uncertainty: the axiom of quantum mechanics which states that it is not possible to precisely measure two related (conjugate) quantities simultaneously. One basic tenet of this principle relates the uncertainty in the measurement of a particle's position (Δx) to that of its momentum (Δp). Another such tenet relates the uncertainty in the measurement of the energy of an event (ΔE) to the uncertainty in the time interval during which that event's energy is measured (Δt). In both cases, the product of these conjugate uncertainties must always be equal to or greater than the quantity $h/2\pi$: [a] $(\Delta x)(\Delta p) \geq h/2\pi$; and, [b] $(\Delta E)(\Delta t) \geq h/2\pi$. Named for Werner Heisenberg.

hemitoroidal: having the shape of a toroid which is bisected through its greatest diameter, exactly like half a bagel.

[A toroid is defined as the volume of rotation of a circle about any line in its own plane that lies outside it.] The nature of the primary drive current about a StarDrive vessel hull is that of a mutually-opposed bihemitoroidal field envelope, each half or *hemitorus* of which rotates through 180° in opposite directions. This unusual but symmetrical current flow produces a magnetic field which is monopolar along the toroidal axis, the other pole emanating in a planar fashion from between the two such hemitoroidal components.

Impulse (FΔt): the product of a force which is applied to an object and the time interval during which the force was applied. The impulse given such an object in newton-seconds (nt-sec) is equal to the *momentum* gained by the object (in kg-m/sec), or the product of its mass and change of velocity during time interval Δt. Thus, $F\Delta t = m\Delta v$.

Impulse, specific: generally, a measurement of the thrust produced by a rocket, reflecting the power and efficiency of the engine and propellant. A rocket's specific impulse I_{sp} is the force produced (in newtons) per unit mass of propellant consumed per second, typically in kilograms. With respect to the StarDrive device, specific impulse is similarly a measure of how much thrust is produced by the collision of each Field electron at the Field Hub.

Inductance: the property exhibited by any conductor of electric current, even vacuum itself, whereby the magnetic field produced by that current resists any change in the magnitude of the current. Inductance is therefore analogous to mechanical inertia, and is measured in henries (see *henry* in *Electronics* above); *magnetically coupled conductors* exhibit joint or *mutual* inductance analogous to the joint inertia two objects have if rigidly fixed together.

Induction: the act of causing a displacement of electron charge, generally in a conductor, via the application of an electric or magnetic field. Induction may therefore be either *electrostatic* or *electromagnetic* in nature. Electrostatic induction refers to the use of one charged object to cause a charge imbalance and resultant electric field to arise upon another object. Electromagnetic induction refers to the use of a changing magnetic field to cause a charge imbalance *within* a conductor, which may result in a flow of current in a closed circuit. For electromagnetic induction to occur, there must be relative motion between the conductor and the magnetic field: in a generator or alternator the conductor is in continuous motion relative to the field; in a transformer the field is in continuous motion relative to the conductor.

Inductive: possessing the property of electrical inductance, or resistance to change in the level of current conducted (by an object or circuit). As used on pg. 15 of the text, refers to the concept that matter is electromagnetic in nature, and therefore mechanical inertia may in fact be simply a consequence of electrical inductance. Some theorists have suggested that gravity itself may be directly related to electromagnetism, in a manner which has so far defied mathematical unification.

inertia: the property of matter which causes it to resist any change in the direction or magnitude of its velocity, as described in Newton's first law of motion: an object at rest tends to remain rest, and an object in motion tends to remain in motion, unless acted upon by an outside force. This law also applies to rotating objects, which resist changes in rotational speed as well as changes in the plane of rotation and thus exhibit gyroscopic inertia. No satisfactory explanation for exactly what inertia is has ever been developed, nor has any means of circumventing it.

inertiomotive: the mechanical force which explains the Hooper effect, or the tendency of electrons located on the outer surface of a thin rapidly rotating conductor to exit that surface simply as a result of centrifugal force.

integral field: refers to the active current-carrying portion of a StarDrive device's Field envelope, wherein such current exhibits rotation in two planes simultaneously. The integral field may be represented by electric lines of force which begin and end on the vessel hull, whereas the leakage current emanates away from the vessel along lines of force which begin on the hull but which extend away from it indefinitely (toward infinity).

ion: an electrically charged atom or group of atoms (radical), formed when an electrically neutral atom or group of atoms either gains or loses one or more electrons in response to chemical reactions, radiant energy, or electrical discharge. An ion engine or rocket is one wherein charged atoms are ejected from the rear of the vehicle by an accelerating electrostatic field to produce thrust by reaction.

ionizing: causing the formation of ions, particularly in a gaseous medium by the action of an electrical discharge.

isometric: referring to equal and opposite forces acting on a body, which cause no motion of the body until an imbalance in the relative magnitude of such forces occurs.

joule (J): (nt-m) [also, kg-m²/sec²] the unit of *work* or energy in MKS units, equal to a force of 1 newton (nt) acting through a distance of 1 meter. One joule is also equal to 1×10^7 ergs (the unit of energy in the cgs system).

Kerr metric space warp: a type of spatial *anomaly* which may be produced by a rotating black hole. New Zealand mathematician Roy Kerr derived a set of solutions to Einstein's Field Equations which presented a more realistic description of black holes than the static Schwarzschild solution (see *Einstein-Rosen bridge* above), by assuming that the star from which the black hole formed must have a finite rotation that the hole would inherit. Such a black hole would collapse to a modified *annular* singularity, which still requires the presence of a wormhole, but in this case it is theoretically possible to enter such a space warp *intact* on a certain trajectory which cuts across the plane of rotation. Since a *metric* is essentially any formula yielding the distance between two points in a given spatial frame of reference, a Kerr metric space warp is then one in which it is actually possible to calculate the length that the wormhole must have if a starship's velocity through it is still limited to a value less than that of light.

kilogram (kg): the unit of mass in the MKS system of units, equal to 2.2046 pounds (lbs) or 1,000 grams.



**A Brief Introduction to the
Kerr Metric Space Warp**

(as extracted from the Glossary of *StarDrive Engineering*)

German physicist Karl Schwarzschild found a solution to Einstein's field equations in 1916 which, roughly speaking, describes the space-time in which a black hole resides. But this solution is strictly valid only for "static" black holes having zero spin (angular momentum) and zero net electrical charge.

An *Einstein-Rosen bridge* is a type of space warp or "wormhole" produced by a static black hole, which is thought to connect the hole with another (and perhaps remote) position in space-time *via an alternate continuum or set of dimensions* and which is a phenomenon that was found to be necessary to preserve the internal consistency of the Schwarzschild solution. A starship cannot traverse an E-R bridge, however, because the black hole *contains a point-like singularity*.

A *Kerr metric space warp* is a type of spatial anomaly which may be produced by a rotating black hole. New Zealand mathematician Roy Kerr derived a set of solutions to Einstein's field equations that presented a much more realistic picture of black hole space-time than the static Schwarzschild solution, by assuming that the star from which the black hole formed must have a finite rotation that the hole would inherit.

Such a black hole would collapse to a modified *annular* (ring) singularity which still requires the presence of a wormhole, but in this case it is theoretically possible to enter such a space warp *intact* on a certain trajectory that cuts across the plane of the black hole's rotation. Since a *metric* is essentially any formula yielding the distance between two points in a given spatial frame of reference, a Kerr metric space warp is then one in which it is actually possible to calculate the foreshortened length the wormhole must have if a starship's velocity through it is still properly limited to a value less than that of light.

- kinetic occlusion:** the maintenance of a virtual vacuum within the Field envelope of a StarDrive device, by means of the extremely energetic collisions of the Field current electrons with the gas molecules in the atmosphere.
- kwh:** kilowatt-hour; a unit of electrical power in the MKS system, equal to the total *work* done or energy transferred at the rate of 1,000 watts for one hour.
- leakage, electric:** refers to the gradual loss of electrical charge from a charged object, or more specifically to the undesirable passage of electrons across the *dielectric* in a capacitor.
- MKS [units]:** the *meter, kilogram, second* system of physical measurement which is now used by international agreement in solving almost all types of scientific problems. This *metric system* was developed in France in the late 19th century, and is referred to as the *Système International* or *SI* (after the French). Also, see *prefixes* below.
- meter (m):** standard unit of length or distance in the MKS system of units, defined in 1983 as the length of the path traveled by light in a vacuum during 1/299,792,458 of a second.
- mole:** (short for molecular weight) the quantity of any substance having a weight in *grams* equal to its molecular weight. The actual number of molecules in a mole of any substance is equal to *Avagadro's constant* (6.022×10^{23}).
- moment of inertia (I):** a measure of the ability to produce rotation of a body about an axis thereof, typically about the axis of symmetry of a uniformly distributed mass (such as a cylinder or disk). An object's moment of inertia is proportional to the product of the mass of the object and the square of the distance over which its mass is distributed, in kg-m^2 . Moment of inertia, angular acceleration (α), and *torque* (τ) are related by the following formula (analogous to $F = ma$): $\tau = I\alpha$.
- moment, magnetic:** the tendency of a magnetic dipolar object to align itself to an external magnetic field, the measure of which is a vector quantity that is a function of the strength and orientation of the magnetic field produced by the object. The electron magnetic moment is quantized, meaning that it may only assume discrete angles with respect to such an external field. The observed magnetic moment of the electron is slightly larger than the theoretical value obtained by Neils Bohr (the Bohr magneton), yielding a *magnetic moment anomaly* which is believed to be related to the electron's continuous interaction with photonic radiation. [See *constants* above.]
- momentum (mv):** the product of an object's mass and its velocity with respect to its inertial frame of reference, measured in kg-m/sec . A change in momentum is always equal to the *impulse* which produced it; conversely, the momentum is also equal to the impulse which must be applied to reduce the object's velocity to zero.
- newton (nt):** (kg-m/sec^2) the unit of force in the MKS system; the amount of force which must be applied to a mass of one kilogram to give that mass an acceleration of one meter/second/second.
- nodal point:** those periodic points in any transverse wave motion where the displacement from the mean or equilibrium value is zero. In the typical graph of a sine curve, these points occur at 0° , 180° , and 360° . Also, any point in a vibrating body or system where the net oscillatory motion is zero.
- no-work force, electron:** the theoretical means by which an electron is able to absorb quanta of photonic radiation *as necessary* when it is forced to continuously output energy by electric or magnetic induction, to prevent its destabilization (and decay). Since a photon has a mass equivalence, the electron is presumed to exert a variable force which accelerates photons through some finite distance to accomplish their absorption. Thus, the electron itself does work to absorb the energy it loses when its angular momentum is properly tapped for output energy, thereby explaining how an *over-unity* device may output more energy than the apparent *outside* work it requires for input. This concept (which might more accurately be called *electron virtual work force*) was developed by magnetic engineer John Ecklin, and is believed to be related to the *electron magnetic moment anomaly*.
- over-unity:** denotes an artificial system or device whose output power is greater than its *apparent* input power (or that attributable to obvious or "normal" sources), and whose efficiency at converting input energy into output energy may therefore be thought of as exceeding 100%. The electron itself, while technically not a *perpetual motion machine*, is capable of continuous energy output without self-decay; it replaces the energy "lost" as necessary via the absorption of photonic radiation. Therefore, it is presumed that any practical over-unity device must take advantage of this capability, generally by electromagnetic induction means, and that the construction and operation of such devices is therefore possible. The Electrodynamic Field Generator is an over-unity device.
- ozone:** an unstable form of oxygen (O_3) which has a pungent smell and is produced by electrical discharges.
- permittivity, electric (ϵ):** ($\text{coul}^2/\text{nt-m}^2$) the ease with which a medium or material carries electric lines of force. All material substances have a higher permittivity than vacuum, whose permittivity $\epsilon_0 = 8.854 \times 10^{-12} \text{ coul}^2/\text{nt-m}^2$.
- perpetual motion [machine]:** an obsolete and often misinterpreted concept which supposes the existence of an as-yet undiscovered type of system or device which, once activated, would somehow be able to perform work indefinitely without any external energy input. Such a machine is undeniably precluded by the laws of thermodynamics.
- Planck's constant (h):** a universal constant discovered by German physicist Max Planck in 1900 as a result of radiant energy emissions studies. The discovery that radiant energy must be emitted and absorbed in miniscule discrete bits became the cornerstone of *quantum* theory. The Planck hypothesis states that the energy (in *joules*) of each wave-equivalent particle or photon of light is equal to the *frequency* of that light times a certain tiny constant h with the value $6.626 \times 10^{-34} \text{ J-sec}$: $E = hf$. A corollary to this concept is that the wavelength λ of light must be equal to h divided by the equivalent photon momentum mv . Since $E = mc^2$, this yields the expression $\lambda = hc/E$.

- polarity, electric:** having either a positive or negative charge with respect to a neutral object which exhibits no external electrostatic field. The protons in the nucleus of the atoms comprising all ordinary matter have a positive charge, and the electrons which orbit those nuclei have a negative charge. However, atoms which are electrically neutral overall, having equal numbers of protons and electrons, may combine to form molecules which exhibit electric polarity (or a dipole moment) in that one end of the molecule may be slightly positive and the other slightly negative due to a non-uniform distribution of charge.
- potential difference:** the difference in voltage between two points in an electric field or electrical circuit.
- potential, electric:** the voltage at any point in an electric field or circuit as measured with respect to *ground*.
- power:** the time rate of doing work or transferring energy in *watts*, equal to the amount of work or energy in *joules* divided by the elapsed time in seconds. One horsepower is equivalent to 746 watts (J/sec).
- prefixes, unit [metric system]:** a Greek or Latin word root which may be attached to a metric system basic unit of measure to raise or lower the unit's value by factors of 10. A condensed listing of these prefixes is as follows: to raise *u*, kilo (k) = $u \times 10^3$, mega (M) = $u \times 10^6$, giga (G) = $u \times 10^9$, tera (T) = $u \times 10^{12}$, peta (P) = $u \times 10^{15}$; and to lower *u*, centi (c) = $u \times 10^{-2}$, milli (m) = $u \times 10^{-3}$, micro (μ) = $u \times 10^{-6}$, nano (n) = $u \times 10^{-9}$, pico (p) = $u \times 10^{-12}$.
- propagation:** specifically, the act of transmitting energy or a change in field potential from one place to another.
- quantum:** (*pl.* quanta) smallest indivisible unit of matter or energy, exhibiting both particle and wave attributes.
- quantized:** any observable entity or quantity which is limited to a multiple of elementary or fundamental units, as expressed in *quantum* theory. It is generally accepted that energy, mass, space, and possibly even time itself are comprised of certain indivisible units or quanta and thus are quantized.
- quantum potential:** the absolute energy level at a given point in *space-time* or *negative quantum time-space*, with "point" in this case being defined not as the mathematical zero-volume/zero-area abstraction but as a smallest possible spatial unit of energy containment which has a circular planar area but zero volume.
- quasi-coherent:** specifically, denoting a flow of electron current in a real or virtual vacuum which exhibits attributes of coherence normally associated with current flow inside a uniform conductor and with laser light. In a StarDrive device's Field envelope current, the combination of uniform ultra-high field intensity, AC voltage component(s), and partial magnetic polarization causes that current to be much less chaotic and more unitized or "in-phase" than an ordinary arc discharge.
- radian:** a unit of angular measurement, representing roughly 57.3° , that is equal to the number of degrees between two radii of a circle which mark off an arc whose length is also equal to the circle's radius. Since an angle is the ratio of two lengths in radian measure, it becomes a dimensionless (pure) number which doesn't usually appear in the algebraic translation of units.
- refractory:** resistant to heat; difficult to melt or work. Tungsten and molybdenum are refractory metals.
- relativistic:** in general, having to do with the relative (non-absolute) nature of mass and time, and of all velocities except that of light; specifically, denoting the interdependence of time, space, and energy such that properties associated with mass begin to markedly deviate from classically-computed (Newtonian) values at velocities approaching that of light. Relativity theory was developed by H. A. Lorentz and Albert Einstein.
- resistivity:** a property of all normal solid conductors of electrical current, whereby the constant collisions of each current electron with the atoms in the conductor cause that conductor to exhibit the phenomenon of electrical resistance. Each substance's resistivity is therefore dependent on its atomic structure, and is usually specified in ohm-cm as a result of a direct measurement of resistance across a one cubic centimeter cube thereof at 20°C .
- roentgens:** a cgs system unit for measuring the quantity of ionizing radiation (in the form of X-rays or gamma rays), equivalent to that which will produce $1/(3 \times 10^9)$ coulomb of charge in one cubic centimeter of dry air at STP.
- sinter:** specifically, to form a shaped solid mass from particles of a mixture of metals by the application of high pressure and heat below the melting points of the constituents. A sintered composite is technically not an alloy.
- specific gravity:** usually defined as the ratio of the weight or mass of one cubic centimeter (1 cc) of a substance to that of 1 cc of water. As it turns out, 1 cc of water at 4°C weighs exactly 1 g (gram), so that specific gravity is actually a measure of the relative density (or mass per unit volume) of all substances including gases.
- specific heat:** generally, the ratio of the amount of heat required to raise the temperature of one gram (1 g) of a substance by 1°C to that required to raise the temperature of 1 g of water by 1°C . Also, the amount of heat required to raise the temperature of 1 g of any substance by 1°C , in calories, with 1 calorie equal to 4.186 J (*joules*).
- spin:** denotes the rotational angular momentum of a mass body or particle, which is *quantized* at the subatomic level. The angular momentum L of a macroscopic body is equal to its *moment of inertia* I times its angular velocity ω in *radians* per second: $L = I\omega$.
- standing wave:** a continuous wave motion between fixed end points, yielding no net transportation of energy. The structure of the atom may be explained by analogy to a system of standing waves in quantum mechanics.
- STP:** standard temperature and pressure: designated as 760 mm of mercury (14.69 lbs/in²) at 0°C .
- superstrings:** the current most popular candidate for a "theory of everything" that is somewhat different in concept than a *unified field theory*, but which likewise endeavors to resolve the mathematical incompatibility of quantum mechanics and general relativity. In superstring theory, all matter, energy, and force is thought to be comprised of

nearly infinitesimal lines of quantum potential which exhibit a variable but tremendous level of inherent tension. The observed spectrum of elementary particles in the Standard Model would then correspond to different quantized states of oscillation of 'closed' strings and fields of force would correspond to 'open strings' which connect the various particle/closed-strings. However, such string theories have to date been unable to eliminate all undesirable infinities and maintain internal consistency unless space-time is comprised of a total of ten dimensions. It can be seen that the dual continuum cosmological model outlined in the text is in essence a modified superstring theory, which might yield a complete logical model of the universe if it is able to accomplish the unification of all forces in such a way that *why* the universe behaves the way it does is explained (therefore making valid test predictions possible). In principle, this unification may be achievable if the *rate of change in tension per change in radius* in each of the particle-, photon-, and force-carrying types of strings (loops) is described by simple algebraic means.

terawatt: equal to one trillion (1×10^{12}) *watts* of power. A terawatt is equivalent to one million megawatts.

thermodynamics: the branch of physics or engineering that deals with the transformation of heat into other forms of energy, particularly mechanical energy, as well as the laws which govern energy conversion. While most such processes are reversible, some are not. The principles of thermodynamics were originally developed to describe the gross physical properties of matter and energy at the *macroscopic* level, such as temperature, pressure, volume, and density. However, the statistical methods of *quantum* mechanics allow averages of mechanical variables like momentum to be assessed at the molecular level. This gave rise to thermodynamic variables such as *specific heat* and thermal expansion coefficient. It is now known that temperature represents a measure of the average kinetic energy of the particles comprising any physical system, and that this kinetic energy corresponds to heat. There are four (4) laws of thermodynamics which govern the processes whereby macroscopic systems such as matter move from one state of equilibrium to another: the zeroth law states that when each of two systems is in equilibrium with a third, the first two systems are not mutually isolated and must come into equilibrium with each other. This yields the precise definition of *temperature* as the property which reflects this equilibrium; the first law gives the precise definition of *heat* as a form of energy which can be stored or converted into mechanical work but which is not a material substance which can be created or destroyed, and is therefore also known as the law of energy conservation; the second law defines entropy as a measure of how close any isolated system is to a state of equilibrium, or alternatively as a measure of the total disorder of the system. The entropy of an isolated system can never decrease, and heat cannot be transferred from a colder environment to a warmer one in the absence of work. A corollary to this statement is that any *heat engine* or device for converting heat to mechanical work must be less than 100% efficient. [This corollary is often misconstrued to include devices which merely convert one or more types of force to another. The StarDrive device actually functions as it does by converting a combination of magnetic force and the interatomic force (inside a charged conductor) to electric field force, in a way that produces thermal energy.]; and the third law states that absolute zero is the thermodynamic equivalent of the speed of light in that it can be approached arbitrarily closely but never equaled.

time dilation: a confirmed relativistic effect demonstrating that time is not a physical constant but is either dilated or slowed-down (in the subjective reference frame) or expanded or speeded-up (in the objective frame of reference) as either a mass body's velocity or its mass increases. Both gravimetric and velocity time dilation were confirmed by the 1970's, the latter using atomic clocks and airplanes flying in opposite directions. Supralight velocity requires that an alternate and intensified scale of relativistic time dilation be applicable during any 'warp jump'.

toroid: see *hemitoroidal* above.

torque (τ): the rotational moment exerted by a force acting at a distance upon a body, equal to the force multiplied by the perpendicular distance between the force's line of action and the center of rotation at which it is exerted. Since torque is measured in nt-m (newton-meters), it is equivalent to *work* or energy in joules (J).

unified field theory: any theory which would unify all four forces that are known to jointly control all of the observed interactions in matter - the strong and weak nuclear forces, electromagnetism, and gravity - and to do so using only a small set of the simplest possible mathematical relationships. Einstein, one of the first and foremost theoretical physicists to unsuccessfully attempt the derivation of such a theory, believed that all physical phenomena should be a function of a fundamental grand design wherein both matter and force could be represented in terms of fields only. It is hoped that someday a grand unified field theory may be developed based on the *dual continuum* cosmology presented in the text (or a variant thereof), wherein the Standard Model may be completed and corroborated mathematically using a simple analytical technique that renders all matter, energy, and force relationships equally valid from any applicable combination of wave, field, and particle-exchange perspectives.

watt (W): (J/sec) the standard MKS unit for power in any form, but particularly with respect to electricity. One watt is equal to one joule per second or to the product of voltage and amperage in an electrical circuit.

wave: an oscillatory disturbance, either transverse or longitudinal, whereby energy is transmitted progressively through a medium without the transference of matter itself.

work: the amount of energy expended or transferred when an applied force accelerates a mass body, the work done being the product of the magnitude of the force and the distance through which the object is moved. Thus, the work done by a force acting on a body is equal to the gravitational potential or kinetic energy gained by the object.

LANGUAGE & SEMANTICS:

- adroit:** clever, expert, or skillful in a creative capacity or difficult situation.
- aficionado:** a devoted and informed follower of a particular doctrine, art form, sport, etc.
- ambient:** having to do with or arising of conditions in a local environment.
- annular:** in the fashion of a ring; generally described as having a shape which is planar, circular, and hollow.
- anomaly:** one or more conditions or properties which appear contrary to convention or to normal rules.
- antipodes:** any two points which are directly opposite each other on the surface of a spherical object.
- apex:** the tip or highest point; a peak or vertex.
- apocrypha:** any collection of stories or written journal which is of dubious or spurious origin or authenticity.
- arcane:** denoting perilous knowledge not shared with others out of concern for their well-being.
- axiom:** a self-evident proposition, or statement which is universally accepted because its truth is obvious.
- coincident:** specifically, to take up exactly the same space or volume at the same time; *bosons* may be coincident.
- concomitant:** an event, object, or condition which accompanies or is attendant to another.
- deductive:** reasoning from a given premise to a logical conclusion, or from a general principle to specific facts.
- duplex:** having a twofold nature; specifically, capable of two modes of operation at the same time (as in telegraphy).
- empirical:** based largely on experiment and observation rather than a specific theory.
- esoteric:** intended for or understood by only a select few; beyond the level of knowledge of most people.
- ethos:** the distinguishing nature, character, mood, and/or attitude of persons or events.
- fuselage:** the main body of an airplane or aerospace vessel (not including wings, engines, or tail assembly).
- inductive:** reasoning from separate facts to a general principle. Also, having to do with the property of *inductance*.
- inherent:** innate, or existing within a thing (or person) as a natural and inseparable quality or characteristic.
- macroscopic:** denoting a large object, group, or system; visible with the naked eye, as opposed to microscopic.
- magnum opus:** the greatest work or largest undertaking of a writer, artist, scientist, etc.
- marginal:** close to a lower limit; or, near an outer boundary. As used in the text, may have either given meaning.
- nominal:** close to an expected or probable value or condition; may also designate an assigned interim value.
- obfuscate:** to obscure, confuse, or make unclear.
- objective:** referring to the reference frame from which a *relativistic* frame of reference originated, or to a condition or property of an object or event in the reference frame of origin.
- prosaic:** matter-of-fact; commonplace or ordinary.
- proximal:** positioned nearest or next to in spatial relationship.
- quasi:** in a general sense or manner of speaking; seemingly, or in part.
- savoir-faire:** knowledge or intuition as to the proper course of action and how best to accomplish it.
- seminal:** like or as a simple or initial stage of development; like or as an early and influential example of basic form.
- subjective:** referring to a particular *relativistic* frame of reference, or to a condition or property of an object or event in that relativistic reference frame.
- synchronous:** to exist, occur, or move at the same time or rate; having the same *frequency* and *phase*, as in waves.
- vignette:** specifically, a brief literary sketch, sometimes used to set the tone of a chapter or section of a book.

MAGNETICS:

- armature:** the *soft ferromagnetic* rotor or rotating central mass in an electric motor, which may be wound (with one or more electrical coils) or unwound. Also, a stationary wound ferromagnetic element that is not incorporated in an electric motor, as in an electromagnet; or the linearly-actuating unwound *core* of a *solenoid*.
- coercivity:** the property of a permanent magnet responsible for its ability to resist demagnetization. In general, the easier it is to magnetize a material, the easier that material can be demagnetized. The *normal coercive force* (H_c) is the field intensity in *oersteds* (Oe) which is required to reduce a saturated magnet's field intensity to zero. Thus, for example, an Alnico 5 magnet can achieve a *residual induction* of 12,400 gauss. The field intensity required to *saturate* the magnet is 3,000 Oe, but that required to fully demagnetize it is only 640 Oe; its coercivity has a lower middle rating of "good". By comparison, Ferrite 5 can achieve a residual induction of only 3,850 gauss. However, the field intensity required to saturate the magnet is 10,000 Oe, and that required to fully demagnetize it is 2,200 Oe; its coercivity has the highest possible rating as "outstanding".
- core:** the form or material upon which an electrical coil is wound, which may or may not be magnetizable. In certain instances, it is more appropriate to call a coil core an *armature*, as above.
- counterflux wafer:** a small disk or tile of a permanent magnetic material having a high *coercivity*, which is used to produce a magnetic field which opposes the *leakage flux* of a primary magnetic element and increase its efficiency.
- coupling, magnetic:** the dynamic linking of two magnetic objects or components solely by the magnetic fields they produce. The primary and secondary coils in a transformer are magnetically coupled while having no direct electrical connection, and are thereby each caused to exhibit an increased level of circuit *inductance*.

- curie point:** the temperature above which a permanent magnet material begins rapidly losing its residual induction.
- degauss:** to demagnetize a material which has acquired a *residual induction*, generally using a current-carrying coil.
- diamagnetic:** having the property of being repelled by either pole of a magnet. When placed in a magnetic field, diamagnetic materials exhibit a *magnetic moment* (see *General Physics*) which opposes the applied field and causes their major axis to align perpendicular to the field. This is now known to result from induced micro-currents at the atomic or molecular level. Many organic compounds are diamagnetic, such as benzene and liquid oxygen. Bismuth, the heaviest non-radioactive metal, is one of the most diamagnetic substances known.
- energy product:** a measure of the greatest energy capability per unit volume of a magnetic material, as plotted in that material's demagnetization curve graph. The magnetic energy product is obtained by multiplying the net or *load-line* flux density (B) produced in a permanent magnet by the corresponding value for the *field intensity* (H) in that magnetic material's demagnetization curve graph (from the manufacturer). This will typically yield an energy product in the millions of gauss-oersteds [e.g., 4.95×10^6 MGO for Alnico NC1 at a load-line of 16.5, where net flux density $B = 9,000$ gauss and the *coercive* force is 550 oersteds (as seen in the graph on pg. A4).]
- ferromagnetic:** denoting any material which, like iron, is strongly attracted to or may become a magnet, including those which exhibit a *residual induction* after an applied magnetic field is reduced to zero. Such substances also exhibit a *magnetic moment* which aids the applied field and causes their major axis to align parallel to that field. A soft ferromagnetic material loses most or all of its induced magnetism when the magnetizing force is removed; a hard ferromagnetic material retains most of its induced magnetism and thus exhibits a high residual induction.
- field, uniform:** a magnetic field in which the *flux density* is essentially constant over most of the length of the field's axis. This is the type of field produced in the flux gap of a ring magnet whose pole faces are plane-parallel. In a non-uniform field, the flux density varies from place to place and has no well-defined major axis.
- flux:** unit lines of force which form closed loops of magnetic "flow", as used to describe a magnetic field since the concept was conceived by Faraday in the early 19th century. The traditional defined properties of magnetic flux lines are as follows: (a) flux lines always follow the path of least *reluctance* ('resistance'), like an electric current; (b) flux lines repel each other if they flow the same direction; (c) flux lines never cross, and generally follow the shortest curved paths; and (d) flux lines must enter and leave a ferromagnetic surface at right angles.
- flux density:** the number of unit lines of *flux* required to depict the strength of a magnetic field per unit planar area. Flux density may be given in *webers/meter-squared* (Wb/m^2) or in *tesla* (T) in MKS units, or in *gauss* in cgs units. One gauss is equal to 1 flux line per cm^2 , and one tesla is equivalent to 10,000 gauss.
- fringing:** the "spreading" of *flux* produced in the air gap of a magnet or magnetic circuit, which causes a portion thereof to bypass the 'load' and reduce the operating efficiency of that magnet or circuit. This phenomenon is a direct result of the defined properties of magnetic flux (above).
- gauss (G):** (mx/cm^2) the unit of magnetic *flux density* in the cgs system, in *maxwells/centimeter-squared*. 1 gauss is equal to 1 flux line per cm^2 , and powerful permanent or electromagnets can produce fields in excess of 10,000 G.
- induction, residual:** the amount of magnetic *flux* remaining in a material when the applied magnetizing force is reduced to zero. Magnet manufacturers specify residual induction after *saturating* a closed ring of a given product.
- leakage:** that portion of the total magnetic *flux* produced by a magnet or magnetic circuit which exists outside the working flux gap; the gross magnetic loss, including *fringing* effects. To illustrate, the net leakage of a closed magnetic ring is quite low around its outer perimeter but is fairly high across its open center. A leakage factor (σ) is used in magnetic circuit design to compensate for losses. In essence, this leakage factor is the ratio of the total flux produced at a magnet's neutral axis to the net useful flux in the air gap. The leakage factor is also the ratio of the circuit's total *permeance* to that of the air gap: $\sigma = P/P_g$.
- load-line, magnetic:** any of a number of lines which may be drawn across the demagnetization graph of a magnetic material to show the relationship between *residual induction* and *coercivity* under circuit operating conditions. This load-line is the ratio of the *flux density* B produced in the magnet to the *field intensity* H which will cause it to be completely demagnetized from that level of flux density. The load-line achieved in a given magnet or magnetic circuit is dependent on the magnet's physical configuration, being the product of the total *permeance* of the magnet or circuit times the ratio of the magnet's length to its pole cross-sectional area: $B/H = P(L_m/A_m)$.
- magneto:** specifically, a simple high-voltage dc generator or dynamo with permanent magnet fields, for producing small arc discharges in an automobile ignition system.
- maxwell (mx):** the unit name given to a single magnetic flux line. Named for British physicist James C. Maxwell.
- oersted (Oe):** the unit of magnetic field intensity in the cgs system. A field which acts on a *unit magnetic pole* with a force of one *dyne* from a distance of one centimeter in a vacuum has an intensity of 1 oersted.
- orientation:** the forced alignment of the random atomic clusters or "domains" in a ferromagnetic material which are responsible for its magnetic properties, by heat treatment, cold-working, curing in a magnetic field, or a combination of such methods. An oriented material is anisotropic, having greatly enhanced magnetic properties in the direction of orientation, and substantially reduced properties in other directions.
- paramagnetic:** denoting a material which is only weakly magnetic or difficult to magnetize, such as platinum. Paramagnetic materials have a *relative permeability* which is only modestly greater than unity (or that of vacuum).

- permeability, absolute (μ ; μ_0):** the ratio of the flux density (B) produced in a magnetized *core* material to the field intensity or magnetizing force (H) producing it, in MKS units. Thus, $\mu = B/H$. The absolute permeability of *vacuum* (μ_0) [see *constants*]. Permeability is a dynamic property which must be rated at a specific level of induced *flux density*.
- permeability, relative (k_μ):** the ratio of the absolute permeability μ of a magnetized material to the absolute permeability of vacuum (μ_0) [see *constants*]; exactly analogous to dielectric constant k . Hence, $k_\mu = \mu/\mu_0$; and $\mu = k_\mu(\mu_0)$. Permeability, absolute or relative, is a dynamic property which must be rated at a specific level of induced *flux density*. However, k_μ for each material is generally determined by graphic analysis of experimental test data plotted in *cgs units*, wherein field intensity H is in *oersteds* and flux density B is in *gauss*. Then, the dimensionless scalar 'multiplier' k_μ may be found directly using formula M3 from DataSheet #16 ($\mu_{cgs} = k_\mu = B/H$), but is equally valid in MKS unit calculations (see pg. 209).
- permeance (P):** a measure of the relative ease with which a material passes or carries magnetic *flux*; the reciprocal of *reluctance*. The total flux Φ in webers equals the magnetomotive force F in amps times permeance P: $\Phi = FP$, where P may be expressed in webers/ampere (Wb/amp).
- polarity, fixed:** referring to the type of magnetic field which is axially oriented and of *uniform field intensity* across much of its axial length, as in that produced between two opposite plane-parallel poles which are closely spaced or that inside the coil windings of an electromagnet or *solenoid*.
- polarize(d):** having a temporary or permanent magnetic field which exhibits a strong *fixed polarity* and which has corresponding and distinct localized 'north' and 'south' magnetic *poles* (like the earth itself). Such magnetic poles are exactly analogous to the two opposite types of electric charge known as 'positive' and 'negative'.
- polar tendency, unfixed:** referring to the type of magnetic field which is radially oriented and which does not have fixed axial poles (like a bar magnet). Such a field is produced around a straight current-carrying electrical conductor, and its direction or polarity is everywhere perpendicular to the axis of the conductor; whereas a bar magnet produces an axial field which has a fixed polarity the direction of which is parallel to its length.
- pole:** in general, either of two areas on the surface of a magnet or at the end of a wound current-carrying coil where the magnetic *flux* has the greatest *density*. Closed loops or lines of magnetic force are usually thought of as emanating out of the 'north' pole and through space into the 'south'.
- reductor:** a *soft ferromagnetic* component in a magnetic circuit or wound *armature* which is designed to limit the passage of a magnetic field to a certain *flux density*, based on the point at which that component will *saturate*.
- reluctance:** a measure of the resistance in a magnet or magnetic circuit to the passage of *flux*, and exactly analogous to resistance in an electrical circuit. Also, the reciprocal of *permeance*, whereby the total flux Φ in webers equals the magnetomotive force F in amps divided by reluctance R: $\Phi = F/R$, where R is in amperes/weber (amp/Wb).
- retentivity:** the property whereby a ferromagnetic material acquires a permanent or *residual induction*.
- saturation:** the condition of maximum possible magnetic *flux density* in a given material, beyond which no increase in applied magnetizing force will produce any higher level of induction.
- solenoid:** an electromagnet whose length is substantially greater than its turns radius, and which often has a *ferromagnetic core* element which is free to move axially in response to the field produced by the coil winding.
- tesla (T):** (Wb/m²), [also, nt/amp-m] the unit of magnetic flux density in the MKS system, equivalent to 1×10^4 *maxwells* per meter-squared (mx/m²). A typical laboratory electromagnet can produce a field of about this strength.
- unit magnetic pole:** any very small magnetic pole which will be acted upon by a force of one *dyne* by an identical (like) pole one centimeter away in vacuum.
- weber (Wb):** (nt-m/amp), [also, J-sec/coul] the unit of magnetic flux quantity in the MKS system, equal to 1×10^8 *maxwells* or unit lines of force.

MATHEMATICS:

- algorithm:** any special method of solving a certain type of problem, used in particular to describe individual groups of complex or repetitive computations which must be performed in a particular order to solve a larger problem.
- asymptotic:** strictly speaking, this term describes a straight line which approaches but never meets an adjacent curve (and is therefore tangent to that curve at infinity); as used in this book, this term is taken to represent the obverse of this relationship, whereby the mass of an object moving at *relativistic* velocity increases on a curve whose slope begins to rapidly approach infinity on the vertical axis of a graph of mass vs. speed.
- connection:** an analytical tool which simplifies the measurement and description of multiple curves in higher-dimensional space; related to geometric *number theory* for finding rational solutions in the study of *quadratic* forms on lattices, such as a uniform distribution of rings or spheres.
- discriminant:** the value computed according to a simple algebraic parameter of a *quadratic equation* which reveals whether the two solutions or 'roots' of that equation are real or imaginary. The typical 2nd degree polynomial has a discriminant, equal to $b^2 - 4ac$, which: (a) is greater than 0 if the roots are real and unequal; (b) equal to 0 if the roots are real and equal; and (c) less than zero if the roots are conjugate imaginary numbers.

- frame field**: an analytical tool from the arithmetic of function fields, dealing with the differential geometry of curves in three dimensions at a limited number of points (or over a finite field). A curve in 3 dimensions is studied by assigning each point a *frame* consisting of 3 orthogonal (mutually-perpendicular) unit vectors. The use of changes of these vectors along the curve may then be expressed according to a certain set of equations (called *Frenet formulas*) and constitutes a description of the curve in "moving" frames.
- geodesic [curve]**: having to do with the shortest distance between two points on a surface, particularly when that surface may be curved, or with the mathematics required for its calculation.
- logarithmic**: specifically, describing the nature of a graph wherein one axis is in linearly-scaled units and another is scaled according to successive integer powers of a unit. A logarithm is the power or exponent to which a given number (or *base*) must be raised to yield a specific reference number (or *antilogarithm*); e.g., $\log_{10}(100) = 2$. The use of logarithms greatly facilitates certain types of computations, given the necessary logarithmic tables. The four fundamental operations with logarithms are as follows: L1. $\log xy = \log x + \log y$; L2. $\log x/y = \log x - \log y$; L3. $\log x^n = n \log x$; L4. $\log \sqrt[n]{x} = (\log x)/n$.
- normal**: in general, meaning perpendicular to the surface. By definition, the normal to the curve $y = f(x)$ at any point $P(x,y)$, is the line perpendicular to the curve's tangent at that point.
- number theory**: specifically, elementary number theory is concerned with the mathematical operation of division, and therefore the Euclidean *algorithm* (or greatest common divisor theorem), the elementary properties of prime numbers and congruencies, Fermat's theorem, and Euler's theorem. Related subjects which are addressed in basic number theory, such as the solution of sets of linear congruence equations or single binary *quadratic* equations, have been used as models in developing sophisticated mathematical tools in other fields.
- quadratic [equation]**: a quadratic equation in one variable is a second degree polynomial expression in algebra, having the general form $ax^2 + bx + c = 0$, which will have a pair of solutions for x that may either be real or imaginary depending on the value of the equation's *discriminant*. In this case, $x = [-b \pm (b^2 - 4ac)^{1/2}]/2a$.
- scalar**: having magnitude in quantity but no specific direction in space, as opposed to *vector*. For instance, the ratio of two lengths is a scalar quantity. The product of two vectors, where the units have cancelled, can also be scalar.
- topology**: the mathematical discipline which studies those properties of space-time which remain unchanged despite any degree of spatial distortion, provided that distortion tears no surface. The concept of "mirror manifolds" can be used to show that coincident continuums will support trans-light velocity, which must cause the topology of the universe to change, in such a way that no significant changes in physical law are entailed *provided* the topological tear in space-time takes the form of the subjective relativistic time expansion discussed in the text.
- vector**: a physical quantity with both magnitude and specific direction, like force or velocity, as opposed to *scalar*.

MECHANICS:

- axial**: parallel with the axis of rotation or symmetry, or with the major longitudinal dimension.
- compressive strength**: the resistance of a material to a decrease in volume as a result of applied pressure.
- dynamic braking**: specifically, the use of permanent magnet dynamoelectric motor-generator units to alternatively produce electrical output when the available torque exceeds the mechanical load. A diesel-electric train's drive units apply a productive counter-torque when descending a grade, due to the magnetic load in generating a current.
- dynamo**: any device for converting input rotary torque to electrical energy, especially high voltage dc power output.
- flexural strength**: the resistance of a material to deformation as the result of a combination of *tensile* and compressive forces, such as those which produce bending or torsion (twisting); often measured in PSI, or lbs/in².
- horsepower**: a British/American unit of mechanical power equal to 550 ft-lbs. of kinetic energy or torque per second, or to 746 *watts* (J/sec) in MKS system units.
- planar**: lying in one plane; denoting a region of a surface within which the net curvature is or approaches zero.
- radial**: extending outward in all directions from a central point or axis. A purely radial field is one which is everywhere perpendicular to the surface of a sphere; the magnetic field around a unit pole is considered radial.
- tensile strength**: the resistance of a material to a linear pulling force or tension that would tend to tear it apart. In general, materials with a very fine and uniform crystalline structure have high tensile strengths, and those with coarse non-homogenous structure have low tensile strengths. Tensile strength is often measured in PSI, or lbs/in².
- thermal expansion coefficient (α)**: a factor which relates the change in linear dimension (ΔL) of a solid to a change in temperature (ΔT): $\Delta L = \alpha L_0 \Delta T$ where L_0 is the original length. Generally given in millionths ($\times 10^{-6}$) per °C.
- thermal conductivity (k_t)**: a proportionality factor which defines the rate at which a material transfers heat across a given contact area (A) and temperature differential (ΔT), as established by direct experimentation. By the Fourier equation: $\Delta Q/\Delta t = -k_t A (\Delta^{\circ}K/\Delta x)$, where ΔQ is the thermal energy conducted (in *joules*), Δx is the thickness of cross section, and k_t is in W/m²·K. Values for k_t range from single digits for ceramics into the hundreds for metals.
- Young's modulus**: also called tensile elastic modulus; the ratio of stress (σ) to strain (ϵ) in a material to which a stretching force (F) is applied. Since stress is the ratio of force to cross-sectional area (A), and strain is the ratio of length increase (Δl) to original length (L_0), the elastic modulus $Y = \sigma/\epsilon = FL_0/A\Delta l$.

Table of Illustrations

	<i>page no.:</i>
<i>acknowl.:</i> StarDrive vessel hull & field w/electric and magnetic field vectors	vi Δ ✓
Chapter 1 }	
Chapter 2 } Fig. 1: side view of 'Eridani' hull design	9 ✓
Fig. 2: side view of 'Pleiades' hull design	10 ✓
Chapter 3 } Fig. 3: Faraday's disk dynamo	20
Fig. 4: triode vacuum tube and basic circuit diagram	22
Fig. 5: primary and rotating electrode arrays	24
Chapter 4 } Fig. 6: a purported Searl levity disc rotor assembly	34
Fig. 7: simplified Primary Power System diagram	39
Chapter 5 } Fig. 8: axial & radial magnetic fields	47
Fig. 9: secondary rotor magnetic field & 'field piece' induction	49 ✓
Chapter 6 } Fig. 10: schematic cross section of the design hull configuration	62
Fig. 11: idealized field envelope configuration	65
Chapter 7 } Fig. 12: simplified Primary Power System electrode array schematic	76
Fig. 13: idealized resistance-coupled 3-stage tube voltage amplifier	76
Fig. 14: polar view of sectorized Zone	86
Fig. 15: Power Resistor & Unit Pentode Array assemblies	89 ✓
Fig. 16: Drive Ring schematic cross section view (complete)	90 ✓
Chapter 8 } Fig. 17: enhanced side elevation of the design hull configuration	94 Δ ✓
Fig. 18: StarDrive vessel hull & bihemitoroidal field	102 Δ ✓
Fig. 19: 3η Drive Unit hull diameter vs. field voltage req'd.	106
Fig. 20: radial rotor segment bandwidths	111 Δ ✓
Figs. 21-23: basic rotor construction & field emitter design	112 Δ ✓
Fig. 24: Neutral Ring cross section & rotor component positioning	123
Fig. 25: Magnetic Ring & Field Coil configuration	127 Δ ✓
Fig. 26: Primary Induction Ring Arrays	173 Δ ✓
<i>special:</i> Tesla Tower and portrait photo	174
Fig. 27: 1η and 3η Primary Power System circuitry	182
Fig. 28: schematic for Field Voltage Control System	183
Fig. 29: induction performance & rotor speed table	191
DataSheet # 8 } Fig. 30: plate characteristics curves graph	355
DataSheet # 9 } Fig. 31: graphic calculations of triode load-line	357
Fig. 32: graphic derivation of load-line for beam power pentode	358
Fig. 33: cutaway showing radial construction of pentode tube	359
DataSheet # 11 } Fig. 34: voltage gain graph	361
DataSheet # 14 } Fig. 35: determination of Zero-Bias Voltage Factor	367
DataSheet # 15 } Fig. 36: tube pre-breakdown phenomena	379
Fig. 37: pentode generic load-line & characteristic curves graph	380
Fig. 38: plate output graph for beam power pentode	381
DataSheet # 16 } Fig. 39: Armature Array quadrant & pole positioning diagram	384
Fig. 40: Armature core configuration	209 Δ ✓
Fig. 41: basic Variable Inductor Array wiring	210

	<i>special:</i> computer-generated representation of the copper atom	388
<i>Mat. SpecSheet A }</i>	Fig. 42: Neutral Ring composite hull construction	392 ✓
	Fig. 43: radial Zone sector partition (side view)	395 ✓
<i>Mat. SpecSheet B }</i>	Fig. 44: Neutral Ring hull section and structural intercooler zone	397
	Fig. 45: Emitter Ring hull plate support bracket	398 ✓
	Fig. 46: Neutral Ring support bracket	399 ✓
<i>Mat. SpecSheet C }</i>	Fig. 47: carrier assembly construction (w/drive motors)	405 ✓
<i>Mat. SpecSheet D }</i>	Fig. 48: electrode array grid wire course patterns	407
	Fig. 49: projected resistivity plot for Steatite 357	409
	Fig. 50: projected resistivity plot for Cordierite 547	410
	Fig. 51: <i>k</i> and <i>ac loss</i> vs. temp. for Sodium Bismuth Titanate	412
	Fig. 52: resistivity vs. temp. for special dielectric materials	413
	Fig. 53: Power Resistor & Unit Pentode Array assemblies	415
<i>Mat. SpecSheet F }</i>	Fig. 54: Ferrite 5 B/H ratio & demagnetization curve graph	418
Chapter 9 }	Fig. 55: power field flux polarity diagram	217 Δ ✓
Chapter 10 }	Fig. 56: combined maximum rotor speed table	241
	Fig. 57: Cuff centrifugal drive (top & side views)	246
	Fig. 58: representation of Pawlicki betatron drive	248
	Fig. 59: theoretical shape of rapidly rotating black hole	252 ✓
Chapter 11 }	Fig. 60: a representation of quantum potential loop-space	265 ✓
Chapter 12 }	Fig. 61: the electromagnetic spectrum	278
	Fig. 62: 3η rotor circuit diagram (per Patent Application)	280
	Fig. 63: unit pentode array control module (per Patent Appl.)	282
	Fig. 64: gm flux cavity detector schematic	288
	Fig. 65: gravitic shadow effect recorded w/cavity detector	289
Chapter 13 }	Fig. 66: stellar spectral classes and characteristics	293
	Fig. 67: local stars of interest (table)	294
	Fig. 68: skymap of local stars discussed	298
	Fig. 69: warp jump turnaround sequence graph	301
	Fig. 70: starmap & galactic coordinates for local reference stars	308
	Fig. 71: dual continuum FitzGerald ratio table	312
	Fig. 72: hull precessional torque vector diagrams	315
	Fig. 73: induced X-ray emissions detection diagram	318 Δ ✓
Chapter 14 }	Fig. 74: behavior of representative cosmological models	333
	Fig. 75: age vs. H_0 for Flat Universe, model 8	335
	Fig. 76: age vs. H_0 for Open Universe, model 7	336
	Fig. 77: age vs. H_0 for Closed Universe, model 12	336
	Fig. 78: simplified proposed quantum matrix structure	339

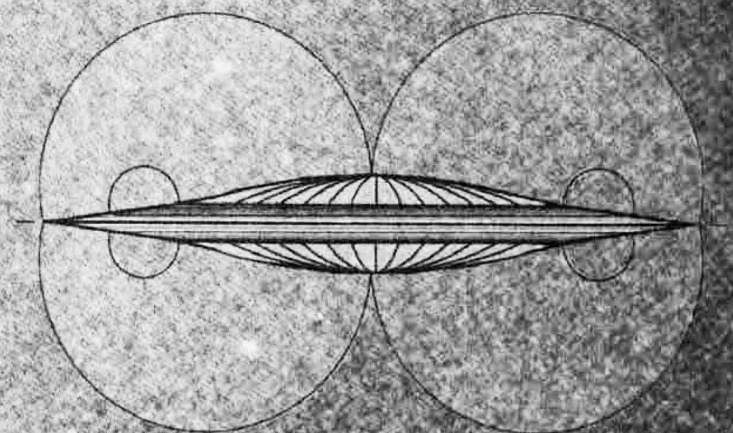
key: Δ = colorized
✓ = shaded

music background research by:

Area Records & Music
74 Seneca St.
Geneva, NY 14456
(e-mail: mail@arearecords.com)

cover photos and flyleaf backdrops by:

Angel Lite Images
8643 Main St., Suite D
Honeoye, NY 14471
(e-mail: alimages@frontiernet.net)



Visit us at www.stardrivedevice.com

ISBN 0-9713727-0-5
51995>



9 780971 372702